The University of Nottingham
Department of Civil Engineering

Wind / Wave Interactions In The Surf Zone

by
Daniel Martin King, B.Eng

Thesis submitted to the University of Nottingham for the degree of Doctor of Philosophy.

October 1994

ABSTRACT

Wind/wave interactions in the surf zone are studied using a wave tank and environmental wind tunnel. The wind simulation is achieved over a relatively short fetch using accelerated growth techniques, at a scale of roughly 1:100. Waves are scaled at approximately 1:50, and consequently there is some scaling mis-match between the wind and wave simulations.

Results show that wind has a significant effect on the breaking of the waves. Both breaker location and breaker type are shown to be affected by the wind. Results are in agreement with those of Douglass (1989 & 1990), who used a wind/wave flume to simulate the prototype conditions, but made no attempt to correctly simulate the turbulence in the air flow. The main findings, are that onshore winds promote spilling waves and increase the surf zone width, whereas offshore winds promote plunging waves, decreasing surf zone width.

Hot-film measurements of the air flow over the waves show that there exists significant differences between the air flow structure of offshore and onshore winds over the surf zone. Under offshore winds, the surf zone exerts a large drag on the air flow, dramatically increasing turbulence intensities, aerodynamic roughness, z_0, and friction velocity, u_*, near the point of wave breaking. Under onshore winds the air flow is less affected and at the point of wave breaking, z_0 for onshore winds is an order of magnitude lower than the value under offshore winds. Phase-averaging techniques indicate large wave-induced perturbations to the mean velocity over the waves, and these are present to heights of up to 5 or 6 times the breaker height over the point of wave breaking. Spectra indicate that for onshore winds large wave-frequency fluctuations are present at the shore.

Additionally, studies of particle motion offshore of the surf zone indicate wind effects on the drift velocities of suspended particles, although the precise nature of the wind effect was not clear.

ACKNOWLEDGEMENTS

Dr Chris Baker for his excellent supervision and support throughout my period of study at Nottingham. Bob McClelland for his technical help and practical ideas during the several months spent assembling and constructing the experimental equipment.

To the Science and Engineering Research Council (now renamed the Engineering and Physical Sciences Research Council) for the financial support for this work.

Grateful thanks to Mr Ian Shepherd of Hydraulics Research Ltd. (Wallingford) for the extended loan of the twin-wire wave probe, without which much of this work would not have been possible.

Also thanks to the other members of the fluids research group, past and present, for comments, suggestions and help in all aspects of this research.

TABLE OF CONTENTS

LIST OF TABLES

LIST OF FIGURES

NOTATION

For The Wind

d	Zero plane displacement
E	Voltage output from anemometer
H_{ref}	Reference height (100mm)
I_u	Longitudinal turbulence intensity
I_v	Vertical turbulence intensity
$\langle I_u \rangle$	Phase-averaged turbulence intensity
K	X-film calibration coefficient
${}^{x}L_u$	Longitudinal turbulent lengthscale
n	Frequency
R_c	Hot-film sensor resistance at t_e
R_H	Hot-film sensor resistance at t_s
R*	Roughness Reynolds' number
S	Sensitivity coefficient for hot-film calibration
S(n,z)	Power spectral density
t_e	Wind tunnel environment temperature
t_s	Hot-film sensor operating temperature
U	Wind velocity
U_{eff}	Effective wind velocity across hot-film
U_i	Instantaneous wind velocity
U_{ref}	Wind velocity at reference height
u*	Friction velocity
$\overline{U}$	Mean wind velocity
$\langle U \rangle$	Phase-averaged mean velocity
V	Vertical wind velocity

V_i	Instantaneous wind velocity in vertical direction
$\overline{V}$	Mean vertical wind velocity
X	Distance from origin
Z	Height
z_o	Aerodynamic roughness
α	Temperature coefficient of resistance (hot-film)
$-\rho \overline{uv}$	Reynolds stress
<uv>	Normalised Reynolds stress
θ	Angle of oncoming flow to hot-film probe
σ^2	Variance of wind fluctuations

For The Waves

C	Wave Celerity
C_b	Wave celerity at breaking
d	Still Water Depth (SWD)
d_b	SWD at point of wave breaking (breaker depth)
d_{pp}	SWD at plunge point
H	Wave height
H_b	Breaker height at the point of breaking
H_o	Deep water wave height
H_p	Wave heights in deepest part of wave tank
L	Wavelength
L_o	Deep water wavelength
m	Beach slope
P_{LS}	Longshore energy flux factor
SWD	Still Water Depth
SWL	Still Water Level
T	Wave period

X	Distance from origin
X_s	Surf Zone Width
ξ	Surf similarity parameter
θ_b	Angle between wave crest and shoreline

General constants

g	Acceleration due to gravity
μ	Dynamic viscosity
μ_a	Dynamic viscosity of air
μ_w	Dynamic viscosity of water
ρ	Density
ρ_a	Density of air
ρ_w	Density of water
ν	Kinematic viscosity
ν_a	Kinematic viscosity of air
ν_w	Kinematic viscosity of water
σ	Surface tension of water

CHAPTER 1

INTRODUCTION & LITERATURE REVIEW

1.1 REASONS FOR THE STUDY

The breaking of waves at the shore is an important aspect of nearshore coastal dynamics and has been extensively studied. The action of the waves is responsible for the movement of large amounts of beach material, both along the coast (littoral drift) and in the onshore-offshore direction (cross-shore drift). Studies have shown that one of the important controlling parameters is the width of the surf zone, since this defines the region of highly turbulent water motions. Another significant factor is the type of breaker that occurs, (Kana (1979), Jiaboa (1989)). These are discussed more fully in section 1.2.

Breaker type is also a principle factor in determining breaking wave induced forces on surf zone structures, for example piers or seawalls, (Silvester (1974a)). Other major factors include the point of wave breaking relative to the structure and wave height.

Despite extensive ongoing research into both nearshore wave breaking and open-ocean wind-waves, the influence of the wind on nearshore breaking waves has only recently been considered. References to its possible effect on the waves have been made frequently, (Kana (1979), Kinsman (1965)), and the existence of wind set-up (or storm-surge) is often quoted as a factor in extreme high tides around the globe.

Two recent studies, field observations by Galloway et al (1989) and a wind-wave flume laboratory experiment, (Douglass & Weggel (1988), Douglass (1989), Douglass (1990)), have shown that there exists a distinct correlation between wind conditions and wave breaking. Not only is the point of wave breaking influenced (which governs the surf zone width), but the breaker type and relative wave height have also been shown to be affected. Thus it would appear that wind conditions are a contributing factor to both nearshore sediment transport and wave-induced forces.

In addition to wind effects on the waves, this research examined the effect of these waves on the nearshore wind profile. No previous work in this area has been discovered by the author, but the literature on open-ocean wind-waves suggests significant modifications to the wind profile may occur, (Banner & Melville (1976), Wu (1968), Banner (1990)). This may have consequences for the wind-induced dynamic loading of nearshore structures.

This research modelled the prototype conditions using a scaled fully turbulent wind, with both offshore and onshore wind conditions being studied. This improved on the wind simulation used by Douglass (1989 & 1990), where no attempt to correctly scale the shear profile or turbulence characteristics of the wind was made. This can significantly affect the results of wind tunnel tests. This criteria resulted in a necessary trade off with respect to model scales. Scaling of wind boundary layers is easier at smaller scales (1/100 is generally the largest scale that can be successfully simulated), while scaling of waves is better at larger scales. Thus while the simulation of the wind is far better than achieved by Douglass, the wave simulation suffered from a smaller scale than preferable.

The main aims were therefore to examine the wind influence on breaking waves with regard to breaker heights, breaker types and the overall surf zone width. Modifications to the wind were also to be studied, with attention paid to changes which may affect structural loading and to the mechanism by which the wind affects the waves.

1.2 BREAKING WAVE INVESTIGATIONS

Waves may be broadly classified into two categories, namely storm waves or swell waves. The former are still being generated or maintained by the wind and are hence still within the confines of the storm affected region. The term swell is applied to waves which have propagated out of the storm fetch and are dispersing across the ocean. For storm waves the sea surface consists of many waves of differing height and length. Swell waves have a roughly sinusoidal profile, with a definable period and wavelength. A full discussion on storm and swell waves is contained in Silvester (1974a). This thesis deals with wind effects on the breaking of these regular swell waves at the shore.

The breaking of waves at the shore has been studied extensively. Shoaling and breaker geometry results are available in the literature for waves at different scales and beach slopes, (Galvin (1968), Ippen & Kulin (1955), Iverson (1952), Wiegel (1950)). Waves breaking on a beach can take any one of several forms or modes at the point of breaking and these are determined by combinations of beach slope, wave height in deep water and wave period, (Silvester (1974a)). The latter two characteristics of the wave determine the wave steepness which is the ratio of wave height to wavelength (or period). For any given wave height a shorter period produces a steeper wave, similarly reducing wave height whilst keeping period constant produces a less steep wave. Wave steepness is fundamental in determining the various forms of breaker type, (Iverson & Hayami (1954)).

There are four recognized modes of breaking wave within the surf zone, (Galvin (1968)). These modes are points in a continuous ordered sequence. For a given wave height, the sequence, in order of increasing wave period, is: spilling, plunging, collapsing and surging, **figure 1.1**. Thus as wave steepness decreases the wave type for a given beach slope changes from spilling through to surging, this sequence is continuous and the named breaker types are merely points of descriptive convenience. Progressing through the sequence one would see for example waves that could not fully be described as either spilling or plunging, but exhibit characteristics of both modes of breaking. The term 'transitional wave' is used here to describe a wave which is between the spilling and plunging modes.

On natural beaches fronting the ocean, the most common breaker types are spilling and plunging respectively, (Galvin (1968)). Spilling waves break by the formation of turbulent flow at the crest of the wave. This turbulent water gradually propagates down the front face of the wave as the wave progresses into shallower water. Eventually the entire front face of the wave is white water and the wave becomes a bore. Plunging waves break in a far more explosive manner. As the wave progresses into shallower water an overhanging lip is formed at the wave crest. The overhang eventually crashes down in front of the wave in a catastrophic event which causes the wave to become a bore. Occasionally these waves form the spectacular 'tubes' favoured by surfers. Plunging waves have a very asymmetrical profile and the breaking process creates an air-entrained roller. This 'horizontal roller' moves

down and along the sea bed sweeping up particulate matter, and as such plays an important role in surf zone sediment transport, (Shibayama & Horikawa (1982)).

Energy dissipation characteristics for spilling and plunging waves are also different. For plunging waves most of the waves' energy is dissipated over a short area where the overhanging lip crashes down in front of the wave. Spilling waves dissipate energy as turbulence gradually over the whole width of the surf zone, (Fuhrboter (1970)). Dissipation of the waves' energy is significant in determining concentrations of suspended sediment in the surf zone.

Peregrine (1983) gives a review of wave breaking on beaches and considers the mechanism by which the breaking process begins to occur. For a majority of waves he notes that part of the water surface becomes vertical, overturns and projects downwards forming a jet of water. The overturning 'lip' may be small with respect to the wave or large as is the case with plunging waves. This is not however always the case and waves may break with no part of the wave becoming vertical. Peregrine notes that "there is reasonable doubt about the initiation of spilling breakers", although in many cases a small overturning is responsible for the initiation of breaking by spilling. Another potential cause of breaking, and one which is applicable to both spilling and plunging waves, is the steepening and subsequent breaking of short waves as they are overtaken by the crest of a longer wave, Kraus (1972). As the short wave breaks, the energy and momentum associated with that wave is transferred to the horizontal component of the long wave's crest.

An often used empirical parameter for calculating wave heights from given breaking depths is given by the equation below:

$$\text{Amplitude-to-depth ratio} = \frac{\text{Breaker Height}}{\text{Breaker Depth}} = \frac{H_b}{d_b} \qquad (1.1)$$

where H_b is the breaker height and d_b is the breaker depth, **figure 1.2**. This equation is frequently used in engineering practice to determine design wave heights for given water depths, and a value of 0.78 is frequently quoted, (Galvin (1972), Iwata and Sawaragi (1982), Weishar & Byrne (1978)). However this parameter takes no account of variables such as beach slope or the incoming wave steepness. Other breaker limits have therefore been

developed to include the variations in amplitude-to-depth ratio resulting from these variables. These are documented by Iwata & Sawaragi (1982).

In recognition of the relatively few factors apparently governing wave breaking, several breaker type parameters have been developed. The aim is to predict for given values of wave height, beach slope and wave period, the form of the wave at breaking. The 'surf similarity parameter', developed by Battjes (1974) is frequently quoted in the literature and it links wave period, (T), beach slope, (m), and wave height (either deep water or at the point of breaking) into a single parameter. This is given below:

$$\text{Surf Similarity Parameter} = \xi = \frac{m}{\sqrt{H_o/L_o}} = \frac{1}{\sqrt{2\pi}} \cdot \frac{m}{\sqrt{H_b/gT^2}} \qquad (1.2)$$

where H_o is the deep water wave height and L_o is the deep water wavelength. Battjes (1974) found this parameter to be a good overall indicator of several surf zone properties including; breaking criteria, breaker mode, distance of breaking from the shore and the number of waves in the surf zone. The values of ξ for which one would expect to find each wave type occuring were determined (at the point of breaking) by Iwata & Sawaragi (1982). The ranges are given in table 1.1.

Wave Type	Surf Similarity Parameter, ξ
Surging	$\xi > 2.0$
Plunging	$0.4 < \xi < 2.0$
Spilling	$0.4 > \xi$

Table 1.1. Breaker type ranges for surf similarity parameter at point of breaking.

However, although this parameter works reasonably well in the laboratory, on naturally occuring beaches investigations have found that it does not categorize the waves so successfully. Several authors have noted that spilling waves appear to occur independently of the parameter, commenting that either non-linear beach slope or the effects of wind are distorting results, (Galloway (1988), Weishar & Byrne (1978)).

A further function of the shoaling process is wave set-up. This occurs shorewards of the breaker region and results in an increase in mean water level. This is important since the increased water level allows higher waves (which would otherwise have broken) to reach shoreline structures.

1.3 WIND/WAVE INTERACTIONS

The interaction between wind and nearshore breaking waves is not well documented and few references to this area of nearshore dynamics are made in the literature. This contrasts with the well documented case of open ocean wind-waves. Over the years this area has been extensively researched; several theories and empirical equations exist for determining wave generation, wave growth, and wave heights. However for this research these are of limited use due to the greatly differing geometry and kinematics of surf zone waves. A review of potentially relevant information is presented later.

Two recent studies, field observations by Galloway et al (1989) and a laboratory wind/wave flume experiment by Douglass (1989 & 1990), have examined the influence of wind on the breaking of waves in the surf zone. Both show that there exists a distinct correlation between wind conditions and wave breaking. Wind strength and direction is shown to affect both where the waves break and how the waves break.

The results from both Douglass (1989 & 1990) and Galloway et al (1989) concerned the effect of wind on the two most common types of breakers; spilling and plunging. Extensive field observations by Galloway et al (1989) suggested that wind conditions impose significant controls on the types of breakers occuring, onshore winds enhancing spilling waves and offshore winds enhancing the plunging mode.

These results were echoed by the laboratory experiments of Douglass (1989 & 1990), with the further result that wind was also significant in determining breaking depths. Using a fan to provide wind over a wave flume Douglass (1989 & 1990) found that offshore winds delayed the breaking process, so that waves would break later, (closer to the shore), and with a tendency towards the plunging mode. This has a marked influence on the 'breaking amplitude-to-depth' ratio (section 1.1). The waves therefore break in shallower water than

they would normally. Waves were found to be particularly susceptible to wind induced variations if they were near the transition point between spilling and plunging waves. Douglass (1989 & 1990) found that 'solid' plunging waves were little influenced by the wind.

Hypothesizing the mechanism of the winds influence on the waves, Douglass (1989 & 1990) observed that the formation of micro-breakers at the wave crest appeared to control the moment of breaking. Wind shear, he supposed, affected wave breaking by retarding the growth of these micro-breakers in offshore conditions and augmenting their growth in onshore winds. Despite this Douglass (1989 & 1990) restricted his wind data to pitot-static tube readings of the mean wind speed: no details of turbulent lengthscale or aerodynamic roughness were presented. This hypothesis corresponds with that given by Peregrine (1983) where the longer wave is caused to break by the transfer of energy and momentum from the breaking of the shorter wave.

There were however some short-comings in Douglass' work. Primarily the ducted air-flow over the tank would not allow the proper development of a wind boundary layer. Simulation of the boundary layer and associated turbulence is important in that this determines the overall drag and pressure forces acting on the waves. Incorrect simulation of the Reynolds stresses can affect the separation and reattachment of the air flow from the waves, and thus the overall drag on the waves, (Cook (1985)). As Douglass made only pitot-static tube measurements of the wind velocity, no details of turbulence characteristics were obtained. Given that 1/100 scale is generally the largest that the wind can be modelled at (even with long fetch wind tunnels), there is likely to be a severe mis-match between Douglass' 1/15 waves and the wind simulation. Thus the wind effects observed by Douglass may differ from those where turbulence characteristics are simulated.

To the author's knowledge no studies of the wind profile over the surf zone have been carried out. The greatest source of information concerning wind flow over waves is for long fetch wind waves or non-shoaling periodic waves, (Bandou & Mitsuyasu (1988); Kawai (1981); Kawai (1982); Kondo, Fujinawa & Naito (1972), Naito (1988)). There are major differences between flow over waves such as these and flow over the surf zone. The primary one is the rapidly changing nature of the surf zone. Waves do not remain homogeneous

in space: they shoal, becoming steeper and closer in profile to cnoidal waves than to the near sinusoidal waves from which they evolved.

Additionally surf zone waves have a very asymmetrical profile. The backs of the waves tend to have a very smooth profile, even once the wave has broken down into a bore. The front face is very different, prior to breaking the front face tends to be steeper and is vertical in the case of plunging waves. Once the wave has broken it is a mass of turbulent water and at full scale this also involves large amounts of air entrainment. It is therefore reasonable to suppose large differences in the air flow over the waves exist for onshore and offshore winds.

Several points from research into wind waves are worth noting. Wu (1968) found the onset of wind wave breaking to be important in determining the shear velocity and aerodynamic roughness for a wind field. It has also been found that local air flow separation occurs concomitantly with wave breaking, (Kawai (1981), Kawai (1982), Banner & Melville (1976)), and that the drag from a breaking wave is an order of magnitude larger than that for a similar sized unbroken wave, (Banner (1990)), which suggests a large drag increment and air flow separation arising from surf zone waves.

Baskaran et al (1991) noted that for a solid curved hill, there is a peak in the values of surface shear at the crest, and given the geometric similarity between their hill and shoaling waves one could suppose a similar shear profile would exist for surf waves. This would support Douglass' hypothesis of the mechanism for the wind/wave interaction.

Takeuchi et al (1977) noted that the variance of the longitudinal velocities just leeward of the wave crest showed a drastic change from the one-wavelength averaged values. Windward of the crest however the values show little deviation from the one-wavelength averaged values. Additionally it was noted that there was a phase-change in the phase averaged velocity profile over the wave. Near the crest velocity is out of phase with respect to the wave height, but as height above the wave increases, a phase change occurs and velocity is in phase with the wave profile (i.e. a peak in phase averaged velocity occurs over the wave crest).

Research by Kondo et al (1972) showed that phase changes can occur for phase-averaged mean velocity over progressive periodic gravity waves if the wind-to-wave speed ratio varies. It was found that for wind and waves in the same direction velocity was in phase with wave height. However for wind and waves flowing in opposite directions (i.e. the wind-to-wave speed ratio has changed) a phase change occurs of 180° occurs.

Over the years several theories for wave generation and growth due to the wind have been proposed. Silvester (1974a) documents four of the theories. These are the: (i) resonance (ii) shear flow (iii) sheltering effect and (iv) breaking theory. Each concerns a different phase of the generation and growth of the wave field. The resonance and shear flow theories deal with the early stages of wave growth when surface perturbations are small and air flow separation is assumed not to occur. These two mechanisms are complementary, with resonance from the air turbulence providing the initial perturbance of the water surface, while shear flow of the mean velocity profile selectively promotes the shorter waves. Once over a certain size, wave growth is due to either the sheltering effect or to wave breaking.

The sheltering effect, which attributes wave growth in the later stages to form drag on the larger components of the wave spectrum, takes over as the mechanism of wave growth once separation from the wave crests begins to occur. Although wave breaking is generally considered to be a dissipating mechanism, energy (possibly in the form of momentum) may be imparted to underlying waves from the breaking of smaller wind-waves at the crest of the larger wave. Also the wind velocity is a maximum at the crest of the longer wave, adding to the momentum of the circular motions of the water particles. This appears to be a similar process to the action of the 'micro-breakers' observed by Douglass (1989 & 1990) in onshore wind conditions, where the extra momentum added to the main wave from the breaking of the smaller wave is sufficent to cause earlier breaking of the wave.

Several points are raised by these theories, which it should be remembered have been developed for open-ocean wind-waves. Firstly the importance of correctly simulating the wind profile is seen to be necessary in order to obtain realistic levels of turbulence and shear flow. The growth of the smaller waves will occur even when generating larger waves, and if the 'micro-breakers' are responsible for the wind/wave effect then the growth of these waves must be

simulated as accurately as possible. A further point is that there is a limit to the smallest wave that will be created, called capillary waves, they have wavelengths of less than 17mm. The problem lies in the fact that at model scale these waves will be proportionally many times larger than for the prototype conditions. At the model scale capillary waves may be a factor in wave breaking, something which is unlikely at prototype scale.

Although capillary waves are generally discussed in the context of wind-induced wave growth, Phillips (1969) noted that capillary waves may exist independently of wind. As wave steepness increases, and the wave crest becomes more curved, it is possible see capillary waves travelling with the primary wave on the front face. These so called 'parasitic' capillary waves may be an important factor in model scale wave breaking, since near breaking the model scale waves will have a large crest curvature.

One other aspect of wind-wave interactions is the storm surge arising from the wind stress on the water surface. Although this is only generally of importance in storm conditions where excessively high tides may be created by strong winds, lower winds may cause a change in mean water level sufficient to affect the breaking of waves. Silvester (1974b) provides a method for calculating the wind setup due to onshore winds. This shows that for a 15m/s onshore wind, over a fetch of some 50km, set-up at the shore is only around 30cm. Although this change in mean water level may affect the position of the breakers with respect to some land based origin, for a constant beach slope the surf zone width will not be affected. The main effect would be for nearshore structures where larger than expected waves may be able to break on the structure. However the set-up due to a 15m/s wind has been shown to be fairly small, and for a 10m/s wind it is lower, at around 12cm. For the wind strengths considered here it can, therefore, be removed from the problem.

1.4 RESEARCH APPLICATIONS

Applications of this research are threefold, probably the most important being the effect the wind may have on nearshore sediment transport. Additionally the winds' effect on wave heights and types may affect surf zone structures, and finally the influence of the waves on the wind profile is considered with respect to possible effects on building dynamics.

Sediment transport within the surf zone is described as either 'longshore' or 'cross-shore'. The former refers to transport of sediment in a direction parallel to the coast, the latter refers to sediment motion in the onshore-offshore direction. Both are significant in determining the nature of transport in the nearshore region.

Studies of suspended sediment in the surf zone, (Kana (1979), Jiabao (1989)), show that one of the principle factors controlling suspended sediment is breaker type. Plunging breakers entrain an order of magnitude more sediment than spilling waves of similar size. This is attributed to the existence of the 'horizontal roller', (Shibayama & Horikawa (1982), which sweeps up particulate matter into suspension. This roller is not present in spilling waves and for these waves sediment suspension results from the downwards diffusion of surface generated turbulence. Secondary factors controlling suspended sediment concentrations include; distance relative to the break point, beach slope, and wave height. Kana proposed that the importance of breaker type suggested dependence on 'relative wave height', $^{db}/_{H_b}$.

Offshore of the point of wave breaking, i.e. outside the surf zone, sediment transport is affected by the net movement of the water particles, (Silvester (1974b)). For swell waves net motion at the bed occurs in the direction of advance of the waves. For storm waves the net bed motion is zero, but is opposite to the direction of the wave propagation just above this level. On naturally occuring beaches one of the characteristics of the offshore zone is the size sorting of the bed material. This occurs as a result of the greater orbital velocities under the wave crests than under the troughs. Further discussion on this is given in Silvester (1974b).

There exists however some doubt as to the possible effects of wind velocity and direction. Kana (1979) notes that "...wave period, longshore current velocity and wind velocity have little or no effect on (sediment) concentration...". Galloway (1988) however calls for detailed categorisation of breaker type which "...accounts for breaker type changes in response to local wind variability". The results of Galloway et al (1989) and Douglass (1989 & 1990) show that wind has the potential to affect both breaker type and amplitude-to-depth ratio (the inverse of 'relative wave height'), therefore influencing two of the major factors determining suspended sediment

concentrations. The author has not found any information linking wind conditions to nearshore sediment transport in the literature.

The potential effect of the wind on surf zone structures such as piers or seawalls should also be considered. These are often subjected to loads arising from breaking waves and are consequently designed to withstand such attack. Silvester (1974a) shows that the point of wave breaking relative to the structure is probably the most important factor governing the forces developed. This is because of the changing geometry of the wave as it shoals. For a vertical seawall the highest forces are developed when the incident wave face is near vertical. Bagnold (1939) developed an expression for the peak dynamic pressure due to a breaking wave based on experimental work. Peak pressure was proportional to breaker height, H_b, and water depth, d, at the toe of the structure.

Silvester (1974a) presents the results of Rundgren's tests on the peak pressures on a vertical wall occuring as a result of wave breaking. During the experiment the water level rose slowly, so that the point of wave breaking relative to the wall changed. Pressure forces due to the waves were measured over time. Peak pressures were observed when wave breaking took place right at the wall, and these forces were around two or three times greater than the forces arising when waves broke before the wall or were reflected from it (without breaking). The location of wave breaking is therefore highly significant in determining forces from a given wave.

Weggel (1972) examines the usual methods of determining the largest breaker height for design purposes. He notes three factors (amongst others) upon which the 'design' wave height for a structure will depend. These are;

i) the depth of water in which the structure is situated,
ii) the beach slope and local bathymetry,
iii) the deep water characteristics of the incident waves.

Clearly, the wind conditions are unable to significantly affect any of these. However, an indirect dependency may occur from the first of these variables. As mentioned in section 1.1 the amplitude-to-depth ratio at the point of breaking is frequently used as a guide to the highest wave that can occur at that point. Thus for a wave which will break with a given wave height, H_b, the depth at which breaking occurs is determined by this ratio. Douglass showed that an offshore wind can significantly affect this ratio, causing waves to

progress further shoreward before breaking. Thus an offshore wind may cause higher waves than expected to break in the region of the structure. Sorensen (1978) gives a formula for the calculation of induced pressures on a vertical wall subjected to wave breaking. Maximum pressure is directly proportional to breaker height, H_b, so any wind induced increase in wave heights breaking on the structure would be reflected in increased wave loading.

Breaker type is also likely to be a factor governing wave induced forces. Minikin (1950) notes that a pocket of air trapped between the structure and wave face can result in extreme high pressures being developed. Such circumstances can only occur for plunging waves, since for spilling waves break without a vertical front face, preventing air entrapment. Reddish & Basco (1987) found that plunging waves resulted in higher forces on slender piles than occured for similar sized spilling waves. Thus the results of Douglass (1989) suggest that the wind, by affecting breaker location and breaker type, may significantly affect wave loading on surf zone structures.

Finally, there also exists the possibility that the action of the waves on the wind will affect the dynamic response of structures in or near the surf zone. For example, piers or buildings close to the shore may be affected. Banner & Melville (1976) note that for wind and waves co-flowing in a wind-wave flume a breaking wave causes serious modifications to the pressure and velocity distributions which are evident at elevations of several times the wave amplitude above the water level. There exists the potential for surf zone waves to affect the air flow in a manner which may be significant for nearshore structures.

CHAPTER 2

DIMENSIONAL ANALYSIS

Waves breaking on a beach at model scale will be scale models of the prototype conditions if the effects of viscosity and surface tension are negligible. For these experiments further scaling effects are imposed by the wind since the profile over the waves must be at the correct scale. This section gives a list of the variables and dimensionless groups which will affect the scaling and modelling of the wind-wave interaction.

The waves depend on the following variables;

H_o	Deep water wave height
T	Wave period
m	Beach slope
L_o	Deep water wavelength
H_b	Wave height at breaking
d_b	Still water depth at the breaking point

Only the first three on this list are independent since deep water wave length, L_o, is determined solely by the wave period, T (see appendix A). Also for the work here beach slope, m, is a constant. Thus, for the work reported here once H_o and T are specified then the other variables will be determined by some function of them.

For the wind, the main variables are;

H_{ref}	Reference height
U_{ref}	Reference height velocity
z_o	Aerodynamic roughness
${}^xL_u$	Longitudinal turbulent lengthscale

In addition to the above variables the following (constant) variables need to be taken into account for certain dimensionless parameters.

σ		Surface tension of water
ρ_w		Density of water
ρ_a		Density of air
μ_w		Dynamic viscosity of water
μ_a		Dynamic viscosity of air
g		Acceleration due to gravity

The following dimensionless groups can therefore be said to be of relevance.

	m	Beach Slope
*	$\frac{H_o}{gT^2}$	Deepwater wave steepness
	$\frac{L_o}{gT^2}$	Dimensionless wavelength
	$\frac{H_b}{gT^2}$	Dimensionless wave height at breaking
	$\frac{d_b}{gT^2}$	Dimensionless water depth at breaking
*	$\frac{H_{ref}}{L_o}$	Ratio of wavelength to wind reference height
*	$\frac{^xL_u}{L_o}$	Ratio of turbulent lengthscale to wavelength
*	$\frac{H_{ref}}{z_o}$	Ratio of reference height to aerodynamic roughness
	$\frac{U_{ref}H_{ref}}{\mu_a/\rho_a}$	Wind Reynolds number
	$\frac{U_{ref}}{L_o/T}$	Wind speed to wave speed ratio
*	$\frac{U_{ref}}{\sqrt{gH_o}}$	Dimensionless wind speed (Froude scaling parameter)

$\frac{\rho_a}{\rho_w}$ Ratio of fluid densities

$\frac{\rho_w L_o^3}{\sigma_w T^2}$ Weber number

Dimensionless wind speed is used as the Froude scaling requirement, using wave height, H_0, as the normalising variable. H_0 was used in preference to H_{ref} because this function is used in the later chapters to specify dimensionless wind speed (see section 4.4). The scaling is not affected by this since H_{ref}, H_0 and L_0 are linked by the above dimensionless groups.

Several problems are thrown up by these dimensionless groups. Firstly in order to fulfill Froude scaling criteria, the wind Reynolds number and the Weber number for the waves must be ignored. In the case of the Weber number this may cause problems for the wave breaking since at this point the waves can become highly curved at the surface (for example the overhanging lip on plunging waves). Thus the large relative difference in surface tension forces may be significant.

Kirschmer (1952) recommends that in order to avoid surface tension effects a minimum wave height of 2cm should be used. Sharp & Khader (1984) conclude that for harbour wave models surface tension and viscous forces are negligable for water depths in excess of 5cm and wave heights greater than 2cm. However for breaking waves the effects of scale may be more pronounced. Stive (1985) examined the the effects of surface tension for breaking waves and concluded that there was no significant deviation from Froude scaling for wave heights in the range 0.1 to 1.5m. Toumazis & Anastasiou (1990) found that surface tension effects were increasingly important with wave heights less than 0.5m, above this height waves were independent of surface tension effects.

Research by Millar (1972) suggests that the effects of surface tension are likely to be felt in terms of position of breaking and the amplitude-to-depth ratio. By using chemical additives Millar reduced the surface tension of water in a wave flume to half that of the original value. He found the reduced surface tension caused a slight increase in breaker heights and that the waves would break consistently closer to the shore. This implies that for the model used here, the

relative increase in surface tension effects compared to the prototype surf will reduce breaker heights and cause premature breaking.

Viscosity forces will also be more significant in the model than at full scale and these are determined by the Reynolds number. A large Reynolds number indicates that inertial forces dominate the viscous forces. Similarly, a small Reynolds number indicates that viscous forces are dominant. Reynolds numbers for the simulation of the boundary layer used here are of the order of 1000 times smaller than in the prototype conditions, indicating an increase in relative viscous forces. Generally however Reynolds number effects are ignored unless the specific area of interest invloves a high degree of flow separation (for example vehicles in cross-winds), and for the modelling here this is necessary due to the precedence of Froude scaling criteria. It is common practice to ignore the Reynolds number scaling in wind engineering models, (Cook (1985)).

Viscosity forces are similarly represented in the scaling of the waves, although according to Le Mehaute (1976), waves at the model scale used here should be minimally affected. The effects of surface tension and viscosity on the validity of the model are discussed further in section 4.8.

The use of a planar beach is potentially a significant deviation from the prototype conditions where beaches tend to have a parabolic profile and may exhibit offshore banks. It's use here is justified by the simplification which arises in terms of interpreting the results and comparing them with previous work. However, a potentially significant problem is the lack of beach porosity at model scale and this is discussed in section 4.8.

The ratio of fluid densities is a constant between model and prototype. Also the beach slope, m, is assumed to be constant between model and prototype. Hence because Reynolds number and Weber number are ignored and the ratio of fluid densities is constant, the problem can be described by those dimensionless groups marked '*'.

Futher discussion into the effects of scale is contained in section 4.8, including a discussion into the possible effects of air entrainment at the model scale.

CHAPTER 3

EXPERIMENTAL APPARATUS

3.1 WIND TUNNEL & ATMOSPHERIC BOUNDARY LAYER SIMULATION

The research was carried out in the Nottingham University Environmental Wind Tunnel. Although the tunnel is a non-return type, air leaving the tunnel recirculates through the building, which is only slightly larger than the tunnel itself, back to the tunnel entrance. Over a period of testing the tunnel temperature tends to rise by a few degrees depending on the fan speed and outside temperature. The tunnel entrance contains a gauze and honeycomb arrangement which smoothes the flow as it enters the tunnel. A contraction speeds up and further smoothes the air between the inlet and entrance to the working section. Air is drawn through the tunnel by a bi-speed fan positioned at the downstream end of the tunnel. Wind speed is varied by two controls, firstly the speed of revolution of the fan is selected, either low constant rpm or high constant rpm. Secondly, a compressor unit connected to a hydraulic circuit is used to change the pitch of the fan blades and thus wind speed.

The tunnel's working section is initially an enclosed jet of area 1.13m high by 2.42m wide. After 6.4m it becomes an open jet for the remaining distance to the fan. The total length of the working section is 11.4m.

Previous work at the University has established that an acceptable 1/100 scale wind can be obtained. However the constraints of space in the tunnel limit the fetch available for boundary layer development to only 5m in the offshore case (6.5m in the onshore case). Consequently accelerated growth methods, (Cook (1985)), were adopted. Simulations of this type are recommended for applications where the benefits of an increased scale are greater than the disadvantage of failing to reproduce the upper two-thirds of the boundary layer, (Cook (1973)). Results show that this provides an adequate simulation with turbulent lengthscales of the order of 0.2m.

The boundary layer in the wind tunnel was developed so that it provided a scaled value of aerodynamic roughness over the wave tank equivalent to that arising from smooth coastal terrain. A full scale value of aerodynamic roughness of 0.003m was selected as being appropriate, (Cook (1985)), and this gives a value of z_o of 0.00003m assuming a 1/100 scale model. The boundary layer is not meant to represent any particular site but to give a 'typical' simulation from which the deviations caused by the waves can be measured. Cook (1985) gives statistical data on U.K. wind climate. For most of the British coastline, at a reference height of 10m, a wind speed of 6m/s (Force 4 on the Beaufort scale) will be exceeded for 50% of the time. A typical coastal wind speed of 10m/s was therefore taken for the purposes of dimensional analysis. The Froude scaling requirement, $U_{ref}/\sqrt{gH_o}$, gives a reference height wind speed of 1-2m/s at the model scale assuming a simulated boundary layer at 1/100 scale.

A further requirement for correct simulation of the boundary layer is the longitudinal turbulent lengthscale, ${}^{x}L_u$, as defined in section 4.3.4. Cook (1978) gives an equation for determining a typical turbulent lengthscale for combinations of aerodynamic roughness, z_o, and height above the ground, Z. Assuming that the zero plane displacement is negligible gives:

$$ {}^{x}L_u = \frac{25Z^{0.35}}{z_o^{0.063}} \qquad (3.1) $$

At a full scale reference height of 10m and taking the value of z_o to be 0.003m, this gives a full scale value of turbulent lengthscale, ${}^{x}L_u$, of 80.7m. Thus assuming a model scale of 1/100 we require a longitudinal turbulent lengthscale of around 0.8m.

The boundary layer was developed using a barrier and two sizes of roughness elements. The final offshore and onshore boundary layer configurations resulted from several 'trial and error' experiments using different combinations of roughness and barrier. The end results are described in section 3.3.

The low windspeeds necessary to fulfil scaling criteria means that experimental scatter may be large and in order to reduce this sampling times were as long as possible. The data acquisition package (Status 74) allows a maximum number of 4096 data points to be taken in one sample. Longer sampling times are

therefore traded against lower sampling frequencies. Details of data sampling frequencies and durations are given in chapter 4.

Details of the atmospheric boundary layer obtained over the flat water are presented in chapter 5.

3.2 WAVE TANK

The wave tank was 1.3m wide and 3.4m long and was of a three sloped design. At the deep end, where the paddle operates, the tank was initially flat, progressing to a steep section of slope 1/8. After this steep section the slope reduced to the 'breaking slope' of 1/20. The side elevation of the wave tank is shown in **figure 3.1**.

For the offshore configuration it was necessary to overlap the shallow end of the tank and wind tunnel floor, and this caused the beginning of the tank to be around 150mm above the level of the wind tunnel floor. In order to ensure a smooth transition of the air flow to the wave tank a sloping surface approximately 2m long was used. A similar overlap in the onshore configuration occurred but obviously required no fairing.

The initial steep slope of 1/8 was necessary due to the constraints of space within the wind tunnel. Wave tanks of similar design have been used by Easson et al (1988) and Izumiya & Isobe (1986). The latter considered the effects of the initially steep slope on the breaking of generated waves on the second shallower slope. Results showed that waves breaking on the second slope were unaffected if breaking occurred sufficiently shoreward of the change in slope. The minimum distance from the slope change at which waves could break unaffected by the change was found to be $5H_b$. The wave tank was therefore designed accordingly.

The tank was constructed of clear perspex sheets supported on an aluminium frame. The waves were generated by the flapping paddle at the deep end of the tank. The paddle was hinged at the bottom of the tank and is driven by a system of pulleys and chains attached to a variable speed motor located beneath the tank. Different wave types could be generated by combinations of paddle motor speed and paddle motion amplitude. Wave periods were directly

controlled by the motor speed. However wave heights were a function of both the motor speed and paddle motion amplitude.

Wave heights in the tank were of the order of 3-5cm, with wave periods of the order of 1 second. This set the scale of the breaking waves at around 1/50 when compared to full scale values. At the deep end the water depth was approximately 230mm, corresponding to a full scale depth of about 11m. Waves in this region had a profile which was roughly sinusoidal. Using Airy wave theory, (appendix A), the wavelengths of the waves in the deep end of the tank were calculated. Results showed waves in this region had wavelengths of around 1m. Comparison of the ratio of water depth to wavelength, (d/L), at this point with Airy wave theory shows that the waves were not strictly 'deep water' waves but were 'transitional', (Silvester (1974a)). Thus the wave heights measured in this portion of the tank were not true values of H_o, the deep water wave height. In order to avoid confusion, the values of wave height measured in the deepest part of the wave tank are referred to as H_p. The exact position of measurement of H_p was at X=-2823mm and a water depth of 190mm. Silvester (1974a) gives tabulated functions of d/L_o, and from this the ratio of H_p/H_o can be obtained. Using d=190mm and the values of L_o given in table 5.2, H_p/H_o is found to be around 0.92.

In order to confirm that the waves within the tank were relatively stable and that wave reflections were not affecting results several preliminary tests were carried out. Firstly the variation of mean wave height within the tank was measured by measuring the heights over a period of time. This test also established how long was needed for the initial transients of wave motion to die away. Over a 15 minute period wave heights were measured initially every 30 seconds and then every 3 minutes. Each sample contained around 20 waves from which the mean wave height was determined, (4096 samples at 200Hz). Results showed that the waves quickly settle to consistent values of mean H_b. After the first two minutes of running time, values of breaker height were within ±1mm for the spilling wave and ±0.5mm for the plunging wave. The speed at which the initial transients decay is probably aided by the relatively low volume of water in the tank.

Repeatability of the experiment was tested by sampling the same wave several times and stopping the paddle between each sampling period. After stopping the paddle several minutes were allowed to elapse in order to let water within

the tank stop moving. After starting the wave generator, the waves were allowed 2 minutes before each set of measurements were taken. Again the results showed good consistency, with both wave types showing maximum deviations from the mean value of H_b of $\pm$1mm. This corresponds to percentage errors of around 2%.

The above two tests investigated the stability and repeatability of *mean* breaker heights. The final area to be investigated was the variation of individual wave heights. A 16 second sample of both spilling and plunging waves was used, giving about 20 spilling waves and 15 plunging waves. For each wave within the data file, H_b was calculated, the mean value and standard deviation from this were then calculated. Results show that H_b is reasonably consistent. Spilling waves gave a mean wave height of 0.0383m and a standard deviation from this of 0.00082m. For plunging waves the mean and standard deviation are 0.0508m and 0.0013m respectively. Thus for both wave cases breaker heights generally fall within $\pm$1mm of the mean value of H_b.

Lateral uniformity of waves at breaking was examined during the onshore phase of the research. For the spilling and plunging waves, at the determined point of breaking, several measurements over the width of the tank were made, including the still water level, (SWL), at the point of breaking. The results showed that this varied across the tank width, with the deepest point being in the centre of the tank. The variation in water depth was basically due to deformation of the tank under the water load. Typically water depth at the edges was 13% lower than in the centre of the tank, although over the central third of the tank the water depth was effectively constant.

Breaker heights measured at the same time showed larger variations. For the plunging wave H_b varied from 58mm in the centre to below 40mm at the edges, for the spilling wave H_b was 50 and 31mm respectively. This translates to a 40% reduction in breaker heights at the tank edges.

Edge effects also probably occur as a result of sidewall friction creating a boundary layer which develops along the tank sides. It is difficult to specify if the variation in tank depth or the boundary layer were responsible for these edge effects. From observations, early breaking of the waves at the edges (almost always by spilling) and the severe reduction in wave height at the

edges, would seem to indicate that boundary layer effects are not insignificant and may dominate the effects due to differences in water depth.

Whether these 'edge effects' affected the waves breaking in the central part of the wave tank is difficult to determine. However the cantilevered traverse mechanism (section 3.4.1.1), from which all probes were suspended, meant that measurements of H_b (and also d_b) were confined to the same lateral position. Thus, the relative changes that occurred are still valid.

3.3 WIND TUNNEL LAYOUT

Details of the wind tunnel layout for the two tank configurations are presented in sections 3.3.1 and 3.3.2. The results for the wind profile over the water, with no generated waves, for the two different tank configurations are presented in section 5.1. Although the water surface is referred to as being 'flat water' for this configuration, small wind-generated ripples were present on the water surface. At higher wind velocities (above the nominal 1.6m/s reference height wind speeds) these ripples developed into recognizable wind-waves.

3.3.1 Offshore Configuration

A schematic diagram of the wind tunnel layout for the offshore phase of work is shown in **figure 3.2**. Due to the tank configuration, the available fetch for boundary layer development was smaller than in the onshore case. The final boundary layer was developed using three sizes of wooden cubes. A single line of 190mm cubes placed with a 20mm gap between adjacent cubes acted as a barrier. These were followed by 1.45m of 100mm cubes arranged at 10% area density, followed by 1.82m of 48mm cubes again at 10% area density.

At the side of the tank boards were placed horizontally at the level of the water, in order to prevent excessive spill-over of the wind. These are shown, along with the rest of the wave tank in **figure 3.3**, which shows the view of the wave tank and wind tunnel from the downstream end of the tunnel.

The overlap of the wave tank into the closed jet working section meant that the end of the tank was some 150mm above the level of the working section. It was therefore necessary to create a sloping fairing in order to promote smooth

transition of the air flow. The roughness elements were placed over this fairing, which at a total length of around 2m had a shallow angle of around 2°.

3.3.2 Onshore Configuration

Figure 3.4 shows the wind tunnel configuration for the onshore wind phase of the research. For the onshore configuration the tank is entirely placed in the open jet working section of the tunnel.

The boundary layer was developed using a similar combination of wooden cubes. The exact configuration was; a single line of the 190mm cubes (the barrier), followed by 1.6m of 100mm cubes at 10% area density, followed by 3.6m of 48mm cubes at 10% area density. The 48mm cubes are followed by a short length of no roughness elements where the fairing over the flapping paddle is.

Two views of the tank and wind tunnel in the onshore configuration are shown in **figure 3.5**, with the fairing used to promote a smooth transition of the air flow to the wave tank shown in **figure 3.5(a)**. The fairing was necessary in order to prevent the flapping paddle interfering with the air flow to the tank.

Following the reconstruction of the wave tank prior to the experiments with onshore winds, some discrepancies in breaker location and type were observed for the same waves as recorded in the 'old' offshore tank position and the 'new' onshore position. After further investigation the differences were narrowed to a slight change in tank slope between the two tank configurations. Unfortunately an exact measurement of the tank slope was not made whilst the tank was in the offshore position, measurements were made simply to check that the slope was close to 1/20. From measurements of the water depth at certain points it became apparent that the tank slope in the offshore configuration was slightly steeper than in the onshore configuration. This discrepancy necessitated slight changes to the waves used for the experiments in order to preserve the breaker types and these changes are noted in subsequent chapters.

3.4 INSTRUMENTATION

The main experimental tool was the hot-film anemometer and details of the anemometers used are given in section 3.4.1. In addition to this a wave probe was also used to measure wave heights within the tank, section 3.4.2. Both anemometry and wave gauge were linked to an IBM compatible personal computer, (Ahkter 486-33MHz), which is in turn linked to the University's main frame computing facilities via the Ethernet system. A data acquisition package (Status 74 Version 2.05) was used to sample the anemometer and wave gauge readings. Sampled data was initially stored on the PC's hard disk before being transferred to the main frame computer for analysis. In addition a VHS camcorder (section 3.4.3) and a conical wave probe (section 3.4.4) were used to obtain data on the effect of wind on the internal characteristics of the waves.

3.4.1 Hot-Film Anemometry

3.4.1.1 Overview Of System

The hot-film anemometer is based on the principle that the heat lost from a heated resistance element is proportional to the velocity of the fluid flowing past the heated sensor. The anemometer controls the sensor temperature and keeps it at a constant temperature, hence the name constant temperature anemometer. The cooling effect of the fluid depends on both the mass flow past the sensor (the product of velocity and density) and temperature difference between the sensor and the fluid. For velocity measurements the best sensitivity is obtained with the largest difference between the sensor and environment temperature. This also makes for the least sensitivity to changes in ambient temperature.

Output obtained from the anemometer is non-linear, with bridge voltage approximately proportional to the quarter power of velocity. However, lineariser circuitry within the anemometer can be used to obtain a linearised voltage output which is directly proportional to velocity. This facility was used for all anemometry measurements in this research.

Three probe types were used for the experiments, a single-film probe (model 1210-20), a single-film boundary layer probe (model 1218-20) and an 'X' configuration double-film probe (model 1241-20) (films were at 45° to each other). All probes were platinum bonded to a quartz substrate. Both the single

film probes were used with Thermo Systems Inc. (TSI) model 1054B constant temperature linearised anemometer with model 1051 monitor and power supply and a model 1056 variable decade. These were connected to the probe using 5m cables. For the X-film probe two TSI model 1054B constant temperature linearised anemometers and two 1056 variable decades were linked to a single model 1051 monitor and power supply.

Probes were held in position over the waves by a cantilevered traverse which allows the probes to be positioned at any fetch and at heights in the range 0-400mm over the tank, **figure 3.6**. The probe holder was graduated in 1cm increments so that once the initial probe height was measured, subsequent heights could be simply determined by subtracting or adding 1cm height increments. The traverse limits the positions of the probe over the width of the tank, and only over the middle third are hot-film measurements possible. The wave gauge (section 3.4.2) is supported from the same traverse.

3.4.1.2 Calibration

Both hot-film systems are calibrated using a pitot-static tube connected to a high resolution Combustion Instruments null reading U-tube manometer. Accurate calibrations are possible since the manometer has a high degree of resolution of 0.001m of water. Calibration was carried out by placing the probe and pitot-static tube in the low turbulence flow at the entrance to the tunnel working section. Data for each calibration point was sampled at 150Hz using 2048 data points. Instruments were re-calibrated regularly, although if the changes in temperature and air pressure over a period of testing were small the same calibration was maintained.

During calibration and periods of testing it was found to be necessary to leave the anemometry equipment on for at least 24 hours before testing. Frequent use of the equipment meant that it was left on for long periods, consequently the drift of the settings on the anemometer should be small.

The single-film probe was calibrated simply by plotting (linearised) voltage output against velocity obtained from the pitot-static tube and manometer. Generally seven or eight points over the range of velocities were used for the calibration with the best fit determined from linear regression of the data points. A typical calibration curve is shown in **figure 3.7**. Wind velocity is

then obtained by simply multiplying the voltage output by the calibration factor (which is given by the slope of the velocity-voltage plot).

The only problem in calibrating the hot-film occurs when attempting to obtain readings from the manometer at wind velocities less than about 1.5m/s. At these velocites the manometer responds very slowly to any changes and small errors in levelling the manometer may be significant. Therefore calibrations were generally made between wind speeds of 2 to 6m/s, and the results extrapolated into the 0-2m/s region. The generally close fit of the observed points to a straight line, as shown in **figure 3.7**, indicates that this will not result in appreciable errors.

Occasionally the linear regression did not pass exactly through the origin, in these cases a slight adjustment to the best fit line was made so that it did pass through this point. This line was then used for the calibration factor. Best fit lines which did not pass close to the origin were not adjusted by this method and the calibration procedure was repeated. The usual reason for this was a poorly adjusted zero span on the linearisor (section 3.4.1.4).

Calibration of the X-film probe is more complicated. For each film the effective flow across the film is assumed to take the following form, (Reynolds (1974)).

$$\frac{E^2}{S^2} = U_{eff}^2 = U^2\left(\cos^2\theta + K^2\sin^2\theta\right) \qquad (3.1)$$

where E=voltage output, S=sensitivity coefficient, U_{eff}=effective velocity, U=actual velocity and θ=the angle of oncoming flow, (**figure 3.8**). The value of K is expected to be small and to be constant with θ. Firstly, for each of the two films the coefficient S was determined. This was done in the same way as for the single-film probes; the probe is aligned in low turbulence flow so that the film to be calibrated first is normal to the oncoming flow. Using the manometer readings coefficient S was determined from a plot of velocity against voltage. This process was carried out for both films. Next the coefficient K must be determined and this was assumed to take the same value for both films. The coefficient K was calculated by measuring the output voltage and velocity (from the manometer) for several angles of oncoming flow

(i.e. flow is not normal to the films). For each case of flow angle the value of K is calculated from equation 3.2.

$$K^2 = \frac{\left[E^2/S^2\right]}{U^2} - \cos^2\theta \Big/ \sin^2\theta \qquad (3.2)$$

The coefficient K was then plotted against incident flow angle, (θ), and from this plot the average value of K was determined. Results showed K to be 0.25, which is consistent with the generally quoted figure of 0.2, (Reynolds (1974)). Once calibrated the X-film probe could be used to measure both vertical and horizontal velocities and turbulent fluctuations. In order to obtain the vertical and horizontal velocities the angle and magnitude of oncoming flow must be known. These are given by the following two formulae, where the subscripts 1 and 2 denote the outputs from each of the two films.

$$U^2 = \frac{\left[U_{eff1}^2 + U_{eff2}^2\right]}{2\left[1+K^2\right]} \qquad (3.3)$$

$$\cos 2\theta = \frac{\left[U_{eff1}^2 - U_{eff2}^2\right]}{U^2\left[1+K^2\right]} \qquad (3.4)$$

From these two equations the horizontal and vertical components of velocity were calculated. These were referred to as the U-component and V-component of velocity respectively.

When setting up the anemometer, the sensor operating resistance was set to the value recommended by TSI and supplied on the sensor box. The over heat ratio, which is the ratio of the sensor operating resistance, (R_H), over the resistance at the environment temperature, (R_C), was typically between 1.6 and 1.7. From this the operating temperature of the sensor could be calculated:

$$\frac{R_H}{R_C} = 1+\alpha(t_s - t_e) \qquad (3.5)$$

where t_s is the sensor temperature, t_e is the environment temperature and α is the temperature coefficient of resistance (quoted as 0.0026/°C for these films). For typical conditions within the wind tunnel, (t_e=13°C), the sensor operating temperature was around 263°C.

3.4.1.3 Signal Filters

For the onshore phase of the work, low-pass frequency signal filters were available for use with the hot-film system. These cut off frequencies higher than a set frequency. For the velocity profile measurements where sampling was carried out at 100Hz they were set to 50Hz. This prevents aliasing of the signal when converted to the frequency domain for spectral analysis.

Potential problems with aliasing only came to light during the final stages of the offshore phase of the experiment. Initially the problem was thought to be one of probe vibration, however testing at higher frequencies (see section 5.1) showed this not to be the case. Therefore for the onshore phase of the work all hot-film measurements from which frequency spectra were to be derived were filtered at 50Hz.

Aliasing is the result of digital sampling where confusion arises between the high frequency and low frequency components of a signal. For example, if a sinusoidal signal of 100Hz is sampled at 100Hz then the output would simply appear as a constant value. Sampling the same source at either 90Hz or 110Hz the signal would appear as one of 10Hz. Hence at least two samples per cycle are necessary to correctly resolve the frequency of a signal. This leads to the requirement that the sampling frequency must be at least twice the maximum frequency of interest which exists in the signal. The cut off frequency is termed the Nyquist or folding frequency.

The 100Hz sampling frequency used for the spectral analysis of the wind data is insufficient to prevent alisasing effects being apparent in the spectra (which are plotted up to 50Hz). However if the signal is passed through a low-pass frequency filter set to 50Hz, then no aliasing effects are observed in the spectra. The effect of using these signal filters can be seen in the high frequency region (30-50Hz) of the non-dimensional spectra if results from the onshore and offshore configurations are compared (for example **figure 5.4(a)** and **(b)**). It should be noted that aliasing only affects frequency spectra, measurements of velocity, turbulence intensity and Reynolds stresses are not affected.

3.4.1.4 Error Sources & Elimination

The main source of error in constant temperature hot-film anemometry is due to the effects of changes in environment temperature. For the work reported here temperature changes occurred due to the wind tunnel heating up during a period of testing and also to a lesser extent from changes in atmospheric weather conditions. Therefore the temperature at testing is often different to that at calibration. However the low wind speed setting used for these experiments means that the increase in temperature is not large. From the experimental records, the differences between temperature at calibration and at testing are generally less than ±2°C. The largest recorded difference was +4°C.

A recommended method of compensating for changes in environment temperature is given in the TSI manual. Although the method is approximate, it is sufficient for small changes in temperature. In order to correct for this type of temperature change, linearised output should be multiplied by:

$$\left[\frac{t_s - t_{e2}}{t_s - t_{e1}}\right]^2 \qquad (3.6)$$

where t_s is the sensor operating temperature, (263°C), t_{e1} is the new environment temperature and t_{e2} is the temperature at calibration. A typical calibration temperature of 14°C, produces an error of ±1.7% if the temperature at testing varies by ±2°C. A 4°C change in temperature produces an error of around ±3.5% in the velocity reading. This was felt to be within acceptable limits, especially since velocities are normalised by U_{ref} which would have the effect of negating the error. The effect of temperature changes on turbulence intensity was shown by Bearman (1971) to be negligible. Similarly spectra obtained from the velocity data will be unaffected. No compensation for temperature effects was therefore attempted.

Another potential source of error is the drift of the settings for the lineariser which can occur over long periods. The two controls for the lineariser are the *zero* and *span* settings. Drift in these settings will affect the calibration of the anemometer. The practice of normalising the velocity data by U_{ref} again will reduce the effects of any drift in linear *span*, but will not correct for changes in the zero-flow setting. Since changes in linear span will not affect the profiles,

the effects of drift can be minimised by checking that the zero-flow point has not moved.

Hot-film measurements for the phase-averaged data and wave data are generally carried out over a short period of time and the drift of the lineariser settings was therefore less problematic.

The final source of error in the hot-film measurements was due to the nature of the films and the turbulence in the air flow over the tank. For a single-film probe, aligned normal to the plane of 2-dimensional flow in order to measure the U-component of velocity, there is no error in effective velocity if V-component fluctuations are zero. However for boundary layers, and in particular for this work, V-component fluctuations are not zero. For a boundary layer with 10% fluctuations in both U and V-components of velocity, the error in U due to V is about 5%, (Wills (1980)). As fluctuations in the V-plane increase, then so does the error in both mean U and I_u.

At high levels of turbulence intensity flow reversal causes further errors since the hot-film cannot distinguish between positive and negative velocities. Extreme caution must be used in interpreting hot-film results in regions prone to separated flow.

X-film probes are particularly susceptible to high turbulence levels. For the film used for these experiments, accurate measurements are made only when the flow direction angle fluctuations are no more than ±15°, which implies turbulence levels of around 10% maximum, (Wills (1980)). The flow angle is the angle of instantaneous velocity with respect to the horizontal (in **figure 3.8** this is equivalent to θ-45°). This creates particular problems for this research, where, due to the wave-induced distortion of the air flow, large fluctuations of the flow angle and in the V-plane are to be expected. Analysis of flow angle data (for spilling waves under offshore winds at H_{ref}) shows this ±15° limit is regularly exceeded. For one wave periods' worth of data, flow angle is generally less than 15°, however at some stage flow angles of between 30 and 40° are recorded. In all out of 75 data points for one complete wave, an angle of ±20° is exceeded 18 times. For the complete data record, the values of I_u and I_v are 0.25 and 0.28 respectively. Below H_{ref} turbulent intensities increase dramatically, consequently errors in the hot-film measurements will also

increase. Above H_{ref} the errors are within acceptable limits, since the flow angle will reduce as the influence of the waves also reduces.

This creates some problems for the definition of mean U, I_u and I_v respectively, which will become more apparent as the results are discussed. The following points can be made about hot-film measurements in this experiment. For the single-film probe, mean horizontal velocity, U, will be over-estimated due to the increase in U_{eff} across the film arising from the fluctuations in the V-component. A similar over-estimation in I_u will also occur as a result of V-component fluctuations. The errors in mean U and I_u will be greatest where fluctuations in the vertical plane are greatest, i.e. near the waves. Errors should decrease with increasing probe height. For the X-film probe, the errors mainly depend on the flow angle, and they will consequently be greatest near the waves.

3.4.2 Wave Gauge

In order to record wave heights and so that time histories of wind and waves could be obtained a wave probe was used. The model used was a Churchill Controls twin-wire wave probe on loan from Hydraulics Research Ltd (Wallingford). The probe works on the basis that the water provides a short circuit between the parallel wires through which an AC current is flowing. A change in water height will therefore alter the resistance of the probe and this is detected by the wave probe unit. Output is in volts and is linear with height. Calibration is carried out by measuring the output voltage at several different water heights. The gauge holder is similar to the hot-film probe holder in that it is graduated in 1cm increments. Calibration of the gauge is therefore simple and can be quickly carried out.

The gauge is simple to use and has only two drawbacks. Firstly the calibration is temperature dependent and must therefore be recalibrated if there is a change in temperature over the duration of the testing period. Secondly, adjusting the *set datum zero* control once the gauge is calibrated will change the sensitivity and the gauge must therefore be re-calibrated. However by simply measuring and noting the voltage of the Still Water Level at each measuring point it was found the same calibration could be maintained for some time.

One minor problem which occurred over time was the growth of limescale or some similar coating on the submerged probe wire. In order to prevent this

growth leading to non-linear calibrations, the probe wires were occasionally rubbed with emery paper.

3.4.3 VHS Camcorder

For the particle path studies, section 4.6, a VHS camcorder was used to record the motions of particles within the waves onto standard VHS video tape. The camcorder was a Canon VC-10 colour video camera. The exact number of frames per second is unknown, but was estimated at 25 by noting the number of frames per wave period. The VHS tape was later played back on a standard domestic TV and VHS video recorder for analysis.

The macro facility on the camcorder, which allows focused close up photography, could not be used due to the width of the wave tank.

3.4.4 Conical Wave Probe

The availability of a conical fluid probe for the onshore phase of this research meant that water velocities under the waves could be measured. The probe used was a TSI miniature conical probe, model number 1264AW, with platinum hot film sensor. The probe is connected to the TSI anemometer used for the regular hot-film measurements, section 3.4.1.

The probe is set up in the same manner as for the hot-film probes, using the anemometer's lineariser. However the lack of suitable facilities for calibration within the wind tunnel meant that the probe output could not be calibrated against water velocity. However, use of the lineariser means that the voltage output will be directly proportional to water velocity over the probe, and can therefore be considered as such.

In use the probe is positioned such that the axis of its body is perpendicular to the plane of water motion as shown in **figure 3.9**. Water velocity across the tip of the sensor cone is then recorded. As only one channel of anemometry was available with this probe no information as to the direction of the water motion is available. Only the magnitude of the velocity vector can be determined.

Problems and errors arising from the use of this probe are similar to those described for the regular hot-film measurements in section 3.4.1.4. However as the probe was used only once, with the measurements being completed within

an hour, problems due to settings drift and temperature fluctuation should be insignificant.

CHAPTER 4

EXPERIMENTAL PROCEDURES & ANALYSIS

4.1 SIGN CONVENTION

In order to retain consistency with references to both on and offshore tank configurations, and also to avoid confusion, the sign convention shown in **figure 4.1** was adopted. The origin is defined to be at the point where the water ends and any distance from this is referred to as 'X'. X is positive in the shorewards direction, making offshore distances negative. This was mainly done so that onshore winds and wave celerity were also positive. Offshore winds are, therefore, negative in sign. Measurement of the surf zone width is from the defined origin to the point of wave breaking. X is generally referred to as the 'offshore distance'.

4.2 STANDARD CONDITIONS

Wind and waves conditions used for the majority of these experiments are standardised in order to reduce the number of variables. These standard conditions are used in all tests, except for the analysis of breaker dimensions and types, (section 4.4).

Two standard waves were defined for the no wind conditions. These were defined as either SPILLING or PLUNGING. The waves had similar heights at breaking, the main difference was in the wave steepness. Spilling waves had a smaller period and were therefore steeper. Results for the breaker dimensions under zero wind conditions for the offshore and onshore tank configurations are given in section 5.2.

Wind speed used for the experiments was 'fixed', except for those experiments described in section 4.4. However it was difficult to set the tunnel wind speed to the same value on subsequent occasions. In order to avoid this problem the wind tunnel was set to provide a nominal wind speed of 2m/s at 400mm above

the still water level and this setting was not altered during the course of the experiments. However, during the first set of experiments, the setting for the single-film velocity profile measurements was slightly different to the for the X-film measurements, with a higher value of U_{ref} used for the single-film measurements. During the onshore phase of the work, careful attention to wind speed ensured that a similar difference was obtained for the onshore phase of work.

4.3 Analysis Of Wind Measurements

4.3.1 Mean Velocites

For both Spilling and Plunging waves, velocity profiles were measured at four locations over the water surface. Initial measurements were made with the single-film hot-film probe and these were later repeated using the X-film probe. The X-film probe was used in the vertical plane so that the horizontal and vertical components of velocity can be measured. As mentioned in the previous section, there was a slight difference in the reference wind speed used for the single and X-film data sets. No horizontal across-wind measurements were taken.

Three of the measurement positions used were common to both the offshore and onshore tank configuration. These were, in order of increasing offshore distance:

a) over the bore of the recently broken wave
b) over the waves at the point of breaking
c) over the waves prior to the point of breaking

The fourth measurement position depended on the tank configuration. In offshore winds, the mean velocity profile over the 'deep' water waves, downwind of the surf zone, was recorded. For onshore winds the profile at the shore (X=100mm) was recorded, this position again being downwind of the surf zone. At this point the probe is over the sloping 'beach', used to prevent wave overtopping, and therefore zero probe height does not correspond to the still water level. This is shown in **figure 4.2**.

The exact positions of measurement are given in table 4.1. The columns are labelled (i) to (v), where (i) refers to the position X=100mm and (v) is over the 'deep' water waves. Positions (ii) to (iv) refer to (a), (b), and (c) (respectively)

as noted above. Velocity profiles over the tank with no generated waves were also measured for reference and the results are presented in chapter 5.

Wave	Wind	Distance From Origin, X (mm)				
		(i)	(ii)	(iii)	(iv)	(v)
PLUNGING	Offshore	-	-912	-1404	-1811	-2640
	Onshore	+100	-912	-1289	-1795	-
SPILLING	Offshore	-	-912	-1177	-1575	-2656
	Onshore	+100	-912	-1554	-1800	-

Table 4.1. Measurement locations for wind profiles.

Velocity profiles were measured from the Still Water Level, (SWL), extending from around 350mm above this level, down to within a few millimetres of the wave crests. Measurements in the lower level were limited by the wave height, but also by the probe holder. Consequently the minimum height down to which it was possible to measure, was around 10-15mm above the wave crests. This was roughly 40mm above the SWL depending on the offshore distance, X. Each point in the mean velocity profile is derived from the mean of 4096 points sampled at 100Hz. This corresponds to a full scale sampling period of around 280 seconds at 15Hz (assuming the 1/50 scale of the waves). Reference height was taken as 100mm and for each profile the reference height velocity, U_{ref}, is used to normalise the velocity axis. A value of U_{ref} was therefore obtained for each profile.

Mean velocity profiles (which are presented as semi-logarithmic profiles) are normalised by dividing all velocities by the reference height velocity, U_{ref}, at that measurement location. Now the semi-log velocity profile can be characterised by two parameters; the aerodynamic roughness, z_o, and friction velocity, u_*. These are determined from the regression results of the semi-log data, which give the least squares best fit to the U/U_{ref} against $\log_{10}$(Height) plot. The semi-log equation for air flow is as follows:

$$U = 2.5\, u_* \log_{10} \frac{Z-d}{z_o} \qquad (4.1)$$

Thus the gradient of the curve is given by 2.5u∗. But since the velocity axis has been normalised to U/U_{ref}, the results of the regression should be corrected to a U against log height plot. Failure to do this results in a lower value of friction velocity than should be the case. From the regression analysis we obtain values for the constants A and B where:

$$\frac{U}{U_{ref}} = A\log_{10}(Z-d) + B \qquad (4.2)$$

But as we require U against log(height), multiply both sides by U_{ref} to obtain the expression

$$U = AU_{ref}\log_{10}(Z-d) + BU_{ref} \qquad (4.3)$$

The values of u* and z_o can then be calculated from the equations 4.4 and 4.5, (assuming that the *zero plane displacement*, d, is zero).

$$\text{Friction Velocity, } u_* = \frac{AU_{ref}}{2.5} \qquad (4.4)$$

$$\text{Aerodynamic Roughness, } z_o = 10^{[-B/A]} \qquad (4.5)$$

Results for the semi-log profiles, aerodynamic roughness and friction velocity are presented in chapters 5 and 6.

The zero plane displacement layer thickness is used where the roughness elements are close together, such that the profile has a zero velocity at some height 'd' above the true ground level. If d is not accounted for then the semi-log profile may exhibit a deviation from a straight line in the lower height regions. Subtracting d from the measurements of height, Z, (from the true ground level), corrects for this. Generally d is found by trial and error, with several values tried until the semi-log plot shows a straight line.

4.3.2 Turbulence Intensities

Turbulence intensity profiles were calculated from the data and presented as plots of height above SWL against turbulence intensity, I. Both longitudinal and vertical turbulence intensities are calculated and these are expressed as I_u

and I_v respectively. Two profiles for I_u are calculated, one from the single-film probe and one from the X-film probe.

Longitudinal turbulence intensity is calculated from the following equation:

$$\text{Longitudinal Turbulence Intensity} = I_u = \frac{\sqrt{\sum_{i=1}^{n}\left[U_i - \overline{U}\right]^2}}{n\overline{U}} \qquad (4.6)$$

where $\overline{U}$ is the mean longitudinal velocity at that height, n is the number of data points (4096), and U_i is the instantaneous velocity. Vertical turbulence intensity is calculated in a similar way, equation 4.7.

$$\text{Vertical Turbulence Intensity} = I_v = \frac{\sqrt{\sum_{i=1}^{n}\left[V_i - \overline{V}\right]^2}}{n\overline{U}} \qquad (4.7)$$

4.3.3 Reynolds Stresses

These are obtained from the X-film probe, and are calculated using the following formula:

$$\text{Reynolds Stress} = -\rho\overline{uv} = \frac{-\rho\sum_{i=1}^{n}\left[\left(U_i - \overline{U}\right)\left(V_i - \overline{V}\right)\right]}{n} \qquad (4.8)$$

Reynolds stress results are presented in chapters 5 and 6 as normalised Reynolds stress against height. Reynolds stress is normalised according to the following formula:

$$\text{Normalised Reynolds Stress} = \langle uv \rangle = \frac{\overline{uv}}{\overline{U}^2} \qquad (4.9)$$

where the mean velocity is the mean velocity for that probe height.

4.3.4 Wind Spectra

A commonly used method of analysing the wind data is to break the data record down into Fourier components to form a spectrum. This is done by fitting sine waves of varying frequency to the original time history of the wind data. This gives an indication of the amount of energy at each frequency.

Spectra for full-scale data show two distinct peaks separated by a region of little wind fluctuation, (Cook (1985)). The lower frequency peak, at about 0.01 cycles per hour, is referred to as the *macrometeorological peak* and corresponds to the passage of weather systems, typically over a period of around 4 days. The second, higher frequency peak at about 50 cycles per hour, (0.014Hz)), referred to as the *micrometeorological peak*, is comprised of the turbulence associated with the prevailing wind. It is the micrometeorological peak that is of interest for this research, since changes over a period of days or even hours are effectively changes in the mean wind velocity.

If spectra are plotted as normalised spectral power (frequency times spectral density divided by the variance of the wind data) against frequency then they can be expected to collapse onto the curve as defined by the von Karman spectrum, (equation 4.10).

Non-dimensional frequency spectra are calculated using fast fourier transform routines available on the University's mainframe computer (VME). Output spectra plot normalised spectral density against the logaritham of frequency. Spectra for the horizontal and vertical components of velocity are obtained. The von Karman spectrum for varying values of turbulent lengthscale, ${}^{x}L_u$, can be plotted for comparison. The empirical von Karman spectrum for the U-component of velocity is calculated from equation 4.10, (Coleman (1990)).

$$\frac{n \,.\, S(n,Z)}{\sigma^2} = \frac{4\left[\dfrac{{}^{x}L_u(Z) \,.\, n}{\overline{U}(Z)}\right]}{\left[1+70.8\left[\dfrac{{}^{x}L_u(Z) \,.\, n}{\overline{U}(Z)}\right]^2\right]^{5/6}} \qquad (4.10)$$

where n is the frequency, ${}^{x}L_u$ is the longitudinal lengthscale at height Z, σ^2 is the variance of the wind fluctuations, and S(n,Z) is the power spectral density.

$^{x}L_u$, the longitudinal integral lengthscale is a measure of the average size of the eddies in the streamwise direction, (Reynolds (1974)), and is a function of aerodynamic roughness, z_o, and height above the ground, Z, (as shown in equation 3.1). Similar lengthscales can be defined for the other components of velocity, (Reynolds (1974)). For the work reported here only $^{x}L_u$ was measured (via the frequency spectra for the U-component of velocity), although it would have been possible to measure $^{x}L_v$ from the spectra for the V-component of velocity using the ESDU empirical spectrum for the vertical component of velocity, (Cook (1985)).

To fit the von Karman spectrum to experimental data, the mean wind velocity and several values of $^{x}L_u$ were input. The best fit to the experimental data was determined by eye. This was done in preference to some form of curve fitting regression as it was felt that the large wave-induced peaks would simply result in the peak in the von Karman spectrum being positioned at the wave frequency.

After conversion to the frequency domain by the program CALCSPEC, the results showed large scatter and some smoothing was required to make the results acceptable. The smoothing routines were incorporated into the program which plots the spectra, (PLOTSPEC). Smoothing was carried out by selecting groups of 10 data points and averaging. The averaged value was then returned to a new array in a position corresponding to the average frequency of the points considered. The next group of data points was selected by 'shuffling' along by one data point. Initially the size of averaging group considered was variable. However a group of 10 data points was found to be sufficient for the high frequency data and did not affect the low frequency data adversely. Smoothed results for the U-component of velocity showed good agreement to the von Karman spectrum.

The availability of 50Hz signal filters for the onshore phase of the research improved the fit to the von Karman spectrum. Evidence of aliasing was present in the data for the offshore spectra (aliasing is discussed in section 3.4.1.3). Although it did not significantly affect the spectra for the horizontal component of velocity, spectra for the vertical component were much improved by the use of the filters.

4.3.5 Errors

Errors arising from the use of the hot-film system are discussed in section 3.4. This section discusses the errors that may occur as a result of the sampling techniques used for this research.

Variations in wind tunnel speed are a potentially large source of error, and would affect both velocities and turbulence intensities. Although these were not directly checked, the fit of the mean velocity data to a semi-log plot indicates no significant changes in tunnel speed during measurements of the velocity profiles. Each profile took around 25 minutes to complete.

The effects of changes in ambient temperature are one of the major sources of error in hot-film anemometry and are discussed in section 3.4. Close checks on the tunnel operating temperature were therefore made. Temperatures were recorded at the beginning and end of each run for calibrations and profile measurements. In the 30 minutes it took to perform calibrations, the tunnel temperature tended to rise by 1 or 2 degrees depending on the external temperature. On cold days the effects of running were greater, and the tunnel was therefore allowed to run for some time prior to calibration.

Once calibrated the temperature must not deviate to far from the calibration temperature otherwise errors in velocity measurement will occur. From the original test records, temperature differences were almost always kept within $\pm 2°$ of the initial calibration temperature. Usually differences were less than $\pm 1°$, reducing the need for temperature compensation (see section 3.4.1.4).

For the velocity profiles, sampling times are as long as possible. The data acquisition package, (Status 74), allows a maximum number of 4096 data points to be sampled. Sampling frequencies were therefore selected to provide a compromise between high sampling frequencies and long sampling times. The necessity for high sampling frequencies is demonstrated in the frequency spectra in the form of aliasing (section 3.4.1.3). Errors in the hot-film measurements as a result of turbulence and the fluctuating water surface are discussed in section 3.4.1.4.

Initial probe height above the SWL is measured using a steel rule, and is determined to the nearest millimeter. The accuracy of ths initial height determination is definitely better than ± 2mm, and probably better than ± 1mm. Subsequent probe heights are determined by moving the probe up or down in

increments of 1cm via the probe holder which was drilled with holes at 1cm intervals (section 3.4.1.1). Therefore overall accuracy of the probe height should remain better than ±2mm.

4.4 ANALYSIS OF WAVE MEASUREMENTS

4.4.1 General

One of the main aims of this research was to obtain information on the winds' influence on the geometry of the waves at breaking. The standard wave conditions defined in section 4.2, were supplemented by other waves with a range of wave heights and periods. Wave periods and heights were selected in order to give a range of breaker types. Due to slight differences in tank slope, (section 3.3), the waves used in the offshore and onshore configuration were not identical. A total of 24 different waves were examined; 12 for the onshore and 12 for the offshore wind configuration. Of the 12 waves used for the offshore configuration, 6 were plunging, 4 spilling and 2 were transition waves in between the spilling and plunging mode of breaking. For the onshore configuration the 12 waves were comprised of 6 plunging, 2 spilling and 4 transition.

Each wave was subjected to four increments of wind, including zero, up to a maximum of around 4.5m/s. Wind velocity was measured using the single-film probe positioned 200mm over the SWL at the point of wave breaking. Wind and waves were sampled using 4096 data points, sampled at 100 and 300Hz respectively. Wave heights were therefore obtained from the average of around 14 waves.

For each wave and increment of wind velocity, breaker depth, breaker height, wind velocity and surf zone width were measured. The type of breaker occuring was also noted and for plunging waves the distance, X, to the plunge point was noted (this is defined in section 4.4.3). The measurement procedures and definitions used for these are given in the sections 4.4.2 to 4.4.4. Data is presented in the results in non-dimensional form, for the variation of the following parameters with normalised wind velocity, $U_{ref}/\sqrt{gH_p}$, and normalised deep water wave height, H_p/gT^2.

$$\text{Normalised breaker height} = \frac{H_b}{gT^2} \qquad (4.11)$$

$$\text{Normalised breaker depth} = \frac{d_b}{gT^2} \qquad (4.12)$$

$$\text{Normalised surf zone width} = \frac{X_s}{H_p} \qquad (4.13)$$

$$\text{Normalised plunge point depth} = \frac{d_{pp}}{d_b} \qquad (4.14)$$

Section 7.3 compares the results from this research to those of Douglass (1989). In order to make a direct comparison wind velocity is normalised by the function used by Douglass. This is given by:

$$\text{Normalised wind velocity (Douglass (1989))} = \frac{U}{\sqrt{g\, d_{b_{(no\ wind)}}}} \qquad (4.15)$$

The testing procedure was as follows. The desired wind and wave conditions were selected and given time to allow the initial transients to decay. Measurements were then made of H_b, wind velocity, distance to plunge point (if necessary), and surf zone width. This was repeated for each of the four wind conditions. Once this was completed, the wind and waves were switched off, and the depth at the point of breaking for each wind increment measured. During testing it was essential that the water in the tank was maintained at the same level. A 1mm change in water depth could potentially shift breaker locations by ±20mm (since the beach slope is 1/20). Regular measurements and adjustments to the water level were therefore made.

4.4.2 Wave Height & Period

Wave heights were measured using the wave gauge described in section 3.4.2. As noted above the waves were sampled at 300Hz for 4096 data points. 'Deep' water wave heights were measured at X=-2800mm, and breaker heights at the defined point of breaking. Breaker height, H_b, is defined in **figure 1.2**.

Recorded values for breaker height are the mean value obtained from the data record.

Wave periods were determined from the paddle motion, using a digital stopwatch. To set the paddle motor to the correct wave period, the time for 10 complete wave periods was recorded and the motor adjusted accordingly. If stopwatch operation is accurate to 0.1 seconds, then using this procedure the wave period should still be accurate to 0.01 seconds. Although the paddle motor speed is infinitely adjustable, wave periods can be determined accurately using this procedure.

4.4.3 Breaker Position, Breaker Depth & Plunge Point Depth

Determination of the correct point of wave breaking was highly important, since all other measurements, except H_p, are based on this point. The defined point of breaking was different for the spilling and plunging waves. For plunging waves the defined point of breaking occurs when the front face of the wave becomes vertical. For spilling waves, breaking is defined by the presence of turbulent water appearing at the wave crest. For transition waves which may break with characteristics of both spilling and plunging waves, breaking was said to occur when either the front face becomes vertical or turbulence appears at the wave crest (whichever occurs first). These definitions are the same as those used by Douglass (1989 & 1990).

Once the point of breaking was determined, the breaker depth, d_b, was simply obtained by measuring the SWD at that point. This is carried out using a steel rule after the wind and waves have been switched off. Care was taken to ensure that d_b was measured as near to the point where H_b is measured as possible. Surf zone width, X_s, was then measured from the origin using a steel tape measure.

For waves which were defined as plunging, an additional measurement was made. Referred to as the 'plunge distance', (Weishar & Byrne (1978)), it defines the distance between the defined point of breaking and the point at which the overhanging crest finally touches/crashes down in front of the wave. Measurements were subsequently converted into depths so that the depth and breaking, d_b, could be compared to the depth at the point of plunging, denoted by d_{pp}. This depth is significant since it defines the point at which the

'horizontal roller' is formed and is therefore important for sediment transort in the surf zone.

4.4.4 Breaker Type & Categorization

Determination of breaker type is difficult in that it is subjective. The definitions of breaker type used for experimental purposes are noted in section 4.4.3. In many cases a wave exhibits both spilling and plunging characteristics. For example, the wave may initially show turbulence at the wave crest, but finally break by forming an overhanging lip. In order to be consistant, it was decided that breakers should be defined as transition waves if they show *any* characteristics of both spilling and plunging waves.

Breaker types should be categorized by normalised 'deep' water wave height, H_p, since this is basically wave steepness. The distribution of breaker types using normalised H_p is considered in the results. Also the Surf Similarity Parameter, ξ, is calculated, from H_b, to see the effect of wind on breaker type distribution (see equation 1.2). Note that ξ is basically a function of dimensionless breaker height.

4.4.5 Errors

The main problems in accurate measurement of the waves derive from the determination of the exact point of wave breaking. The small scale (and therefore rapid breaking) of the waves means that precise determination is difficult with the naked eye. This potential error has consequences for the breaker height, H_b, as this is measured at the point of breaking. In order to obtain some estimate of the expected errors, a rudimentry error analysis was carried out.

After consideration, an error margin in determining the point of breaking of ±50mm was felt to be representative. This value is used in order to obtain estimates of the percentage errors in breaker height, breaker depth, amplitude-to-depth ratio and the surf zone width. Errors are calculated from the 'true' value of the variable. An error of -10% therefore means that the measured variable is smaller than the true value by 10% (i.e. is 90% of the true value). Error bars scaled to represent these errors are presented in chapter 6.

For the surf zone width, X_s, the breaker location error was calculated as a percentage of each value of surf zone width. Percentage errors ranged from ±3% to ±6%, but were generally around 4%. A value of ±4% was therefore used for plotting purposes. For breaker depth, the 1:20 beach slope means that an error in breaker location of ±50mm leads to an error in the measured value of d_b of ±2.5mm. Expressing this value as a percentage of a 'typical wave' breaker depth, (d_b=0.05m), leads to a typical error of around ±5%.

For the breaker height, H_b, the twin-wire wave probe allows accurate measurement of wave height assuming that the probe is positioned correctly. Errors occur from the probe not being correctly positioned at the point of breaking. So what effect does a ±50mm error in estimated breaker location have on H_b? An estimate for this error was calculated from the phase-averaged data, where measurements of wave height, H, were made at the point of breaking and approximately 300mm on either side of it. An estimate of error for a ±50mm error in probe location was obtained by linear interpolation. In theory H is a maximum at the point of breaking, so errors in breaker height should always be negative. However the two plunging waves show wave heights slightly larger than H_b at approximately 300mm offshore.

From the linear interpolation it was apparent that the error is not symmetrical about the point of breaking. If the probe was positioned before the wave breaks ($d > d_b$), then the error is much smaller than if the measurement is taken after the wave has broken, ($d < d_b$). This leads to two values, expressed as percentages of the breaker height. If the probe is positioned before breaking, then the error is small, around ±3%. If the probe is measuring the wave after breaking, then the error is of the order of -7% to -10%. Generally, whether the wave has broken or not can be determined from the sampled wave time history, and therefore it is more likely that the waves are measured prior to the point of breaking.

Finally the error in amplitude-to-depth ratio is calculated from the errors for H_b and d_b. If the probe is positioned after the point of breaking then the error is around -6%. Offshore of the point of breaking gives a value of either -7% (assuming an error in H_b of -3%) or -1% (assuming H_b error is +3%). Thus it appears that errors in amplitude-to-depth ratio are always likely to be negative. That is the measured value of H_b/d_b is less than the true value.

These values represent percentage errors for any single measurement of wave properties. The figures presented in chapter 7 show the percentage change in these properties from the value in zero wind. For example the percentage change in breaker height, H_b, is calculated from:

$$\text{Percentage change in breaker height} = \frac{H_{b\,wind}}{H_{b\,no\,wind}} \times 100\% \qquad (4.16)$$

Errors may be present in both numerator and denominator, compounding the original error. In order to reflect this 'compounded errors' have been calculated from the single measurement errors and it is these values that are presented in chapter 7. These were calculated simply by working out the combinations of positive and negative errors for the numerator and denominator which give rise to the greatest overall error for the percentage change in each variable. A summary of the single and compounded error values is presented in table 4.2.

	Maximum Estimated Error in Single Measurement	Maximum Estimated Compounded Error For Percentage Change
Breaker Height, H_b	Prior to wave breaking: ±3% After wave has broken: -7%	±10%
Breaker Depth, d_b	±5%	±10%
Surf Zone Width, X_s	±4%	±7%
Amplitude-To-Depth Ratio, H_b/d_b	-6%	±8%

Table 4.2: Estimated errors in wave measurements.

Estimated maximum errors for the percentage changes in surf zone and wave characteristics are thus all around ±10%.

In addition to the measurement errors there also exists potential for error in the classification of the breaker types. This is more difficult to quantify since the allocation of a particular wave to a certain breaker type is subjective. In order

to reduce errors of this sort to a minimum then the following convention was adopted: if the wave has characteristics of both wave types, (spilling and plunging) then it is classified as a transition wave, even if it is, for example, more spilling than plunging.

4.5 PHASE-AVERAGED WIND & WAVE MEASUREMENTS

Simultaneous recordings of wave height and wind velocity were made at three fetches and either three or four probe heights over the waves, (table 4.3). The fetches correspond to the point of wave breaking and to points approximately 300mm on either side of this point. At each fetch the anemometer probe (single-film) was positioned over the waves with the twin-wire wave probe positioned at the same fetch but so that it would not interfere with the air flow to the hot-film probe. Probe height was measured from the still water level.

Wind	Wave	X (mm)	SWD (mm)	Probe Heights (mm)
OFFSHORE	**Plunging**	-1136	45	48 / 63 / 83
		-1450	59	47 / 63 / 83
		-1705	71	47 / 63 / 83
	Spilling	-1183	47	43 / 63 / 83
		-1370	54	43 / 63 / 83
		-1738	74	43 / 63 / 83
ONSHORE	**Plunging**	-1289	54	43 / 63 / 83 / 103
		-1589	70	42 / 62 / 82 / 102
		-1889	84	38 / 58 / 78 / 98
	Spilling	-1254	50	46 / 66 / 86 / 106
		-1554	70	42 / 62 / 82 / 102
		-1854	83	41 / 61 / 81 / 101

Table 4.3. Phase-averaging: details of measurement locations.

For each each tank configuration, the experiment was repeated twice, once each for the PLUNGING and SPILLING waves. The 4096 data points were sampled at 250Hz, giving a data record of just over 16 seconds. This means that for the Plunging waves 14 or 15 complete wavelengths were recorded, and

for the Spilling waves the number was around 20. Phase-averaging involved obtaining values of mean velocity and turbulence intensity over all parts of the wave, so that the variation of these values with instantaneous water depth could be observed.

4.5.1 Phase-Averaged Mean Velocity

The method for obtaining phase-averaged velocity was as follows. The original data record was taken and the number of complete wavelengths within the record established. Next the number of data points per wave period was found. Then the velocity data is divided up so that the data points lying over the same part of the wave could be summed and averaged. Thus if there are 16 complete wavelengths in the data file then the mean value of velocity at any point over the wave crest is the average of 16 velocity data points. Thus, sampling at 250Hz (i.e. once every 0.004 seconds) meant that a value of mean velocity was obtained for each 0.004 second interval over the wave period.

In addition to the plots of phase-averaged mean velocity, the results are also expressed in tabular form. This shows the ratio of the maximum recorded value of phase-averaged mean velocity over the minimum value.

4.5.2 Phase-Averaged Turbulence Intensities

The method for calculating the turbulence intensity was slightly different because we were dealing with deviations from the mean. The raw data file was divided and the wind velocity data stored in matrix form, with each column representing data for one wavelength. Each column of velocity data was then divided up into small sections each with 10 data points (i.e. 0.04 second sections), and for each section the mean velocity and turbulence intensity, (I_u), were determined. The I_u values corresponding to the same phase of the wave were then averaged to give the phase-averaged turbulence intensity for that particular phase of the wave. For the plunging waves this meant the final I_u values were the average of 14 individual I_u values, (i.e. 14 complete wavelengths in the matrix); for the spilling waves final values were derived from 20 initial values. It will be seen later that these small sections were necessary because of the rapidly changing nature of the mean velocity over the wave. For both phase-averaged velocity and turbulence intensity, the results are plotted using double y axis graphs with an example wave form at that fetch for comparison.

4.6 ANALYSIS OF PARTICLE PATH MEASUREMENTS

In order to determine if the wind affects sediment transport, particle paths were examined using the two wave conditions (Spilling & Plunging) and three wind conditions (zero and approximately ±2m/s) at three locations in the wave tank. The method for data acquisition was simple. Using a powerful photographic lamp and cardboard sheets to provide a 'blackout', a vertical plane or corridor of the wave tank was illuminated. This corridor was approximately $1\frac{1}{2}$" wide (45mm) as shown in **figure 4.3**. A VHS camcorder was then used to record the motion of particles held in suspension by the water, (the nature of these particles is discussed below). Analysis of the video was carried out using a video recorder with a 'pause' and 'frame-by-frame advance' facility. A suitable particle was selected and the picture advanced a frame at a time. This allowed the locus of the particle paths to be traced and measured.

The three points of measurement selected are listed in table 4.4. Unfortunately, the turbulent flow of water after the point of wave breaking caused particles to move out of the illuminated corridor and to disappear from view. Measurements were therefore confined to points offshore of the point of breaking.

Offshore Distance, X (mm)	SWL (mm)	Bottom Slope
1525	60	1/20
1755	74	1/20
2000	102	1/8

Table 4.4. Points of data measurement for particle motion study.

For the offshore configuration, two sachets of Optimage 30μ seeding powder were used to seed the water with suitable particles. However the fineness of the particles meant that whilst they could be seen during normal playback of the video, it was not possible to distinguish individual particles once the video was paused. This was probably due to the light plane not being powerful enough to allow sufficient light to be reflected from the particles. It was therefore necessary to obtain the data from the locus of the particles of dust and debris

which had accumulated in the tank. These were larger than the seeding powder particles and reflected sufficient light. An obvious disadvantage of this is that no information on the size or density of the particles is available. For the onshore phase of the experiment no attempt to seed the tank with particles was made.

Study of the video reveals that the majority of particles remain actively in suspension, and only a few are obviously heavier than the water. Examination of the particles under flat water conditions revealed that the fall velocities of the particles were sufficiently small to be considered negligible over one wave period.

The method of recording the particles was simple. The desired wind and wave conditions were selected and switched on, and the camera was moved to the first point of measurement, allowing time for the initial transients of the wave motion to decay. The camera was set up as in **figure 4.3**, as close to the illuminated corridor as focusing and the wave tank allowed.

At each point of measurement two camera positions were necessary in order to ensure that particles at the top and bottom of the waves were in view. Particle motion was calibrated against a metre rule placed vertically into the illuminated corridor so that it touched the bottom of the tank, the camera recorded the ruler in this position before it was removed. The particle paths were then recorded for about 90 seconds and this process was repeated for each case of fetch, wind and wave.

Data was retrieved from the VHS cassette using a colour TV and video recorder as mentioned above. The method was as follows. Firstly the entire 90 second period at each measurement point was viewed in 'real-time', which allowed suitable particles to be determined and also gave an overall feel for the nature of the motion. Suitable particles were those which reflected enough light for their motion to be followed for at least one complete wave period. Particles which were obviously observed to fall during each wave period were neglected and large particles were avoided if possible. Next, a blank over-head projector acetate was taped to the TV screen and was calibrated by marking off 10mm increments from the recorded picture of the metre rule. The tape was then played and when suitable particles were spotted it was rewound and paused. Using the 'frame-by-frame advance' facility the locus of the particle

was plotted onto the acetate. This was repeated for around 30 particles at different heights.

The TV used for the tracing of particle locii onto acetate enlarged the motions by a factor of about 3, and gave a field of view of approximately 150mm by 100mm at full scale. This had the effect of reducing measurement errors, since it was possible to determine amplitudes correct to about 1mm, i.e. 0.33mm at full scale. More mention of errors will be made later (section 4.6.3).

4.6.1 Measurement Definitions

A typical locus is shown in **figure 4.4**, along with the definitions used to describe the particle locus. Firstly, the particle motion is divided into two halves according to whether the cycle of the wave is a crest or a trough. A crest causes the particle to move onshore, a trough causes an offshore motion. For the purposes of this thesis, *UPRUSH* is defined as the locus of the particle in the crest phase of the wave, *BACKWASH* is the locus during the trough phase. The particle reaches its maximum height above the tank bottom during the crest phase and its minimum during the trough phase. Between each crest and trough the horizontal velocity of the particle is momentarily zero, at this point the particle is represented as a dot on the acetate. The uprush or backwash path heights are the average height of the particle during the crest or trough phase, respectively. Particle height is defined as the mean of the uprush and backwash path heights.

Uprush/Backwash amplitude was defined as the horizontal distance between the two 'stationary points' during the particle cycle, i.e. uprush amplitude was the horizontal distance between the end points of the uprush locus. Vertical amplitude was defined as the maximum vertical distance between the uprush locus and the backwash locus.

The presented results show the effect of the wind on the three 'components' of the particle motion, namely the uprush, backwash, and vertical amplitudes plotted against particle height above the bed. In addition plots to show the wind effect on the particle drift velocity are presented. These are calculated from the uprush and backwash amplitudes. Data for uprush and backwash is 'binned' into height ranges of 0-10mm, 10-20mm, 20-30mm etc, and then averaged. For each height range the average backwash amplitude is subtracted from the average uprush amplitude, giving a net drift in mm per wave period.

The drift velocity is then found by simply dividing the net drift (in mm) by the wave period (in seconds). This gives the drift velocity, (mm/s), with positive values indicating onshore movement of the particles. These drift velocities are then plotted against the mid-point of the height ranges, for example 5, 15, 25mm etc.

4.6.2 Statistical Analysis

Due to the large scatter of the data it was felt that some form of statistical analysis should be carried out in order to determine the significance level at which the two distributions, (wind and no wind), could be said to be different. A 2-D, two sample, Kolmogorov-Smirnov test, (Press et al (1992)), was used to provide this statistic. The statistic, which lies between 0 and 1, is referred to as the 'K-S value' or the significance level. The nearer this values is to 1, then the more likely it is that the two samples are from the same population. For example, if comparing two distributions of particle motion, identical except for an offshore wind in one case, a significance level of 0.7 would indicate strongly that the wind has no effect on the particle motion, whilst 0.04 would indicate that the wind has had an effect on the motion. Details of this analysis are given in appendix B.

The results of the statistical analysis are presented in chapter 8, but it should be remembered that the test is not exact, and it is not possible to distinguish between significance levels of say 0.7 and 0.4. The statistic provides only an indication of distribution similarity, to be checked with observations by eye.

4.6.3 Errors

The simple methods used to obtain this data may have resulted in errors being present. In order to gain an appreciation for the magnitude and likely affect of these errors on the results, probable causes of these errors have been examined. The source of these errors can be divided into three main areas. Firstly, during the filming of the particles, secondly during the tracing of the particle loci from TV to acetate, and thirdly whilst measuring and recording data from the traced particle loci. Some of the errors are systematic and unavoidable with the methods used, others may be to due to human error.

Errors may occur in the first place due to particles following the water motion to differing degrees. Two particles which look the same may have differing densities, consequently one will follow the water particle motions better than

the other. No details of particle densities or variation of particle densities are known. Consequently it is not possible to estimate the variation in how well particles track the surrounding fluid. This is potentially a large source of error. It is hoped that significant variations have been minimised by carefully selecting the particles to be traced beforehand. However, even if the particles do not closely follow the water motion, but all follow the motion to the same degree of 'closeness', results will validate the effect of the wind.

Some difficulties were encountered in positioning the camera due to the tank's construction and supporting frames. Camera alignment is a potentially large source of error due to parallax-type errors. These occur when the viewed object is at a different distance from the camera compared with the ruler against which the object motion is to be measured. They can be minimised in two ways, firstly by ensuring that the calibrating ruler is placed in exactly the same plane as the observed particles. Secondly the further away the camera is from the area of interest then the smaller the error due to parallax since the light rays are nearer to being parallel. As the camera is positioned over 1m away from the relatively small area of interest then both types of error can be minimised. A typical error in measured particle amplitude (horizontal and vertical) due to alignment of the calibrating ruler was estimated at ±4mm (full scale) by simple geometric considerations.

Plotting the loci from the TV screen onto the OHP acetate can also cause parallax-type errors. This is due to the small gap between the TV image and the curved front glass. These can be reduced by viewing the image from directly in front. Problems in tracing the particle loci mainly resulted from the particle velocity rendering the video image of the particle nothing more than a faint vector streak. This was especially so nearer to the water surface where the particles were subjected to the greatest amplitudes and velocities. Often only one or two suitable particles could be traced near the surface.

Errors in plotting the particle motions onto OHP acetate were estimated at ±4mm for both horizontal and vertical amplitudes, although the exact distance between TV image and front glass is not known.

Once plotted onto the OHP acetate, measurement of the amplitudes of particle motion was straightforward and errors here should be small, typically around

±2mm) . The main problem was the correct determination of the particle path height. Errors may have occured here for two reasons;

i) Measurement of the path height becomes more difficult for highly curved loci.

ii) As the particles move in an ellipse they move horizontally and the bottom slope means that they are experiencing a continually changing depth. Particles whose ellipse does not centre the line of the calibrating ruler are therefore either in slightly deeper or shallower water than measured.

Typical errors from these two sources were estimated at ±6mm in total.

Overall the errors can be divided into two areas: the amplitudes of the particle motion and the average height of the particle. Table 4.5 gives a summary and expected total for these errors.

Error in:	Source	Error	Total Error
Amplitude of motion	Camera parallax & ruler alignment	±4mm	±10mm
	Particle tracking of fluid	unknown	
	TV plotting onto acetate	±4mm	
	Measurement of loci on acetate	±2mm	
Particle height	Measurement of loci on acetate	±6mm	±6mm

Table 4.5. Summary of errors for particle motion study.

Error in the drift velocity results is far harder to estimate because of the way in which the drift was calculated. For each height 'bin' the number of uprush and backwash data points will vary. As each data point is calculated from the average uprush minus the average backwash, and errors may be present in both amplitudes, the error in the final value for drift velocity will be dependent on the sum of individual uprush and backwash amplitude errors and the number of points from which the average is taken. This is represented in equation 4.17,

$$\text{Drift velocity} = \frac{\left[\frac{\sum_{i=1}^{N}(Uprush + error)}{N}\right] - \left[\frac{\sum_{i=1}^{M}(Backwash + error)}{M}\right]}{T} \qquad (4.17)$$

where N is the number of uprush data points in the height range considered, M is the number of backwash data points and T is the wave period. It is easy to see that where drift is small the errors may dominate or conversely they may cancel out. If a value for total horizontal amplitude error of ±10mm (table 4.5) is used, then the resulting error for drift velocity (assuming errors are opposite) is large: 18mm/s and 27mm/s for plunging and spilling waves, respectively. However, these extreme values are the worst case, with the unlikely combination of extreme and opposite errors in uprush and consecutive backwash. Errors are more likely to be spread randomly.

After much consideration, the following procedure for presenting drift velocity error was adopted. An assumption was made that the typical error in any one value of drift velocity would be ±20mm/s. In order to account for the benefits of averaging several values of uprush and backwash amplitude, this value would then be factored by the inverse of the number of values in each height range (if N and M were not equal, then the smaller number was used). Thus as the number of data points used to obtain averaged uprush and backwash increases from 1, to 2, to 3 etcetera, so the estimated error in drift velocity decreases from ±20, to ±10, to ±7mm/s etc. For the drift velocity results the error in the height of the particles is assumed to be small with respect to the error in drift and is not plotted.

4.7 Analysis Of Water Velocity Measurements

Water velocities under the waves were measured using the conical hot film probe, in order to compare the differences between no wind and onshore winds. The probe was not available during the offshore phase of the research. For both spilling and plunging waves, the probe was positioned at X=-1755mm, which corresponds to the middle measurement point for the particle path measurements described in section 4.6. The probe was positioned at three heights above the bed; 10, 30 and 50mm. The probe is positioned as indicated in **figure 3.9**, so that the probe body is normal to the plane of water particle motions.

Simultaneous sampling of the wave height at that fetch meant that the output could be phase averaged in a similar manner to the phase-averaged wind velocity measurements described in section 4.5.1. Sampling was carried out for 2048 data points at a frequency of 150Hz, giving a data record of just under 14 seconds. For the spilling waves this meant that a total of 18 complete waves were recorded and 12 complete plunging waves being obtained. Both water velocities and wave heights were phase-averaged in order to examine any wind influence.

At the time of the tests, which was at the end of the experimental programme, there was a lack of suitable equipment for calibrating the probe against actual water velocity. This does not however affect the relative changes in output voltage and the linearised output is therefore directly proportional to the actual water velocity.

The results are presented in section 8.2 to show the effect of the onshore wind on phase-averaged water velocity at each measurement location.

4.8 MODELLING LIMITATIONS

This section looks at how well results from this experiment can be expected to apply to the real surf zone. Several limiting factors, including scale effects are discussed.

Firstly there was the wave tank itself, which for several reasons makes the model unlike the prototype conditions. The perspex base which was smooth and totally impermeable behaves unlike the sand or pebble beaches occuring at full scale. Bed friction would hence be lower (no sand ripples were able to form) and the water was unable to penetrate the bed. On natural beaches the wave run-up tends to sink into the sand, percolating gradually back to the sea. The perspex bed used here means all wave run-up was forced to flow back down into the path of incoming waves, increasing the volume flowing back. Iverson (1952) notes that this backwash is a factor in the breaking action. High backwash velocities tend to retard the base of the wave promoting the wave to break in a plunging manner.

Sidewall friction also occurs and this has the effect of reducing wave heights. The tank used for these experiments is reasonably wide and this may render the effects of this negligible at the measurement points (over the centre third of the tank). It has been noticed that waves are affected at the edges, but the region of interference does not appear to extend into the centre third of the tank, (section 3.2). For this experiment the ratio of wave height to tank width is smaller than occurs for typical wave flume experiments.

Generation of the waves by the paddle may also cause problems. Douglass (1989) noted problems with secondary waves occuring as a results of the paddle motion. Measurements of H_p, the wave height in the tank deep end show no indication of secondary waves or reflections. Generally in wave tank experiments the tank is long with plenty of distance between the wave generation mechanism and the point at which shoaling begins. Limitations of space within the wind tunnel have meant that this is not possible. Not only is the paddle very near to the point where wave shoaling begins, but the length over which the waves shoal has had to be reduced, (by using a preliminary steeper beach slope), again due to space considerations. Previous research indicates that the initial steeper beach slope should pose no significant problems, but the effects of having the paddle so close to the point of breaking are unknown.

One other consequence of the limits on space is that of fetch limitation. In other words the nearer that the waves are generated to the point of breaking then the less time the wind has to influence them. In the experiments here wind can only really affect the waves very near to the point of breaking. This applies especially in the onshore configuration. Douglass (1989) used a proportionally much longer tank, allowing the wind to affect the waves much further offshore. If part of the winds influence on the waves derives from affecting the waves in deeper water then this will not be reproduced in this experiment. This will be discussed later.

The scale of waves produced in the tank also limits the applicability to full scale. Waves at the scale used here (1/50) have viscous and surface tension forces proportionally many times larger than in the real surf. How this affects the waves is difficult to assess without conducting further tests at different scales. From the literature it would appear that the effects of viscosity can be ignored, (LeMehaute (1976)). For breaking waves the effects of surface

tension are more difficult to quantify. If the mechanisms of breaking are considered then for spilling waves surface tension may be significant, probably retarding the formation of turbulence at the crest, and therefore delaying the onset of breaking. Plunging waves are probably affected to a lesser degree since breaking is less dependent on small scale features, but rather on the overall geometry of the wave. In deeper water surface tension may act to reduce wave heights by damping the amplitude of motion. This however is of minor importance compared to the effects at the point of breaking.

The work of Millar (1972) suggests that the exaggerated surface tension effects in the model will affect breaker heights and the position of wave breaking. However the magnitude of changes occuring as a consequence of the wind will still be of relevance, as will the qualitative results from the experiment.

A major aspect of scale is the vastly reduced, or possibly non-existent, air-entrainment by the model-scale breakers. Although little is known about the concentration and distribution of entrained air bubbles, Fuhrboter (1970) points out possible effects of this entrainment. He notes that energy stored in the entrained air bubbles is released as turbulent mixing and eddy production as the bubbles rise to the surface. Although this is unlikely to affect the actual breaking of the waves, sediment transport in the region of the breakers may be affected. The amount of air-entrainment is probably dependent on not only Froude and Reynolds numbers, but also the Weber number (i.e. surface tension).

For this experiment the presence or otherwise of air-entrainment is unlikely to affect results as it does not affect the waves prior to breaking. However, the entrainment of air may affect the way in which the air flow interacts with the wave and hence the overall drag of the wave. Peregrine & Svendsen (1978), note that even for breakers of 1-2cm, the turbulent flow has all the qualitative characteristics of breaking irrespective of the entrainment process. In the absence of any other details on this phenomenon the effect of air-entrainment is considered to be of minor significance compared to suitably turbulent flow after breaking.

Wind scaling is also of significance, and the Reynolds' number is not correctly simulated at the model scale. This means that inertial wind forces in the model are proportionally smaller than in the prototype. Again the effects of this are

difficult to judge without tests at different scales, and depend on the mechanism of the winds' influence on the waves. If wind shear is the primary agent then the Reynolds' number is unlikely to be significant. If however the form drag of the wind on the waves is the primary agent then Reynolds number effects may be significant.

In addition there is a scaling mis-match between the wind and the wave simulations. Where the waves are scaled at approximately 1/50, the wind is simulated at nearer 1/100 scale (with the exception of ${}^{x}L_{u}$ (see below)). Cook (1982) notes that this is a common error where the 'model' (i.e. the waves) is too big for the simulated boundary layer. The effects of this are to underestimate the mean and fluctuating components of surface pressure. Conceptually this mis-match could be interpreted as a 1/50 scale model with a poor representation of the wind boundary layer.

A major point about the wind scaling is the correct simulation of the turbulent lengthscale, ${}^{x}L_{u}$. As noted in section 3.1, a scaling mis-match of a factor of about 4 exists for ${}^{x}L_{u}$, and normally this is acceptable for wind tunnel experiments (since the frequencies of interest are not near the spectral peak). However in this case an unfortunate consequence is that the frequency of the waves corresponds closely to the frequency of the spectral peak in the developed boundary layer. The effect of this is shown in **figure 4.5**. The two smooth lines are the von Karman spectrum for ${}^{x}L_{u} = 0.2$ and 0.8m respectively. The lower value corresponds to the best fit to the experimental data, while the larger value is that which should be ideally obtained for modelling similarity. The frequency of the waves is about 1Hz. Thus the largest energies in the fluctuations of the wind are contained at the wave frequency, which as shown by the line for ${}^{x}L_{u} = 0.8$m, should not be the case. The effects of this are further discussed in section 9.1.

PAGE MISSING
IN ORIGINAL

Chapter 5

PRELIMINARY RESULTS

5.1 ATMOSPHERIC BOUNDARY LAYER

Measurements of the wind profile over the nominally flat water were made at three locations for both offshore and onshore configurations using both single and X-film anemometry probes. Generally the air flow changed little over the length of the tank, with the exception of aerodynamic roughness, (z_o), and friction velocity, (u_*), which decreased with increasing downstream distance. Turbulence intensities, frequency spectra and Reynolds' stresses remained roughly the same.

Wind	Probe Type	U_{ref} (m/s)	z_0 (m)	u* (m/s)	$\frac{u_*}{U_{ref}}$	${}^{x}L_u$ (at H_{ref}) (m)
Offshore	Single	-1.687	0.000012	0.177	10.5	0.2
	X-film	-1.091	3×10^{-10}	0.051	4.7	0.2
Onshore	Single	1.714	0.000048	0.205	12.0	0.16
	X-film	0.951	0.0000015	0.082	8.6	0.16

Table 5.1. Simulated boundary layer: results for flat water at X=-1265mm.

Semi logarithmic velocity profiles (as defined in section 4.2) over the flat water at X=-1265mm are shown in **figure 5.1**. The results for z_0 and u_* in table 5.1 were obtained from the semi-log velocity profiles. Corresponding results for other values of X are presented in table C.1 in appendix C. The data for the profiles was fairly scattered, mainly as a result of the low wind speeds dictated by the Froude scaling requirement.

The large discrepancy between single-film and X-film measurements of z_0 and u_* appears to be a result of the differences in U_{ref}. The larger reference height velocity for the single-film measurements gave rise to significantly larger values of z_0 and u_* when compared to the X-film results. Possibly this reflects greater capillary wave growth at the higher wind velocity which would effectively 'roughen' the water surface. As no wave measurements were made on the 'flat' water under wind forcing this hypothesis cannot be verified. However, the semi-log velocity profiles of section 6.1 show good agreement of the X-film and single-film results when the waves are running (with the same U_{ref} difference). This supports the notion that capillary wave growth differences are the reason for this, as the small difference in surface roughness would be insignificant in comparison to the roughness due to the waves. For the friction velocity results, normalisation by U_{ref} reduces the discrepany somewhat.

For the single-film results aerodynamic roughness, z_0, is close to the desired model scale value of 0.00003m for both onshore and offshore configurations. As mentioned in section 3.2, the waves produced in the experiments are at approximately 1/50 scale and this gives a required simulated model scale roughness of 0.00006m. Consequently for aerodynamic roughness there exists some degree of scaling mis-match between the wind and the waves.

Horizontal turbulence intensity profiles over the flat water at X=- 1.265m are shown in **figure 5.2**. Results from the X-film probe showed intensity levels consistently higher than those from the single-film probe. One would not expect the differences in U_{ref} for the two sets of measurements (X-film data set has lower U_{ref}) to account for this since these differences usually vanish when the results are normalised. It was therefore felt that the differences were the results of the V-component fluctuations introducing errors into the hot-film measurements (section 3.4.1.4).

A slight variation between the two wind directions was also observed. The offshore configuration showed values of I_u typically around 0.2, with onshore values of I_u around 0.15. Otherwise the two profiles are similar.

Vertical turbulence intensities can only be determined from the X-film probe. The profiles corresponding to the above results are presented in **figure 5.3**. For I_v differences in the profile were observed, the onshore profile showed no variation with height above H_{ref}.

The non-dimensional frequency spectra at the reference height at X=-1.265m are shown for both tank configurations in **figure 5.4**. The longitudinal lengthscale, ${}^{x}L_u$, required by scaling criteria is of the order of 0.8m (section 3.1). The results from measurements over flat water give a best fit to the von Karman spectrum with lengthscales of about 0.2m in the offshore configuration and 0.16m for the onshore configuration. There is, therefore, a scaling mis-match of about 4 for longitudinal lengthscale.

For the offshore spectra, **(figure 5.4(a))**, for frequencies above 20Hz, the experimental data shows larger energies than normal and in order to ensure that these were not the result of probe vibration several tests were carried out. The tests used higher sampling frequencies (up to 1000Hz) and several probe heights above the still water. They showed no indication of probe vibration in this frequency region. It was therefore felt that these higher than expected energy levels at the high frequency end of the spectrum resulted from aliasing effects (aliasing is discussed in section 3.4.1.3). The availibility of low-pass frequency signal filters, (section 3.4.1.3), for the onshore phase of the work improved the high frequency fit to the von Karman spectrum. This can be seen by comparing **figures 5.4 (a)** and **(b)**. Despite this for spectra derived from the U-component of velocity, the effects of aliasing present no significant problems for the areas of interest.

Non-dimensional frequency spectra are also presented for the vertical components of velocity. **Figure 5.5**(a) and (b) shows the corresponding figures for the V-component of velocity. In this case aliasing effects are more significant since the spectrum is shifted to the right (higher frequencies) when compared to the U-component spectrum.

Figure 5.6 shows Reynolds stress profiles at X=-1265mm. For a boundary layer in equilibrium a vertical Reynolds' stress profile is expected in accordance with the existence of a region of constant shear stress. A change in roughness, for example to a rougher surface, leads to an increase in the Reynolds' stress in the lower heights which is convected to the upper height levels with increasing fetch. Substantial scatter of the calculated Reynolds stress data points is common and expected, (for example see Dalley (1993)). Presented results are normalised according to the equation given in section 4.3.3.

For the offshore profile (**figure 5.6(a)**) the distribution was not quite vertical, even after allowing for the scatter usually associated with Reynolds stress measurements. At H_{ref} a value of about 0.012 was obtained. **Figure 5.6(b)** shows the corresponding onshore profile, which showed a value of about 0.01 at H_{ref}.

Overall the flat water profiles of wind characteristics showed similar results for the onshore and offshore tank configurations. The fairing used to smooth the onshore air flow over the flapping paddle (section 3.3.2) has no significant effect on the air flow at X=-1265mm. Measurements of the wind profile approximately 630mm downstream of the fairing also confirm this.

Checks on the lateral variation of the air flow over the wave tank were made in the onshore configuration. These showed that differences in mean velocity and turbulence intensity over the central third of the wave tank were small, but that larger differences were recorded at the edges. Mean velocity at X=-1694mm was around 2.2m/s in the centre compared to 1.9m/s at the edges. However at X=-284mm the position was reversed with larger mean velocities recorded at the edges (2.3m/s) than in the centre of the tank (2.0m/s). Turbulence intensities in both configurations tended to be greater at the edges, typically 0.2 at the edge compared to 0.15 at the centre.

Although similar checks were not made in the offshore configuration, one could expect less variation since the tank is mainly positioned within the closed-jet section of the tunnel.

The results indicate that the simulated boundary layer suffers from a scaling mis-match of between 2 and 4 with respect to the waves. This represents a common mis-match error, where the model is too big for the simulated boundary layer. Cook (1982) notes that the effects of this are to severely underestimate the mean and fluctuating components of surface pressure.

5.2 STANDARD WAVE RESULTS

Results for the two standard waves, as described in section 4.2, under zero wind conditions are shown in table 5.2.

It can be seen from the table that there were differences in the breaker dimensions between the onshore and offshore conditions for the waves. As noted in section 3.3 there were slight differences in the tank slope between the two sets of experiment and slight changes were required to the spilling wave in order to ensure the wave remained spilling. The period was shortend to 0.72 seconds and the paddle throw was also modified slightly. The result was that in zero wind the onshore spilling wave was slightly bigger than the offshore wave. Although the paddle amplitude and period settings for the plunging wave were not altered, similar differences in the wave dimensions occured. Deepwater wavelength, L_o, was calculated from the wave period using Airy wave theory, (appendix A).

	Wind Condition	H_b (mm)	d_b (mm)	X_s (mm)	T (seconds)	L_o (m)
Spilling	Offshore	41.1	54	1383	0.75	1.171
	Onshore	47.6	67	1444	0.72	1.124
Plunging	Offshore	50.6	64	1615	1.10	1.889
	Onshore	42.7	53	1174	1.10	1.889

Table 5.2. Breaker dimensions under zero wind for the standard waves.

CHAPTER 6

AIR FLOW OVER THE WAVES

6.1 VELOCITY PROFILES

Results in sections 6.1, 6.2 and 6.4 are presented in the same format. In each section four figures are presented in the order: spilling offshore; plunging offshore, spilling onshore, and finally plunging onshore. Each figure presents four profiles (a) to (d) in order of increasing offshore distance, (X). For the offshore wind the point of breaking is always represented by plot (b), while for onshore winds the point of breaking is shown in plot (c). Results for normalised wind spectra, section 6.3, are presented slightly differently. The results from the velocity profiles for U_{ref}, z_0 and u_* are presented in tabular form in appendix C.

Figures 6.1 to **6.4** show the normalised semi-logarithmic velocity profiles for the spilling and plunging waves in the offshore and onshore configurations respectively. In order to prevent the analysis from becoming confusing, the offshore configuration results are discussed first, followed by the onshore results. The two sets of results are then compared and contrasted. The values of aerodynamic roughness and friction velocity obtained from the best fit regression lines are presented in a graphical form and are discussed later in this section.

For the offshore configuration, **figures 6.1** and **6.2**, the semi-log profiles indicate little difference between the two wave types. The general trend was of increasing z_0 with increasing negative distance from the origin, i.e. aerodynamic roughness increased through the surf zone. Aerodynamic roughness reached a maximum immediately downwind of the point of breaking, **figures 6.1(c)** and **6.2(c)**. For both wave types, z_0 reached a value of 0.002m, almost 100 times larger than the initial value (at X=-912mm).

Over the 'deep' water waves, (X approximately -2650mm), the profiles indicated a reduction in z_0. In the case of the plunging waves a 'kink'

developed in the profile, **figure 6.2(d)**. This is a result of the flow adjusting to the smoother surface of the deeper water waves, and means that the air flow is still adjusting to the new roughness at the end of the tank. Further reductions in z_o with increasing distance offshore are therefore to be expected.

The kink noted above also occurs, for both wave types, at the point of breaking, **figures 6.1(b)** and **6.2(b)**. Again this have may been due to the rapid changes in surface roughness that occured or to the effects of separation from the waves crests on the zero plane displacement layer. The data points lying below the reference height, H_{ref}, indicated much larger values of z_o and u_* than were obtained from the best fit line to the whole of the data. The profiles indicated in the figures have assumed a negligible zero plane thickness, which may not be valid at the point of breaking. The kinks may have been a result of dramatic changes in surface roughness or a positive zero plane displacement layer arising either due to the height of the waves or as a result of air flow separation from the waves. If some displacemant of the zero velocity height occured then it would be unlikely to be steady with time (d will certainly be zero at the wave crests). It is felt that these kinks are a result of either the sudden changes in surface roughness or due to the effects of air flow separation in the lee of the wave. For the spilling wave, **figure 6.1(b)**, the gradient becomes nearly infinite and hence the friction velocity becomes extremely large.

For the onshore winds, lower values of z_o and u_* were expected, because since the wind and waves are co-flowing the wind 'sees' fewer roughness elements. There is also the asymmetry of the waves themselves to consider. Plunging waves especially are very asymmetrical at breaking, the front face becomes vertical while the back face retains a reasonably smooth profile. The dramatic changes observed for the offshore conditions were not expected to be repeated.

Onshore semi-log profiles for spilling and plunging waves are shown in **figures 6.3** and **6.4**. Note that for the onshore profiles figure (c) always corresponds to the point of wave breaking (as apposed to figure (b) in the offshore case). Problems in terms of analysis arose beceause of the fairing used to promote smooth flow onto the tank. Ideally the wind coming onto the tank should have a profile consistant with that naturally occuring over a large fetch of sea in a state of swell. In practice this was difficult to achieve and some adjustment of the air flow was therefore expected.

The general trend was common to both wave types. Immediately upwind of the breakers, the profiles indicated values of z_o of the order of 0.0002m for the plunging waves and 0.0008m for the spilling waves. The profiles remained very similar over the point of wave breaking, (**figures 6.3(c)** and **6.4(c)**), and also immediately downwind of this point, (**figures 6.3(d)** and **6.4(d)**). On the 'shore' at X=100mm, the profiles indicated a much smoother surface profile, with z_o values of around $1x10^{-7}$m for the plunging wave and $5x10^{-7}$m for the spilling wave. From an engineering perspective, it is the wind conditions at the shore (where wind loads on structures must be considered) that are of particular interest.

In order to compare more easily the results for aerodynamic roughness and friction velocity, they are plotted against distance from the origin, X, showing the variation with offshore distance.

Figure 6.5 shows the logarithm of z_o against X. Differences between the values of aerodynamic roughness for the onshore and offshore tank configurations were not great. The largest difference occurs at the point of wave breaking, where z_o is generally larger in the offshore case by a factor of about 10. At X=-912mm (where the wave has already broken), the position is reversed with onshore winds showing larger values of z_o. Differences in the single and X-film measurements which were observed over flat water are not apparent with the waves running. This supports the notion that the slightly differing U_{ref} values made some small difference to the roughness of the 'flat' water, a difference which is negligible with the waves running.

As previously mentioned one of the foreseeable problems for the onshore configuration was the development of the boundary layer and fairing required to promote smooth flow to the water. Comparing the onshore results at X=-1850mm with the offshore values at X=-2700mm reveals similar values of z_o. In the offshore case the profiles indicated that the flow would become smoother still over the deeper water waves. However in general it suggests that the onshore boundary layer is not too far removed from that which would have occured over a large fetch of swell waves.

Normalised friction velocity, u_*/U_{ref}, is shown in **figure 6.6**. The general trends were similar to those for z_o. In the onshore case u_*/U_{ref} remained fairly constant with X, with lower values recorded at X=100mm. For offshore winds

a large increase in u_*/U_{ref} is observed downwind of the point of wave breaking. Differences between the two wave types were small, generally spilling waves have larger values of u_*/U_{ref}. The exception to this occurs in offshore winds downwind of the point of breaking where the largest values of u_*/U_{ref} were recorded for plunging waves.

6.2 TURBULENCE INTENSITIES

6.2.1 Horizontal Component

Turbulence intensity profiles for the horizontal component of velocity are shown in **figures 6.7 to 6.10**. Each profile shows the results for the single-film and X-film probe. As noted in section 5.1, the values of turbulence intensity obtained by the X-film probe tend to be higher than those from the single-film probe.

Flat water profiles indicate values of I_u of the order of 0.2 in offshore winds, and 0.15 in onshore winds. **Figures 6.7** and **6.8** show the offshore results for the spilling and plunging waves. At X=-912mm, over the bore of the broken waves, the profiles indicated little change from the flat water case. The biggest changes occured over the point of breaking, (**figures 6.7(b)** and **6.8(b)**). For both waves I_u values below the reference height (100mm) rose to over 0.4, and up to 0.5 for the spilling waves. Intensities in the upper levels, above about 150mm, remained similar to those upwind.

As offshore distance, X, increases the profiles indicated progressive increases in I_u in the upper levels. Below the reference height, I_u values decreased from the large values observed over the point of wave breaking. However they remained larger than those observed upwind of the point of breaking. Overall differences between the two types of wave were small, spilling waves showing peak values of intensity slightly larger than for plunging waves.

The extreme values of I_u observed in the offshore case were not present in the profiles for onshore winds, **figures 6.9** and **6.10**. Although I_u increases were recorded in the lower levels downwind of the breaker point, the increases were much less than those observed in the offshore configuration. The maximum recorded value of I_u was 0.25 for both wave types, and generally changes in I_u from the flat water case were small.

Generally, hot-film measurements of intensity values above 0.3 are to be regarded with some caution. Large I values often imply some degree of flow reversal (separation). Hot-film probes, and especially the X-film probe, are susceptable to errors if the flow direction is not within the boundaries of reliable measurement as discussed in section 3.4.1.4. This problem is discussed further with the phase-averaged results in section 6.5.

6.2.2 Vertical Component

Vertical turbulence intensity profiles are presented in **figures 6.11** to **6.14**. Flat water profiles indicated values of I_v at H_{ref} of around 0.2 in the onshore case and 0.25 for offshore winds. For the onshore configuration the profile for I_v was nearly vertical above H_{ref}, but below this height I_v reduced to a minimum at the lowest measured height. For the offshore case the profiles exhibited a linear profile of increasing I_v with probe height.

Overall the profiles for I_v with generated waves followed similar trends to those observed for the U-components of velocity presented above. In offshore winds peak values of I_v (over the point of wave breaking) were around 0.48. Values in the upper levels, above 200mm, remained fairly constant at 0.3. Recorded values of I_v in the onshore winds were lower, as for I_u, and did not exceed 0.3 at any fetch (for either wave type).

Peak values of I_v occured in the lower levels (in contrast to the flat water profiles), as a result of the wave-induced fluctuation. At X=100mm the profiles changed to resemble the corresponding profile in the flat water case.

6.3 FREQUENCY SPECTRA

6.3.1 Horizontal Component

Frequency spectra for the horizontal components of velocity are presented in **figures 6.15** to **6.22**. Due to the large number of spectra obtained some restriction on the numbers presented was felt to be necessary. Therefore the spectra at probe heights of approximately 100 and 200mm above the SWL are presented for both offshore and onshore conditions at all measurement locations. The von Karman spectrum (calculated from equation 4.10) for

$^{x}L_u$=0.2m is also plotted on the figures to provide a reference point for comparisons.

Offshore results for spilling and plunging waves are presented in **figures 6.15** to **6.18**. In the lower height levels, below 100mm and irrespective of wave type or fetch, the spectra were dominated by peaks at the frequency of the generated waves. In some cases harmonics of the wave frequency were also present, **figure 6.17(b)**. For the spilling waves the peak occurred at a frequency of 1.3Hz or 1.4Hz depending wind direction (different periods for spilling wave under onshore and offshore winds), plunging waves caused a peak at 0.9Hz. As height increased the peak became less dominating and eventually disappeared.

Although the bores of broken waves had some affect on the wind, spectra were most noticeably affected at the point of breaking. At this point the waves reached a maximum height and the gradient at the front face of the wave reached maximum steepness (vertical for plunging waves). **Figures 6.15(b), 6.16(b), 6.17(b)** and **6.18(b)** show the spectra over this point for the spilling and plunging waves. Results show that spilling waves significantly affect the wind to a height of 197mm, and the plunging waves to a height of 252mm. This is roughly proportional to the wave heights at breaking and in both cases spectra are affected to heights of 5 or 6 times the breaker height, H_b. In other respects spectra for the two wave types were similar.

For the offshore winds, immediately downwind of the point of breaking (X=-1575mm for plunging and -1811mm for spilling), the spectral peaks were still present but dominated the spectra to a lesser degree. For the plunging waves spectral peaks were present up to 253mm above the SWL.

Over the deep water waves one would expect the influence of the waves to be reduced, partly because of the reduced wave heights, but also because they presented a smoother profile to the wind. Peaks at the wave frequency were still significant and are observed at heights of 148mm and 309mm for the spilling and plunging waves, respectively. This represents an affected height of 3.6 and 6.1 times H_b for spilling and plunging waves respectively. At this fetch it was noticeable the spilling waves affected the wind to a lesser degree than the plunging waves. This possibly indicates that the spectral peaks at this

measurement point are the result of the upwind wave-induced disturbances and not the waves in deeper water.

Results for the onshore configuration are shown in **figures 6.19** to **6.22**. At X=100mm for the plunging waves, (at the shore), spectra showed large peaks at the wave frequency at 250mm above the ground. These were still present, but less obviously at over 300mm. Nearer the ground, below 100mm, the peaks were not present, possibly as a result of the slight incline prior to the probe at X=100mm, (**figure 4.2**). This slope would have the effect of smoothing the air flow near the ground, reducing turbulent fluctuations.

Immediately downwind of the point of breaking, the spectra showed strong peaks present at up to 200mm over the SWL. Over the point of breaking the peaks were much less dominant than in the offshore case and were mainly constrained to below 200mm, although they could still be observed at up to 250mm.

Results for the spilling waves were similar. At the 'shore', X=100mm, large wave frequency peaks were observed at 146mm, and smaller peaks could be observed up to 246mm. Again no peaks were observed below 100mm. At X=-912mm few large peaks were observed except at 53mm. However at the point of breaking large peaks dominated all spectra up to 200mm above the SWL. At 300mm they were no longer present.

Upwind of the point of breaking, at X=-1795mm, there was little evidence of the wave frequency peaks, which augments the hypothesis that the peaks over the deep water waves in the offshore configuration were the result of the waves' effect on the wind at the point of breaking. However the results for spilling waves contrasted with this, and upwind of the point of breaking, peaks were observed to extend from the SWL to 190mm. The peaks appeared to be of similar magnitude to those over the point of breaking. Possibly this reflects the larger wave steepness for the spilling wave in deeper water.

In both cases the spectra showed wave effects on the wind at the 'shore' in the height range of 100-200mm. The lack of wave effects in the lower heights may have been a direct result of the sloping beach, mainly used to prevent overtopping of the waves. In some ways this simulates the prototype conditions well since beaches are often steeper away from the high tide line.

The results indicated that wave induced effects on the wind may be felt at the shore, at heights of 4 or 5 times the breaker height, H_b.

Apart from the peak at the wave frequency, spectra were changed little from the spectrum for wind flowing over the water with no generated waves. No significant increases in higher frequency turbulent energies were seen to result from the waves' effect on the air flow. The spectra retained similar levels of energy as shown in the case over flat water, **figure 5.4**.

6.3.2 Vertical Component

Frequency spectra for the vertical component of velocity are presented in **figures 6.23** and **6.26**. Aliasing effects in the offshore spectra were more significant, compared to the horizontal component of velocity, since the turbulent fluctuations occured at higher frequencies, whilst the sampling frequency (and therefore the niquist frequency), remained constant at 100Hz. Spectra are presented at the reference height, H_{ref}, at all measurement locations.

Offshore results echoed those for the horizontal component of velocity. Large peaks at the wave frequency occured at, and downwind, of the point of breaking for both wave types, **figures 6.23(c) & (d)** and **6.24(c) & (d)**. Over the deep water waves, X=-2640mm, these peaks were still present for both wave types.

In the onshore case large peaks were observed at the point of breaking, **figures 6.25(c)** and **6.26(c)**. At X=100mm these peaks were no longer apparent at this height, although from the U-component spectra, results indicated that wave effects may be present at heights between 100 and 200mm. Upwind of the point of breaking, X=-1800mm, spectra for the plunging waves showed no peaks at H_{ref}. However spectra for the spilling waves did show a large peak at this height. As previously noted it is felt that this difference is probably a result of the differences in wave steepness offshore of the point of breaking. The effects of this are more likely to be felt in the onshore configuration as the differences in the amount of roughness seen by the wind are more apparent.

6.4 REYNOLDS STRESS PROFILES

Figures 6.27 to **6.30** show the Reynolds stress profiles over the tank with generated waves. Flat water Reynolds' stress profiles are shown in chapter 5.

For offshore winds and generated waves, **figures 6.27** and **6.28**, the Reynolds stress profiles indicated large adjustments of the boundary layer immediately downwind of the breakers. In contrast to the semi-log velocity profiles, profiles at the point of breaking remained similar to those over the bores of the broken waves at (X=-912mm). Over the 'deep' water waves the profiles showed large reductions in <uv> in the lower heights, reflecting the smoother profile presented to the wind by the deeper water waves.

The onshore results, **figures 6.29** to **6.30** were clouded by the effects of the transition from the tunnel floor to the water surface. Immediately downwind of the fairing the profile was sloped, with larger values in the lower heights. Further downwind the values in the lower levels reduced, and the profile became near vertical. Nearest to the fairing, the profiles for spilling, **(figure 6.29(d))** and plunging **(figure 6.30(d))** waves were similar to that in the flat water case at X=-2800mm. Generally values for the spilling waves were greater than for the plunging waves.

At the far downwind end, (X=100mm **(figures 6.29(a) & 6.30(a))**), profiles were nearly vertical (albeit with some degree of scatter). At this point values of normalised Reynolds stress for the flat water, plunging and spilling cases were; 0.009, 0.010, and 0.012 respectively, indicating that the profile at this point was still affected by the waves upwind, although the values of <uv> were not very different from the no wave case.

6.5 PHASE-AVERAGED WIND AND WAVE MEASUREMENTS

All results for phase-averaged velocity and turbulence intensity in **figures 6.31** to **6.54** are plotted alongside a typical wave profile at that fetch for comparison. In each case the wave is plotted such that the wave crest occurs at t=0.3 seconds, and the direction of wave advance is from right to left. Thus

onshore winds are also blowing right to left, whilst offshore winds blow left to right.

6.5.1 Phase-Averaged Velocity

Results for phase-averaged velocity are presented in **figures 6.31** to **6.42**. Each figure shows three plots of phase-averaged mean velocity, <U>, at heights of approximetely 45, 65, and 85mm above the SWL. The three figures for each combination of wave type and wind direction show <U> results at the point of breaking and approximately 300mm on either side of this point.

Figures 6.31 to **6.36** show results for <U> for the offshore configuration. The general trends were common to both spilling and plunging waves. All plots showed a good correlation between instantaneous wave height and <U>. Peak values of <U> occurred near the crest of the waves, with distinct phase-differences becoming apparent with increasing probe height. At the point of breaking peak values of <U> were typically double the values of <U> over the trough. Largest variations occurred over the point of wave breaking. For plunging waves at 47mm above the SWL peak crest velocity was 3.8m/s compared with typical trough values of 1.3m/s. At 83mm above SWL the difference had reduced to 3.0m/s compared to 1.5m/s. Spilling waves at the point of breaking showed similar, if not quite so large, variations over the wave.

Downwind of breaking, **figures 6.33** and **6.36**, (i.e. in deeper water) the correlation for spilling waves appeared to be better than at the point of breaking. For plunging waves the correlation begins to break down with increasing height, and at 83mm above SWL crest peak velocities were only slightly larger than those over the trough.

For spilling waves the correlation over the bores of the broken waves was also good. At 83mm above SWL <U> values near the crest were around 2.0m/s compared to typical trough values of 1.6m/s, **figure 6.31(a)**. Although the correlation for plunging waves was not so good at this point, the difference between crest and trough velocities was still marked, 1.9m/s compared to 1.6m/s, **figure 6.33(a)**.

In all cases a phase-lag was apparent with increasing height above the waves. At 83mm above SWL, the phase-lag was of the order of 0.05 to 0.1 seconds,

(**figures 6.32(a)** and **6.35(a)**). As probe height above the SWL increased then so did the phase difference between the wave height and <U>. The lag reflects the time for the wave-induced fluctuations to reach the probe height as the wave continued to propagate forward. Essentially the phase-lag represents a spatial difference between the instantaneous wave crest position and the maximum <U> at a given height and is due to the movement of the waves. If the waves were not moving then one would expect the maximum <U> to occur at the wave crest. As a result the phase-lag is opposite for the offshore and onshore waves (although for the onshore waves this is highly dependant on the wave-to-wind speed ratio).

In all cases for the offshore phase-averaged velocity, significant wave-induced perturbations to the air flow were in evidence at the maximum height measured (around 83mm). Hence, for the onshore phase, an additional measurement at around 105mm above SWL was made. However the results showed that the wave to <U> correlation was not so good for this case and therefore the presented results are confined to roughly the same three probe heights as in the offshore case.

Figures 6.37 to **6.42** show the <U> results for the onshore configuration.

Figures 6.38 and **6.41** show the <U> results over the point of breaking. Slight modifications to the air flow were observed for plunging waves, where a peak in <U> is observed in the lee of the wave crest, (in front of the wave for onshore winds). The changes in <U> were small however, 2.3m/s at the crest, compared to a typical trough value of 1.9m/s. At 103mm (not shown) the effect of the wave on <U> was minimal to the eye, indicating that the effect on the waves was less than in the offshore case. For spilling waves at the point of breaking the correlation was not as good as in the offshore case and it rapidly decayed with height, (**figure 6.38**). At 102mm above SWL the changes in <U> over the wave period were almost zero.

Upwind of the point of breaking (in deeper water) the results are shown in **figures 6.39** and **6.42** for spilling and plunging respectively. For plunging waves the effects were felt up to 102mm, where <U> values were observed to decay in the lee of the wave crest. However the correlations were still weaker than those that occured in the offshore case. For spilling waves, the correlation

was better upwind of the break point than it was over the point of breaking, although the effects were becoming noticeably weaker at 101mm above SWL.

Downwind of the breakers, over the bores of the broken waves, wave induced variations in <U> for the plunging waves, **figure 6.40**, almost vanished to the eye, except at the lower probe heights. For spilling waves the correlation was better, **figure 6.37**.

A simple way to show the wave influence on the air flow is to present a ratio of the maximum phase-averaged mean velocity over the minimum value. The results are presented in table 6.1 for the plunging wave and table 6.2 for the spilling wave.

Approximate probe height (mm)	Over the bore of the broken wave		At the point of breaking		Over the waves before breaking	
85	1.26	**1.61**	1.33	**2.51**	1.17	**2.00**
65	1.37	**1.76**	1.24	**2.49**	1.17	**2.05**
45	1.34	**1.76**	1.35	**4.70**	1.23	**3.10**

Table 6.1. Ratio of $\frac{<U>_{max}}{<U>_{min}}$ for plunging waves. Results for offshore winds are shown in bold, onshore results are in normal type.

Approximate probe height (mm)	Over the bore of the broken wave		At the point of breaking		Over the waves before breaking	
85	1.28	**1.36**	1.26	**1.50**	1.30	**1.59**
65	1.26	**1.74**	1.33	**2.07**	1.36	**1.82**
45	1.39	**2.01**	1.40	**3.56**	1.35	**1.75**

Table 6.2. Ratio of $\frac{<U>_{max}}{<U>_{min}}$ for spilling waves. Results for offshore winds are shown in bold, onshore results are in normal type.

Each table shows clearly the difference between the onshore and offshore wind conditions. The greatest variations in <U> were recorded for the plunging

wave under offshore winds. Table 6.1 also indicates that for the plunging wave, and for both wind conditions, the ratio of $<U>_{max}$ to $<U>_{min}$ downstream of the break point tended to be larger than the corresponding value upwind of the point of breaking. This would suggest that the waves at the point of breaking provide the greatest influence on the wind. For the spilling wave this trend did not occur and values of the ratio were similar upwind and downwind of the point of breaking, indicating that the spilling wave affects the wind both before and after the point of breaking.

Overall the correlation between wave height and <U> was much better for offshore winds than for onshore conditions. The major reason for this is probably the difference in wind speed relative to wave celerity. Assuming that wave speed at breaking is approximately given by;

$$c = \sqrt{g.d} \qquad (6.1)$$

where c is wave celerity and d is water depth, (see appendix A). Then at the point of wave breaking, where d_b was typically 0.06m, wave celerity was around 0.77m/s. If onshore and offshore wind speeds were +2 and -2m/s respectively, then the wind speed relative to wave speed was 1.33m/s for onshore winds and 2.77m/s for offshore winds.

These results have implications for the non phase-averaged turbulence intensity values in section 6.2. The significant fluctuations of <U> over the wave period will have been included as turbulent fluctuations from a static mean. Actual turbulence intensity levels may not have been affected by the waves at all. However, this does not mean that the problems in using the hot-film, as discussed in section 3.4.1.4, did not apply. Significant fluctuations in the V-component were probably still present as a result of the fluctuating water surface level.

6.5.2 Phase-Averaged Turbulence Intensities

Phase-averaged turbulence intensities, $<I_u>$, are presented in **figures 6.43** to **6.54**.

For the offshore configuration, **figures 6.43** to **6.48**, phase-averaged turbulence intensity was shown to be little affected by the waves, except over the point of breaking. **Figures 6.44** and **6.47** show $<I_u>$ results for the plunging and

spilling waves at this point. For both waves $<I_u>$ values at 83mm above SWL showed no correlation with wave height. For the lower probe heights, $<I_u>$ levels in the lee of the wave crests were seen to rise. In the case of the plunging waves $<I_u>$ increased by a factor of around 3. Downwind of the point of breaking, intensity levels showed no changes with wave height, although $<I_u>$ levels were generally larger than those upwind of the point of breaking.

Onshore results are presented in **figures 6.49** to **6.54**. The additional measurement made at a height of approximately 105mm is not presented, although results are discussed. Results for spilling waves showed no significant correlation to wave height, except over the point of breaking at 42mm above SWL. $<I_u>$ values upwind and downwind of the point of breaking were similar.

For plunging waves under onshore winds, no consistent changes in $<I_u>$ over the wave period were observed, **figures 6.52, 6.53 & 6.54**. Again values of $<I_u>$ remained fairly constant, with no significant changes observed with increasing offshore distance.

From the figures it can be seen that the recorded values of $<I_u>$ were far lower than those obtained in the turbulence intensity profiles of section 6.2. Typical values of $<I_u>$ from these results were around 0.006. Significantly larger values were only obtained in the offshore configuration, in the lee of the wave crests, where $<I_u>$ reached 0.04 for both wave types. This compares to a typical flat water value of I_u of 0.2 from the velocity profiles, (section 5.1).

The low values of $<I_u>$ obtained were due to the small time period over which the intensity was calculated. This was necessary in order to ensure that the intensity was calculated from the mean velocity at that point over the wave. It should be noted that in the I_u profiles of section 6.2, the large variations in phase-averaged mean velocity recorded above were included as fluctuations from the overall mean and hence contributed towards the value of I_u. This explains the very large I_u values (up to 0.5) obtained.

The results for $<I_u>$ show that for the onshore configuration little change in intensity levels occured over the wave period. In offshore winds, large increases were observed in the lee of the wave crest, but only in the lower two

heights measured. This provides an indication of separation at the wave crests, although is not conclusive. For onshore winds no evidence of air flow separation at the wave crests is seen.

CHAPTER 7

WIND EFFECT ON EXTERNAL WAVE CHARACTERISTICS

7.1 BREAKER DIMENSIONS

The results in this chapter deal with the effect of the wind on the geometry of the waves at breaking. Non-dimensional results are presented for breaker height, breaker depth, surf zone width, plunge point depth and amplitude-to-depth ratio at breaking. Results for the above are also presented as percentage changes from the no wind case. Error bars are plotted for breaker height, breaker depth and amplitude-to-depth ratio, showing the maximum estimated error in the measured variable. These errors are calculated in section 4.4.5. The data from which the figures in sections 7.1 and 7.2 were obtained is presented in tabular form in appendix D.

7.1.1 Breaker Height

Non-dimensional results for breaker height, (H_b/gT^2), against wind velocity, $(U/[gH_p]^{0.5})$, are shown in **figure 7.1**. No real trend is seen to emerge, although individual waves may show a trend towards increasing or decreasing wave height. Overall the influence of the wind on breaker height is minimal.

Figure 7.2 shows the same data expressed as percentage changes of breaker height from the no wind case. Results are categorized into three wave types, where the category is determined by the form of the wave in the no wind case. Data points are scattered fairly symmetrically around the zero percentage change mark, with the majority lying within the range -5% to +5%. Scatter of the data points appears to increase with increasing wind velocity No discernable trend can be seen.

This distribution must be compared with the estimated errors in determining H_b (section 4.4.5). Except for two cases in the offshore configuration and seven in the onshore configuration, all data points show error bars crossing the *zero percentage change* line. Therefore there exists the possibilty that for the

majority of observed breaker heights, the recorded change is a result of measurement errors and not true changes in H_b.

7.1.2 Breaker Depth

Similar graphs are presented for breaker depth. **Figure 7.3** shows the non-dimensional results for breaker depth, (d_b/gT^2), against normalised wind velocity. A general trend of increasing normalised breaker depth with increasing onshore normalised wind velocity is observed. Offshore winds appear to cause a corresponding reduction in breaker depth. The trend becomes more apparent when plotted as percentage changes from the no wind value of d_b, **figure 7.4**.

At normalised wind velocities in the range -3 to +3, the data is affected little by the wind. For this wind range, the observed changes are of similar magnitude to the estimated errors (obtained in section 4.4.5). At higher wind speeds larger changes, of 20-30%, are observed.

In the offshore case the data exhibits reasonable sorting according to initial breaker type. Plunging waves (with the exception of one data point) are little influenced, and often no detectable change in breaker location (and therefore breaker depth) occurred. With one exception, all plunging wave data points show a reduction of less than 11% due to the offshore wind. Spilling and transition waves are more affected, with reductions in d_b of around 10% occurring even at lower wind strengths.

The onshore data set is dominated by two results for one of the transition waves (Wave 7 in table D.2 (appendix D)), where increases in breaker depth of 60% occur. Otherwise large increases in d_b occur mainly for the plunging waves, which show 20-35% increases in d_b for a normalised wind strength of +4.

Overall a clear trend is observed: onshore winds increase d_b, offshore winds decrease d_b.

7.1.3 Surf Zone Width

Results for the wind influence on normalised surf zone width, (X_s), are presented in **figure 7.5**. X_s is normalised by dividing by the 'deep' water wave height, H_p. The results clearly show differences between the onshore and

offshore configurations. These differences are not apparent if non-normalised surf zone width is plotted against wind velocity. That is actual measured values of X_s are similar for both tank configurations, the differences in normalised surf zone width arise from a slightly larger range of values of H_p used in the onshore configuration. This discrepancy is probably a result of the slight difference in the tank slope for the two tank configurations (section 3.3).

Data is quite well sorted according to breaker type in the offshore configuration, but less so for onshore winds. In both cases the effect of the wind can be seen, decreasing X_s for offshore winds, and increasing X_s under onshore winds.

Figure 7.6 plots the percentage change in surf zone width against normalised wind velocity. Results here are nominally indentical to those for breaker depth, since on a constant gradient beach, breaker depth is proportional to distance from the shore. The comments regarding breaker depth, made in section 7.1.2, are therefore valid. Error bars were not plotted on **figure 7.6** in order to retain clarity; they are discussed later in this section.

The results show that waves are affected differently between the offshore and onshore configurations. Offshore winds appear to mostly affect the spilling and transition waves. In onshore winds the largest changes in X_s were recorded for plunging and transition waves. For both wind configurations the problem of determining the exact point of breaking meant that in many cases there was no recorded change in breaker location until the second or third wind increment. This problem is discussed elsewhere, but may account for the large concentrations of data on the zero change line in **figure 7.6**.

Section 4.4.5 calculates the maximum error in the percentage change of surf zone width, based on the an error margin in determining the point of breaking of ±50mm. The error for surf zone width was estimated at ±7%. Although there is a concentration of data on the zero change line (for reasons expressed above), wind affected data is shown to be clear of the zero change line when the error is accounted for.

7.1.4 Amplitude-To-Depth Ratio At Breaking

Results for amplitude-to-depth ratio at breaking are shown in **figure 7.7**. For the onshore configuration waves have values of H_b/d_b ranging from 0.65 to

1.15, whilst the waves used in the offshore configuration range from 0.69 to 0.98. Generally plunging waves show larger values of H_b/d_b than either spilling or transition waves. Weishar & Byrne (1978) note that from their field observations an average value of H_b/d_b of 0.78, with plunging and non-plunging waves having average values of 0.87 and 0.68 respectively. For this experiment the corresponding averages of H_b/d_b are 0.83, 0.86 and 0.79.

Although it can be seen that there is a general trend of increasing H_b/d_b for offshore winds and a decreasing trend in onshore winds, it is also apparent that for each wave H_b/d_b is quite variable. It is difficult to determine any specific trends from **figure 7.7**. Therefore the results are plotted as percentage changes in H_b/d_b from the zero wind value, **figure 7.8**. The trends observed above become clearer. There is some scatter around the zero percentage change line, mainly as a result of the scatter in H_b. The larger changes in H_b/d_b are a result of changes in breaker location (i.e. d_b) since changes in H_b were mainly constrained to less than ±5%. For offshore winds no clear trend regarding breaker type is observed. Onshore winds show plunging waves to be more affected than either spilling or transition waves. 8 out of the 11 data points showing a reduction greater than 10% are for plunging waves.

Overall onshore winds show the greatest effect on H_b/d_b with several points showing decreases in excess of 15%. However they also show more scatter about the zero percentage change line, again due to the influence of H_b. For offshore winds only three data points show an increase in excess of 15%. Error bars show that although at the lower wind speeds the observed changes may be due to errors, this is unlikely for higher wind speeds where changes in excess of the maximum estimated errors were recorded.

7.1.5 Plunge Point

Plunge point is defined and measured as in section 4.4.3 for all plunging waves, including those which were initially non-plunging. It is converted into a depth, d_{pp}, which is equivalent to the still water depth at the point where the 'horizontal roller' is formed. Although errors for plunge point are not discussed in section 4.4.5, they will be of similar magnitude to those for breaker depth, d_b. This is mainly because determination of the plunge point is subject to the same inaccuracies as the point of wave breaking. Thus for **figure 7.11**, errors in the vertical scale are of the order of ±10%.

Figure 7.9 shows the effect of the wind on the ratio of plunge point depth, d_{pp}, to breaker depth, d_b. This shows for each plunging wave, the relative depth in which the horizontal roller is formed with respect to the breaker depth at the same wind velocity. Wind appears to have very little influence on this ratio, with values remaining reasonably constant at between 0.83 and 0.75 irrespective of wind strength or direction. This also applies to the waves which were initially non-plunging, but became plunging under the action of the wind. This ratio does not however take into account the actual depth of water in which the roller is formed, it simply shows that the ratio of depth at plunge point to breaker depth is roughly constant with wind velocity.

In order to reflect the actual depth in which the wave finally plunges with respect to the initial breaker depth, the data is plotted as in **figure 7.10**. This shows the ratio of the depth at plunge point for each wind condition, (d_{pp}), with respect to the breaker depth in the no wind condition, ($d_{b\ no\ wind}$), against wind velocity. For the offshore configuration, a clear trend of decreasing $d_{pp}/d_{b\ no\ wind}$, is observed. The trend for the onshore wind is less clear, consequently the data is re-plotted as the percentage change in d_{pp} from the zero wind value, in **figure 7.11**. Since a zero wind value of d_{pp} does not exist for the initially non-plunging waves these waves have been omitted from this plot. The results show that for the onshore configuration the majority of the points lie on the zero percent line. Partly this is because the onshore wind caused a change in breaker type away from plunging. Offshore winds cause a reduction in d_{pp} with increasing offshore wind velocity. Maximum reductions in d_{pp} are of the order of 20%, similar to the wind affected changes for breaker depth, d_b.

In summary the wind is shown to be a factor in determining the point of plunging. Offshore winds cause a reduction in this depth in line with the changes in breaker depth, d_b. Onshore winds have little effect on the value of d_{pp} for waves which remain plunging. However the significant effect of onshore winds on breaker type is not shown in the figures. The winds' effect on breaker type is discussed in the next section.

7.2 BREAKER TYPE

This section investigates the effect of the wind on the type of breaking wave formed. Before dealing with the winds' effect on the wave, the distribution of breaker types under zero wind conditions will be considered. **Figure 7.12** shows the distribution of breaker type determined by non-dimensional 'deep' water wave height, (H_p/gT^2). In order to give some idea of scale, H_p/gT^2 is plotted against 'deep' water wave height, H_p. Theoretically breaker type should be categorized by H_p/gT^2 alone (assuming a constant beach slope). The range of values of H_p used for the two configurations is different, for the offshore configuration; $24<H_p<44$mm, and for the onshore configuration, $35<H_p<53$mm.

Breaker classification is moderately well predicted by wave steepness. One would expect the spilling waves to occur at the largest values of H_p/gT^2 . Plunging waves from both wind cases are mainly grouped below values of H_p/gT^2 of 0.006. The majority of spilling and transition waves occur at values above 0.005. No significant differences between the spilling and transition wave classifications appear.

There are however some discrepancies. Firstly, there are the two spilling waves, from the offshore configuration, which are grouped to the left of the plunging waves, some distance from the other spilling waves. Since H_p for these waves is significantly smaller than for the other spilling waves (these waves were also the smallest overall), it is felt that this discrepancy may be the result of scale effects. Similarly, the outlying plunging wave at $H_p/gT^2 = 0.0103$, is the largest plunging wave by some 25%. Removing these three waves, so that H_p is effectively restricted to $30<H_p<55$mm, much improves the classification of the waves by H_p/gT^2. This implies some scale effects on the mode of wave breaking.

Figure 7.13 shows the effect of the wind on breaker type by plotting H_p/gT^2 against normalised wind velocity. Note that H_p is assumed to be unchanged by the wind. The initial breaker type (i.e. in zero wind) is indicated by the shape of the icons. The breaker type at a particular wind strength/direction is indicated by the colour of the icon. It is apparent that the onshore configuration covers a greater range of wave steepnesses than the offshore configuration.

The general trend is towards plunging waves in offshore conditions and spilling waves in the onshore winds. Under offshore conditions, out of the 6 initially non-plunging waves, at the maximum wind speed all were either plunging (3) or transition (3). Similarly for the onshore conditions, out of the 10 initially non-spilling waves, 5 became spilling and 3 became transition waves.

Figure 7.14 shows the distribution of breaker types from this experiment according to one of the recognised breaker parameters, the surf similarity parameter, ξ. The breaker types are indicated by the same system of icons as in **figure 7.13**. Since calculation of H_o from the values of H_p is not really appropriate, the inshore version of the parameter (section 1.2) is used. Thus ξ is calculated from the breaker height, H_b, and assuming a beach slope of 1/20.

From section 7.1.1 the effect of the wind on breaker height is shown to be minimal, the purpose of plotting the data is to examine the effect of the wind on the breaker category boundaries. Iwata & Sawaragi (1982) quote value for ξ of 0.4 for the spilling-plunging boundary, with spilling waves occuring at values of ξ less than this. The maximum value of ξ observed here is 0.33. Thus according to ξ all waves in this experiment should be spilling. No real improvement in the grouping of the breaker types is seen to occur, although there is some change in ordering.

Spilling and transition waves occur consistently for values of ξ less than approximately 0.23 in zero wind conditions. Under onshore winds, only two waves remain plunging at the top wind velocity. For offshore winds all waves except three plunge. To quote a boundary value of ξ is therefore pratically impossible, since the effect of the wind is apparently greater than the range of waves used.

Breakers were examined for signs of the micro-breakers observed by Douglass (1989). During the onshore phase, distinct ripples could be seen at the crests of the waves. Sometimes the ripples would be left behind by the advancing wave, at other times they would 'ride' the wave crest until the wave broke. However, it was not possible to observe whether these micro-breakers were responsible for the breaking of the main wave as noted in section 1.3. Under offshore winds, the micro-breakers appeared on the front face of the wave, resulting in a convoluted appearance. The size of the micro-breakers means

that they were capillary waves. The effects of these waves are discussed further in section 9.2.

In summary, wave breaker types are classified reasonably succesfully by normalised H_p in zero wind conditions, (with some reservations). Under the wind, the trend for breaker type is clear and undoubtably significant, but boundaries between spilling and plunging are not well enough defined to quote firm figures. The surf similarity parameter, calculated from breaker height shows no improvement in breaker type classification over normalised H_p.

7.3 COMPARISON WITH THE RESULTS OF DOUGLASS (1989)

In this section the results for breaker height, amplitude-to-depth ratio and surf zone width are compared to those of Douglass (1989). Examination of the experimental results showed that waves in the experiment, where H_b was between 0.1-0.15m, were simulated at a scale of approximately 1/15. This is three or four times larger than the waves used for these experiments and allows for more accurate measurement of breaker dimensions. Other differences include the wind simulation, overall length of wave tank and model beach slope. Douglass (1989) used a model beach slope of 1/25, compared to the 1/20 slope used here. This difference will affect the results, but the trends should still be comparable. Also the longer wave tank means that the wind can begin to affect the waves further offshore than is possible with the equipment configuration here. The potential effects of this are further considered in the discussion.

Douglass used three waves in his experiment, one each of plunging, spilling and a transition wave between the plunge and spill modes. These waves were denoted by; Wave P, Wave I and Wave S, for the plunging, transition (intermediate) and spilling waves respectively. Results for wind velocity have been normalised according to the dimensionless group used by Douglass (1989) and given in section 4.4.

7.3.1 Breaker Height

Results for breaker height, **figure 7.15**, show similar changes due to the wind. Douglass's results show changes in the offshore configuration of between -6 to +10%, agreeing well with the magnitude of changes observed here. Onshore winds caused changes in H_b of around -3% for all three waves, which corresponds to the results here since most data lies within ±5% of the zero change line.

7.3.2 Surf Zone Width

Results for the wind's influence on surf zone width, **figure 7.16**, show good agreement. Observed changes are of similar magnitude, although there is some disagreement concerning breaker types.

For the offshore results, section 7.1.3 notes that the data is reasonably sorted by breaker type. Spilling waves tend to be most affected and plunging the least affected. Data from the two transition waves falls in between that for spilling and plunging. The overall fit of Douglass' data is good for Waves S and P. Wave I is the exception to this showing a greater degree of dependance on the wind than results from this experiment would suggest.

For the onshore winds Douglass' results fall into the region of observations from this experiment. Wave S is shown to be most affected, followed by Wave I, then Wave P. This is somewhat contradictory to results here, where plunging and transition waves were observed to be most affected. However Douglass' Wave I shows good agreement this time with the data for transition waves.

For both wind configurations, Douglass observed only small changes in X_s for Wave P, and these would explain the large number of recorded 'zero change' results for plunging waves in this experiment. It has been previously mentioned that at the scale used here some difficulty was experienced in determining the exact position of wave breaking. The ±2% changes in surf zone width observed by Douglass for Wave P, represent at the scale of these experiments a shift in breaker location of approximately 30mm. This is within the estimated ±50mm margin of error for breaker location estimated in section 4.4.5.

7.3.3 Amplitude-To-Depth Ratio

Figure 7.17 shows percentage change in amplitude-to-depth ratio, (H_b/d_b), against normalised wind velocity. Agreement between the two sets of data is good for both wind configurations except for Wave I. At the highest wind speed in the offshore configuration an 80% increase in H_b/d_b is recorded, this far exceeds any other results recorded either by the author or Douglass himself. Also, for Wave S in the offshore condition there is an initial reduction in H_b/d_b from the no wind case. At the next wind speed, the change is shown to be positive following the general trend. From the results of this experiment the trends from individual waves often show deviations from the general trend. If fewer numbers of waves had been used, then the results could potentially look very different. Error limits calculated in section 4.4.5 show that the potential errors are quite large, especially for amplitude-to-depth ratio where error may be present in both H_b and d_b. Calculating the percentage change from the no wind value, as shown in equation 4.16, also amplifies potential errors, since opposite errors in numator and denominator will be compounded.

Overall there is good agreement between the results of this investigation and those of Douglass (1989). The wind is shown to be a potentially significant factor in influencing breaker amplitude-to-depth ratios and also the surf zone width. The general agreement shows that the differences in modelling, (wind simulation and model scale), have not been significant.

CHAPTER 8

WIND EFFECT ON INTERNAL WAVE CHARACTERISTICS

The results in sections 8.1 and 8.2 are used to test the hypothesis that the action of the wind, either by it's influence on the breaking of the waves or by the formation of a wind drift layer, will affect the motion of the water particles and consequently the net drift of particles beneath the waves. The two methods of testing this hypothesis, particle path studies, (section 8.1), and measurements of water velocity, (section 8.2), are discussed in the context of this hypothesis.

8.1 PARTICLE PATH ANALYSIS

In section 8.1 the results are presented, and are generally discussed, in the order plunging-offshore, plunging-onshore, spilling-offshore, and spilling-onshore.

8.1.1 Effect Of Wind On Particle Amplitudes

The wind effect on the three 'components' of particle motion, as defined in section 4.6.1, is shown in **figures 8.1** to **8.12**. Figures are presented to show comparisons between the *wind* and *no wind* data sets for uprush amplitude, backwash amplitude and the vertical amplitude of motion. The onshore and offshore results are presented separately. The errors estimated in section 4.6.3 are not plotted on the figures in order to retain clarity.

Results for the Kolmogorov-Smirnov statistical analysis described in section 4.6.2. are shown in table 8.1. Each value indicates the significance level at which the distribution of data for the wind and no wind conditions can be said to be different. The smaller the value, then the more likely it is that the two distributions are different, and that the wind has had an effect. Generally wind effects only become apparent to the eye at K-S values lower than 0.1, and

values above about 0.2 indicate no significance differences between *wind* and *no wind* data sets.

Wave	Configu-ration	Amplitude	K-S significance level		
			X=-1525mm	X=-1755mm	X=-2000mm
PLUNGING	Offshore	Uprush	0.024	0.698	0.084
		Backwash	0.017	0.00008	0.401
		Vertical	0.603	0.791	0.940
	Onshore	Uprush	0.118	0.604	0.241
		Backwash	0.00197	0.00239	0.00171
		Vertical	0.0286	0.328	0.4
SPILLING	Offshore	Uprush	0.121	0.009	0.221
		Backwash	0.675	0.527	0.350
		Vertical	0.926	0.822	0.915
	Onshore	Uprush	0.0000163	0.00279	0.0196
		Backwash	0.293	0.274	0.643
		Vertical	0.643	0.505	0.923

Table 8.1. Results of the K-S significance test for the correlation between *Wind/No Wind* data sets.

8.1.1.1 Vertical Amplitudes

Vertical amplitudes of the particle motions are shown in **figures 8.1** to **8.4**. The distributions show a linear increase in amplitude with height above the bed as expected from Airy wave theory.

No significant differences between the *wind* and *no wind* cases were observed. This is verified by the statistical analysis (table 8.1). The K-S values exceed a value of 0.5 in the majority of cases, with only one recorded value lower than 0.3. This occured for the plunging wave at X=-1525mm **(figure 8.2(a))** in the onshore configuration and can be attributed to large scatter of the *wind* data points at a height of approximately 40mm above the bed.

For the spilling waves under an offshore wind, **figure 8.3(b)**, there appears to be some wind effect on the amplitudes near the water surface at X=-1755mm. With the wind affected data showing lower values of vertical amplitude than

the *no wind* data would suggest. Overall however the K-S value of 0.527 indicates no wind effect.

Overall, the results indicate that there is little or no wind effect on the vertical amplitudes of the particles. However the results, by virtue of the low levels of scatter, give an indication that the method of obtaining the data does not give rise to significant experimental errors. The estimate of ±10mm error in amplitude is significantly larger than any observed deviations from the general trend. The estimate of error for particle height, (±6mm), is nearer to the variations in measured path height. Thus although the results for vertical amplitude indicate no wind effects they do suggest that errors due to the experimental technique are reasonably small.

8.1.1.2 Uprush Amplitudes

These are presented in **figures 8.5** to **8.8**. A distinct difference between the results for plunging and spilling waves is apparent and the results are discussed separately.

For the plunging waves differences between the *wind* and *no wind* data sets were small **(figures 8.5 and 8.6)**. No general trend for the winds' effect on the particle uprush amplitudes was apparent. These observations were confirmed by the results for the statistical analysis given in table 8.1. However in the case of the offshore configuration, at X=-1525 and -2000mm, **(figure 8.5(a)** and **(c))**, the results indicated some wind effect due to the K-S values of 0.024 and 0.084 respectively. Despite differences in the waves used, (section 4.2), differences between the results for the onshore and offshore wind conditions were small, although generally amplitudes in the offshore case were 5-10mm greater than corresponding amplitudes in the onshore configuration.

For the spilling waves, **figures 8.7** and **8.8**, uprush amplitudes were about 2/3 the size of those for the plunging waves. Scatter of the data points was also greater, possibly on account of the shorter wave period for spilling waves. Differences between the *wind* and *no wind* data sets could observed by eye, for example **figure 8.8(a)**, where a clear difference is observed. These differences were reflected in the recorded values of the K-S significance level in table 8.1.

At X=-1525mm the offshore wind, **(figure 8.7(a))**, increased uprush and the onshore wind, **(figure 8.8(a))**, decreased uprush. At first sight this is

contradictory (considering the wind direction) however it is probable that the particles in the wind drift layer were not measured due to the difficulties noted in section 4.6.3. A simple hypothesis for these observations is therefore that the net particle motion due to the wind drift layer must be matched by a balancing opposite drift below this layer which is superimposed onto the particle motions.

Differences between the onshore and offshore configurations were again apparent. Under the onshore wind uprush amplitudes were observed to be affected more significantly than under offshore winds. This was reflected in both the figures and the K-S values.

Overall scatter of the data points for amplitude of motion is less than that estimated in section 4.2.

8.1.1.3 Backwash Amplitudes

Backwash amplitudes are shown in **figures 8.9** to **8.12**. Again distinct differences between the spilling and plunging waves were observed, with plunging waves showing greater effects of the wind. Scatter of the data points was noticeably less than occured for the uprush data, especially for the spilling wave.

For the plunging waves distinct wind effects were observed for both wind directions at X=-1525 and -1755mm, **figures 8.9** and **8.10 (a** and **b)**. At X=-2000mm wind effects were only apparent in the onshore case **(figures 8.9(c)** and **8.10(c))**. K-S values were all lower than 0.017 with the exception of the offshore case at X=-2000mm, **(figure 8.9(c))**. However the effects of the wind on the particle amplitudes appears to be the same irrespective of direction. In both **figures 8.9** and **8.10** the effect of the wind was observed as an increase in the backwash amplitudes irrespective of the wind direction. The reason for this is not known.

For the spilling waves, **figures 8.11** and **8.12**, no significant differences due to the wind were observed. This was again verified by the statistical analysis, with the K-S values all greater than 0.27.

8.1.2 Effect Of Wind On Particle Drift

The above results for particle amplitudes indicate wind effects on the motion of the suspended particles. For spilling waves uprush amplitudes were affected, whilst for plunging waves the backwash phase was affected. For engineering applications however it is the drift velocity of these particles which is of importance. Plots of height above bed against drift velocity were therefore obtained as described in section 4.6.1. These are presented in **figures 8.13** to **8.16**. All figures show the estimated errors in drift velocity, as obtained in section 4.6.3, in the form of error bars.

Overall there should be a zero net drift, since for any given point the law of continuity must apply with the amount of water moving onshore equalling the amount moving offshore. This assumes that measurements have been made right up to the surface, and that the particles follow the water particle motions exactly, (this is unlikely due to the size and density of the suspended particles). At low velocities and accelerations the particles are likely to track the surrounding fluid well. It is at high velocities and accelerations that the inertia of the observed particles will cause them to deviate from following the water particles closely.

The results for plunging waves are considered first; **figures 8.13** and **8.14**. In all cases it was apparent that drift velocities were generally positive, indicating a net onshore movement of the particles. Only close to the surface did the particles exhibit offshore drift.

Wind effects on the drift were difficult to determine in general terms. However for all figures the wind affected drift velocities in the mid height regions tended to be lower than the zero wind case.

With the exception of the two figures at X=-1525mm, (**figures 8.13(a)** and **8.14(a)**), drift velocities near the surface showed trends as expected from the influence of the wind drift layer. The error bars also indicate that measurements in this region were sparse and this should be bourne in mind. For onshore winds (**figure 8.14(b)** and **(c)**) near surface drift velocities were increased, and for offshore winds (**figure 8.13(b)** and **(c)**) near surface drift velocities were decreased. Near to the bed the results indicated increased onshore drift under onshore wind conditions. For offshore winds the net onshore drift was reduced (although only by a small amount).

Overall the results for the plunging waves support the hypothesis, although the results do not permit a clear conclusion as to the effect of the wind.

Results for spilling waves are presented in **figures 8.15** and **8.16**. When compared to plunging waves the positive drift which is encountered at the bed, changes to negative drift at a lower height above the bottom. Also the error bars are generally smaller, indicating larger amounts of data from which the average drift was calculated.

At X=-1525mm (**figure 8.16(a)**) onshore winds appeared to make a significant difference to the particle drift velocities, with the wind affected data exhibiting large negative values (indicating offshore particle drift) in the mid height levels. At the same point in the offshore wind case differences between the *wind* and *no wind* case were minor (**figure 8.15(a)**). The onshore results showed changes in near surface drift velocities from net offshore to net onshore X=-1525 and X=-2000mm, (**figure 8.16(a)** and **(c)**). Offshore winds appeared to increase the offshore drift of particles near the surface, except in **figure 8.15(c)**.

Near bed drift velocities for the spilling waves were not significantly affected, but generally tended to be lower than the zero wind drift velocities. This occurred irrespective of wind direction.

8.2 WATER PARTICLE VELOCITY MEASUREMENTS

These measurements were made at X=-1755mm in the onshore configuration only. **Figures 8.17** and **8.18** show the effect of the onshore wind on water velocity at three probe heights above the bed; 10, 30 and 50mm. **Figure 8.19** shows the wind effect on the average wave profile at this point for both the spilling and plunging waves. Results have been phase-averaged to show the average wind effect over one complete wave period. For all three figures the 'time' axis corresponds to the same phase of the respective wave, which allows direct comparison of water velocity and wave height at any point over the wave period. Clarity prevents the results being included on one graph.

The lack of suitable calibration facilities means that the water velocity is presented as voltage, however the lineariser on the anemometer meant that the voltage output was directly proportional to the water velocity at any time. It should however be remembered that the velocity is the absolute velocity of the water, which is equivalent to the square root of the sum of the squares of the horizontal and vertical components.

Figure 8.17 shows the onshore wind effect on the water velocity within the spilling wave. Minimum velocity corresponds to the two points on either side of the ellipsoid locus. Near the bed, **figure 8.17(c)**, the particles were momentarily stationary at this point as indicated by zero velocity. Higher up, where the locus is more circular, the particles did not become stationary, but a minimum velocity was experienced nonetheless. The central peak, approximately between t=0.2 and 0.45 seconds corresponds to the uprush phase, elsewhere the particles were in the backwash phase.

Distinct differences were observed between the zero wind and onshore wind results. At 10 and 30mm above the bed **figures 8.17 (b)** and **(c)** show changes to the uprush phase as well as the backwash phase. The areas under the 'uprush' and 'backwash' curves, which are proportional to the total arc distance travelled by the water particles, were reduced. This corresponded to the uprush amplitudes presented in **figure 8.8(b)**, where in the lower heights uprush amplitudes were generally lower with the wind running.

At 50mm above the bed, the difference between *wind* and *no wind* uprush is minimal. Again this corresponded to the results for uprush amplitude shown in **figure 8.8(b)**, where differences between the *wind* and *no wind* conditions decreased with increasing height above the bed. However significant differences in the backwash are apparent at 50mm above the bed. This was not reflected in the backwash amplitudes on **figure 8.12(b)**, where no wind effects can be seen.

Figure 8.18 shows the wind effect on water velocity for the plunging wave. At probe heights of 10 and 30mm above the bed, differences between the two wind conditions were small. At 50mm above the bed, uprush velocities are shown to be slightly smaller, while backwash velocities have increased. Again this corresponds to the observations made in section 8.1. Backwash velocities under onshore winds were observed to increase, and uprush velocities were

generally unaffected. The only source of discrepancy is the lack of wind effect on backwash amplitudes at 10 and 30mm above the bed. The particle path results, **figure 8.10(b)**, indicate that wind effects should be present.

Figure 8.19(a) shows the effect of the onshore wind on the phase-averaged wave profile at X=-1755mm for the spilling wave. A distinct increase in wave height was observed, from 0.038 mm to 0.046mm effectively increasing the wave steepness. Onshore wind effects on the plunging wave profile, figure **8.19(b)**, were small however. Changes to the crest height above the SWL were almost non-existent, while only minor changes to the overall wave height were observed. The wave heights for *no wind* and *onshore wind* were 0.043mm and 0.046mm respectively. The overall change in wave height coming from the slightly lower trough height under the onshore wind. Again this would cause an increase in wave steepness.

Overall the results for water particle velocities, while not being quantative in themselves, show that the wind effects observed in the particle path study are real and therefore support the stated hypothesis. Wave heights offshore of the point of breaking are shown to be affected by the wind, significantly in the case of the spilling wave. The method of data aquisition is more reliable than the methods used in section 8.1, even when the lack of calibration is considered. Errors are similar to those obtained from regular hot-film measurements (section 3.4.1.4).

8.3 SUMMARY

This section contains a summary of the results from section 8.1 and 8.2, with reference to the earlier stated hypothesis. It should be noted however that it is difficult to make generalisations as to the effect of the wind on the waves. Therefore this section will simply summerise the main points and areas where wind has been shown to be a factor in the particle motions.

In all cases the 'best' results were obtained at X=-1755mm. At X=-1525mm the results in section 8.1 showed significant amounts of scatter which will have affected the particle drift results in section 8.1.2. At X=-2000mm the effects of the wind were small and this was reflected in the K-S values of table 8.1. As previously mentioned, the low scatter in the other results indicates that scatter

at this point was not a result of experimental error, but was a function of the turbulence generated by the waves. Silvester (1974b) gives a method for determining if the drift boundary layer formed by the waves is laminar or turbulent. This depends on relatively few parameters, and showed that at X=-1755mm the flow is turbulent. This has implications in that the drift may well have some fluctuating component adding to the difficulties in accurate measurement of the mean drift. Certainly the results in section 8.1.1 show some indication of variation in particle amplitudes (for example **figure 8.10(a)**). The scatter in the results at X=-1525mm was therefore almost certainly a result of turbulence.

A clear distinction between the spilling and plunging waves appeared. For plunging waves the backwash phase was affected by the wind, whilst for spilling waves, the uprush phase showed wind effects.

Overall the results suggest wind effects on the water motions. The effects of the wind were clearest when the particle motion was broken down into uprush, backwash and vertical amplitudes, and these results confirm the earlier stated hypothesis. By comparison the results for drift velocity are less conclusive, they indicate wind effects near the surface and bed, but do not show clear trends.

These results were probably due largely to the method of obtaining data. The changes in drift velocity due to the wind in the lower height levels were likely to be small and the methods used may not have been accurate enough to reflect these changes. In the upper height regions wind effects appeared more consistently in deeper water, however problems occured in that the particles near the surface were the most difficult to follow due to the large amplitudes of motion and higher velocities.

The following four sections note the main effects of the wind for both wave types and both wind directions.

8.3.1 Offshore Wind, Spilling Wave

For the spilling waves under the offshore wind results for vertical amplitude and backwash amplitude showed no wind effects on the data. Results for uprush showed clear wind effects on the data at X=-1755mm, with uprush amplitude reduced by the action of the wind. Some wind effects were observed

at X=-1525mm but at X=-2000mm wind induced changes were small. This was reflected in the drift velocity results, where the biggest wind effects were observed at X=-1755mm. At this point the drift near the surface is lower, (which corresponds to the reduced uprush). Near surface drift is also reduced by the wind at X=-1525mm.

8.3.2 Offshore Wind, Plunging Wave

In this case the wind effects were observed in the backwash amplitude, with vertical and uprush amplitudes unaffected. Backwash amplitude at X=-1525 and 1755mm was clearly increased by the wind. Results for the drift velocity, showed little wind effects except at X=-1755mm, where changes were observed both near the surface and bed. The wind affected drift is more 'offshore', especially near the surface where a change in the direction of drift was observed.

8.3.3 Onshore Wind, Spilling Wave

This showed similar results to the spilling wave in the offshore case, with the uprush amplitudes showing the effects of the wind. Vertical and backwash amplitudes appear to be little affected. At all three measurement points uprush is seen to reduce due to the wind, although the changes are only significant at X=-1525mm. Thus the onshore wind appears to have the same effect as the offshore wind on uprush, section 8.3.1. Near surface drift at X=-1755 and 2000mm is increased in the onshore direction. At X=-1525mm the wind has increased offshore drift at all levels, although there is some evidence that the near surface drift would be increased in the onshore direction.

The water velocity measurements of section 8.2 show wind effects at X=-1755mm at heights of 10, 30, and 50mm above the bed, although the biggest difference is observed at 50mm above the bed. The result at 50mm above the bed indicates that uprush is unaffected, but that backwash is reduced by the wind.

8.3.4 Onshore Wind, Plunging Wave

Results show reductions in backwash due to the onshore wind at all three measurement locations. At X=-1525mm scatter in the wind affected backwash data is noticably greater than for the no wind data. The reductions in backwash amplitude show in the drift velocity results as the wind affected data generally shows lower drift velocities than the no wind data. Near the surface there is no

real evidence of wind effects, but near the bed wind affected drift is greater (more onshore) at all locations.

At X=-1755mm the water velocity results indicate little wind effect at 10 and 30mm above the bed. At 50mm above the bed uprush appears to be reduced, backwash increased by the wind, contrary to the results from section 8.1.

CHAPTER 9

DISCUSSION

9.1 AIR FLOW OVER THE WAVES

This section discusses the results from chapter 6, for the air flow over the waves.

Mean velocity profiles for offshore winds indicate the large drag on the air flow due to the breaking waves. For onshore winds the drag is much lower. For the offshore configuration, changes to the wind profile downwind of the breakers indicate that the drag due to the breakers is significantly larger than that due to the same waves in deeper water. This was expected from previous research into wind-waves, (Banner (1990), Wu (1968)). For the onshore configuration, differences in surface drag over the tank were much less marked.

The aerodynamic quality of the surface can be determined from the roughness Reynolds number, Donelan (1982), which is classified as either *smooth* or *rough*. Smooth implies that the tangential stress is transmitted to the surface entirely by the action of molecular viscosity, rough flow occurs if the transfer is dominated by form drag on the roughness elements themselves. The roughness Reynolds number is given by:

$$\text{roughness Reynolds number} = R_* = \frac{u_* z_o}{\nu} \qquad (9.1)$$

Calculating the values of R_* from the single-film results in section 6.1 gives the results shown in table 9.1; where the positions (i) to (v) are as shown earlier in table 4.1. The value of dynamic viscosity, ν, is taken as 1.15×10^{-5} m^2/s. Aerodynamically rough flow occurs for values of R_* above about 2.0, (Donelan (1982)).

The results in table 9.1 show that at all measurement locations over the waves, the flow is aerodynamically rough. Distinct differences between both the

onshore and offshore wind conditions and the two waves types are however apparent. At the point of breaking, (position (iii)), large differences between the onshore and offshore winds are apparent. The difference is most marked for the plunging wave. Overall the results indicate that the transfer of tangential stress to the surface is dominated by form drag on the waves.

Position		(i)	(ii)	(iii)	(iv)	(v)
Plunging	Offshore	-	44	1807	7292	580
	Onshore	0.3	78	33	303	-
Spilling	Offshore	-	332	663	6699	90
	Onshore	1.0	1245	541	1457	-

Table 9.1. Roughness Reynolds number values for the surf zone.

Two possible explanations exist for the observed differences between offshore and onshore wind results presented in chapter 6 and table 9.1. Firstly, there is the differing wind speed relative to the wave speed. At the point of breaking the relative wind speed for the offshore winds is approximately twice that for the onshore conditions. This fact alone is likely to be responsible for significant discrepancies.

A second factor is the asymmetry of the waves as they approach breaking and also once they have broken. Plunging waves show a significantly steeper front face as the wave nears the break point. Once the waves have broken forming a bore, the front of the waves is a mass of highly turbulent water while the rear face is still relatively smooth. Thus for offshore winds, the air flow is incident on the steep turbulent face of the wave bore. Under onshore winds, the air flow follows a much smoother surface. This may have significant consequences in terms of the air flow separation from the wave crests and in offshore winds early separation of the air flow from the wave would be 'encouraged' by the steep turbulent face of the bore. This is illustrated schematically in **figure 9.1**.

Air flow separation is usually accompanied by increased turbulence intensities downstream of the separation point. Turbulence intensity profiles in section 6.2 show large values of both I_u and I_v occurring over and downwind of the point of breaking. However, these values cannot be taken as an indication of

separation, since the phase-averaged results from section 6.5 indicate large variations in mean velocity over the waves. The phase-averaged results for I_u provide a better indication of turbulence due to air flow separation. These results indicated for offshore winds large increases in $<I_u>$ in the lee of the waves at breaking occured at heights below about 85mm above the SWL. Some corresponding increases were observed in the onshore configuration, however they were less significant and generally turbulence intensities were lower than in the offshore configuration (although this may reflect the overall lower turbulence intensity in the simulated boundary layer). For both wind directions, the results over the waves prior to breaking (approximately 300mm offshore of this point), showed no wave-coherent increses in $<I_u>$, (although significant changes in <U> were still apparent).

The low overall values of $<I_u>$ were felt to be due to the small size of sampling sections used, which each span 0.04 seconds (10 data points sampled at 250Hz). As the mean velocity from which the fluctuations are measured is calculated for each section, fluctuations below 25Hz may be included with the mean. Assuming that fluctuations below about 1Hz (the wave frequency) are bona fide changes in the mean velocity, then there potentially exists a 'missing' band of turbulent fluctuations between 1 and 25Hz. Frequency spectra in section 6.3 show large amounts of energy contained within this region. There therefore exists the possibiltity that the results do not indicate the complete effect of the waves on the turbulent intensities. In retrospect a better method would have been to calculate the turbulent fluctuations from the phase-averaged mean velocity profile.

The phase-averaged mean velocity results showed large variations in <U> over the waves and distinct differences were again apparent between the offshore and onshore winds. The largest differences between maximum and minimum <U> values occured for offshore winds over the point of breaking. For onshore winds this ratio changed little over the measurement region. These fluctuations in <U> are responsible for the large I_u and I_v measurements in section 6.2. They also account for the peaks present in the frequency spectra presented in section 6.3, and therefore spectra indicate variations in <U> exist higher over the waves than measured during the phase-averaged testing. Krugermayer et al (1978) noted that for wind-waves the wind profile is distorted up to about three wave heights above the water surface. From these results spectra indicate that over the point of breaking wave-frequency peaks

are still in evidence at heights of up to $6H_b$. The wave-frequency peaks in the spectra are present over the waves in deeper water for both the offshore and onshore wind directions, although they do not appear as high above the SWL as at the point of breaking.

Phillips (1969) shows that the wave-induced streamline distortions comprise an additional shear stress which decreases with increasing height, refering to this stress as a wave-induced Reynolds stress. The Reynolds stress profiles of section 6.4 therefore include this stress in the results. This would explain the non-vertical profile, since the largest values of <uv> are recorded in the lower heights. Profiles over the flat water indicate near vertical profiles. Attempts at obtaining phase-averaged <uv> plots were not made because of the large amounts of data that would be required.

The results indicate the problems of defining what are "mean" velocities and what are "turbulent" or "wave-induced" fluctuations. This problem is further complicated by the limitations of the hot-film probes discussed in section 3.4.1.4. The large V-component fluctuations, caused mainly by distortion of the air flow by the waves, leads to errors in the measurement of U and I_u for the single-film probe and to also to accuracy problems for the X-film probe. This problem should be borne in mind for any further work in this area.

The measurement of the air flow over the waves poses several problems, some arising as a result of the hot-film system. The combined effects of wind, water and a fluctuating water surface throw up several problems of which a major one is the correct resolution of the U and V-components of velocity. A further point is that measurement of the air flow beneath the level of the wave crests was not possible with the probes available. This limitation meant that information about the air flow in a critical region was lacking. From the literature ruggedized hot-wires have been used successfully where they were exposed to periodic submersion, (Wills (1980)), although certain precautions were necessary to prevent the wire from burning out. Recent developments in Laser Doppler Anemometry and Particle Image Velocimetry mean that non-intrusive simultaneous analysis of air flow, wave heights and even the particle motions beneath the waves are feasable. Kawai (1981 & 1982) used simple PIV techniques to examine the structure of air flow separation from wave crests. A fibre-optic LDV system was used by Nadaoka et al (1988) to examine sediment suspension due to eddies from surf zone waves.

The non-dimensional frequency spectra presented in chapter 6 show distinct wave effects on the wind, with significant increases in energy at the frequency of the waves. However the scaling mis-match as noted in section 4.8 means that a discrepancy between these results and full scale measurements is likely. Model scale spectra show increases in energy due to the waves at, or very close, to the spectral peak, but otherwise the spectra appear to be unchanged from the typical von Karman spectrum. The value of turbulent lengthscale, ${}^{x}L_{u}$, also appears to be unchanged between the spectra for flat water and over the waves.

At full-scale the waves would provide additional energy at frequencies significantly higher than the spectral peak (as shown in **figure 4.5**). Effectively this reduces the *proportion* of energy associated with the spectral peak, creating a new 'peak' at a higher frequency. Thus fitting the von Karman spectrum to the resulting spectra may lead to a smaller value of lengthscale than over flat water.

A further point concerns the way in which the waves affect the wind. If the wave-induced spectral peaks were the result of vortex shedding then one could expect the wave-induced turbulence to also affect the higher frequencies as the fluctuations decay. However, the phase-averaged results from section 6.5 indicate that the peaks are due to fluctuations in mean velocity over the wave and, except close to the surface, turbulence intensity changes little over the wave period. Thus one could expect that little energy from the wave-induced peak will be transferred to the higher fequencies, and therefore the overall shape of the spectrum will be relatively unaffected.

9.2 Influence Of The Wind On The Waves

The results show clear wind effects on the breaking waves. All aspects of the waves considered were affected with the exception of breaker height, H_b. The general trends that arise can be simply summarised; offshore winds delay the moment of breaking (decreasing breaker depth, d_b, and surf zone width, X_s, and increasing H_b/d_b) and cause a tendency to break by plunging. Onshore winds promote earlier breaking of the waves by spilling, increasing the surf

zone width, and d_b, and decreasing H_b/d_b. The results showed good agreement with those of Douglass (1989).

9.2.1 Mechanism Of The Winds' Influence On The Waves

This poses the question of how the wind is affecting the waves. If the energy of the waves is considered, and assuming that breaking for a given wave is dependent on the energy associated with the wave, it is reasonable to suppose that adding to a wave's energy would lead to earlier breaking of the wave. Conversely decreasing the wave energy would allow the wave to continue into the shallower water before breaking. For waves of a given period, wave energy is a function of wave height, H, and therefore any changes to H will affect the breaking of the wave.

The wind's effect on the waves may therefore originate offshore in deeper water, where changes to the wave height are small but become significant close to breaking. Wind-wave theory indicates that the incoming wave amplitudes would be damped, (either by form drag or the effects of the wind drift layer), by an offshore wind, eventually to be replaced by wind-waves travelling in the opposite (offshore) direction. Similarly onshore winds would lead to increased wave heights.

However Douglass' (1989) data for the shoaling of his three experimental waves shows that the effects of the wind are confined to the shallower water. For his Wave P no significant changes to shoaling wave heights were observed. For Waves S and I shoaling wave heights were affected, but only as d/L_o reached a value of 0.035. This is not far offshore of the point of breaking, (at X=-1755mm values of d/L_o are 0.04 and 0.07 for plunging and spilling waves respectively). However **Figure 8.19** shows (onshore) wind effects on wave height at this point, which contrasts with the results of Douglass. A corresponding measurement for the offshore winds was not made however, making further comment difficult. Although due to the relatively short length of the wave tank used for these experiments, the observed changes in wave breaking must be the result of wind affecting the waves reasonably close to the point of breaking.

Given the instability of waves approaching the point of breaking, it is possible that small changes or perturbations may encourage or delay the breaking process. Douglass (1989) hypothesised that wind shear was the main agent of

the winds' influence on the waves. He noted that the formation and subsequent breaking of micro-breakers at the wave crest under onshore winds added sufficient impetus to the underlying wave to cause early breaking. This is analogous to the growth of wind waves by the breaking of smaller waves riding at the crest, (Silvester (1974a)). Results here provide an indication that this may be correct, however there is also evidence to support form drag on the waves as the mechanism of the winds influence.

The large distortions to the mean streamlines caused by the waves indicates that there will be pressure differentials affecting the waves. Also the increases in phase-averaged I_u in the lee of the waves provides an indication of air flow separation, which requires the presence of an adverse pressure gradient. Work on a qualitatively similar curved hill, (Baskaran et al (1987)), suggests that this pressure gradient would act favourably upwind of the wave crest and adversely in the lee of the crest, with a low pressure region over the wave itself. This low pressure region over the crest could be expected to promote an increase in wave height. The results in section 8.2, where for onshore winds the wave profile was measured offshore of the point of breaking, showed a distinct increase in wave height for the spilling wave. Although the plunging wave height did increase it was by a much smaller amount. It is unfortunate that it was not possible to obtain directly comparable results for offshore winds.

A similar result for the offshore winds could be expected, however the differing wind-wave speed ratio may be significant in determining where the low pressure region acts. Shemdin & Hsu (1967) measured aerodynamic pressure over simple progressive gravity waves and reported distinct phase-changes with increasing wind speed relative to wave speed. That is at different wind-wave speed ratios the position of the low pressure region over the wave crest changed. It was also noted that the role of tangential stress in the transfer of energy from the wind the waves appeared to be of secondary importance. This further points towards changes in form drag as the mechanism responsible for the winds' effect on the waves.

However, the presence of the waves also has the effect of increasing mean wind velocities at the wave crest. Crest mean velocities are shown to be significantly larger than those over the trough regions. At the point of breaking (at approximately 45mm above SWL) crest values of <U> are larger than the general trough values by a factor of about 3 in offshore winds and 1.3 in

onshore winds. Since the trough values tend to be closer to the overall mean value of velocity, then these increases in <U> at the crest represent values of surface shear roughly 9 and 1.7 times larger than those indicated by the mean velocity profiles.

In offshore winds the shear at the crest will retard the orbital motions of the particles near the surface, reducing the orbital momentum of the wave. In onshore winds the shear acts to increase the motions of the particles at the wave crest, adding to the waves overall momentum. This is tied with the formation of the wind drift layer and results from the particle path study show some evidence for the influence of the wind drift layer on the particle paths. Thus offshore winds effectively dampen the incoming waves via the wind drift layer, allowing them to progress further shoreward before breaking, and onshore winds provide a supply of momentum to the waves.

From the particle path study, the wind-induced surface drift was measured at ±10 to 20mm/s, although this value is almost certainly an under-estimate since it was increasingly difficult to measure particles close to the surface. A drift of 20mm/s represents roughly 1% of the reference height velocity U_{ref}.

By placing punch-outs from hole-punches on the water surface Douglass (1989) observed drift velocities of 3% of the wind speed for the wind blowing over flat water. Similar values were obtained by Wu (1968). This suggests that assuming drift with the waves running is similar to that in the flat water case, drift velocities at the surface should be around 48mm/s (assuming U_{ref}=1.6m/s). This drift velocity is larger than any recorded in section 8.1.2 at any height above the bed. The superposition of such a drift on the water surface would certainly have some effect nearer the bed simply from consideration of the continuity law.

Douglass (1989) made some attempts at measuring surface drift with the waves running. For an offshore wind and using the paper punch-outs placed close to the point of breaking, some were caught by the breaking wave but others moved offshore riding the wave crests. Despite this Douglass quoted no figures for drift with the waves running.

It is difficult to separate the effects due to form drag and wind shear as the wave approaches the point of breaking. One possibility is that the mechanism

for offshore winds is different to that in onshore winds as a result of the differing wind-wave speed ratio and the asymmetry of the waves themselves. Certainly drag in the offshore case was significantly larger than for onshore winds. However this was also the case with wind shear at the wave crests as a result of the large <U> values. Wind-wave theory, (Silvester (1974a)), attributes wave growth to form drag on the larger components. This suggests a complimentary mechanism, whereby form drag provides the initial change in wave height, with surface shear only becoming important in the final stages of breaking. At this point where the wave is unstable, small changes, such as to the wind drift layer, or the formation of micro-breakers may provide significant controls on the moment of breaking. In this respect determination of the point at which separation and reattachment of the air flow occurs is important.

The formation of a wind drift layer will have other effects on the nearshore region, since a net drift at the surface in either direction must be balanced by a corresponding net movement of particles lower down. The net drift and water velocity plots in chapter 8 certainly show wind effects on the wave motion beneath the surface. However, scatter and problems in measuring particles actually within the wind drift layer means that firm conclusions on the effect of the wind below the water surface are not possible.

9.2.2 General Discussion On The Experiment And Techniques

Whatever the mechanism by which the wind affects the waves, distinct trends are observed. These have been summarised above. Scatter of the data points for the wave characteristics is fairly large, although this did not prevent the trends from being apparent. Most of this scatter can be accounted for by errors present in the measuring techniques (section 4.4.5). The good agreement between these results and those of Douglass (1989) lends credence to the notion that the errors and small scale of the model waves has not significantly affected results.

However the effects of scale are apparent elsewhere. The failure of the breaker parameters to correctly account for breaker type is noted in section 7.2, and it is felt that scale effects have influenced these results. If the results are limited to waves within certain limits, excluding those waves larger or smaller, then the grouping of the waves according to the breaker parameters is improved. As a result of these apparent scale effects it is not possible to comment further on the performance of the surf similarity parameter. Despite this the effects of the

wind on the breaker type were clear, offshore winds enhanced plunging waves and onshore winds caused a tendency to break by spilling. The main problem in determining breaker type, other than the small size of the breakers, was due to the subjectivity involved.

The micro-breakers observed by Douglass (1989 & 1990), were observed at the wave crests for both wind directions. However, the detailed observation of Douglass that the breaking of a micro-breaker was the catalyst for breaking of the underlying wave was not verified. The generation of these waves, is an aspect of the model that suffers from the effects of scale. At the model scale, capillary waves which are insignificant at full scale, become proportionally much larger. For modelling similarity similarly proportioned waves must also be present at full scale.

However, even when these uncertainties are considered, for engineering purposes the most important results are the effect on breaker type, surf zone width and amplitude-to-depth ratio, and the results for these parameters are clear.

Despite the fact that wind effects were observed, the results from chapter 8, for the particle path analysis, were disappointing in that no real conclusions could be made. There are however several points which are worth noting.

Firstly, although the scatter of the data for the amplitudes of motion was relatively small, it was large with respect to the actual drift of the particles per wave period. The experimental error, (which from the low scatter appears to be small), was also significant in relation to the actual drift. Certainly the estimate of error for particle amplitude made in section 4.6.3 was often larger than the obtained values of drift per wave period.

Definite wind effects were observed in the 'raw' data for particle amplitude, and these observations were verified by the K-S significance test. However there were some curious results, for example, uprush for the spilling wave at X=-1525mm, where the effect of the offshore and onshore winds appears to be the same. The reason for this is not known.

The results for the drift velocity, derived from the uprush and backwash amplitudes, were poor compared to the results from which they were derived.

This was most probably due to the scatter in the measurements of uprush and backwash amplitude. Although there was evidence for significant wind effects near the water surface, and to a lesser extent near the bed, general trends were not apparent. Unfortunately, the measurement of the particles near the surface proved to be the most difficult. Problems were experienced in simply videoing the motion, in addition to the tracing of the particles (from the TV) which had larger amplitudes and velocities than those lower down.

The water velocity measurements of section 8.2 certainly improved on accuracy and ease of measurement, however they were limited by the inability to perform a calibration for the probe and to resolve the horizontal and vertical components of the motion. Nevetheless where the measurements were carried out, distinct changes to the flow past the probe were recorded as a result of the wind. These results agreed with those of the particle path study to some extent but discrepancies were also apparent. These may have resulted from the fact that the particle path study measured the locii of the particles, while the conical probe measured the velocity of the water past the sensor tip. Also there was the problem that the components of the flow could not be separated and so it was not possible to obtain an estimate of drift from these results. Some discrepancy between the two sets of results was therefore to be expected.

9.3 IMPLICATIONS OF RESULTS

The main applications of this research have been discussed in the first chapter. This section examines the implications of the research findings for the prototype conditions.

9.3.1 Sediment Transport

Previous research has identified several factors governing the suspension of sediment in the surf zone. Surf zone width, breaker type and amplitude-to-depth ratio have all been shown to be significant, (Kana (1979), Jiabao (1989), Galloway et al (1988)).

Sediment transport is either longshore or cross-shore, with cross-shore movement of sediment giving rise to the 'swell' and 'storm' built beach profiles frequently referred to in the literature, (Silvester (1974a)). No measurements of particle drift velocities were possible in the surf zone, but results obtained

outside the surf zone indicate wind effects. Longshore currents arise because waves are incident to the shore at some angle other than perpendicular. This sets up a current within the surf zone which is frequently responsible for the transport of large quantities of sediment along the coast, for example the stretch of coastline to the north of Spurn Point in Humberside. Determination of the wind effect on longshore sediment transport was outside the scope of this experiment as only 2-D effects were considered.

Although conclusions from the direct measurement of the wind's effect on the particle paths and water motion cannot be made, the results from chapter 7 are significant. Several equations concerning the longshore current and sediment transport are available in the literature. Douglass (1989) presents Longuet-Higgins equations for the longshore current velocity and longshore volume rate of water transport. The longshore current velocity is shown to be a function of breaker height, H_b. Thus, wind does not significantly affect this parameter. However the volume rate of water transported in the surf zone in the longshore direction is a function of the product of H_b and d_b. Therefore changes to the volume of water transported will be proportional to the change in breaker depth due to wind. This assumes that the effect of an offshore or onshore wind is the same for waves approaching at some angle to the shore. In addition to this, the wind may not be directly shore-normal, so that both wind and waves approach at an angle to the shore. As only shore-normal wind and waves have been considered in this research the extrapolation of these results for wind and wave conditions other than shore-normal should be considered as providing only an indication of possible wind effects.

The main interest is the movement of sediment, usually sand or silt, within this region. The CERC equation (US Army (1984)) gives the longshore sand transport rate as proportional to the longshore energy flux factor, P_{LS}, (equation 9.2).

$$P_{LS} = \frac{\rho_w g}{8} H_b^2 C_b \sin\theta_b \cos\theta_b \qquad (9.2)$$

where C_b = wave celerity at breaking and θ_b = angle between the wave crest and the shoreline. By approximating the wave celerity at breaking by equation 6.1, equation 9.2 can be re-written as;

$$P_{LS} = \frac{\rho_w g^{1.5}}{8} H_b^2 d_b^{0.5} \sin\theta_b \cos\theta_b \qquad (9.3)$$

Thus the longshore sand transport rate is proportional to the product of H_b^2 and $(d_b)^{0.5}$. Typical results from this research, would therefore suggest that the longshore sand transport rate in moderate offshore winds is between 3 and 5% lower than in zero wind. In onshore winds the effect on transport is a similar increase in sediment transport. This assumes that the wind effect on the waves is similar for waves at some angle to the shore (as opposed to parallel with it). It should be noted however that none of these equations account for the change in breaker type also seen to occur. Increased levels of suspended sediment resulting from a change in breaker type from spilling to plunging will almost certainly have an effect on sediment transport. Similarly the equation takes no account of the effect of the wind drift layer on nearshore currents or circulation.

Cross-shore sediment transport is primarily dependent on the characteristics of the incoming wave train and the beach slope. This will also determine the breaker type of the incoming wave. The results of the particle path study in chapter 8 show wind effects on the motion and drift of particles offshore of the surf zone.

9.3.2 Wave Forces On Coastal Structures

Wave forces on surf zone structures such as piers, seawalls, or revetments would also be affected by changes in wave geometry due to the wind. The factors affecting wave forces on these structures are discussed in section 1.4.

The limiting amplitude-to-depth ratio, equation 1.1, is noted as a design criteria. For moderate offshore wind speeds increases in this ratio were of the order of 10-20%. This is equivalent either to larger values of H_b occurring at the same value of d_b or to the same H_b in shallower water. In either case the effect on loading can be significant. For onshore winds amplitude-to-depth ratio tended to decrease by around 10%. Wave forces are generally proportional to wave height squared, and the recorded changes in H_b/d_b mean that for the same water depth in front of the structure, waves which would otherwise have already broken, will be breaking on the structure. The presence of an offshore wind may therefore increase the maximum value of H_b incident on the structure by around 20%.

The effects of breaker type are more difficult to quantify. The highest pressures (and therefore forces) are developed on a structure when the wave is stopped abruptly by the structure, (Silvester (1974a)). Highest pressures are therefore developed by plunging waves when the incident front face is vertical. Occasionally extremely high intensity, short duration pressures are developed when a thin 'lens' of air is trapped between the wave face and the structure, (Sorensen (1978)).

The breaking of waves by spilling is far less explosive, and even if incident on a structure at the moment of breaking, their geometry dictates that the wave is not stopped abruptly. Thus spilling waves present a far less significant threat to surf zone structures than plunging waves do. Hence onshore winds are beneficial in that waves may be caused to break by spilling further offshore. Overall the effects of the wind on breaker type may be more significant in terms of the forces developed, than the effect on the wave height (via the amplitude-to-depth ratio).

Few design methods incorporate wave type as a variable, and generalised quantitative details of the difference between spilling and plunging waves in terms of wave forces could not be found in the literature. In designing seawalls, Thomas & Hall (1992) acknowledge the dependency of hydrodynamic loading on breaker type and refer to the surf similarity parameter (or Iribarren number as they call it) as a tool for determining breaker type. The results from this investigation indicate that the prevailing wind may significantly affect prediction of breaker type by this parameter. Chadwick & Morfett (1986) note that preliminary design of such breakwaters may be based on the Hudson formula. This expresses the required weight of the armour unit as proportional to the design wave height cubed. Hence changes to the value of design wave height may result in significant changes being required for the armour units.

For waves breaking on a sloping surface, forces due to plunging waves are localised in the region of plunging, (the plunge point). Wind induced changes to the plunge point may significantly affect wave forces due to the changed water depth into which the lip plunges (since H_b is unaffected). Again breaker type is extremely significant, since such forces due to spilling waves are almost non-existent as no plunging overhang is formed.

Cylindrical members are frequently used for maritime structures, although in the surf zone their use is generally restricted to supports/foundations for piers or jetties. Forces on these members due to the waves are comprised of drag, inertial and impact forces. Silvester (1974a) notes that overall forces on slender cylinders are 2 to 4 times higher for breaking waves than from equally sized non-breaking progressive waves. He presents Halls' equation which gives overall force to be proportional to H_b^2. This implies the significance of breaker location. Although breaker type is not considered, the effects are probably similar to those noted generally above. Reddish & Basco (1987) considered the effects of breaker type on slender piles, finding that the highest forces are developed by plunging waves.

9.3.3 Wind Forces On Coastal Structures

The final area of potential application to the prototype conditions is the air flow over the waves. Results show that significant deviations to the mean streamlines occur which in turn set up wave-frequency fluctuations about the mean. These are shown to occur in both vertical and horizontal planes to several wave heights above the water. The question is, will they be significant for structures and/or boats in the affected area. For offshore winds, the main influence of the waves on the wind occurs near the point of breaking and downwind of it. This effectively limits the type of structure occuring to piers or jetties. For onshore winds spectra showed that wave-induced fluctuations were still present at the shore. Potentially therefore all structures near the surf zone may be subject to wind fluctuations at the wave frequencies.

For a 1 second wave period at model scale, the equivalent full scale wave period is 7 seconds, which equates to a frequency of 0.14Hz. The effect of strong velocity fluctuations at this frequency are considered.

As structures respond dynamically only to periodic loads at the same frequency as their own natural frequency, the vibration of a particular structure is caused by a small part of the total wind turbulence, (MacDonald (1975)). From the literature, buildings generally have natural frequencies of 5-10Hz, much higher than the wave-induced fluctuations observed here. Although the combined effects of weight and slenderness means that some tall blocks have low natural frequencies in the range 0.1 to 1Hz, (Sachs (1978)). Other structures which will have natural frequencies of around 0.14Hz include masts and lattice

towers. The author has not been able to locate in the literature details of the dynamic response of piers or jetties to the wind.

An immediate extension of these findings is in the combined effects of wind and wave loading. Again this will limit the type of structures to piers, jetties and seawalls, although wind effects on seawalls are likely to be negligible in comparison to the design wave loads.

DAMAGED TEXT IN ORIGINAL

CHAPTER 10

CONCLUSIONS AND SUGGESTIONS FOR FURTHER WORK

10.1 CONCLUSIONS

The wind is shown to be a significant factor in the breaking of the waves at the shore. Both the breaker type and the point of breaking are affected by the wind. Offshore winds shift the breaker type seawards, decreasing the breaker depth, d_b, and the surf zone width. Onshore winds shift the point of wave breaking seawards (offshore), increasing the surf zone width. The magnitude of the observed changes is similar for both wind directions. For the breaker type, offshore winds promote spilling towards plunging waves, and onshore winds towards wave breaking.

Breaker height, H_b, is shown to be unaffected by the action of the wind. However, the amplitude-to-depth ratio is shown to be affected by the wind. Offshore winds increase the ratio, onshore winds decrease the ratio. The change in H_b/d_b is a result of change in d_b since H_b is relatively unaffected.

There is good agreement between the Douglass (1989 & 1990) and those obtained from this research. The changes to surf zone width, breaker height and amplitude-to-depth show very similar trends.

The surf zone is shown to exert a drag on the air flow over the waves. Differences between onshore and offshore winds are significant, with offshore winds showing the greatest levels of drag. Calculation of the roughness Reynolds number indicates that the drag arises from the form drag on the waves and not tangential stress. Thus the drag on the air flow changes over the width of the surf zone. For offshore winds the largest drag is recorded over the point of breaking, and the drag due to waves near the point of breaking is significantly larger than the drag over waves in deeper water. Under

onshore winds the drag on the air flow changes less significantly, although the largest drag still occurs in the region of the break point.

Differences between the air flow over spilling and plunging waves were small compared to the differences between offshore and onshore winds. The difference between onshore and offshore winds was attributed to two factors:

i) the differing wind speed relative to the wave speed

ii) the asymmetry of the waves at and after breaking

Differences to the air flow between the two wave types are a result of the differing geometries of the waves, i.e. steepness and form at breaking.

Phase-averaged measurements of velocity show large variations in the mean velocity over a wave period. Peak values of velocity were recorded near the wave crests. Offshore winds showed the largest variations in velocity over the wave, with peak velocities over 100% larger than those near the trough. In onshore winds the differences in velocity over the wave were smaller.

Peaks in the frequency spectra over the waves were attributed to the variations in mean velocity over the waves. Spectra showed that the waves influence the wind up to 5 or 6 wave heights above the water surface at the point of breaking. Under onshore winds wave-frequency peaks were observed in the frequency spectra at the shore, indicating that the structure of the wind at the shore is affected by the breaking waves.

Evidence exists to suggest that both surface shear and form drag are responsible for the wind's influence on the waves. The large values of velocity recorded at the wave crests indicate correspondingly large values of surface shear in this region. This may have resulted in the micro-breakers or capillary waves which were observed on the waves for both offshore and onshore winds. These were noted by Douglass (1989) as a possible mechanism of the winds' influence on the waves. However, due to the small scale of the waves it was not possible to tell if they were resposible for the early breaking of the waves under onshore winds.

Recorded values of non-phase-averaged turbulence intensity over the waves show extremely large values, up to 0.5. These are shown to be a result of the wave-induced variation in mean velocity over the wave period. Phase-

averaged turbulence intensity shows evidence of air flow separation in the lee of the wave crests near the point of breaking.

The waves were not successfully grouped according to breaker type by either wave steepness or the surf similarity parameter. Some scale effects were apparent in the classification of the waves by these parameters.

A study of the paths of particles suspended in the water, reveals wind effects on the motions of the particles offshore of the surf zone, and resulting in changes to the cross-shore drift of the particles. However, the results were not clear enough to draw firm conclusions. Late in the experiment the use of a conical probe to measure orbital water velocities beneath the waves also indicated wind effects. Although these results could not be directly compared to the particle path results due to the inability of the probe to resolve the components of the water motion, it is felt that they indicate potentially significant changes to nearshore sediment transport.

10.2 SUGGESTIONS AND RECOMENDATIONS FOR FURTHER WORK

The results from this experiment and that of Douglass (1989) show that the winds' influence on the waves is significant. Several areas are apparent which it is felt require further investigation.

Further investigations into the possible wind effect on sediment transport are required. The particle path study indicates that wind effects may be significant offshore of the point of breaking, however no measurements were made inside the surf zone. Inside the surf zone, which has been shown to be significantly affected by the wind, littoral currents are set up by waves breaking at some angle to the shore. If the wind effect is similar for waves breaking in such a manner then changes to the littoral current are to be expected. Thus the wind may be a factor in both cross-shore and littoral sediment transport. This is an important aspect of nearshore dynamics, with ongoing research into the problem.

Also further examination into the influence of the wind drift layer is needed, with regard to both wave breaking and to the subsequent superimposed drift velocity on the water particles nearer the bed.

One of the major problems associated with this work, was the conflicting scaling requirements of the wind and the waves. Further investigation into the winds' effect on the waves at the scales used here is not recommended due to the difficulties in measuring and generally observing the breaking of the waves. If the correct simulation of the wind can be shown to be unimportant to the effect on the waves, then this would allow a significant improvement in the simulation of the waves. Comparison of the results from this experiment to those of Douglass (1989) shows good agreement despite the differences between the two modelling simulations. Further study into the effects of turbulence on the waves are needed to assess the problem. Although the observations of Galloway et al (1989) indicate wind effects on breaker type at full scale, it is felt that some form of near full-scale experiment should be set up, ignoring the wind scaling if necessary, in order to confirm that the observed results at model scale are repeated with larger waves.

Further it is suggested that field measurements of breaking wave heights and breaker types should also include measurements of the prevailing wind. Simple measurements of wind speed and direction would allow for comparison of breaker types under consistent wind conditions, which may account for the apparent independence of spilling waves to breaker type parameters such as the surf similarity parameter.

The results have implications for the use of the breaker type parameters, such as the surf similarity parameter. The apparent dependence of breaker type on the wind may explain the problems in correctly predicting breaker types in the field. The results strongly indicate that wind direction and strength should be accounted for when considering field investigations into breaker type.

Recent advances in the use of Laser Doppler Aemometry and Particle Image Velocimetry, (PIV), mean that information in both the air flow and water velocities can be obtained in the areas that pose problems for hot-film anemometry. Specifically this refers to the region close to the water surface where separation of the air flow and subsequent re-attachment may be fundamental to the effect of the wind on the waves. The other major problem in this region in using hot-films is the large fluctuations in the V-component of

velocity. In particular these techniques may be applied to determine the effect of the wind on the wind drift layer and on the drift of particles nearer the bed.

REFERENCES

BAGNOLD, R.A. (1939) *'Interim report on wave pressure research'* J. Inst. Civil Engineers, 12.

BANDOU, T., MITSUYASU, H., MARUBAYASH, K. & ISIBASI, M. (1988) *'The structure of turbulent air flow over a wavy wall. Part 1'* Reports Res. Inst. Applied Mechanics v.XXXIV n.103

BANNER, M.L. (1990) *'The influence of wave-breaking on the surface pressure distribution in wind-wave interactions'* J. Fluid Mech. v.211 p.463-495

BANNER, M.L. & MELVILLE, W.K. (1976) *'On the seperation of air flow over water waves'* J. Fluid Mech. v.77 p.4 p.825-842

BASKARAN, V., SMITS, A.J. & JOUBERT, P.N. (1987) *'A turbulent flow over a curved hill, part 1. Growth of an internal boundary layer'* J. Fluid Mech. v.182 p.47-83

BASKARAN, V., SMITS, A.J. & JOUBERT, P.N. (1991) *'A turbulent flow over a curved hill, part 2. Effects of streamline curvature and streamwise pressure gradient'* J. Fluid Mech. v.232 p.377-402

BATTJES, J.A. (1974) *'Surf similarity'* Proc. 14th Conf. Coastal Eng. Publ. American Soc. Civ. Eng., New York p.466-480

BEARMAN, P.W. (1971) *'Corrections for the effect of ambient temperature drift on hot-wire measurements in incompressible flow'* DISA Information, No. 11, May 1971 p.25-30

CHADWICK, A. & MORFETT, J. (1986) 'Hydraulics in civil engineering' Allen & Unwin Ltd (Publishers)

COLEMAN, S.A. (1990) *'The aerodynamics of vehicles in cross-winds'* PhD Thesis, University of Nottingham, Dept. Civil Engineering

COOK, N.J. (1973) *'On simulating the lower third of the urban adiabatic boundary layer in a wind tunnel'* In: Atmospheric Environment, Pergammon Press, v.7, p.691-705

COOK, N.J. (1978) *'Determination of the model scale factor in wind-tunnel simulations of the adiabatic atmospheric boundary layer'* J. Ind. Aerodynamics 2 (1977/1978) p.311-321

COOK, N.J. (1982) *'Simulation techniques for short test-section wind tunnels: roughness, barrier and mixing device methods'* Wind Tunnel Modelling for Civil Engineers, Ed. Reinhold, p.126-136

COOK, N.J. (1985) 'The designer's guide to wind loading of building structures. Part 1' Butterworths

DALLEY, S.J. (1993) *'Wind tunnel measurements on a low rise building and comparison with full-scale'* PhD Thesis, University of Surrey, Department of Civil Engineering

DEIGAARD, R. FREDSOE, J. & HEDEGAARD, I.B. (1986) *'Suspended sediment in the surf zone'* ACSE J. Waterway, Port, Coastal & Ocean Eng. v.112 n.2 Jan 1986

DONELAN, M.A. (1982) '*The dependance of the aerodynamic drag coefficient on wave parameters*' 1st Int. Conf. Meterology and Air/Sea Interaction of Coastal Zone. May 10-14 The Hague p.398-404

DOUGLASS, S.L. (1989) '*The influence of wind on nearshore breaking waves*' PhD Thesis, Drexel University, Dept. Civil Eng., (America)

DOUGLASS, S.L. (1990) '*Influence of wind on breaking waves*' ASCE J. Waterway, Port, Coastal & Ocean Eng. v.116 n.6 Nov/Dec

DOUGLASS, S.L. & WEGGEL, R.J. (1988) '*Laboratory experiments on the influence of wind on nearshore wave breaking*' Proc. 21st Conf. Coastal Eng. Publ. American Soc. Civ. Eng., New York p.632-643

EASSON, W.J, GRIFFITHS, M.W.P., & GREATED, C.A. (1988) '*Kinematics of breaking waves in coastal regions*' 21st Coastal Eng. Conf. v.1 p.871-883 ASCE

FUHRBOTER, A. (1970) '*Air entrainment and energy dissipation in breakers*' Proc. 12th Int. Conf. Coastal Eng. p.391-399

GALLOWAY, J.S. (1988) '*Field investigation of suspended sediment clouds under plunging breakers*' Esturine, Coastal & Shelf Science, Aug., 27(2) p119-130

GALLOWAY, J.S., COLLINS, M.B. & MORAN, A.D. (1989) '*Onshore/offshore wind influence on breaking waves: an empirical study*' Coastal Eng. 13 Publ. American Soc. Civ. Eng., New York p.305-323

GALVIN, C.J. (1968) '*Breaker type classification on three laboratory beaches*' J. Geophysical Research v.73 p.3651-3659

GALVIN, C.J. (1972) '*Wave breaking in shallow water*' In: Waves on beaches and resulting sediment transport. Ed. R.E.Meyer Acad. Press, New York, London

IPPEN & KULIN (1955) '*Shoaling and breaking characteristics of the solitary wave*' MIT Hydrodynamics Laboratory. Tech. Rep. 15

IVERSON, H.W. (1952) '*Laboratory study of breakers*' US National Bureau Standards Circ. 521 p9-32 Ed. H.W. Iverson

IVERSON, H.W. & HAYAMI, S. (1954) '*Mechanics of wave breaking*' Proc. 2nd Japanese Conf. Coastal Eng. 13-15

IWATA, K. & SAWARAGI, T. (1982) '*Wave deformation in the surf zone*' Memoirs Fac. Eng., Nagoya Univ. v.34 n.2

IZUMIYA, T. & ISOBE, M. (1986) '*Breaking criterion on non-uniformly sloping beach*' Coastal Eng. 10 Publ. American Soc. Civ. Eng., New York p.318-327

JIABAO, Z. (1989) '*A discussion on currents and suspended load transport in the surf zone*' China Ocean Eng. v3 n2 p195-202

KANA, T.W. (1979) '*Suspended sediment in breaking waves*' Coastal Res. Div., Dept. Geol. Univ. S. Carolina, Tech. Rep. 18-CRD

KAWAI, S. (1981) '*Visualization of air flow separation over wind-wave crests*' J. Fluid Mech. v.77 p.825-842

KAWAI, S. (1982) '*Structure of air flow separation over wind wave crests*' Boundary Layer Meteorology v.23 p.503-521

KING, D.M. & BAKER, C.J. (1993) '*Offshore wind influence on breaking waves*' University of Nottingham, Department of Civil Eng. Internal report no. FR 93038 Dec. 1993

KINSMAN, B. (1965) 'Wind waves: their generation and propagation on the ocean surface' Prentice-Hall, Englewood Cliffs, N.J.

KIRSCHMER, O. (1952) '*Die theorie der meerswollen als grundlage von modelluersuchen fur seebauten*' MAN Forschungsheft 2 Halbjahr

KONDO, J., FUJINAWA, Y. & NAITO, G. (1972) '*Wave-induced wind fluctuation over the sea*' J. Fluid Mech. v.51 n.4 p.751-771

KRAUS, E.D. (1972) 'Atmosphere-ocean interaction' Oxford Uni. Press

KRUGERMEYER, L., GRUNEWALD, M. & DUNKEL, M. (1978) '*The influence of sea waves on the wind profile*' Boundary Layer Met. v.14 p.403-414

MACDONALD, A.J. (1975) 'Wind loading on buildings' Applied Sci. Publishers Ltd

LE MEHAUTE, B. (1976) 'An introduction to hydrodynamics and water waves' Springer Verlag, New York

MILLAR, R.L. (1972) '*The role of surface tension in breaking waves*' Proc. ASCE 13th Conf. Coastal Eng. Publ. American Soc. Civ. Eng., New York p.433-449

MINIKIN, R.R. (1950) 'Winds, Waves and Maritime Structures' 2nd Rev Ed. Griffin London

NADOAKA, K., UENO, S. & IGARASHI, T. (1988) '*Sediment suspension due to large scale eddies in the surf zone*' Coastal Eng. Publ. American Soc. Civ. Eng., New York p1646-1660

NAITO, G. (1988) '*Turbulent properties and spectral behaviours of ocean winds observed at an off-shore tower*' J. Wind Eng. and Ind. Aerodynamics v.28 p.51-60

PEREGRINE, D.H. (1983) '*Breaking waves on beaches*' Ann. Rev. Fluid Mech. v.15 p. 149-178

PEREGRINE, D.H. & SVENDSEN, I.A. (1978) '*Spilling breakers, bores and hydraulic jumps*' Proc. 16th Int. Conf. Coastal Eng. ch.30 Publ. American Soc. Civ. Eng., New York p.540-550

PHILLIPS, O.M. (1969) 'The dynamics of the upper ocean' Cambridge Uni. Press

PRESS, W.H., TEUKOLSKY, S.A., VETTERING, W.T., & FLANNERY, B.P. (1992) 'Numerical receipes in fortran: the art of scientific computing' 2nd Ed. Cambridge University Press

REDDISH, H.J. & BASCO, D.R. (1987) '*Breaking wave force distribution on a slender pile*' Coastal Hydrodynamics Speciality Conference , Newark, Delaware , June, p184-195

REYNOLDS, A.J. (1974) 'Turbulent flows in engineering' Wiley-Interscience Publ.

SACHS, P. (1978) 'Wind forces in engineering' 2nd Ed Pergamon Press

SHARP & KHADER (1984) *'A review of scale effects in harbour wave models'* Dock & Harbour Authority, v.64, n.757, Jan 1984, p.190-192

SHIBAYAMA, T. & HORIKAWA, K. (1982) *'Sediment suspension due to breaking waves'* Coastal Engng. in Japan v.25, p.163-176

SHEMDIN, O.H. & HSU, E.Y. (1967) *'Direct measurement of aerodynamic pressure above a simple progressive gravity wave'* J. Fluid Mech. v.30 p.403-416

SILVESTER, R. (1974a) 'Coastal Engineering 1: Generation, propagation & influence of waves' Elsevier Sci. Pub. Co.

SILVESTER, R. (1974b) 'Coastal Engineering 2: Sedimentation, estuaries, tides, effluents & modeling' Elsevier Sci. Pub. Co.

SORENSEN, R.M. (1978) 'Basic coastal engineering' Wiley-Interscience Publication

STIVE, M.J.F. (1985) *'A scale comparison of waves breaking on a beach'* Coastal Eng. 9 Publ. American Soc. Civ. Eng., New York p.151-158

TAKEUCHI, K. LEAVITT, E. & CHAO, S.P. (1977) *'Effects of water waves on the structure of turbulent shear flow'* J. Fluid Mech. v.80 p.3 p.535-559

THOMAS, R.S. & HALL, B. (1992) 'Seawall design' CIRIA Butterworth-Heinemann.

TOUMAZIS & ANASTASIOU (1990) *'Scale effects in breaking waves'* Coastal Engineering Vol 1, Proc.22nd Coastal Eng. Conf. Publ. American Soc. Civ. Eng., New York p973-985

US ARMY CORPS OF ENGINEERS / (1984) 'Shore Protection Manual' Coastal Engineering Research Center, Vicksburg, Mississippi, 2 volumes

WEGGEL, R.J. (1972) *'Maximum breaker height'* J. Waterways, Harbours & Coastal Eng. Division, Proc. ASCE Nov v98

WEISHER, L.L. & BYRNE, R.J. (1978) *'Field study of breaking wave characteristics'* Proc. 16th Int. Conf. on Coastal Eng. Publ. American Soc. Civ. Eng., New York p.487-506

WIEGEL, R.L. (1950) *'Experimental study of surface waves in shoaling water'* Transactions, American Geophysical Union, v.31, n.3, June 1950, p.377-385

WILLS, J.A.B. (1980) *'Hot-wire and hot-film anemometry'* Lecture notes from a course at Stanford University, California, July/August 1979

WU, J. (1968) *'Laboratory studies of wind-wave interactions'* J. Fluid Mech. v.34 p.91-111

FIGURES

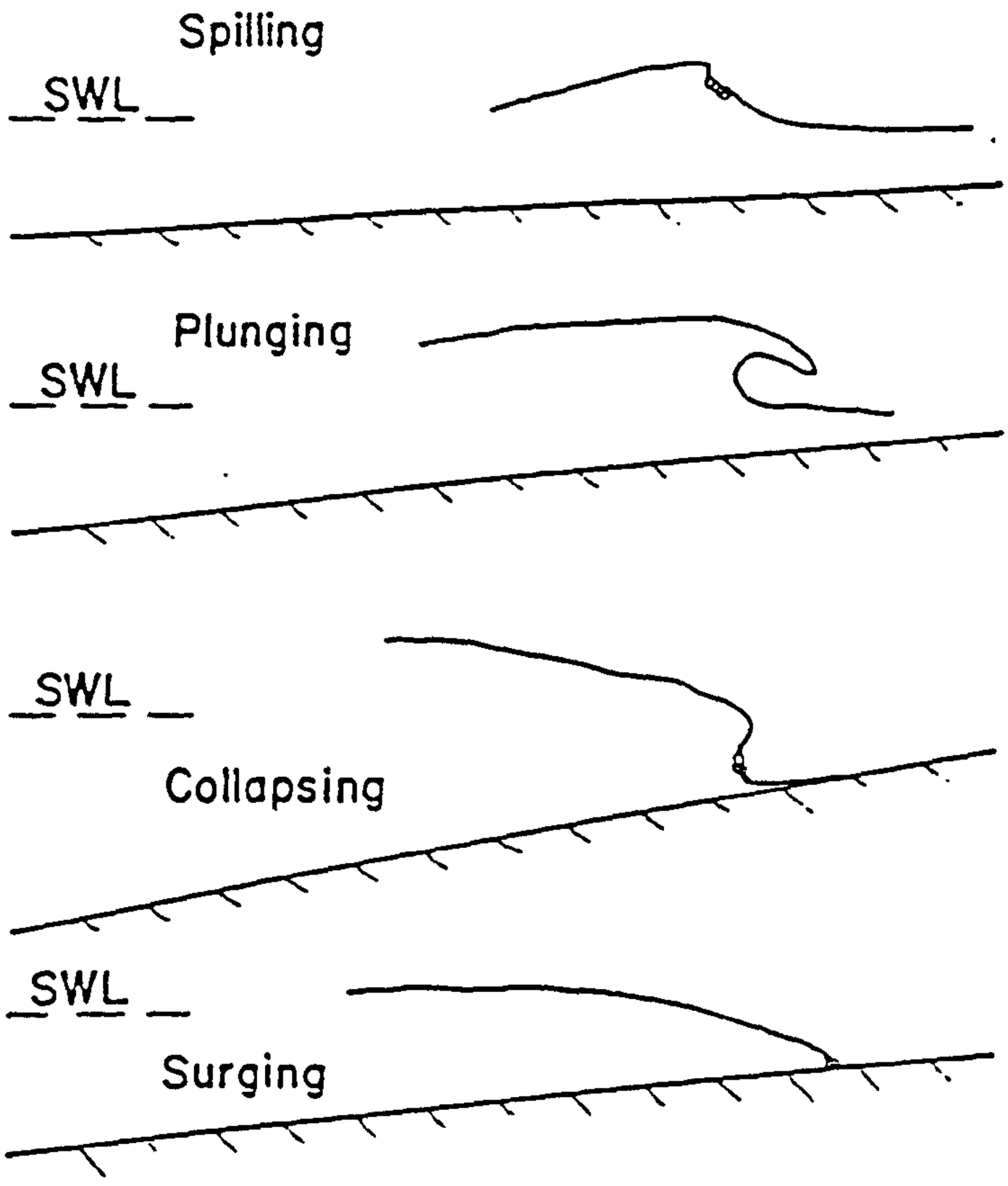

Figure 1.1 The four recognized breaker types according to Galvin (1968).

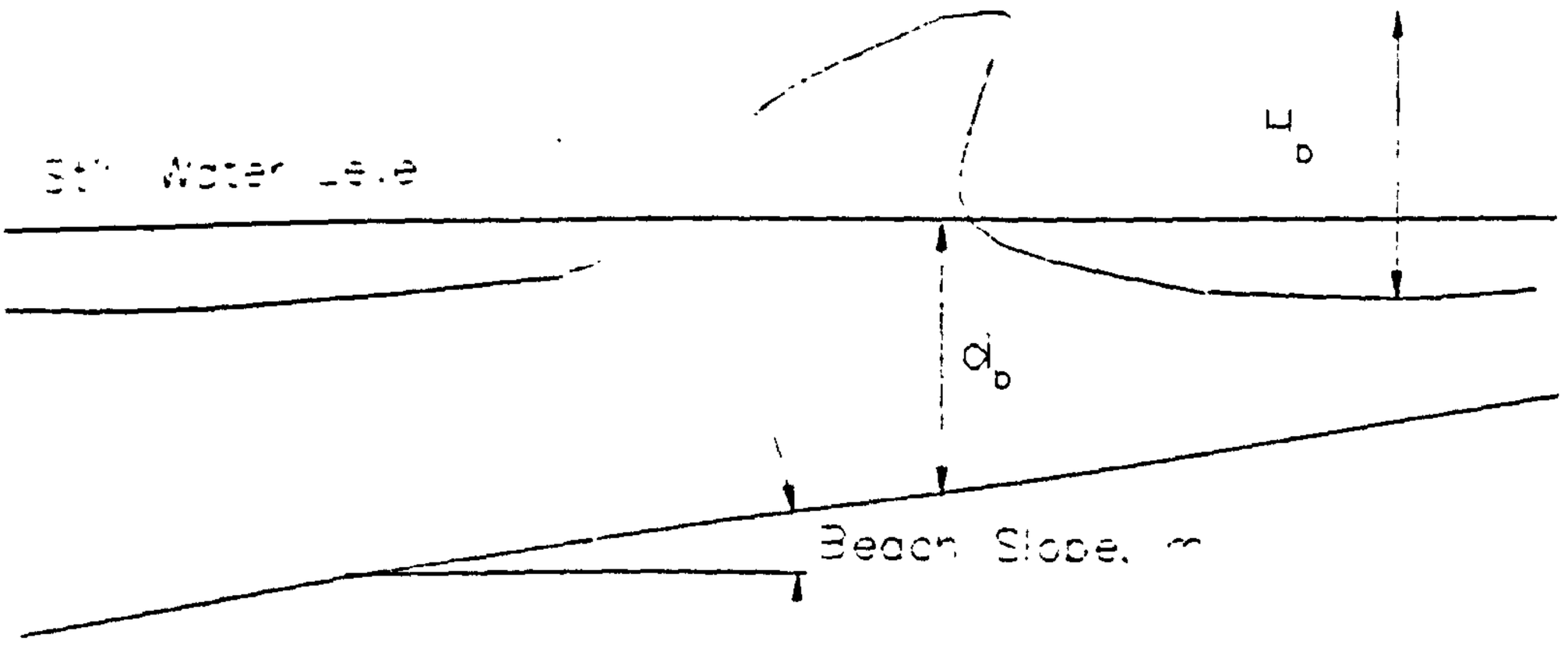

Figure 1.2 Definition of breaker height, H_b, and breaker depth, d_b.

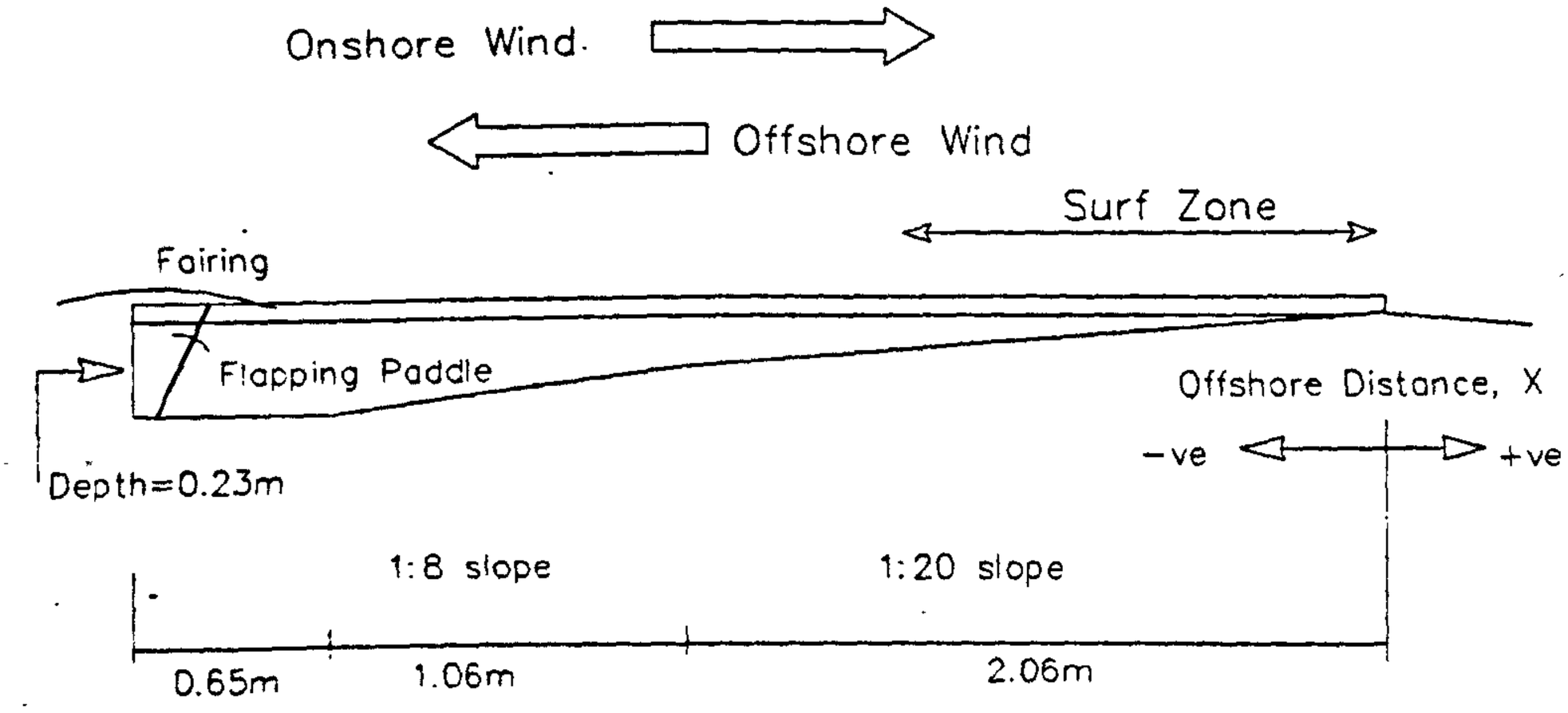

Figure 3.1 Side elevation of wave tank.

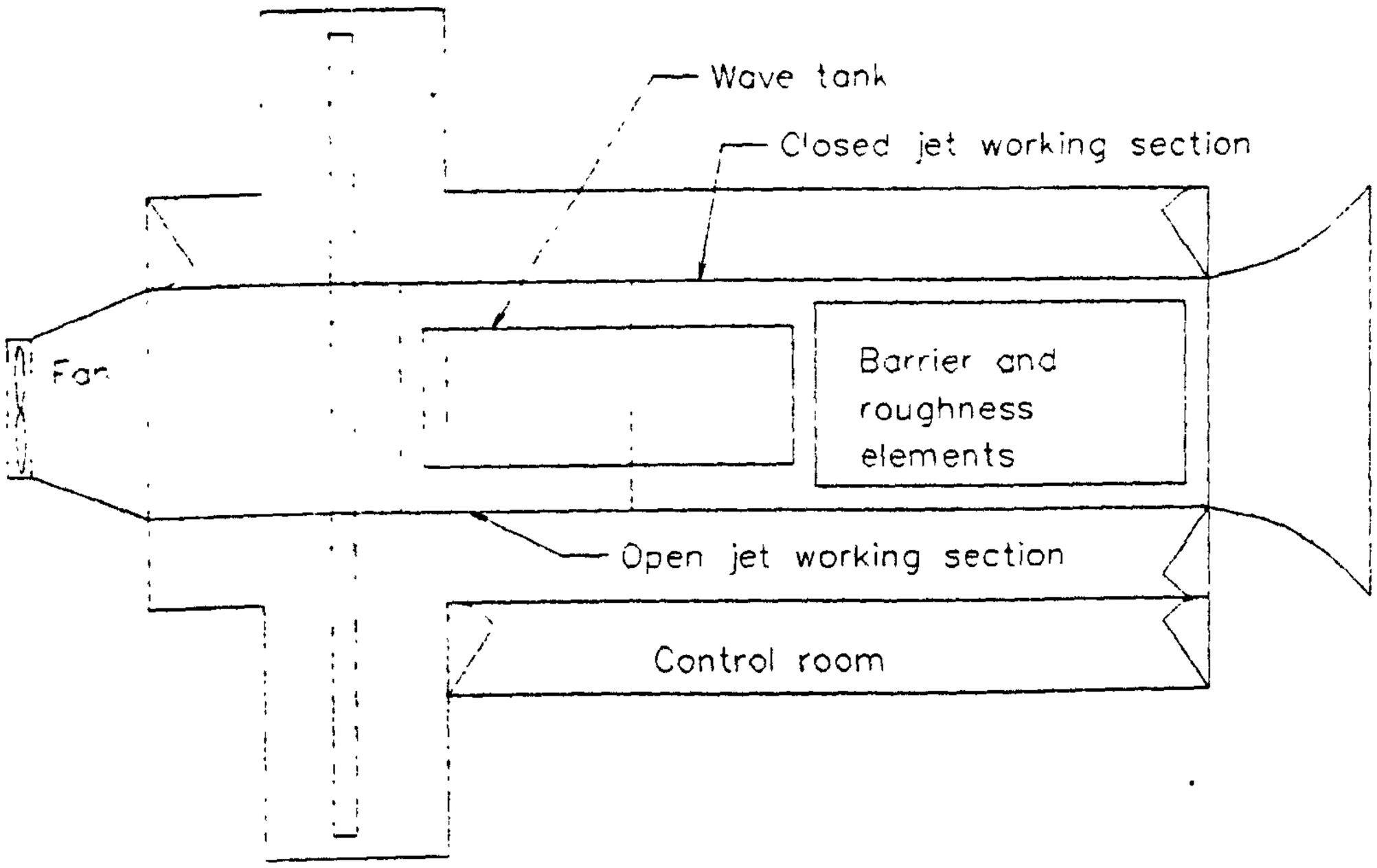

Figure 3.2 Schematic diagram of wind tunnel layout for offshore winds.

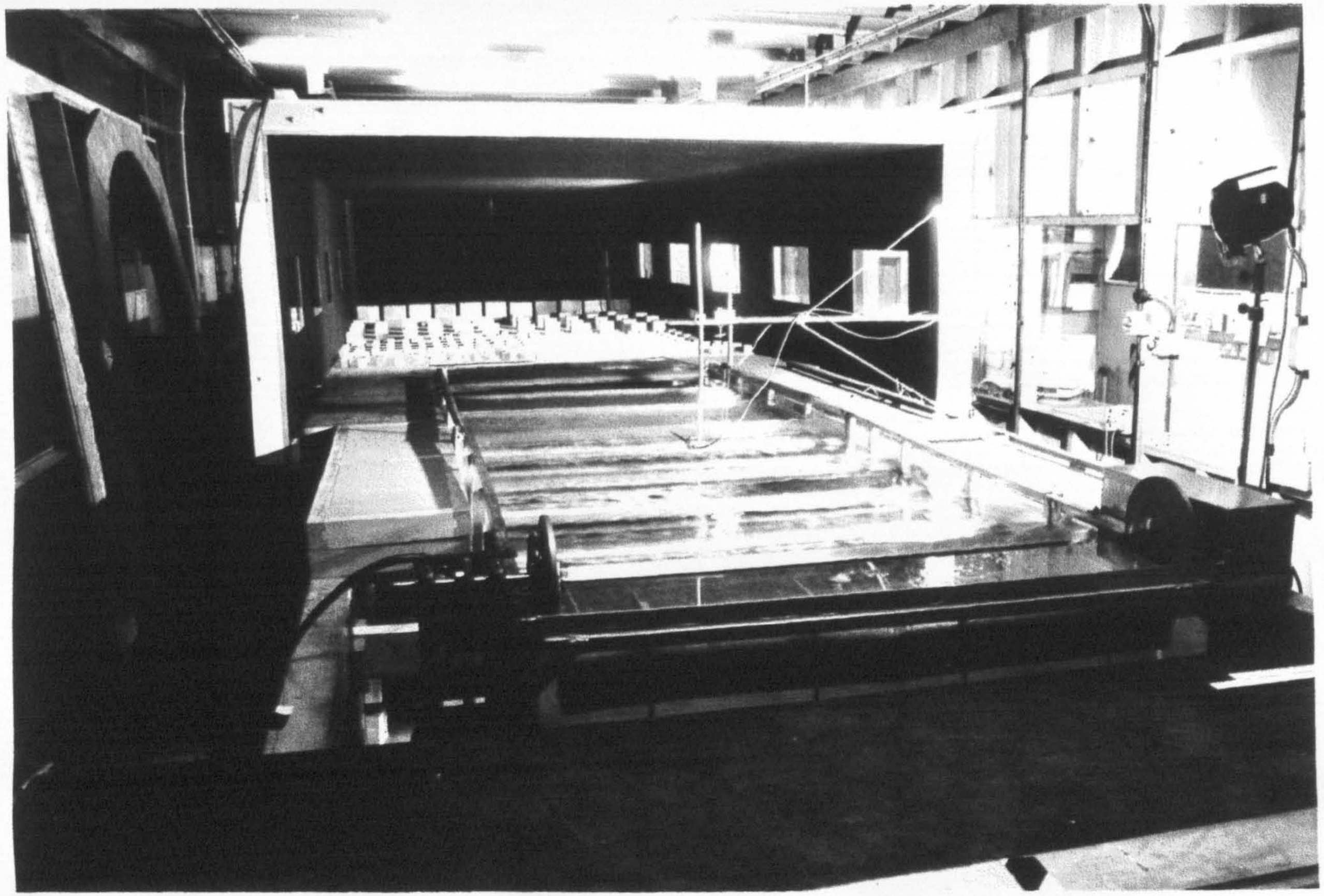

Figure 3.3 Wind tunnel layout for offshore winds. View of wave tank and boundary layer roughness elements looking upwind. Flapping paddle wave generator is in foreground.

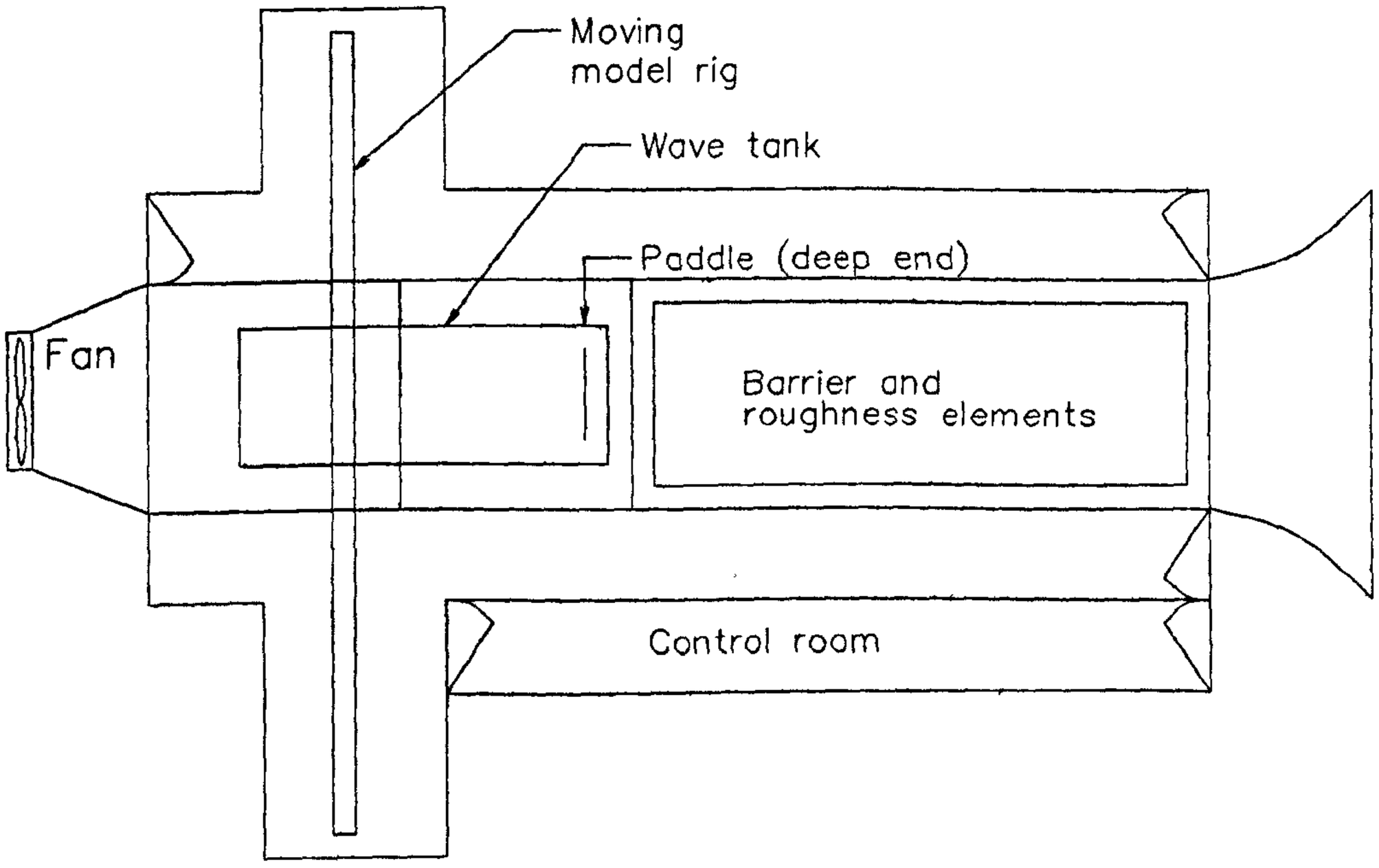

Figure 3.4 Schematic diagram of wind tunnel layout for onshore winds.

a)

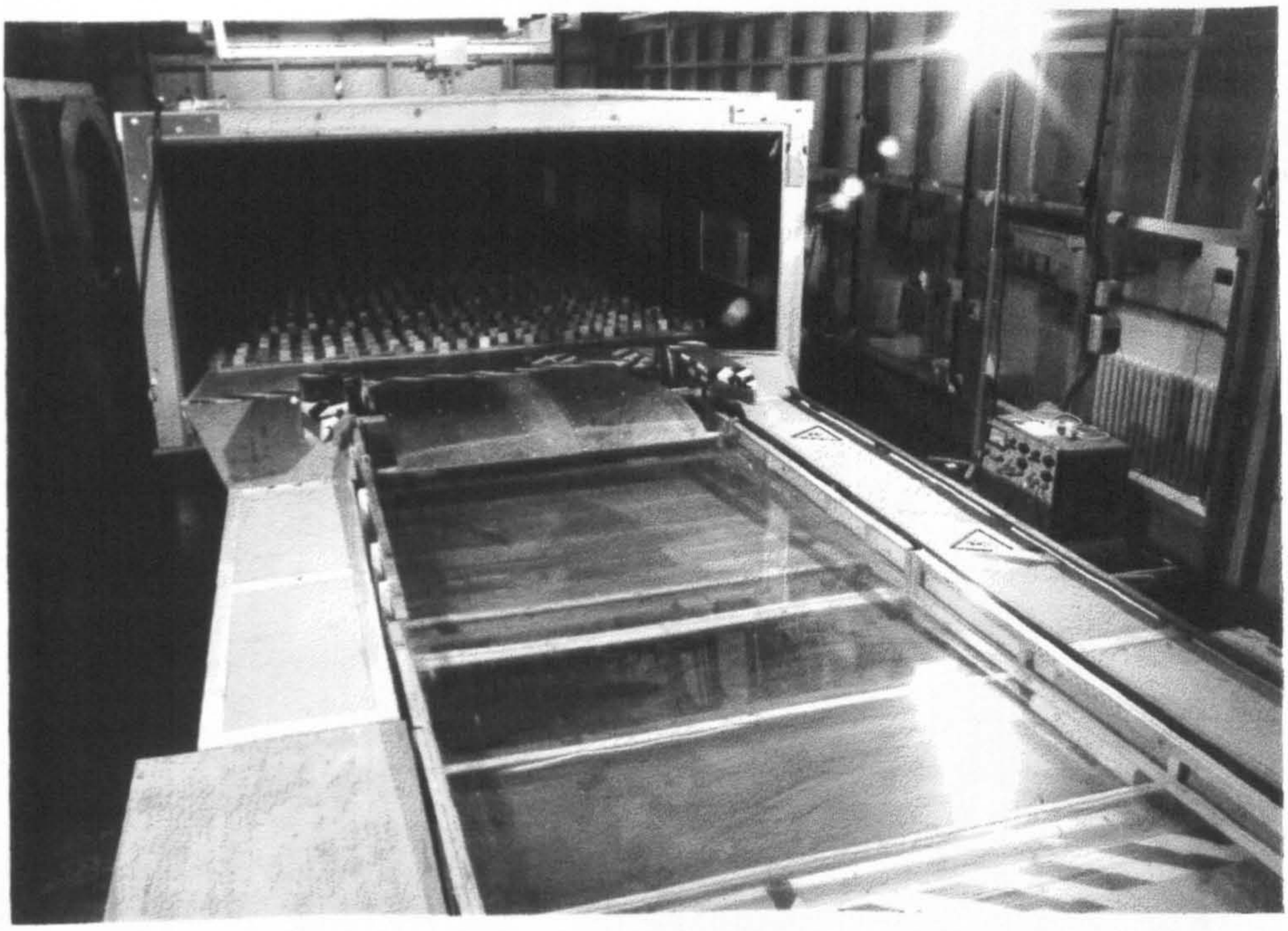

b)

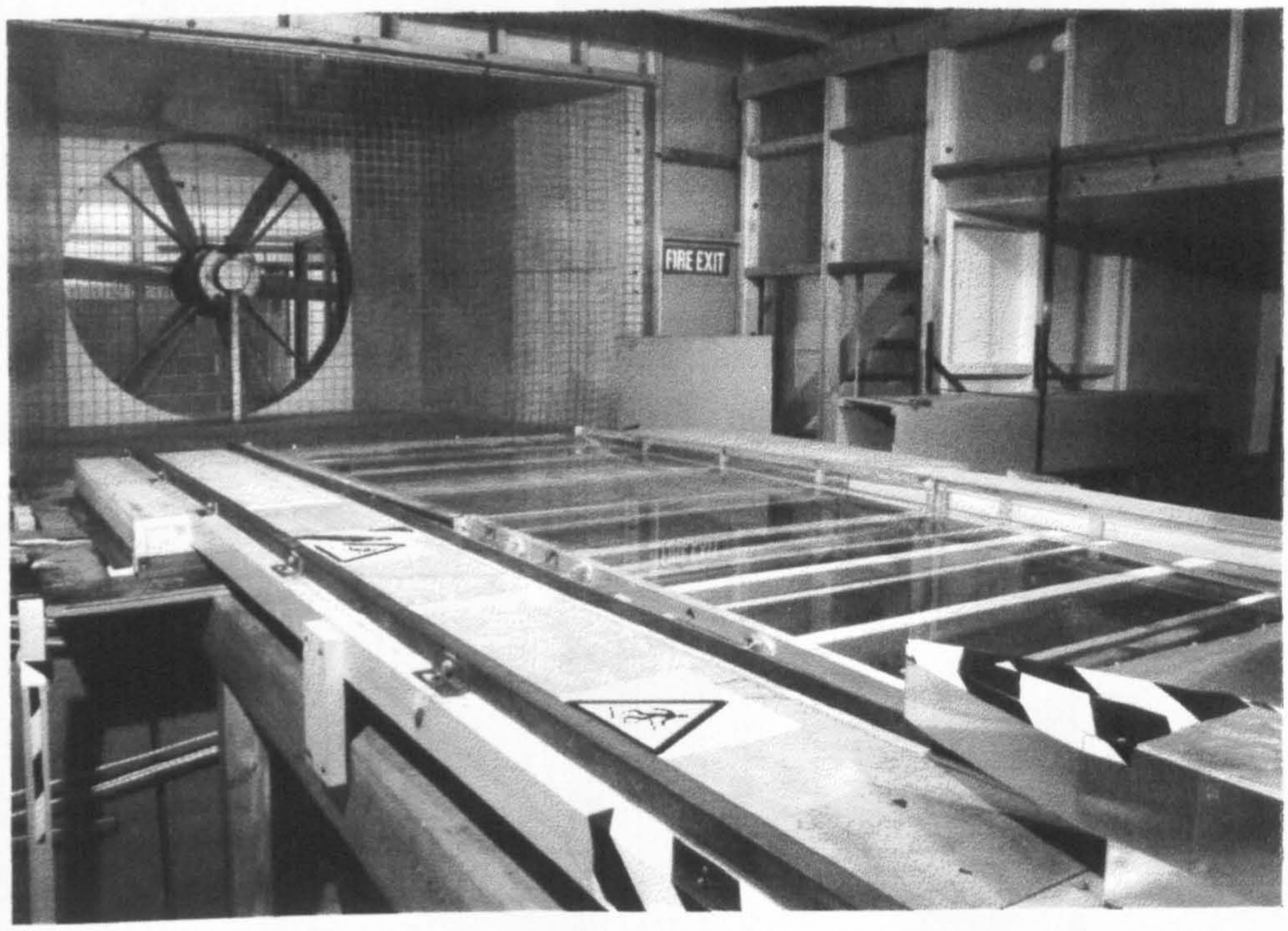

Figure 3.5 Wind tunnel layout for onshore winds: a) view looking upwind b) view looking downwind. Aluminium fairing over the flapping paddle is visible in (a).

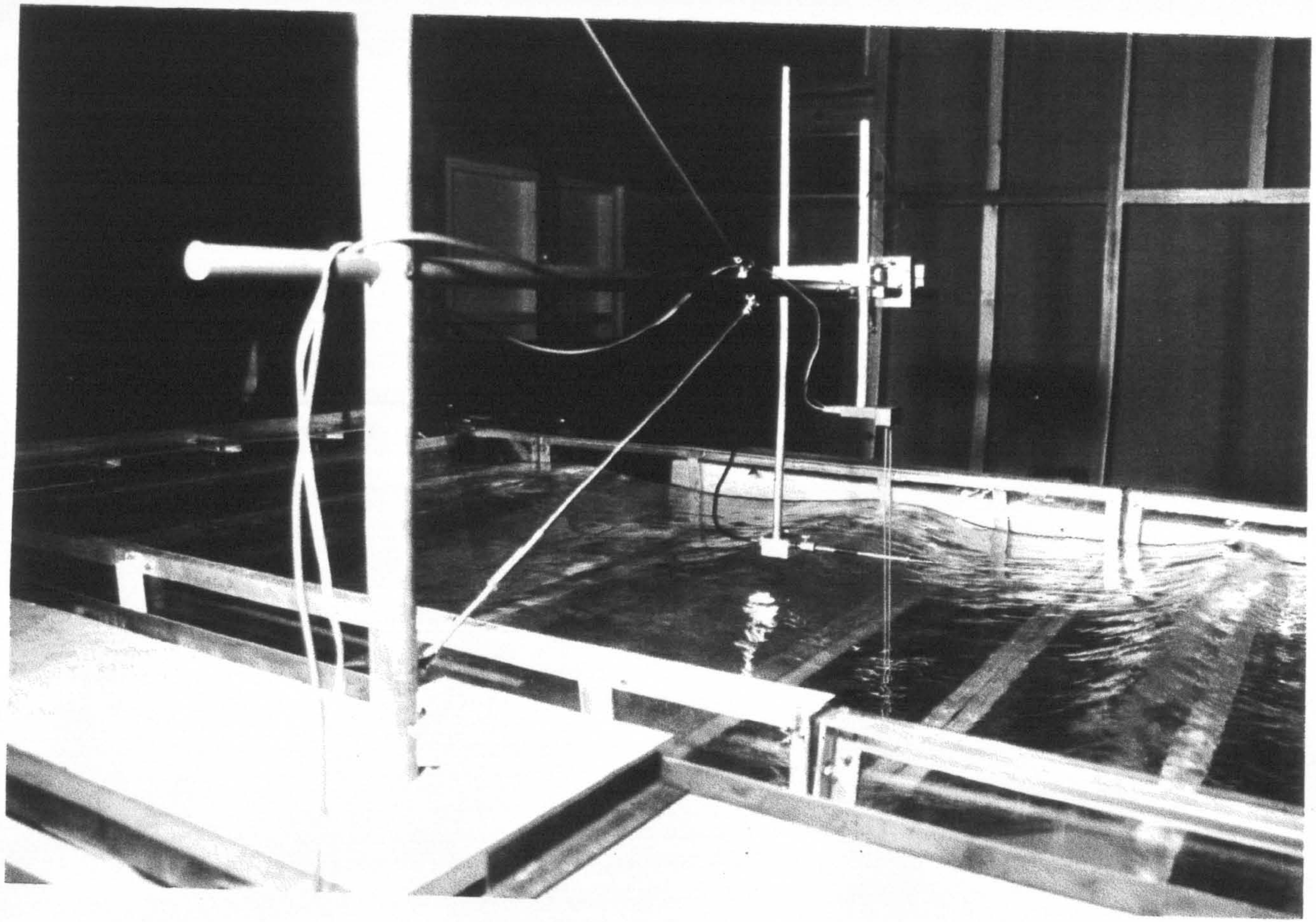

Figure 3.6 The cantilevered traverse being used with the hot-film probe and twin-wire wave probe for offshore winds.

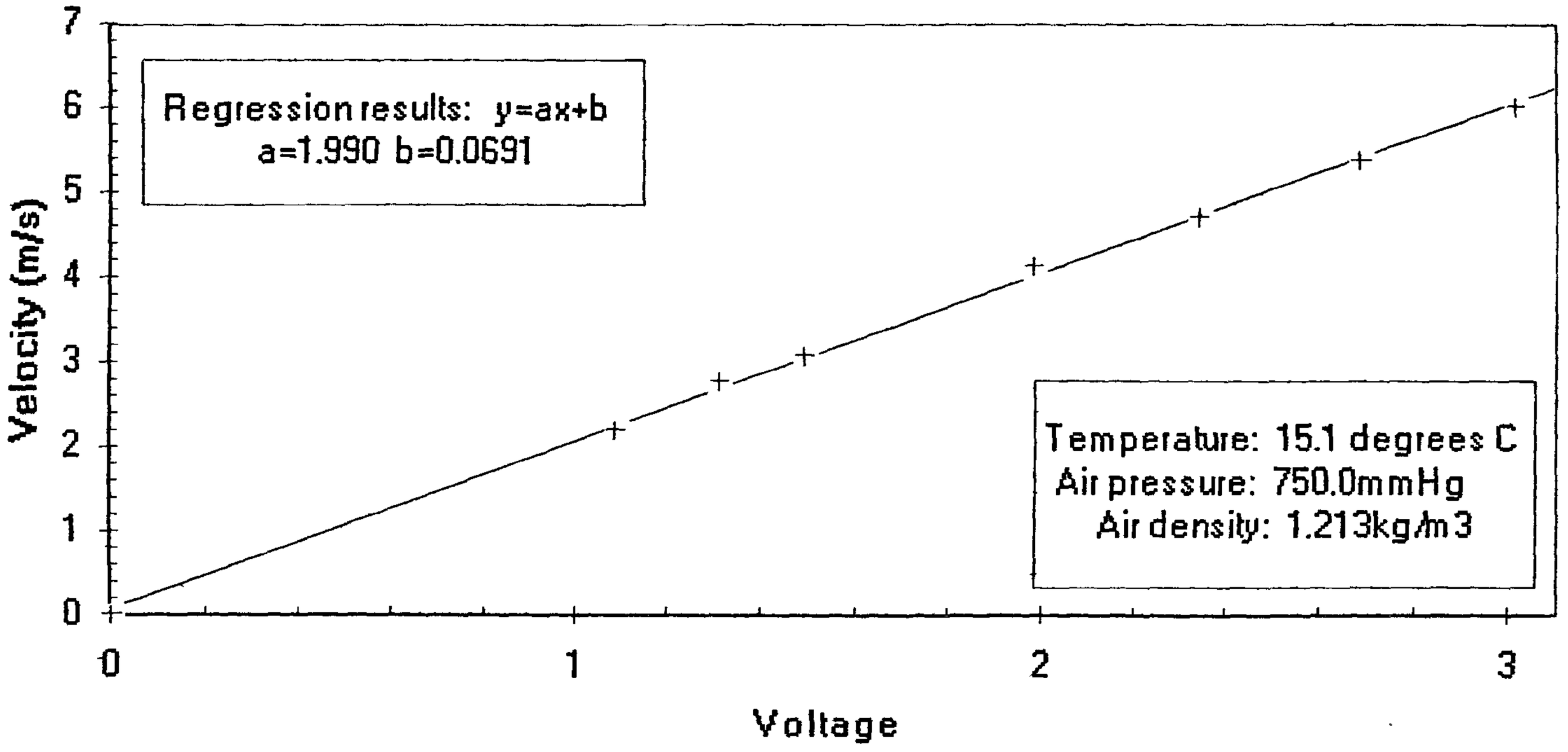

Figure 3.7 Typical linearised calibration curve for the hot-film probe.

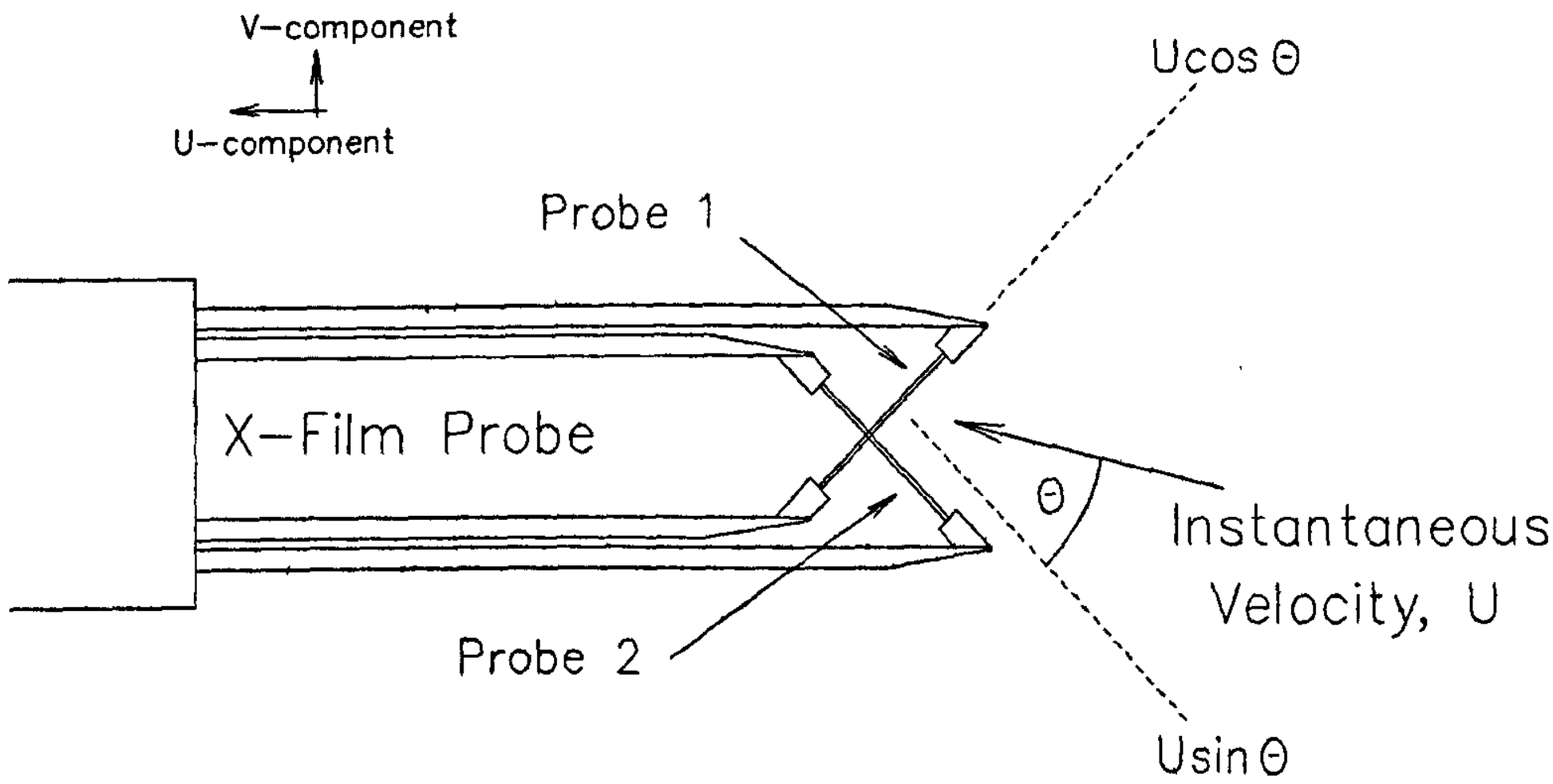

Figure 3.8 Definition diagram for the twin-channel X-film probe. Diagram indicates resolved velocity vectors for probe 1.

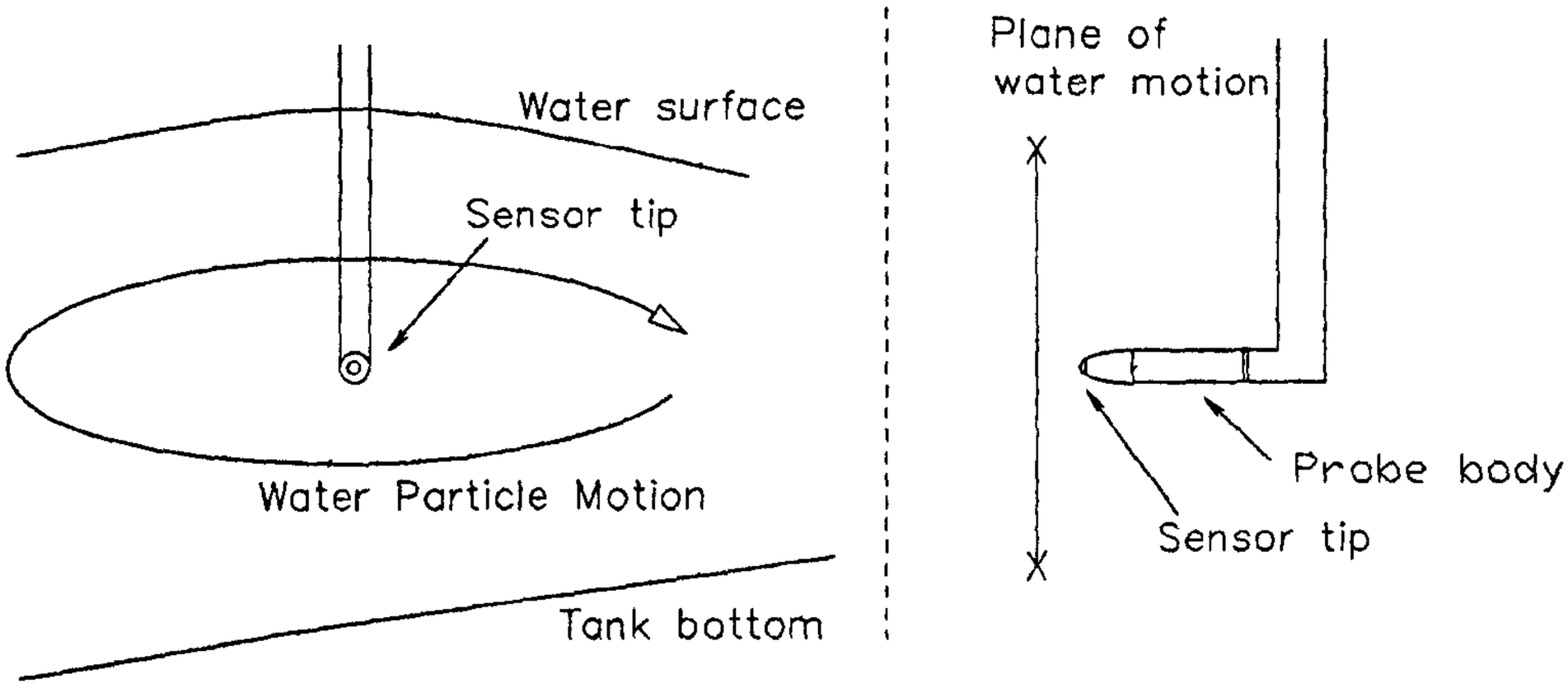

Figure 3.9 Conical water probe: arrangement of probe for water velocity measurements.

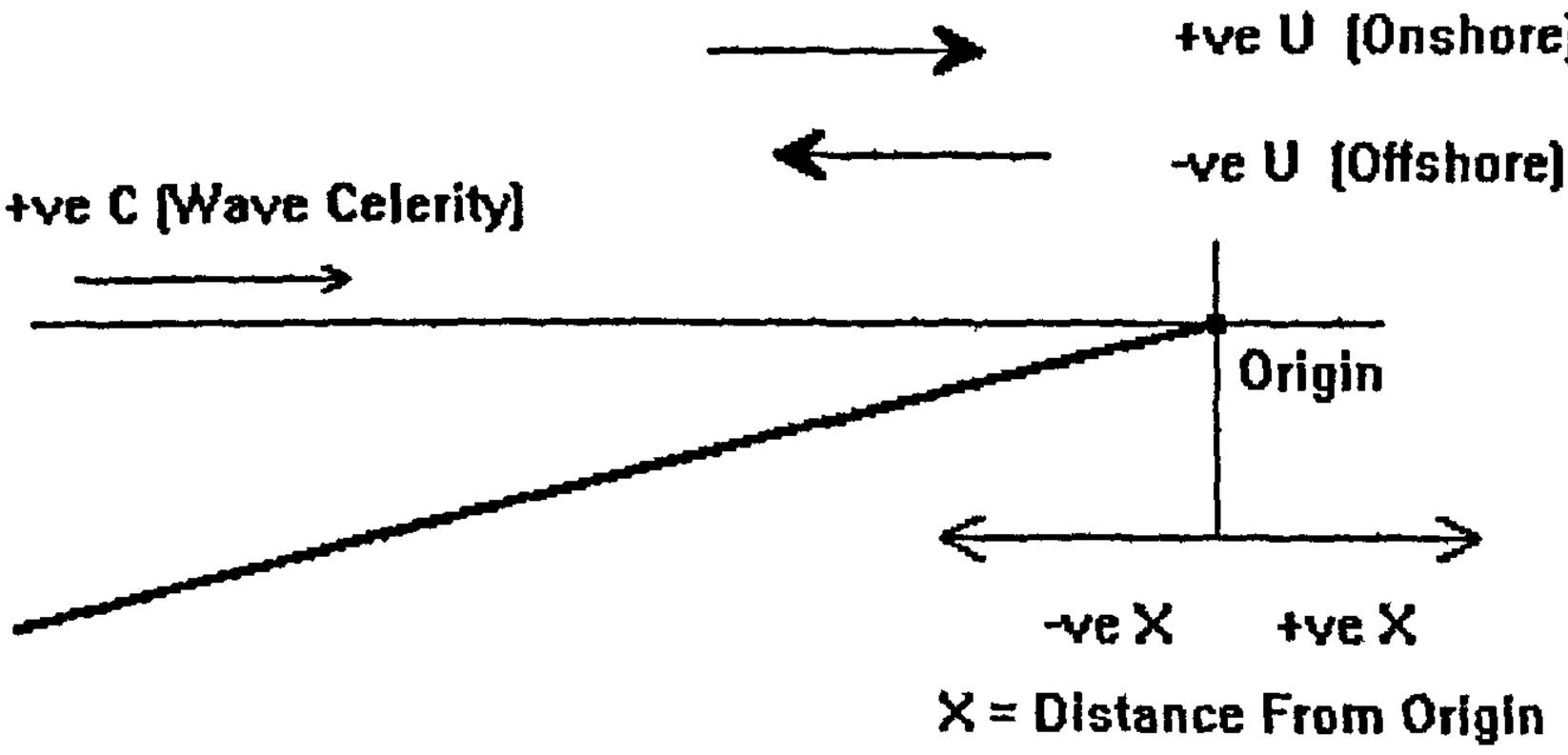

Figure 4.1 Adopted sign convention for all measurements.

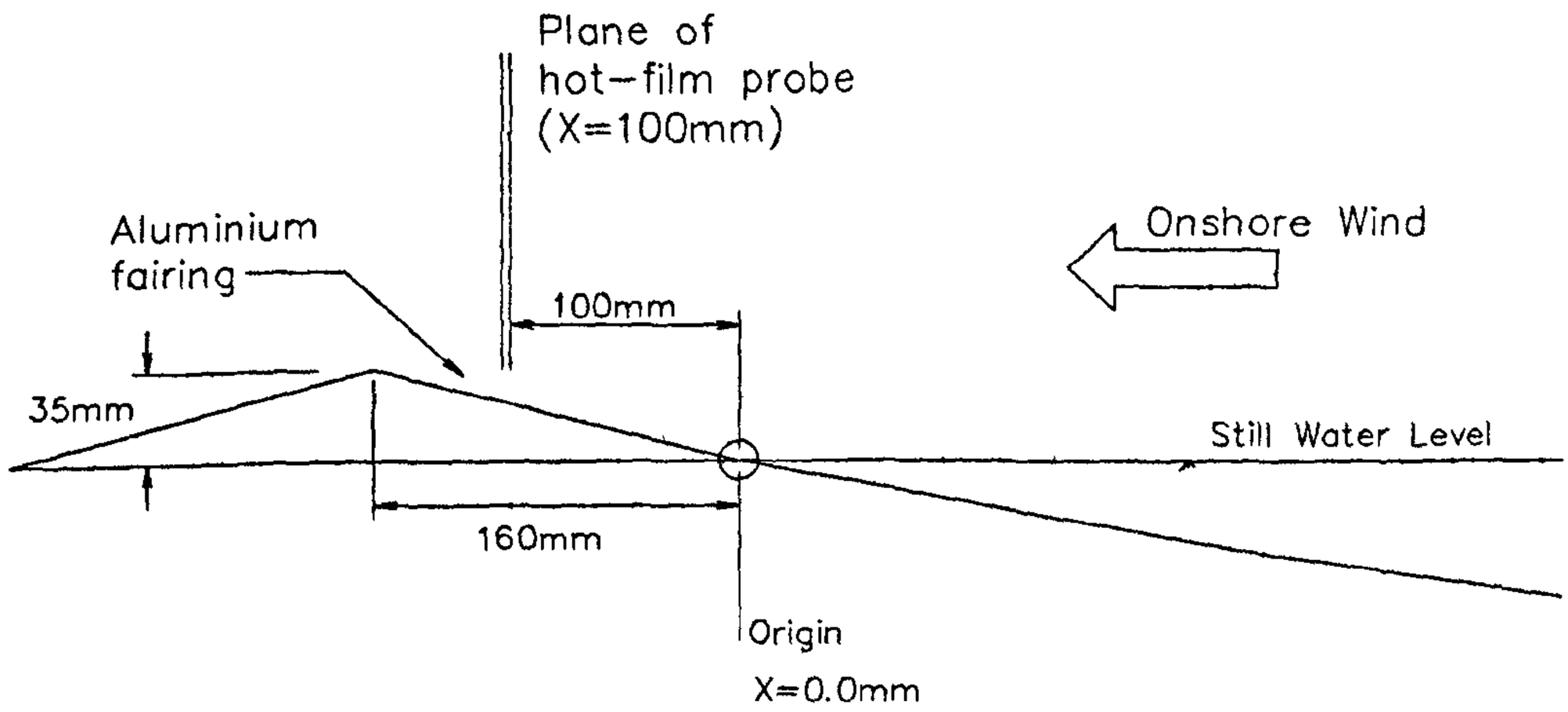

Figure 4.2 Arrangement of hot-film probes at X=100mm.

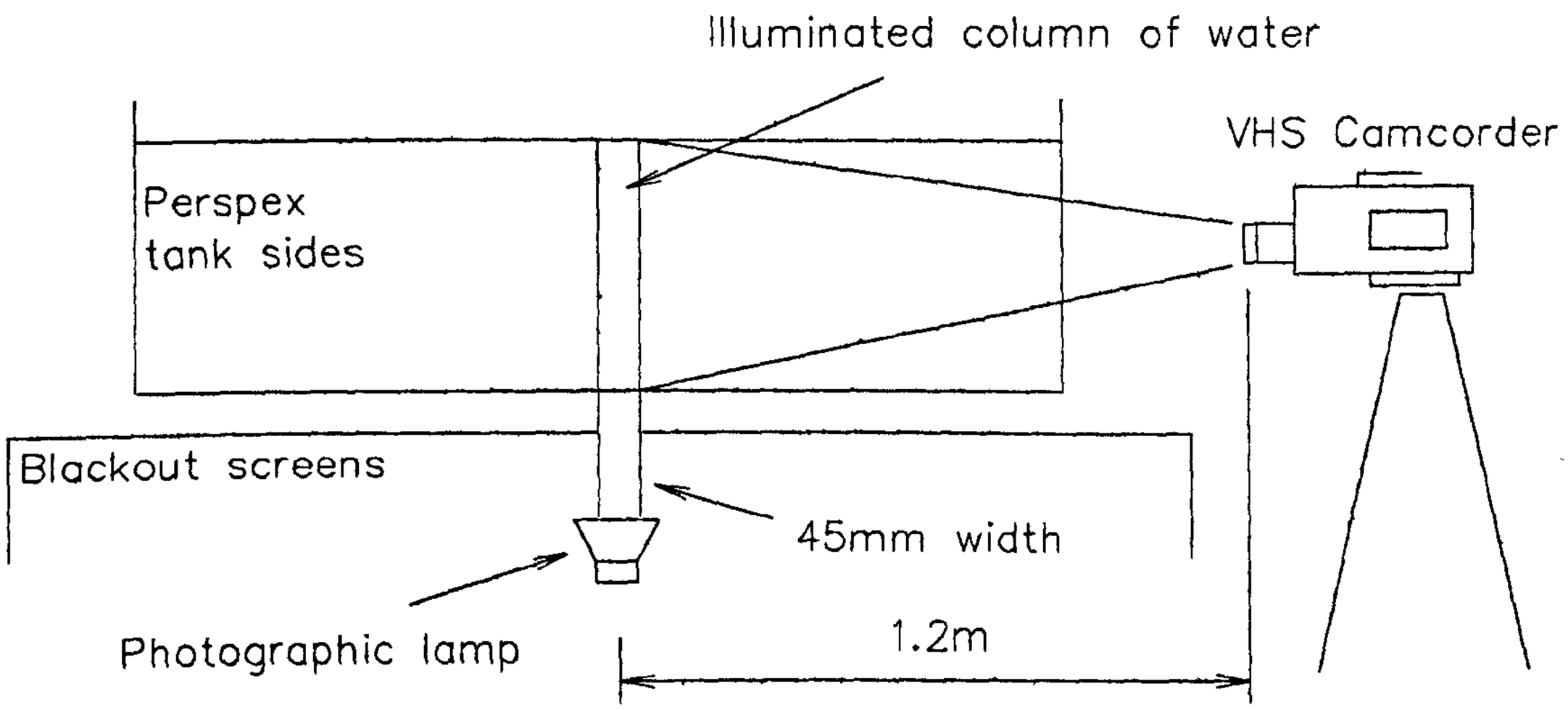

Figure 4.3 Camcorder set up for particle path study.

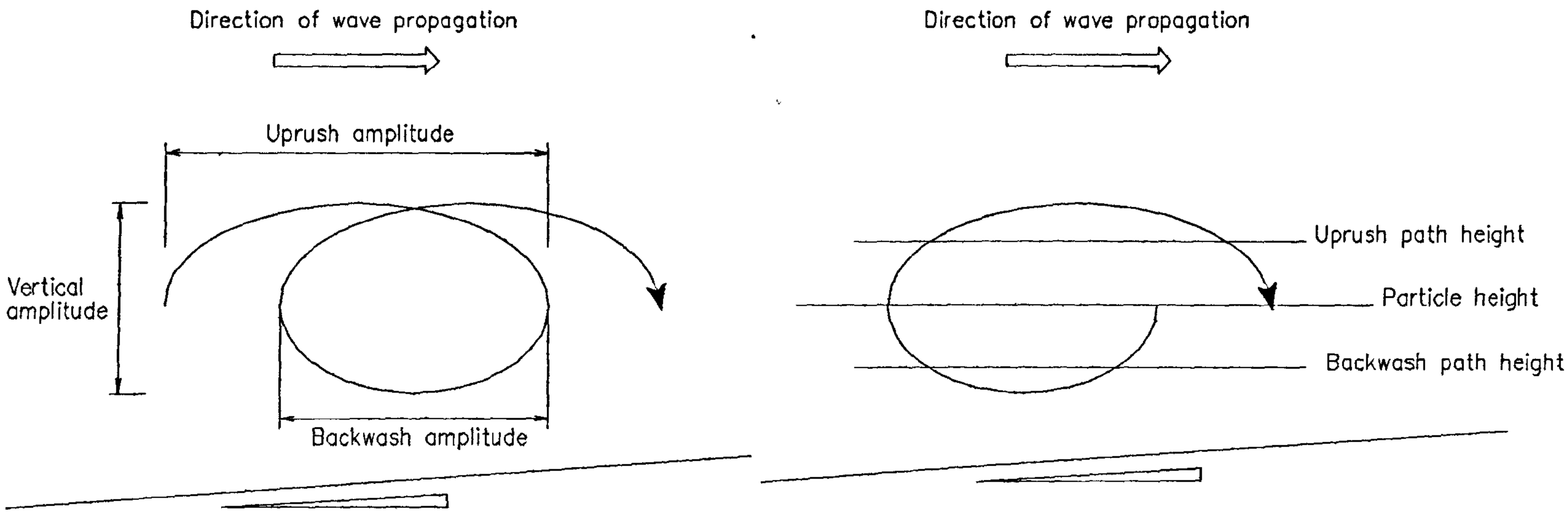

Figure 4.4 Particle path study: Definitions of uprush, backwash, and vertical amplitude, plus associated path heights.

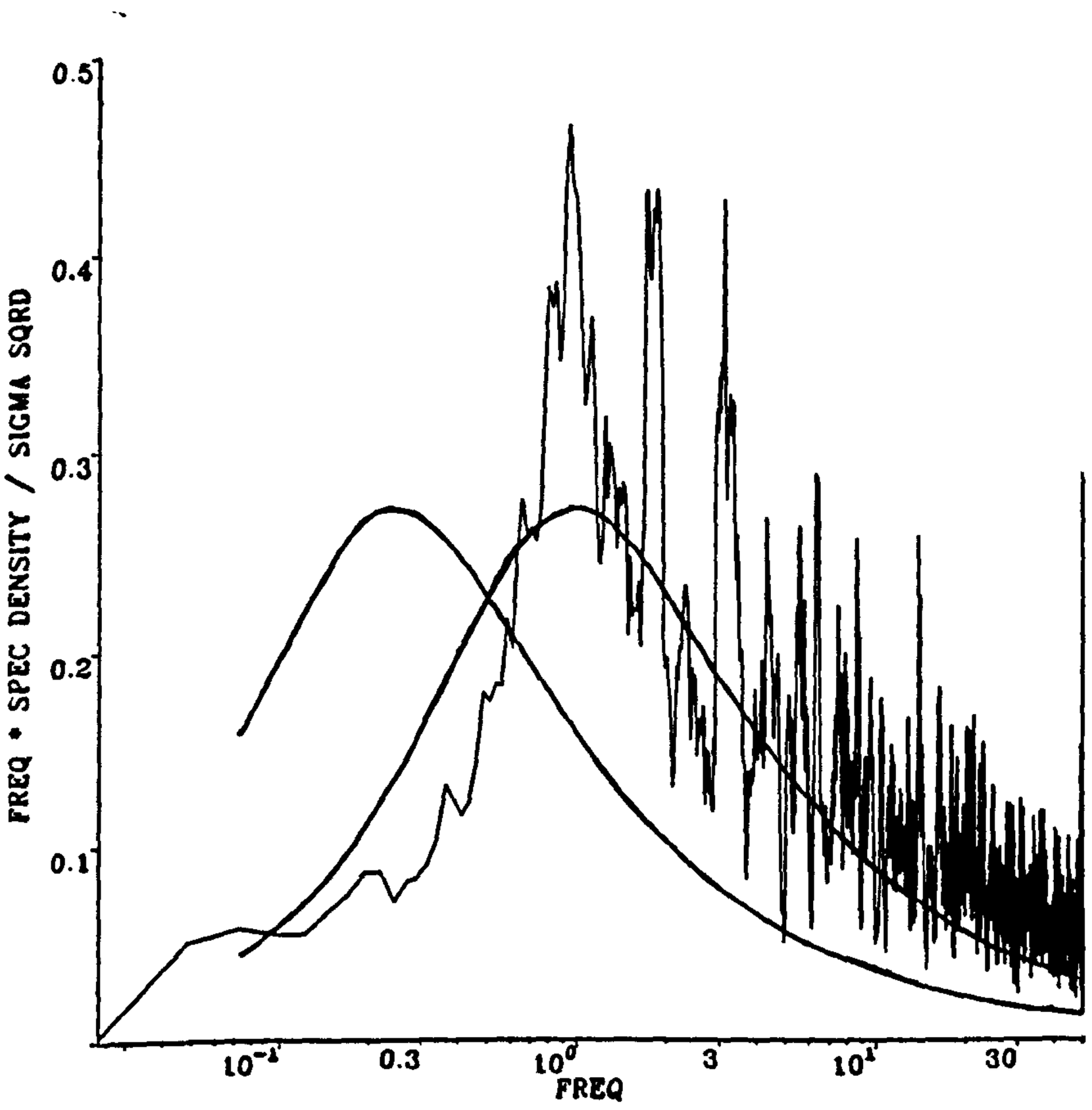

Figure 4.5 Frequency spectrum showing scale mis-match of ${}^{x}L_u$ with respect to wave-induced frequency peak (for plunging waves at point of breaking under onshore winds). Smooth lines are Von Karman spectra for ${}^{x}L_u$=0.2m and 0.8m.

a)

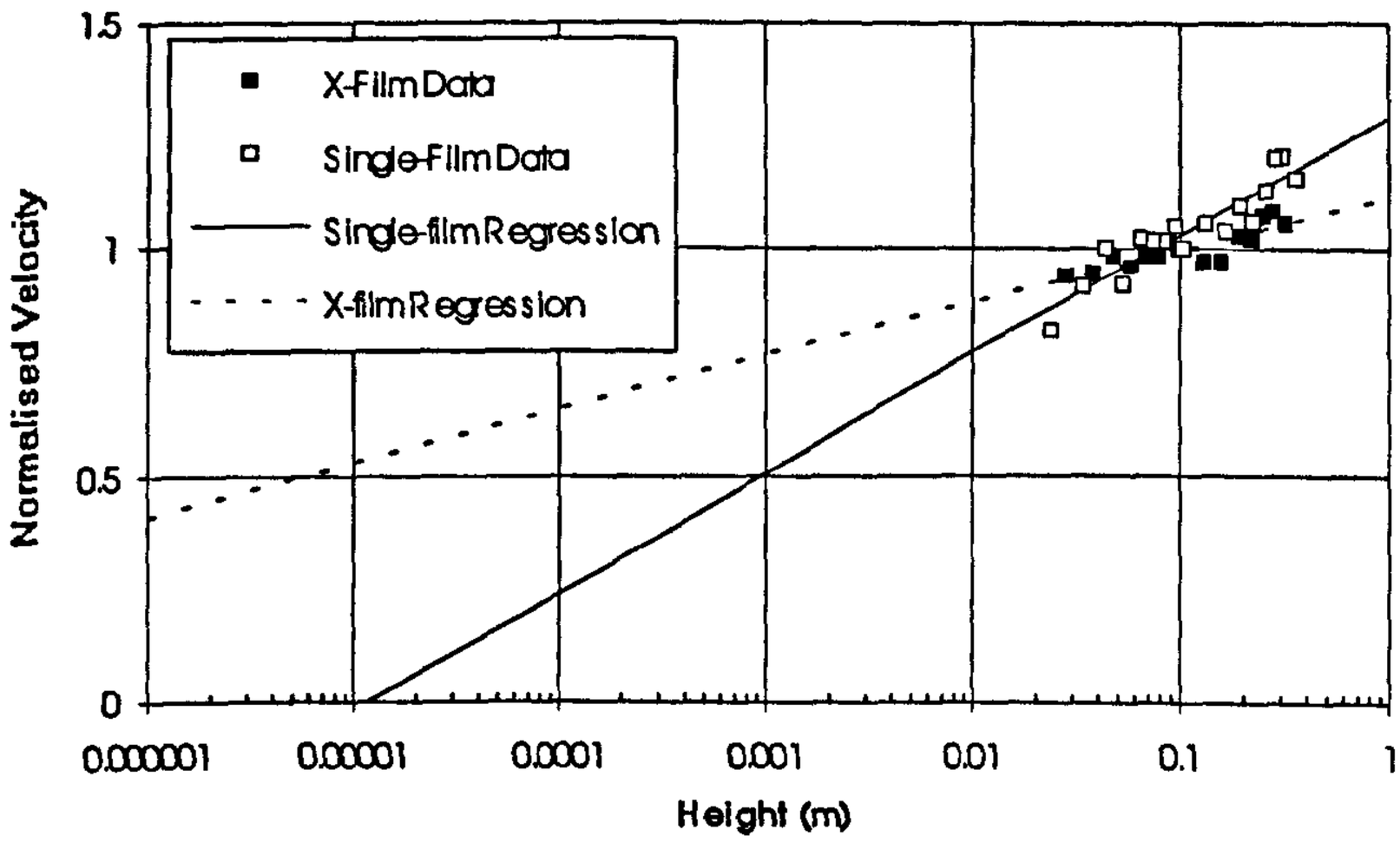

b)

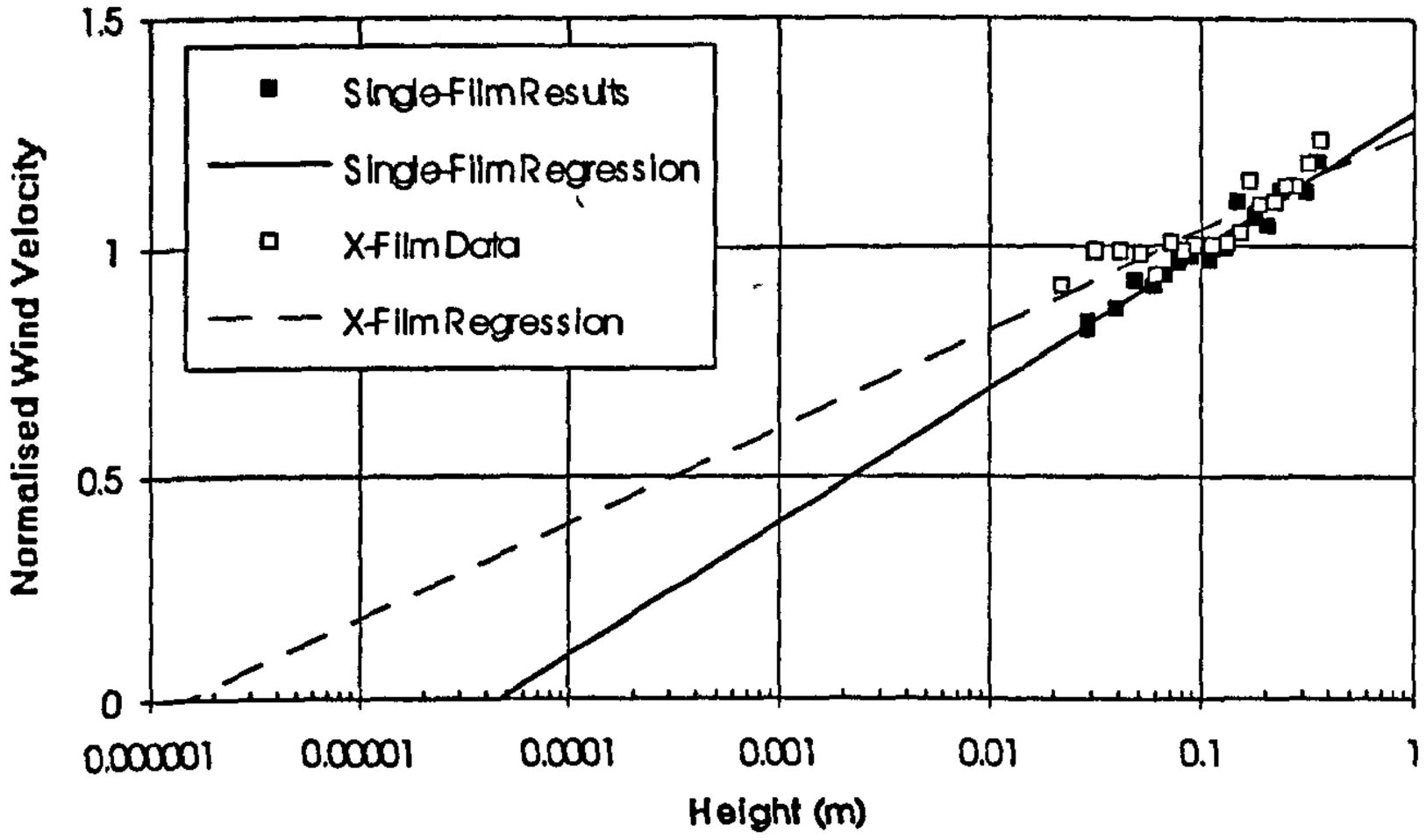

Figure 5.1 Semi-log velocity profiles for flat water (no generated waves) at X=-1265mm. a) Offshore winds b) Onshore winds

a)

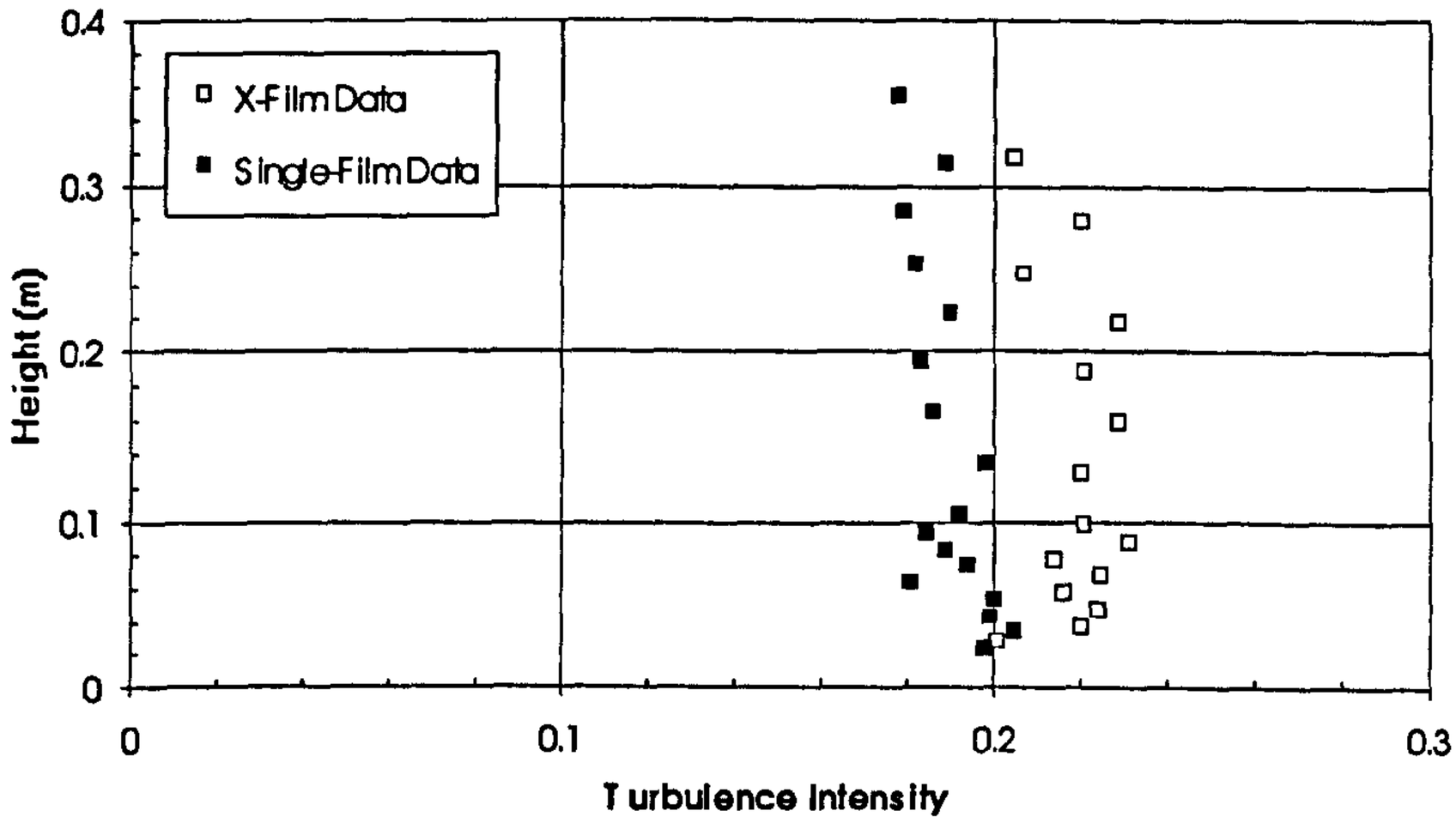

b)

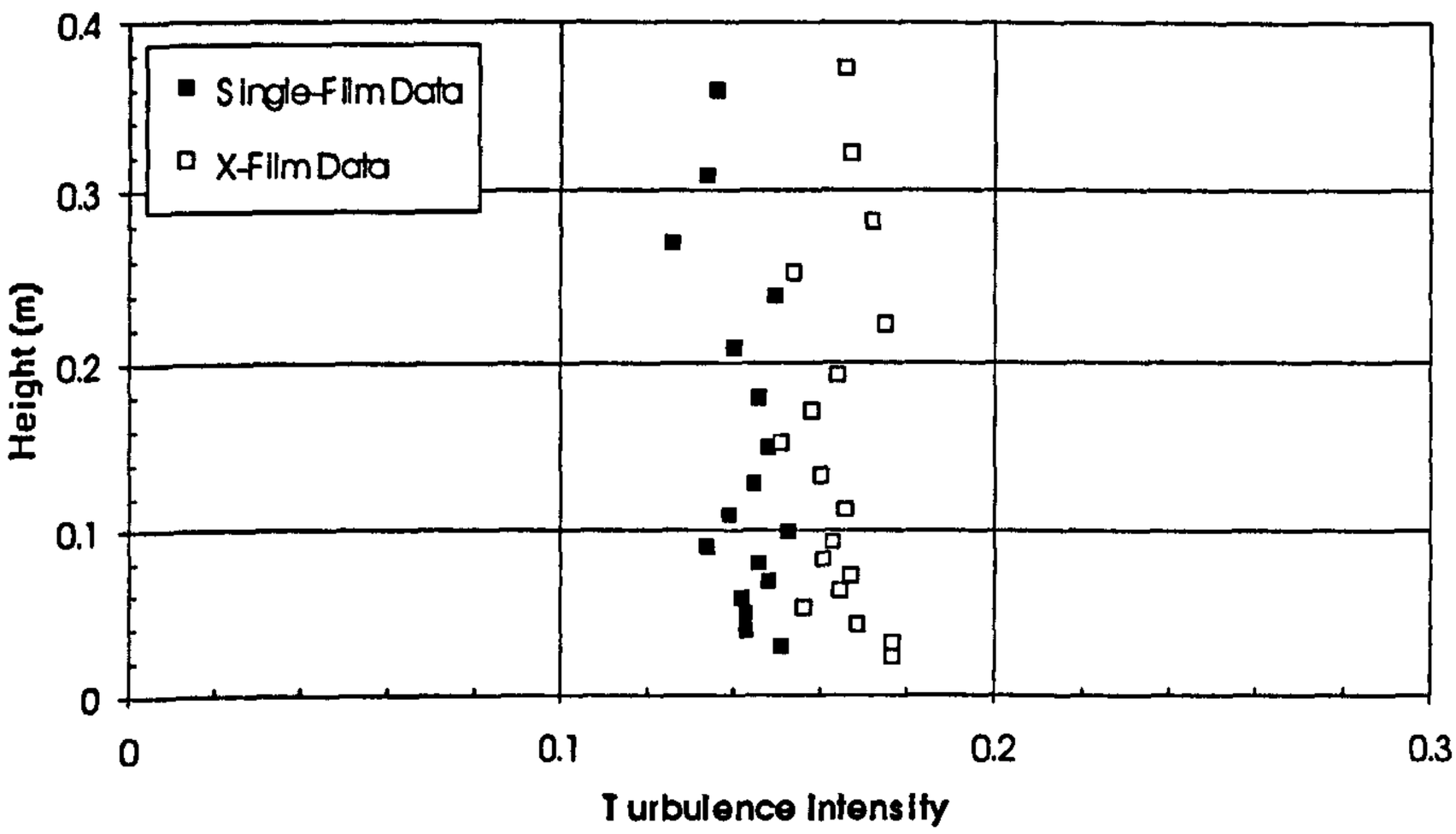

Figure 5.2 Turbulence intensity profiles for flat water (no generated waves) at X=-1265mm for: a) Offshore winds b) Onshore winds

a)

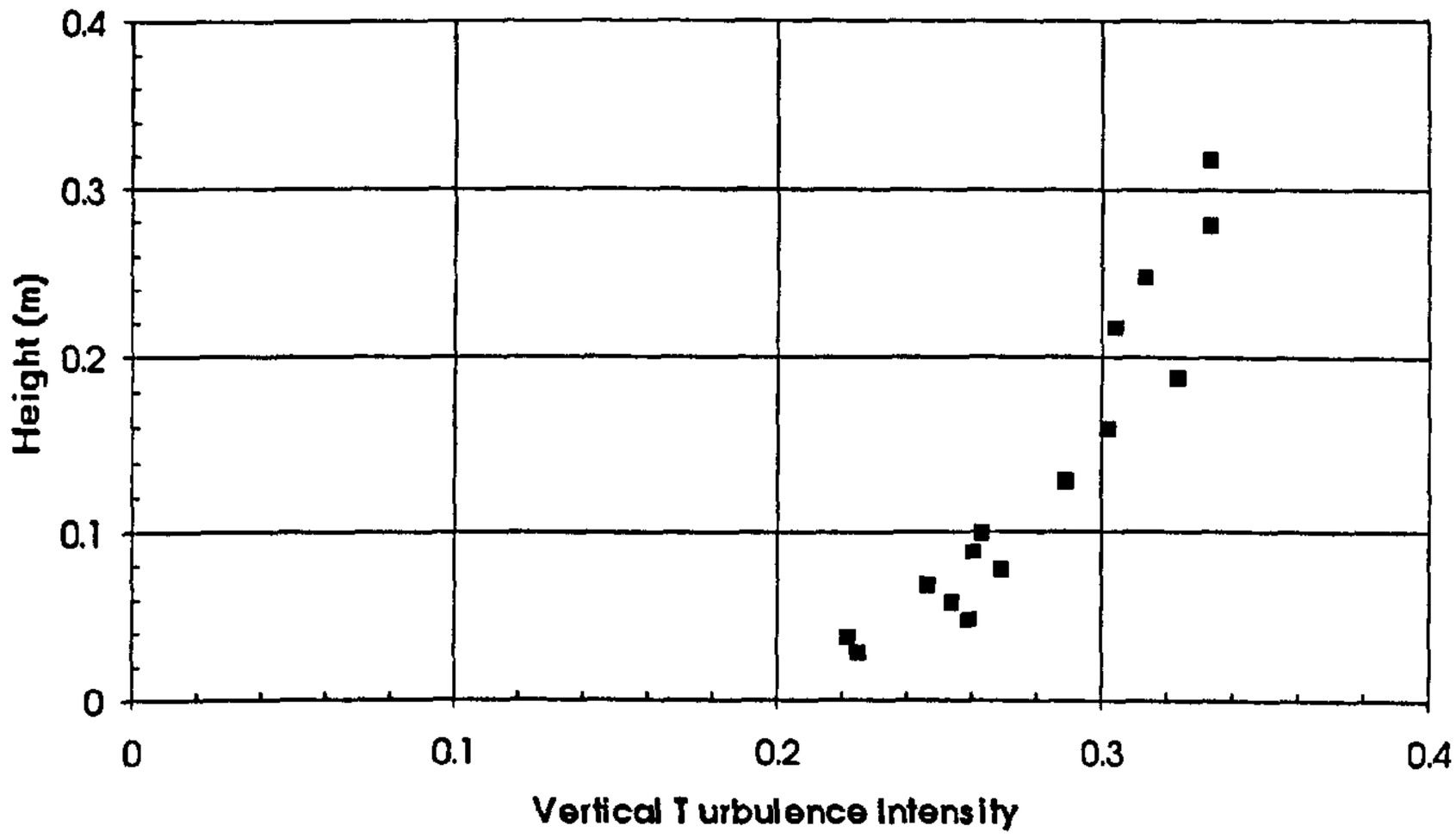

b)

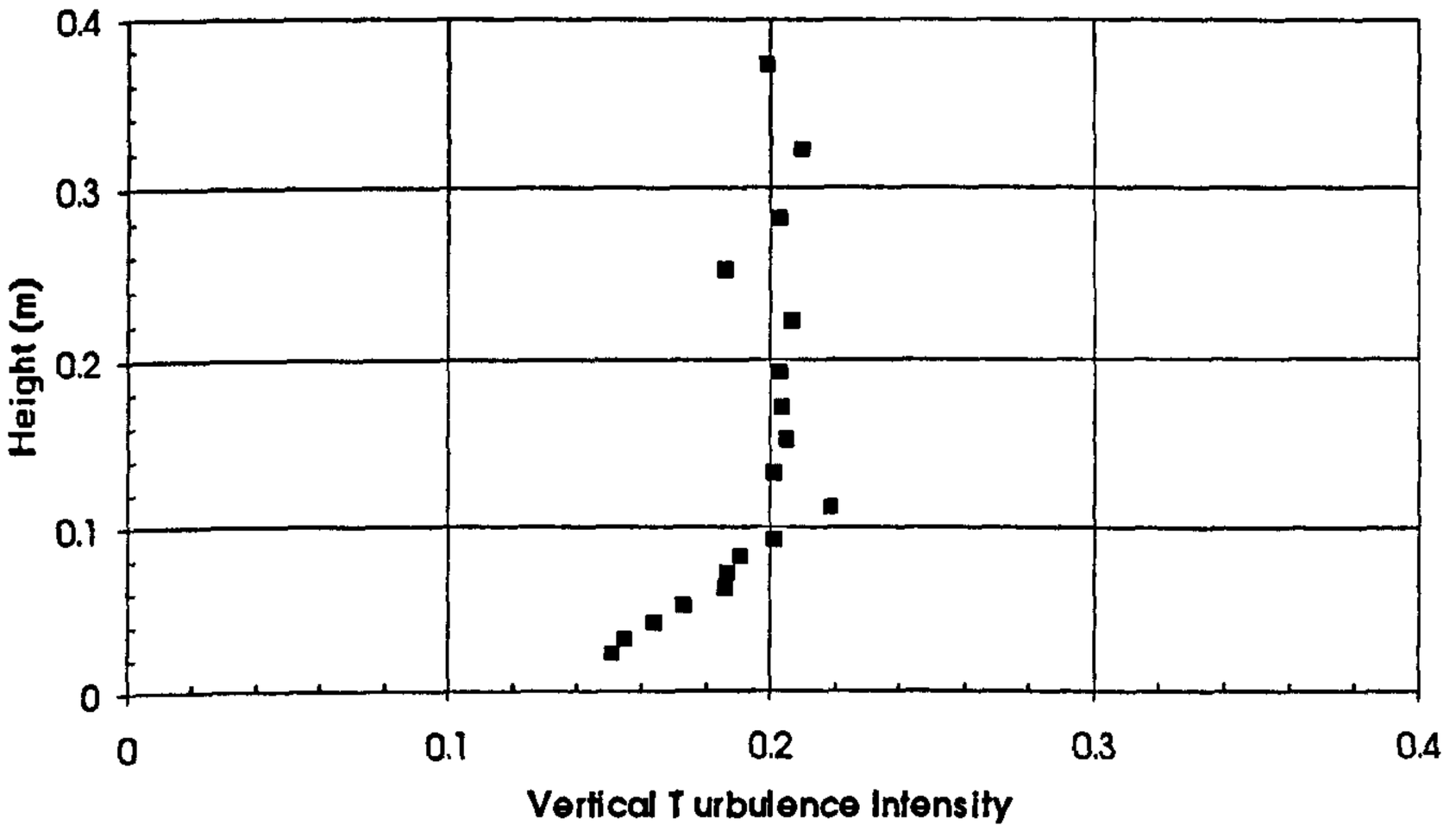

Figure 5.3 Turbulence intensity profiles for the vertical component of velocity over flat water (no generated waves) at X=-1265mm for: a) Offshore winds b) Onshore winds

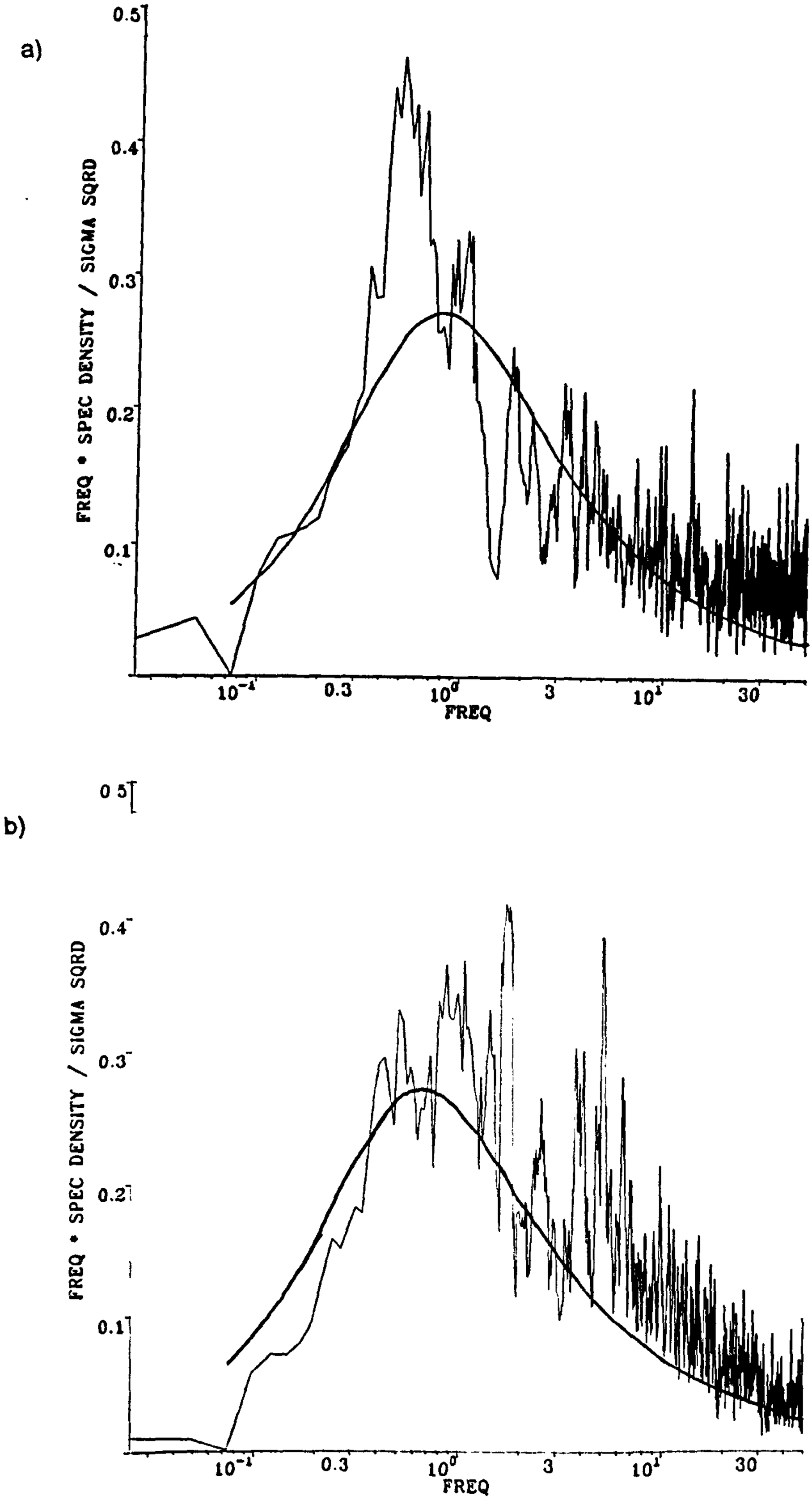

Figure 5.4 Non-dimensional frequency spectra for the U-component of velocity at X=-1265mm at H_{ref}: a) Offshore winds b) Onshore winds. Smooth line is Von Karman spectrum for ${}^{x}L_{u}$=0.2m.

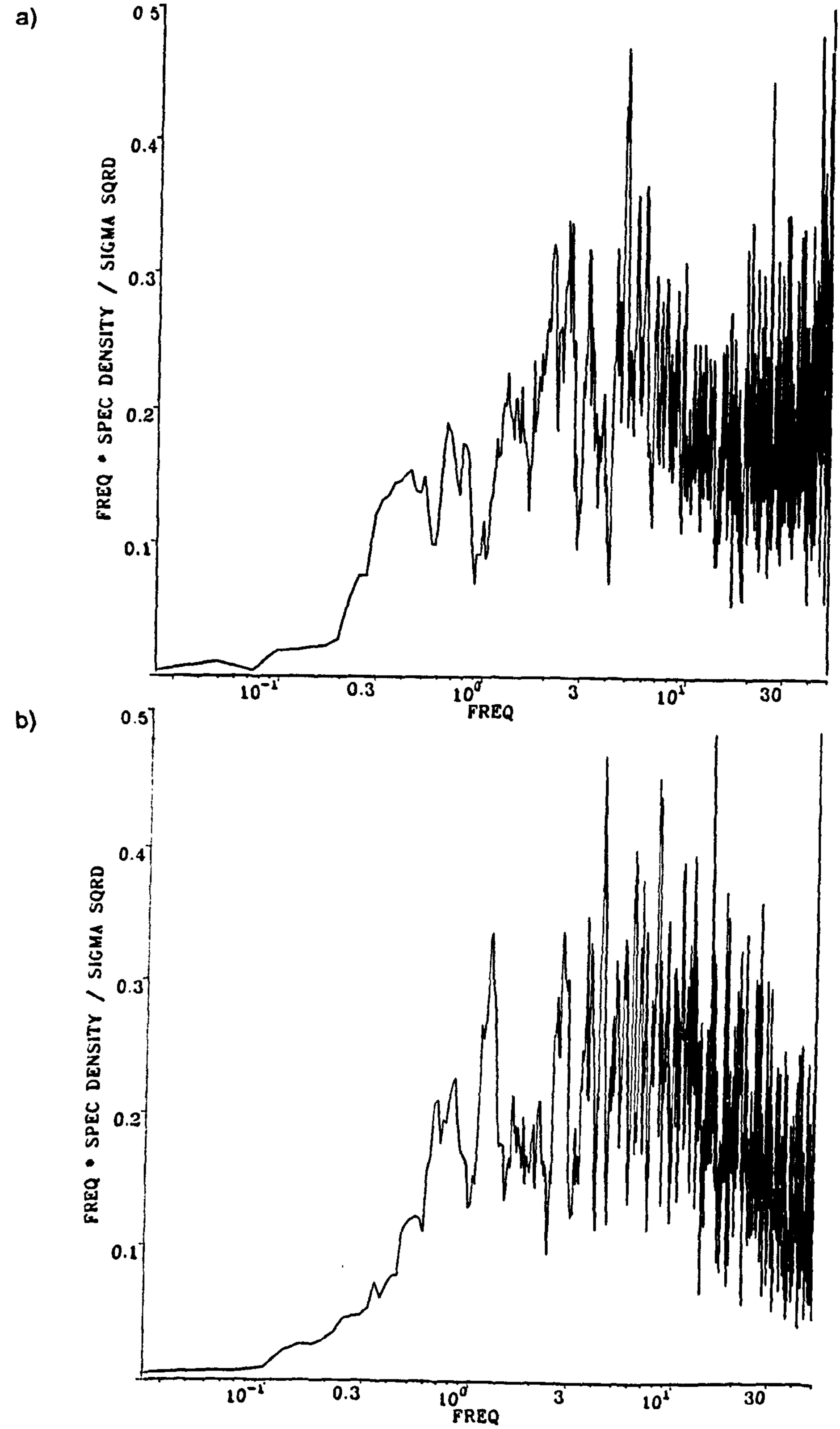

Figure 5.5 Non-dimensional frequency spectra for the V-component of velocity at X=-1265mm at H_{ref}: a) Offshore winds b) Onshore winds

a)

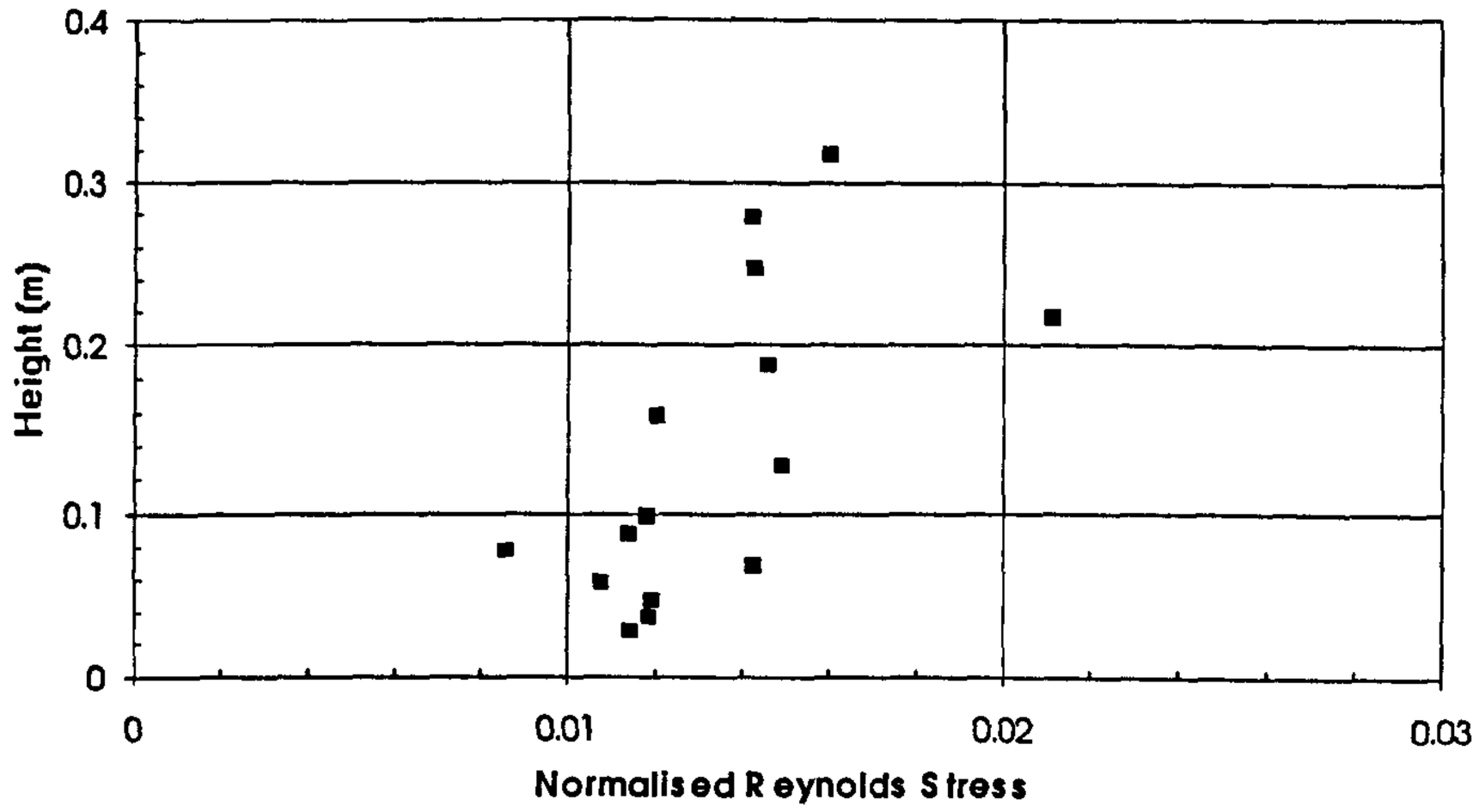

b)

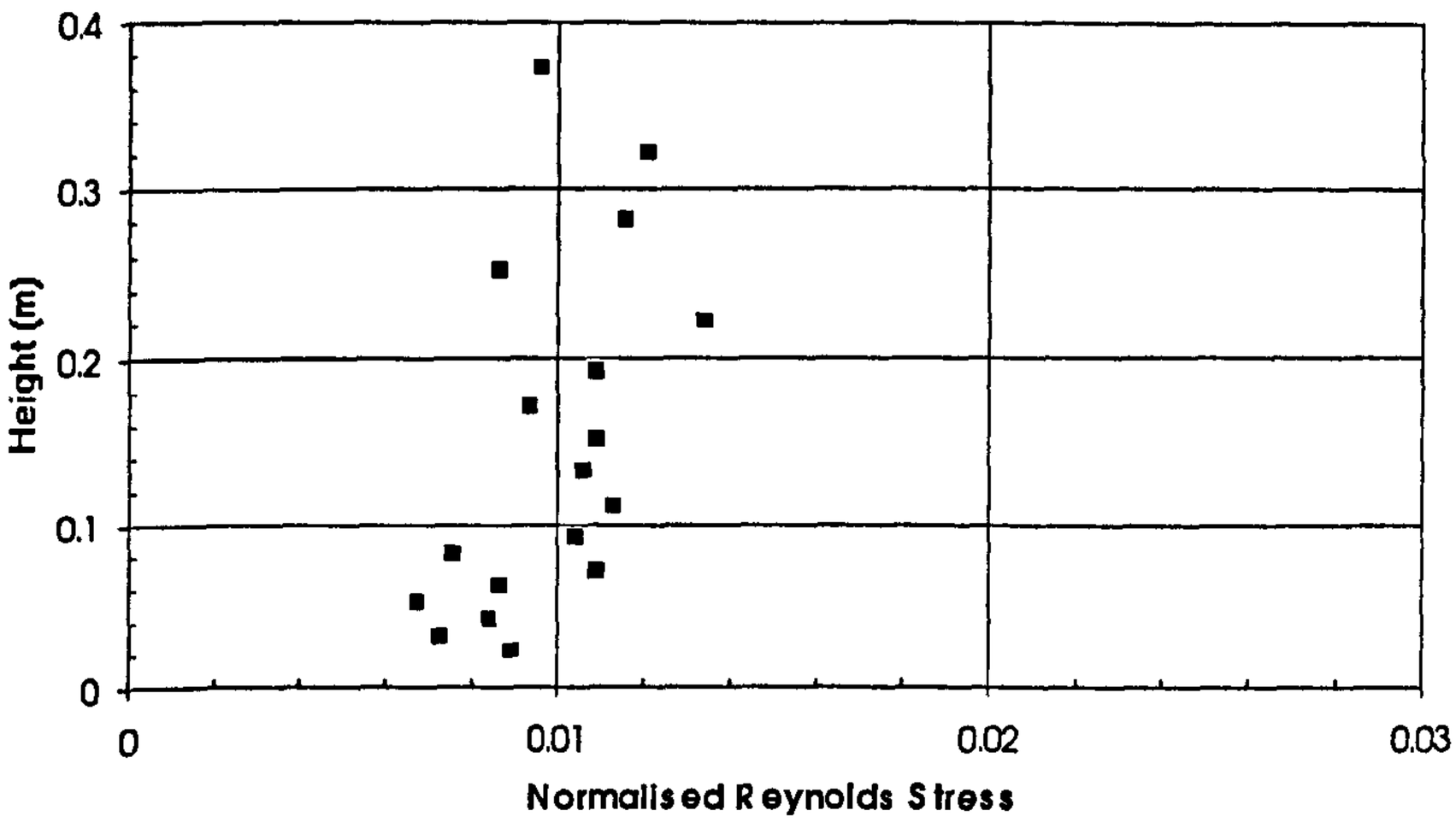

Figure 5.6 Normalised Reynolds stress profiles over flat water (no generated waves) at X=-1265mm for: a) Offshore winds b) Onshore winds

a)

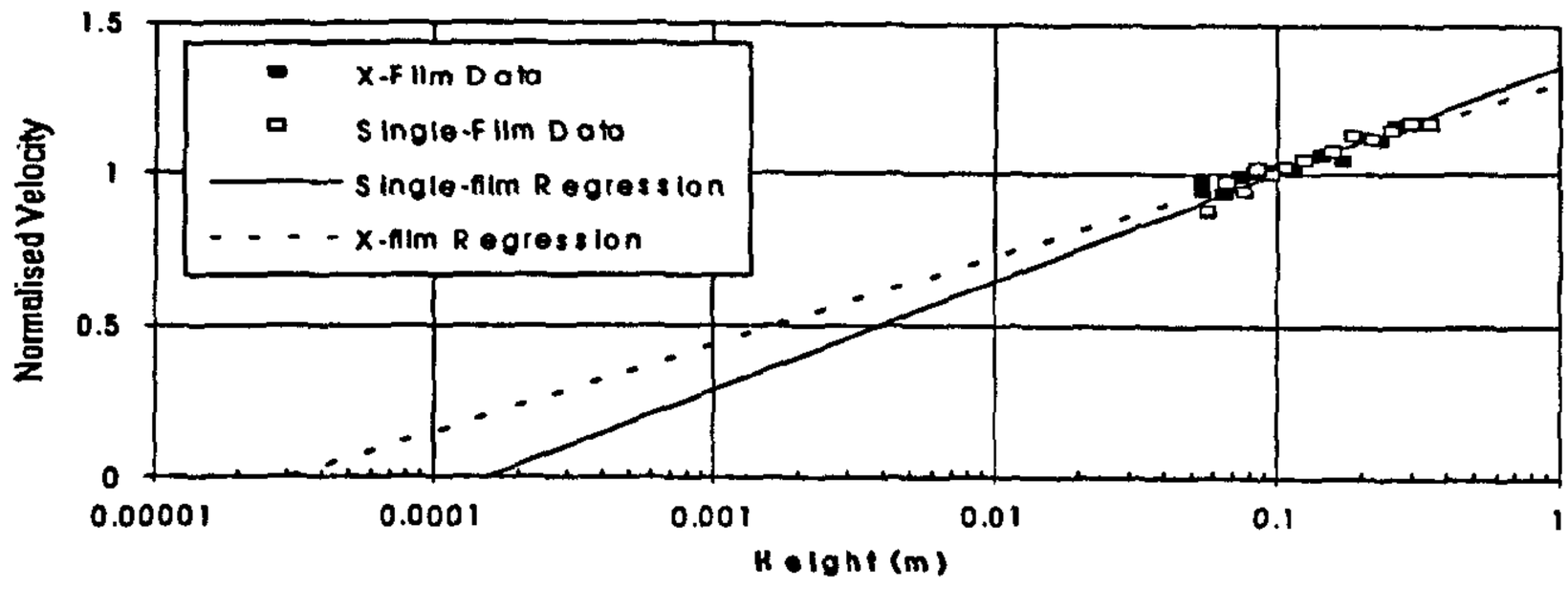

b)

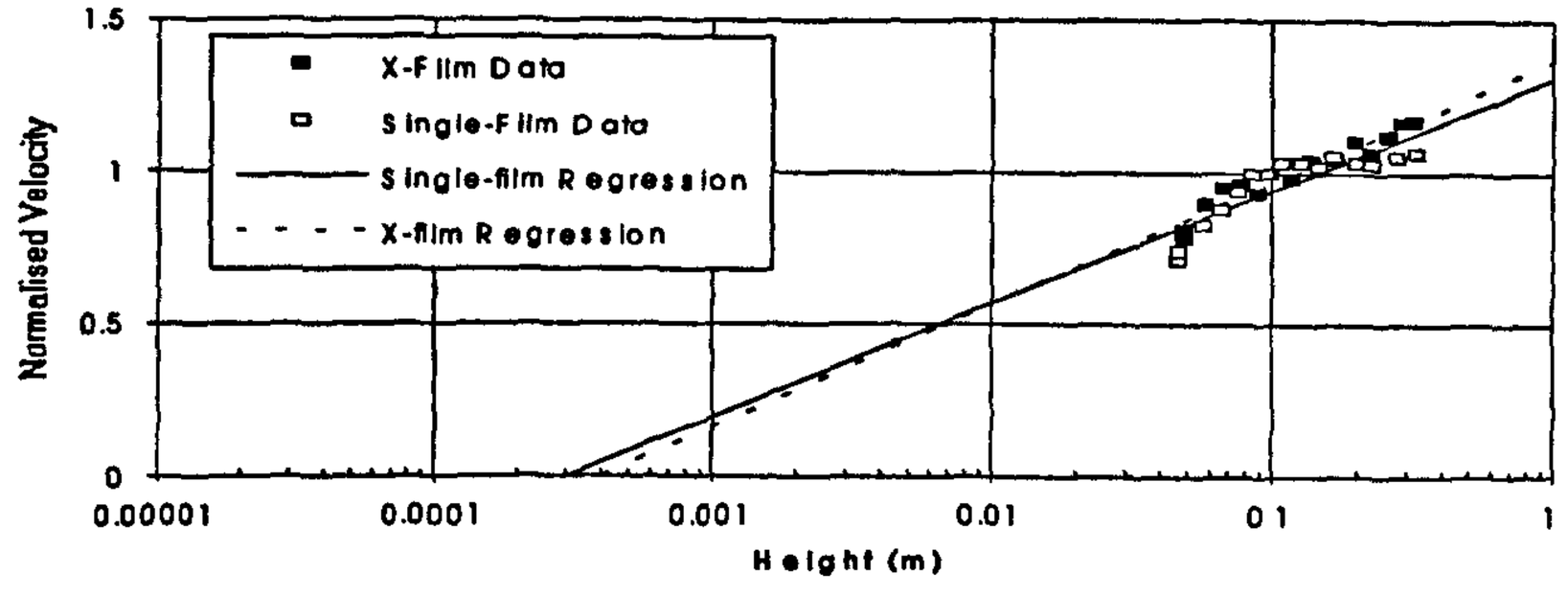

c)

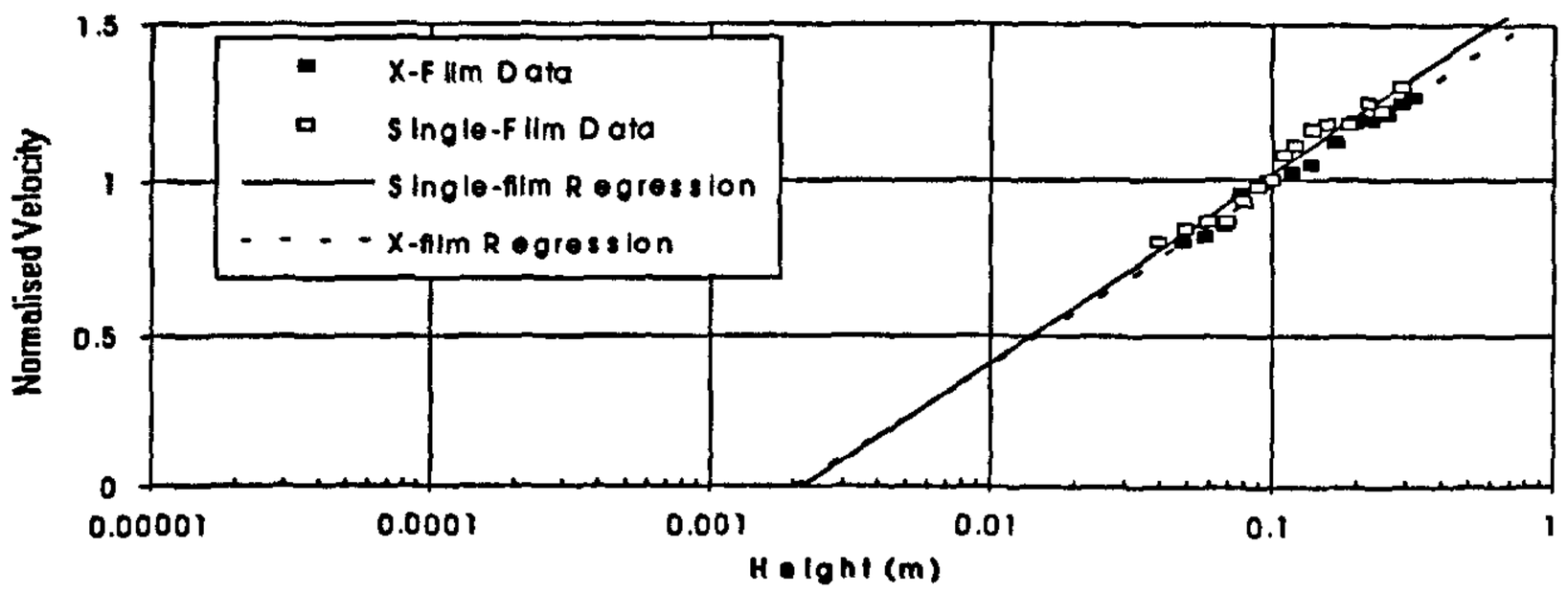

d)

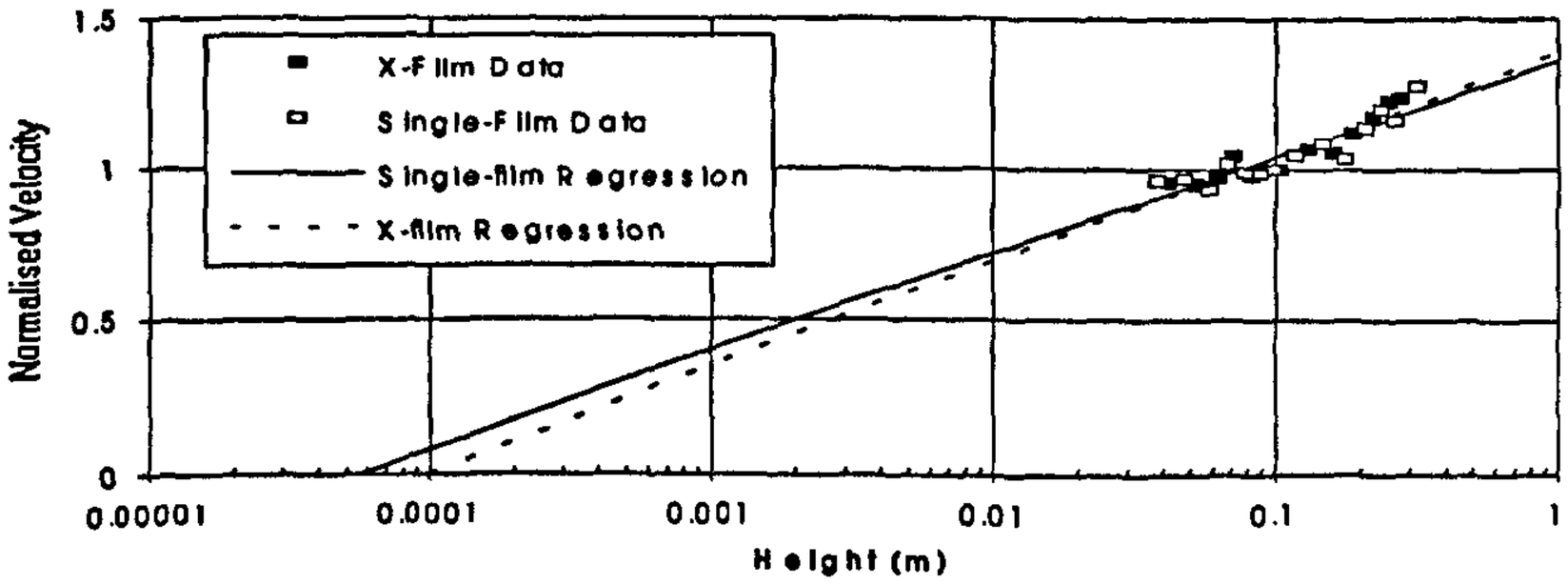

Figure 6.1 Semi-log velocity profiles for spilling waves under offshore winds:a) X=-912mm b) X=-1177mm c) X=-1575mm d) X=-2646mm

a)

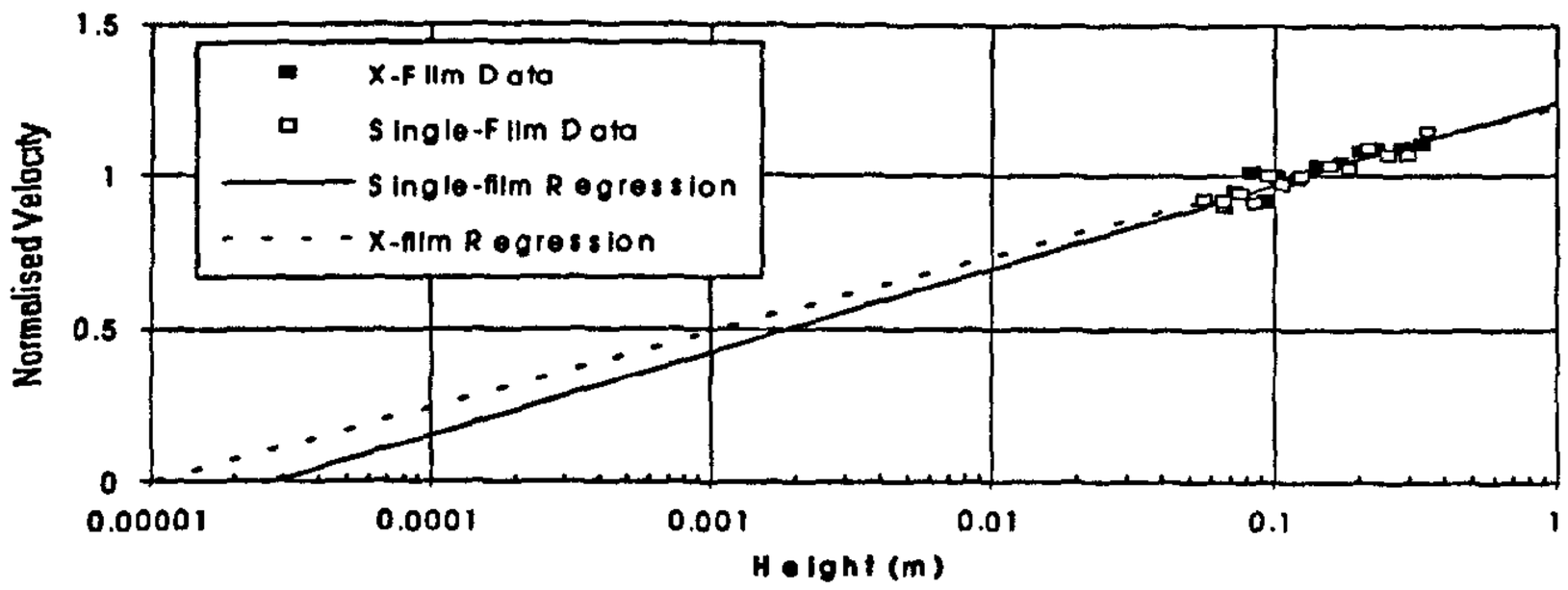

b)

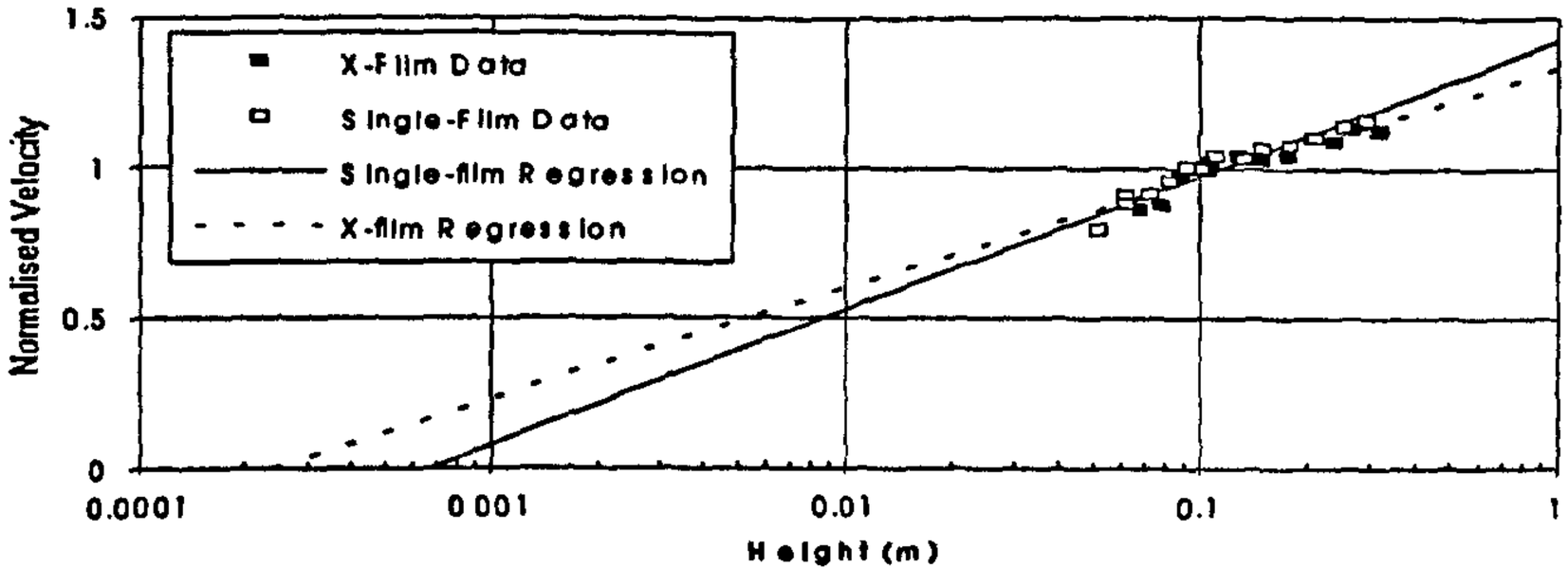

c)

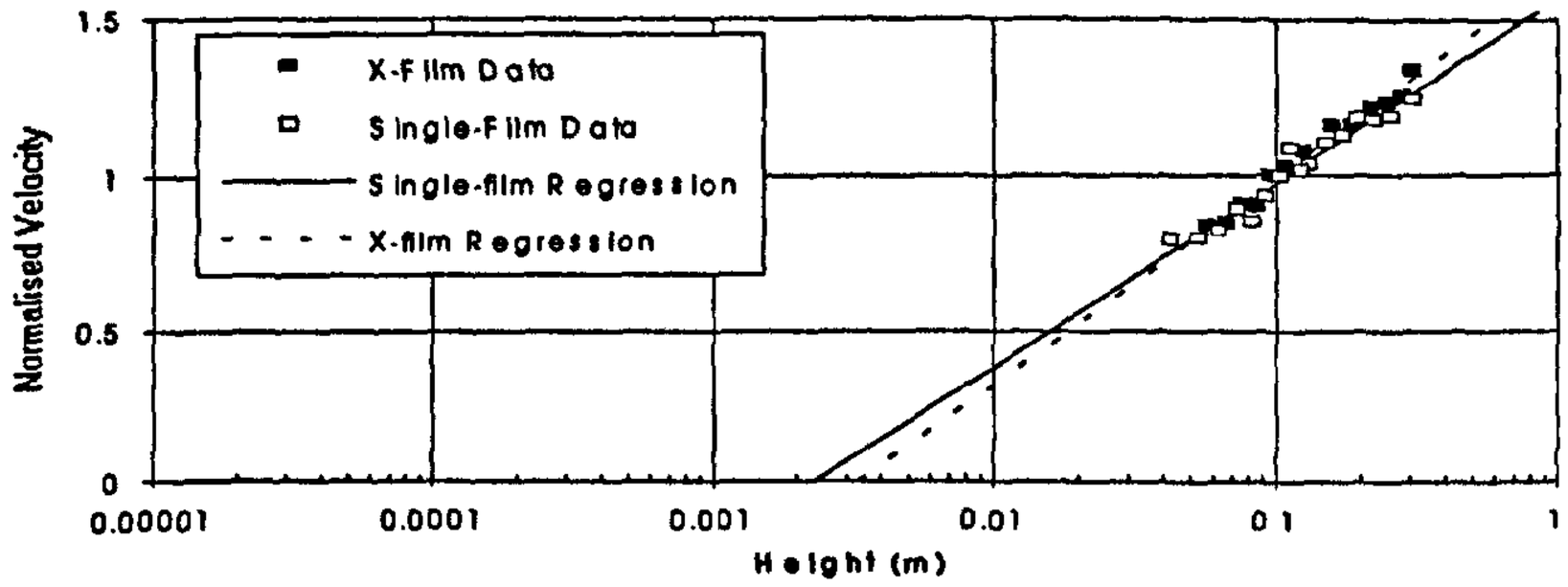

d)

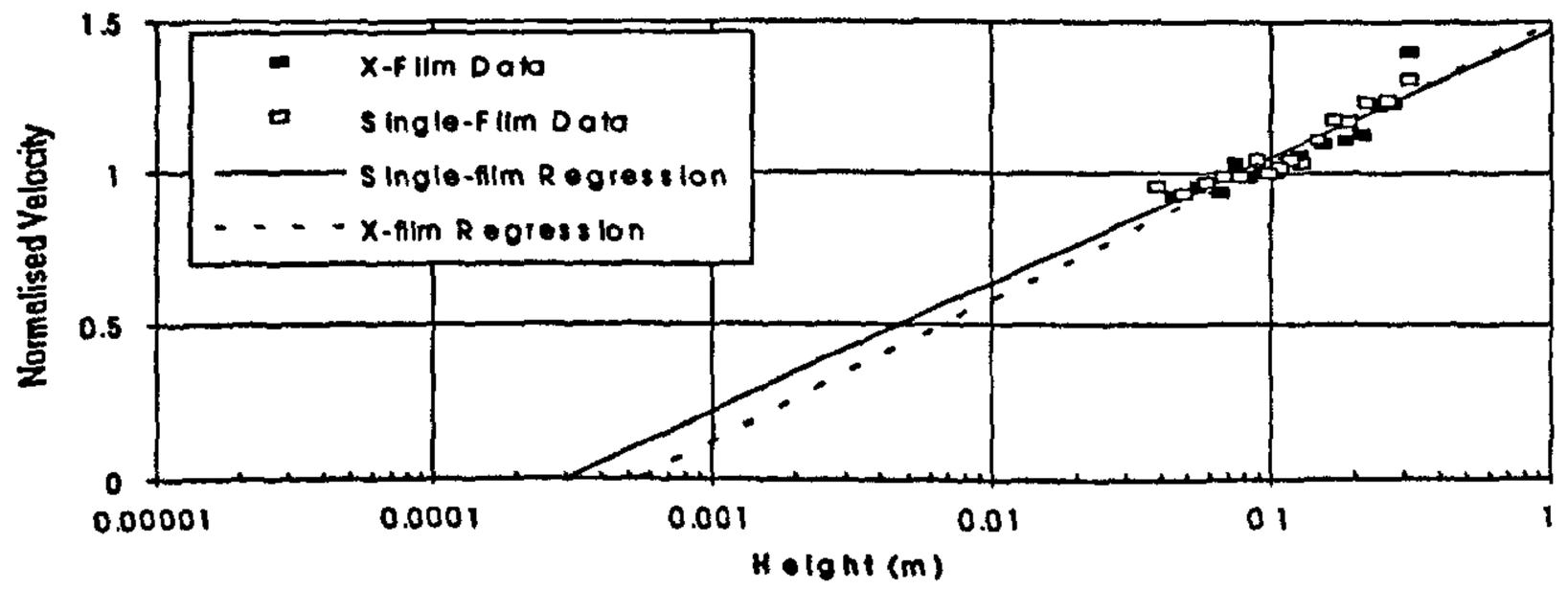

Figure 6.2 Semi-log velocity profiles for plunging waves under offshore winds: a) X=-912mm b) X=-1404mm c) X=-1811mm d) X=-2640mm

a)

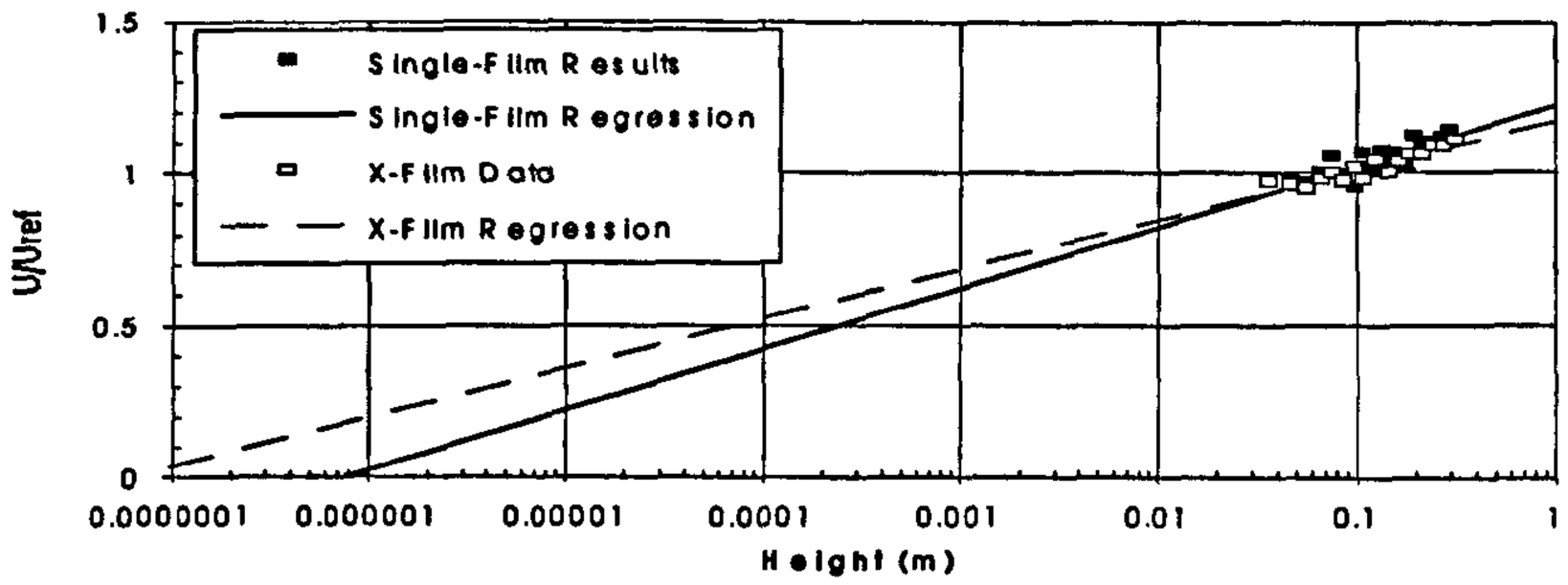

b)

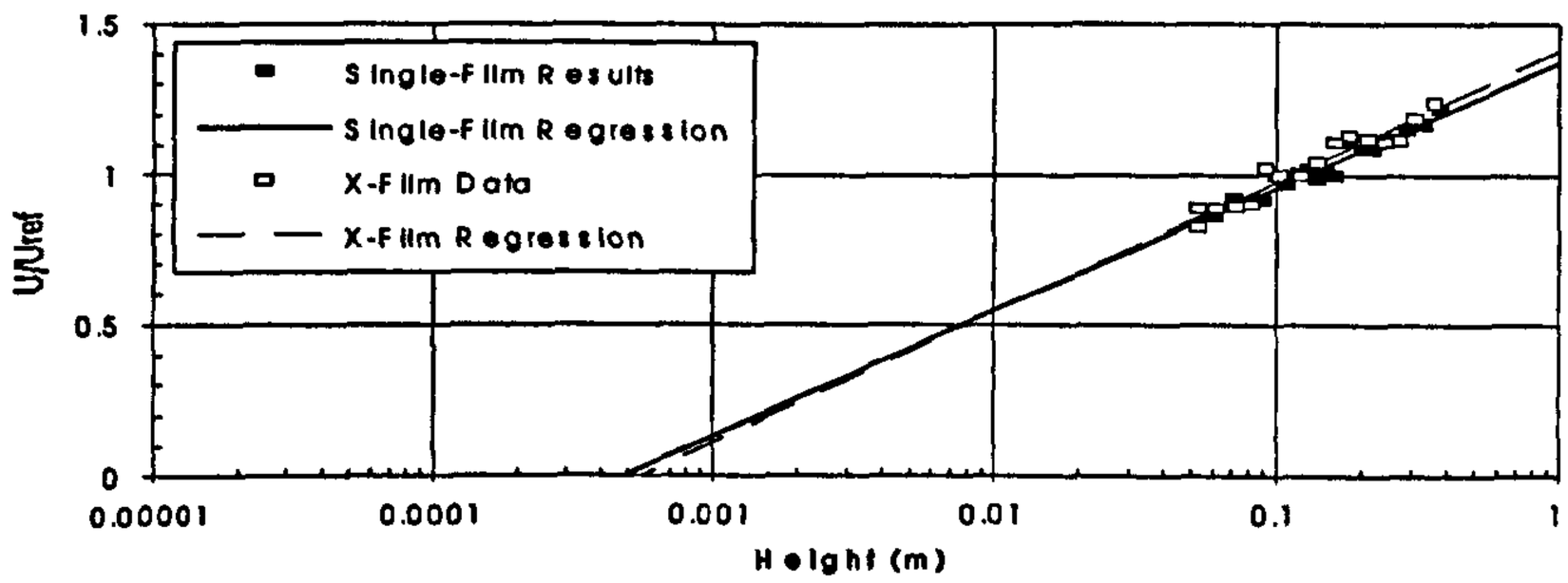

c)

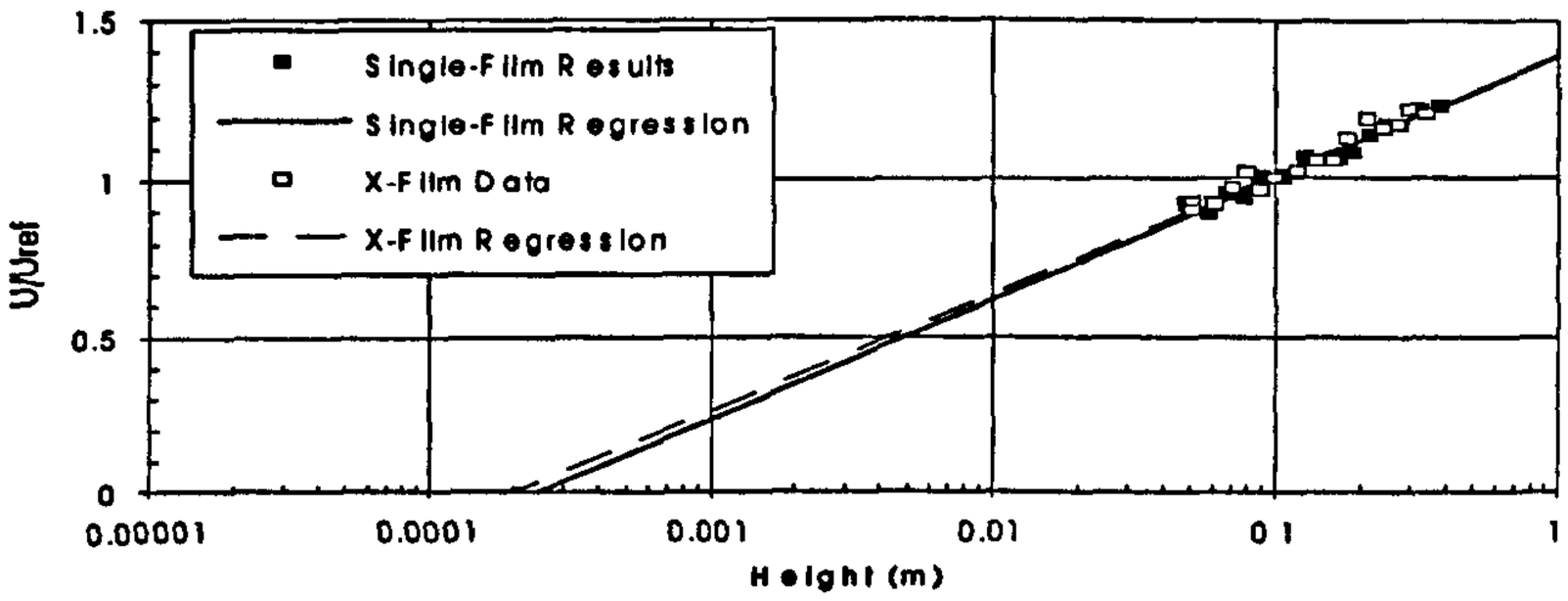

d)

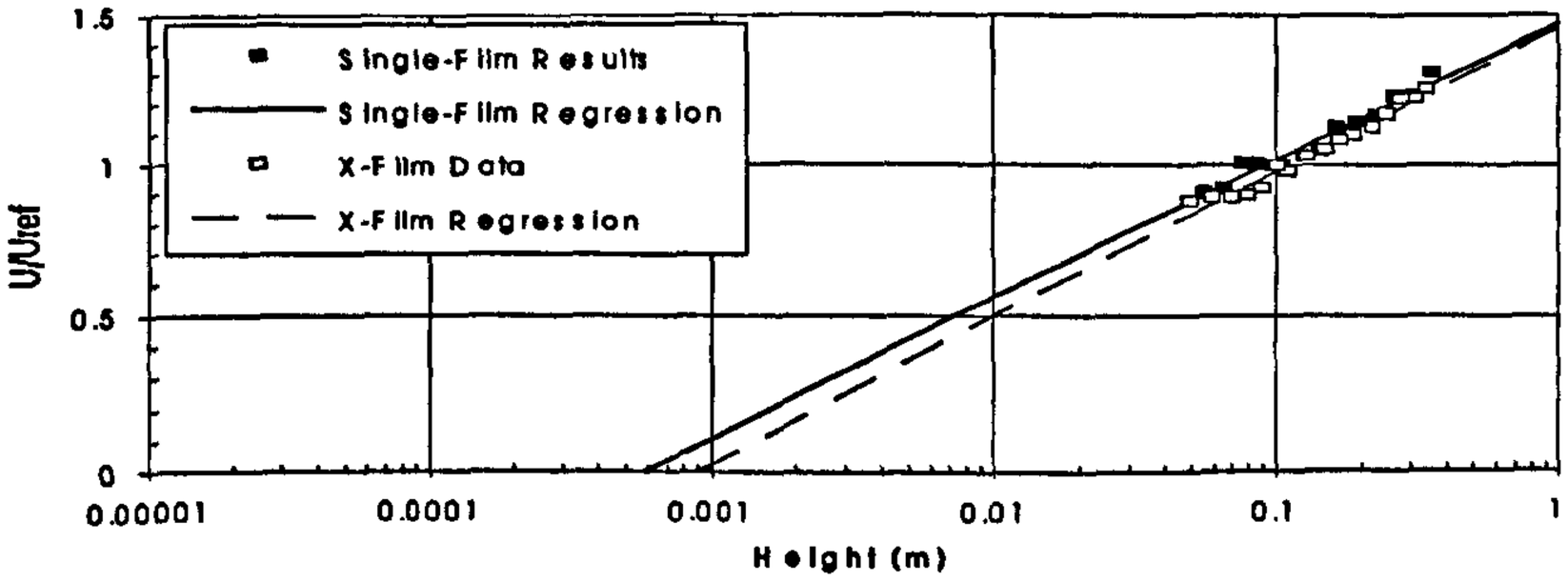

Figure 6.3 Semi-log velocity profiles for spilling waves under onshore winds: a) X=100mm b) X=-912mm c) X=-1554mm d) X=-1800mm

a)

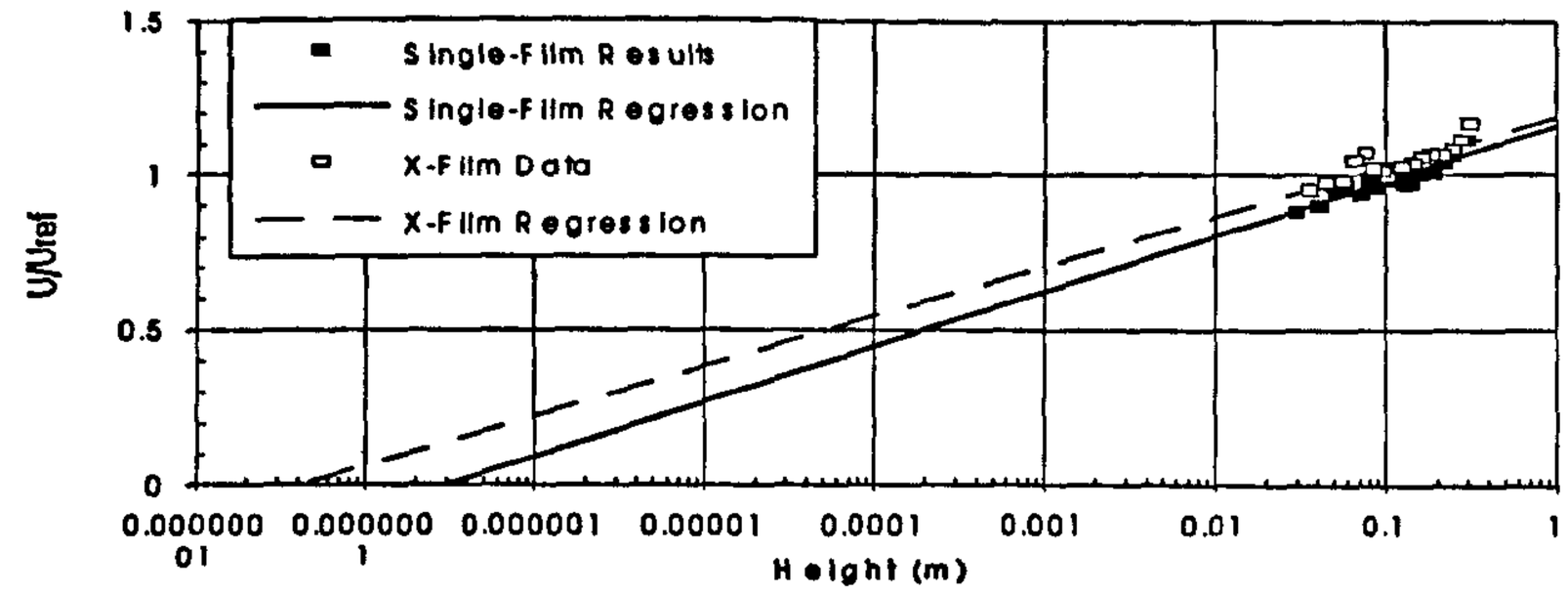

b)

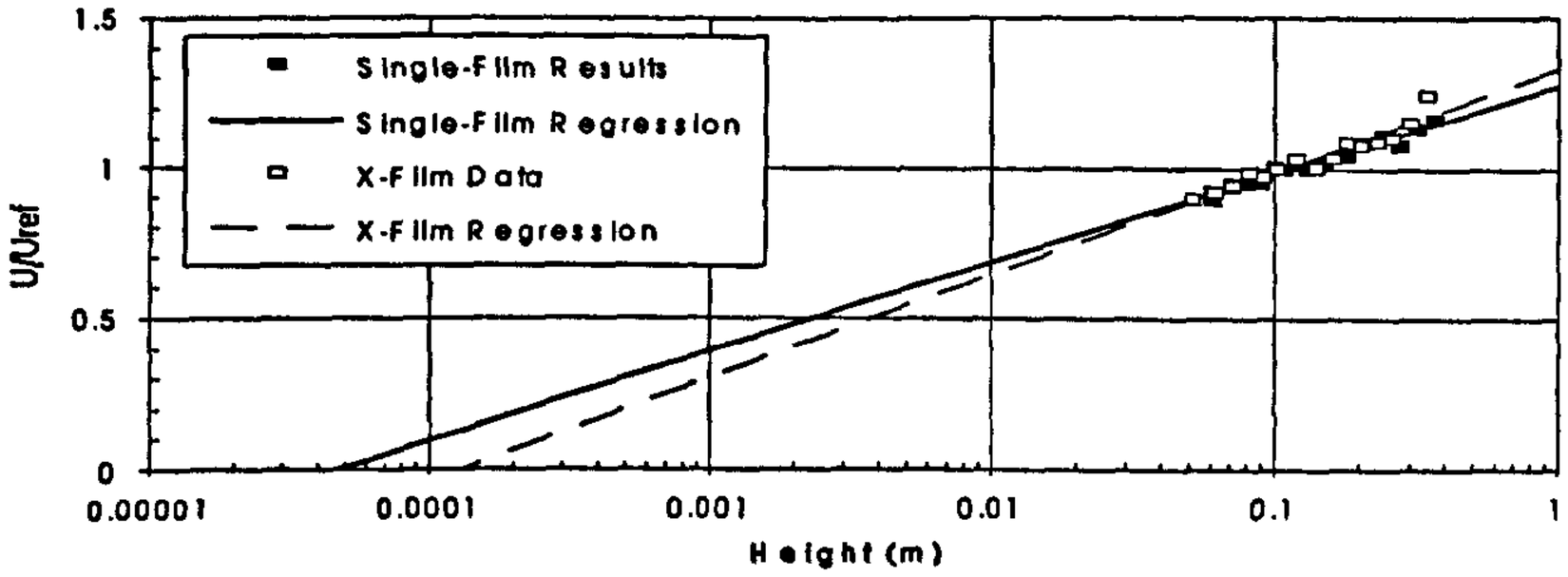

c)

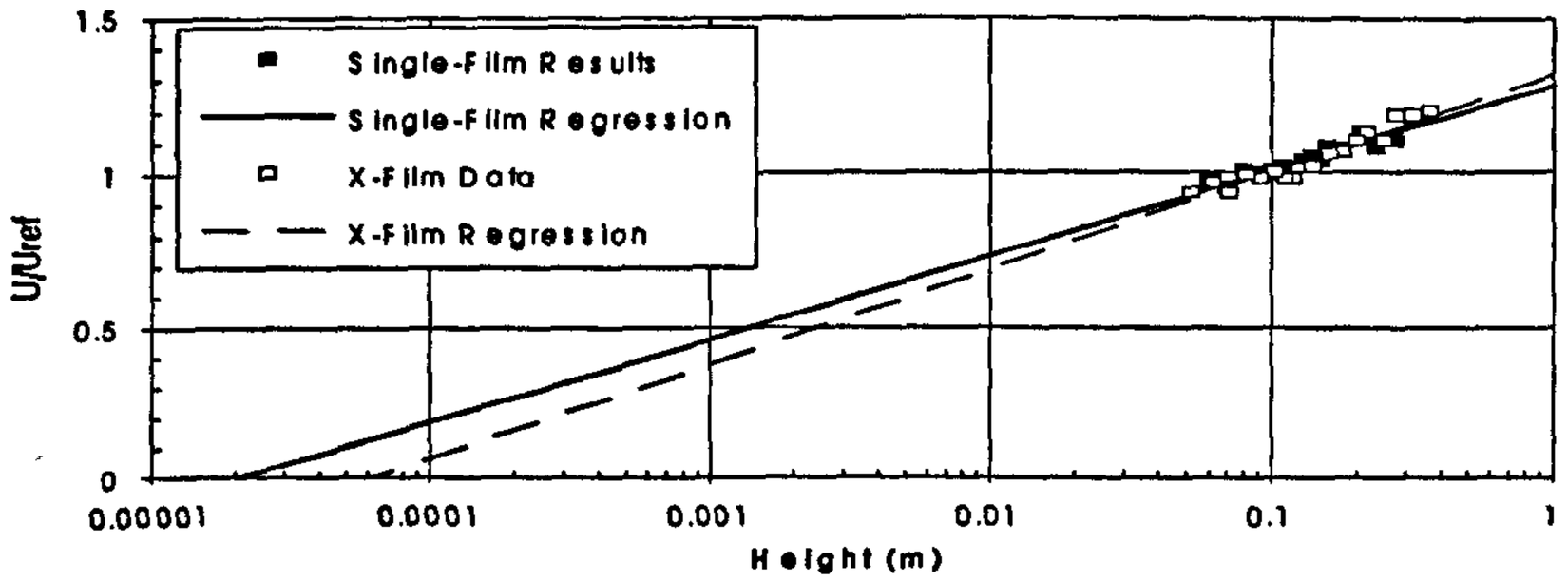

d)

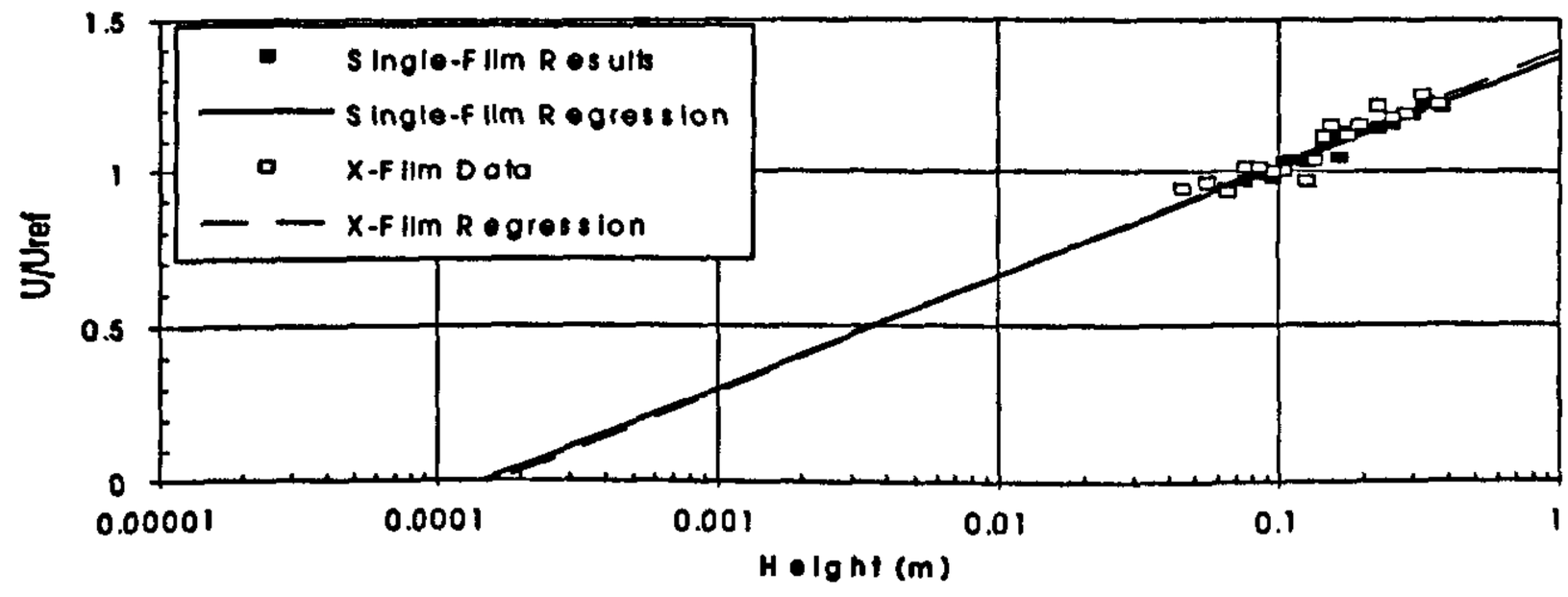

Figure 6.4 Semi-log velocity profiles for plunging waves under onshore winds: a) X=100mm b) X=-912mm c) X=-1289mm d) X=-1795mm

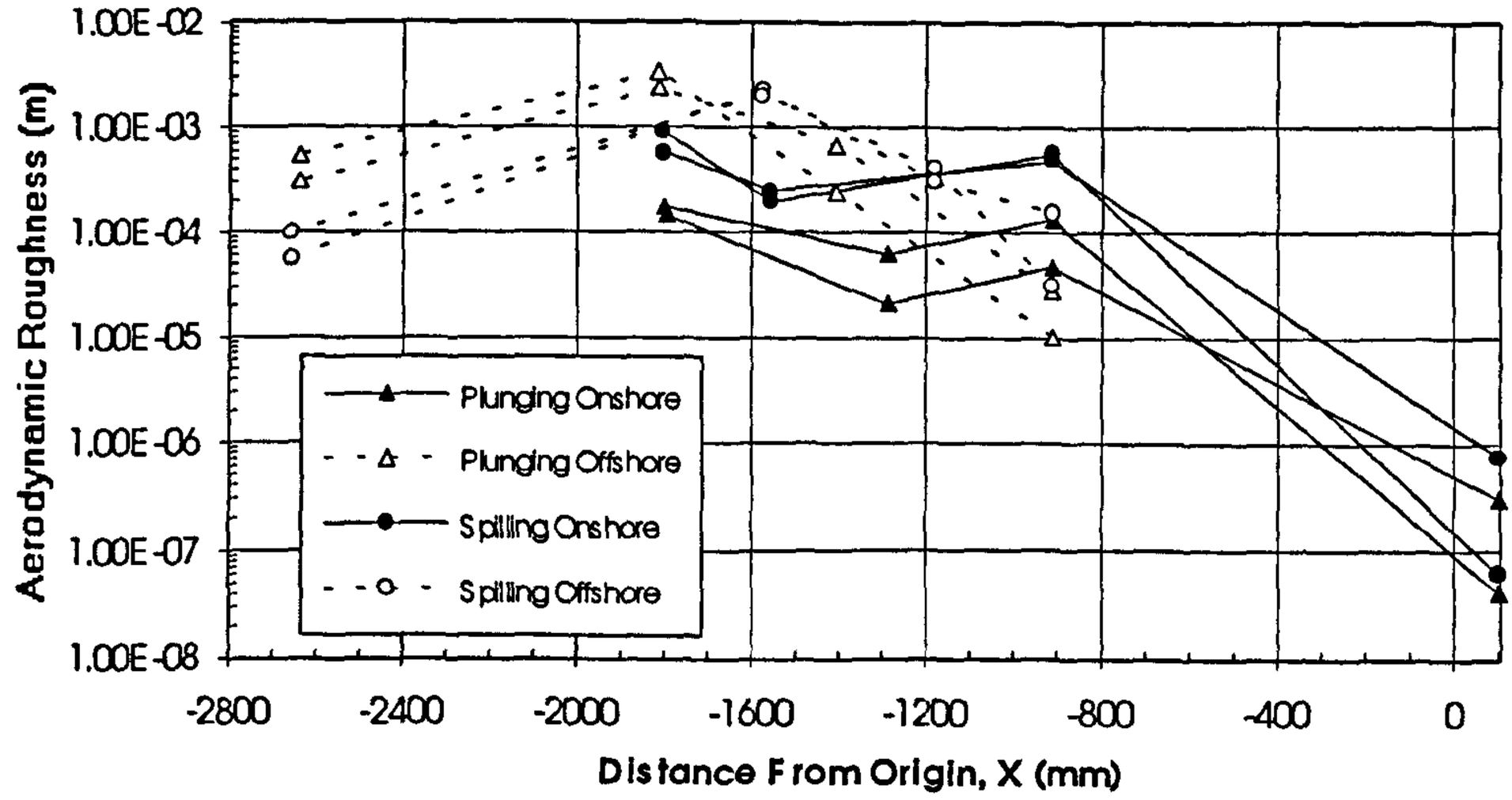

Figure 6.5. Aerodynamic roughness, z_o, over the waves for both onshore and offshore winds against offshore distance, X.

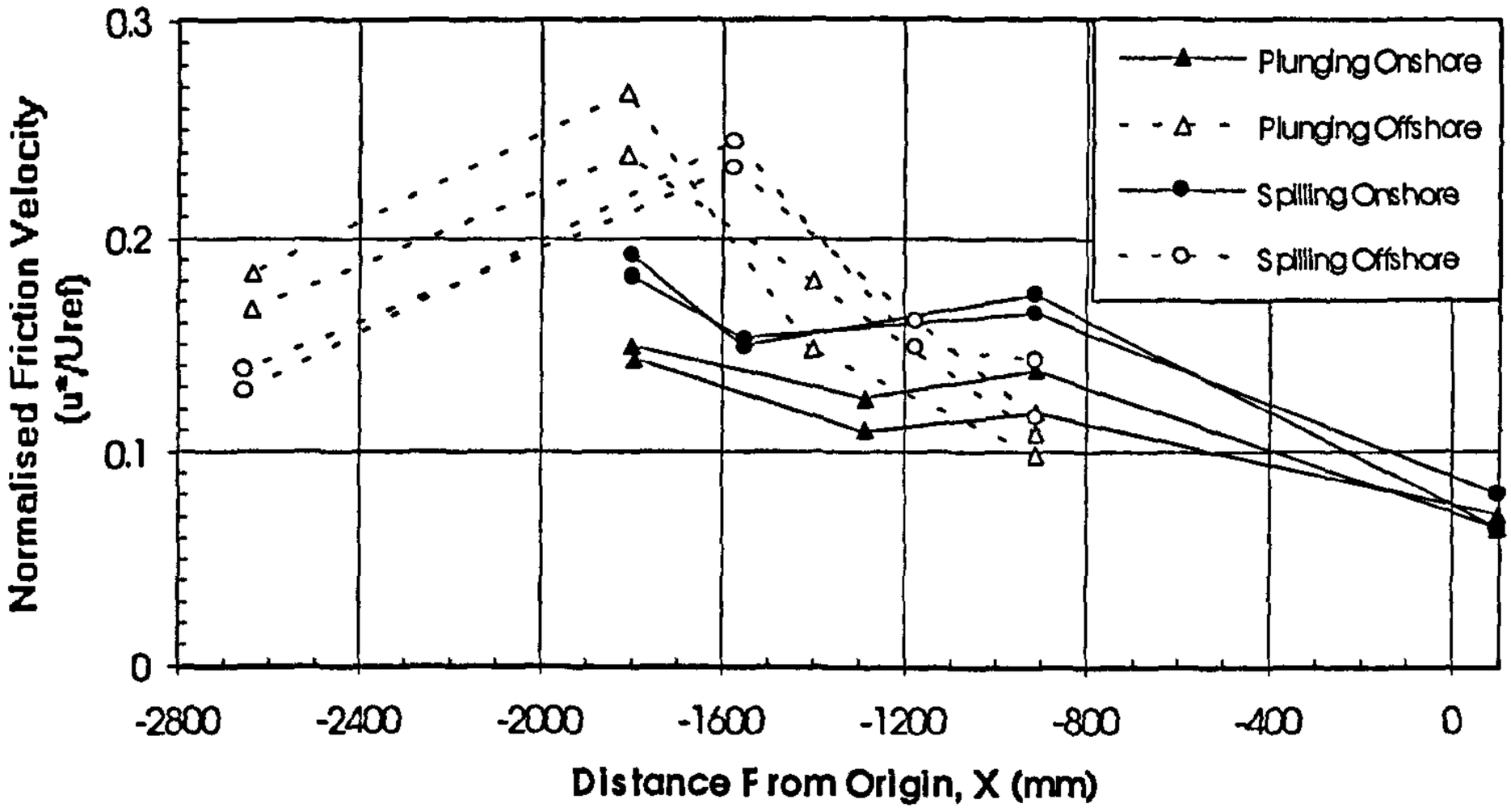

Figure 6.6 Normalised friction velocity over the waves for both onshore and offshore winds against offshore distance, X.

a)

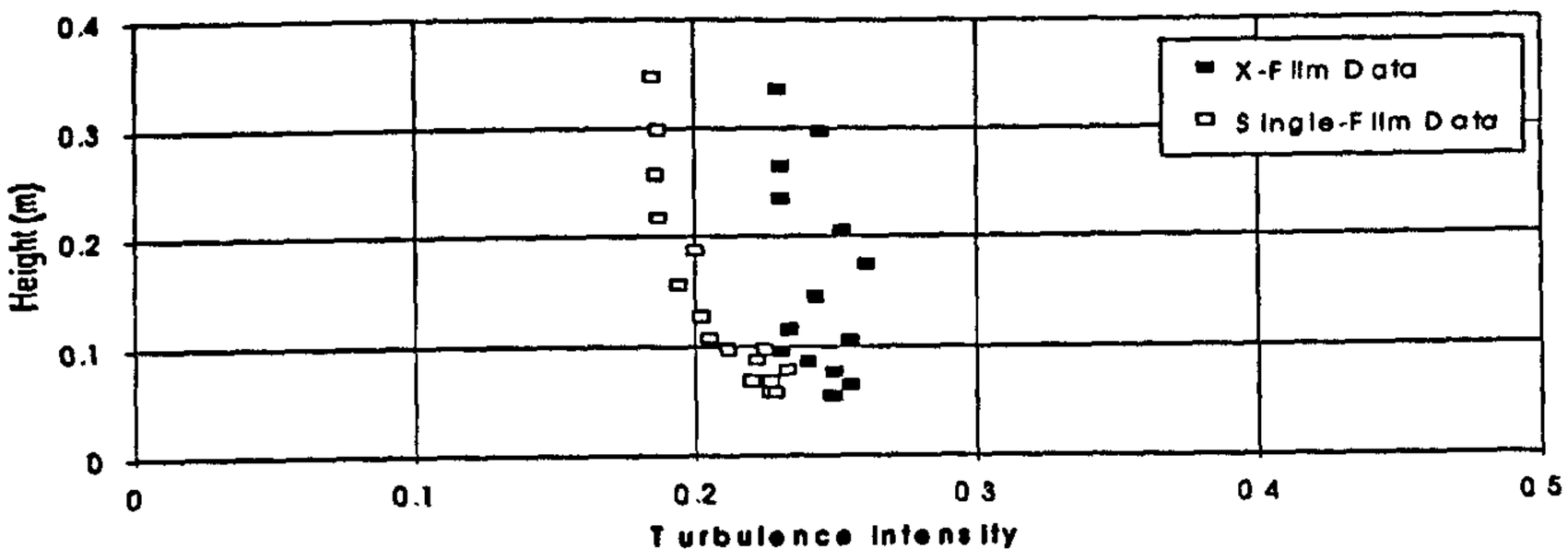

b)

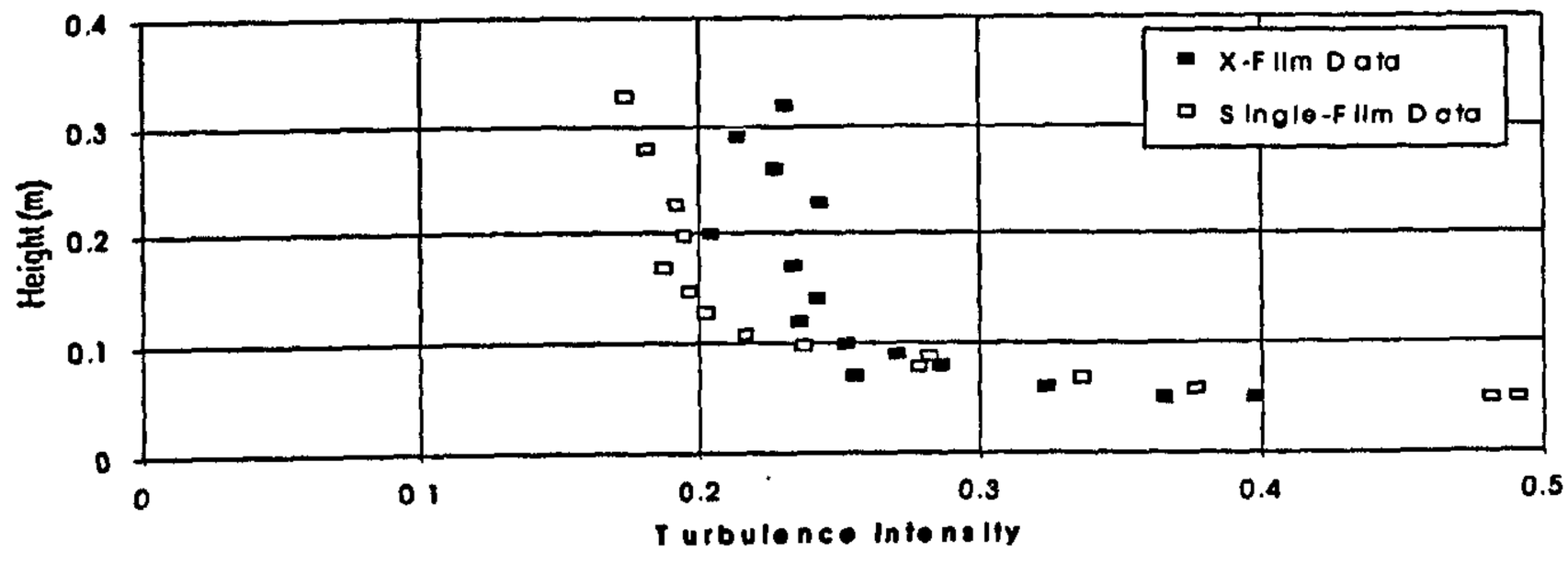

c)

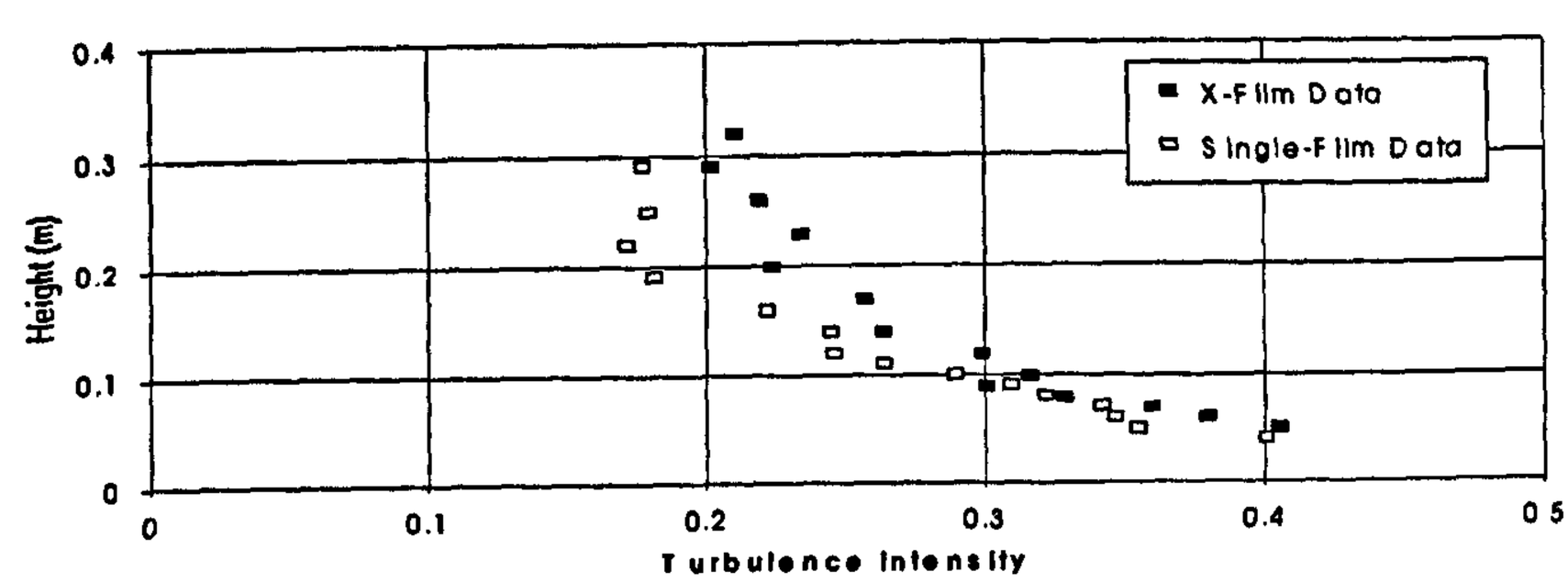

d)

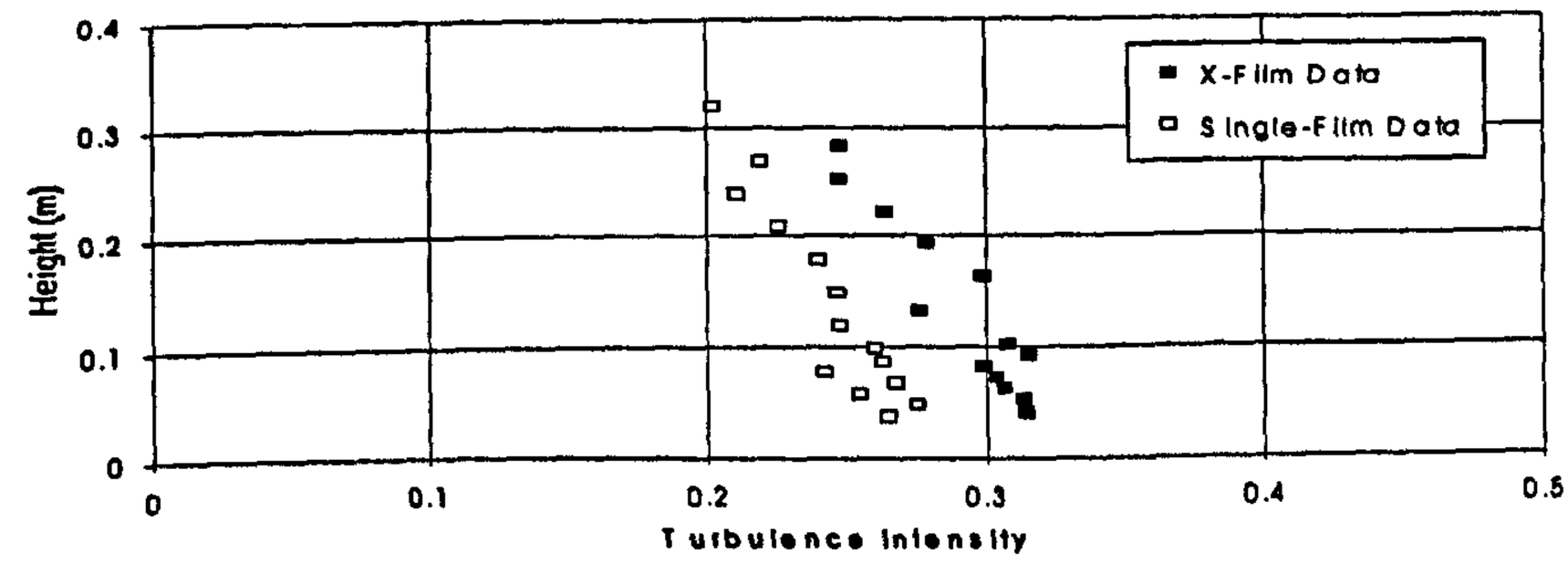

Figure 6.7 Turbulence intensity profiles for spilling waves under offshore winds: a) X=-912mm b) X=-1177mm c) X=-1575mm d) X=-2646mm

a)

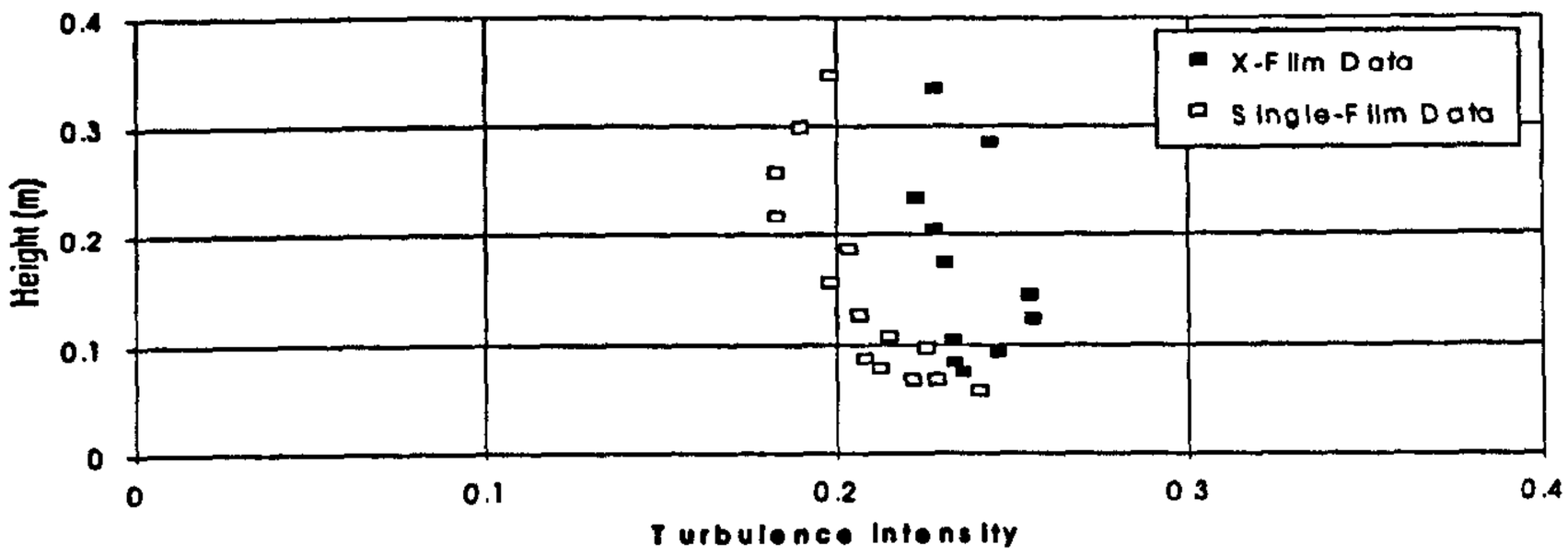

b)

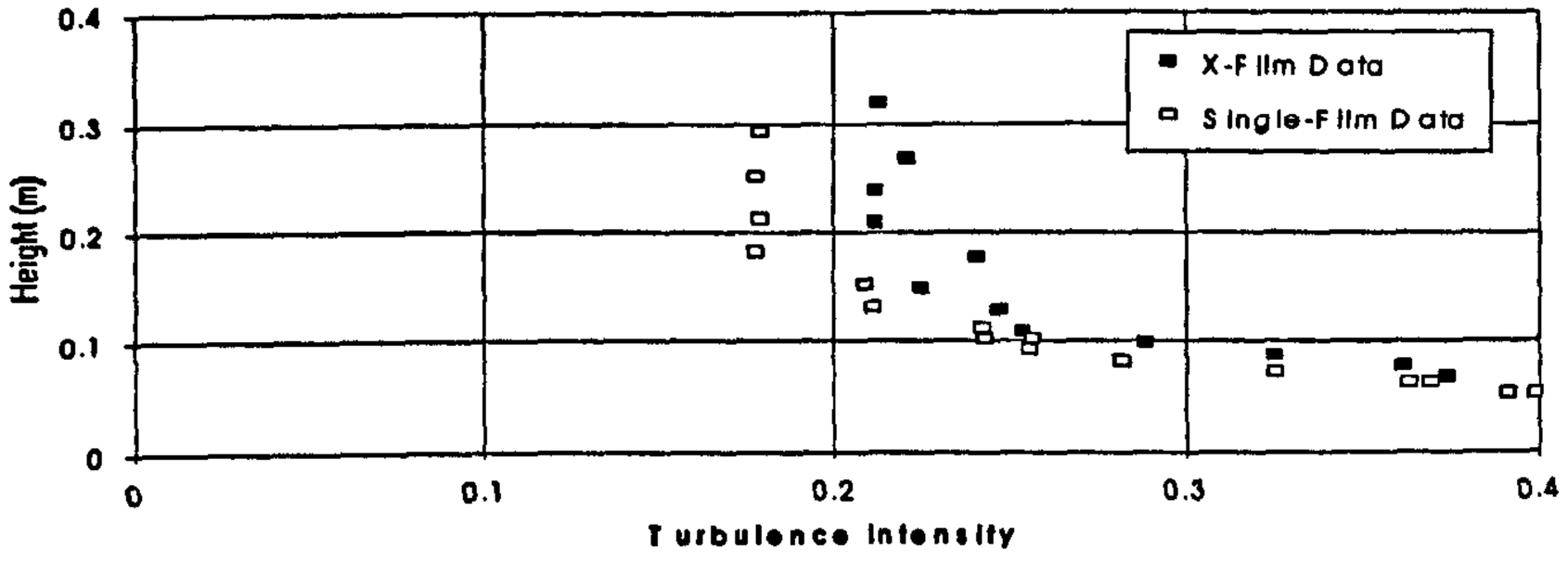

c)

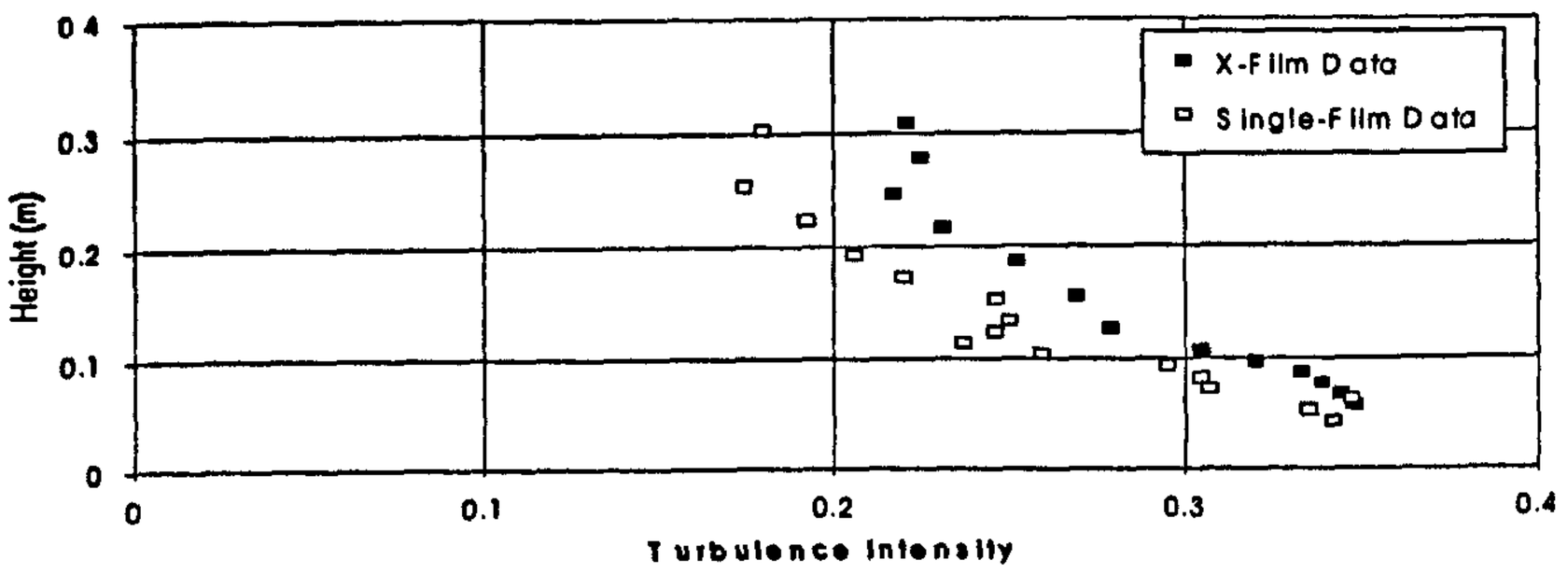

d)

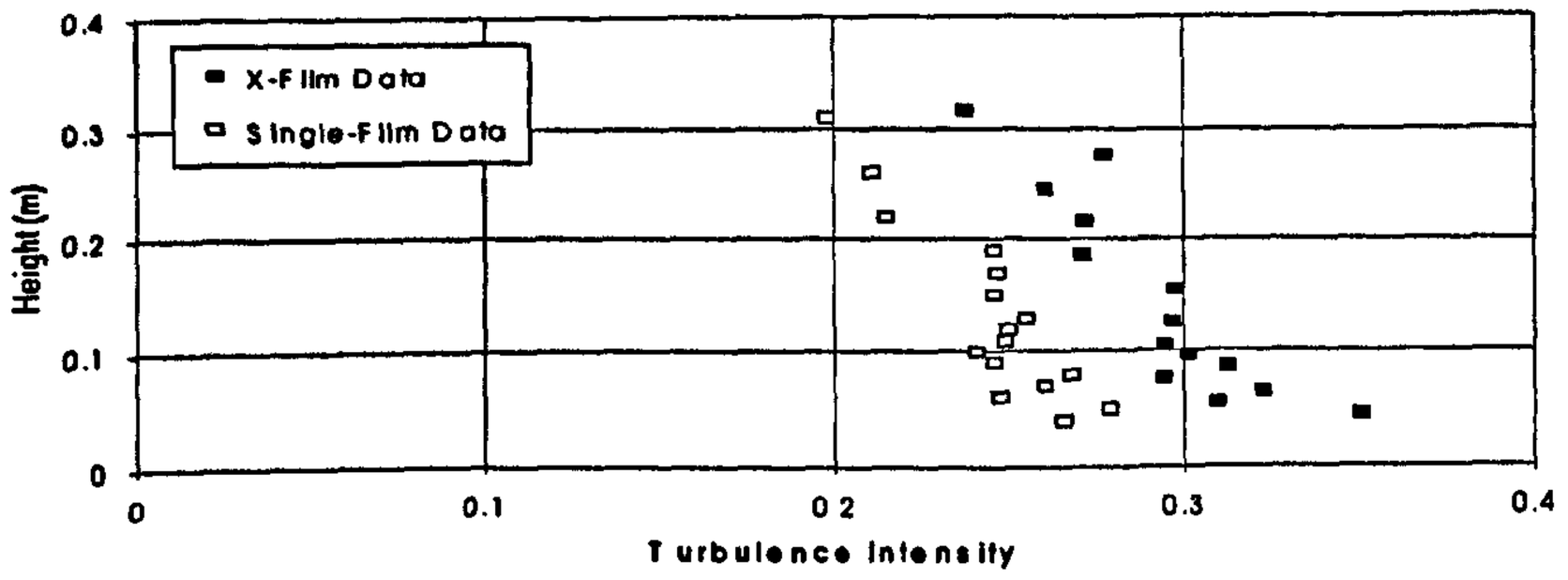

Figure 6.8 Turbulence intensity profiles for plunging waves under offshore winds: a) X=-912mm b) X=-1404mm c) X=-1811mm d) X=-2640mm

a)

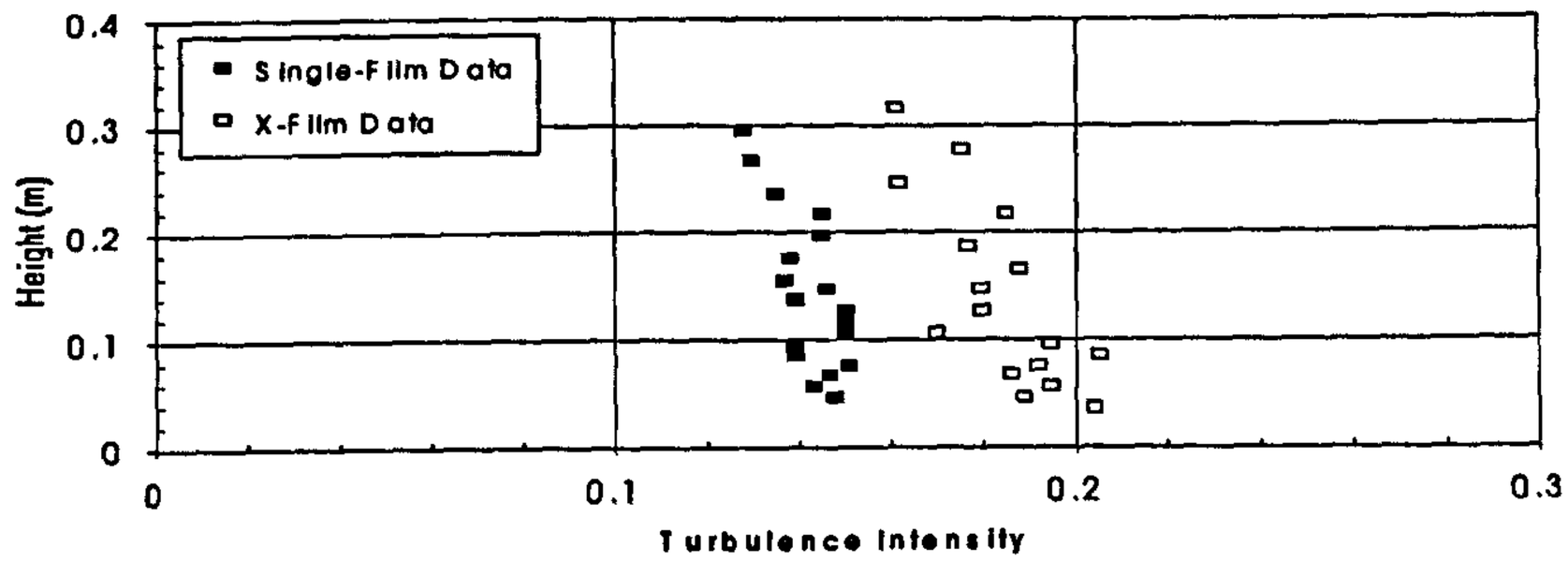

b)

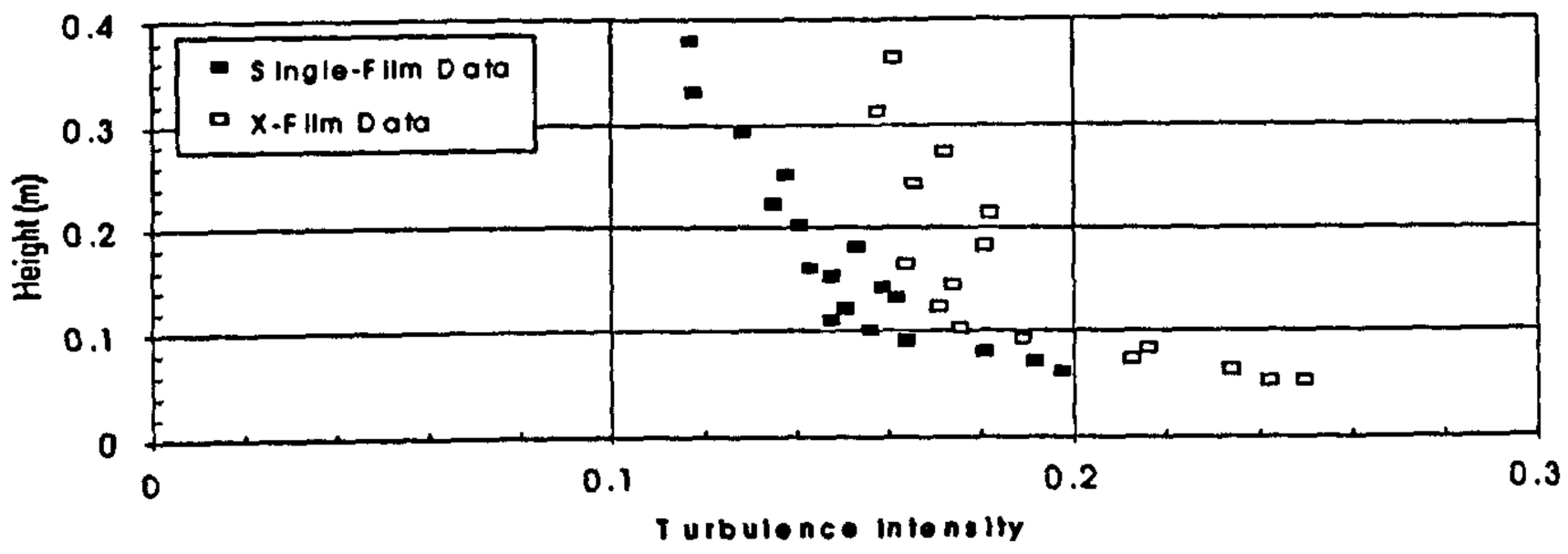

c)

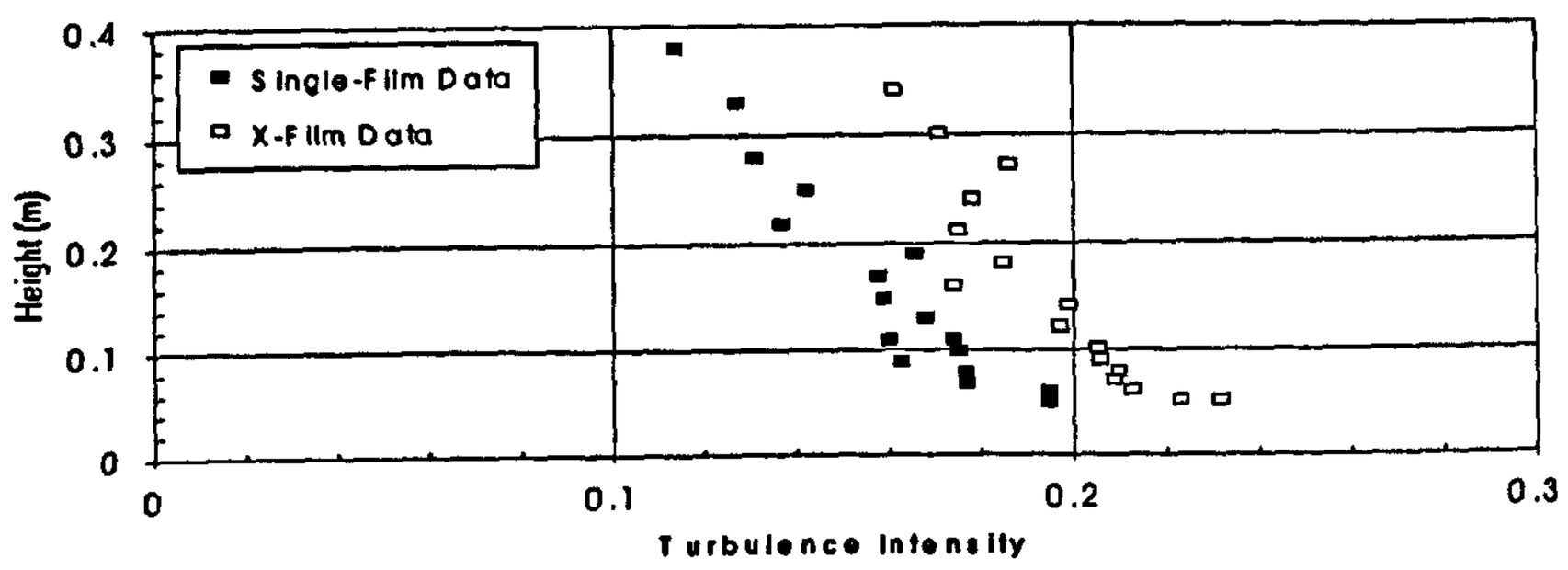

d)

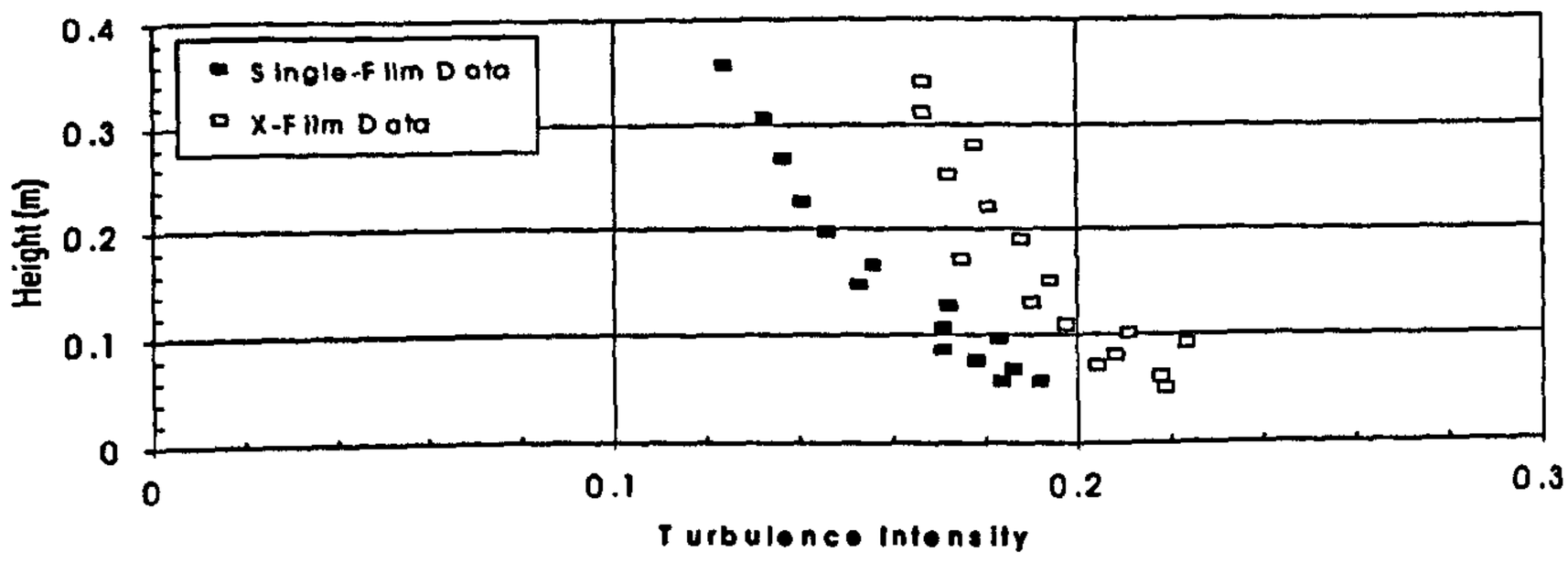

Figure 6.9 Turbulence intensity profiles for spilling waves under onshore winds: a) X=100mm b) X=-912mm c) X=-1554mm d) X=-1800mm

a)

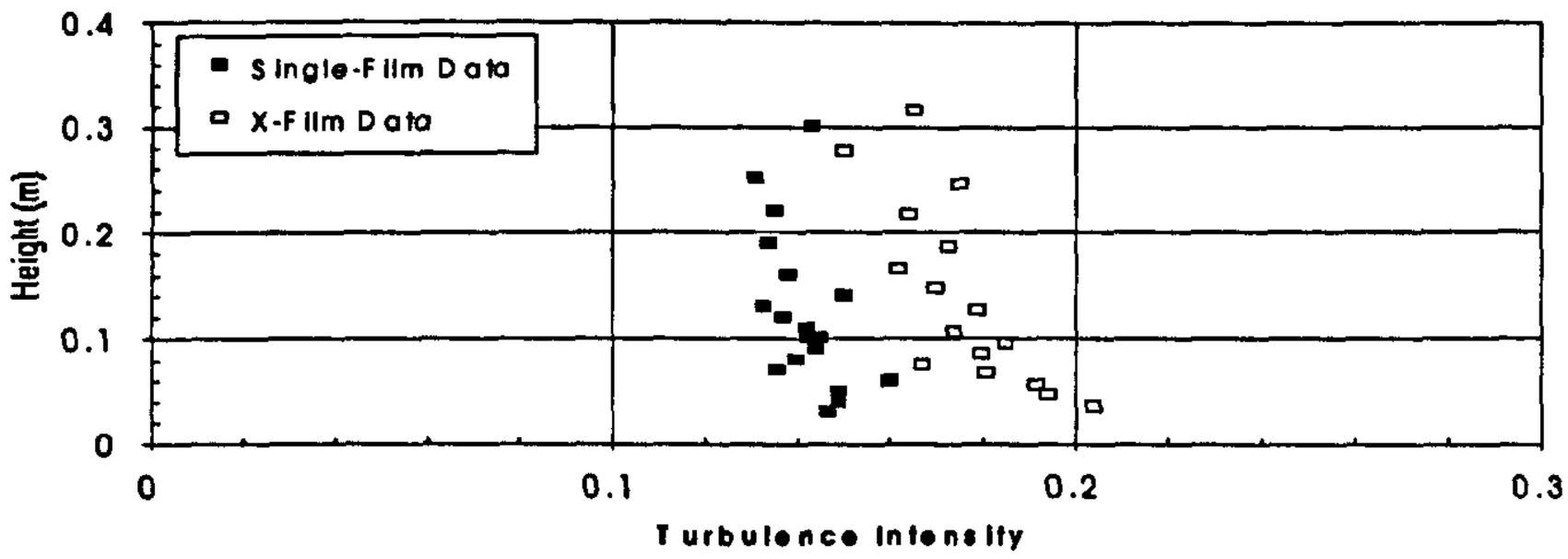

b)

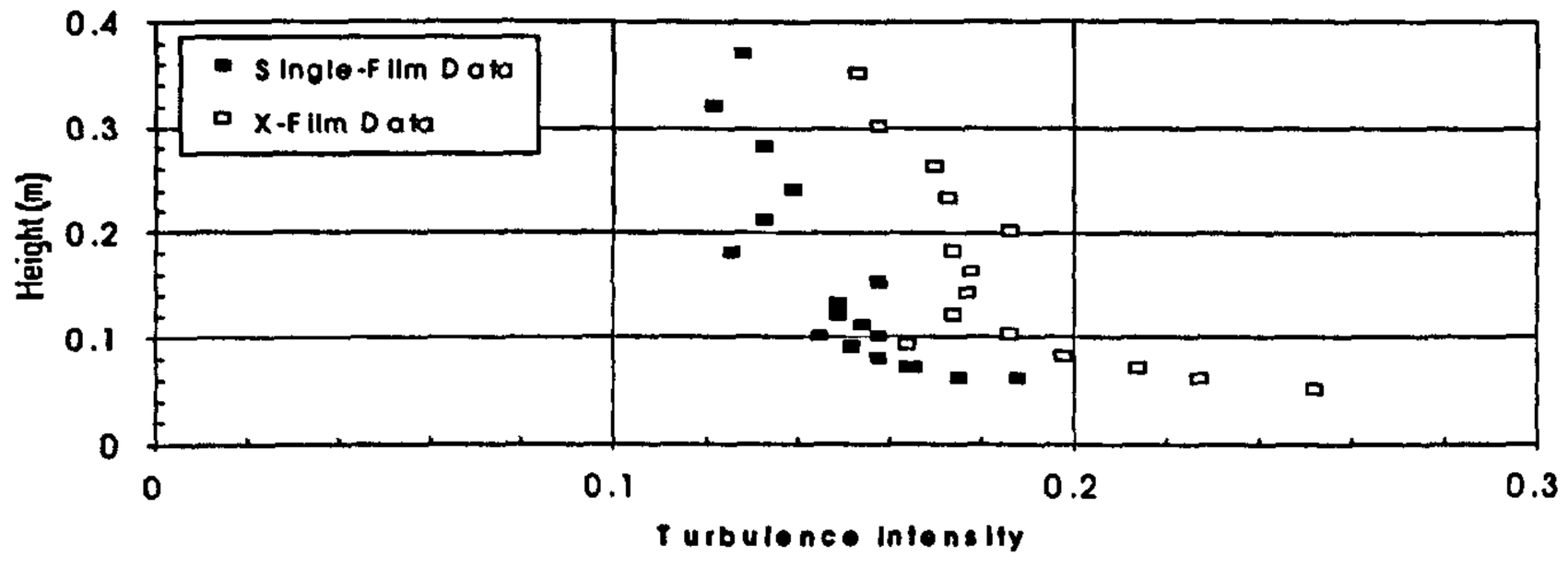

c)

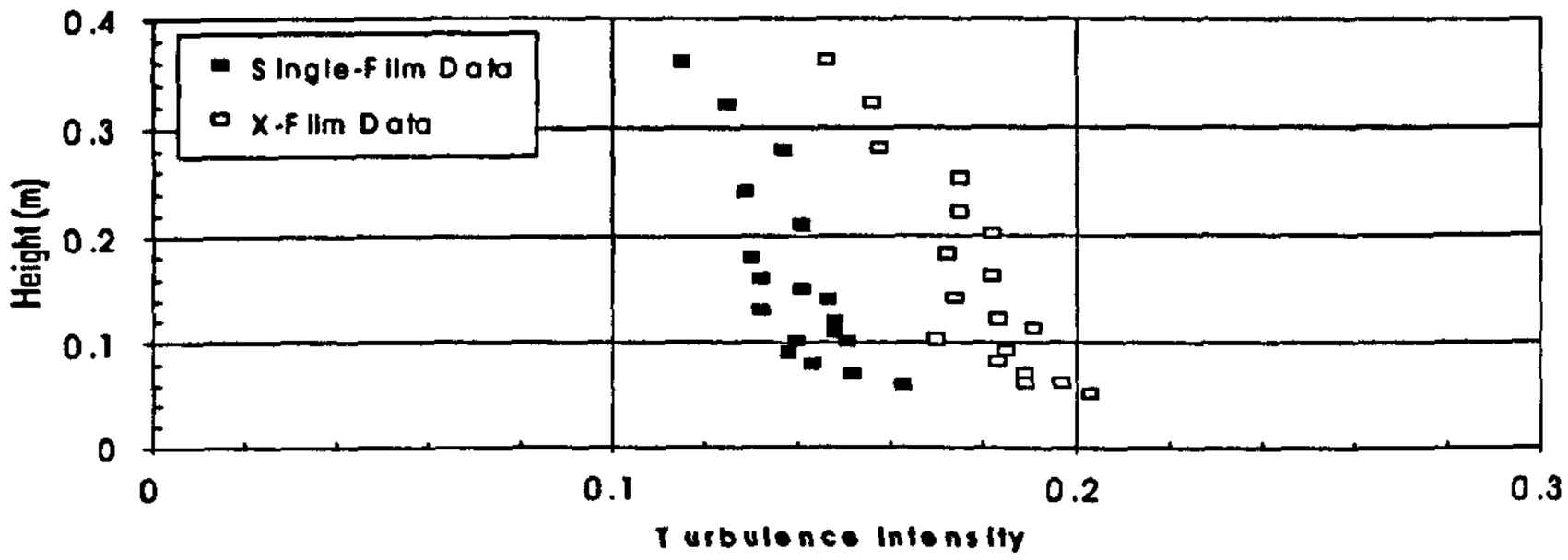

d)

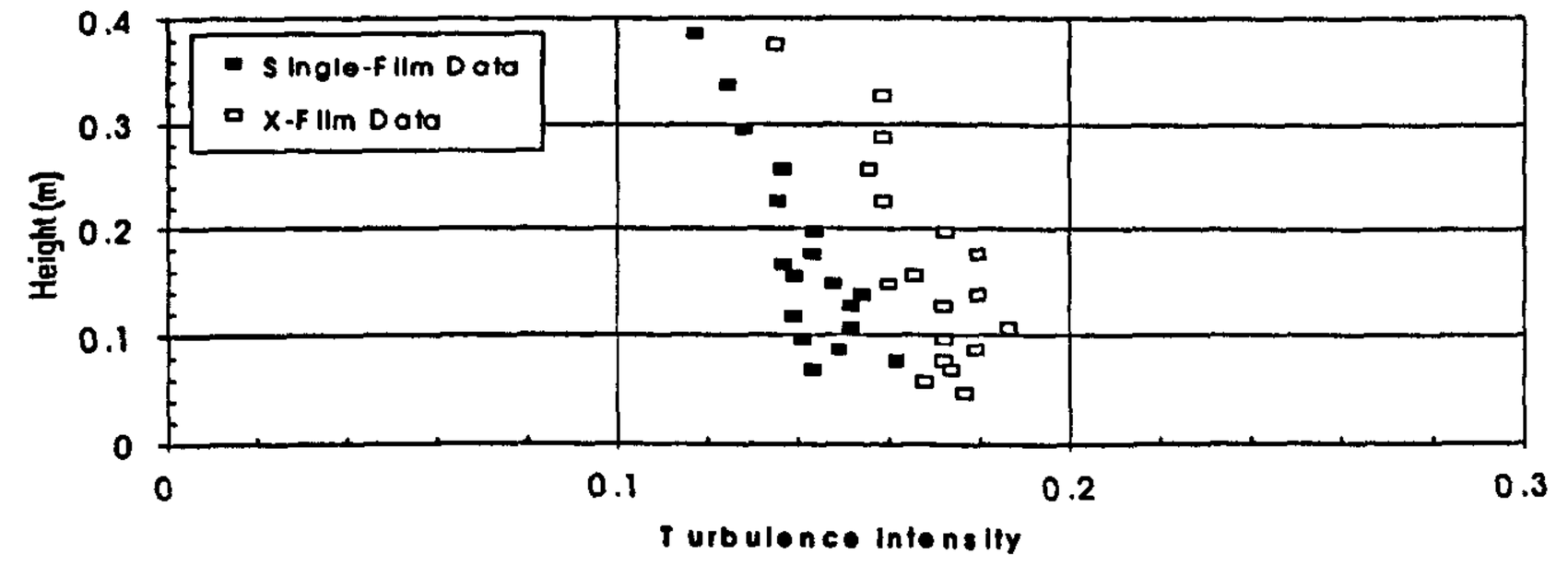

Figure 6.10 Turbulence intensity profiles for plunging waves under onshore winds: a) X=100mm b) X=-912mm c) X=-1289mm d) X=-1795mm

a)

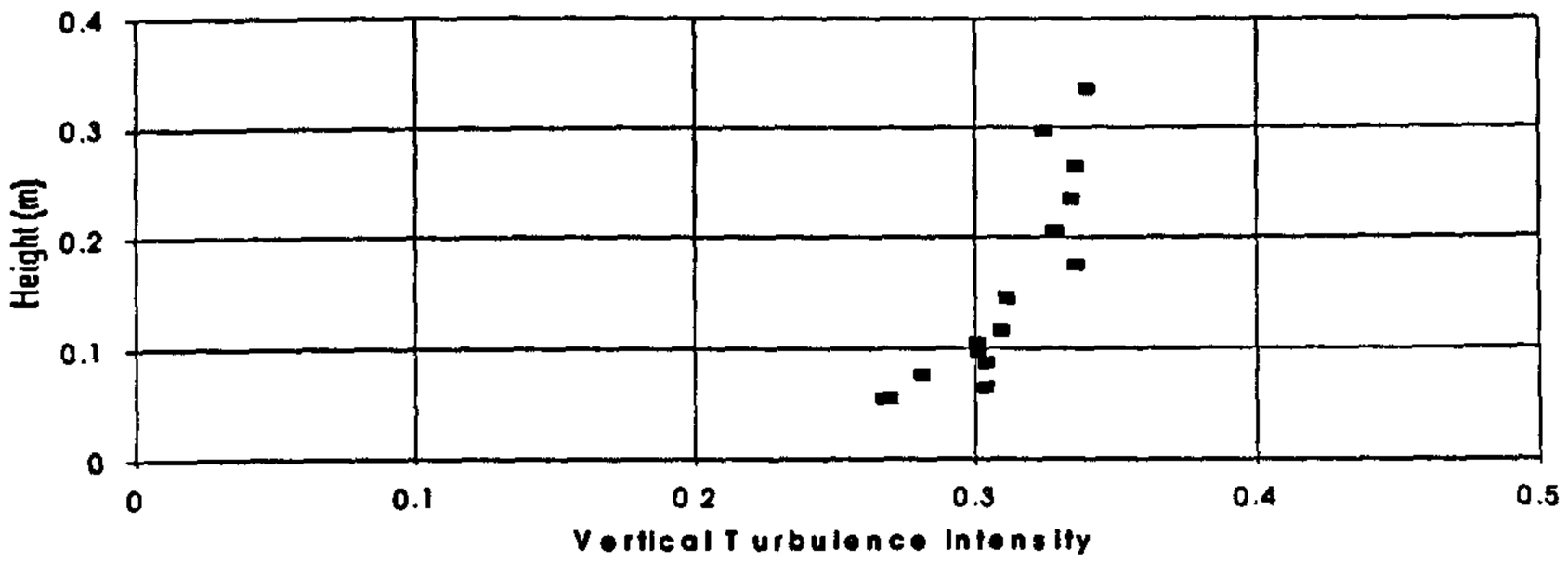

b)

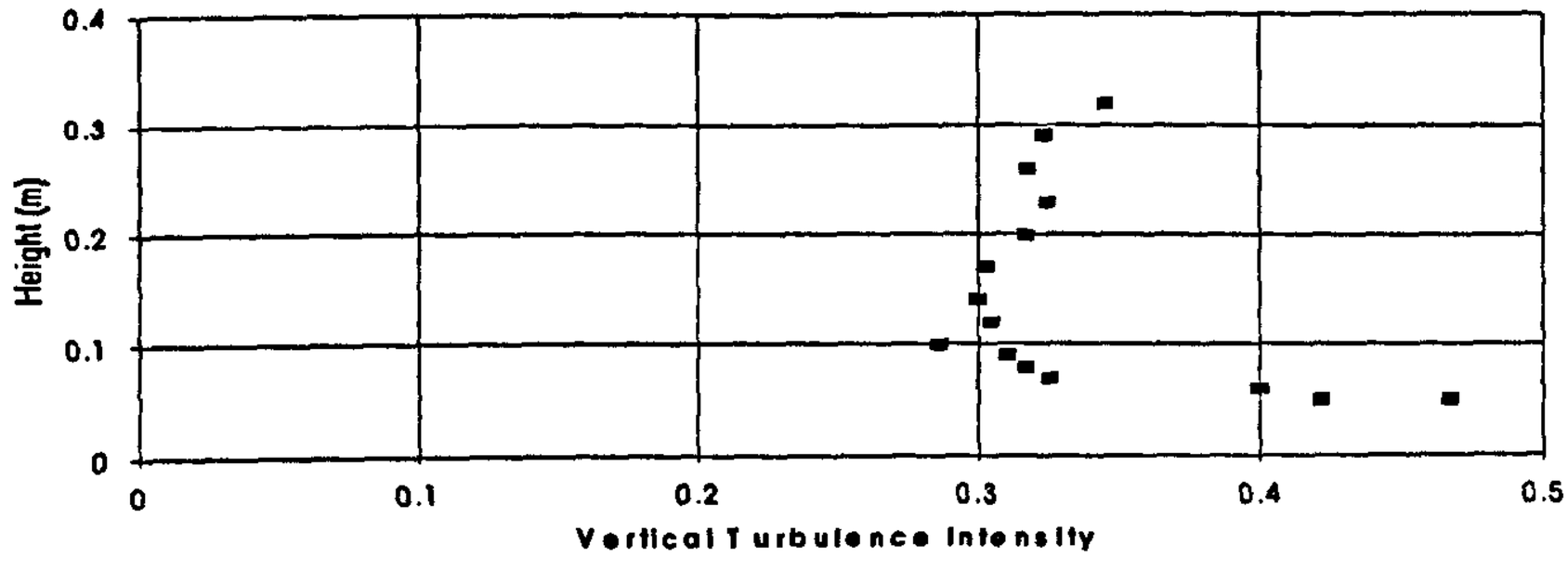

c)

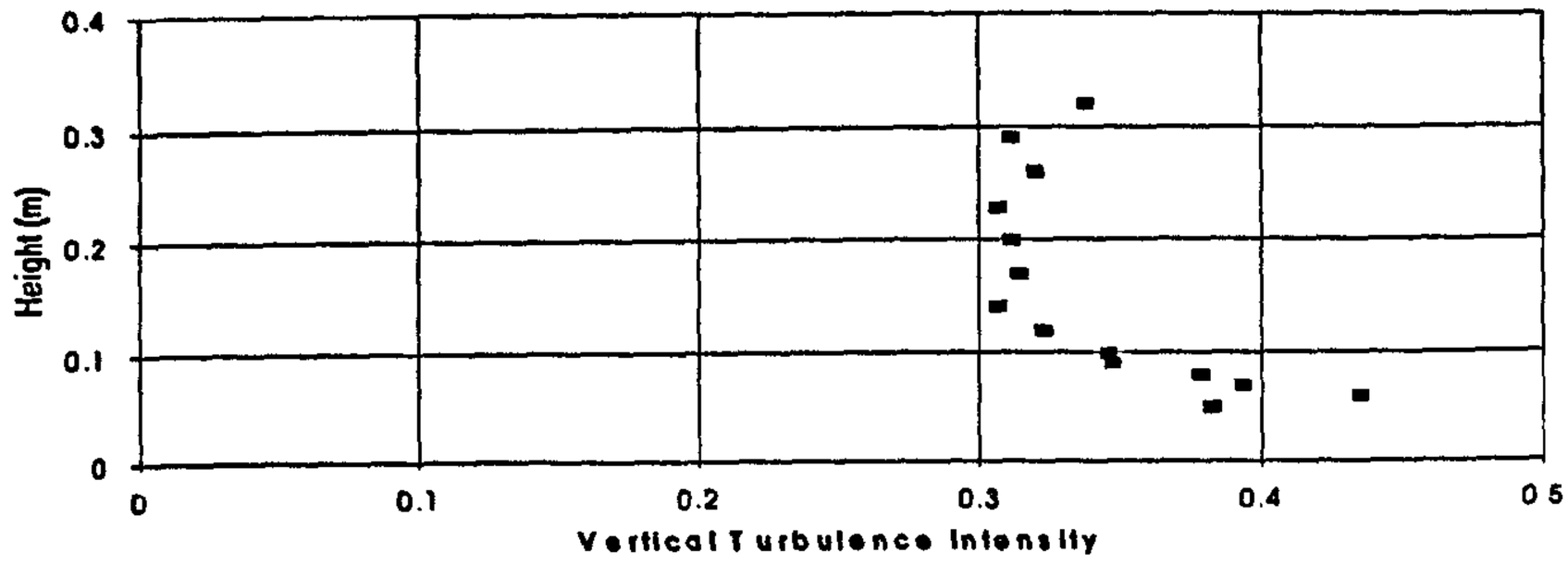

d)

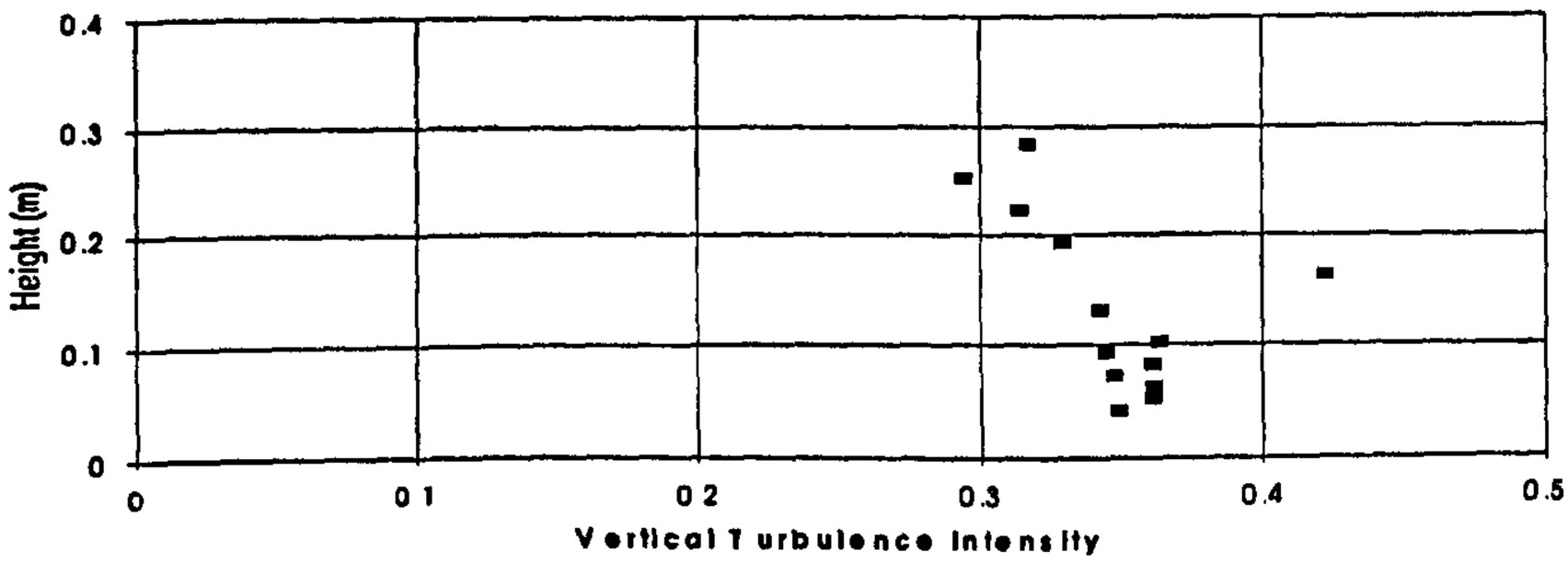

Figure 6.11 Turbulence intensity profiles for the vertical component of velocity, spilling waves under offshore winds: a) X=-912mm b) X=-1177mm c) X=-1575mm d) X=-2646mm

a)

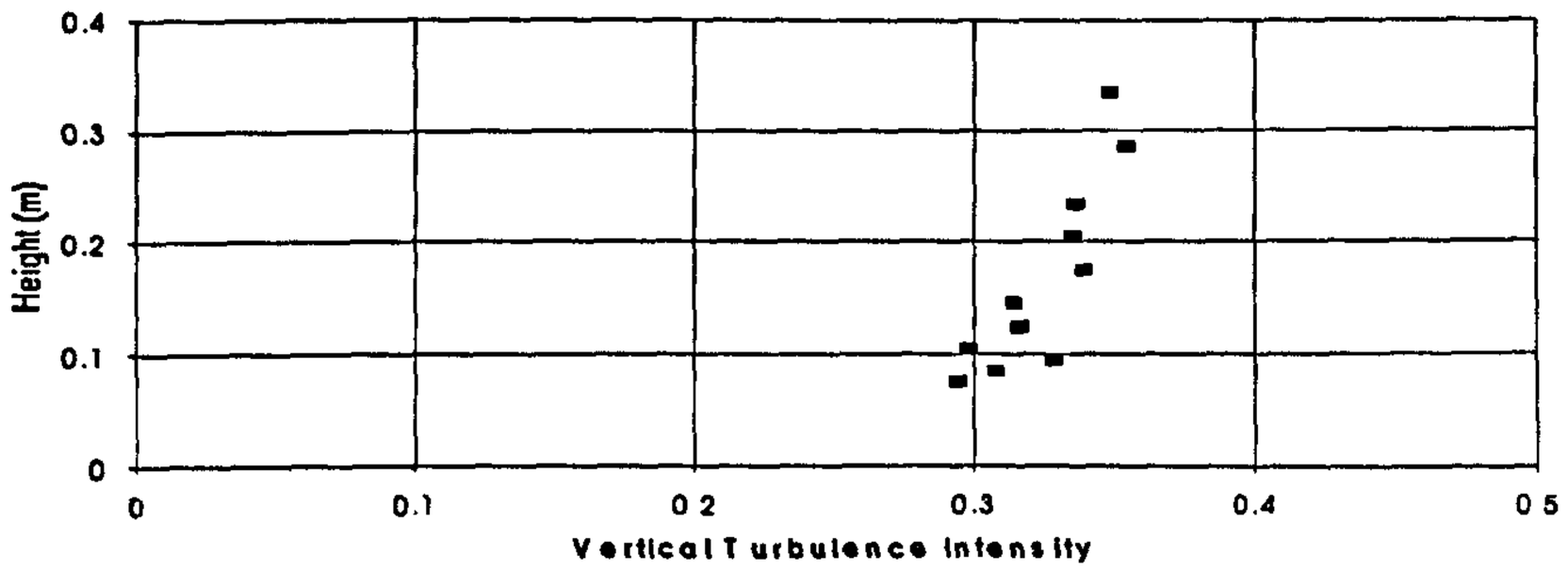

b)

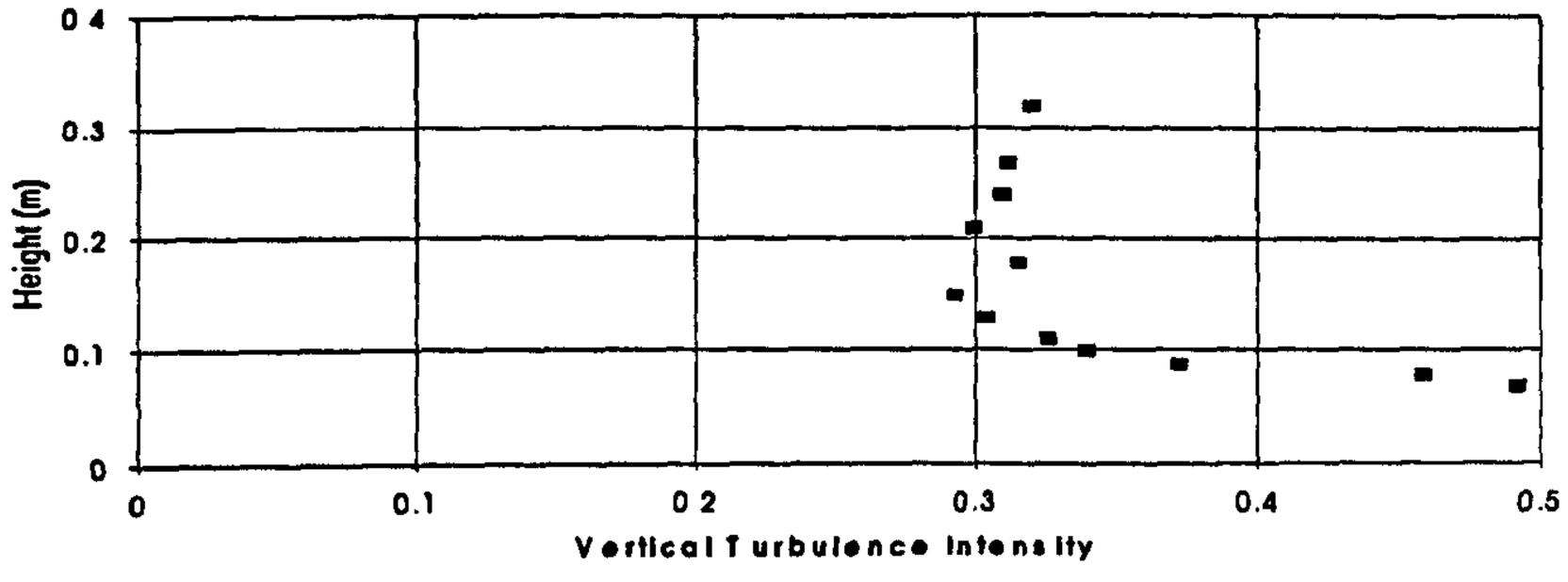

c)

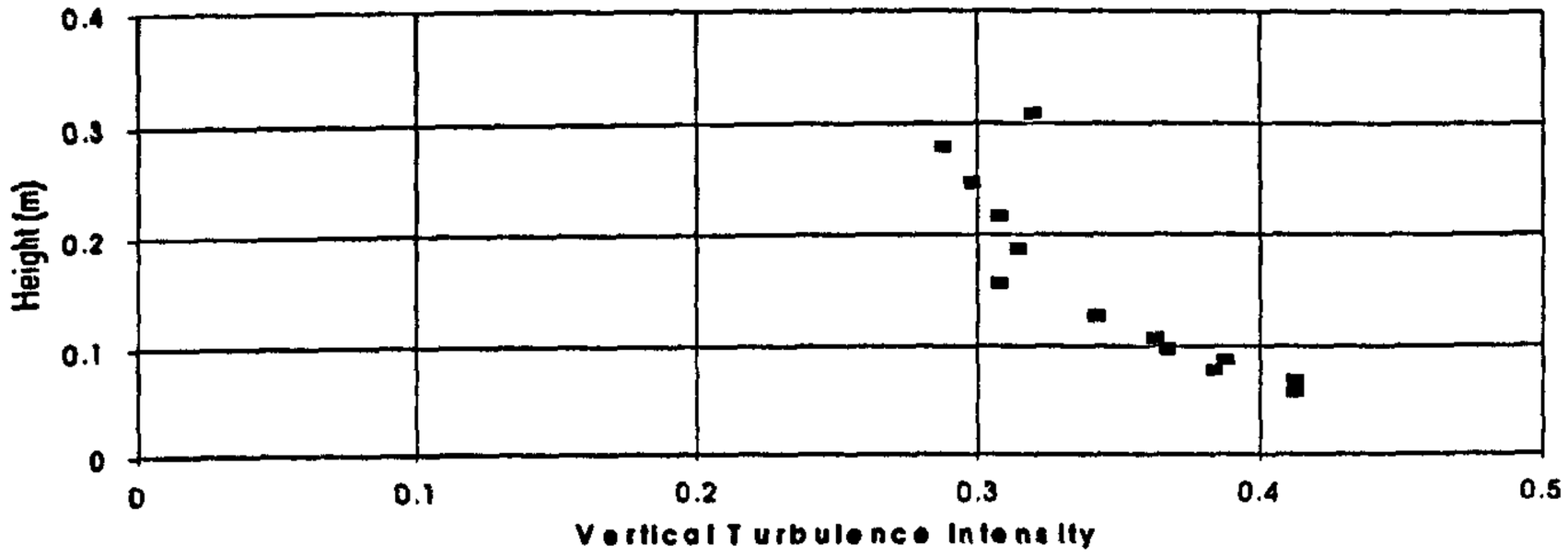

d)

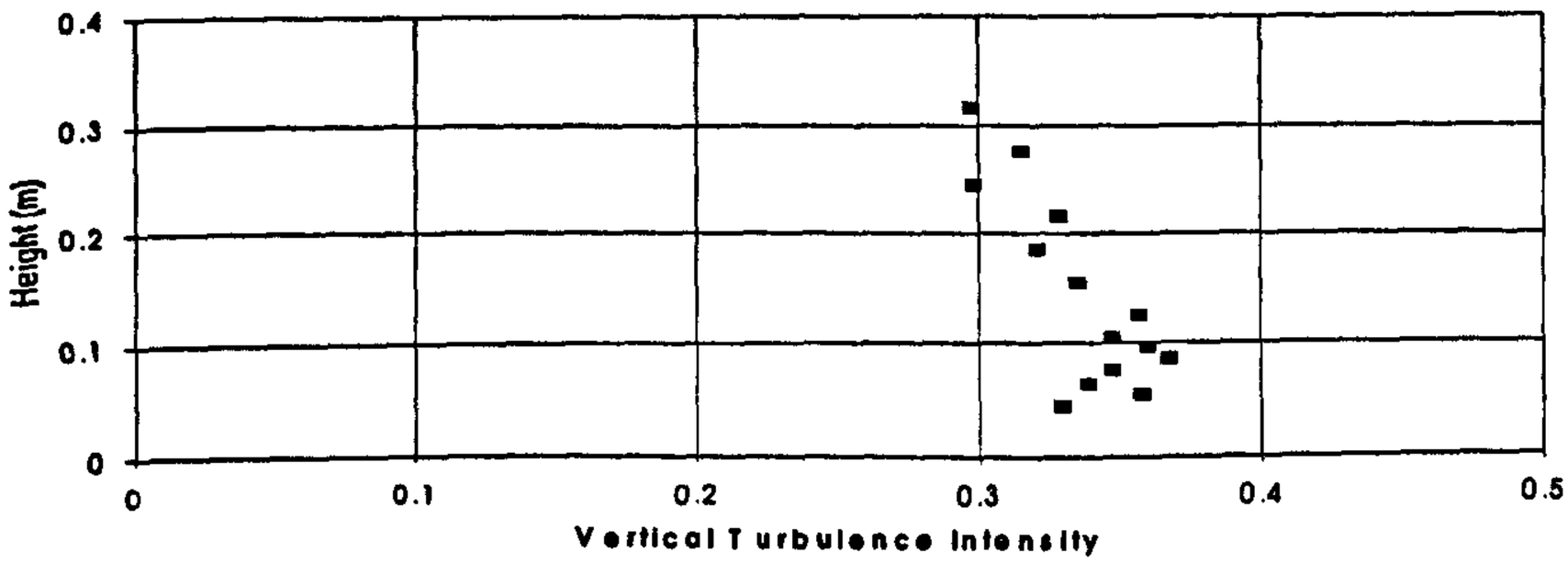

Figure 6.12 Turbulence intensity profiles for the vertical component of velocity, plunging waves under offshore winds: a) X=-912mm b) X=-1404mm c) X=-1811mm d) X=-2640mm

a)

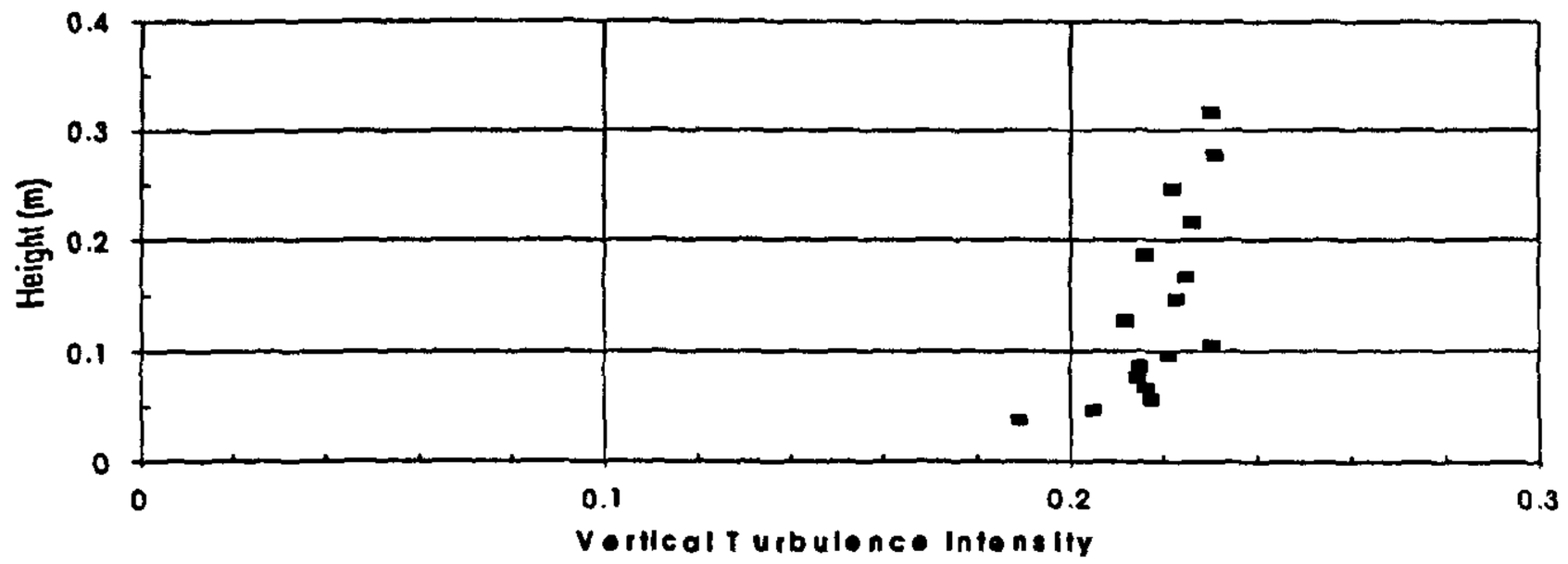

b)

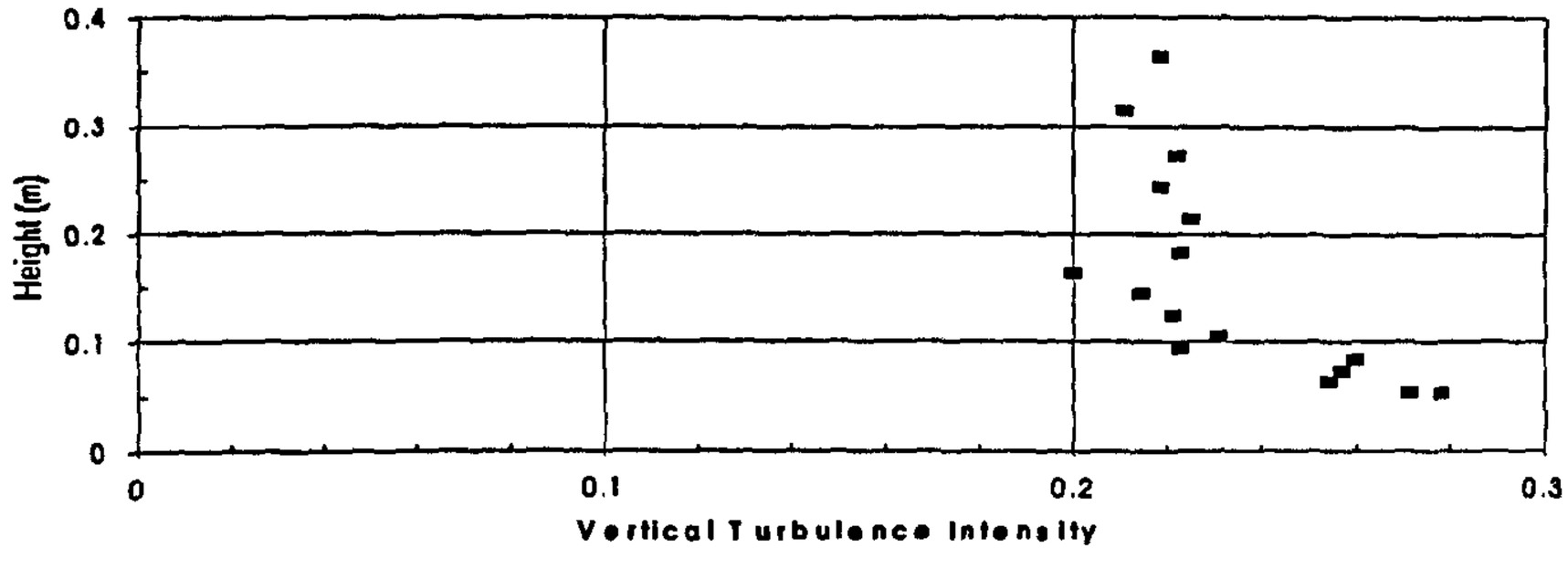

c)

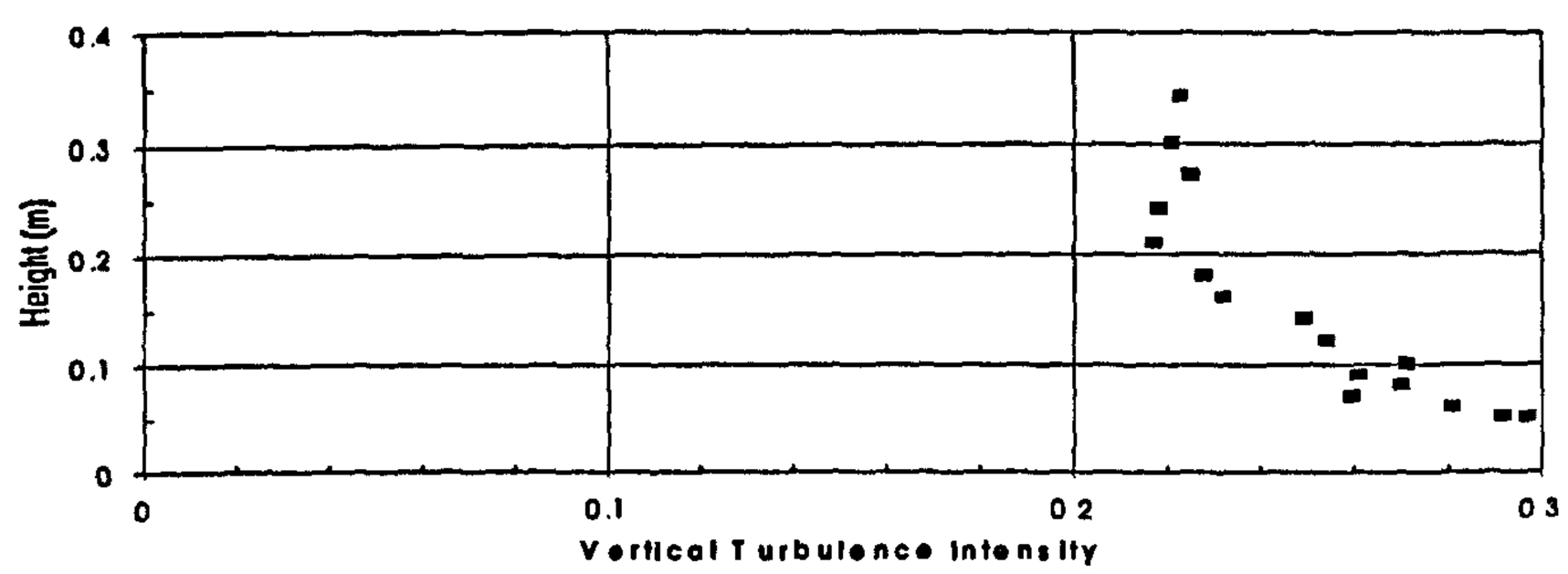

d)

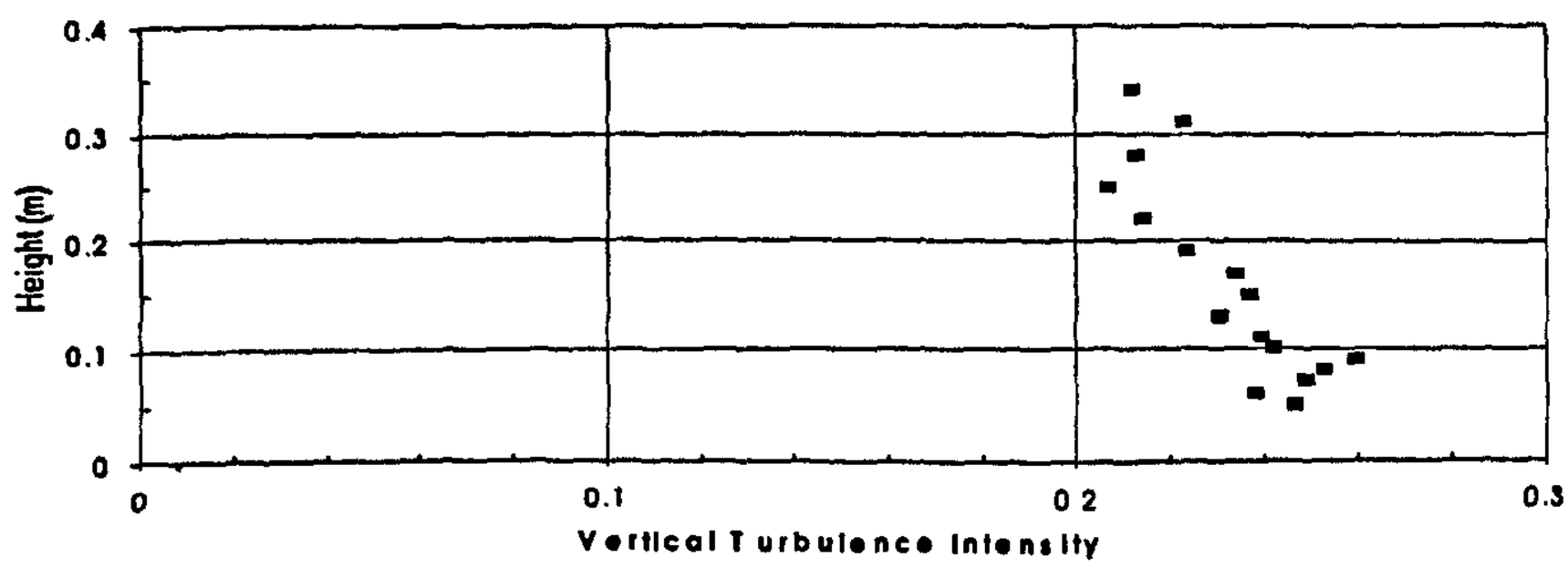

Figure 6.13 Turbulence intensity profiles for the vertical component of velocity, spilling waves under onshore winds: a) X=100mm b) X=-912mm c) X=-1554mm d) X=-1800mm

a)

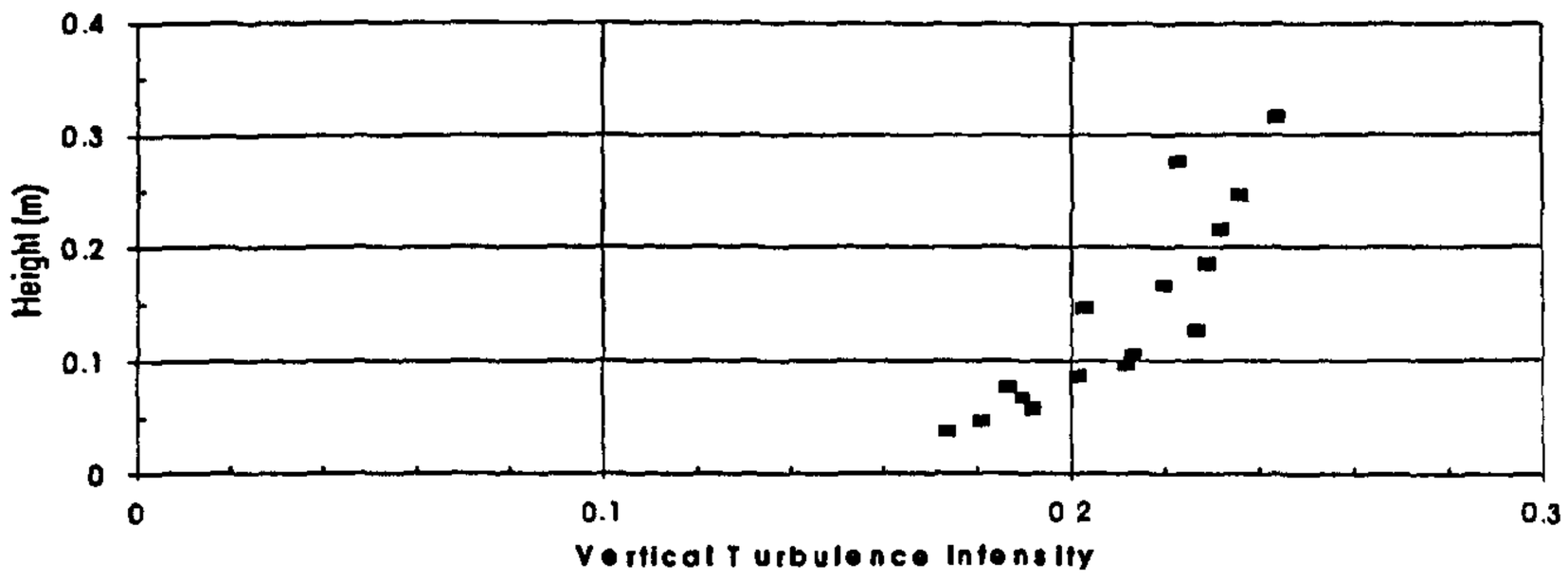

b)

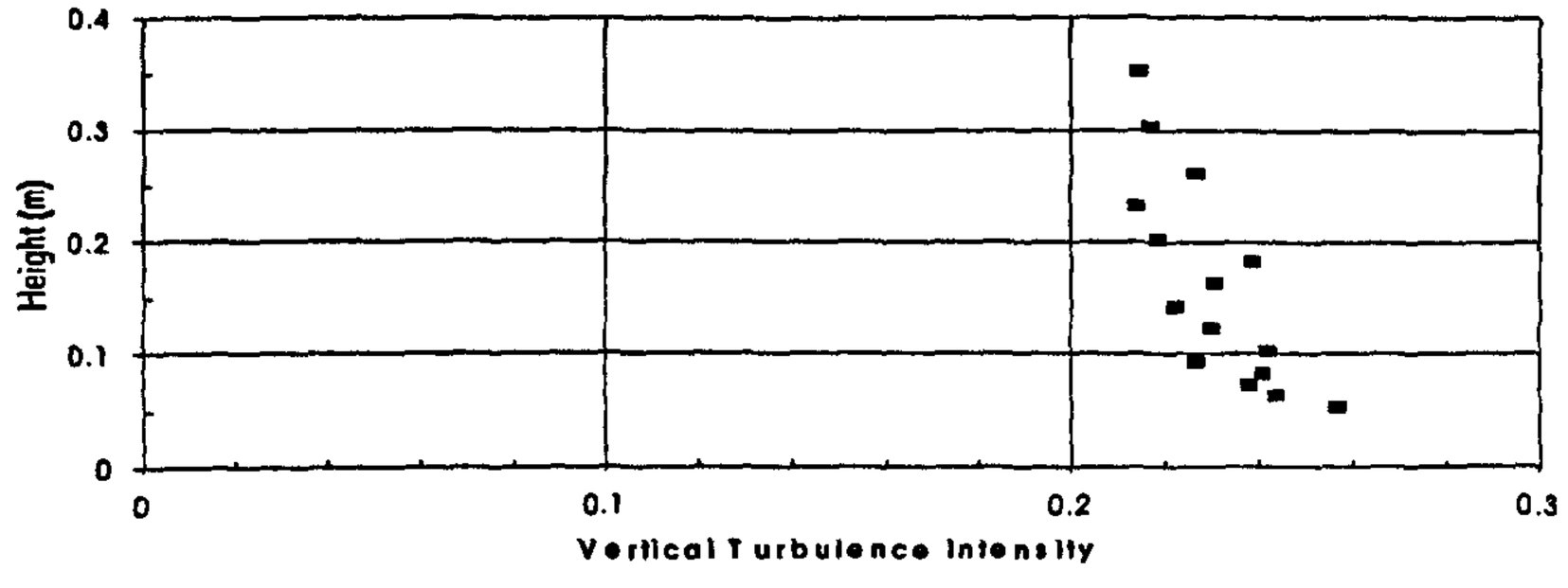

c)

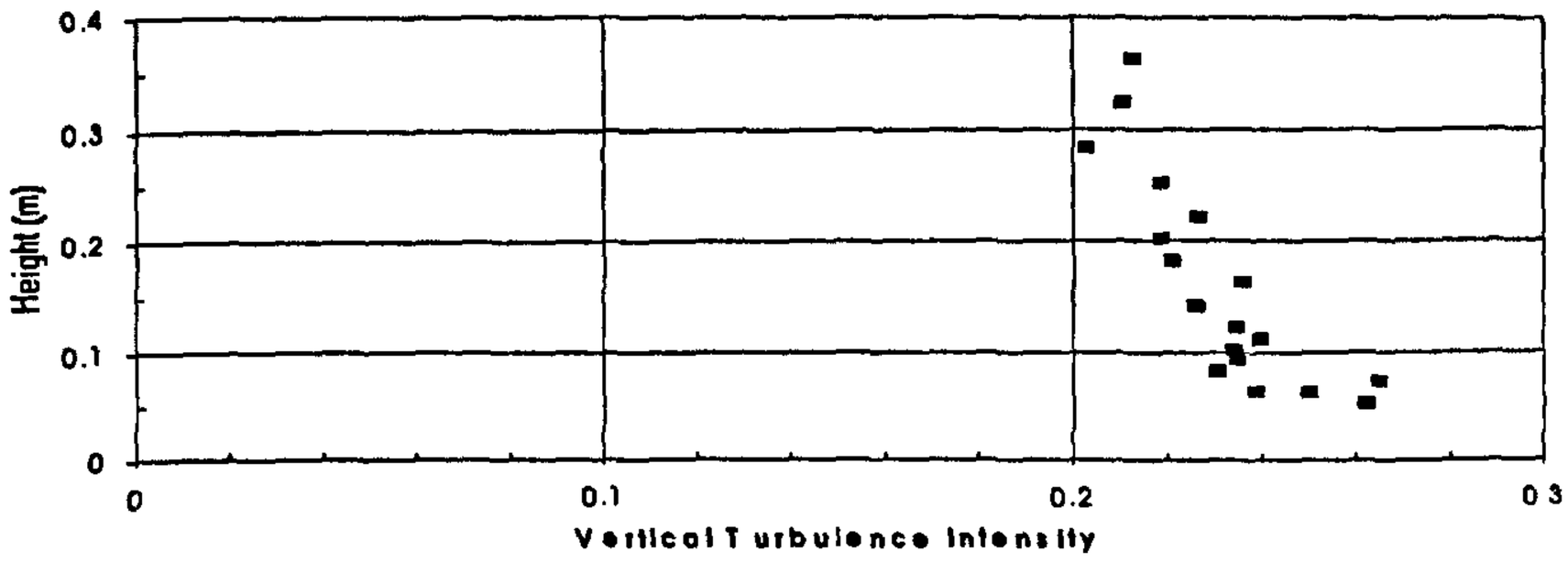

d)

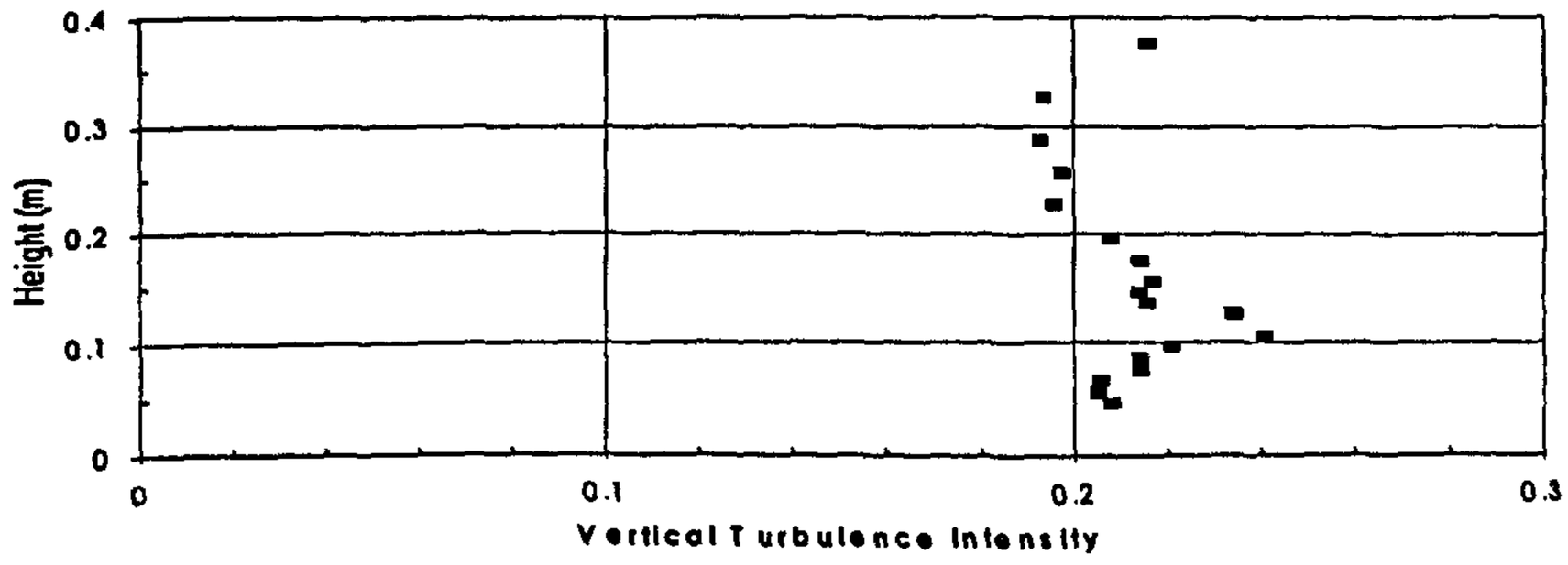

Figure 6.14 Turbulence intensity profiles for the vertical component of velocity, for plunging waves under onshore winds: a) X=100mm b) X=-912mm c) X=-1289mm d) X=-1795mm

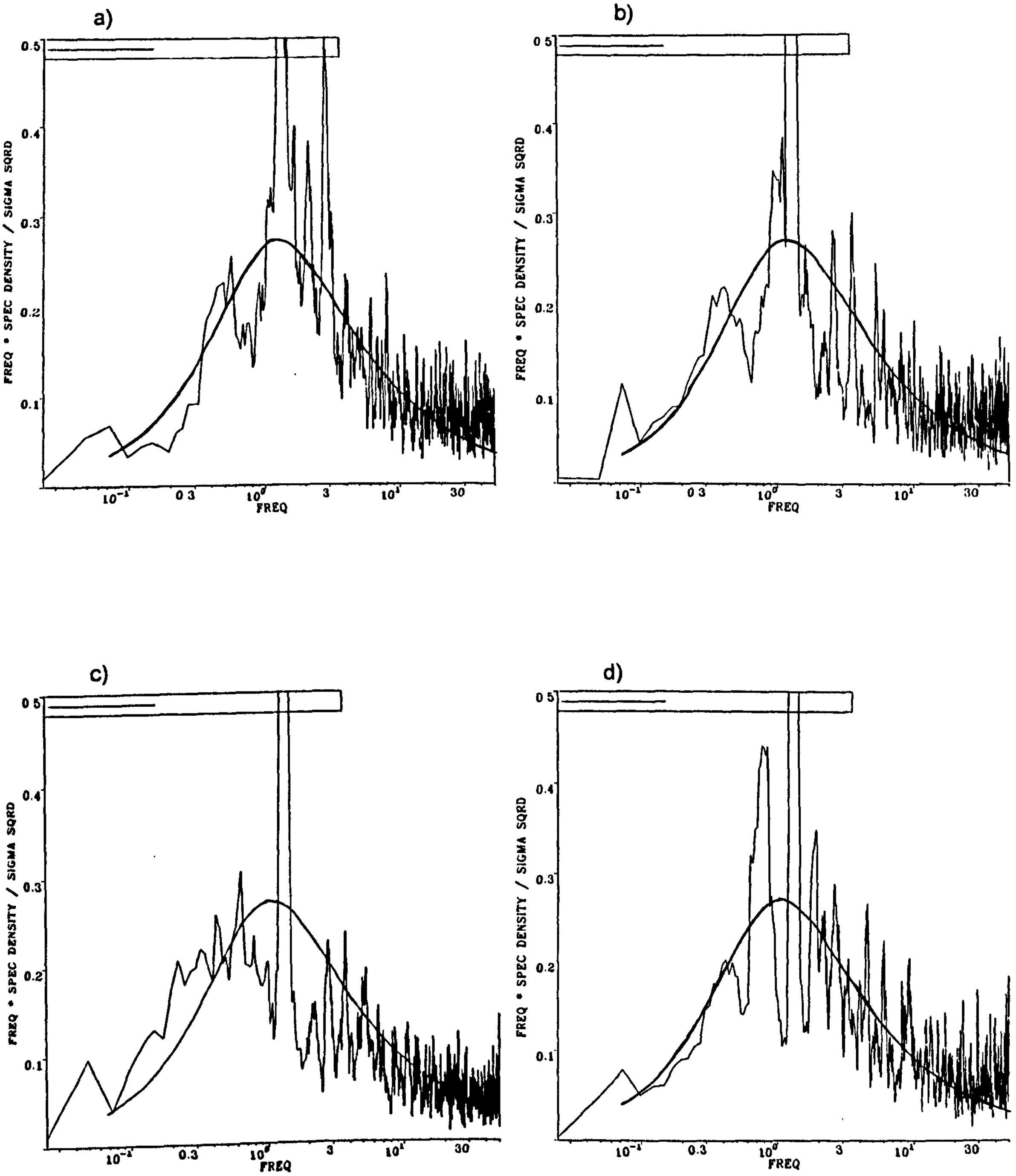

Figure 6.15 Non-dimensional frequency spectra for spilling waves under offshore winds at H_{ref}. Smooth line is Von Karman spectrum for ${}^{x}L_{u}$=0.2m: a) X=-912mm b) X=-1177mm c) X=-1575mm d) X=-2646mm

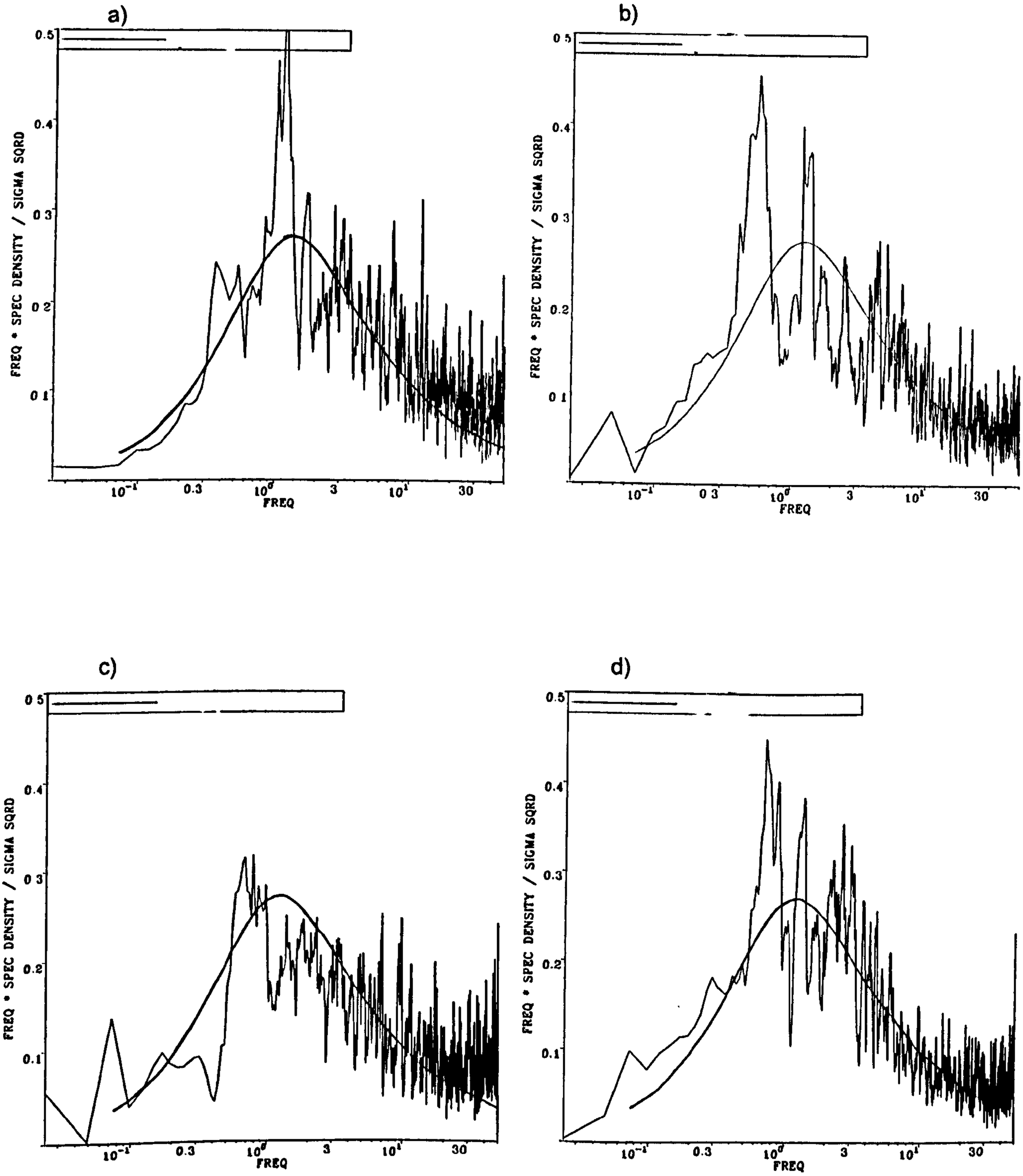

Figure 6.16 Non-dimensional frequency spectra for spilling waves under offshore winds at 200mm above SWL. Smooth line is Von Karman spectrum for ${}^{x}L_{u}$=0.2m: a) X=-912mm b) X=-1177mm c) X=-1575mm d) X=-2646mm

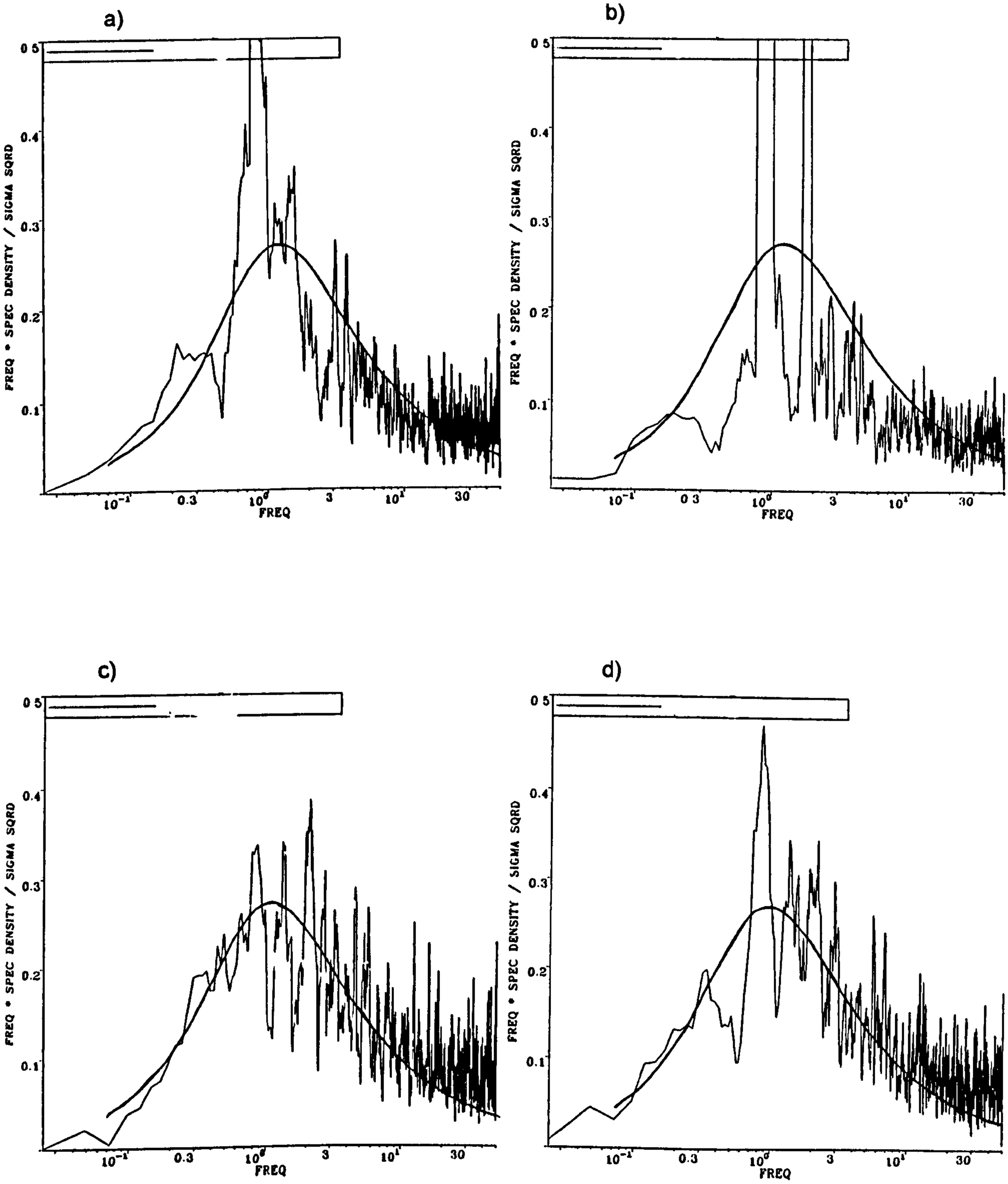

Figure 6.17 Non-dimensional frequency spectra for plunging waves under offshore winds at H_{ref}. Smooth line is Von Karman spectrum for ${}^{x}L_{u}$=0.2m: a) X=-912mm b) X=-1404mm c) X=-1811mm d) X=-2640mm

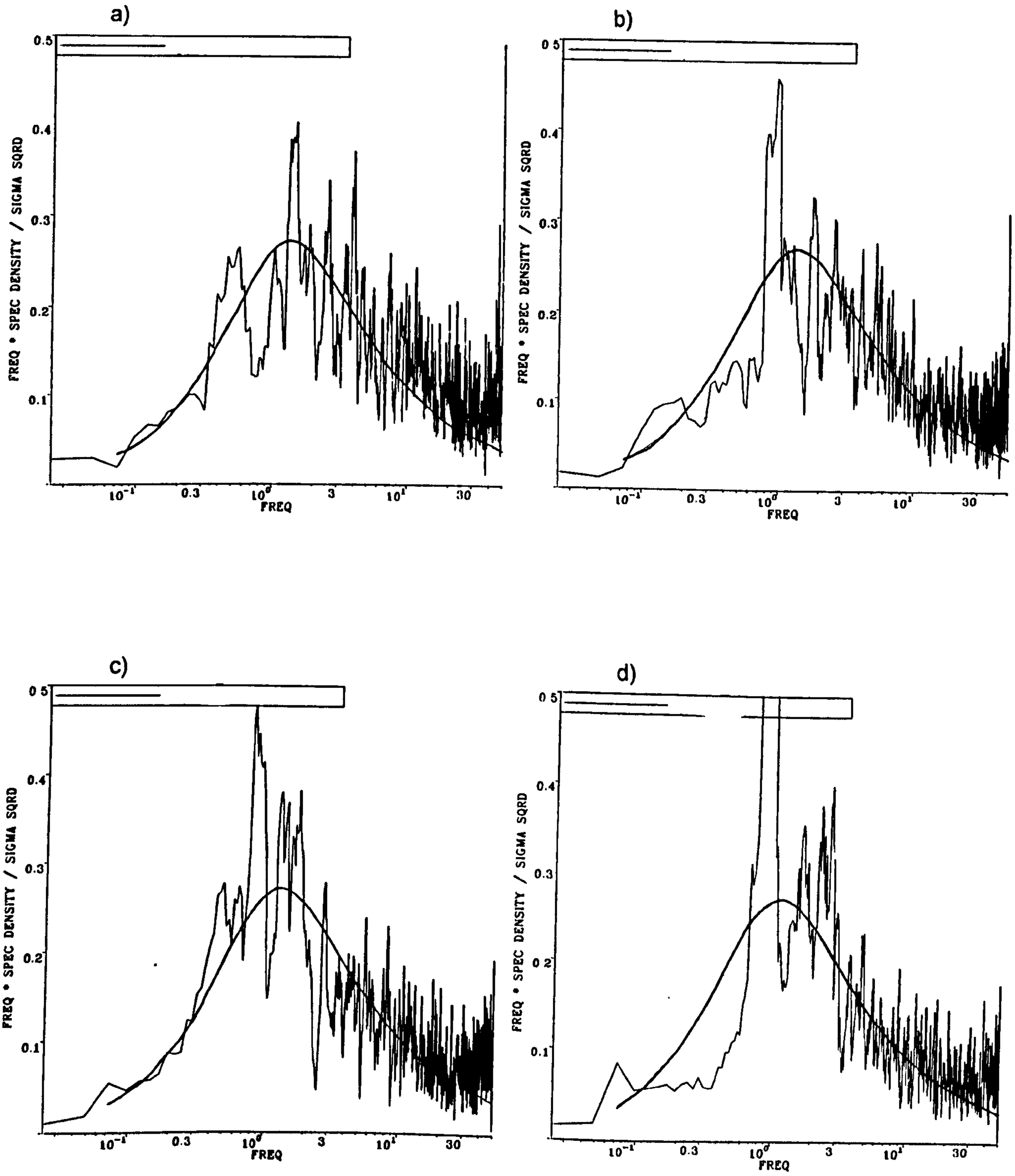

Figure 6.18 Non-dimensional frequency spectra for plunging waves under offshore winds at 200mm above SWL. Smooth line is Von Karman spectrum for ${}^{x}L_{u}$=0.2m: a) X=-912mm b) X=-1404mm c) X=-1811mm d) X=-2640mm

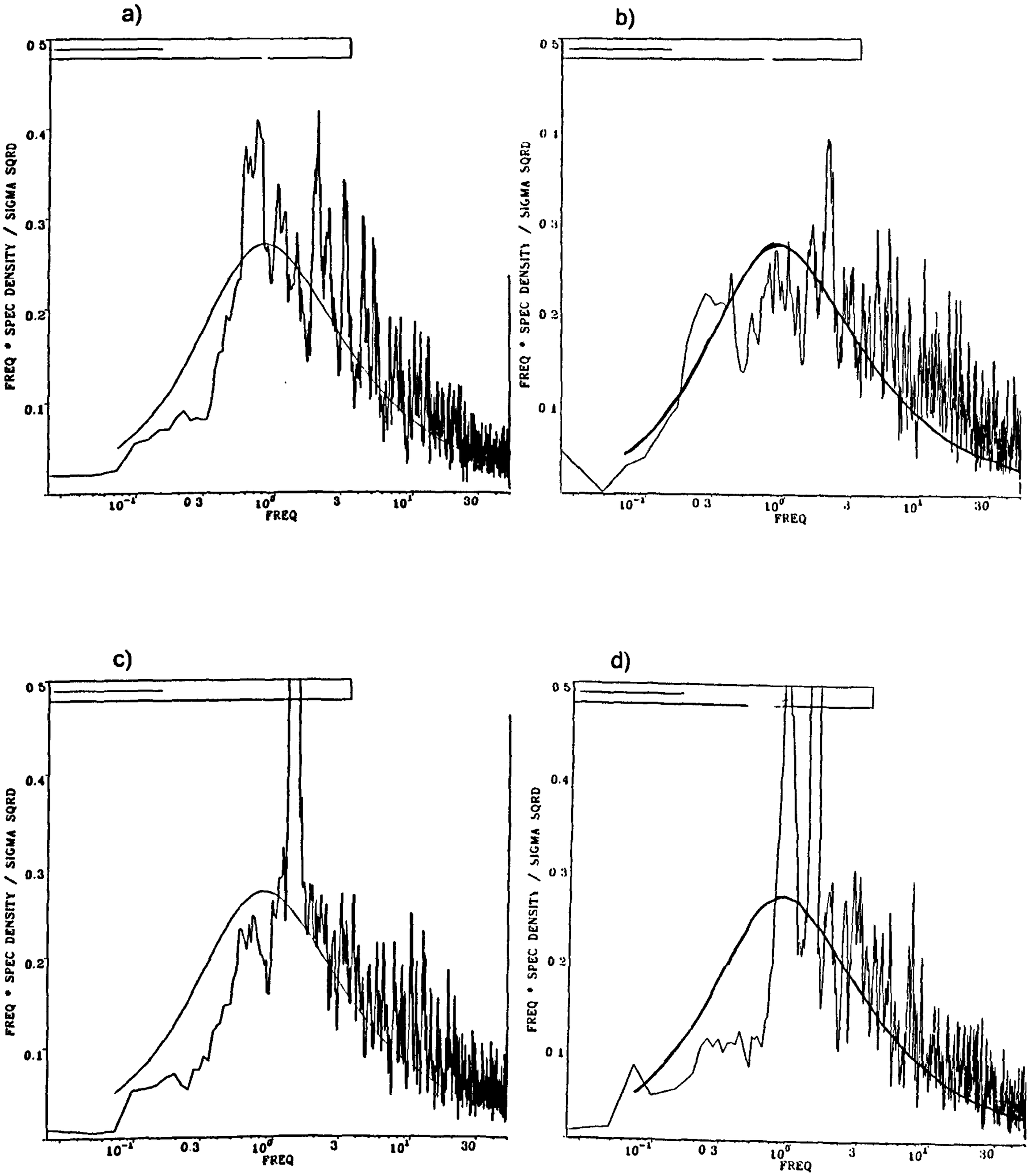

Figure 6.19 Non-dimensional frequency spectra for spilling waves under onshore winds at H_{ref}. Smooth line is Von Karman spectrum for ${}^{x}L_{u}$=0.2m: a) X=100mm b) X=-912mm c) X=-1554mm d) X=-1800mm

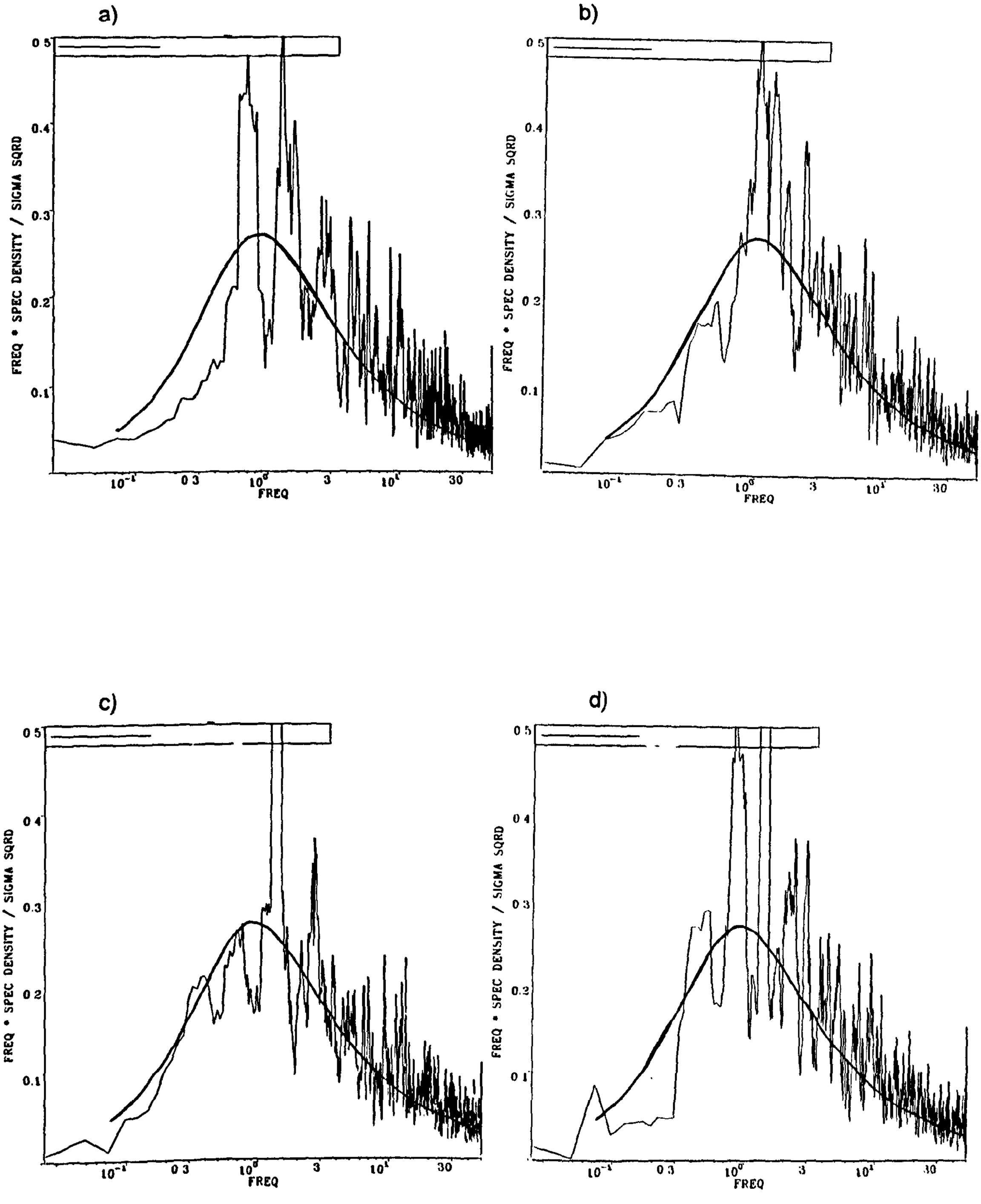

Figure 6.20 Non-dimensional frequency spectra for spilling waves under onshore winds at 200mm above SWL. Smooth line is Von Karman spectrum for ${}^{x}L_u$=0.2m: a) X=100mm b) X=-912mm c) X=-1554mm d) X=-1800mm

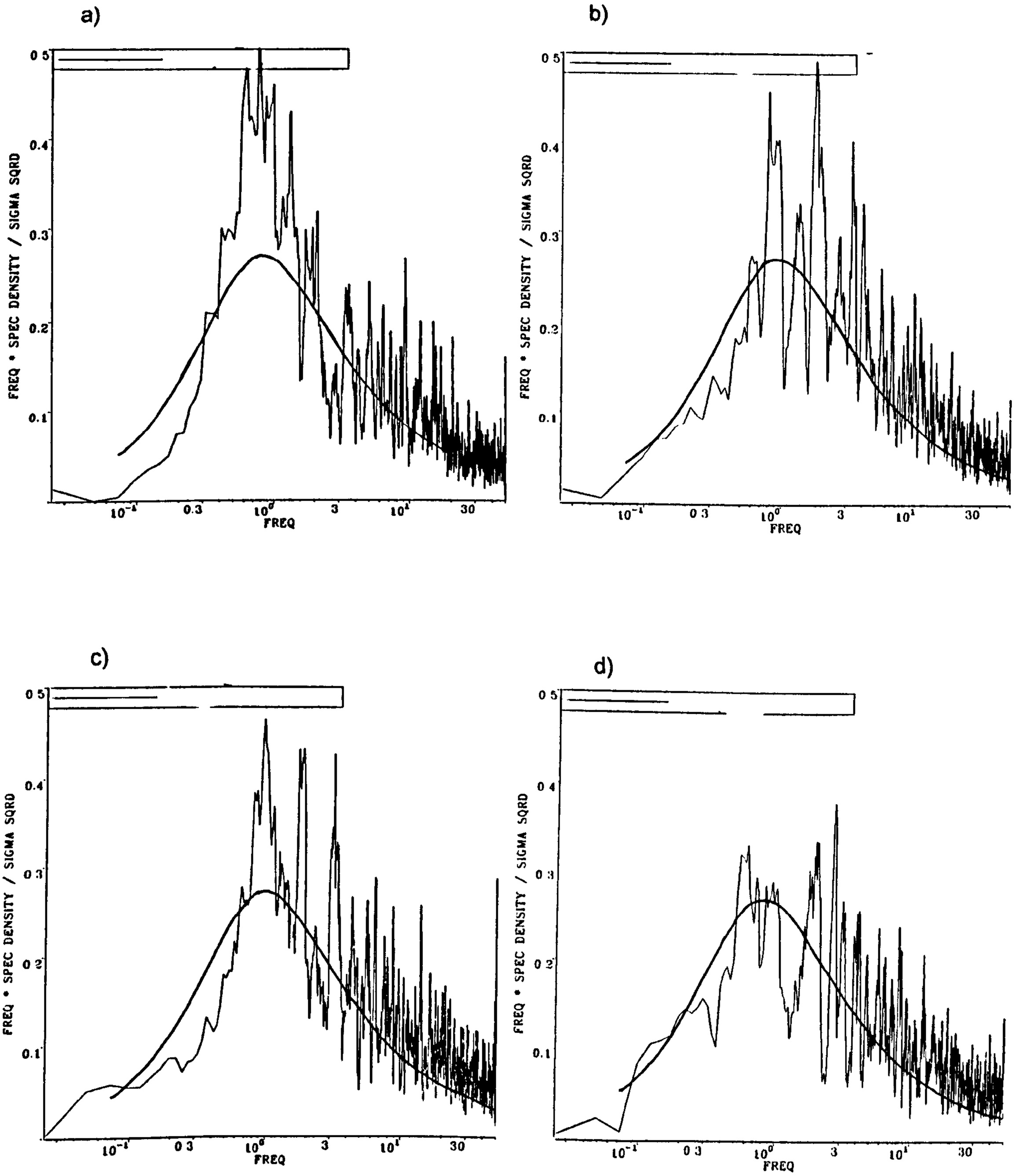

Figure 6.21 Non-dimensional frequency spectra for plunging waves under onshore winds at H_{ref}. Smooth line is Von Karman spectrum for ${}^{x}L_u$=0.2m: a) X=100mm b) X=-912mm c) X=-1289mm d) X=-1795mm

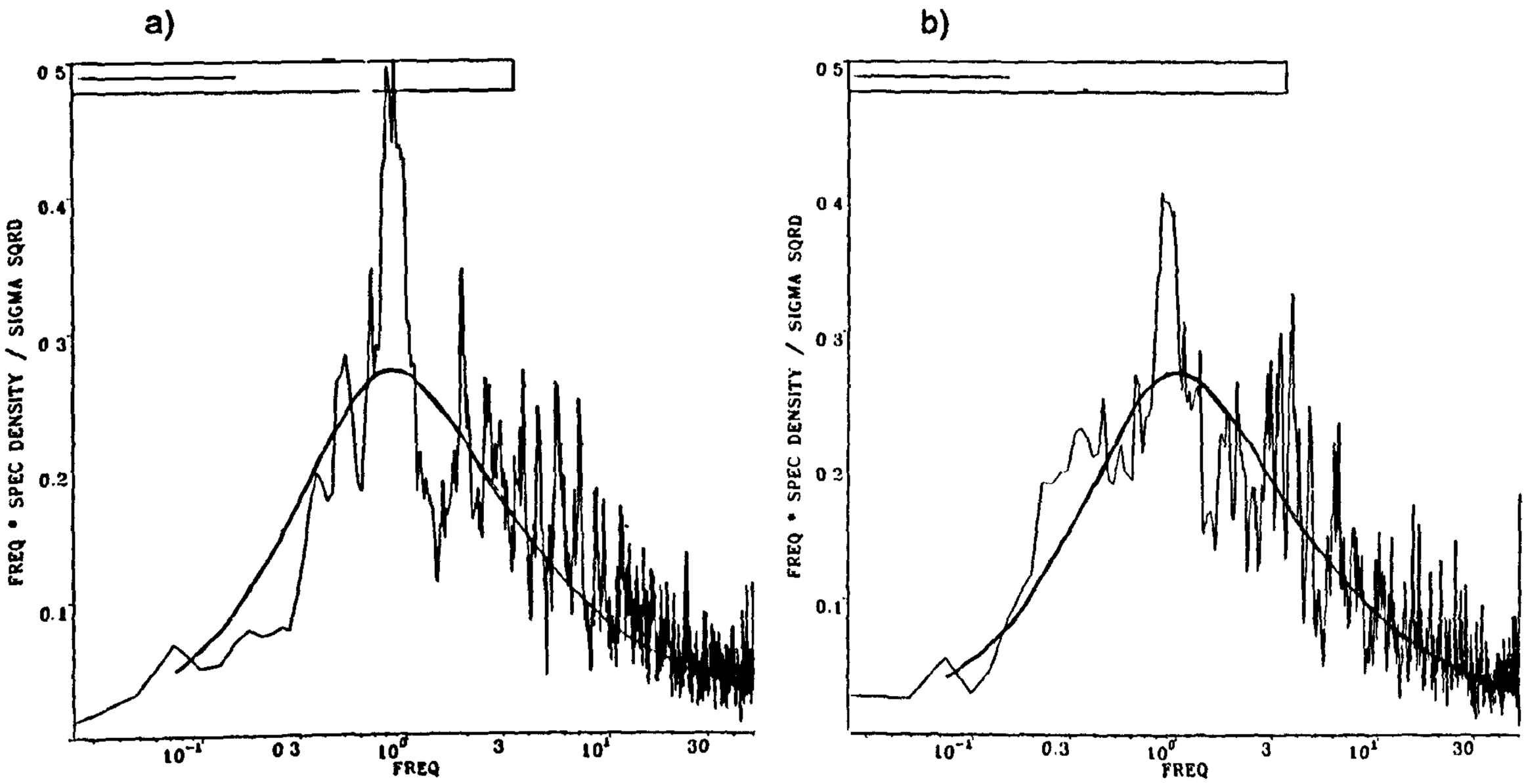

Figure 6.22 Non-dimensional frequency spectra for plunging waves under onshore winds at 200mm above SWL. Smooth line is Von Karman spectrum for ${}^{x}L_{u}$=0.2m: a) X=100mm b) X=-912mm c) X=-1289mm d) X=-1795mm

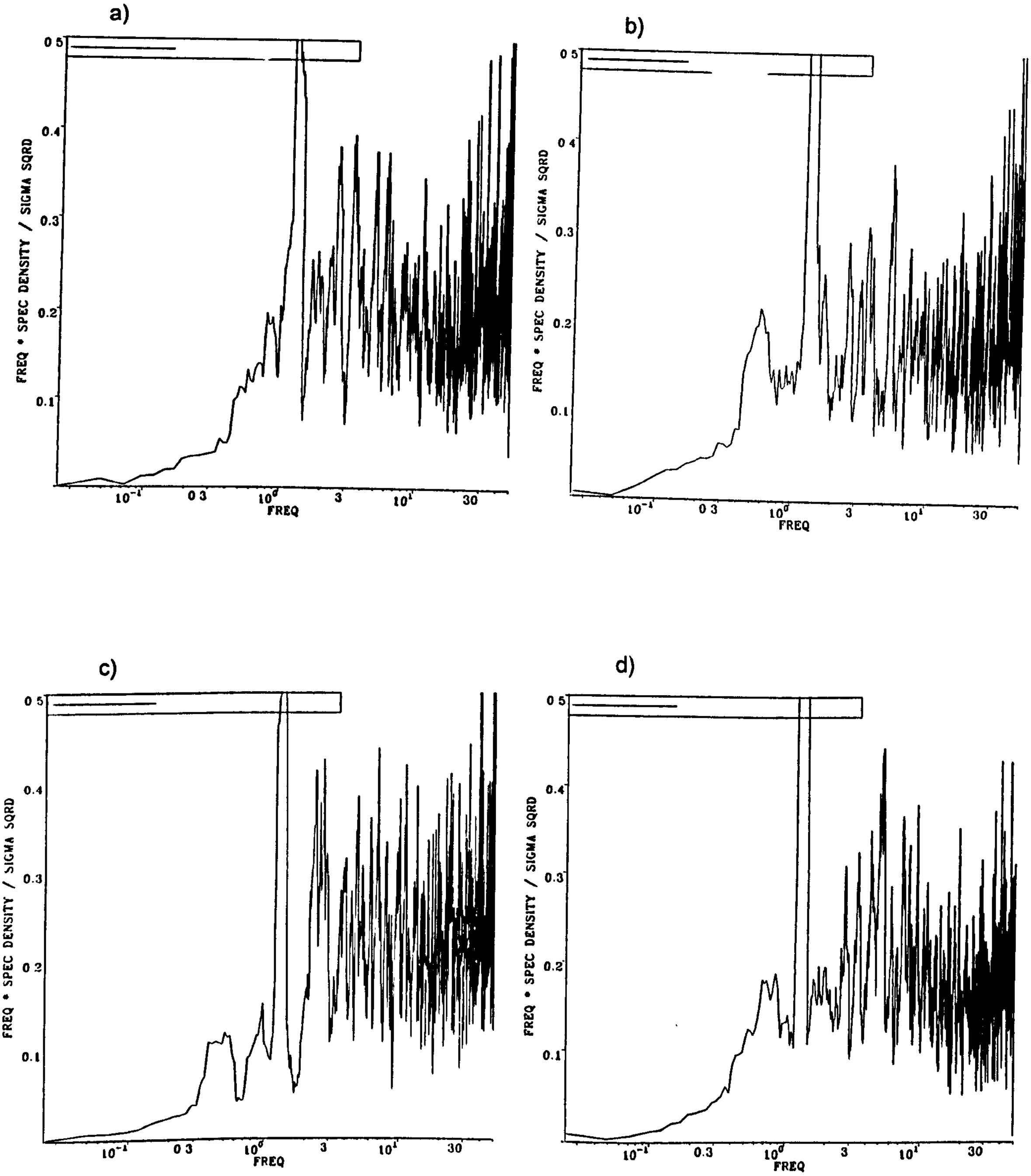

Figure 6.23 Non-dimensional frequency spectra for the vertical component of velocity for spilling waves under offshore winds at H_{ref}:
a) X=-912mm b) X=-1177mm c) X=-1575mm
d) X=-2646mm

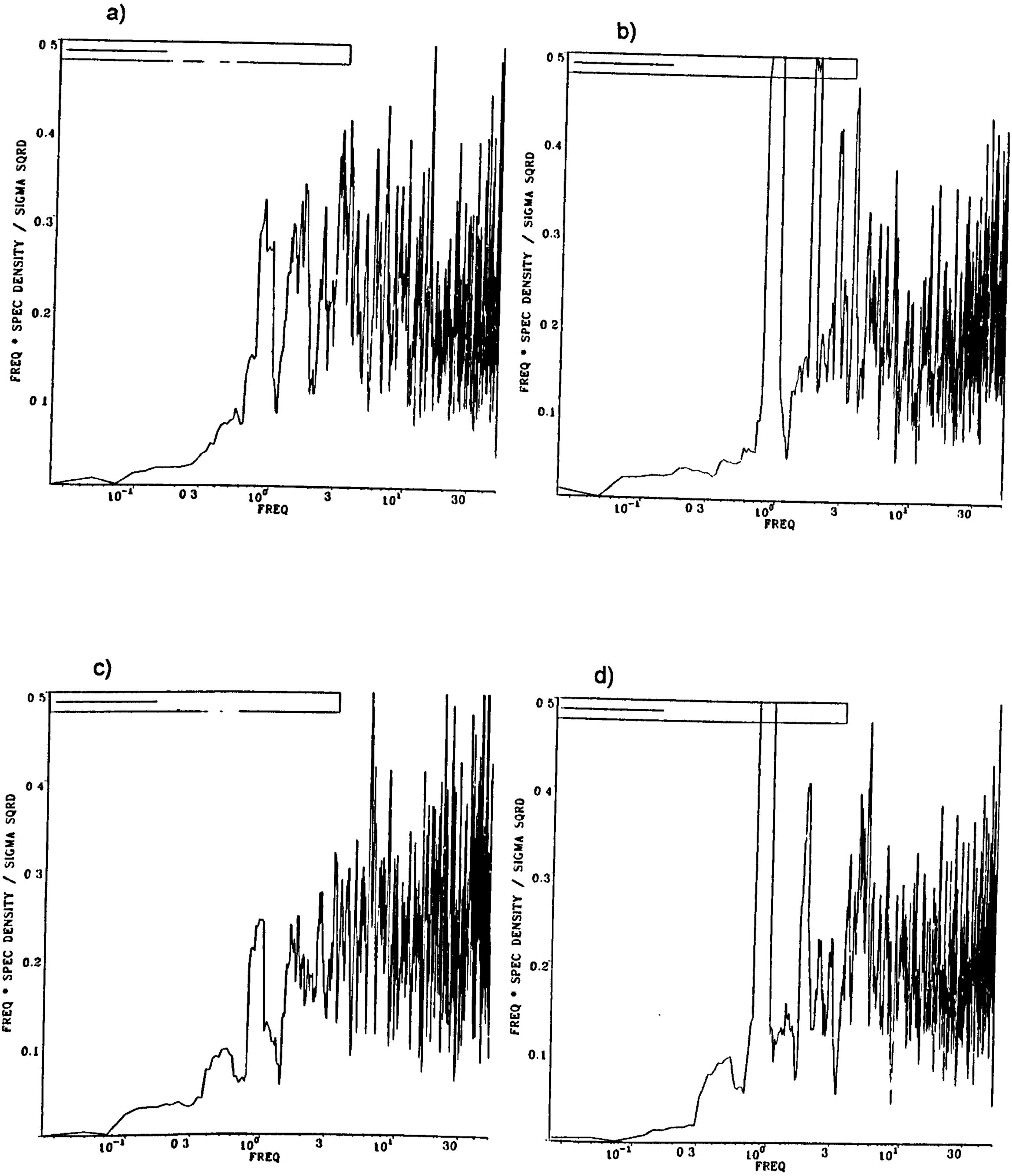

Figure 6.24 Non-dimensional frequency spectra for vertical component of velocity for plunging waves under offshore winds at H_{ref}:
a) X=-912mm b) X=-1404mm c) X=-1811mm
d) X=-2640mm

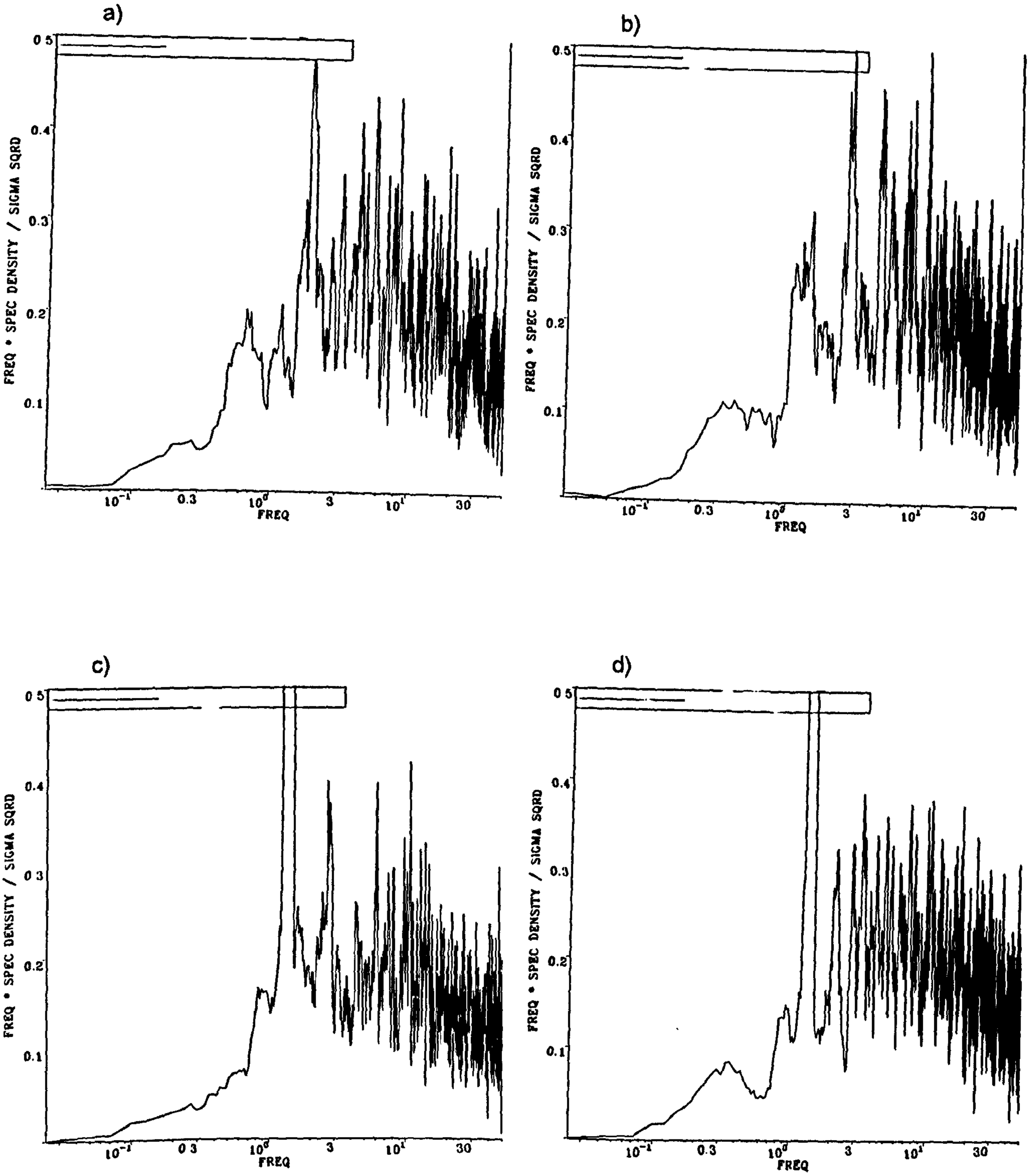

Figure 6.25 Non-dimensional frequency spectra for the vertical component of velocity for spilling waves under onshore winds at H_{ref}:
a) X=100mm b) X=-912mm c) X=-1554mm d) X=-1800mm

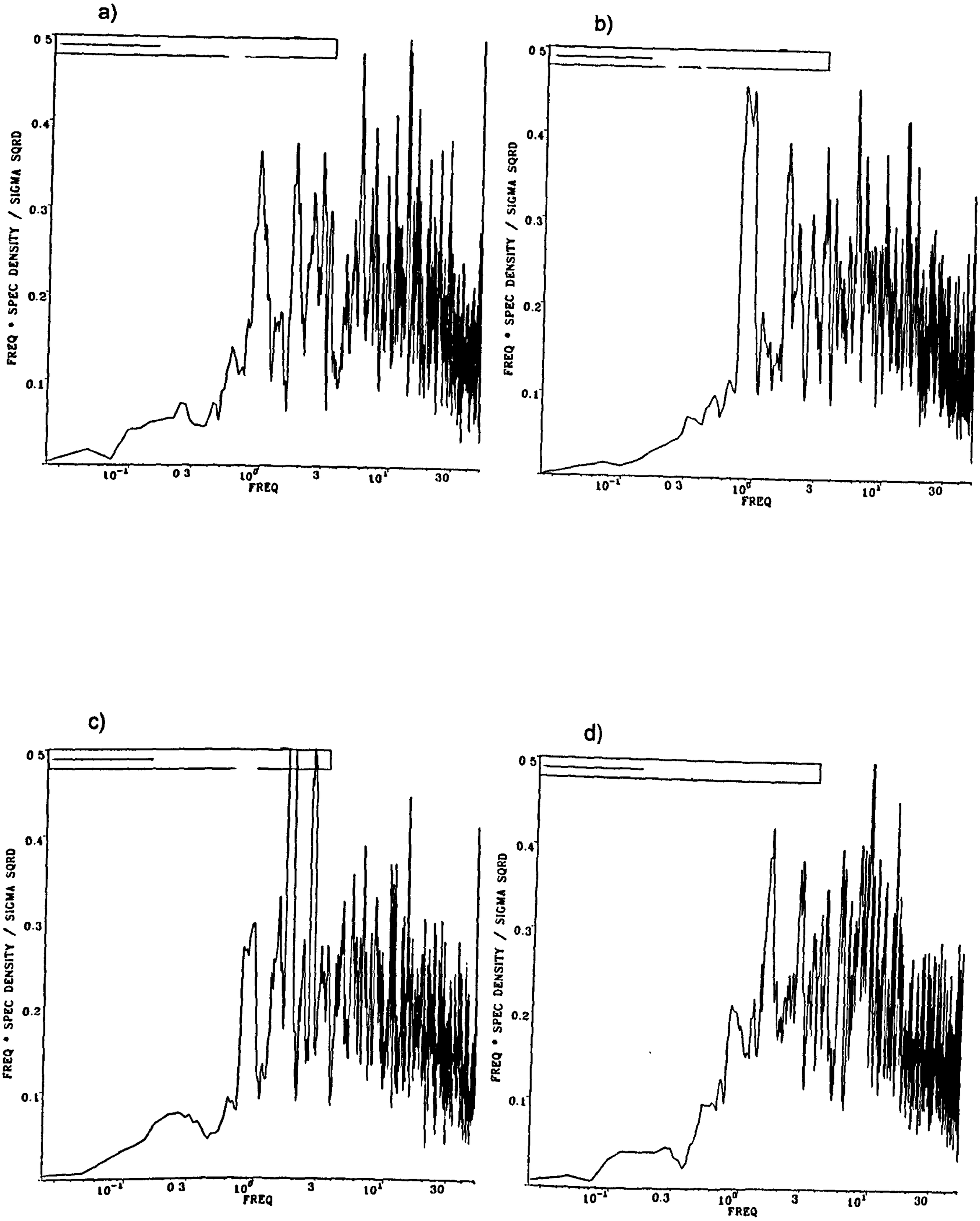

Figure 6.26 Non-dimensional frequency spectra for vertical component of velocity for plunging waves under onshore winds at H_{ref}:
a) X=100mm b) X=-912mm c) X=-1289mm d) X=-1795mm

a)

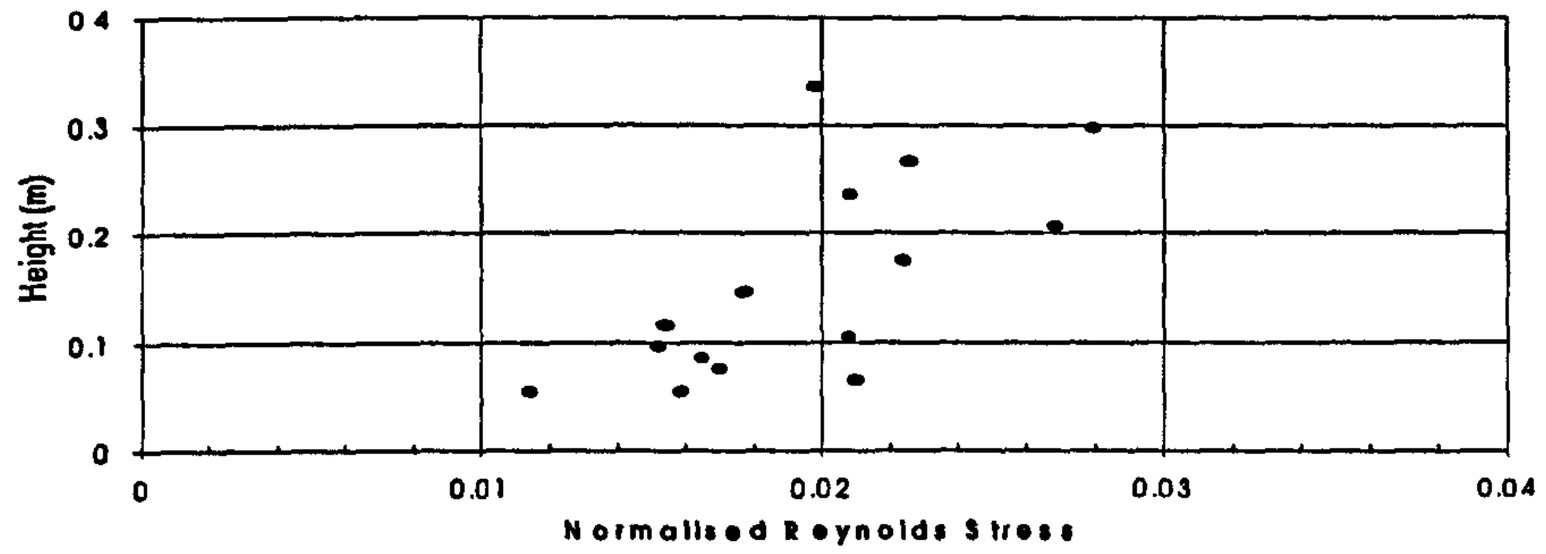

b)

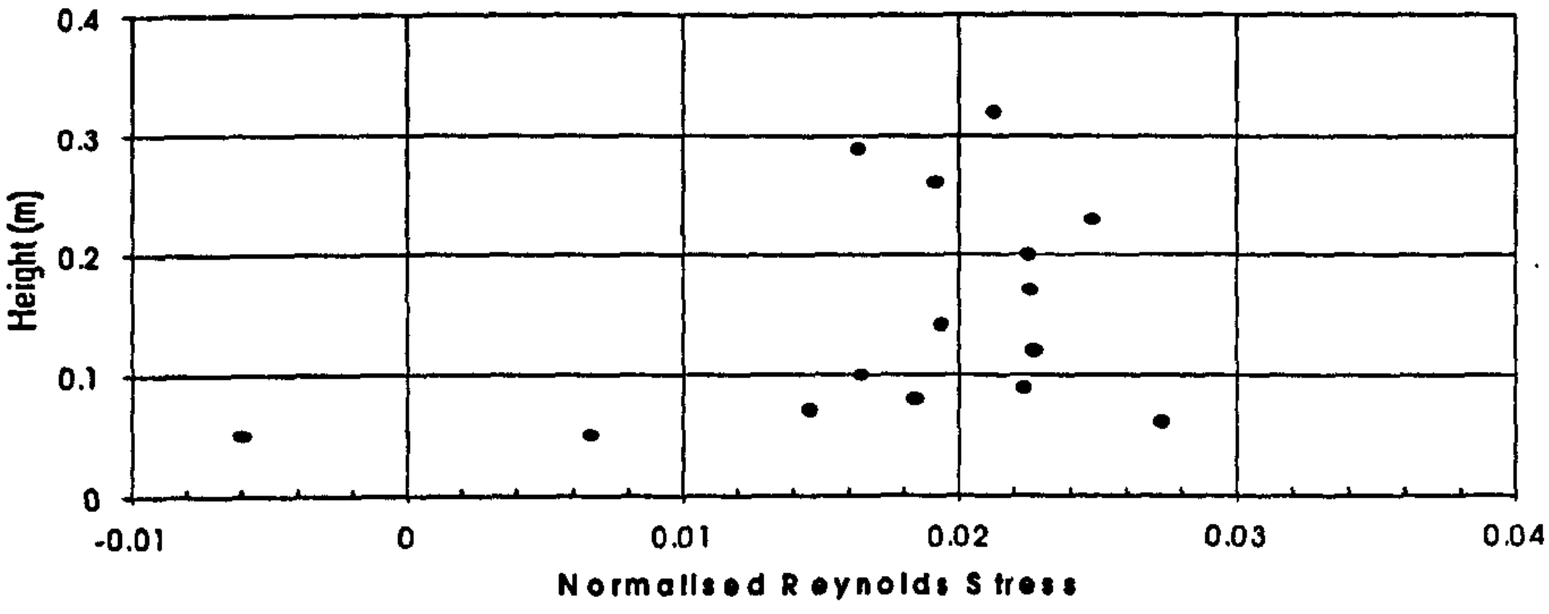

c)

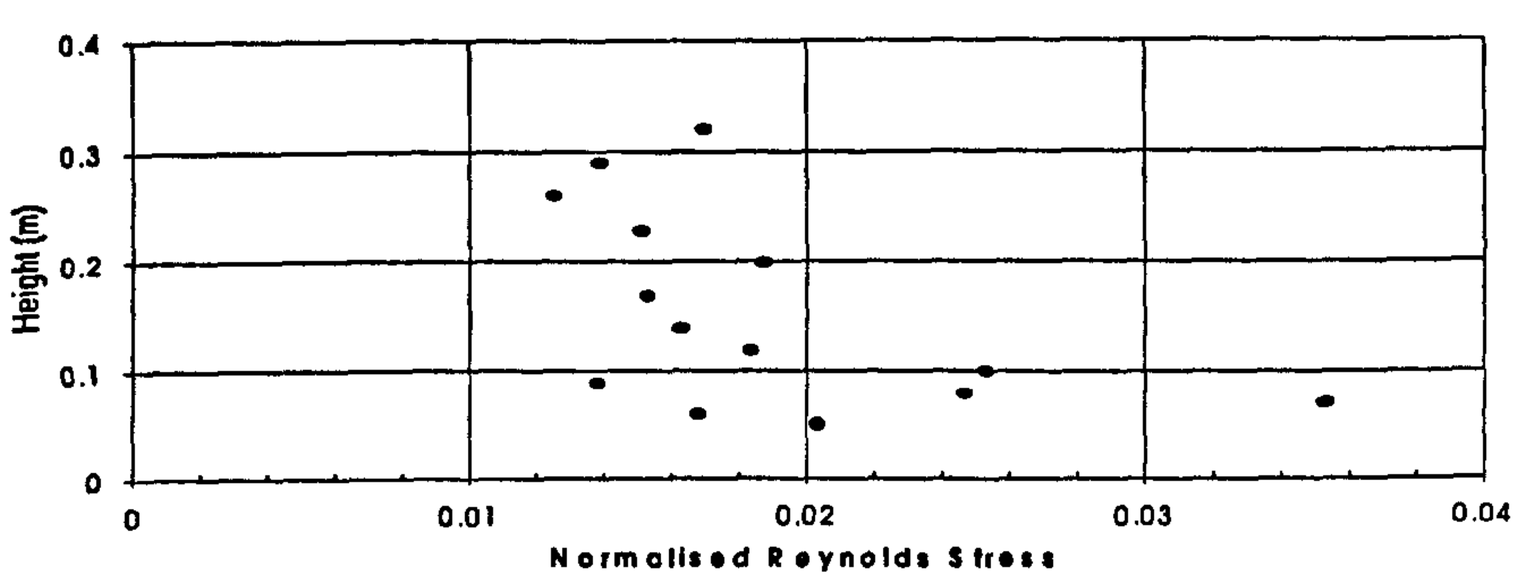

d)

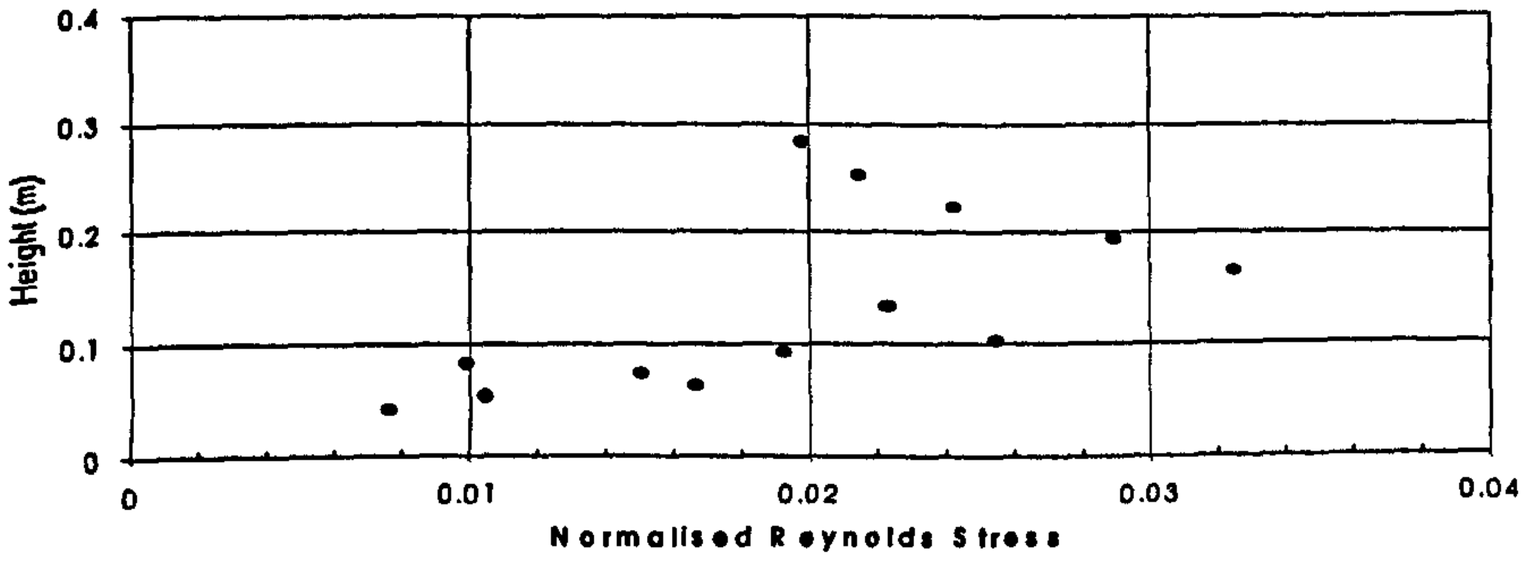

Figure 6.27 Normalised Reynolds stress profiles for spilling waves under offshore winds: a) X=-912mm b) X=-1177mm c) X=-1575mm d) X=-2646mm

a)

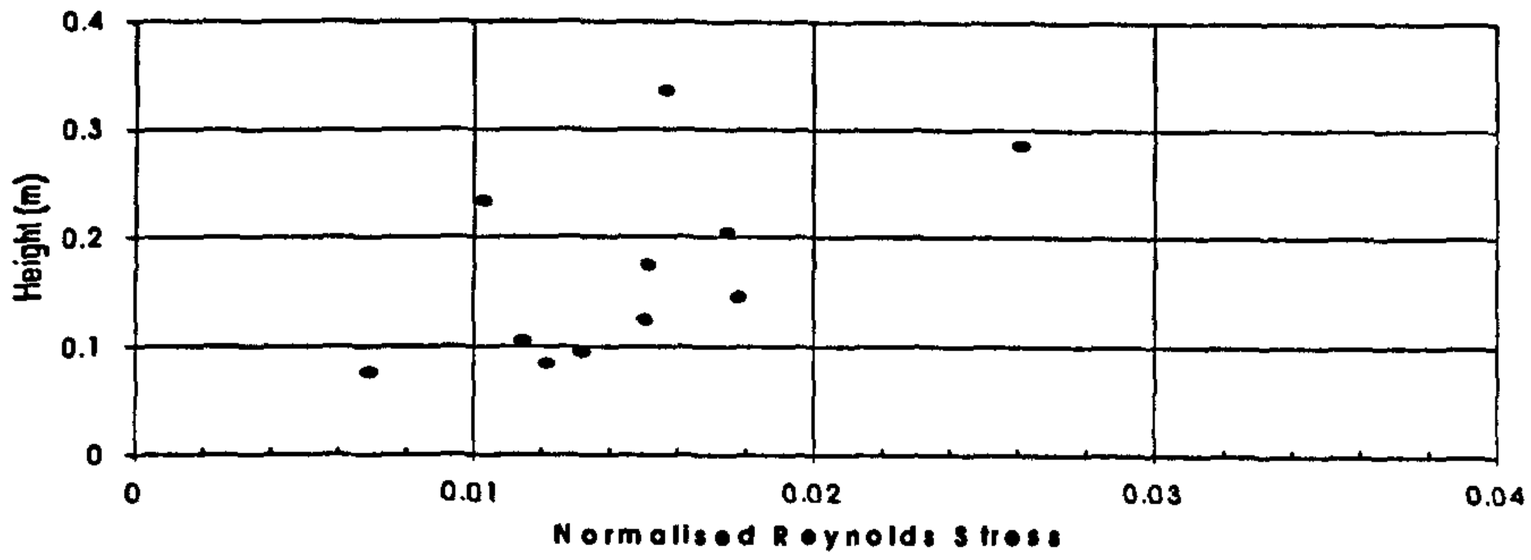

b)

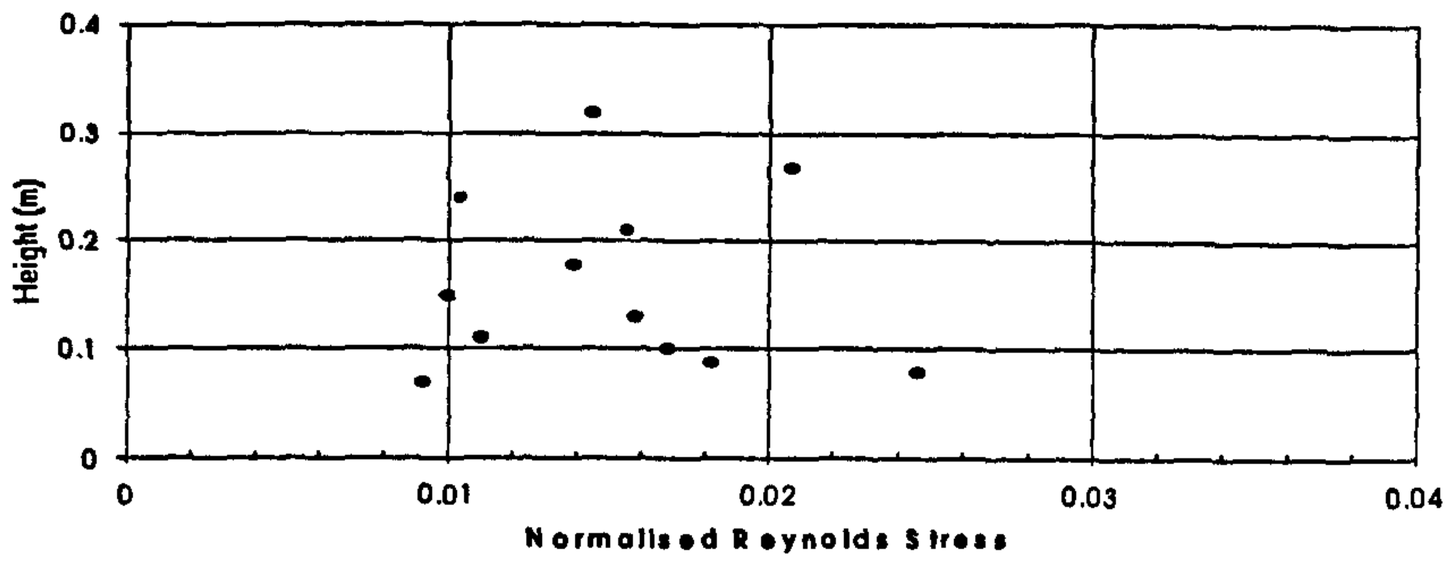

c)

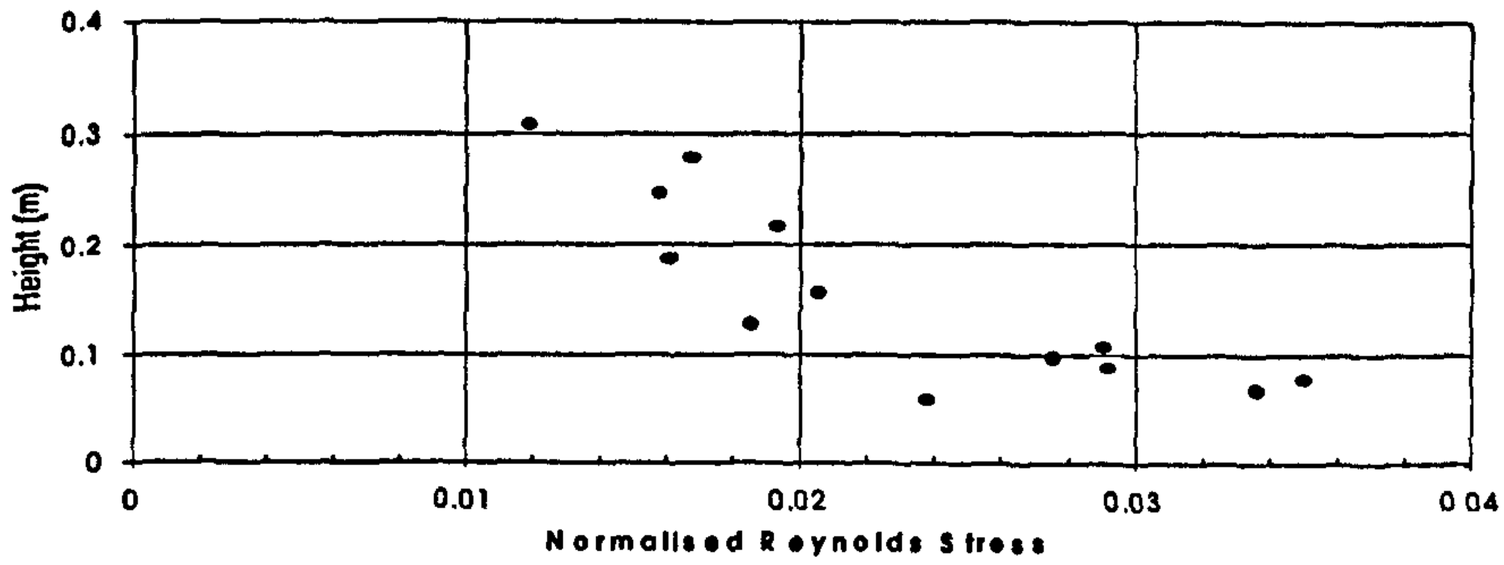

d)

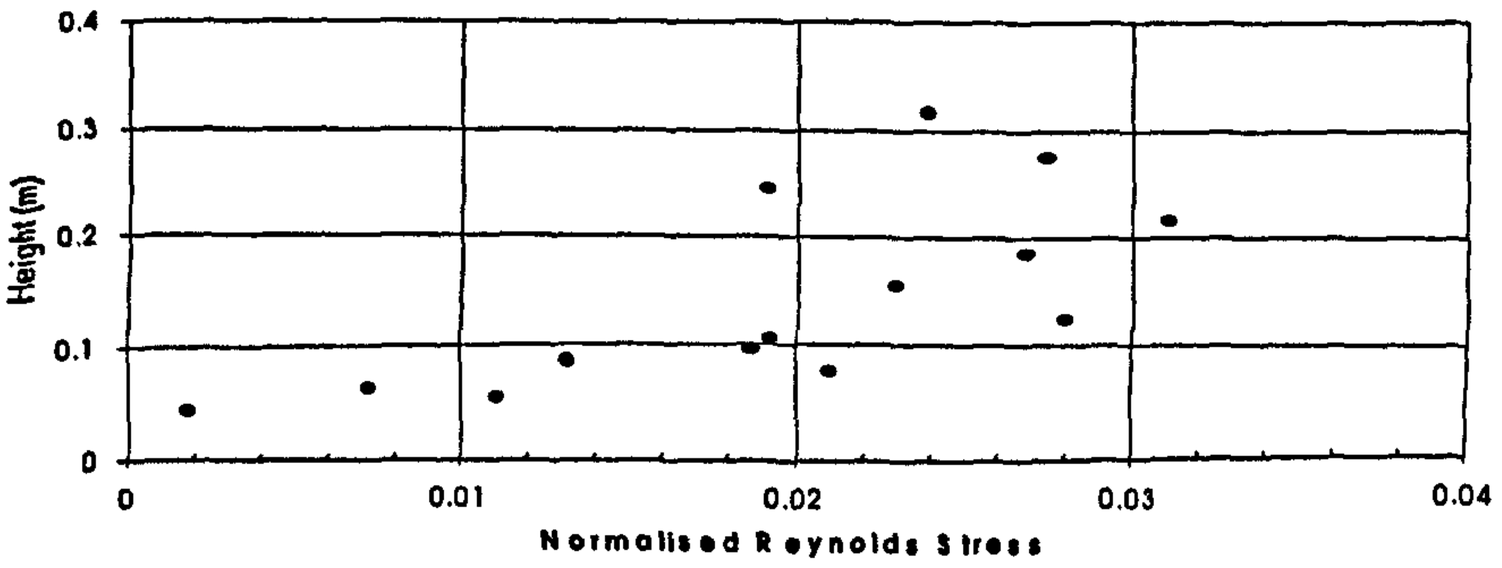

Figure 6.28 Normalised Reynolds stress profiles for plunging waves under offshore winds: a) X=-912mm b) X=-1404mm c) X=-1811mm d) X=-2640mm

a)

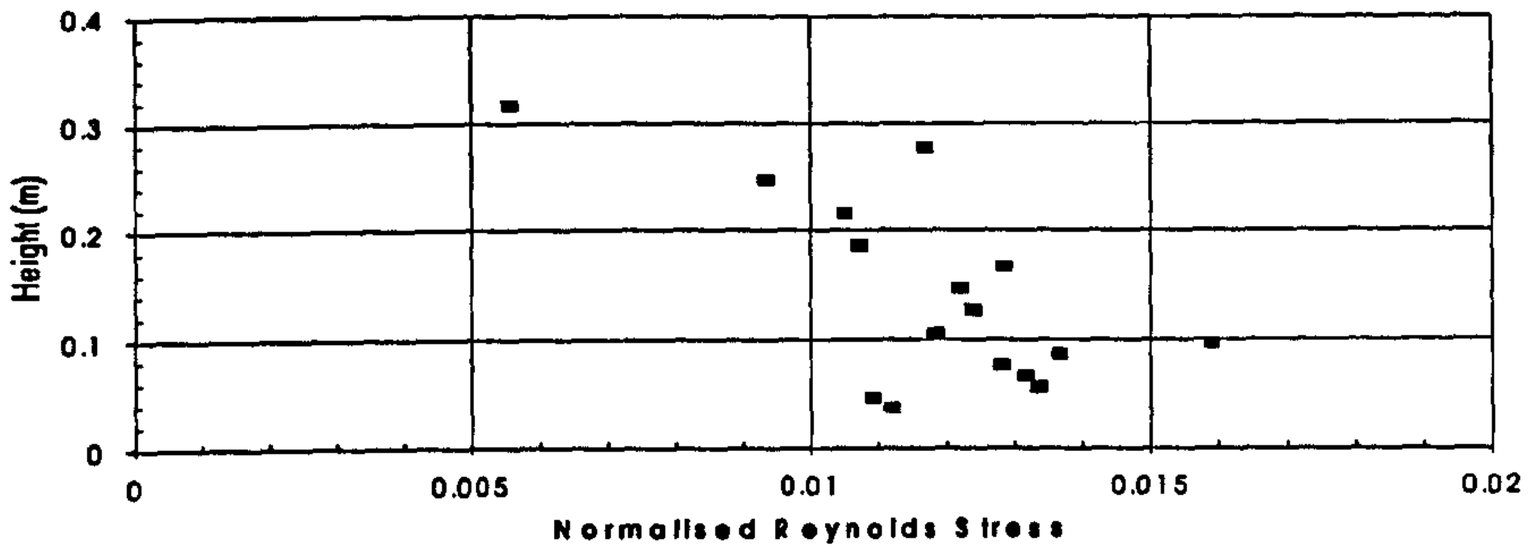

b)

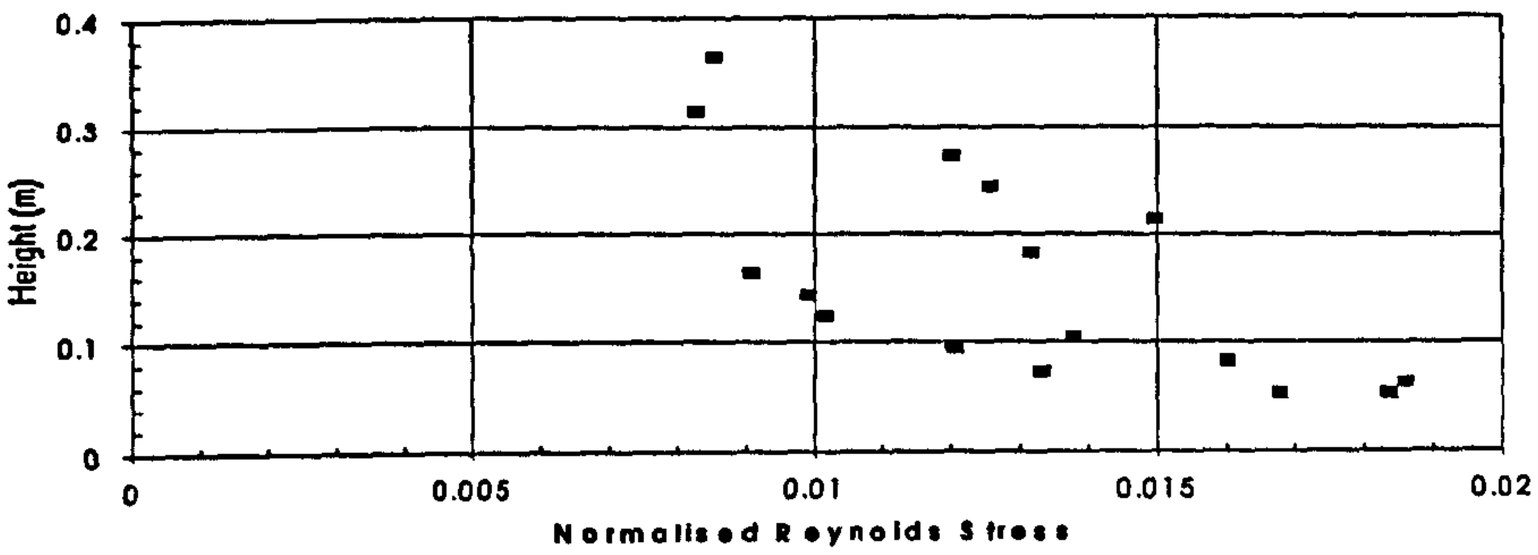

c)

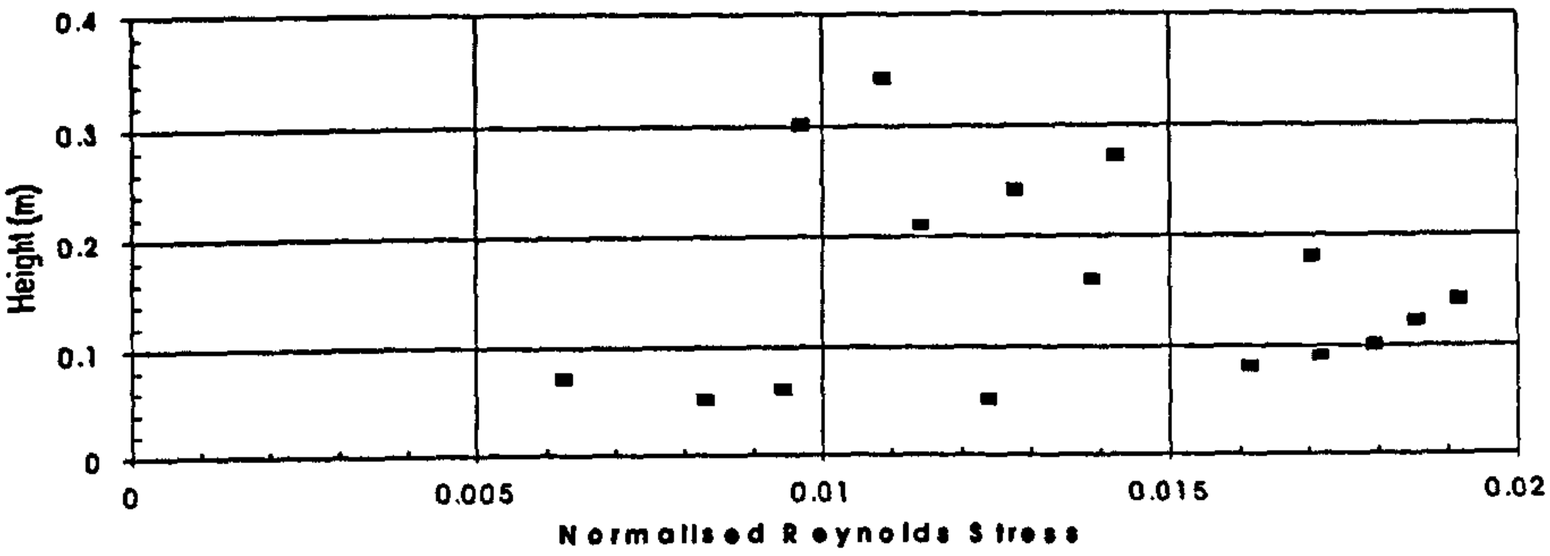

d)

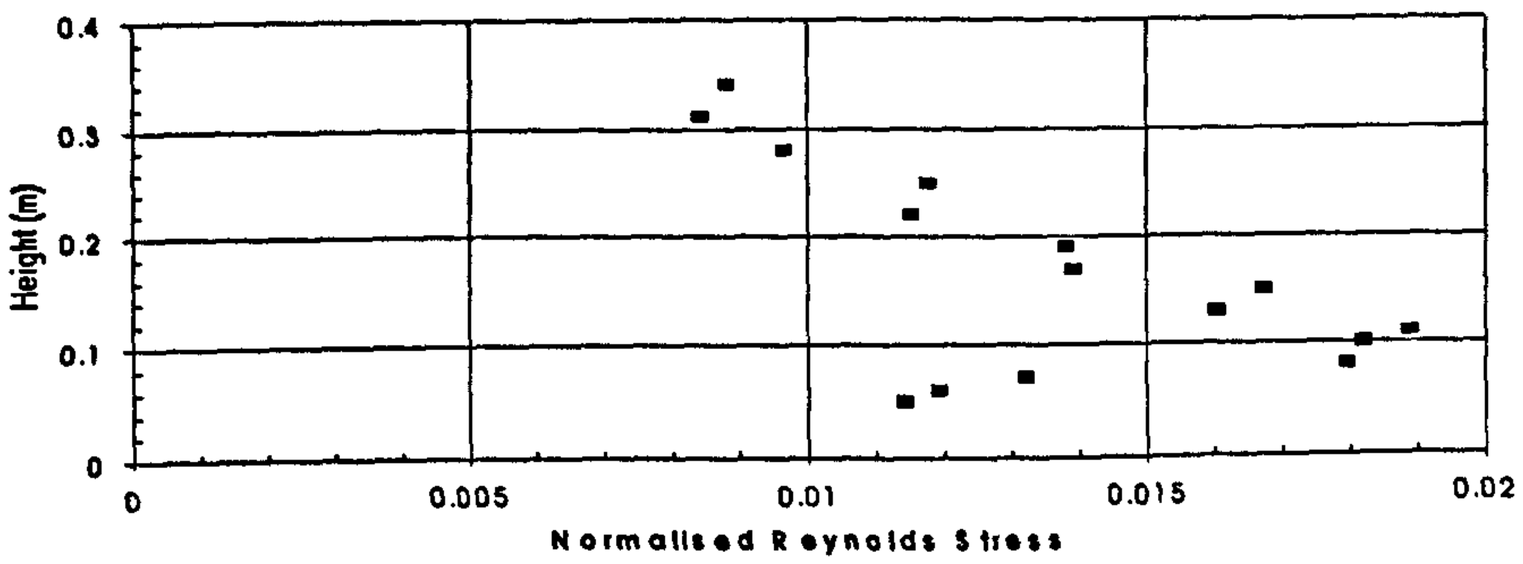

Figure 6.29 Normalised Reynolds stress profiles for spilling waves under onshore winds: a) X=100mm b) X=-912mm c) X=-1554mm d) X=-1800mm

a)

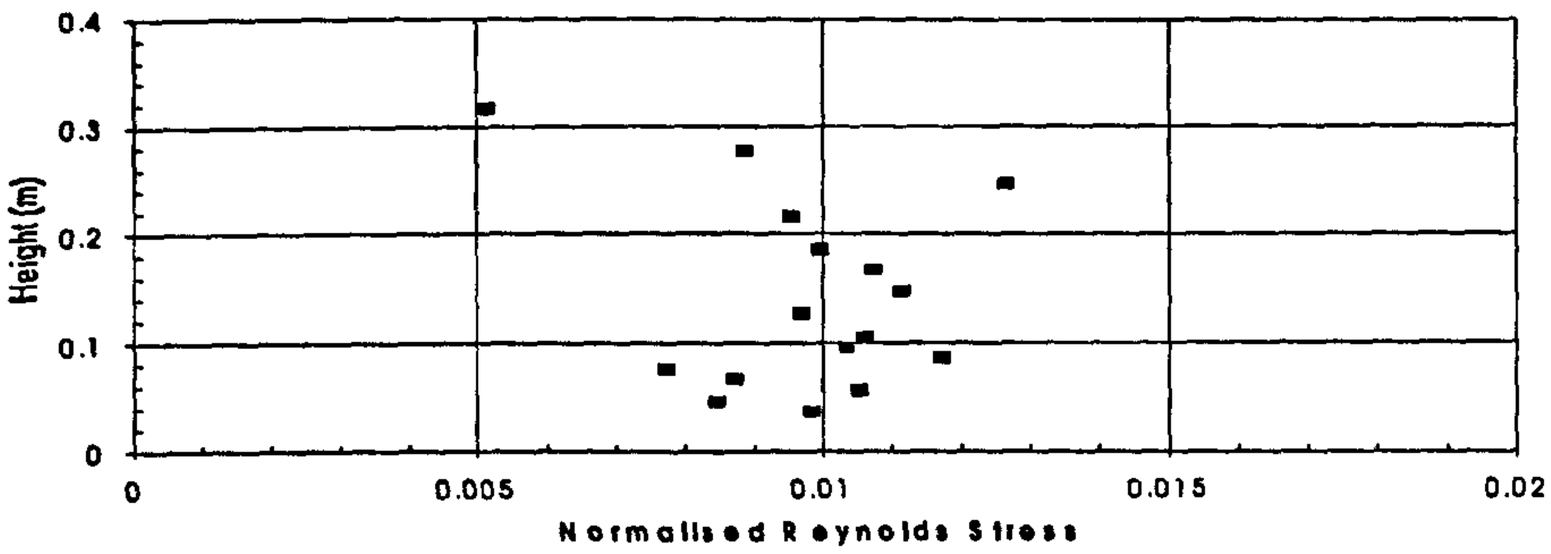

b)

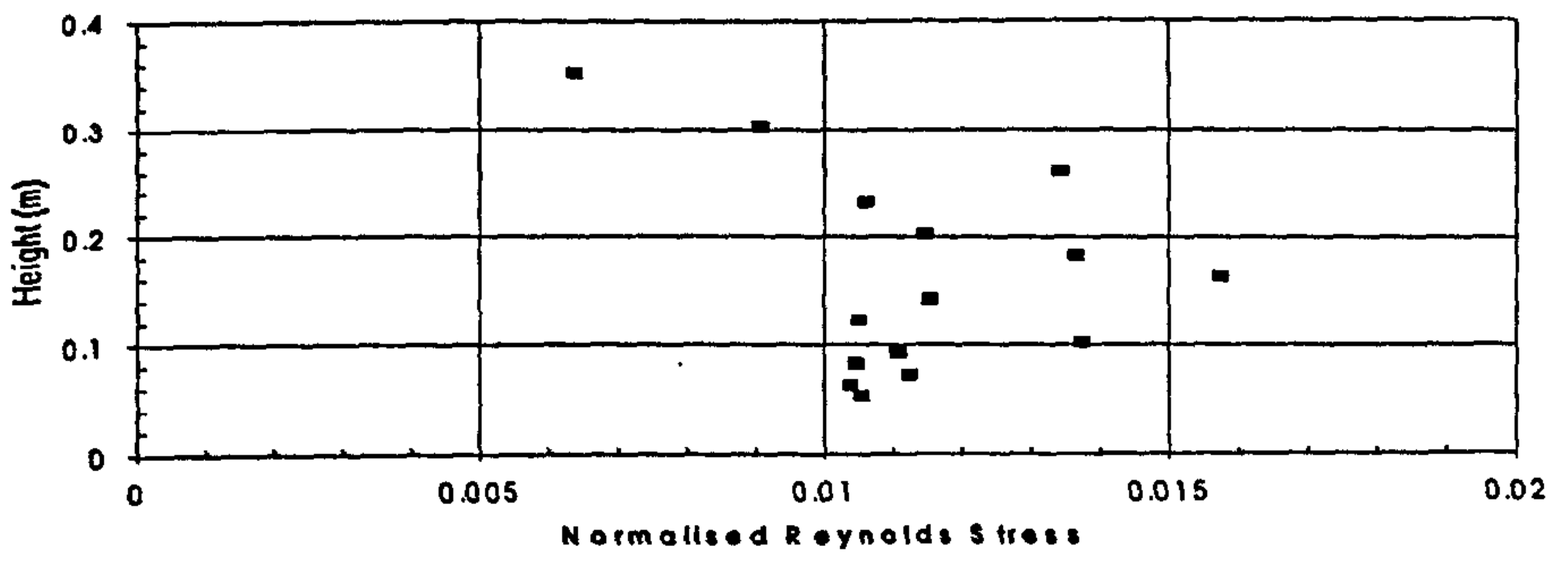

c)

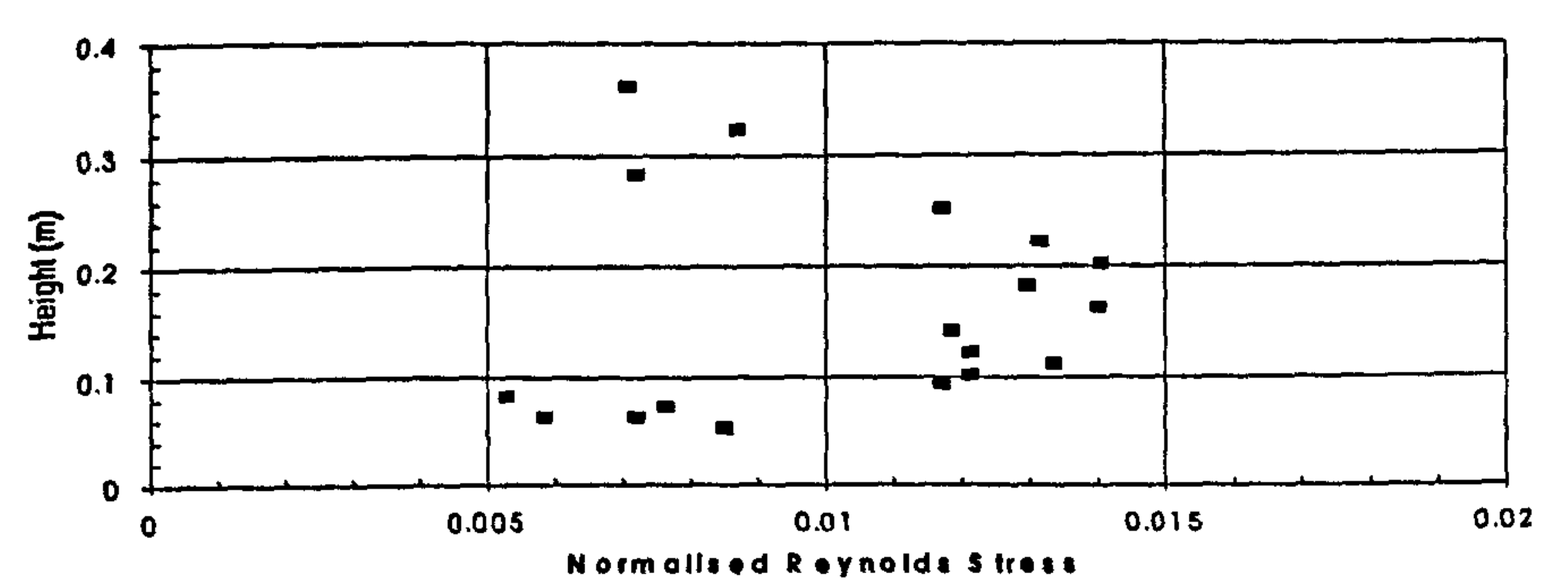

d)

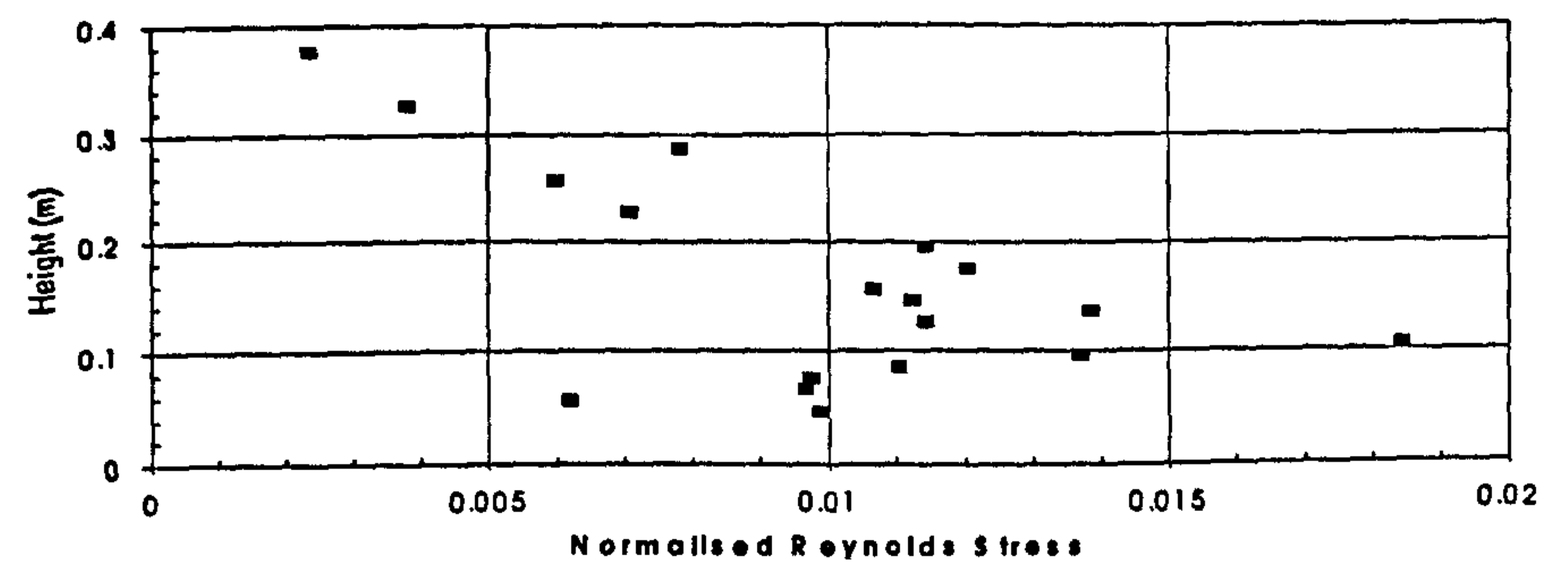

Figure 6.30 Normalised Reynolds stress profiles for plunging waves under onshore winds: a) X=100mm b) X=-912mm c) X=-1289mm d) X=-1795mm

a)

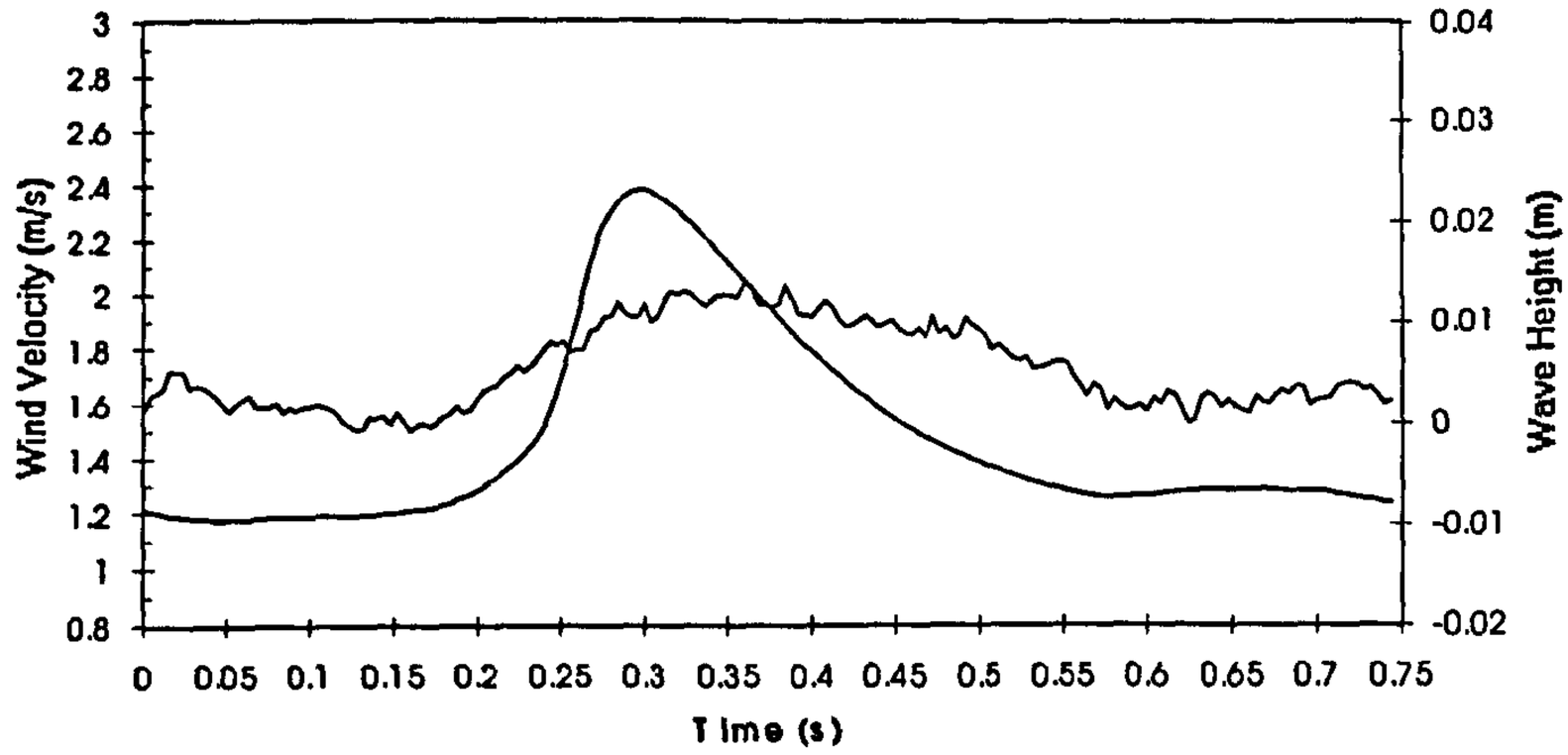

b)

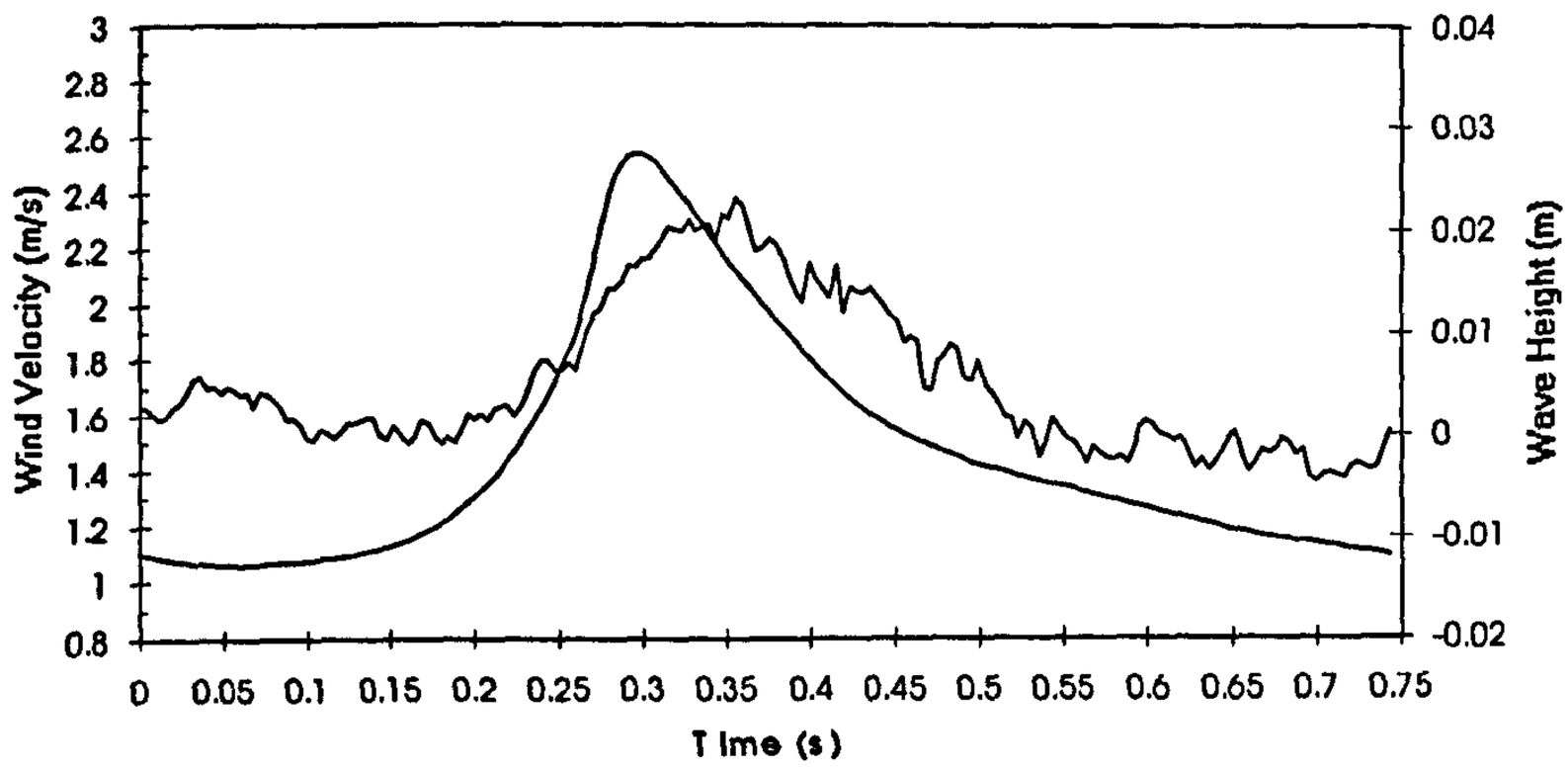

c)

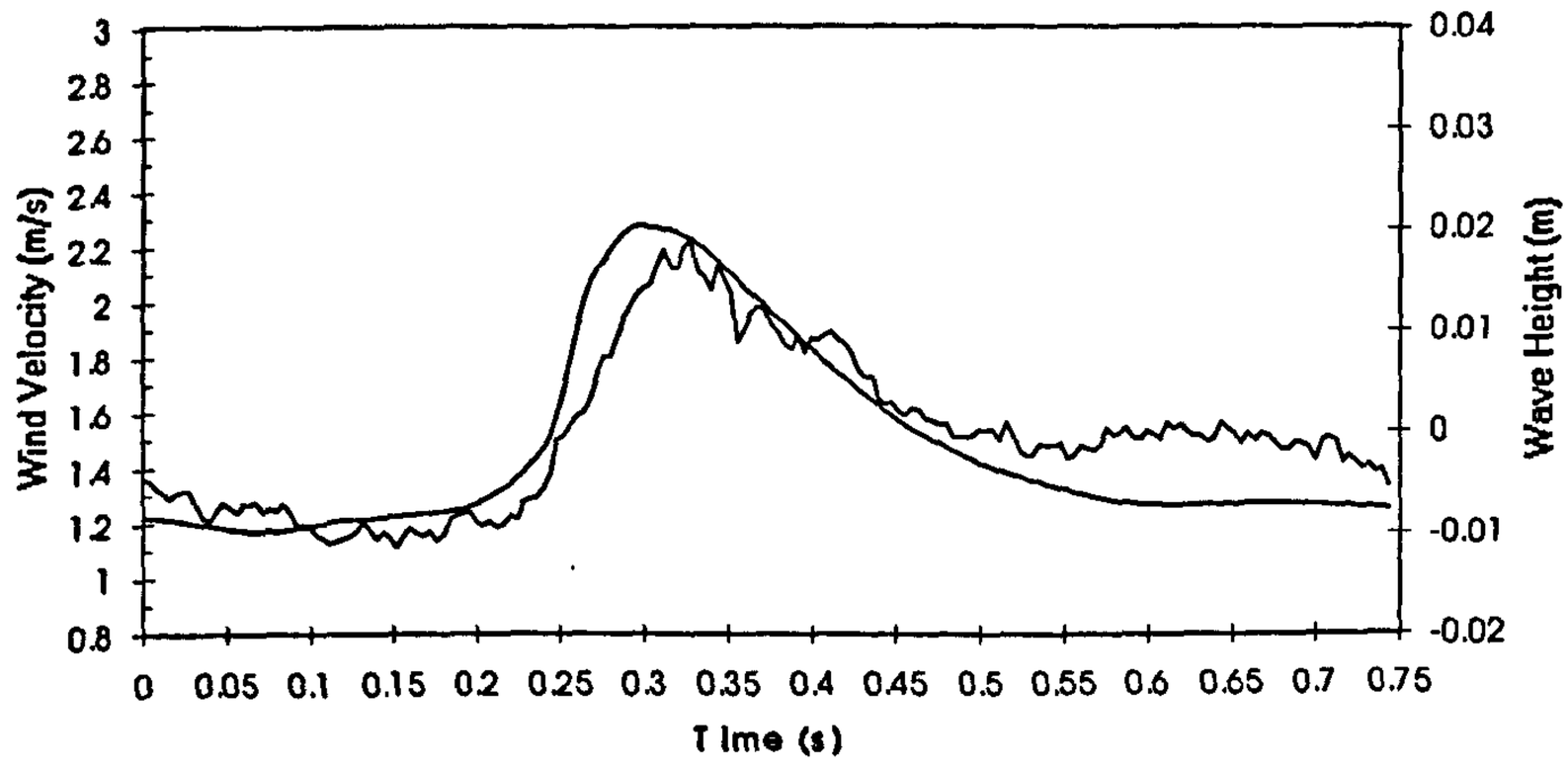

Figure 6.31 Phase-averaged results for spilling waves under offshore winds at X=-1183mm. Probe heights: a) 83 b) 63 c) 43mm

a)

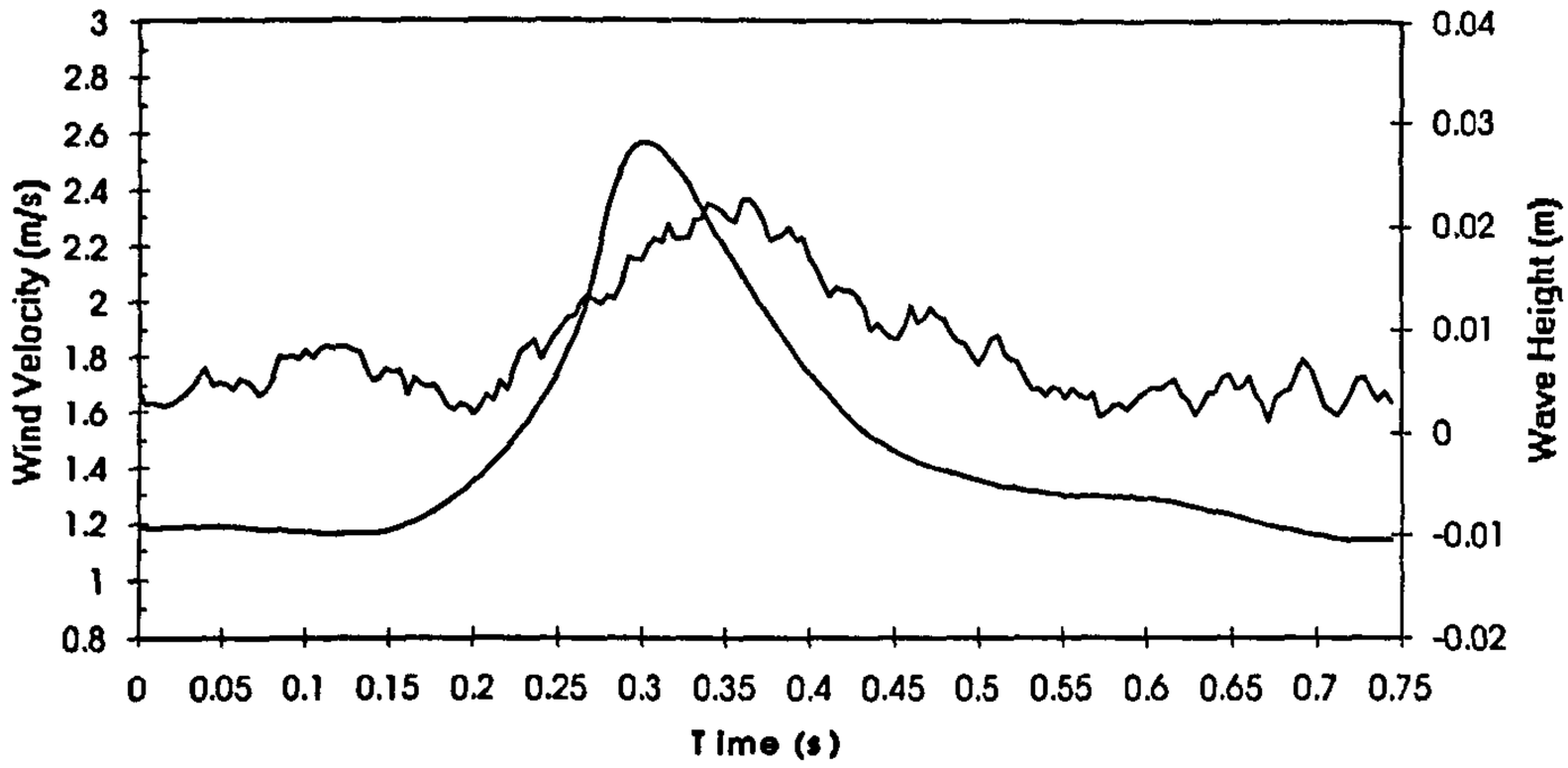

b)

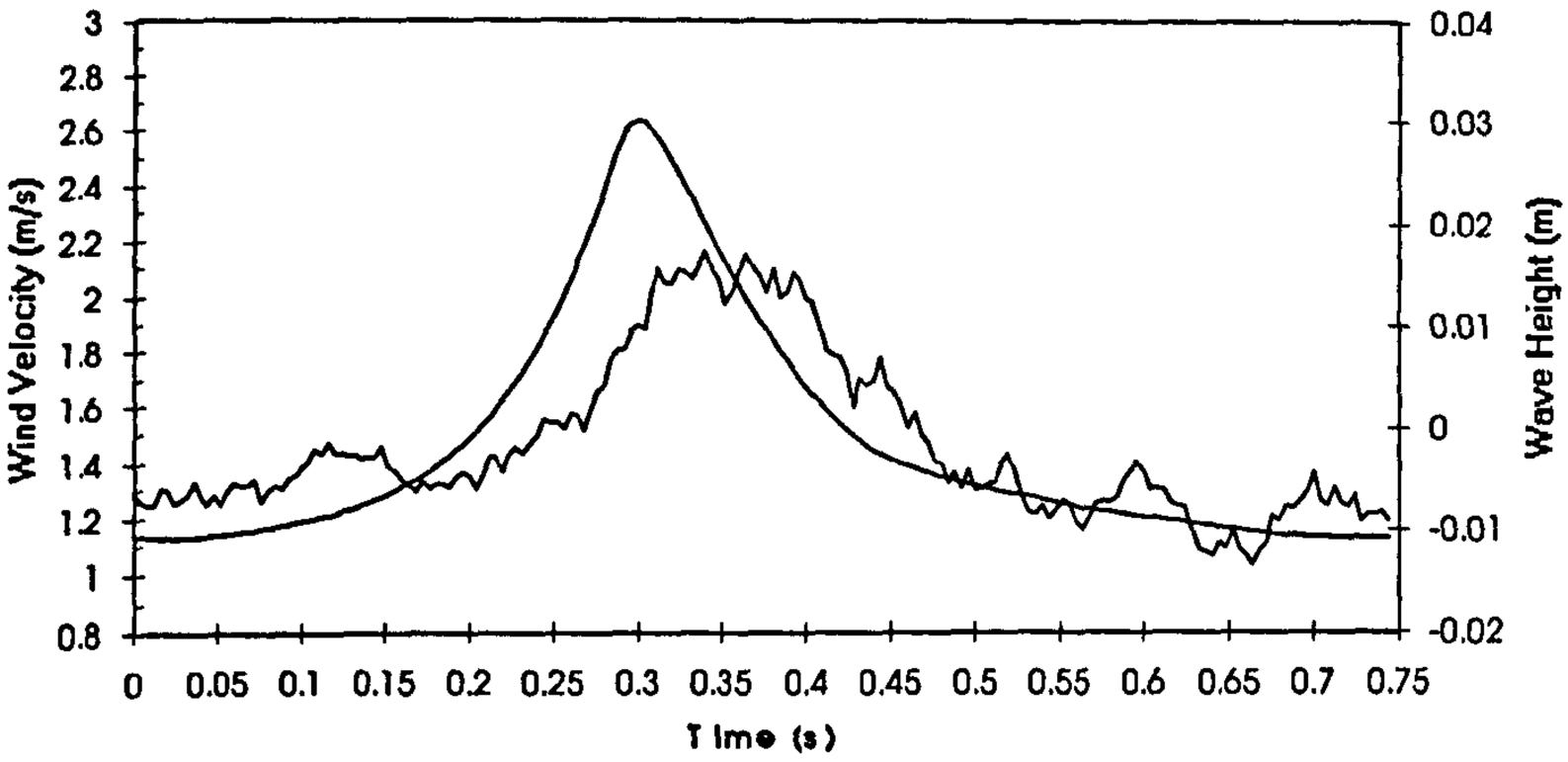

c)

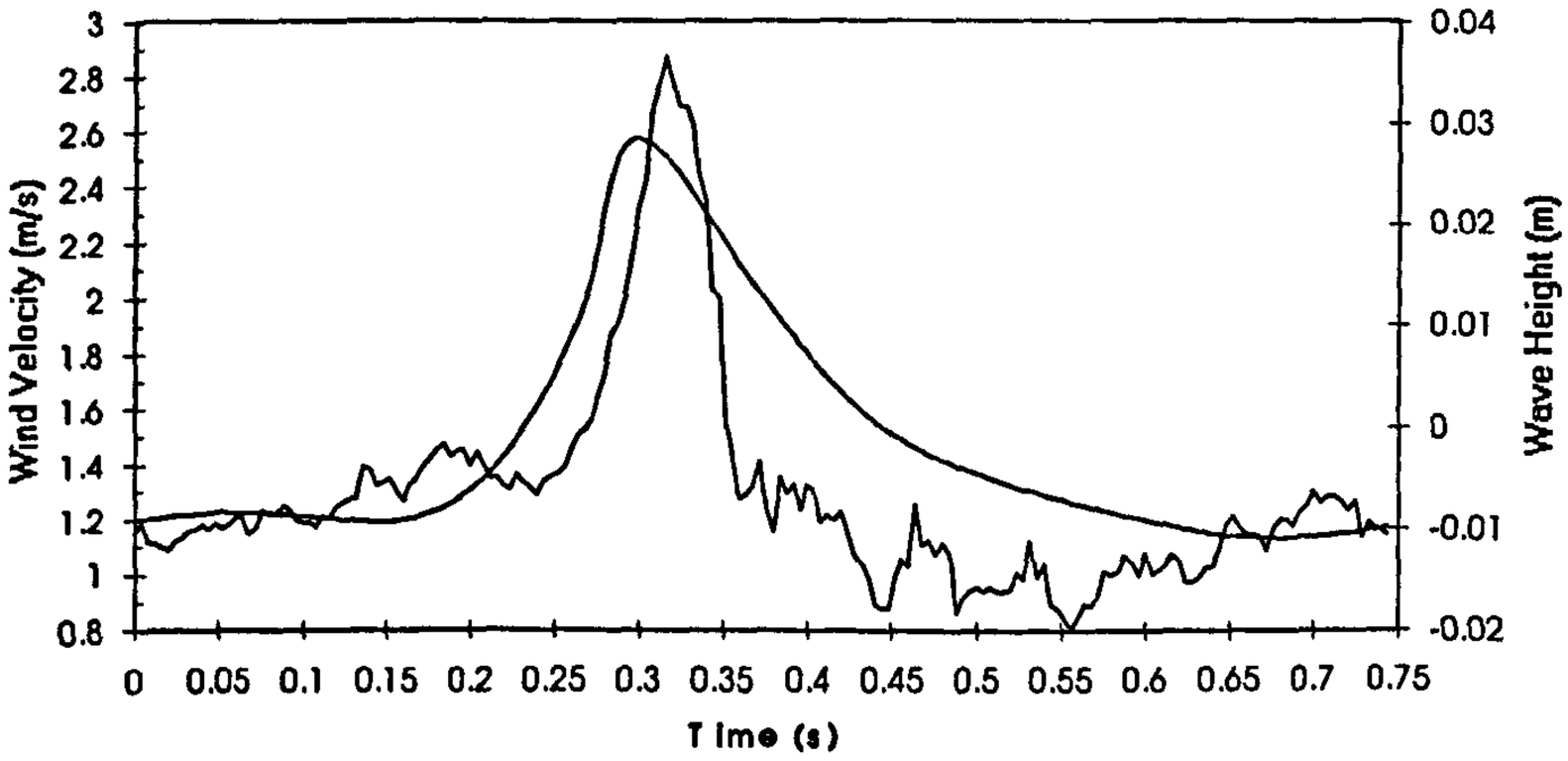

Figure 6.32 Phase-averaged results for spilling waves under offshore winds at X=-1370mm. Probe heights: a) 83 b) 63 c) 43mm

a)

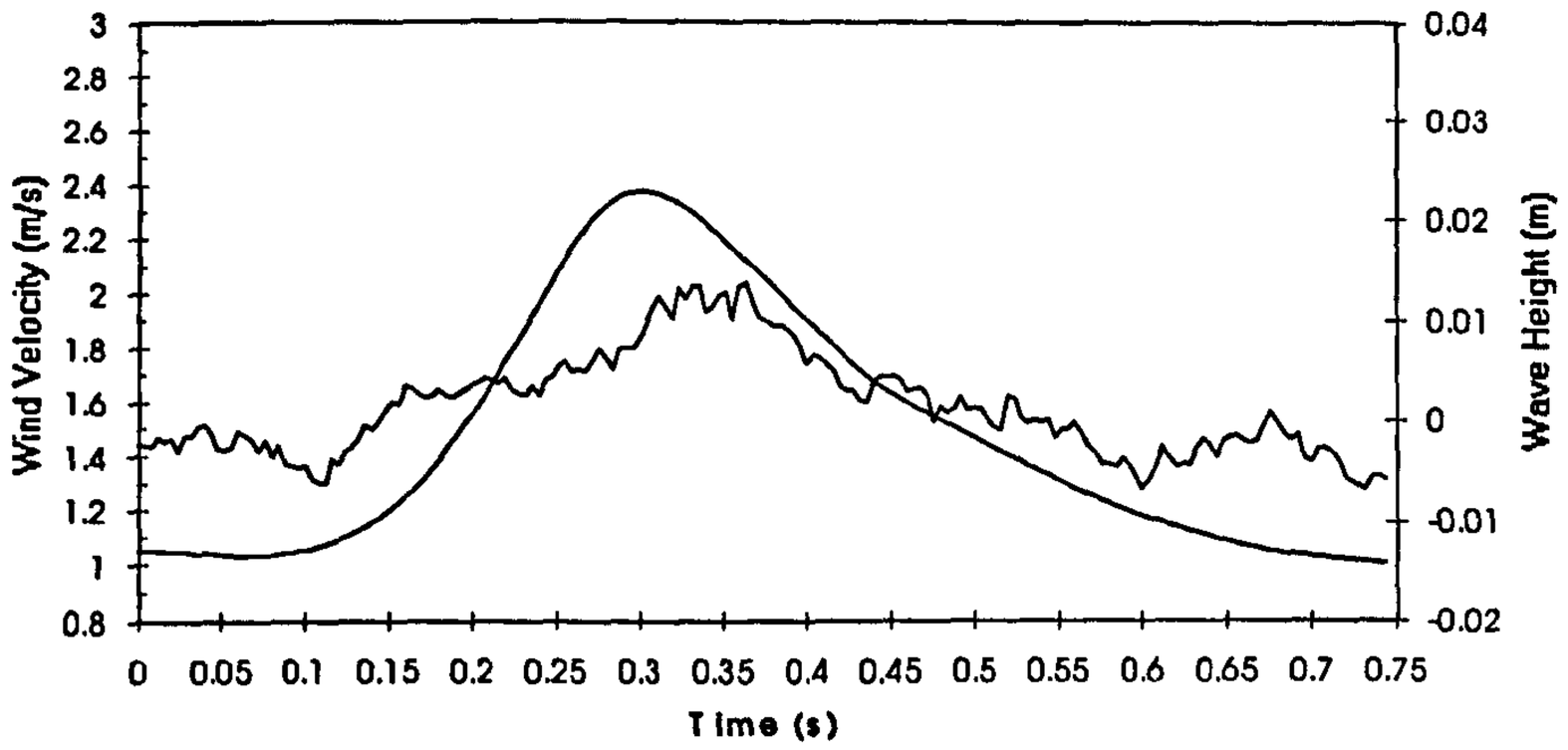

b)

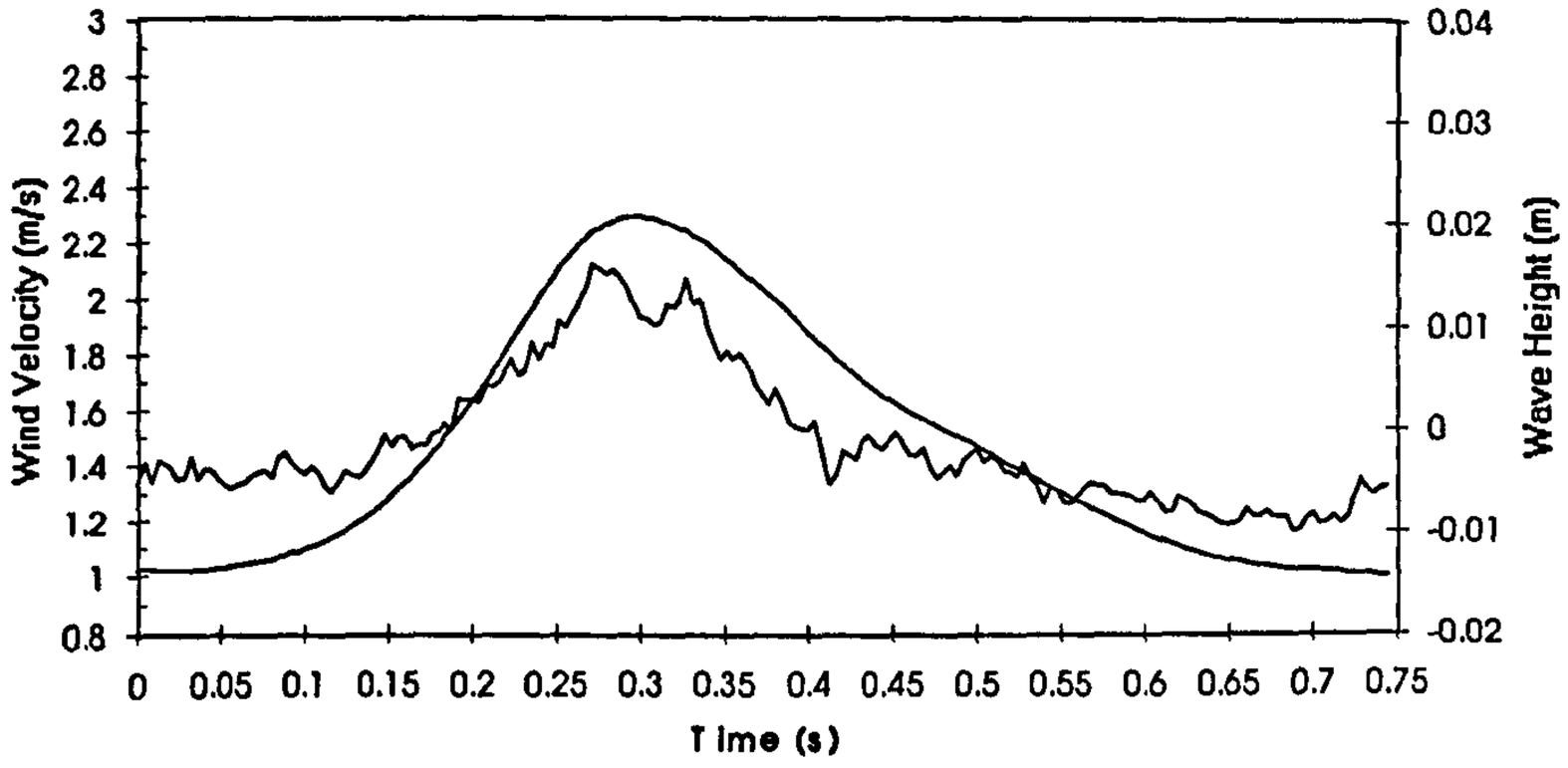

c)

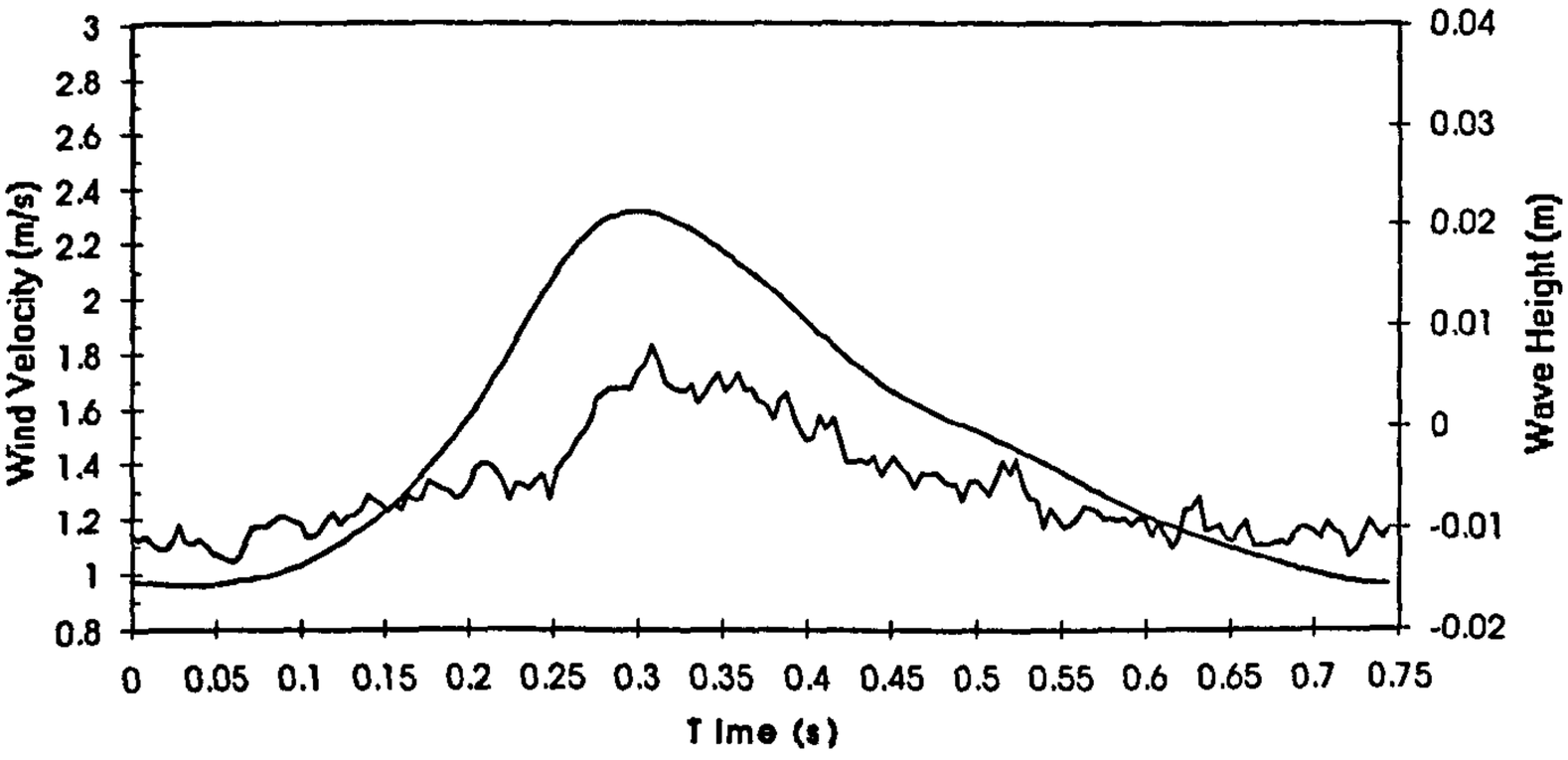

Figure 6.33 Phase-averaged results for spilling waves under offshore winds at X=-1738mm. Probe heights: a) 83 b) 63 c) 43mm

a)

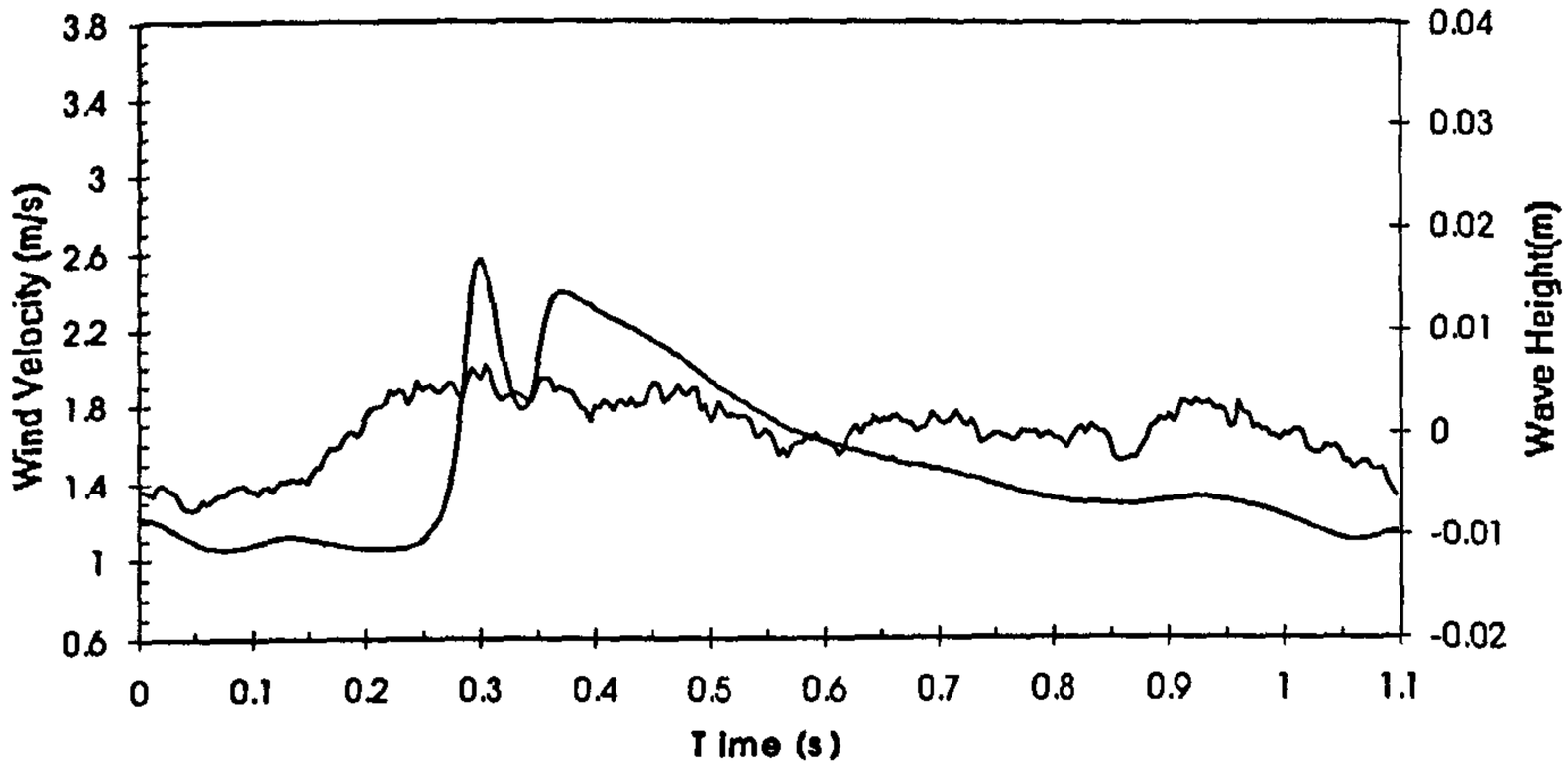

b)

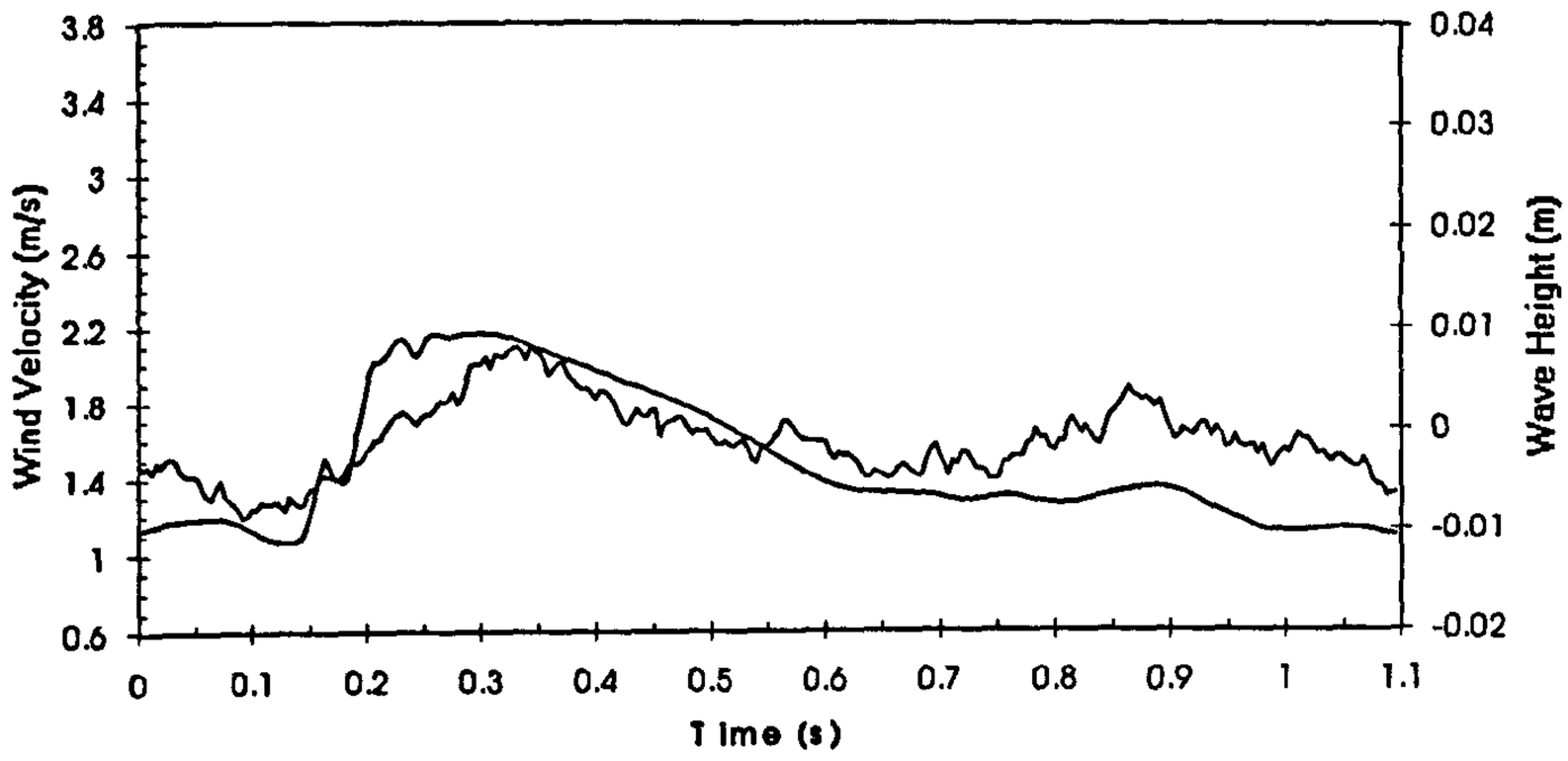

c)

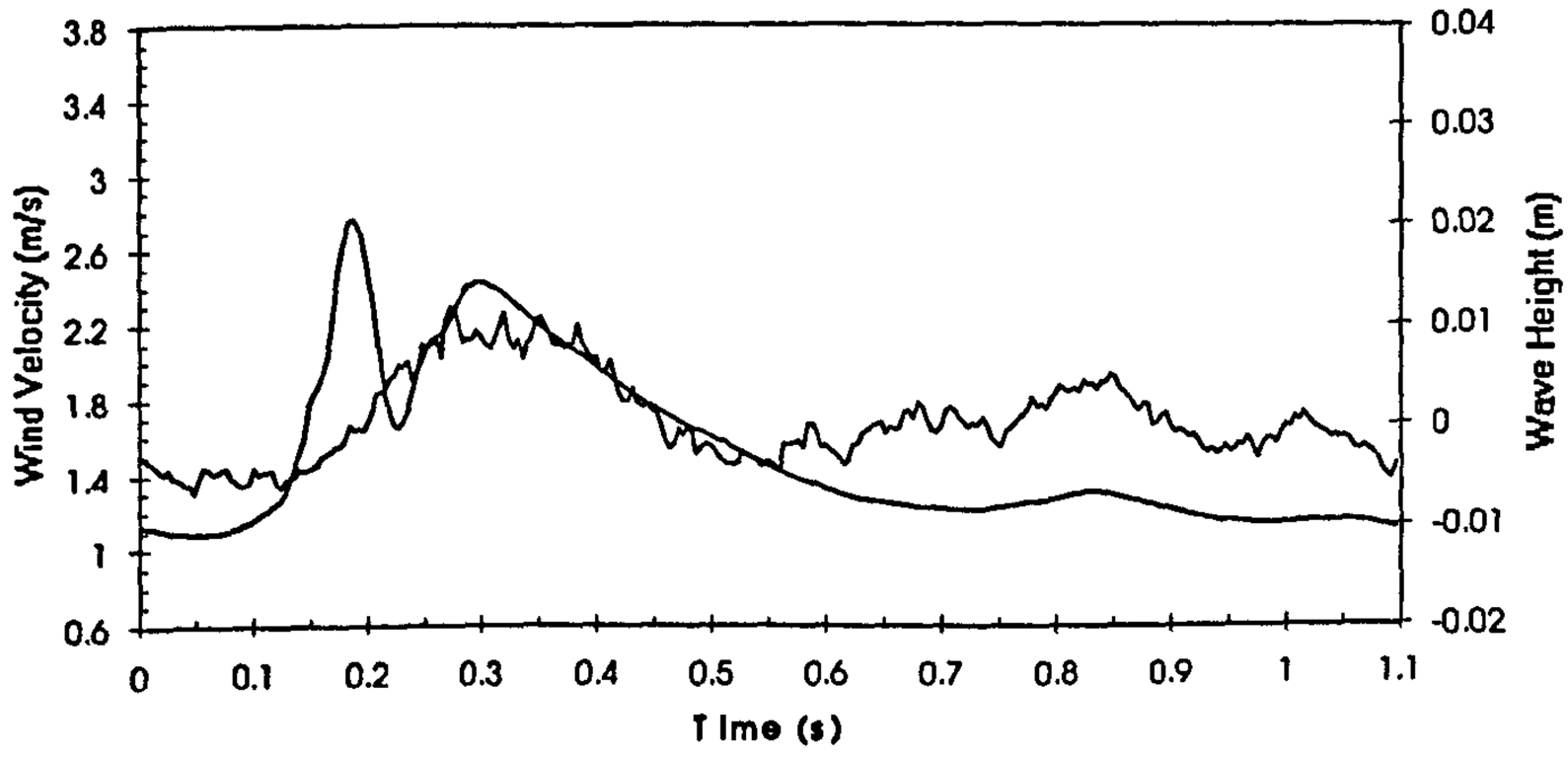

Figure 6.34 Phase-averaged results for plunging waves under offshore winds at X=-1136mm. Probe heights: a) 83 b) 63 c) 48mm

a)

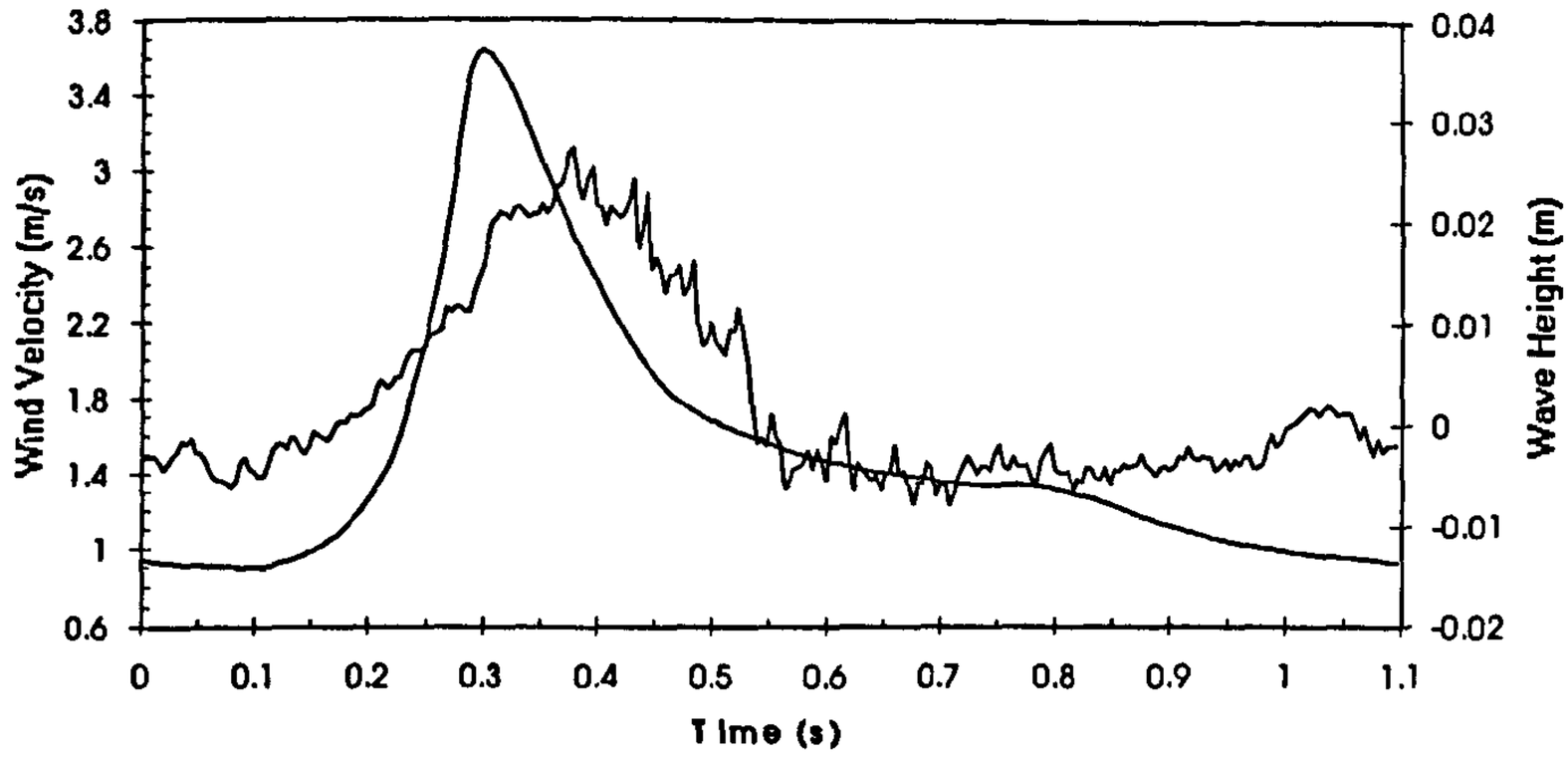

b)

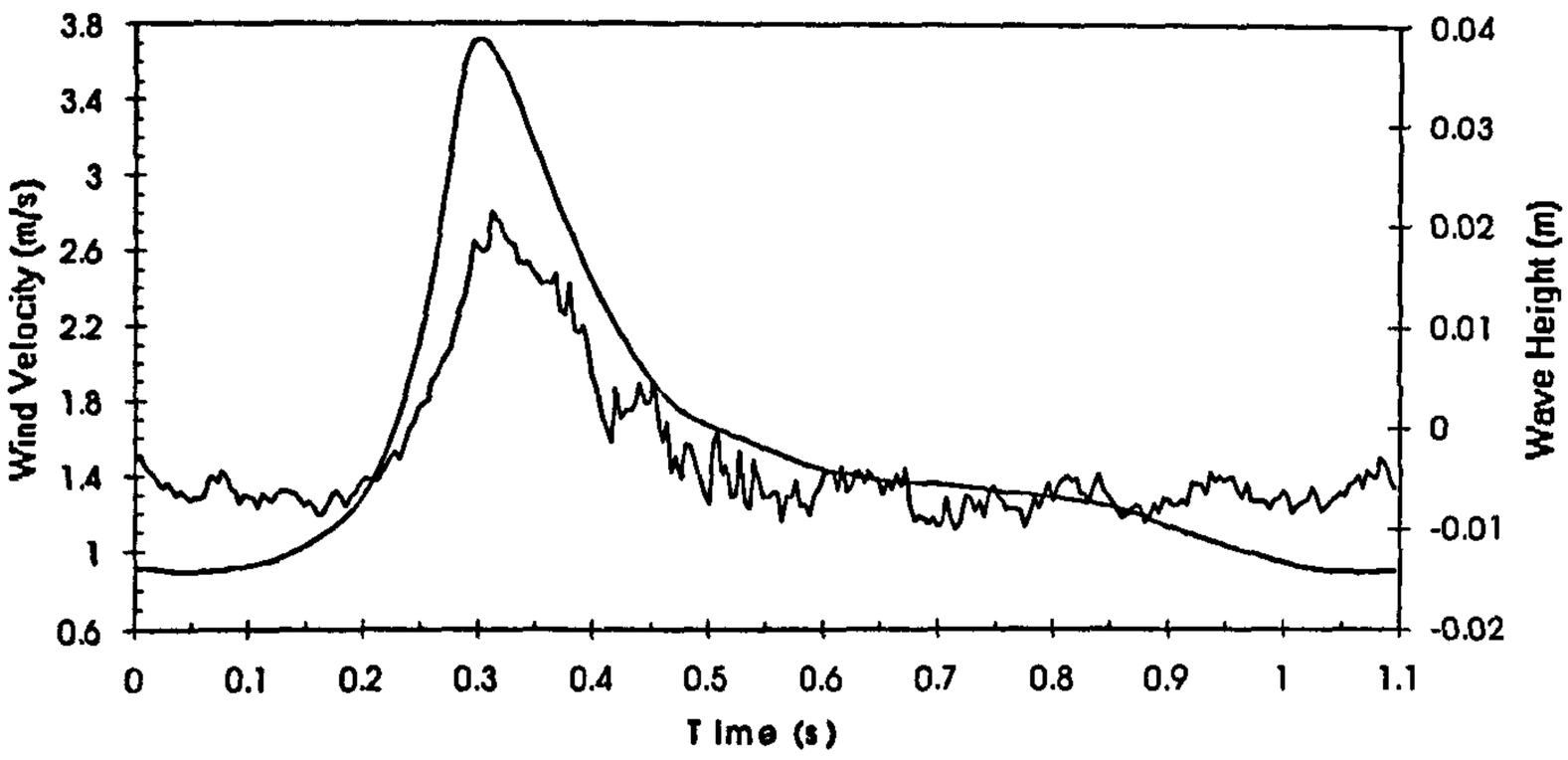

c)

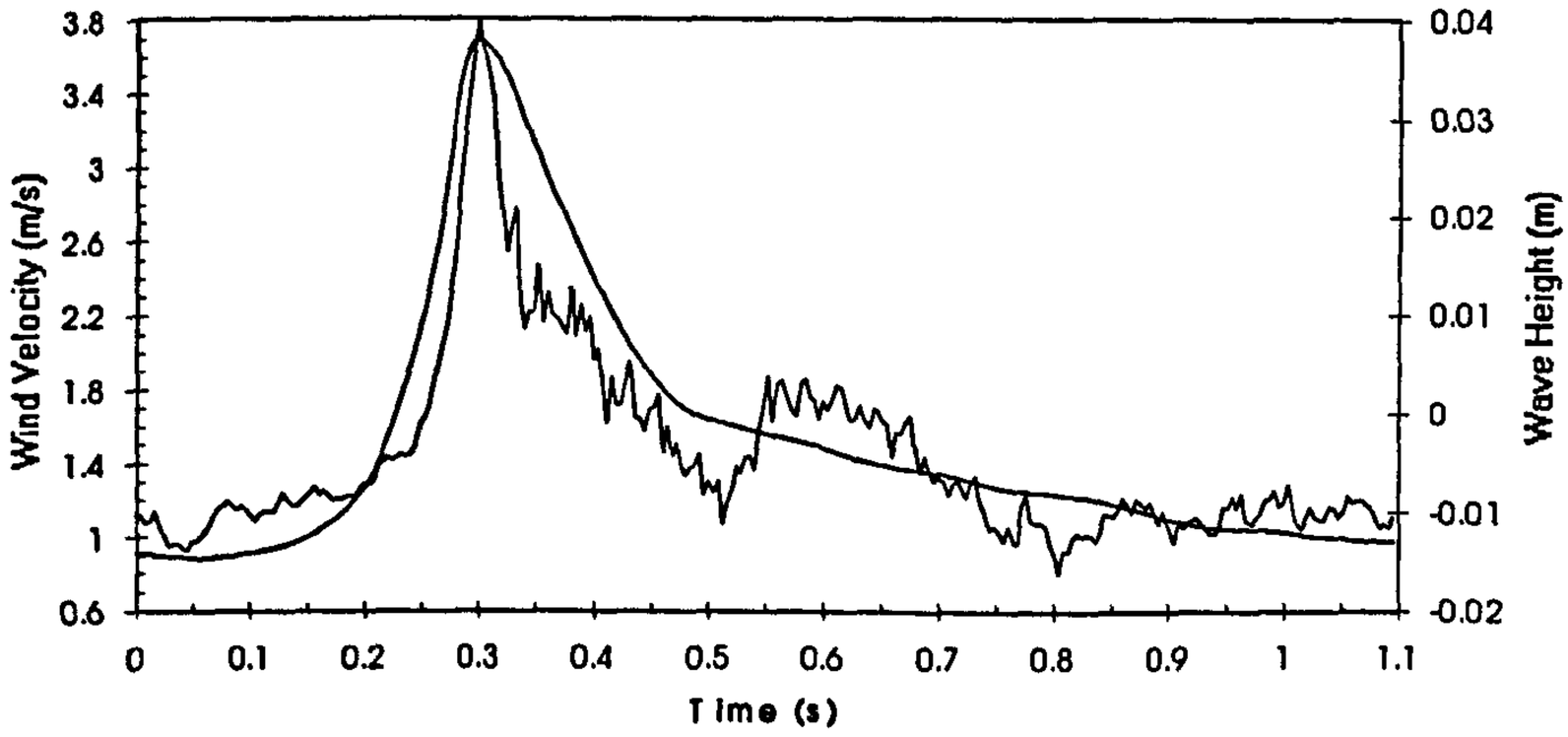

Figure 6.35 Phase-averaged velocity results for plunging waves under offshore winds at X=-1450mm. Probe heights: a) 83 b) 63 c) 47mm

a)

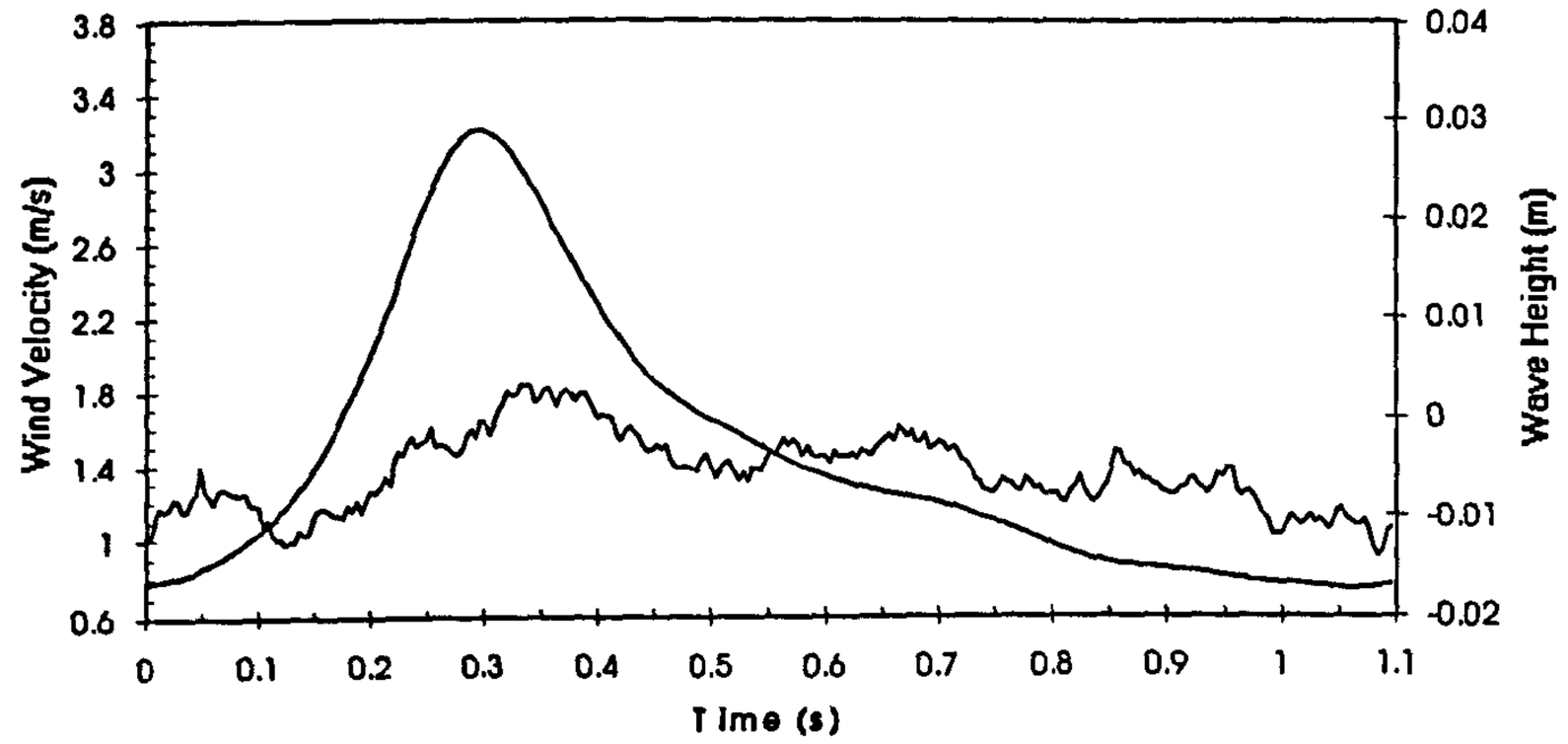

b)

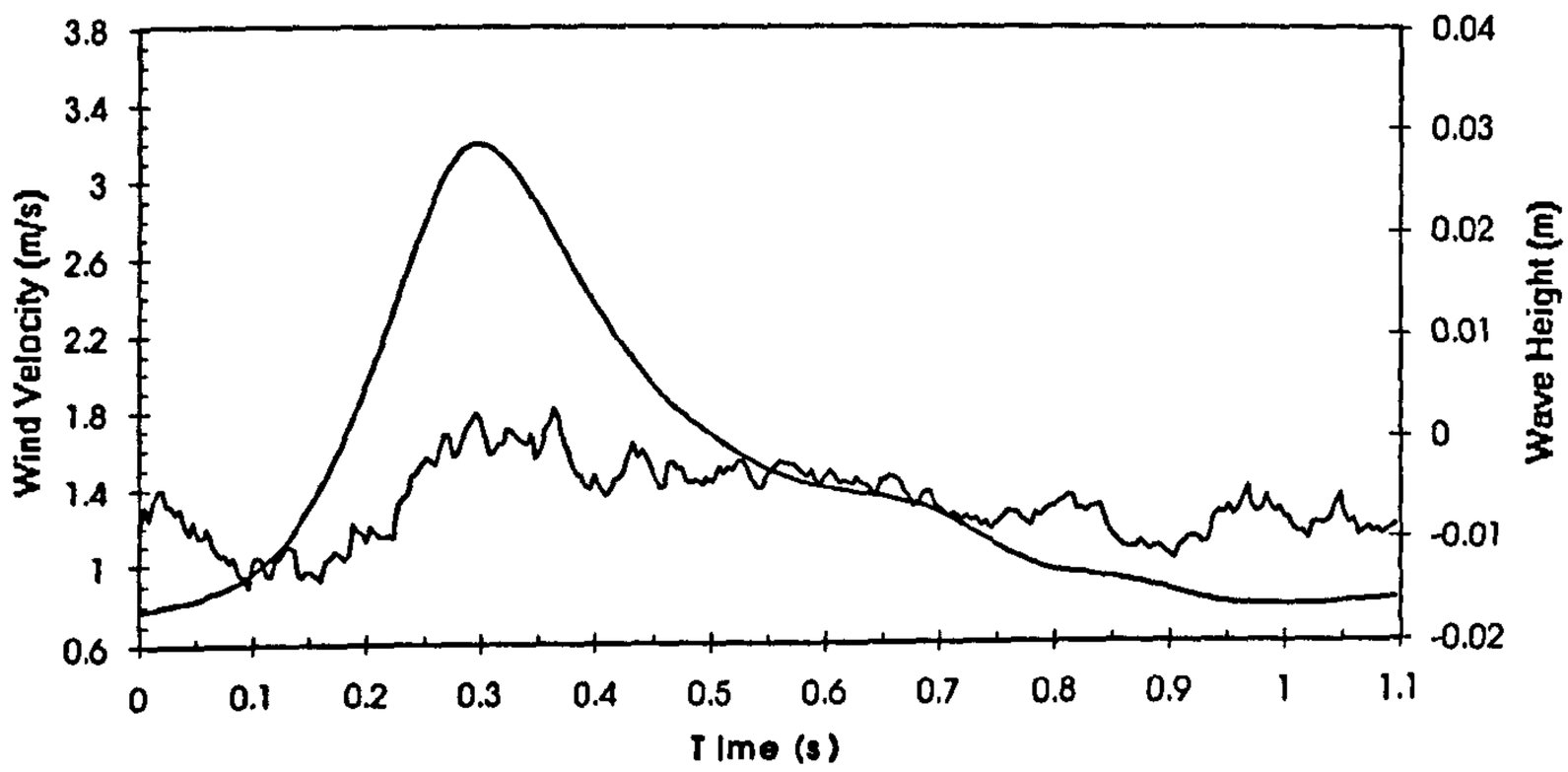

c)

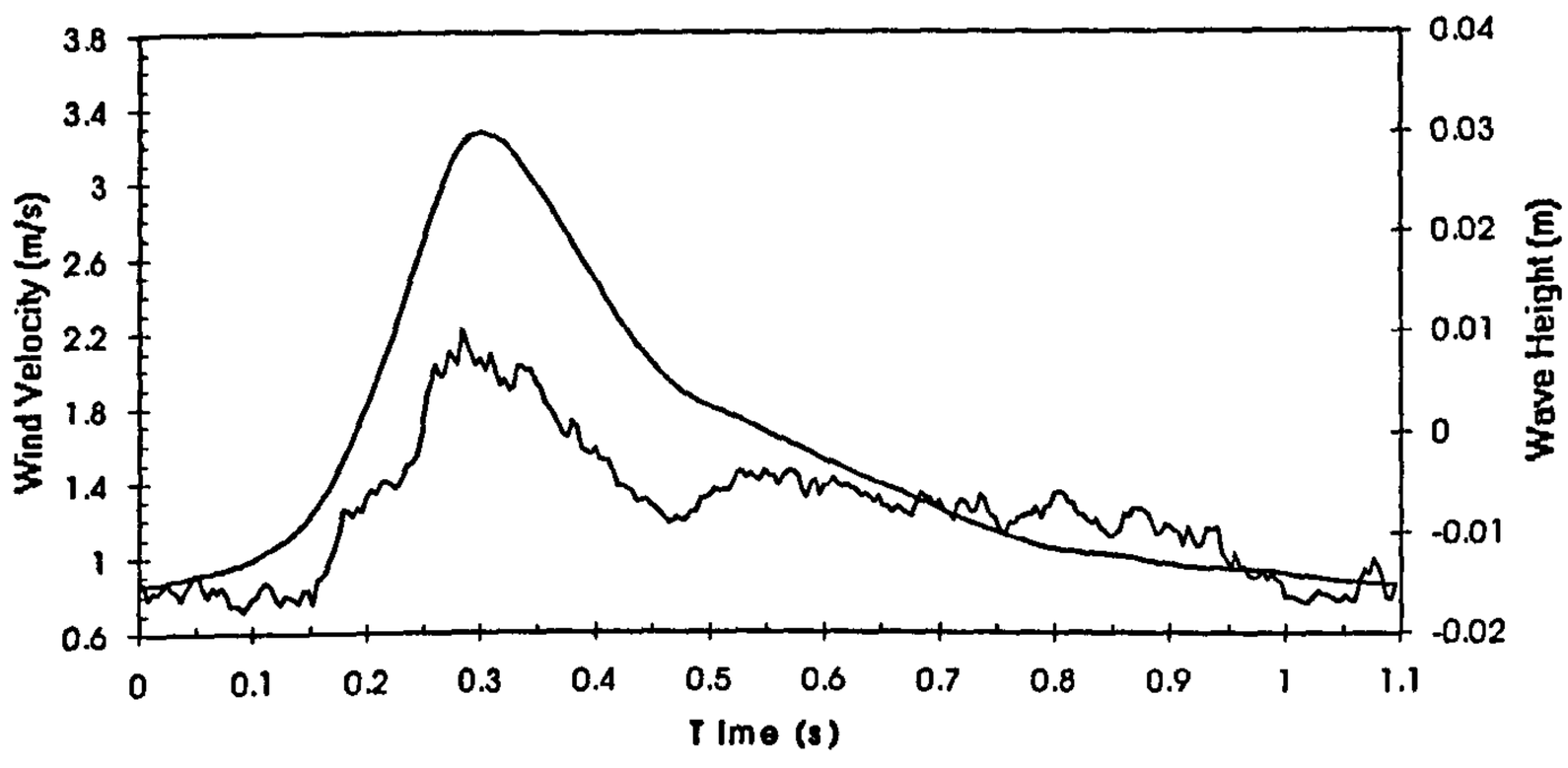

Figure 6.36 Phase-averaged velocity results for plunging waves under offshore winds at X=-1705mm. Probe heights: a) 83 b) 63 c) 47mm

a)

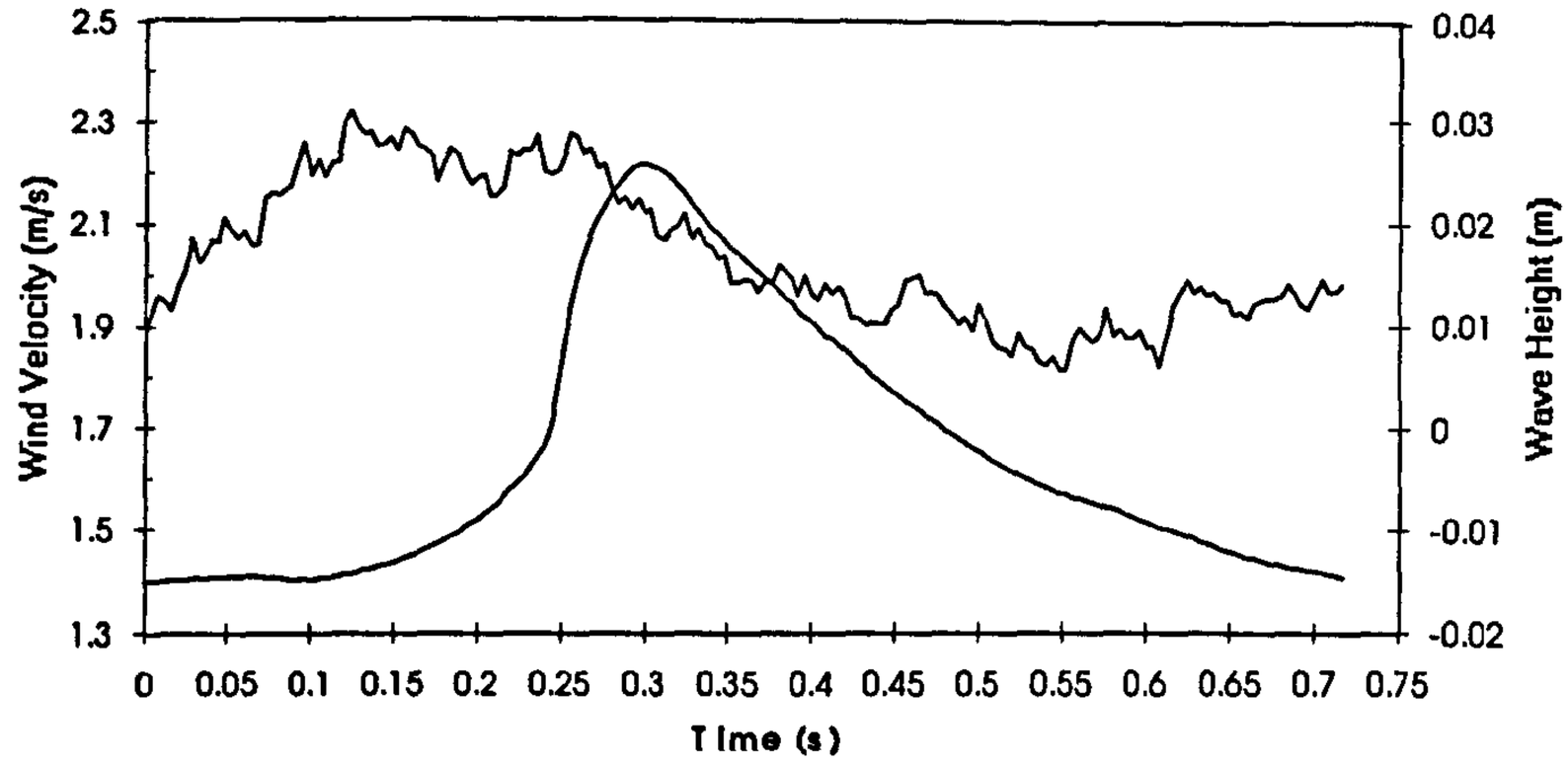

b)

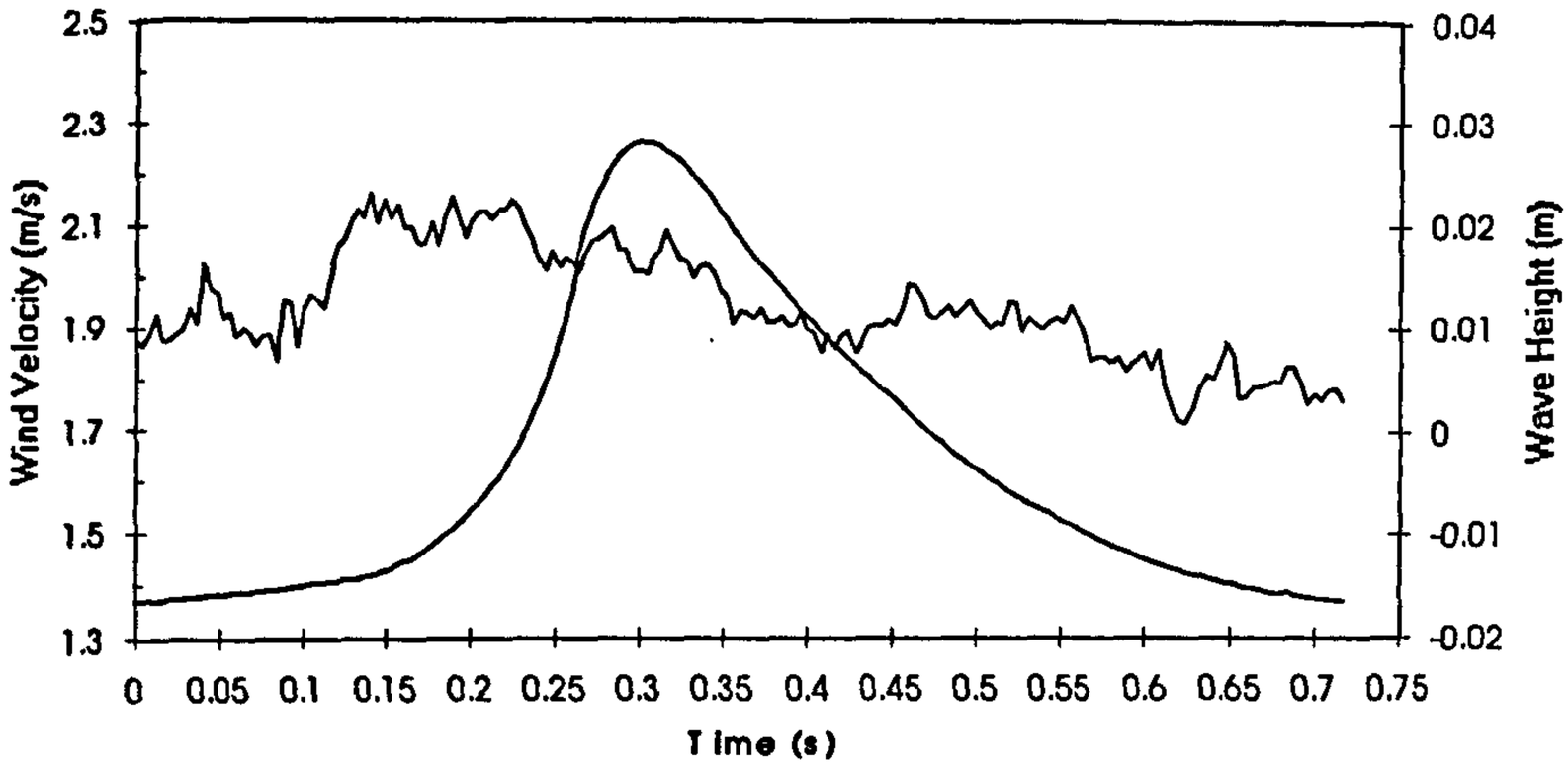

c)

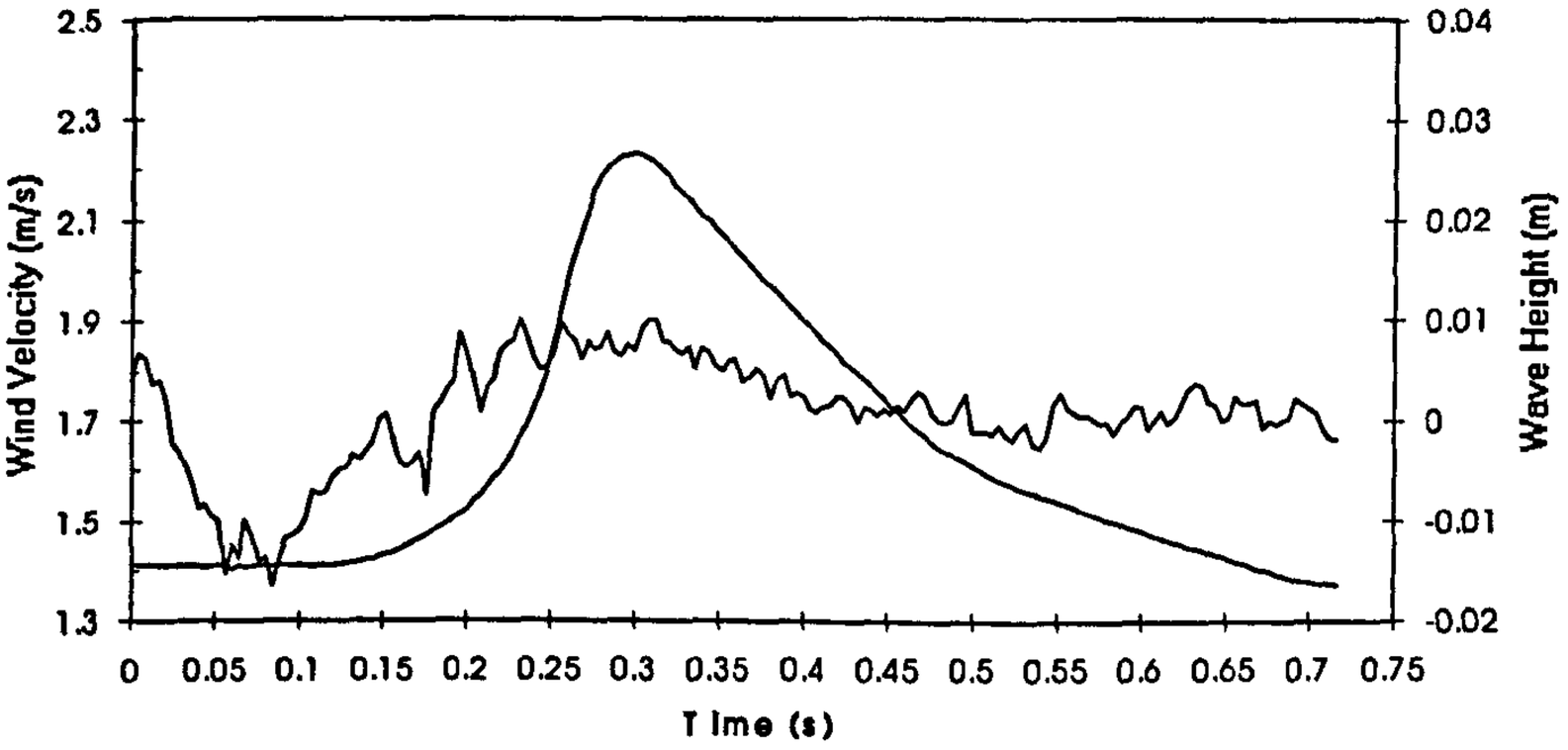

Figure 6.37 Phase-averaged velocity results for spilling waves under onshore winds at X=-1254mm. Probe heights: a) 86 b) 66 c) 46mm

a)

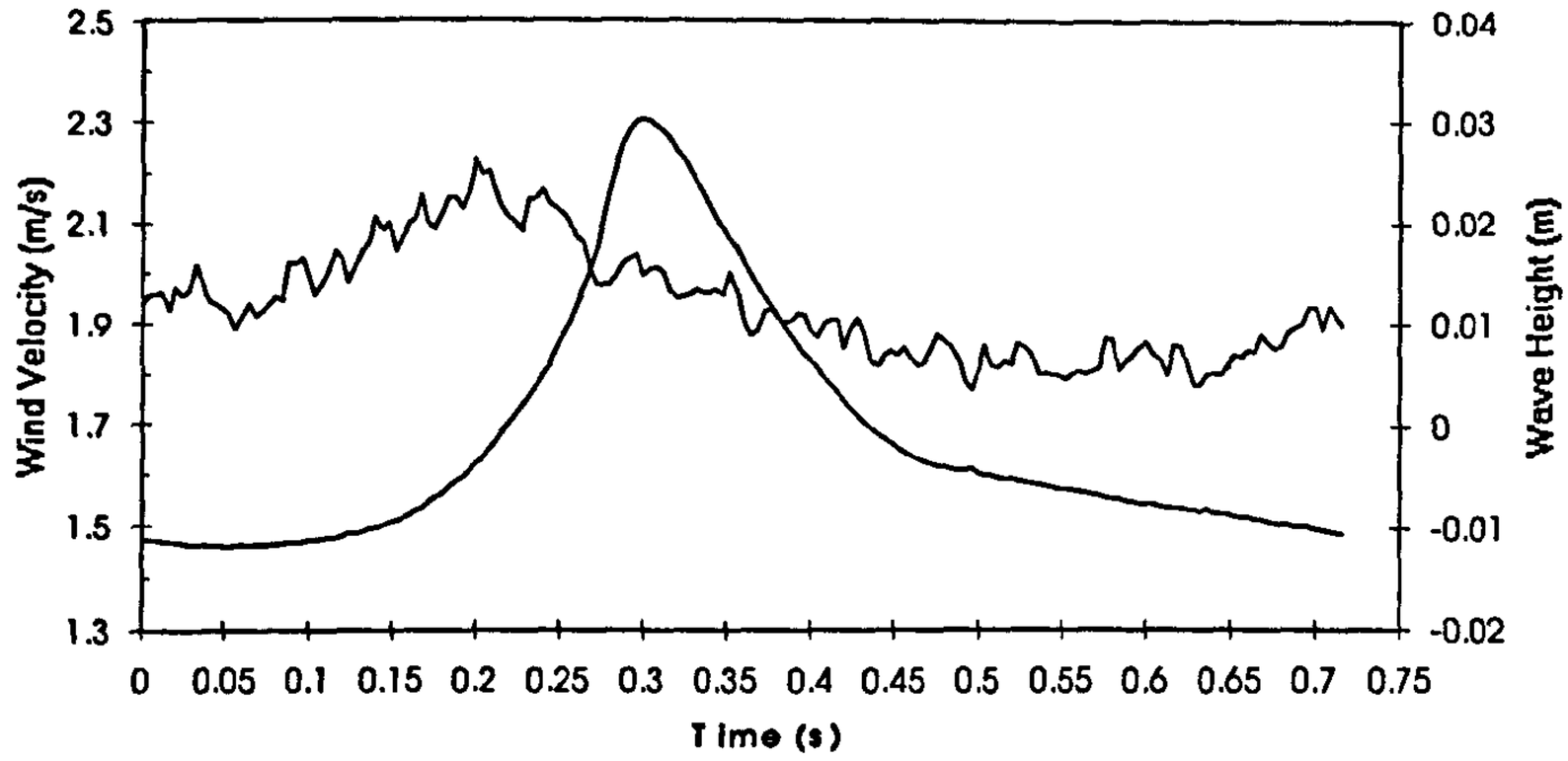

b)

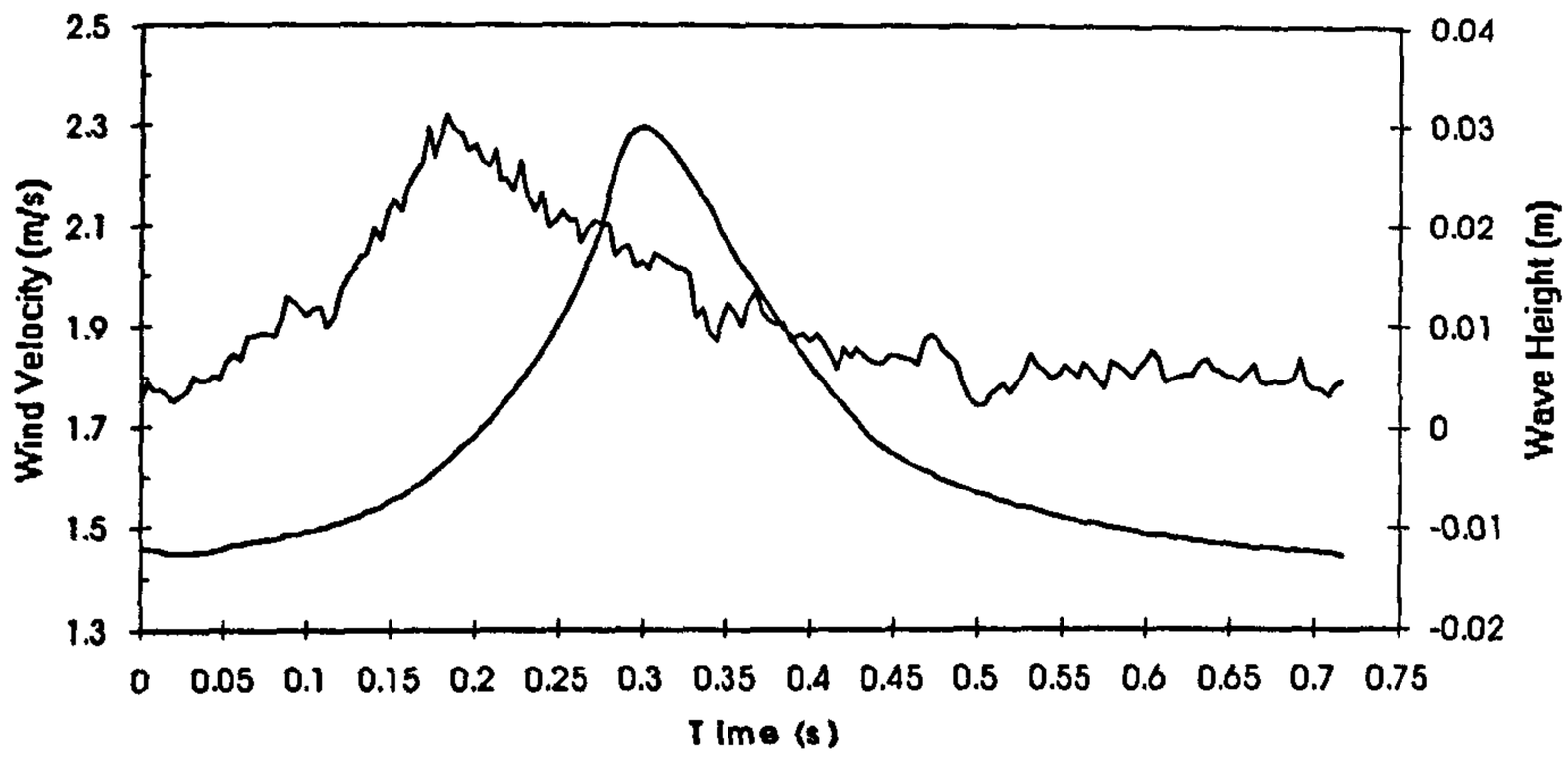

c)

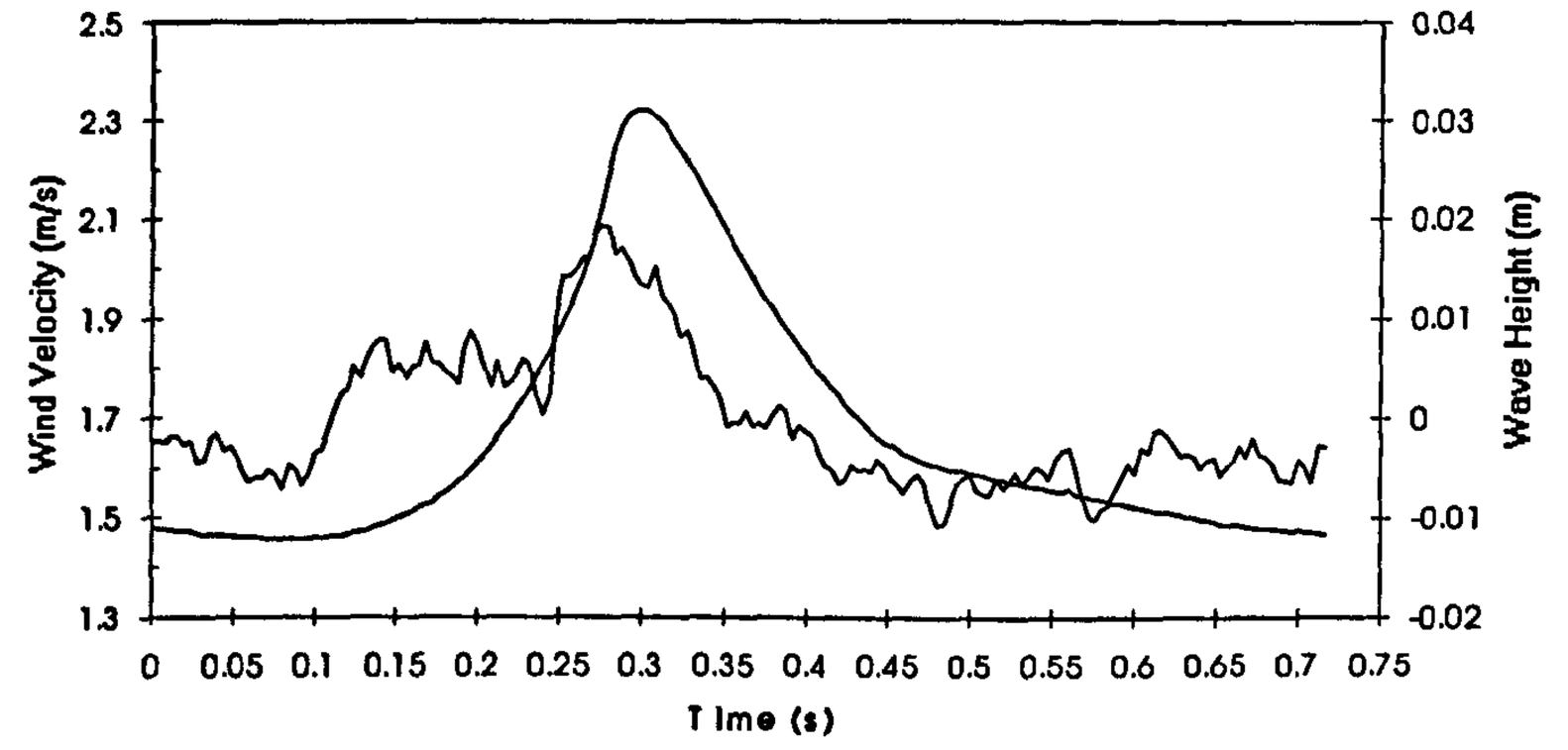

Figure 6.38 Phase-averaged velocity results for spilling waves under onshore winds at X=-1554mm. Probe heights: a) 82 b) 62 c) 42mm

a)

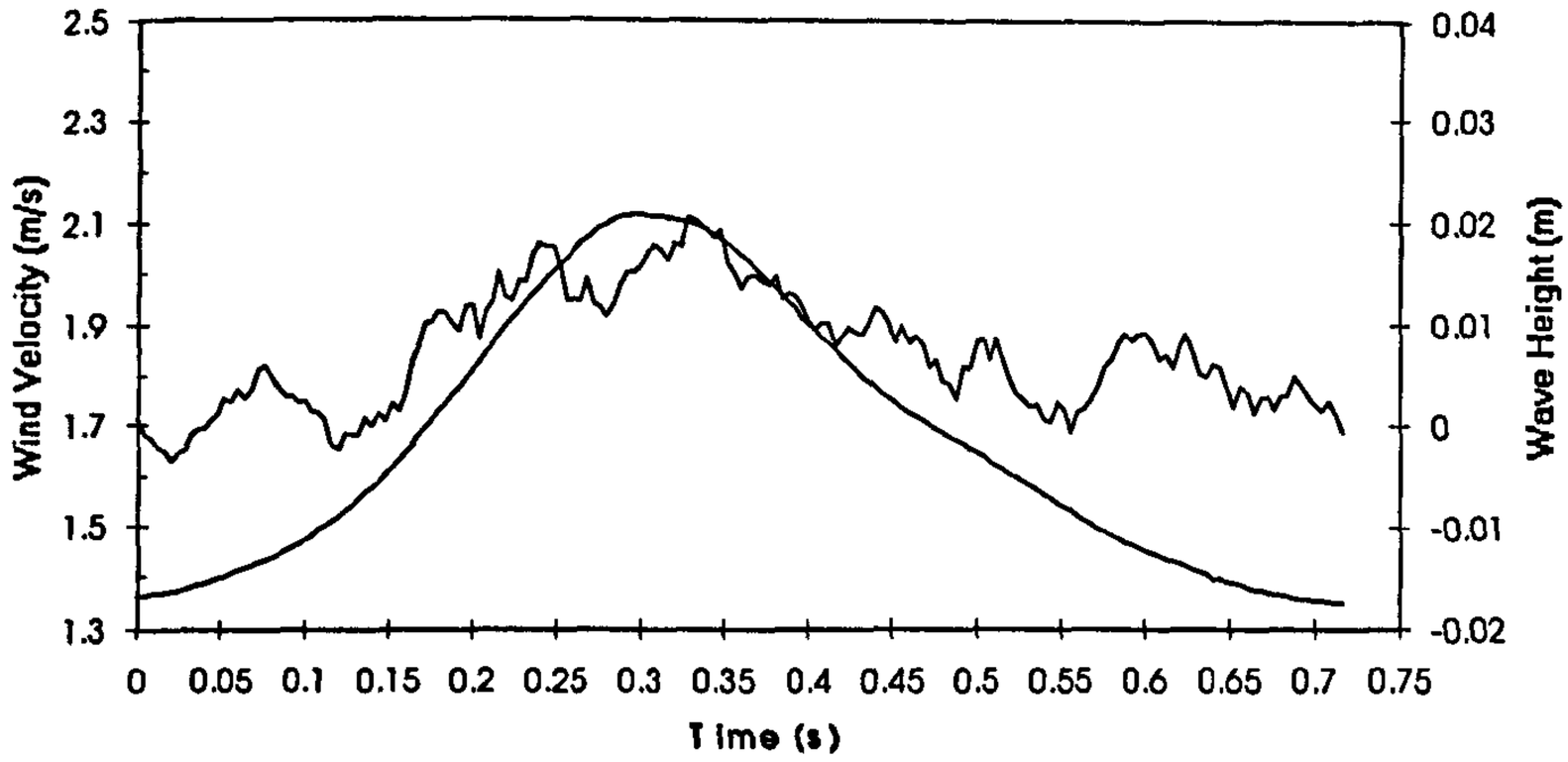

b)

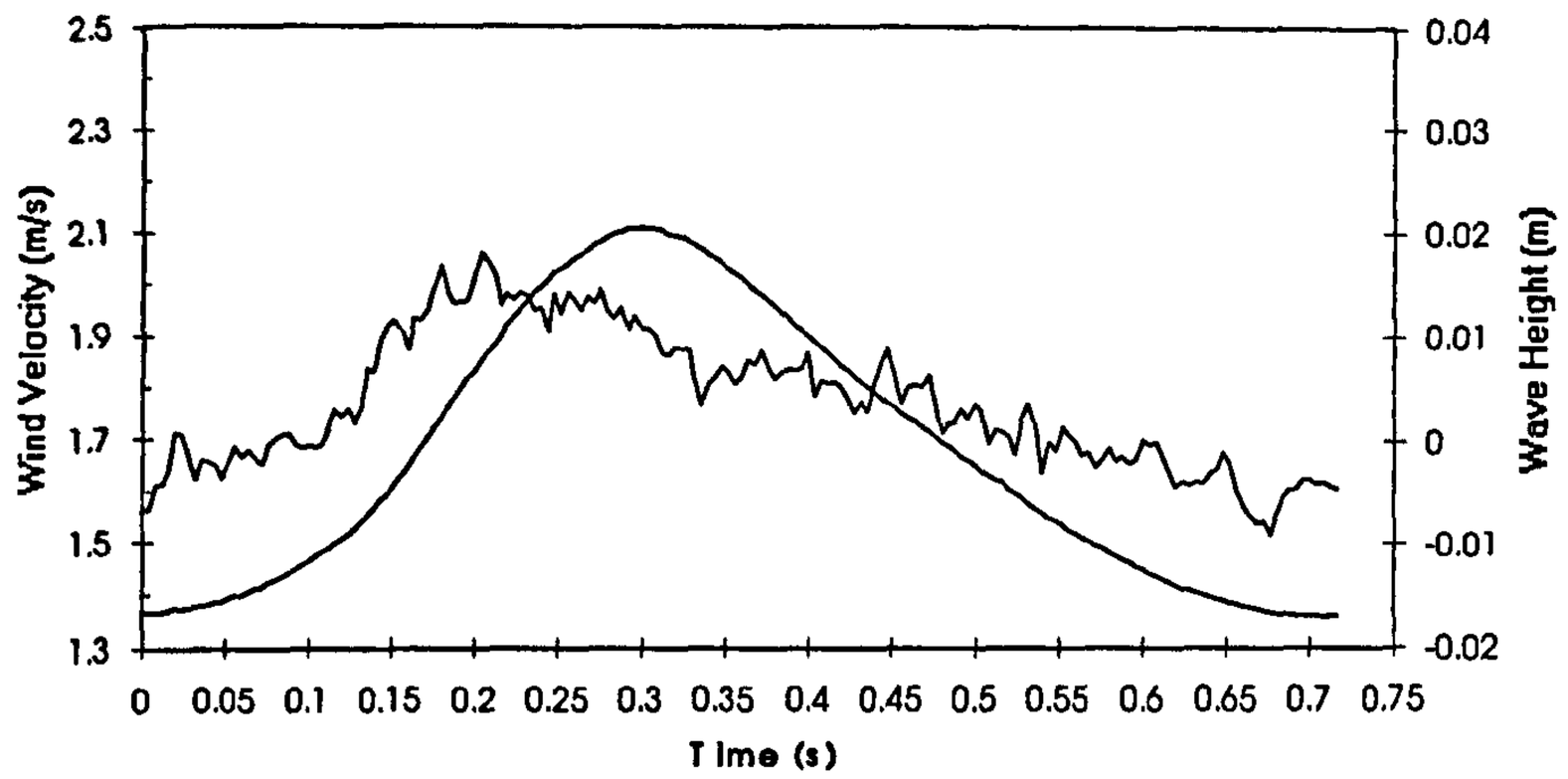

c)

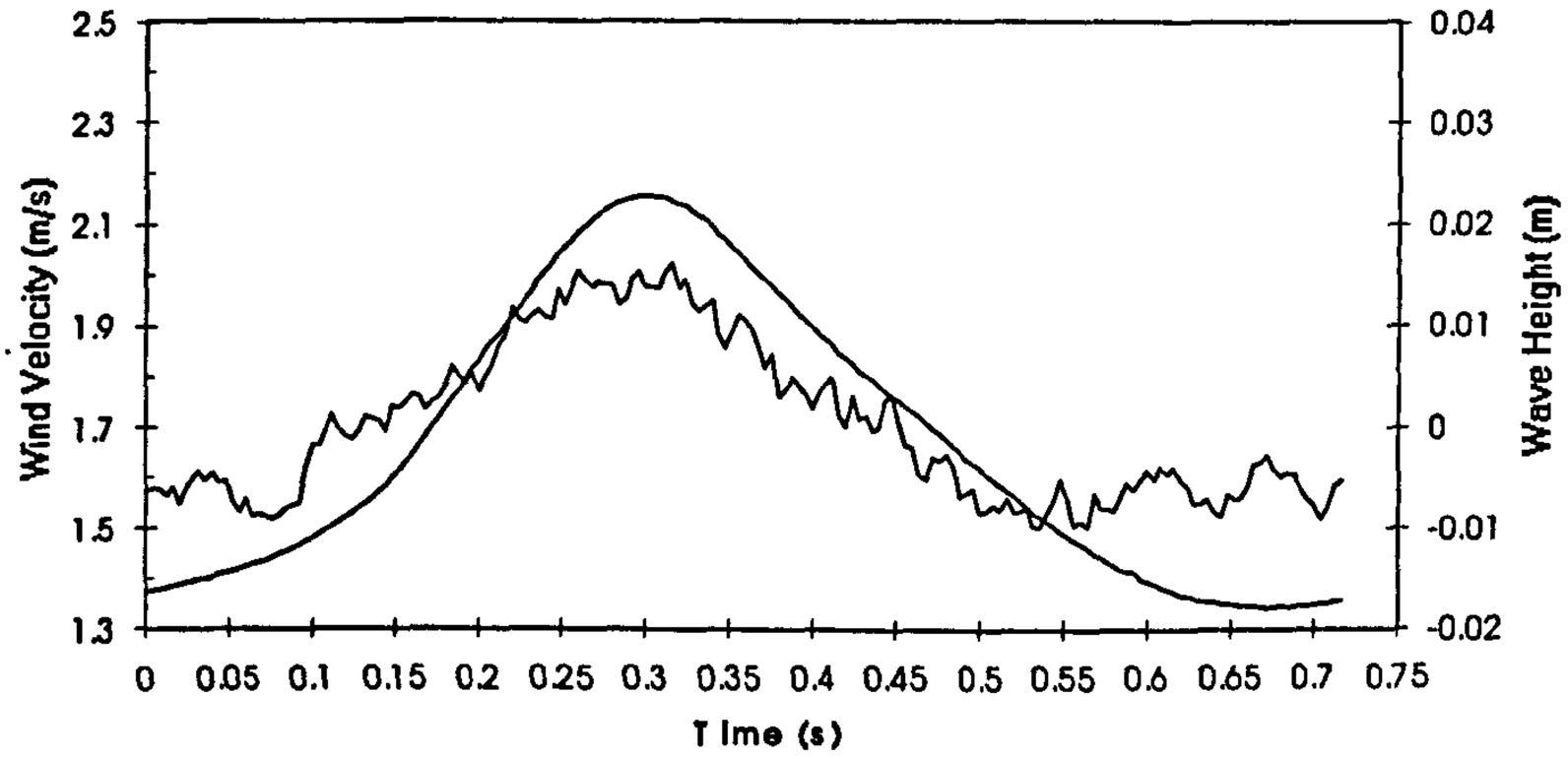

Figure 6.39 Phase-averaged velocity results for spilling waves under onshore winds at X=-1854mm. Probe heights: a) 81 b) 61 c) 41mm

a)

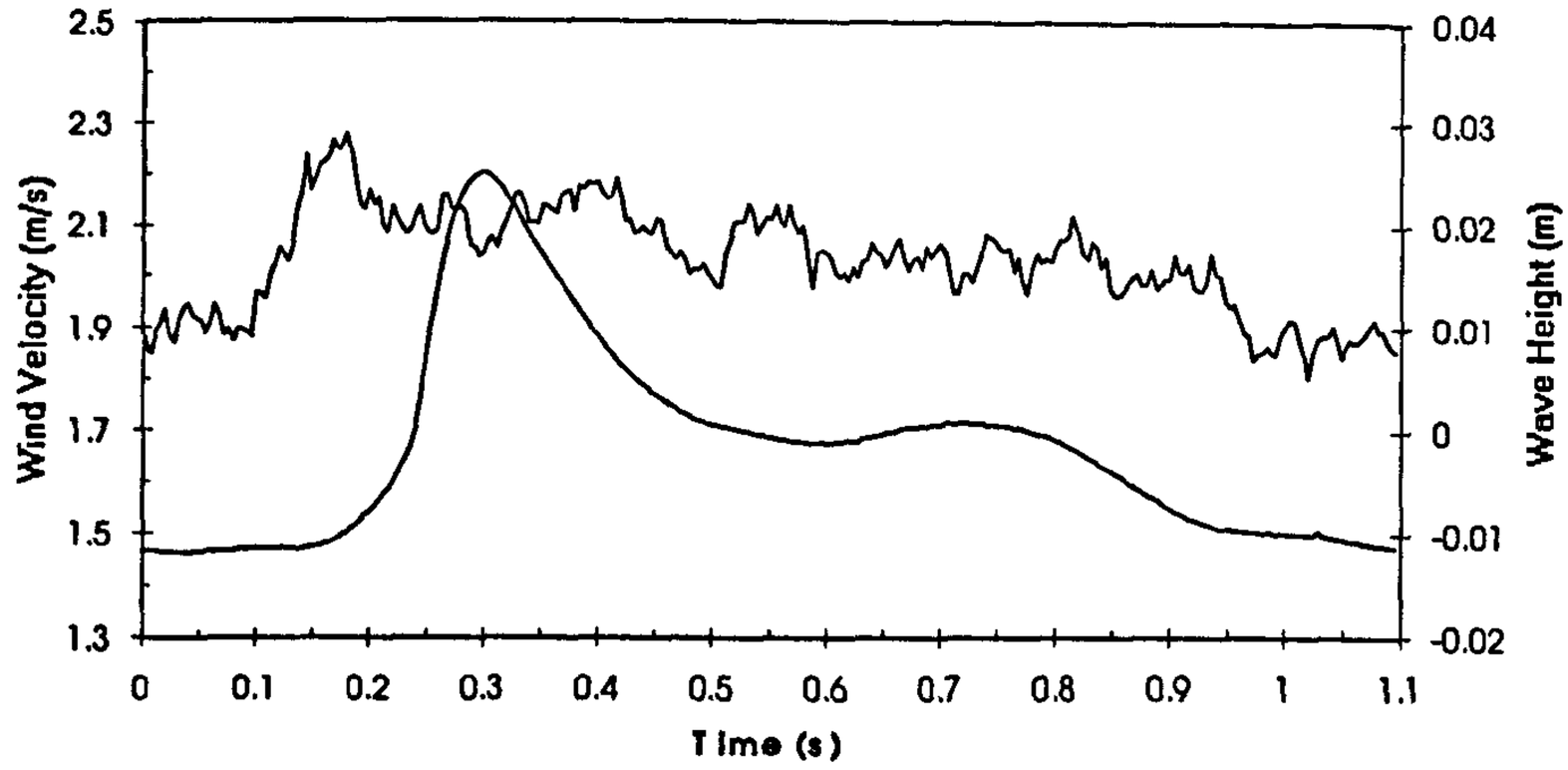

b)

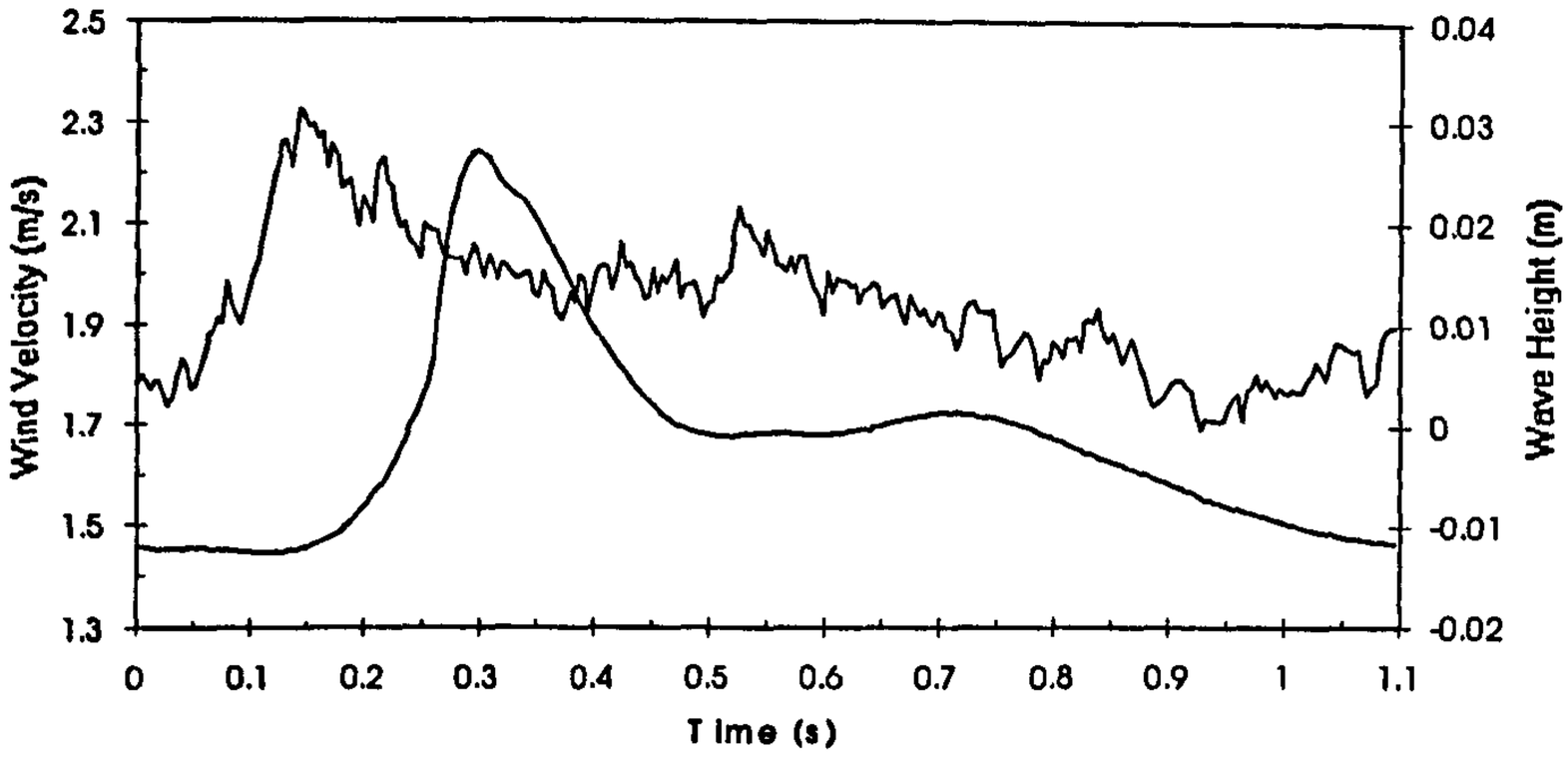

c)

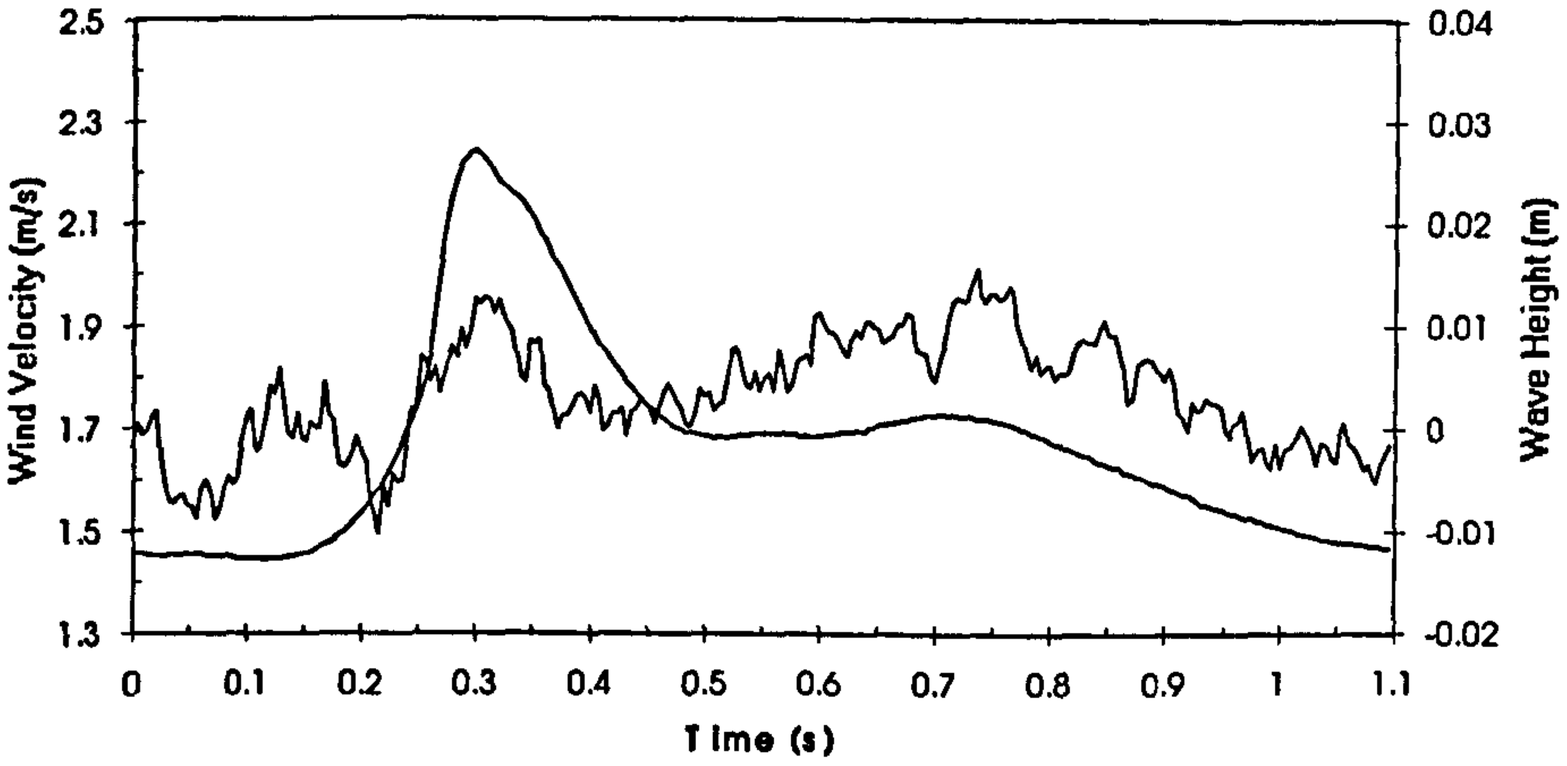

Figure 6.40 Phase-averaged velocity results for plunging waves under onshore winds at X=-1289mm. Probe heights: a) 83 b) 63 c) 43mm

a)

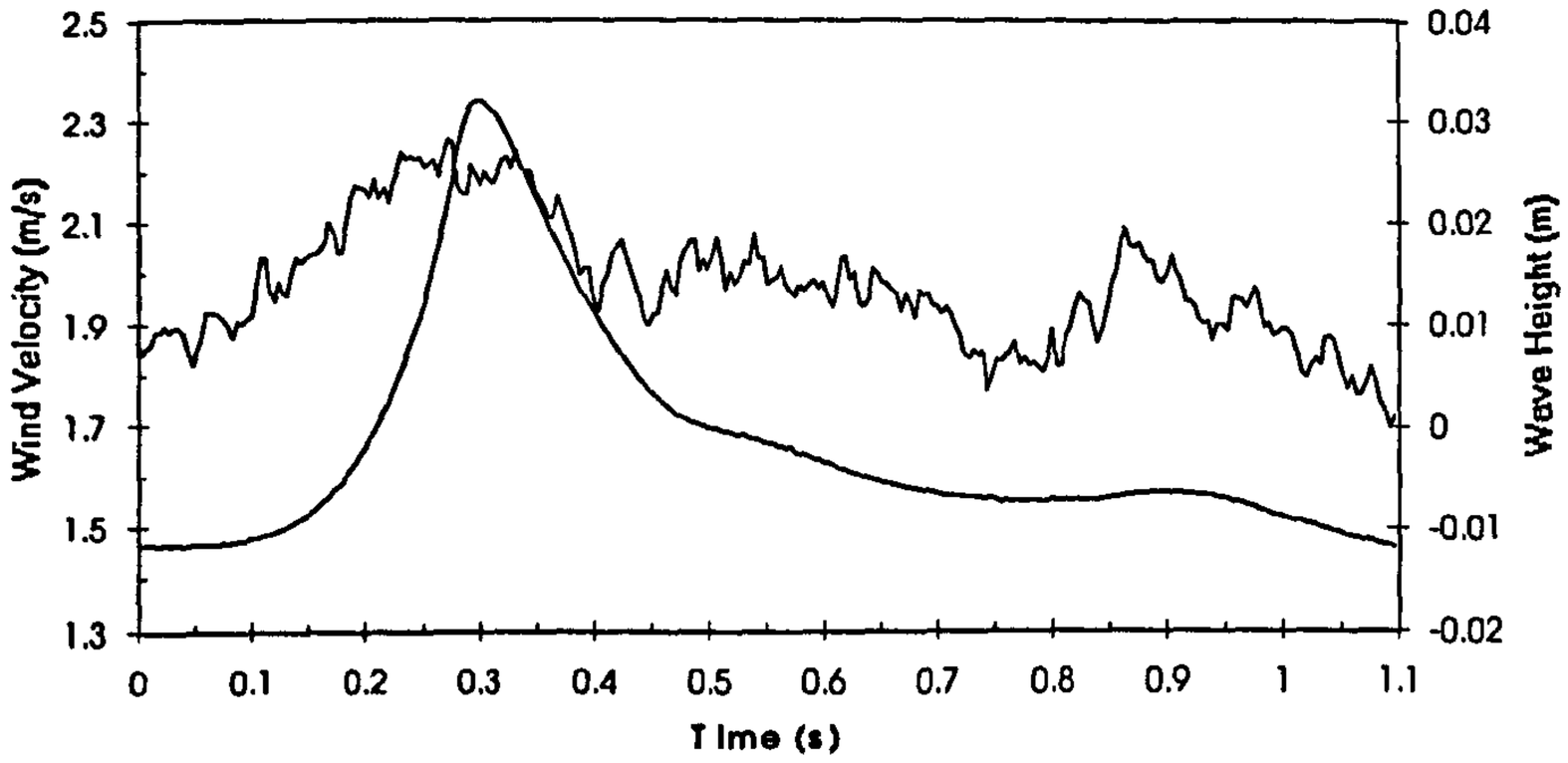

b)

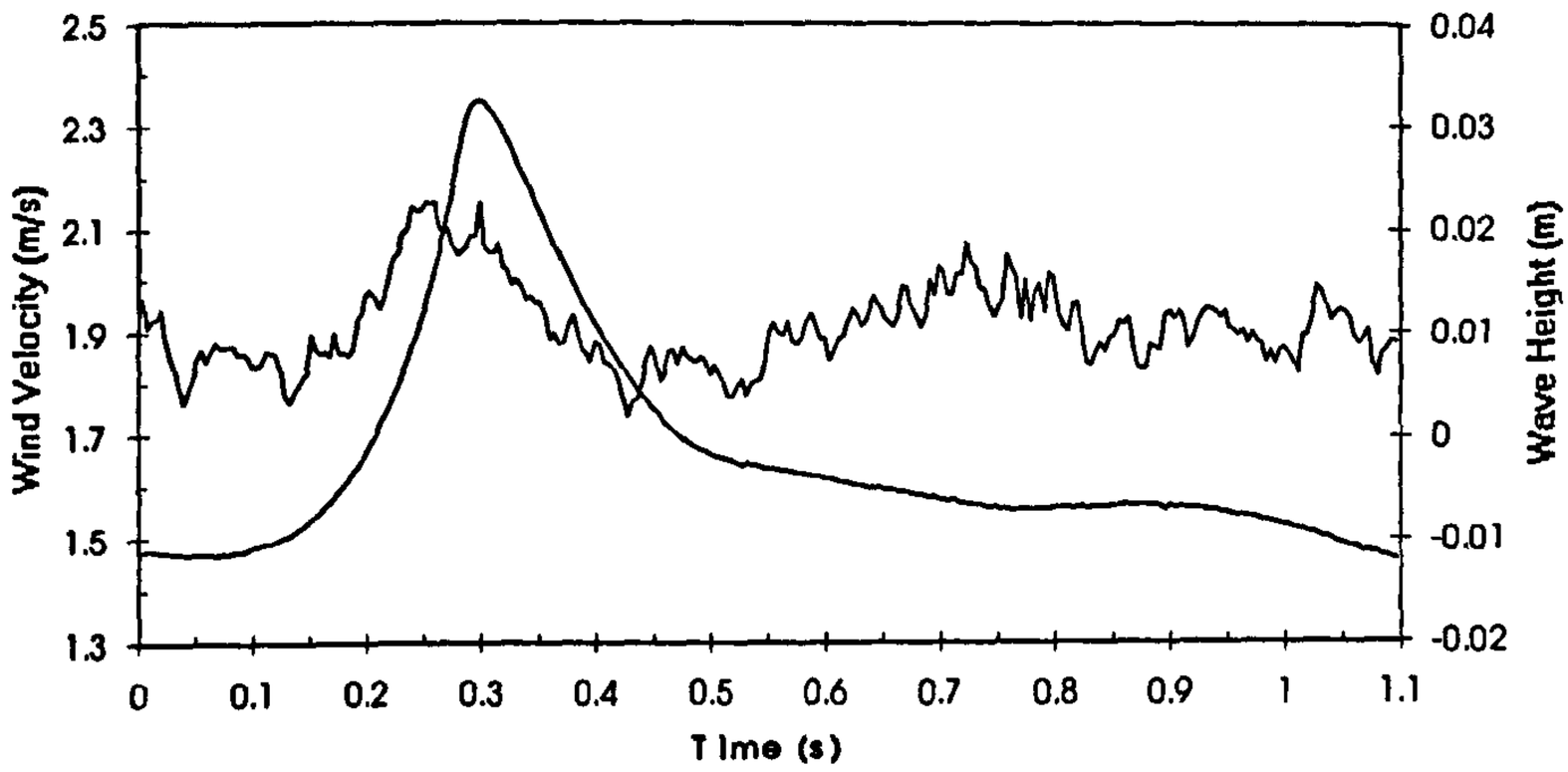

c)

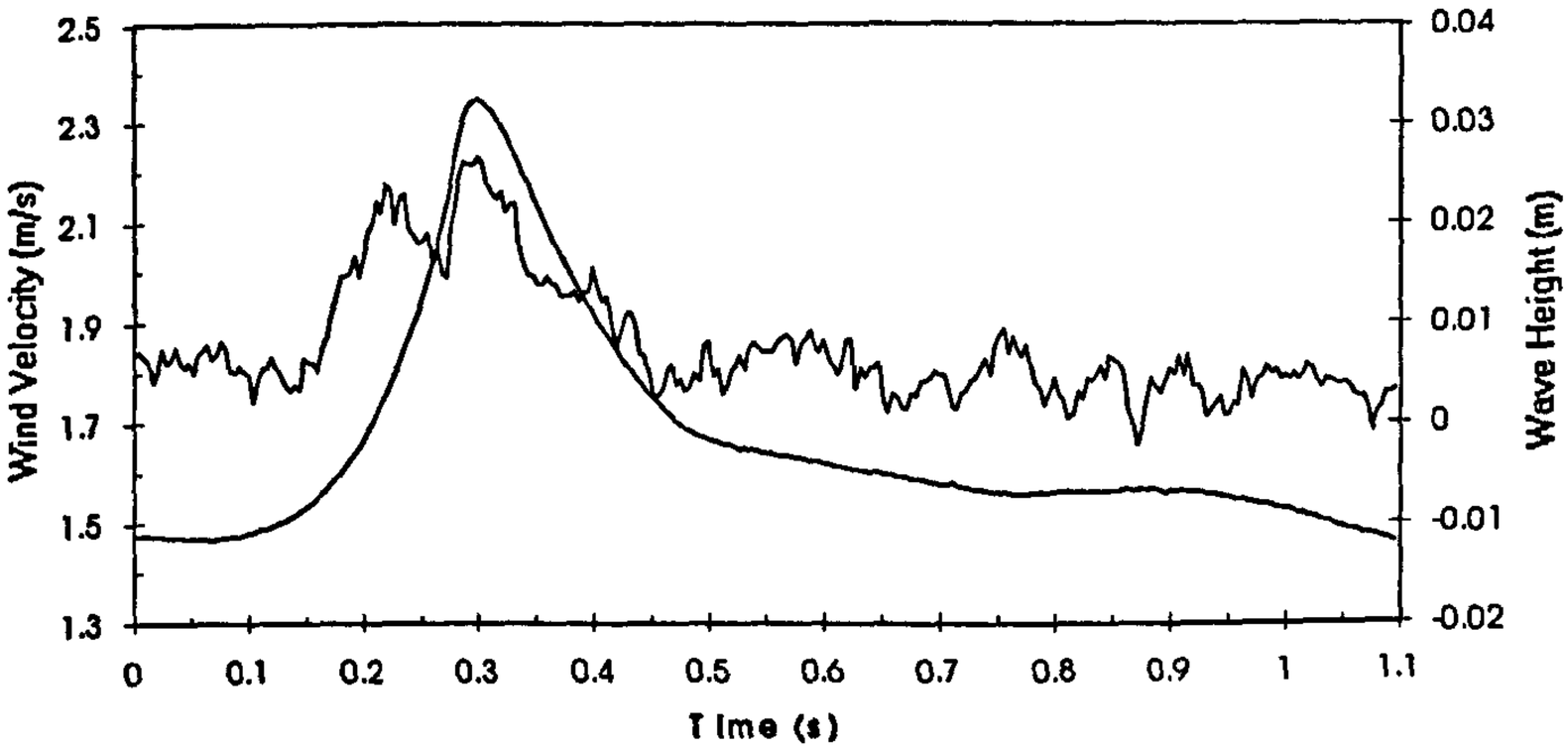

Figure 6.41 Phase-averaged velocity results for plunging waves under onshore winds at X=-1589mm. Probe heights: a) 82 b) 62 c) 42mm

a)

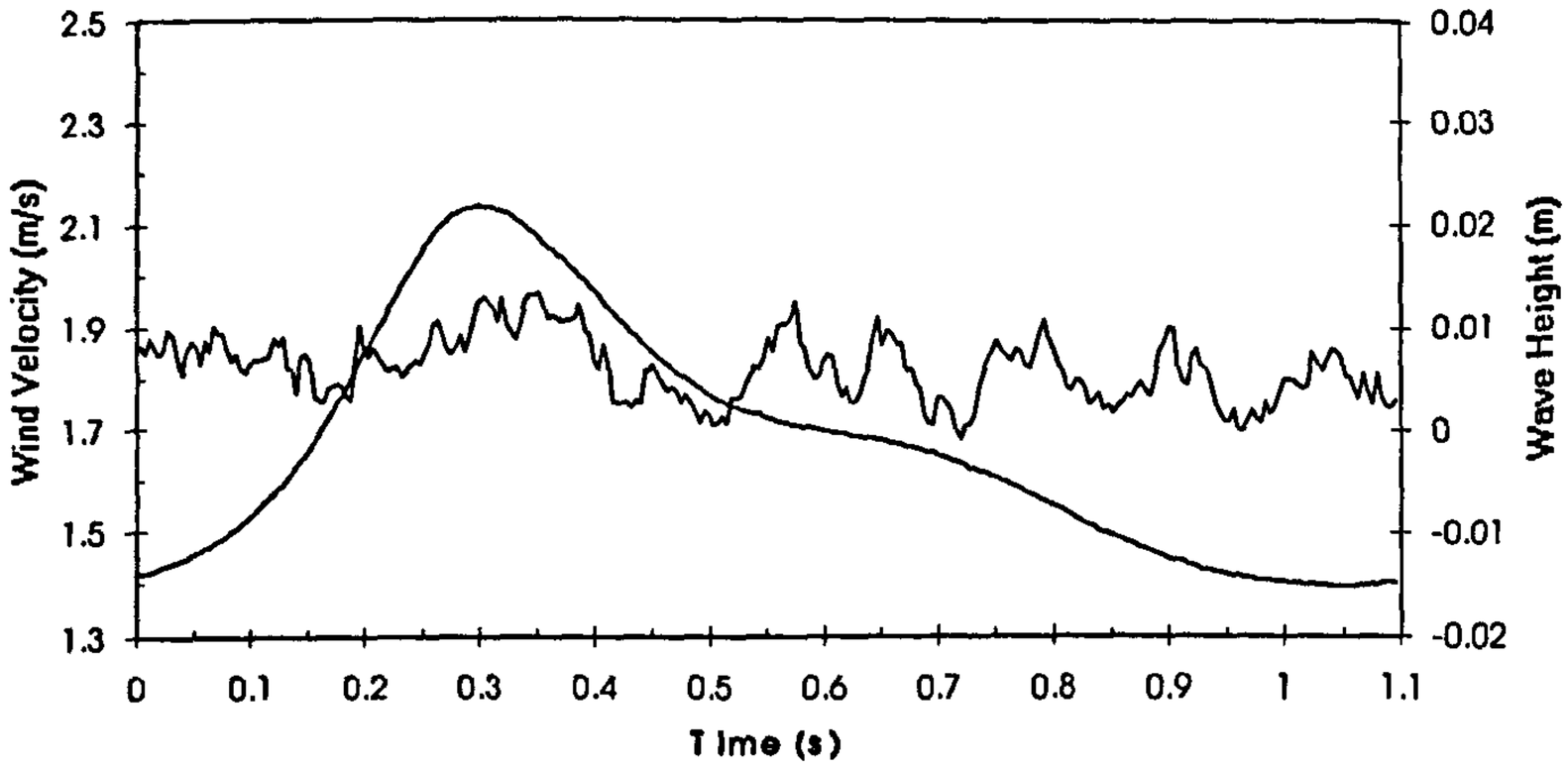

b)

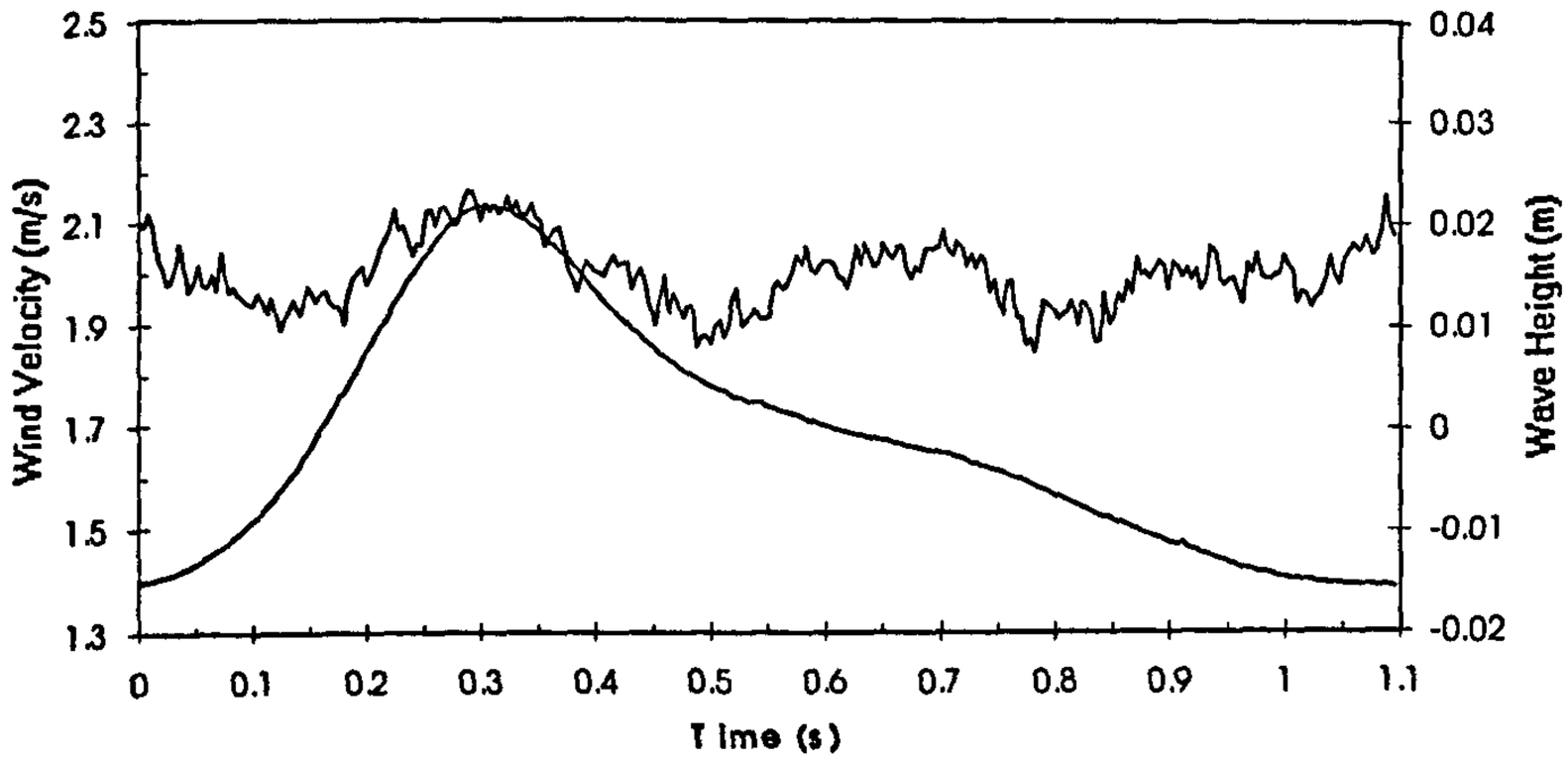

c)

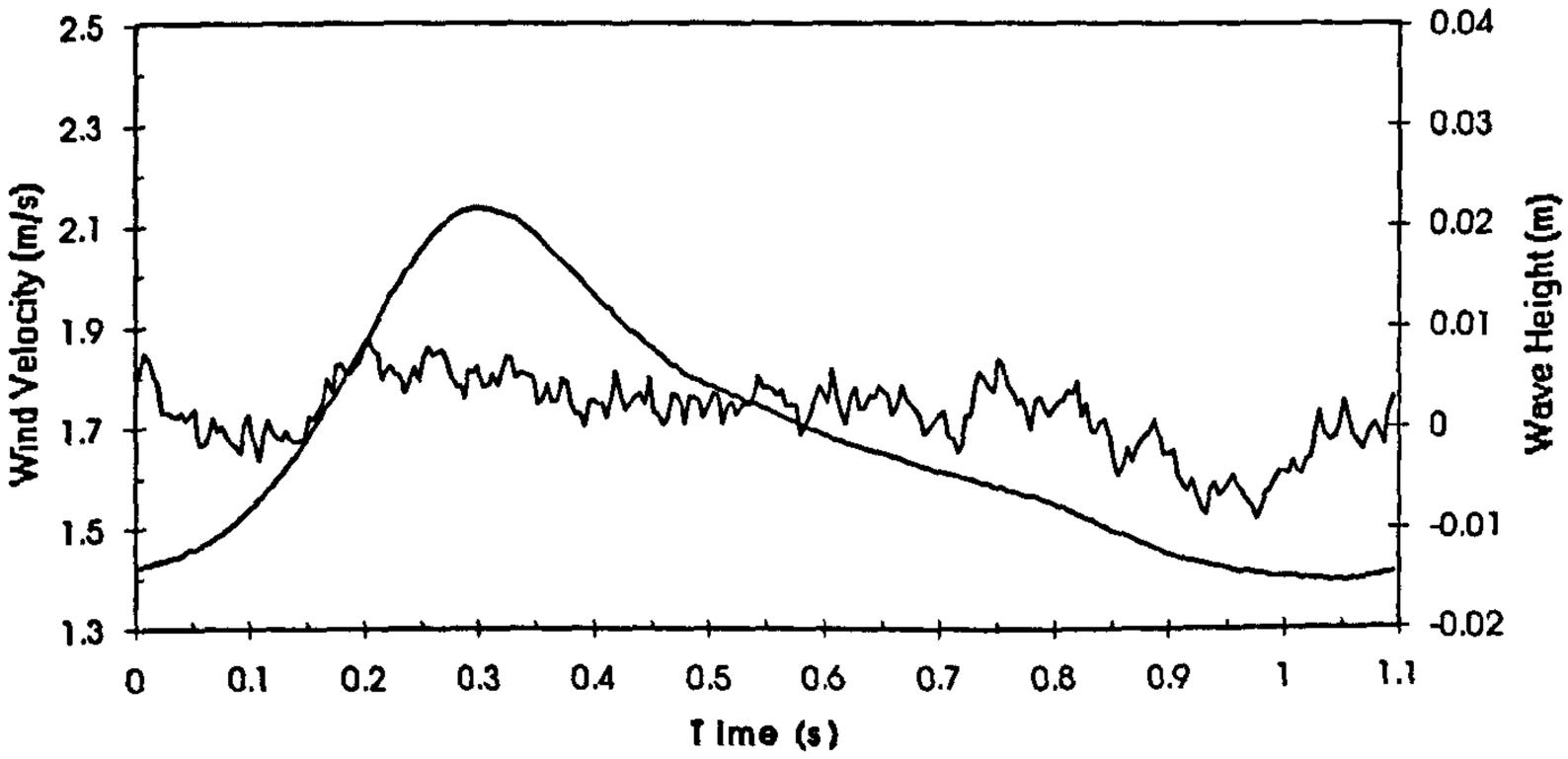

Figure 6.42 Phase-averaged velocity results for plunging waves under onshore winds at X=-1889mm. Probe heights: a) 78 b) 58 c) 38mm

a)

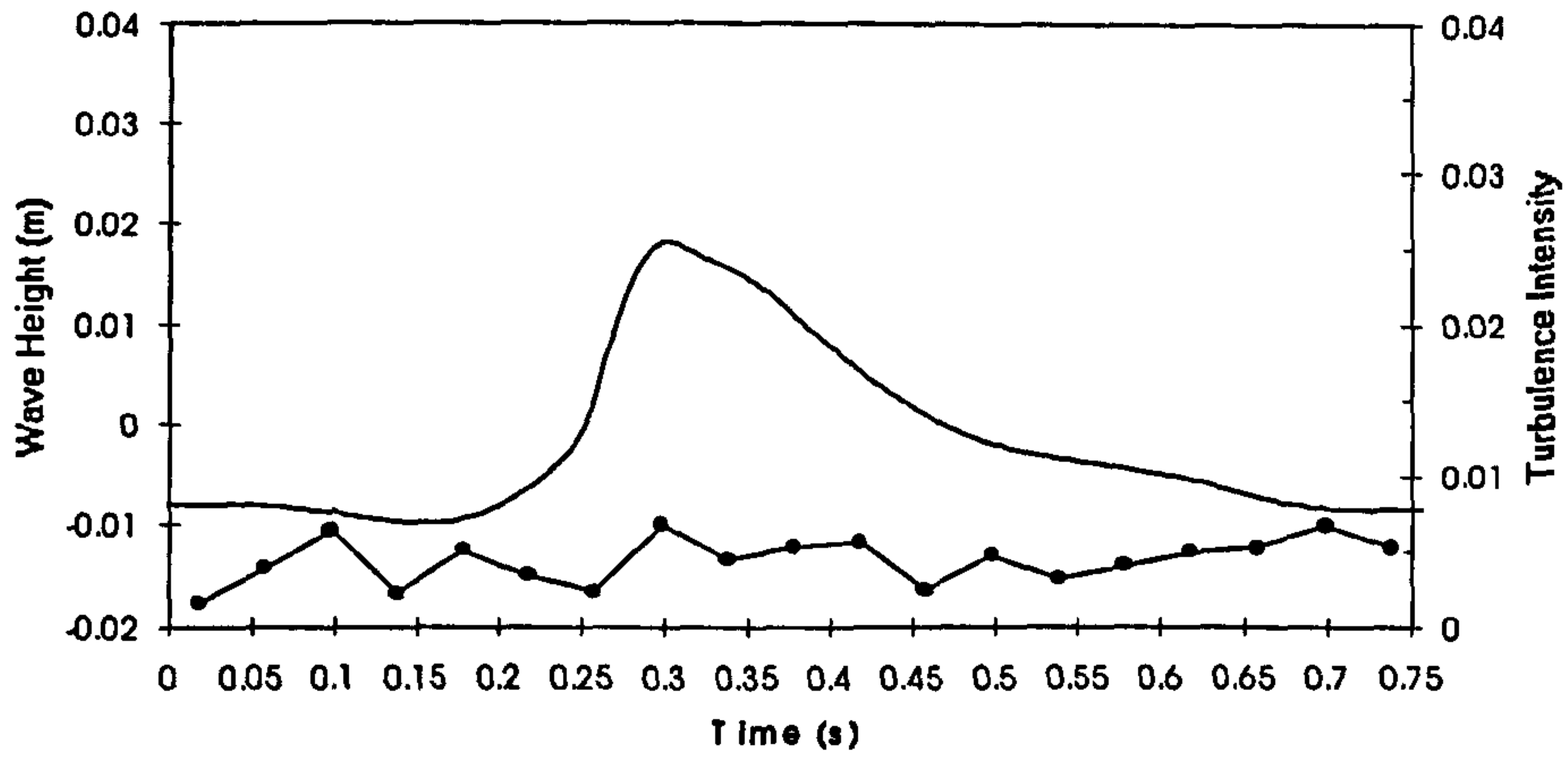

b)

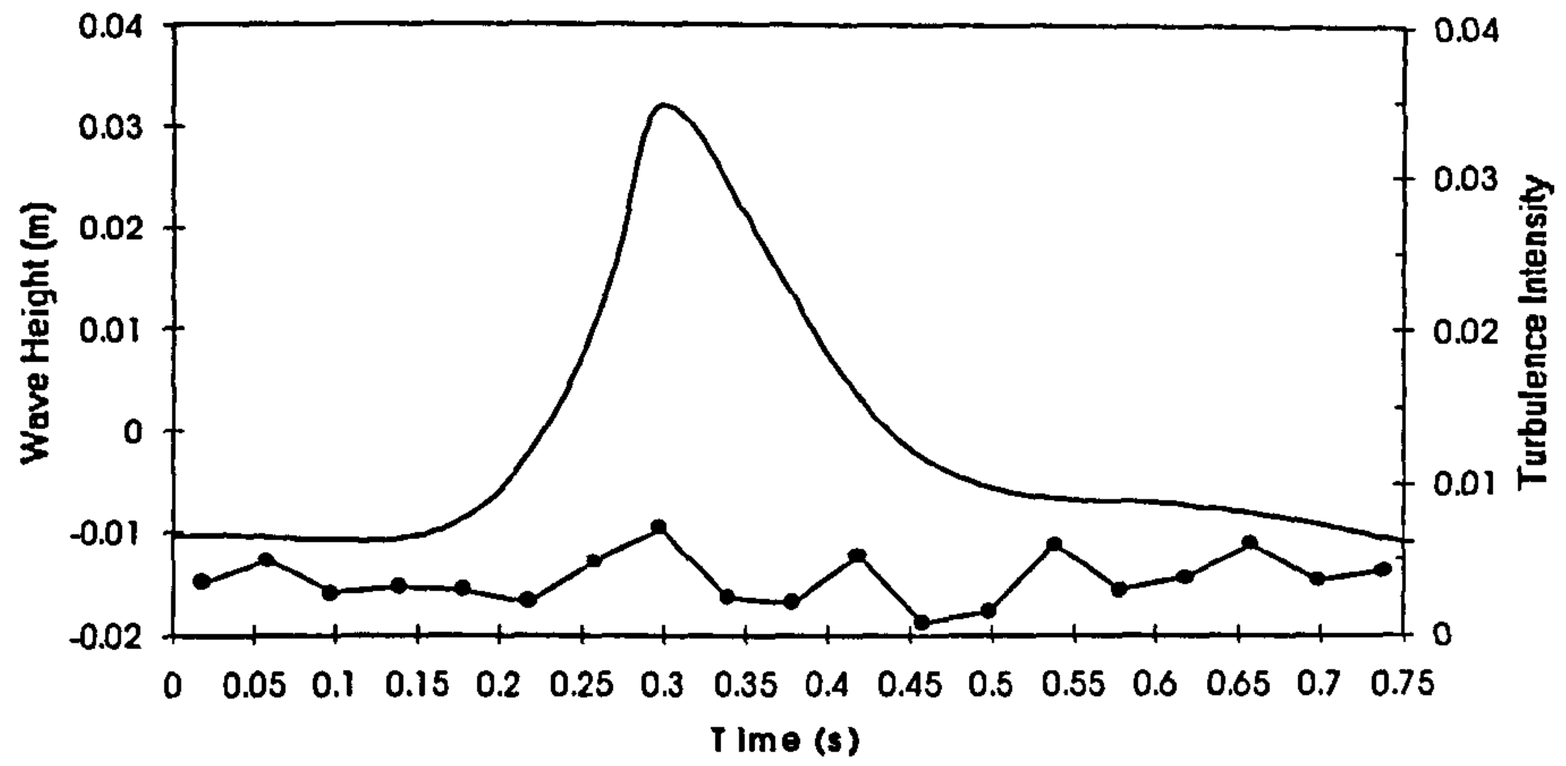

c)

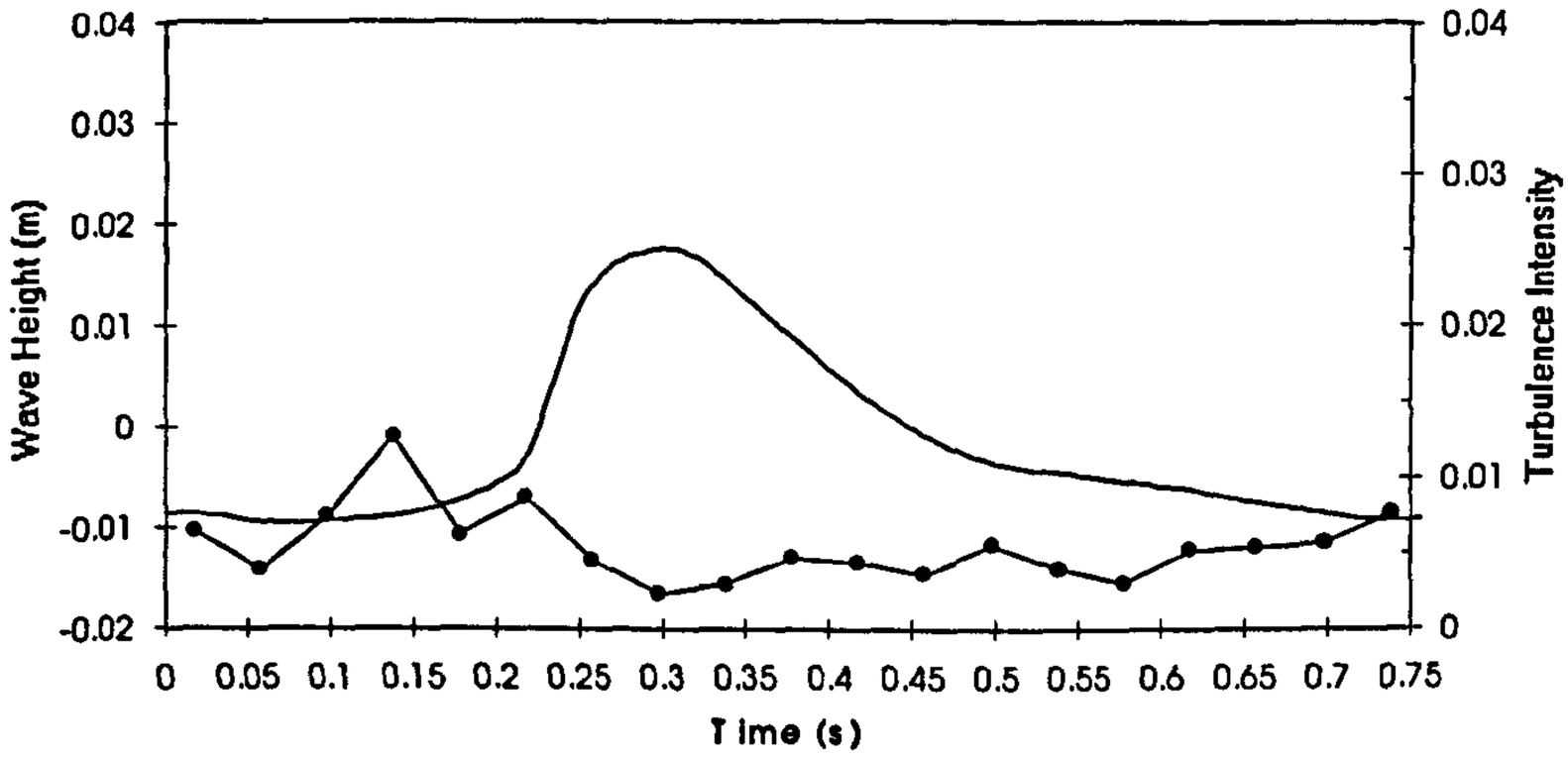

Figure 6.43 Phase-averaged turbulence intensity results for spilling waves under offshore winds at X=-1183mm. Probe heights: a) 83 b) 63 c) 43mm

a)

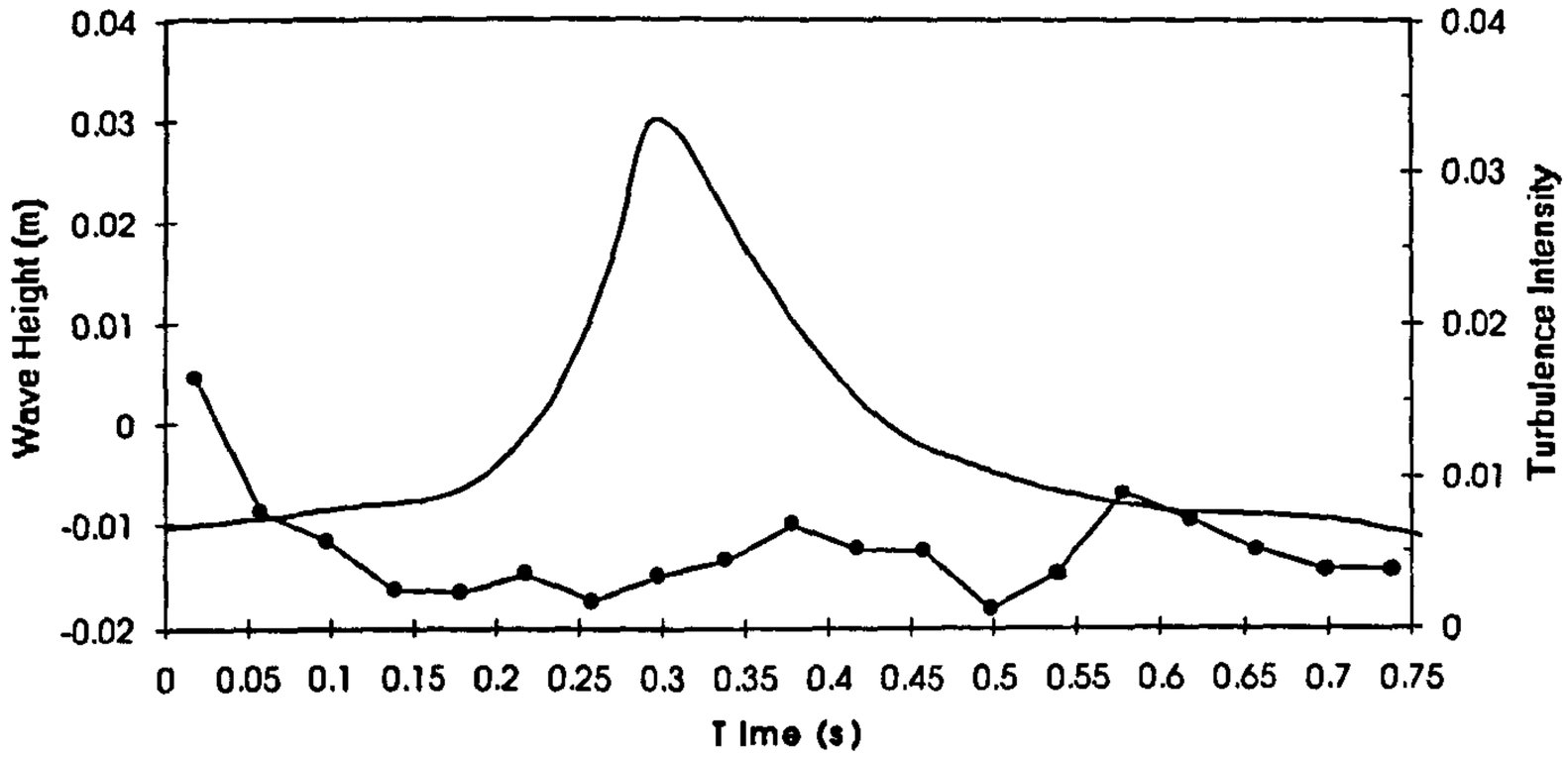

b)

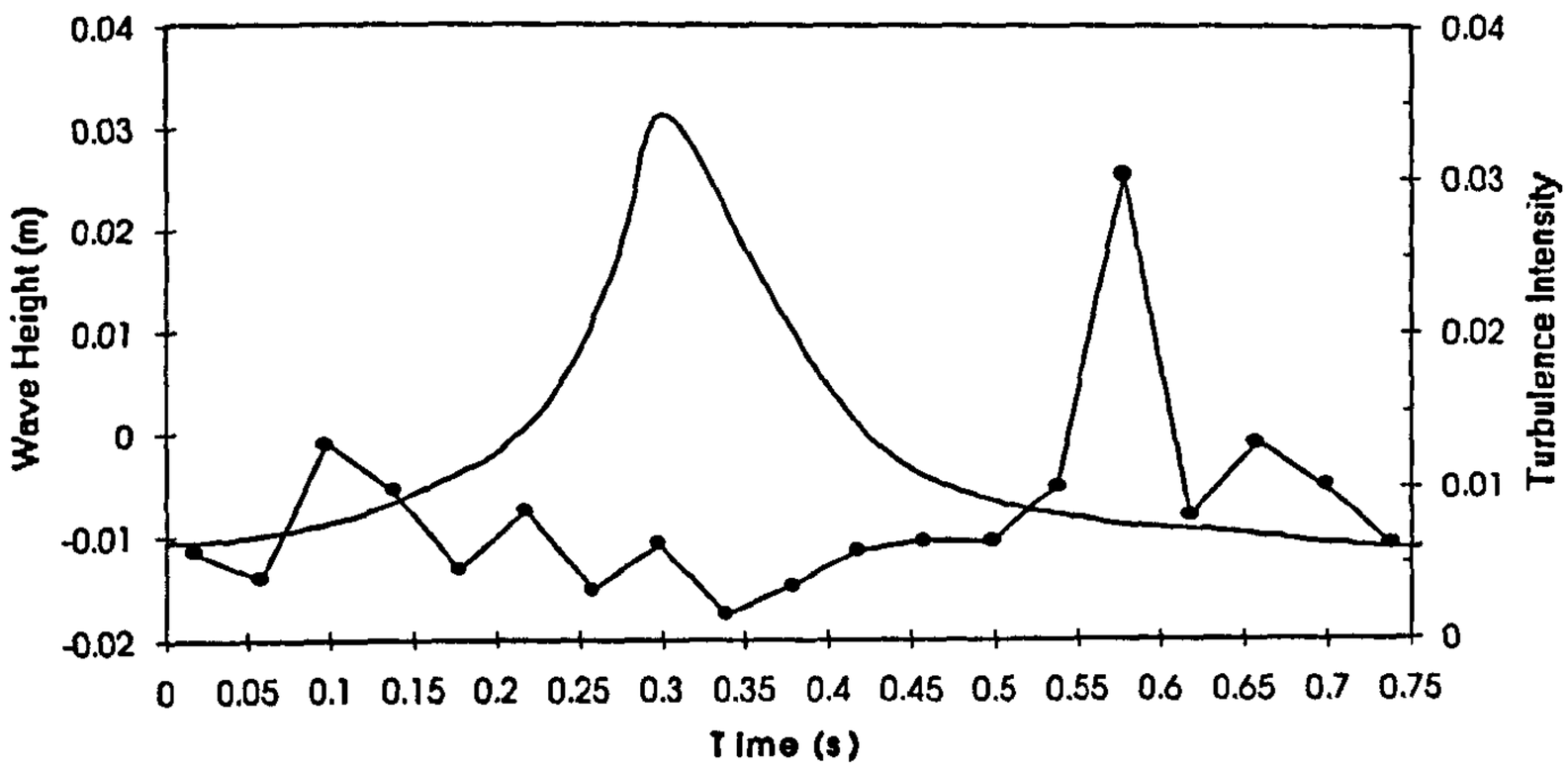

c)

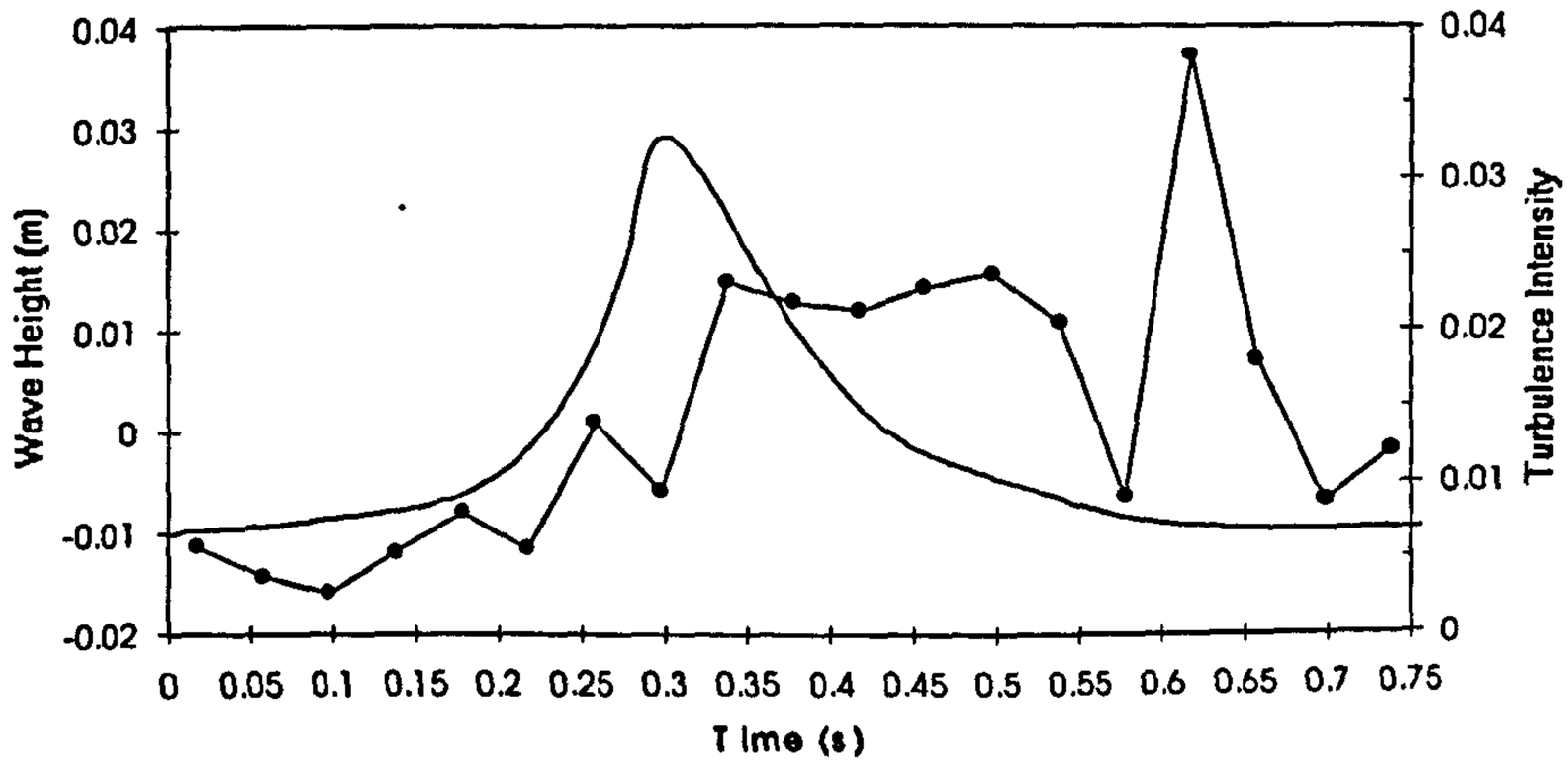

Figure 6.44 Phase-averaged turbulence intensity results for spilling waves under offshore winds at X=-1370mm. Probe heights: a) 83 b) 63 c) 43mm

a)

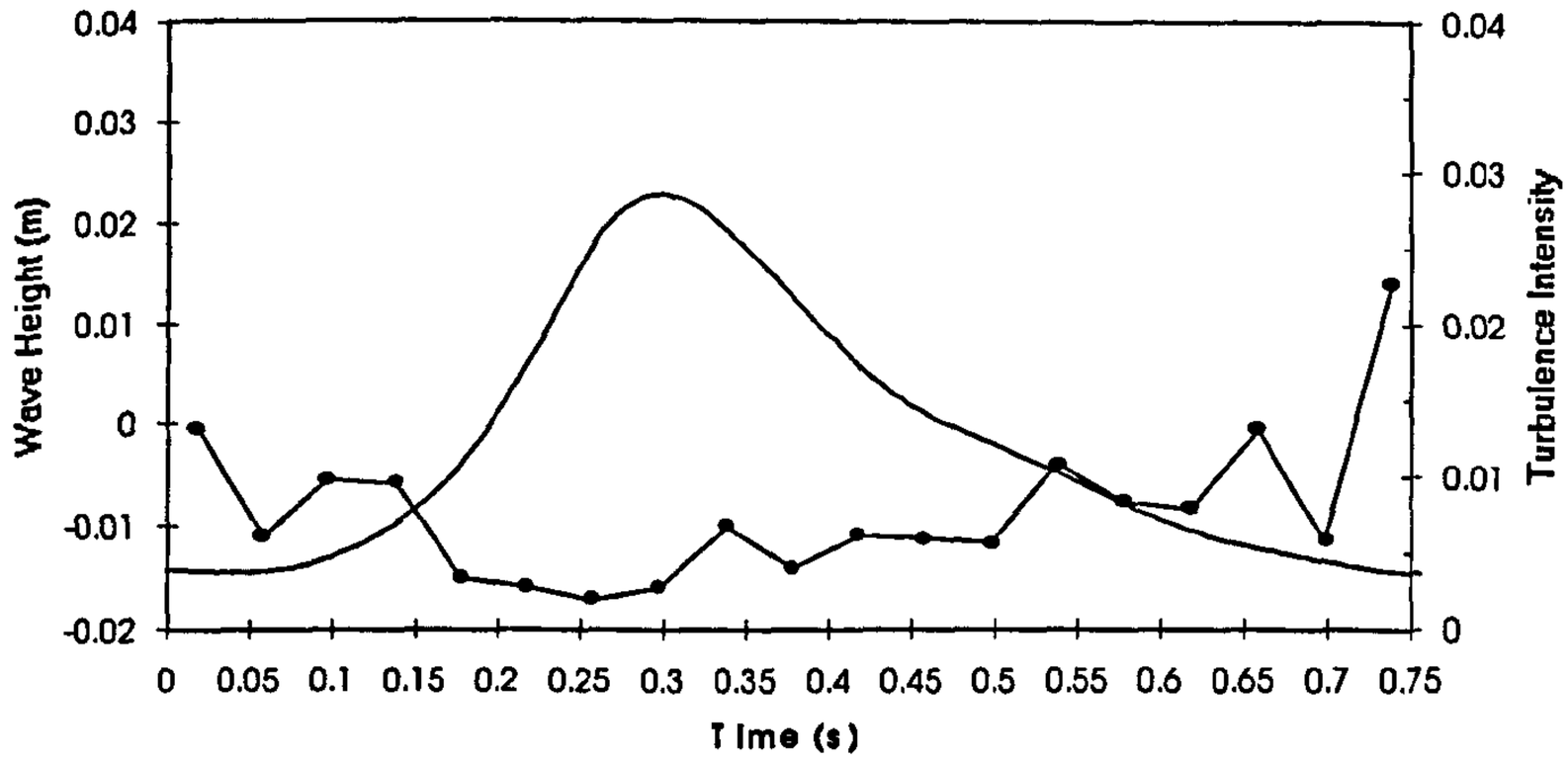

b)

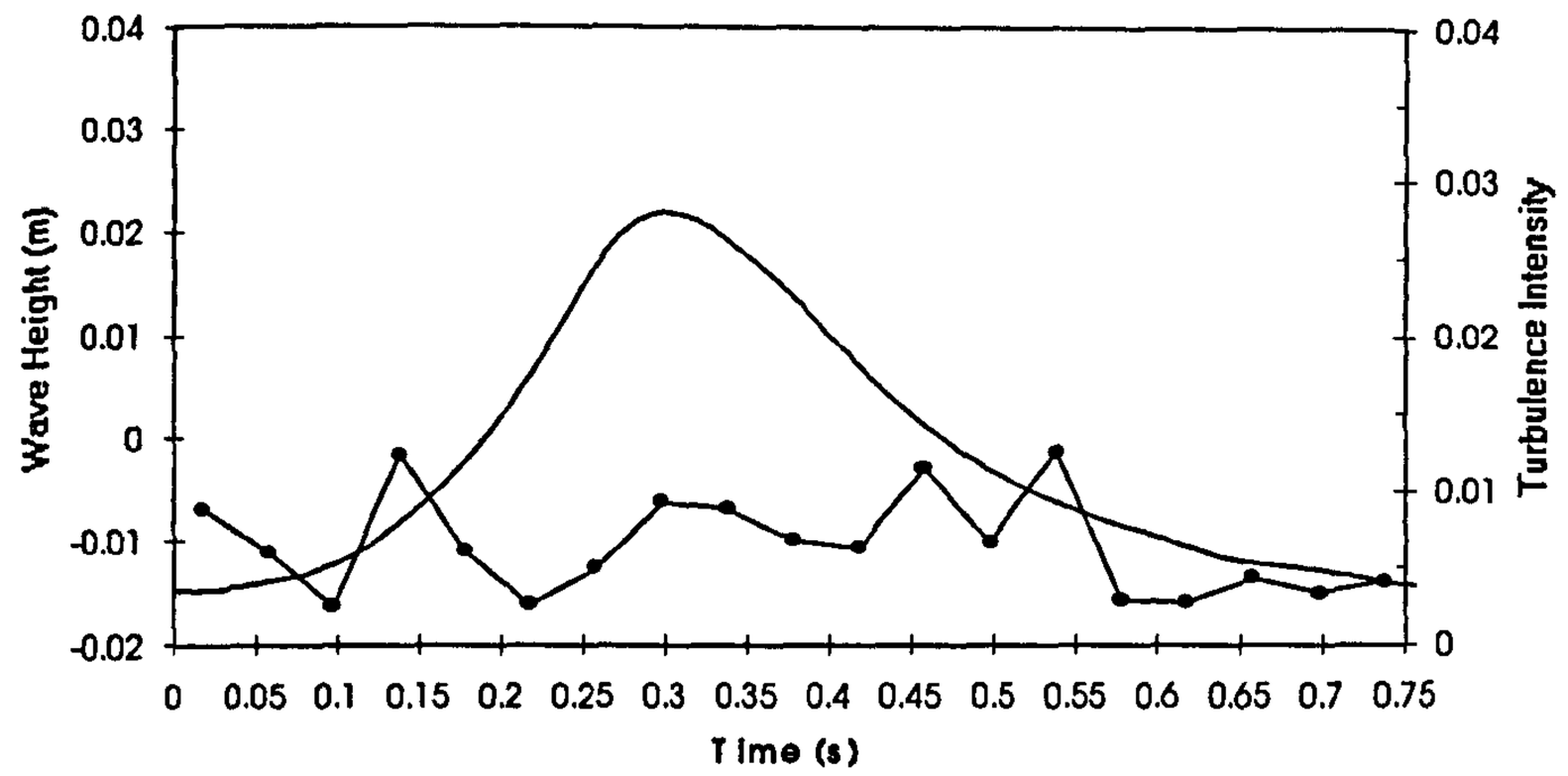

c)

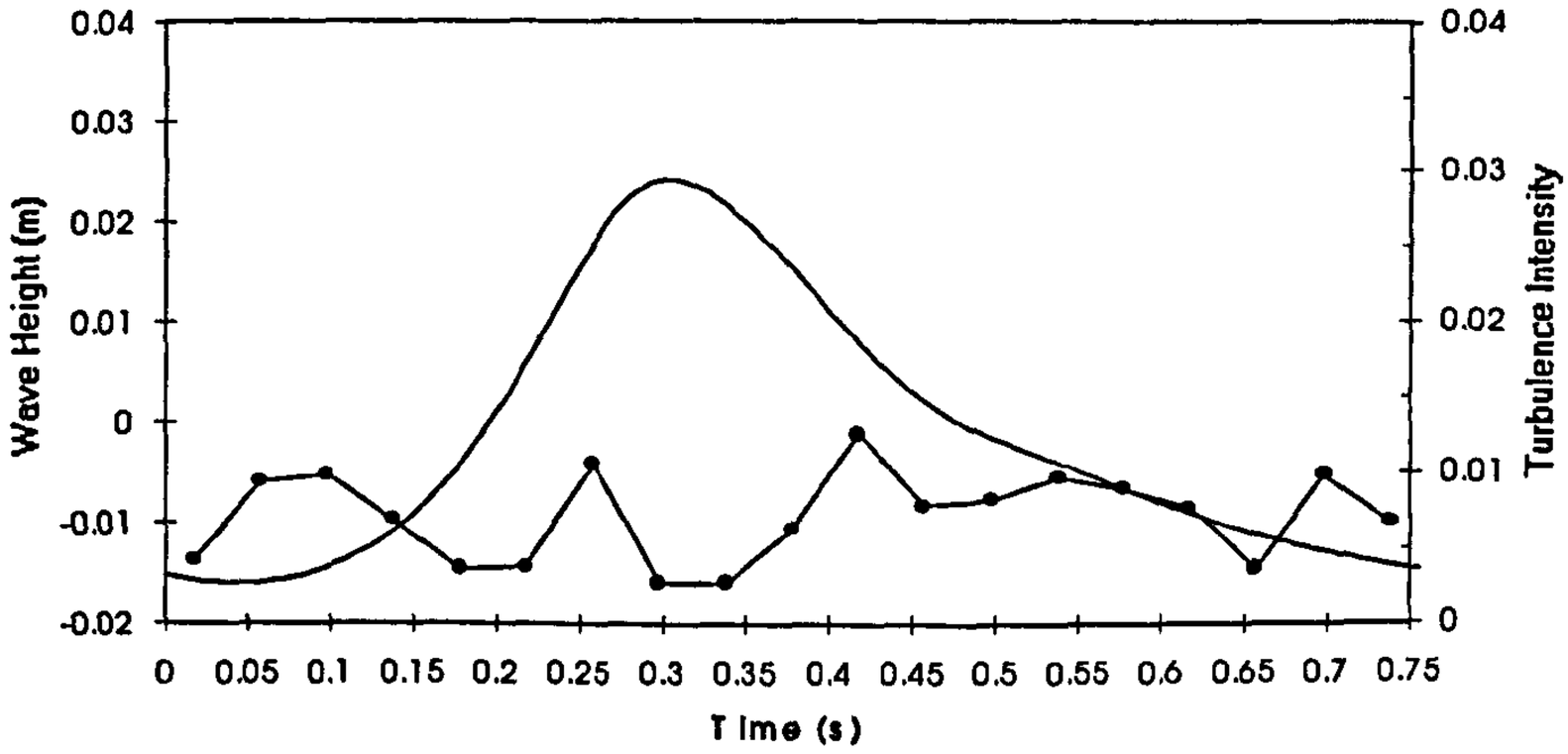

Figure 6.45 Phase-averaged turbulence intensity results for spilling waves under offshore winds at X=-1738mm. Probe heights: a) 83 b) 63 c) 43mm

a)

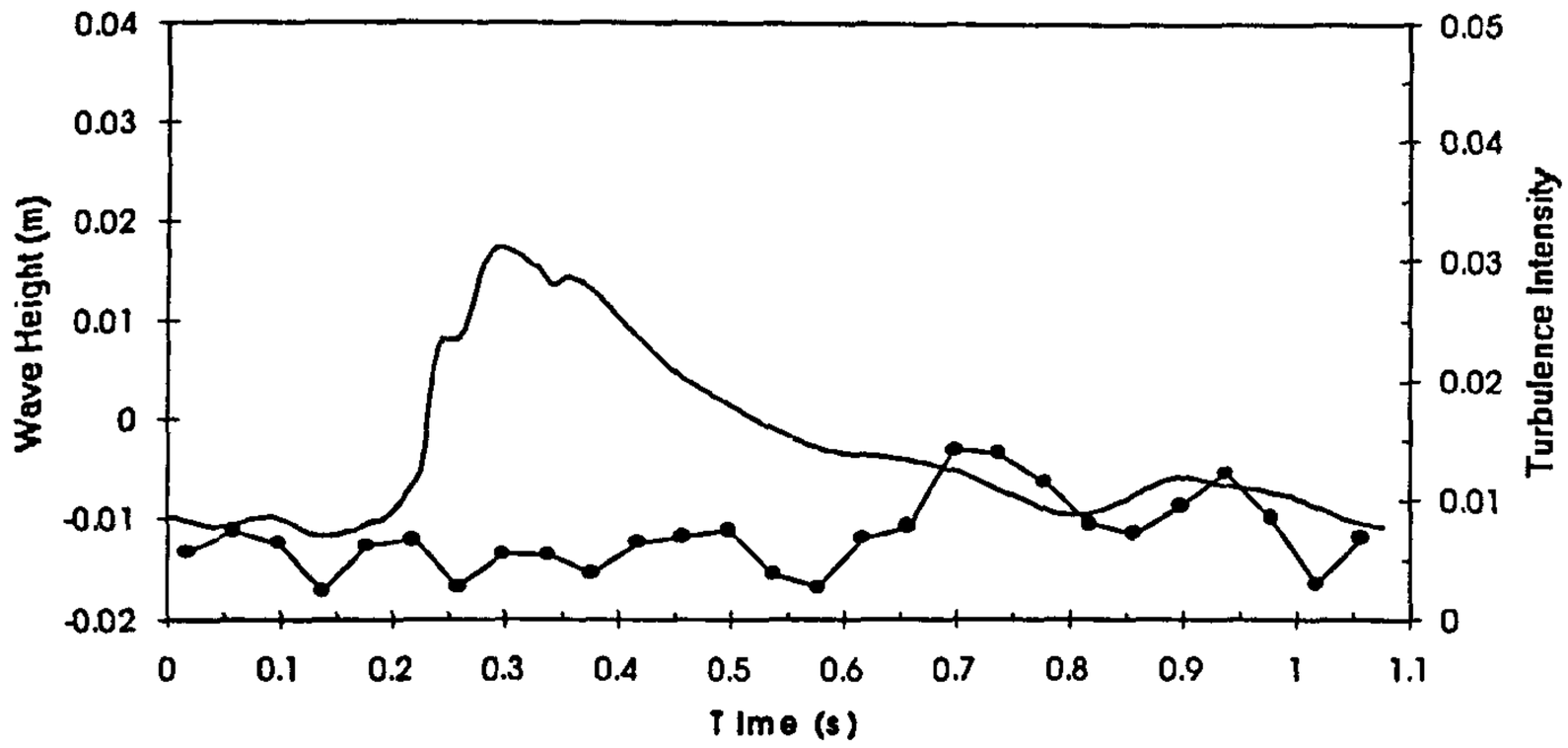

b)

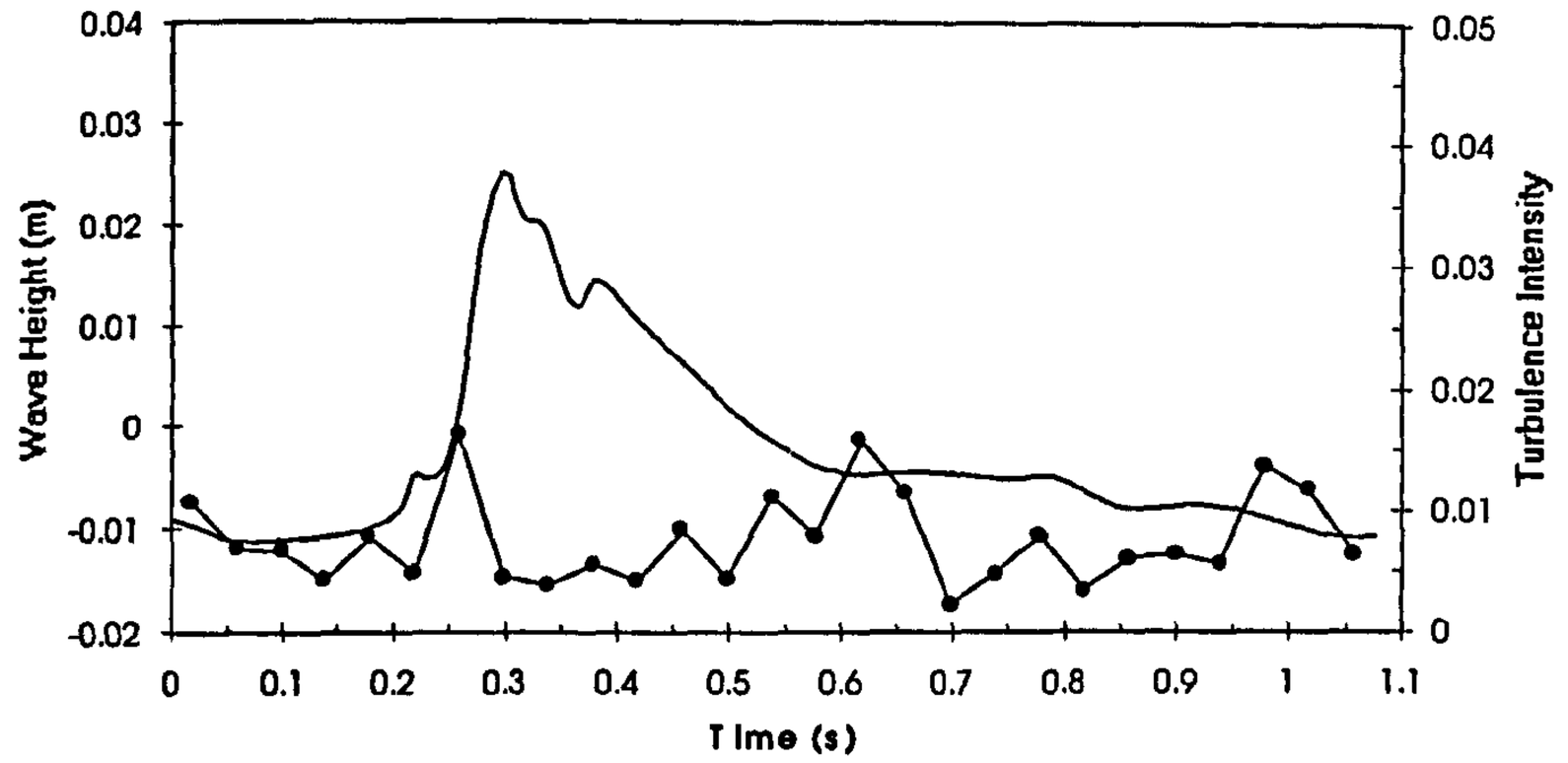

c)

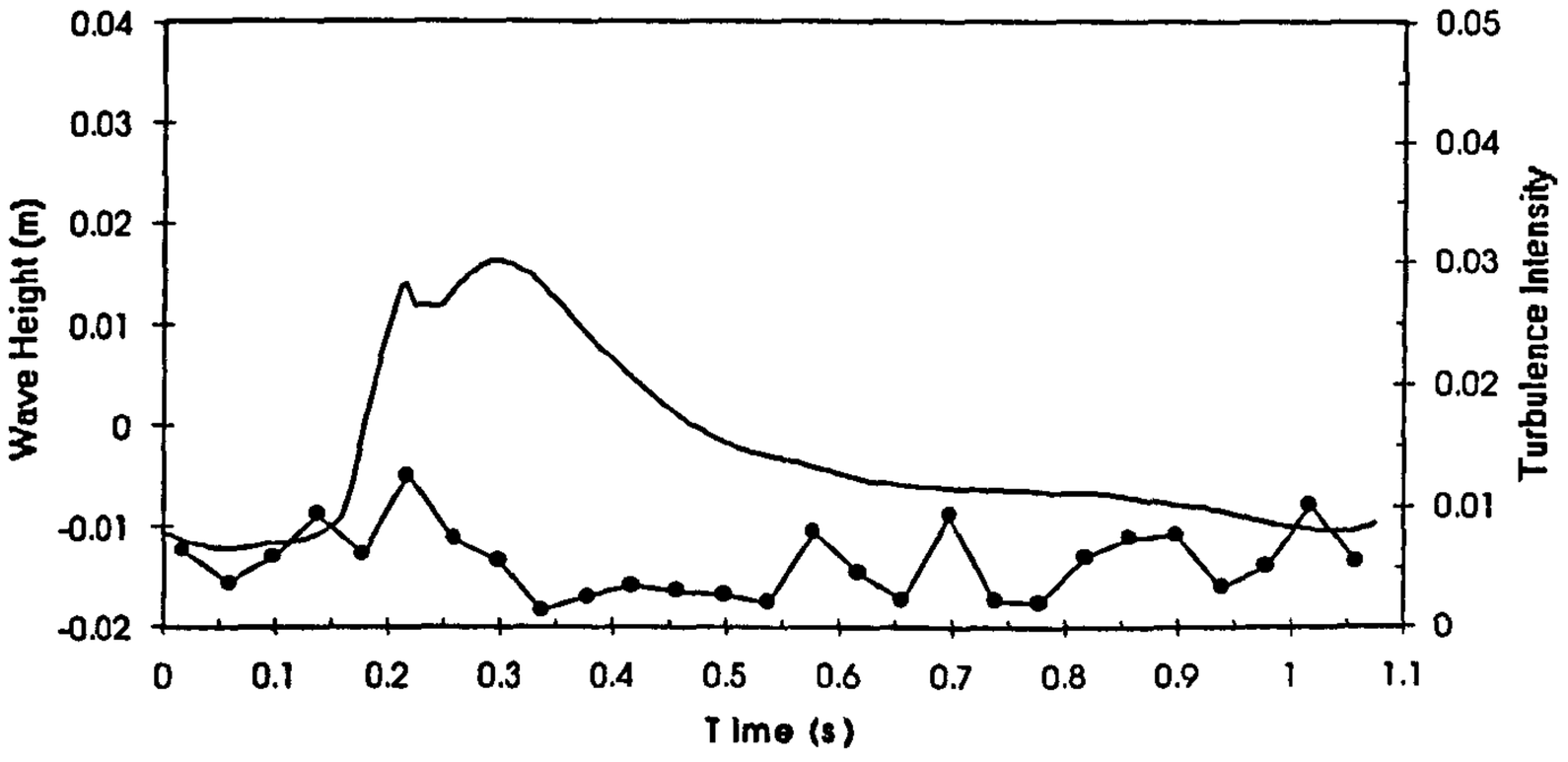

Figure 6.46 Phase-averaged turbulence intensity results for plunging waves under offshore winds at X=-1136mm.
Probe heights: a) 83 b) 63 c) 48mm

a)

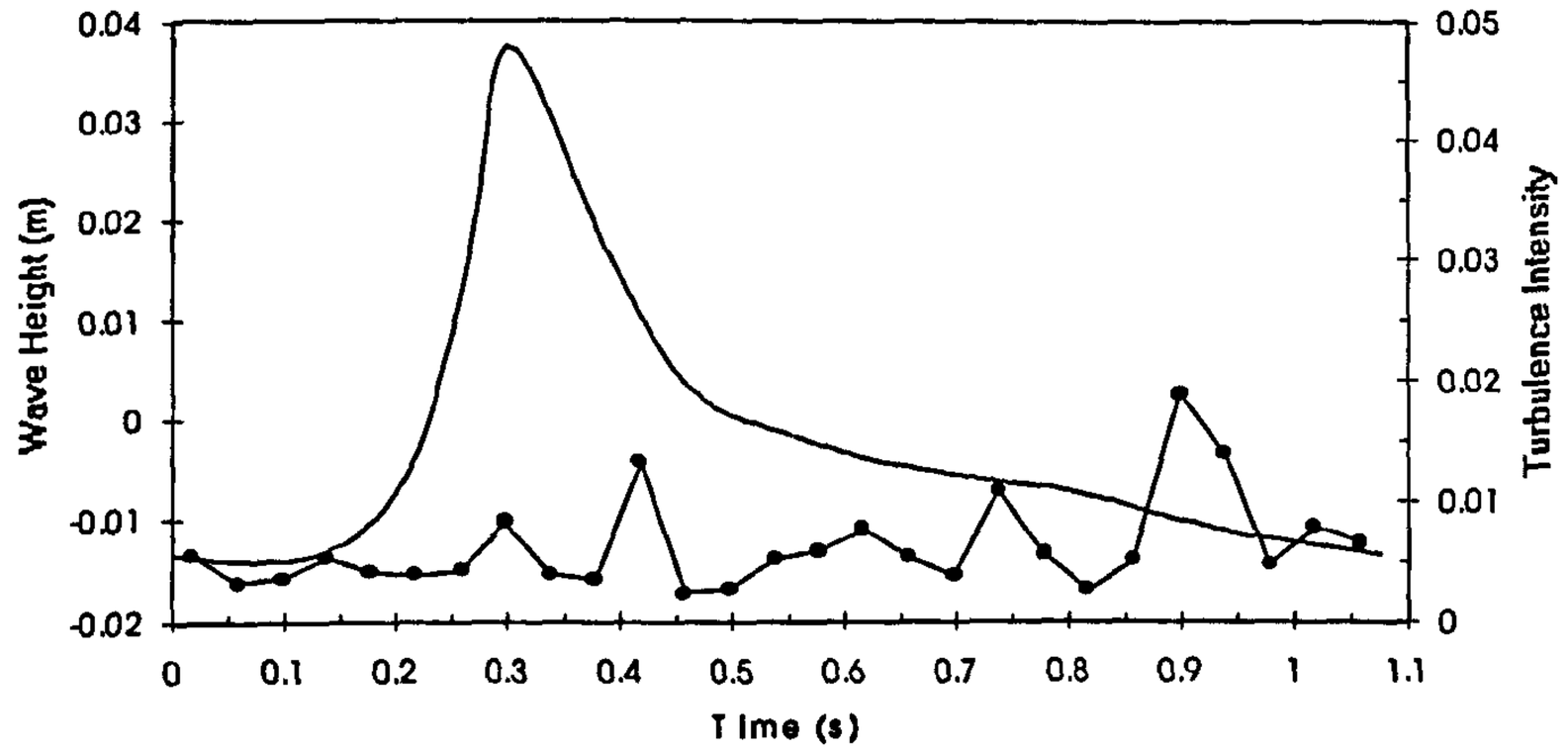

b)

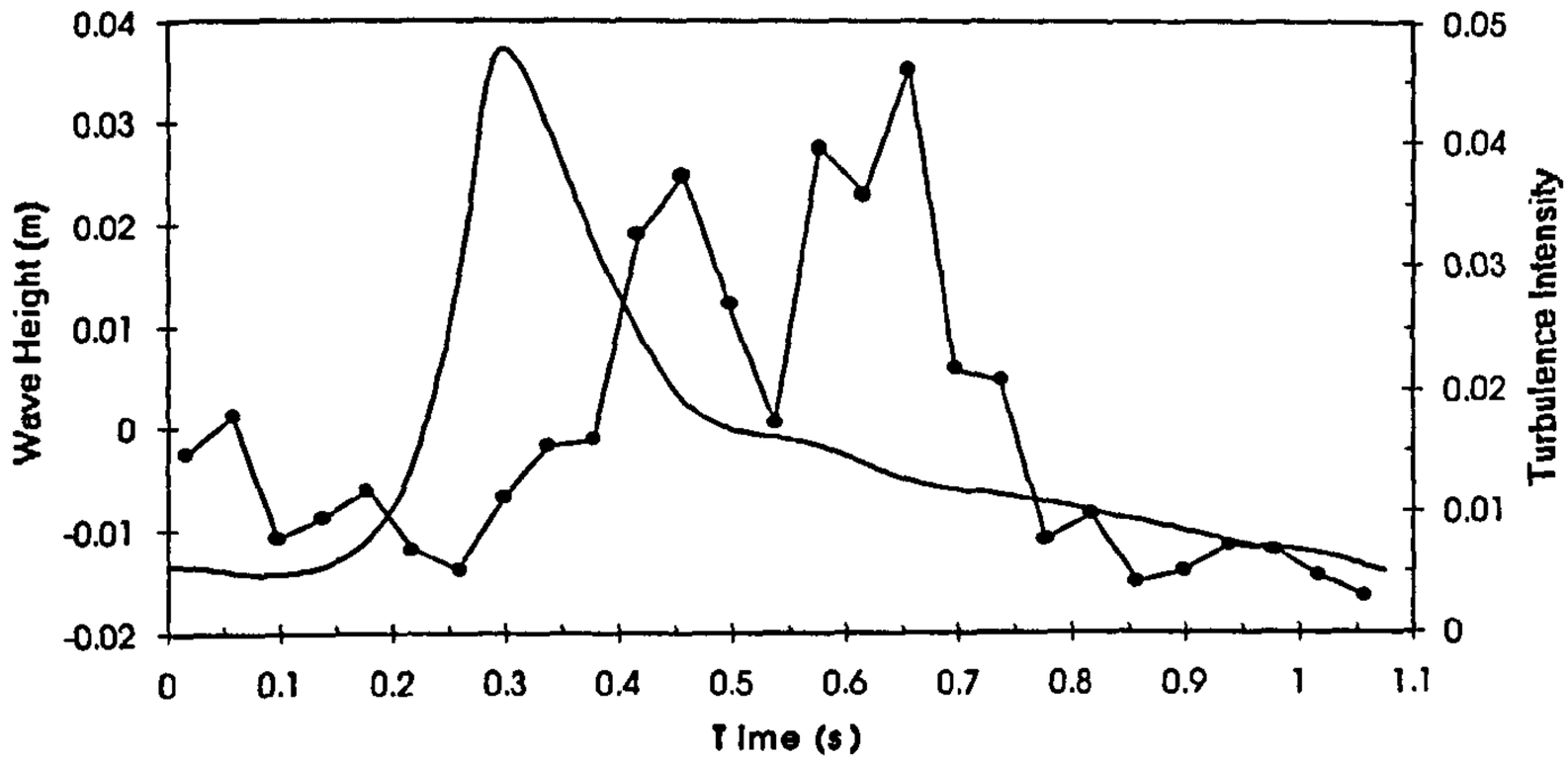

c)

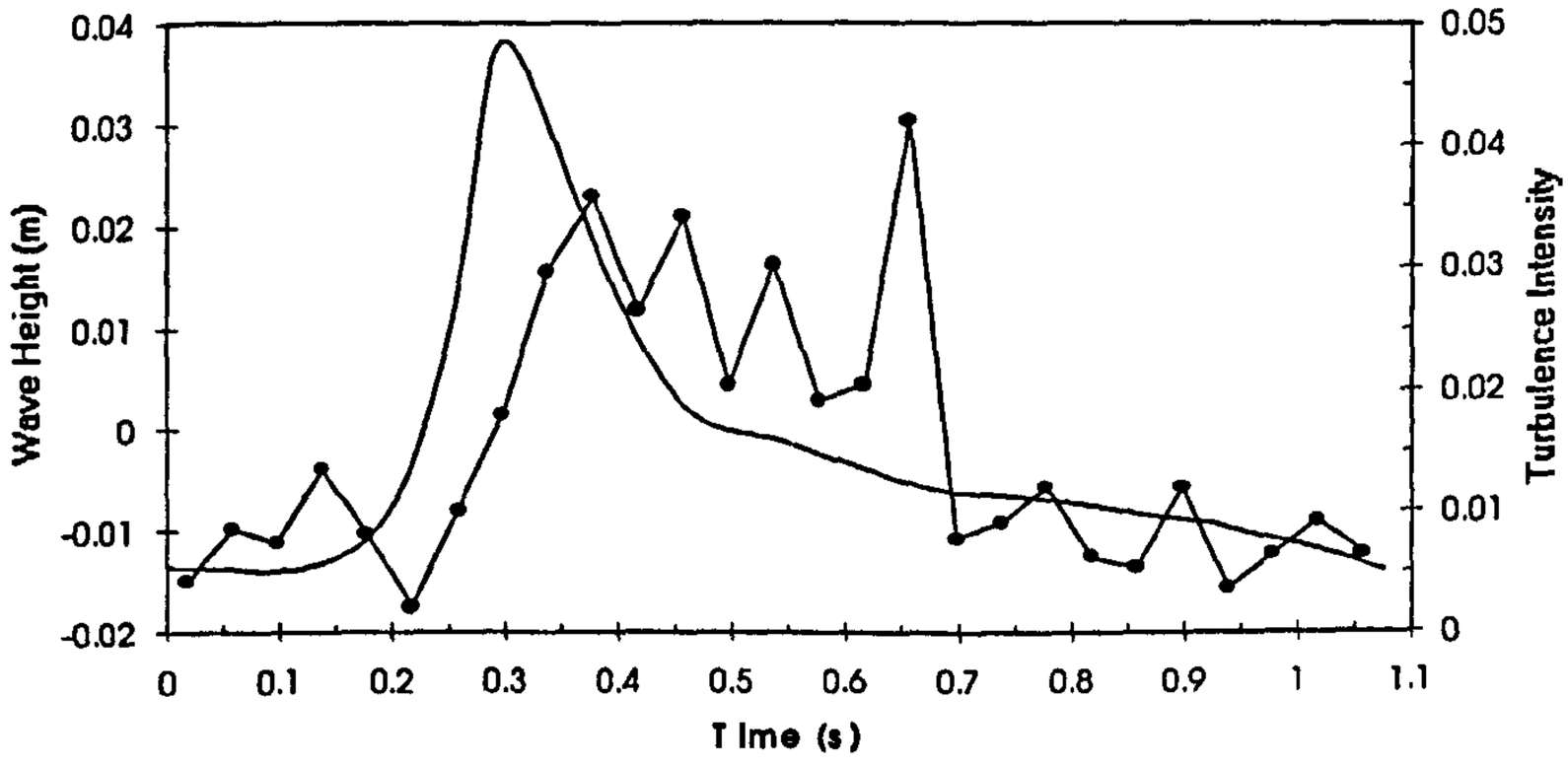

Figure 6.47 Phase-averaged turbulence intensity results for plunging waves under offshore winds at X=-1450mm
Probe heights: a) 83 b) 63 c) 47mm

a)

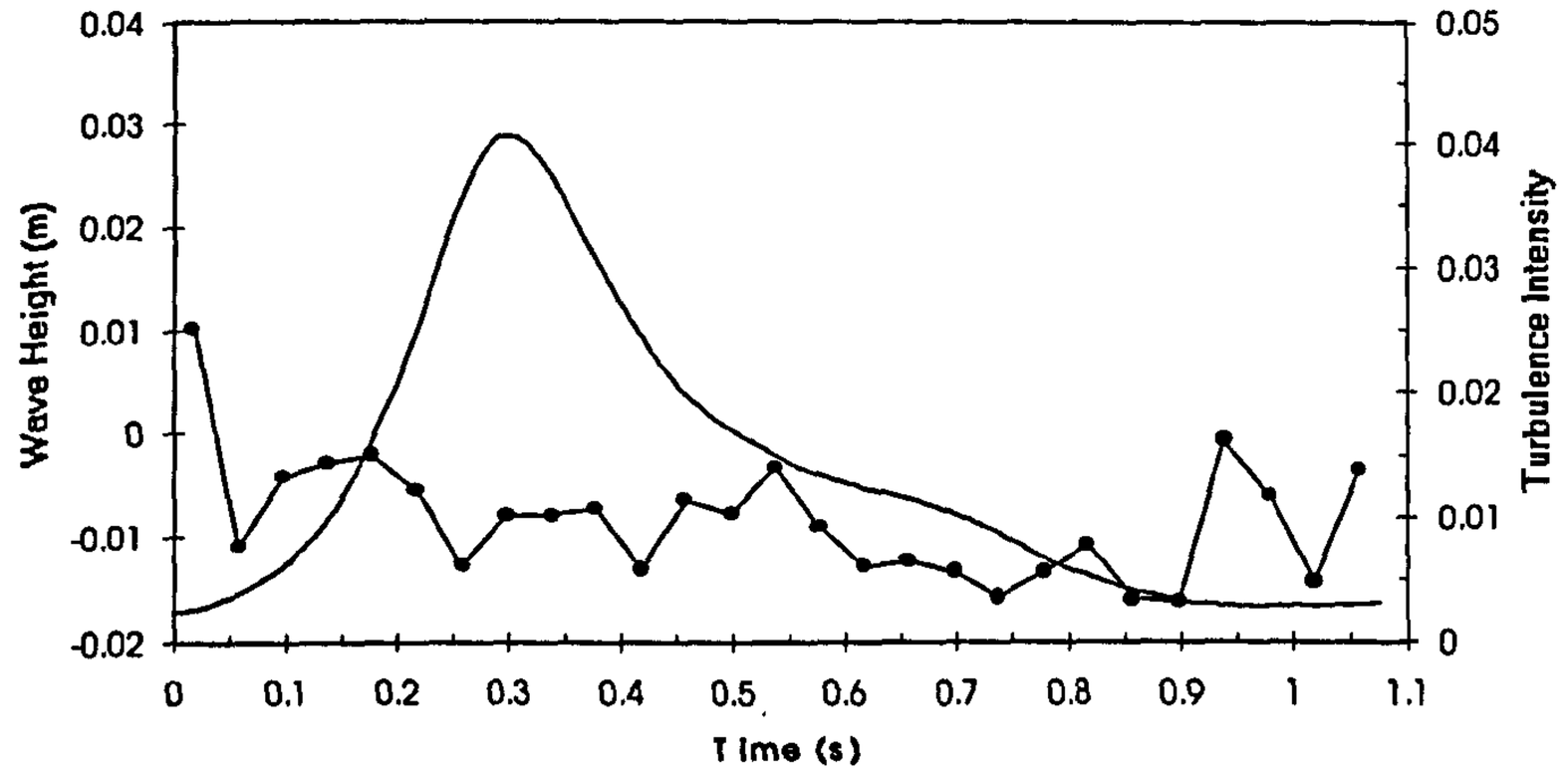

b)

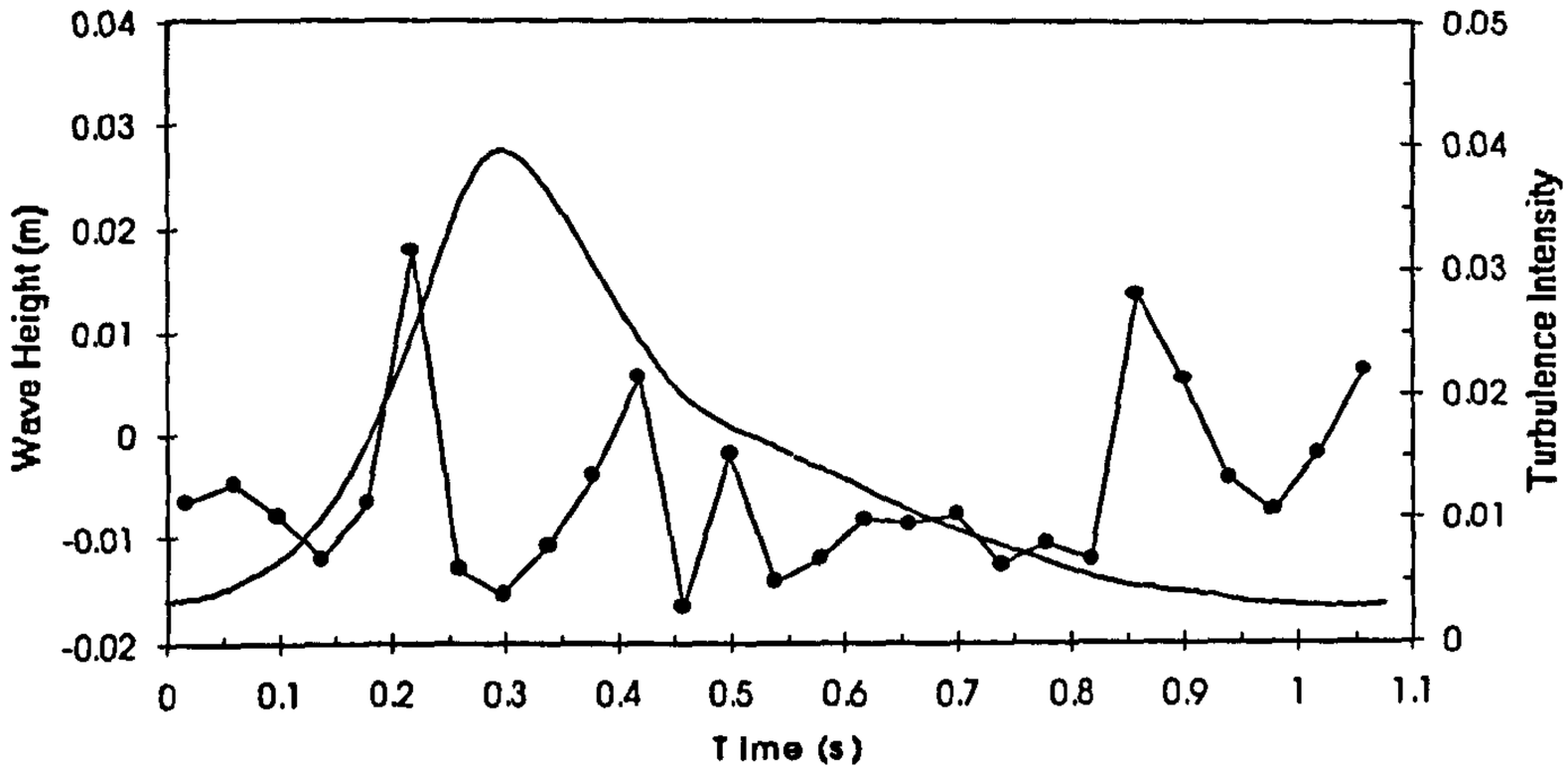

c)

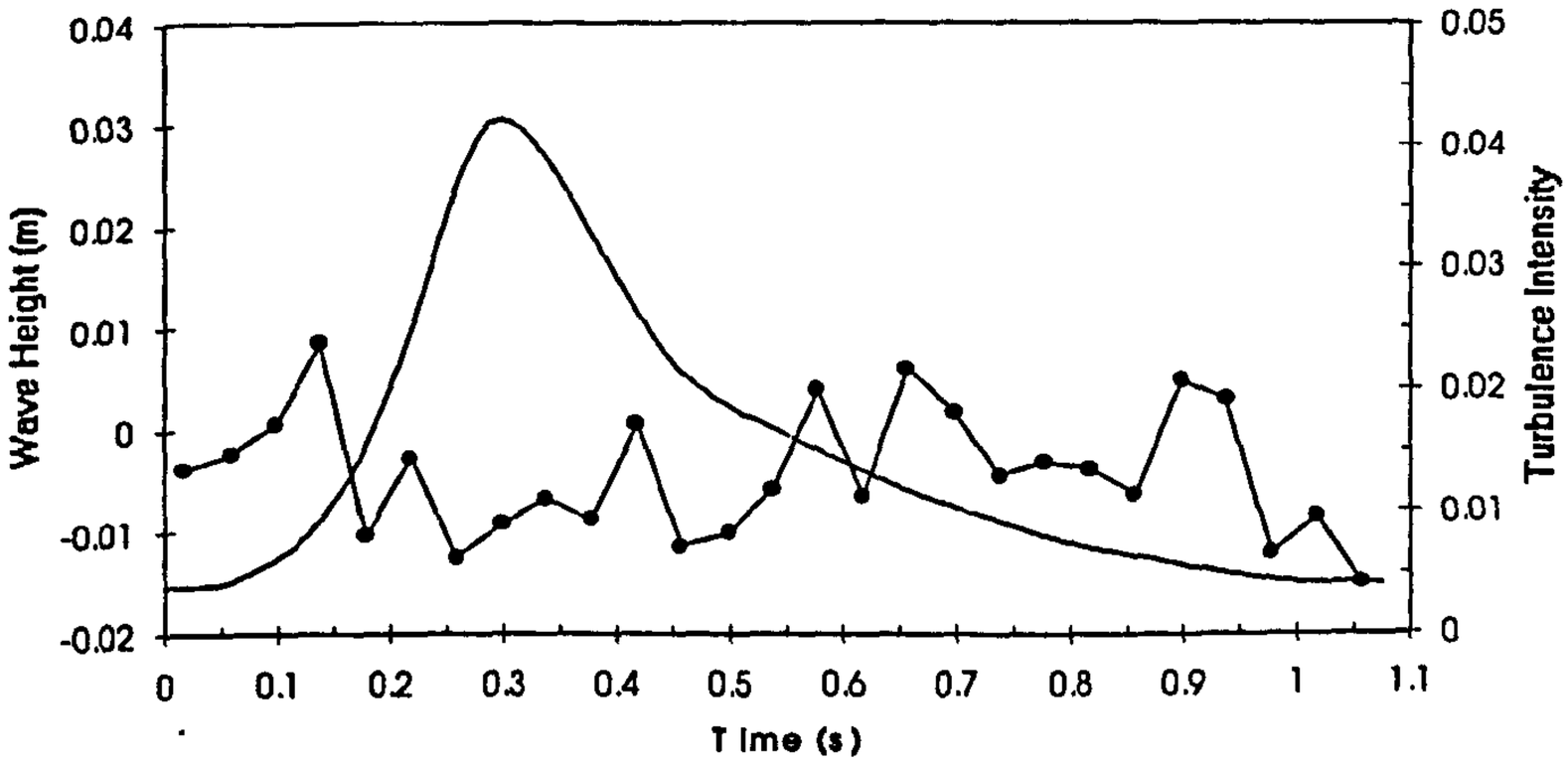

Figure 6.48 Phase-averaged turbulence intensity results for plunging waves under offshore winds at X=-1705mm
Probe heights: a) 83 b) 63 c) 47mm

a)

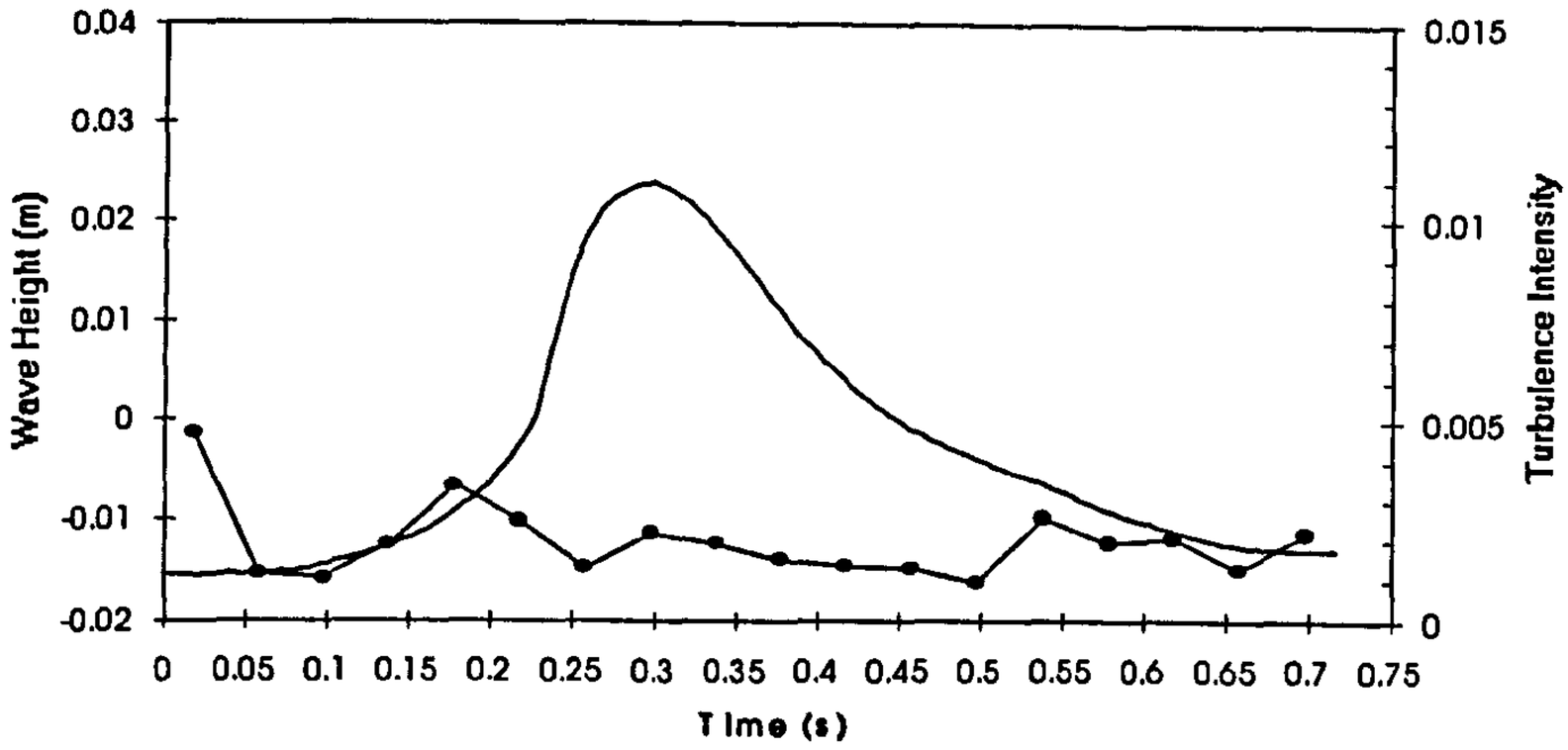

b)

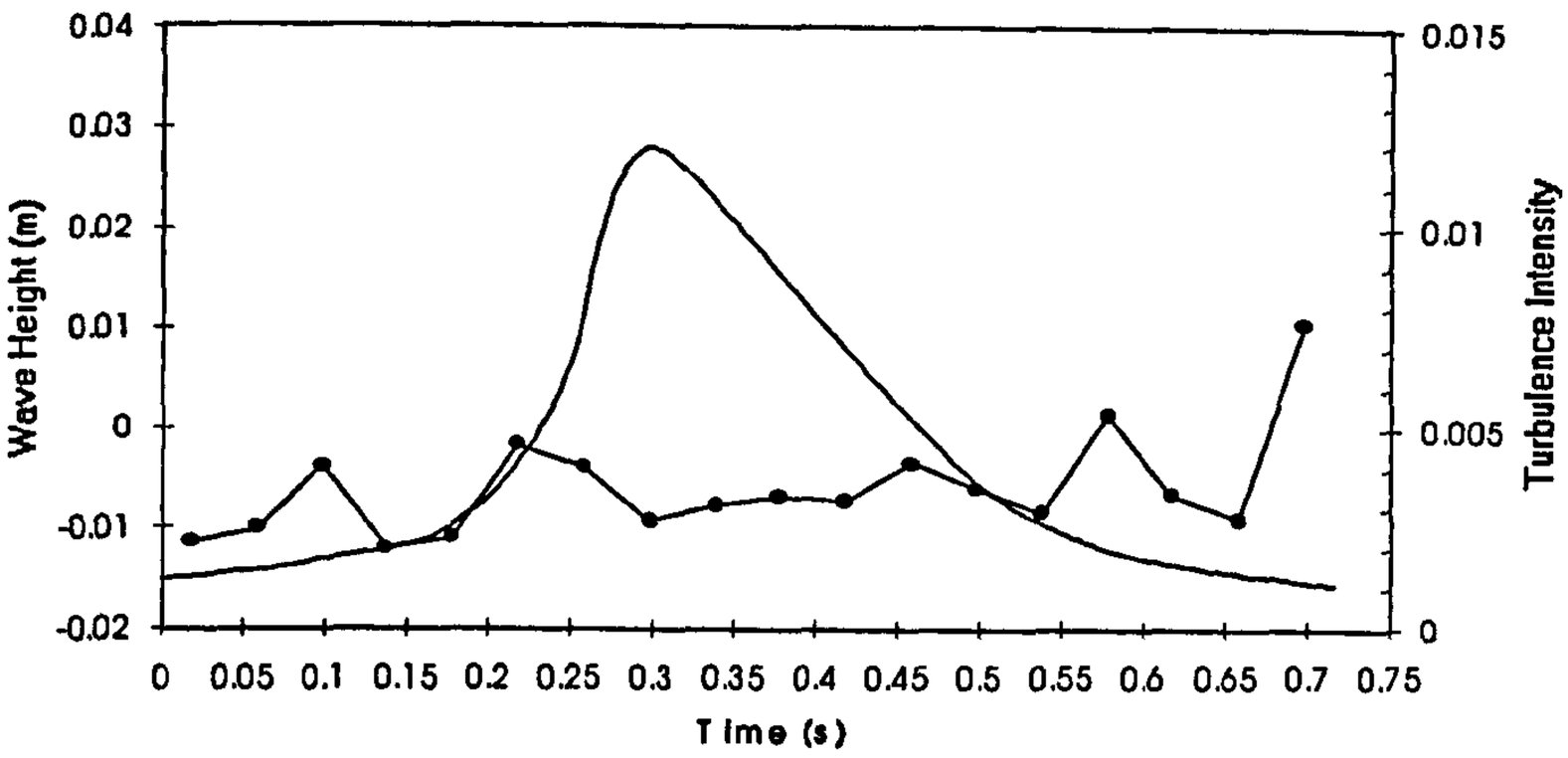

c)

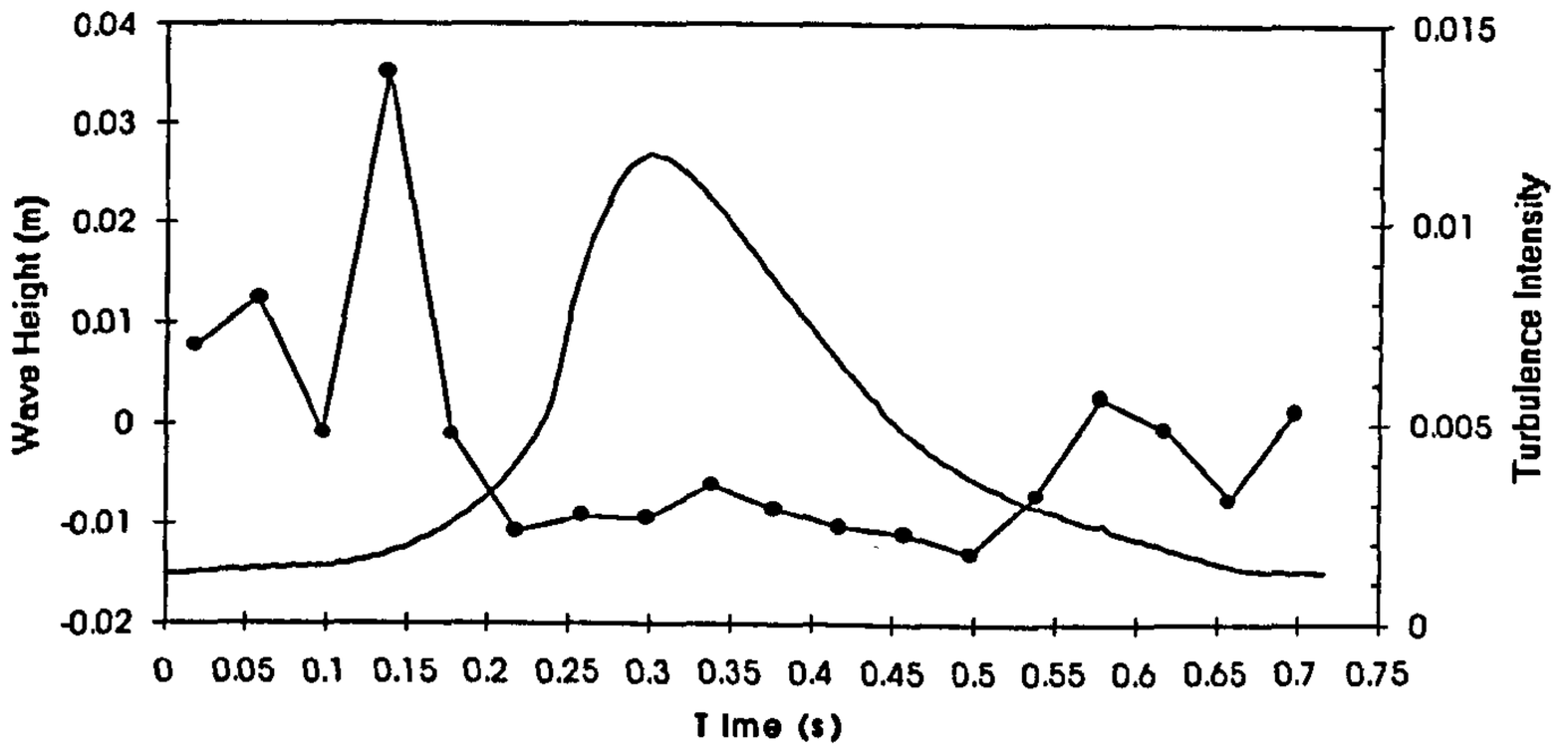

Figure 6.49 Phase-averaged turbulence intensity results for spilling waves under onshore winds at X=-1254mm. Probe heights: a) 86 b) 66 c) 46mm

a)

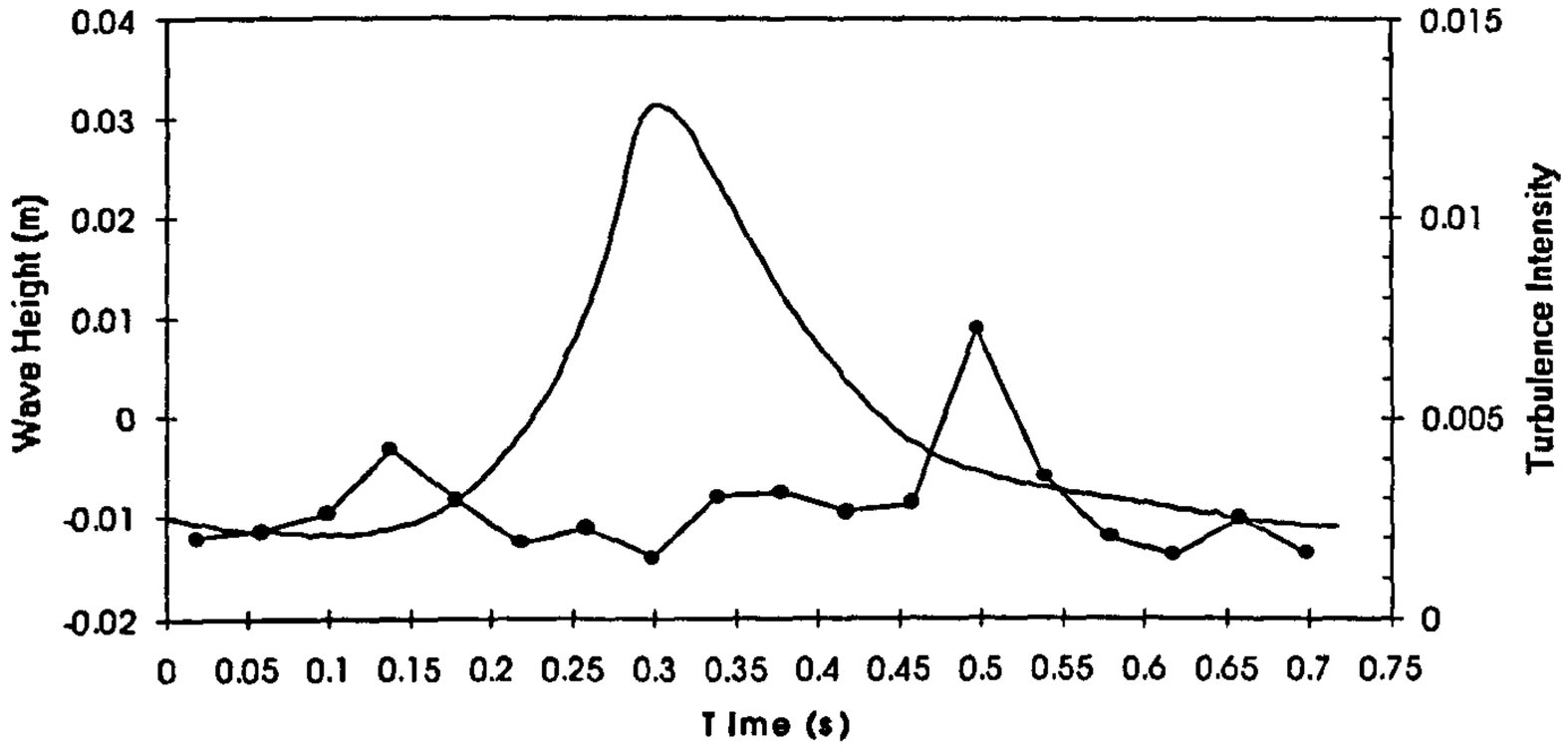

b)

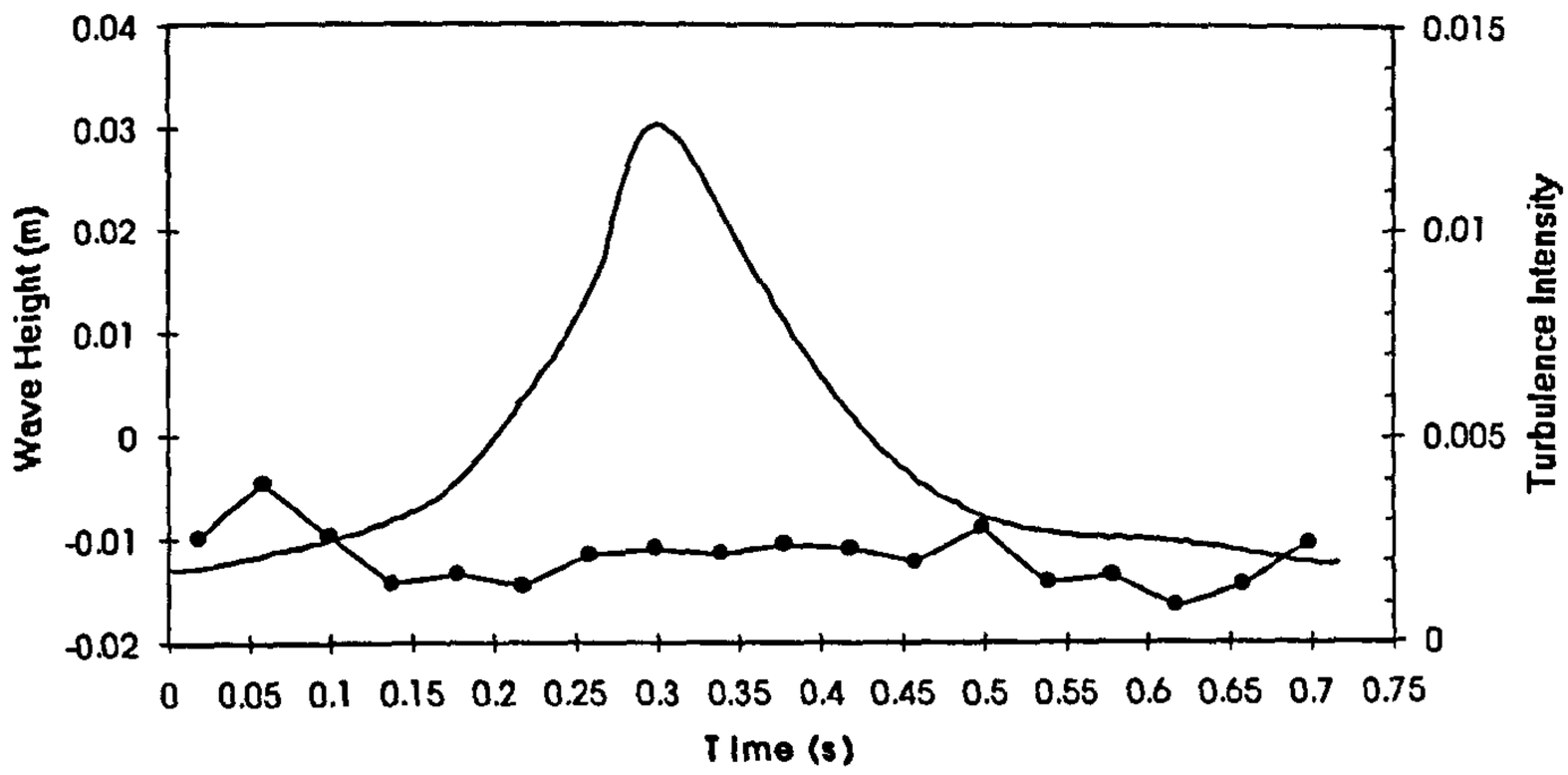

c)

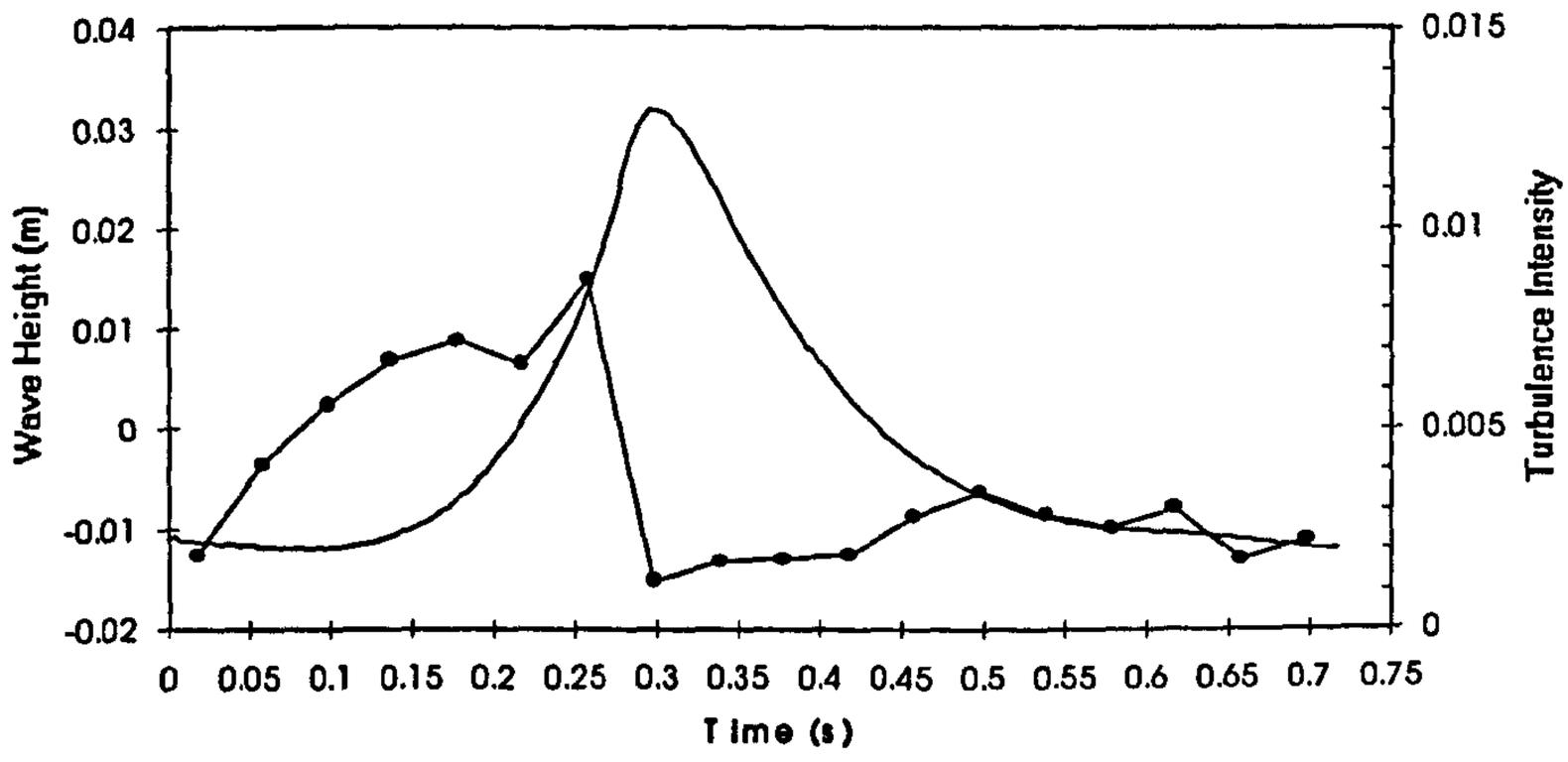

Figure 6.50 Phase-averaged turbulence intensity results for spilling waves under onshore winds at X=-1554mm. Probe heights: a) 82 b) 62 c) 42mm

a)

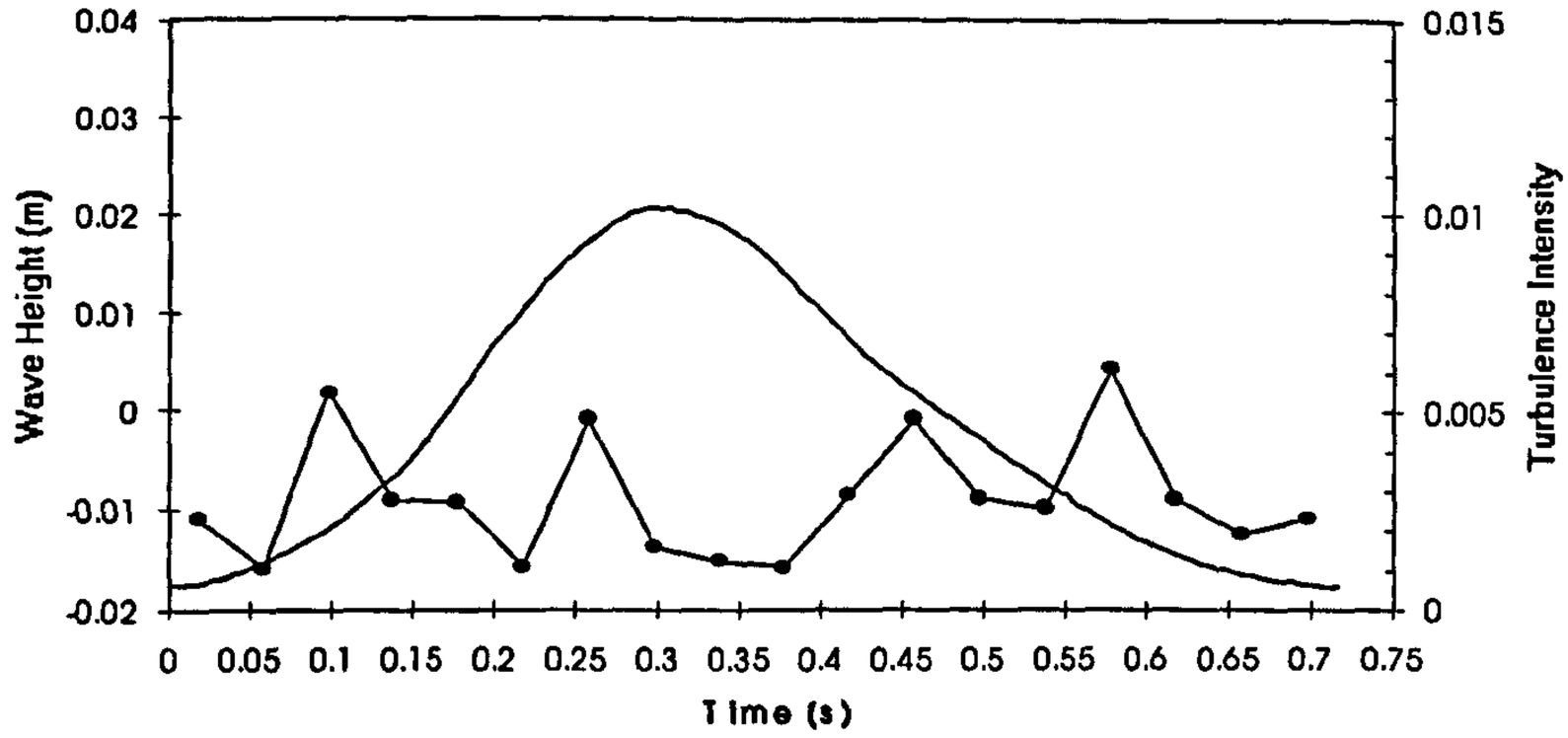

b)

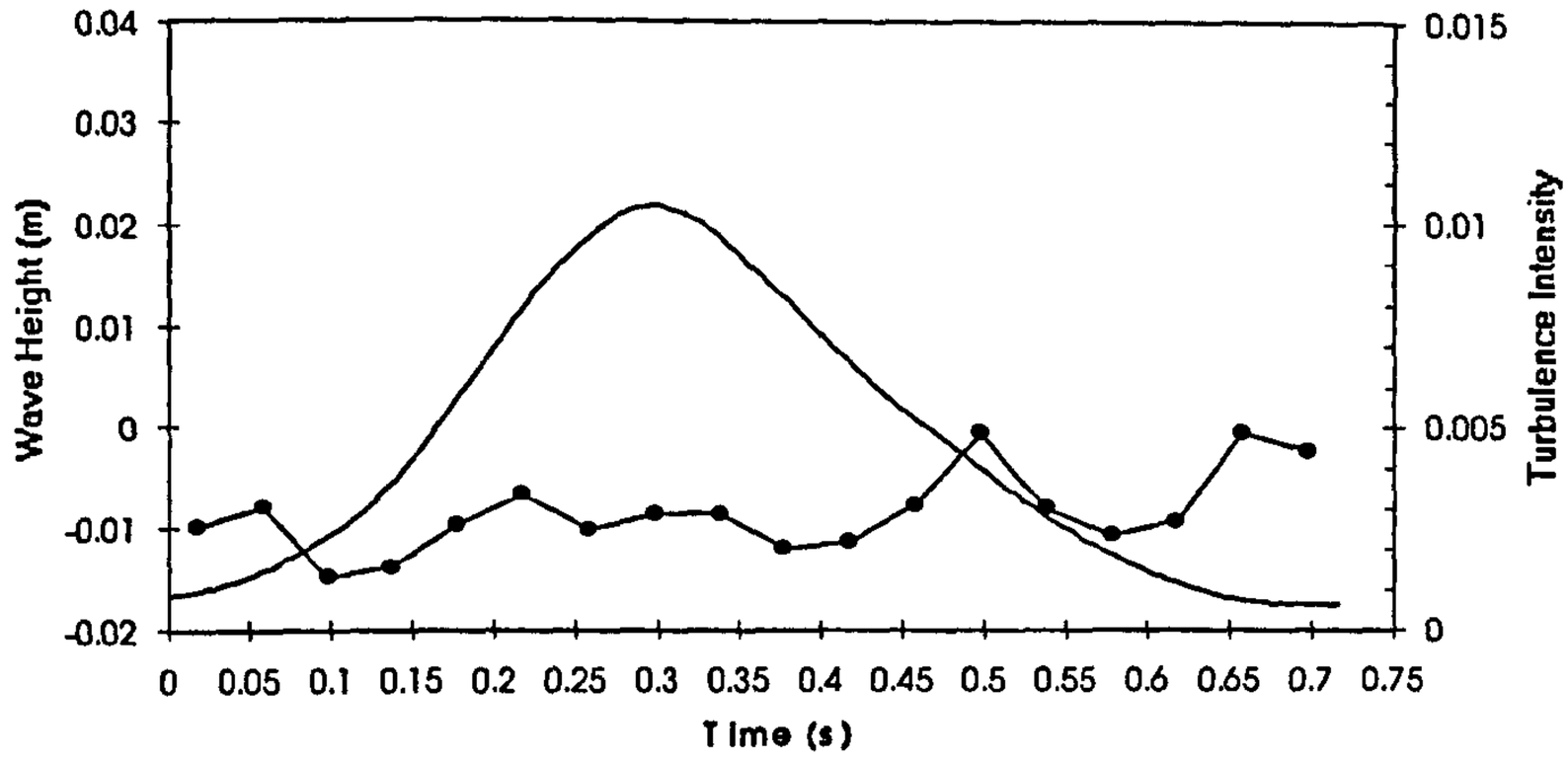

c)

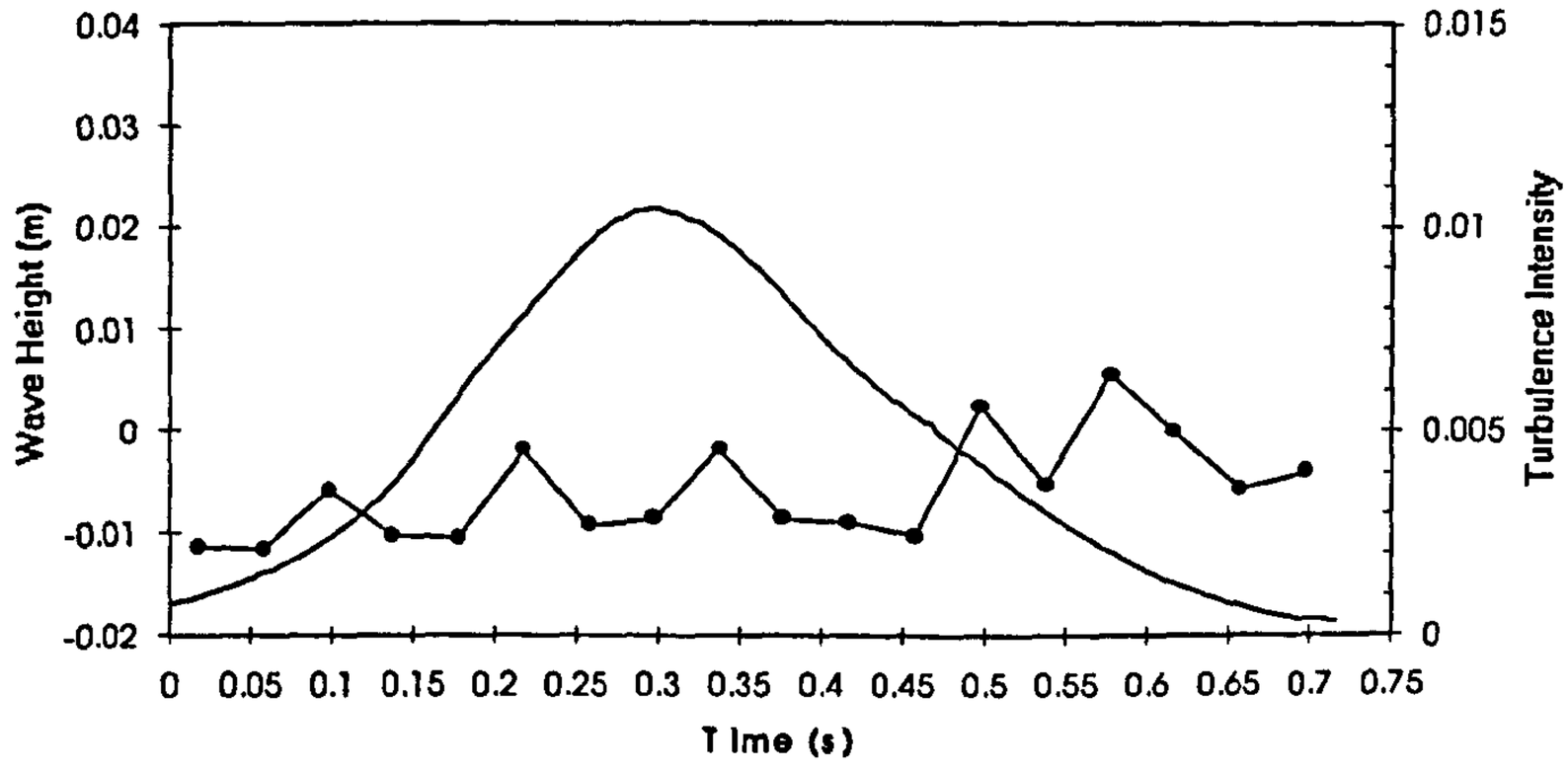

Figure 6.51 Phase-averaged turbulence intensity results for spilling waves under onshore winds at X=-1854mm. Probe heights: a) 81 b) 61 c) 41mm

a)

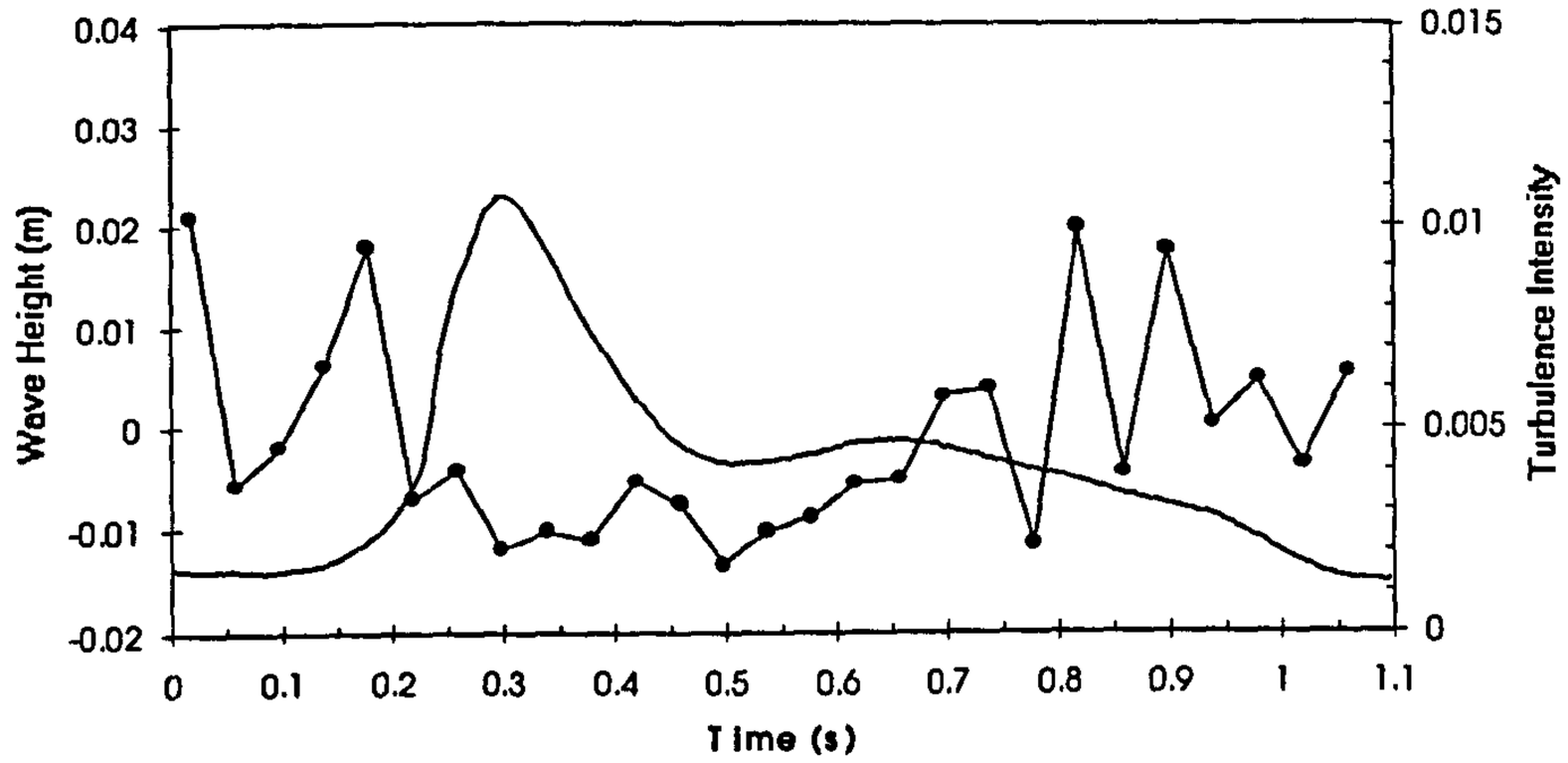

b)

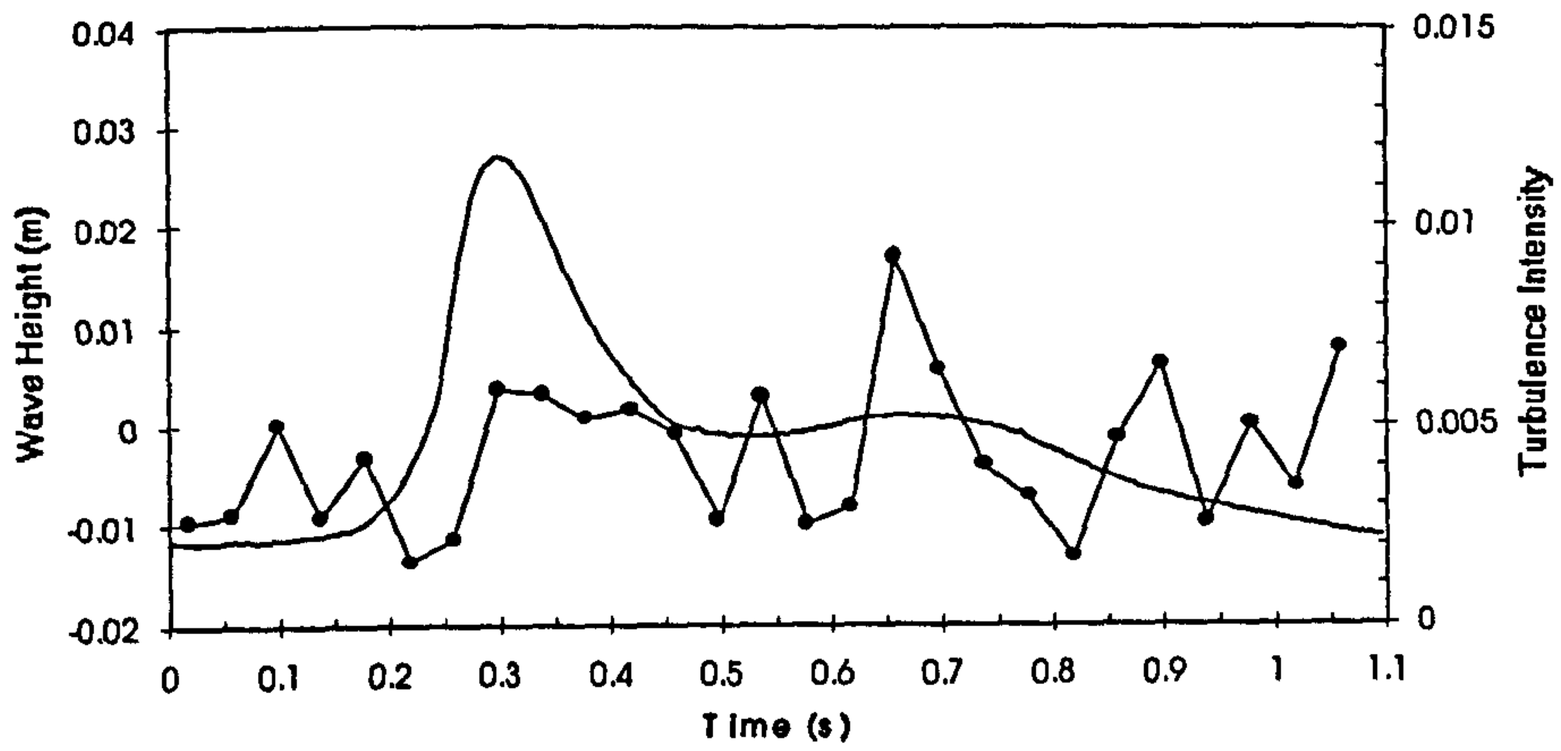

c)

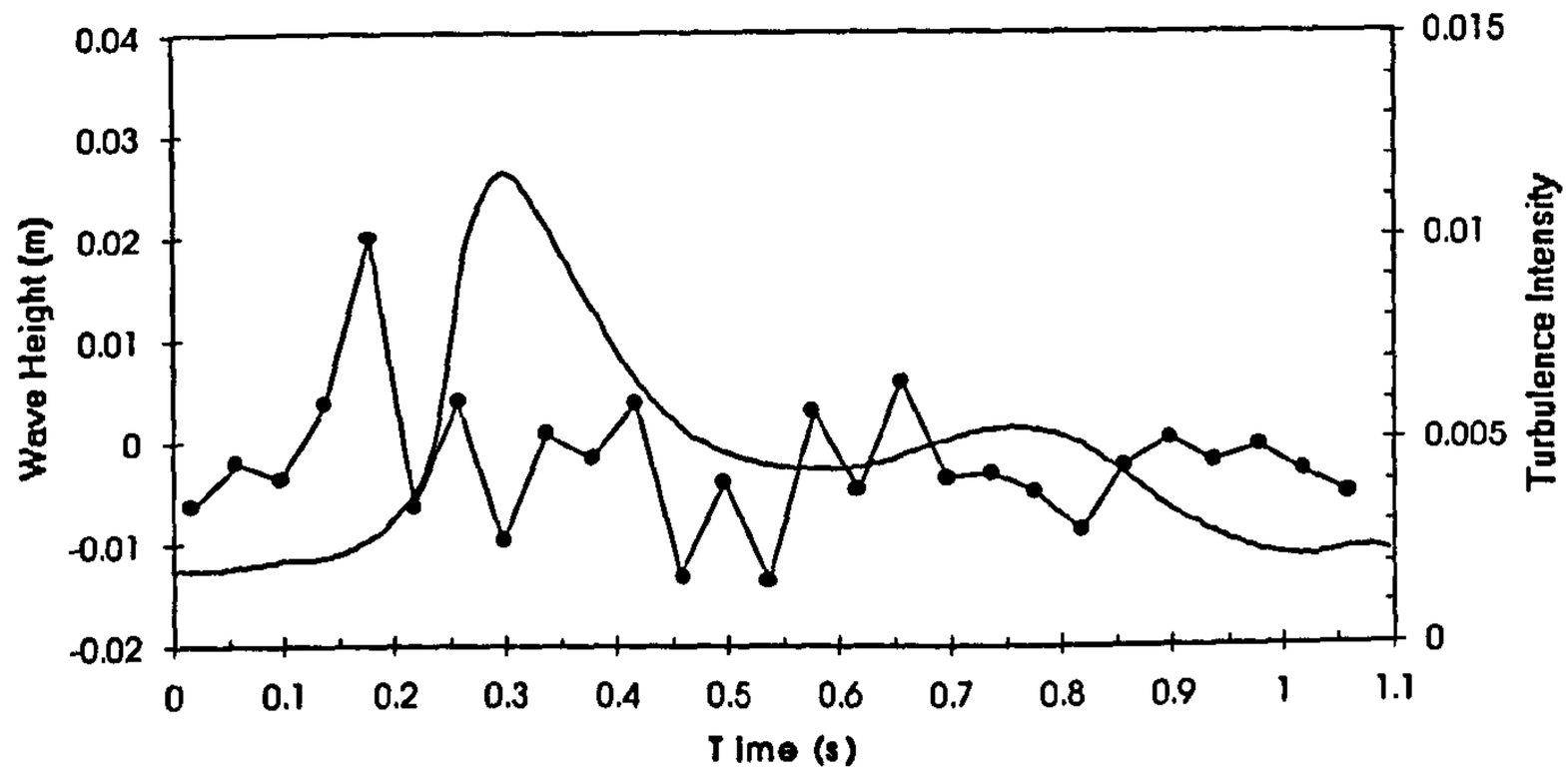

Figure 6.52 Phase-averaged turbulence intensity results for plunging waves under onshore winds at X=-1289mm.
Probe heights: a) 83 b) 63 c) 43mm

a)

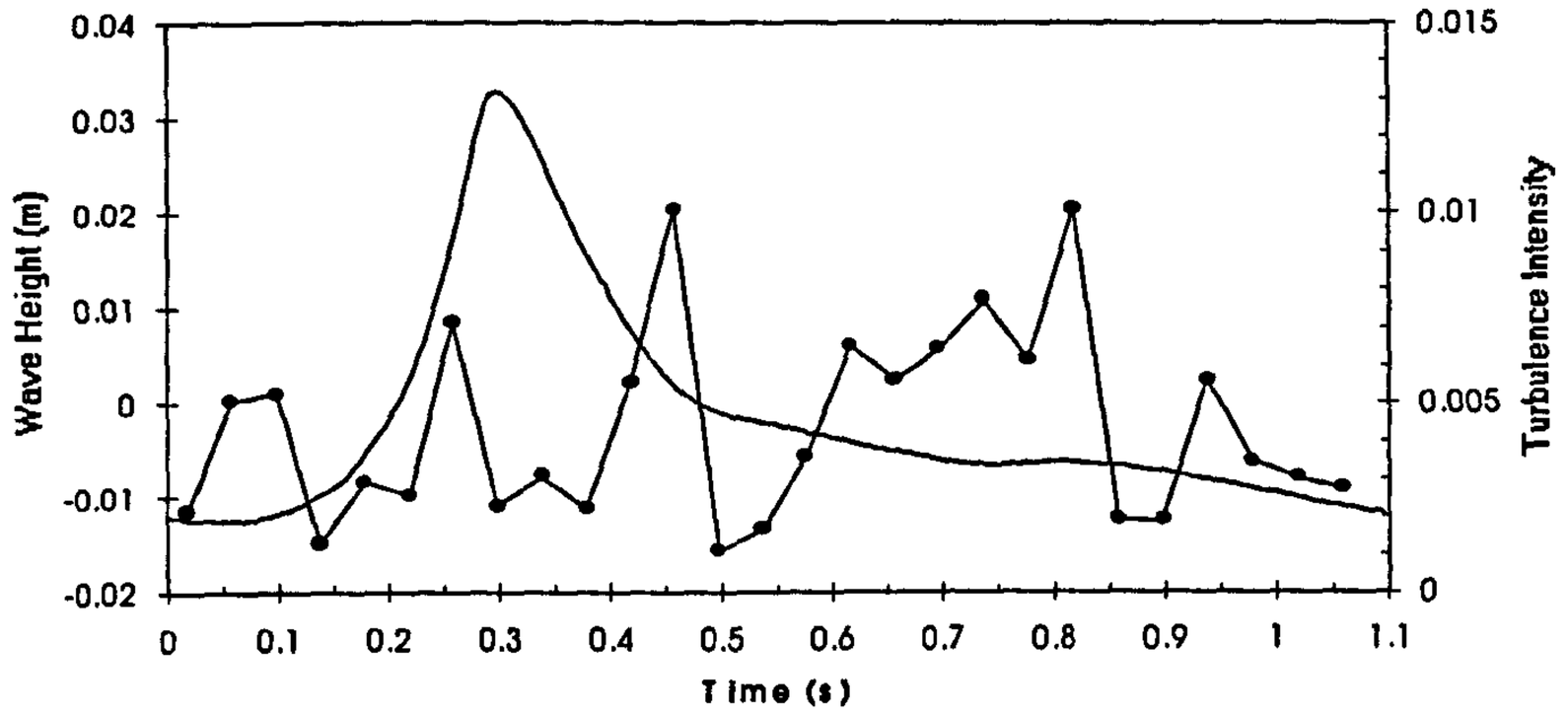

b)

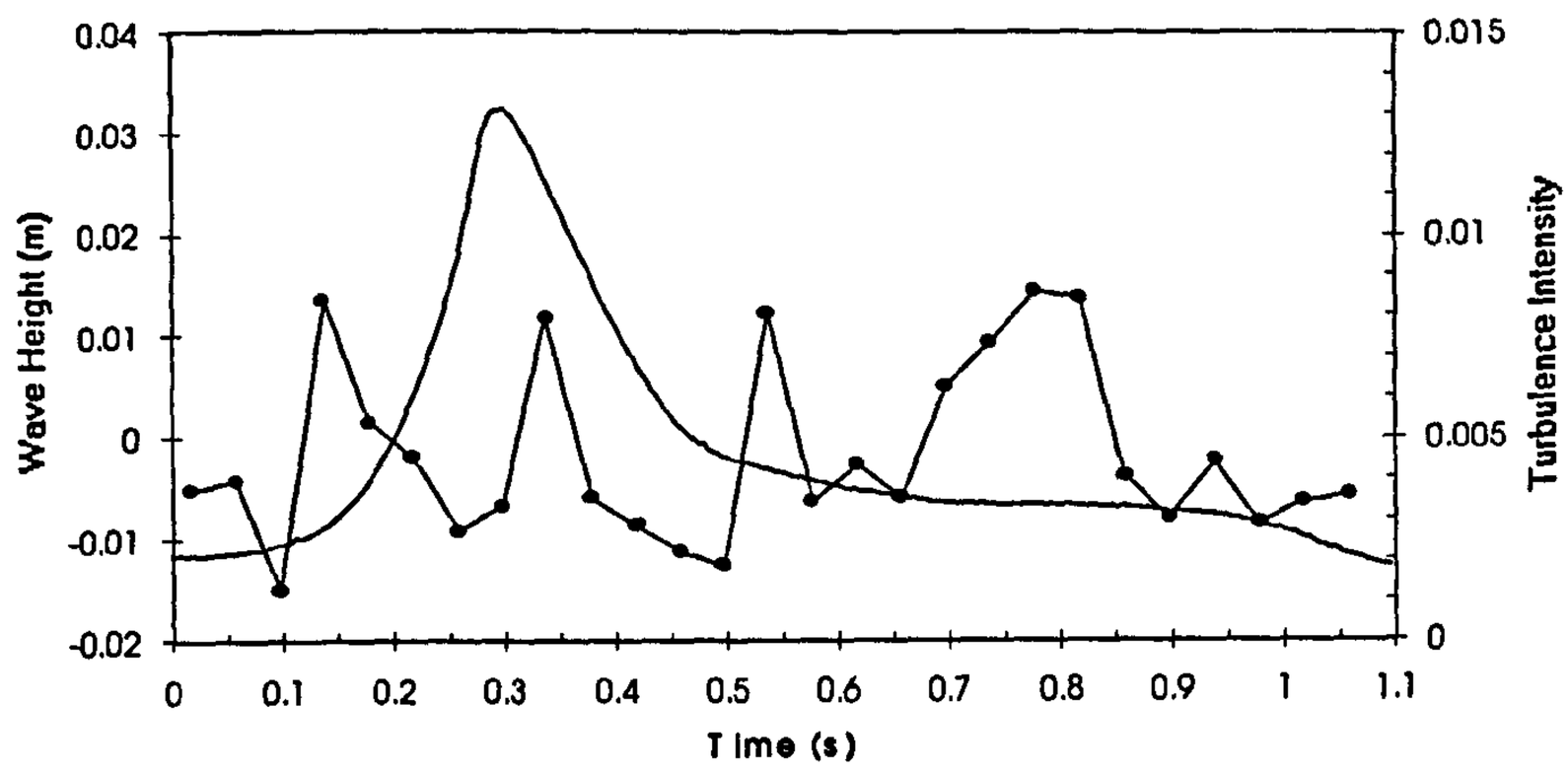

c)

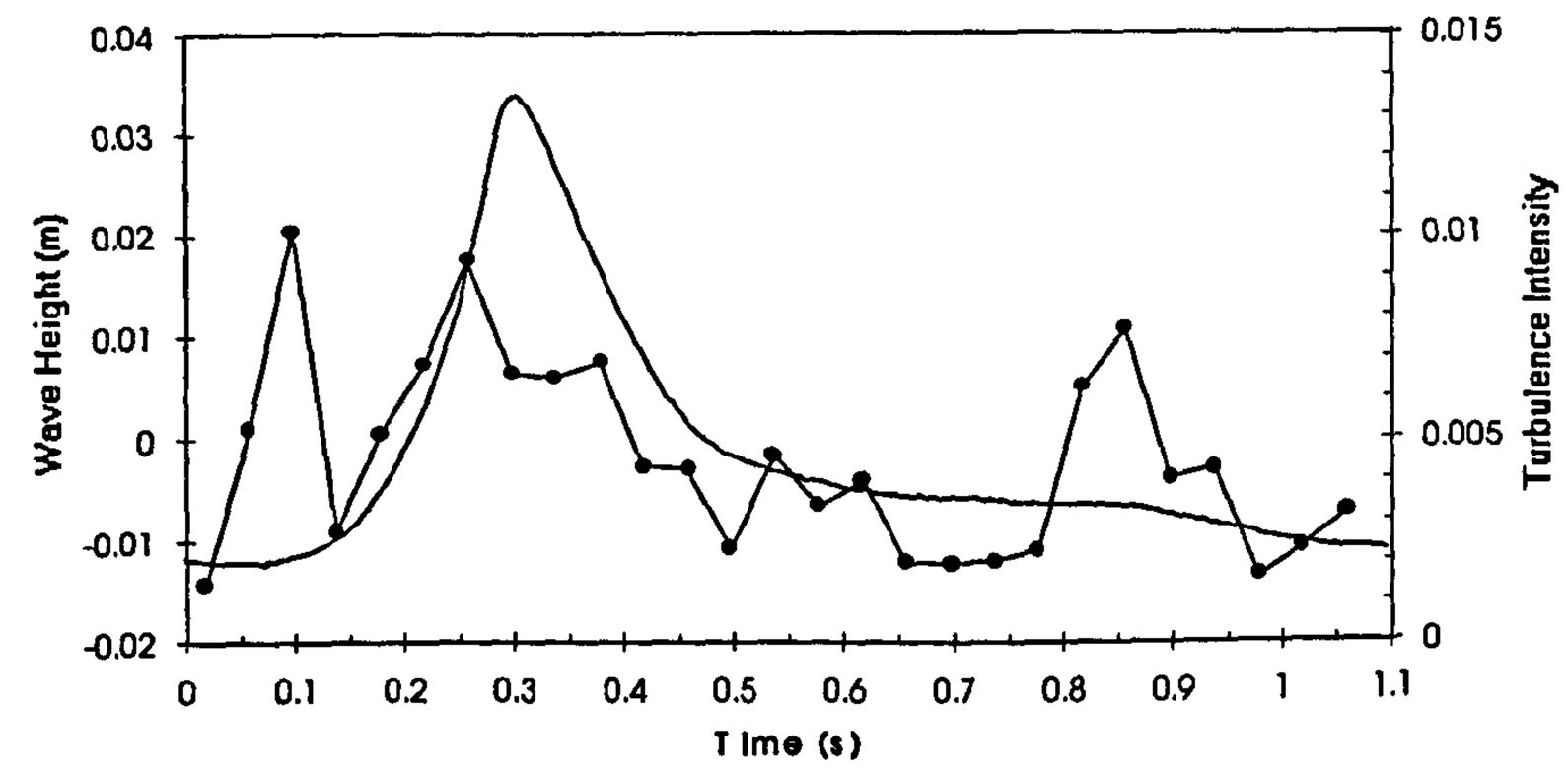

Figure 6.53 Phase-averaged turbulence intensity results for plunging waves under onshore winds at X=-1589mm.
Probe heights: a) 82 b) 62 c) 42mm

a)

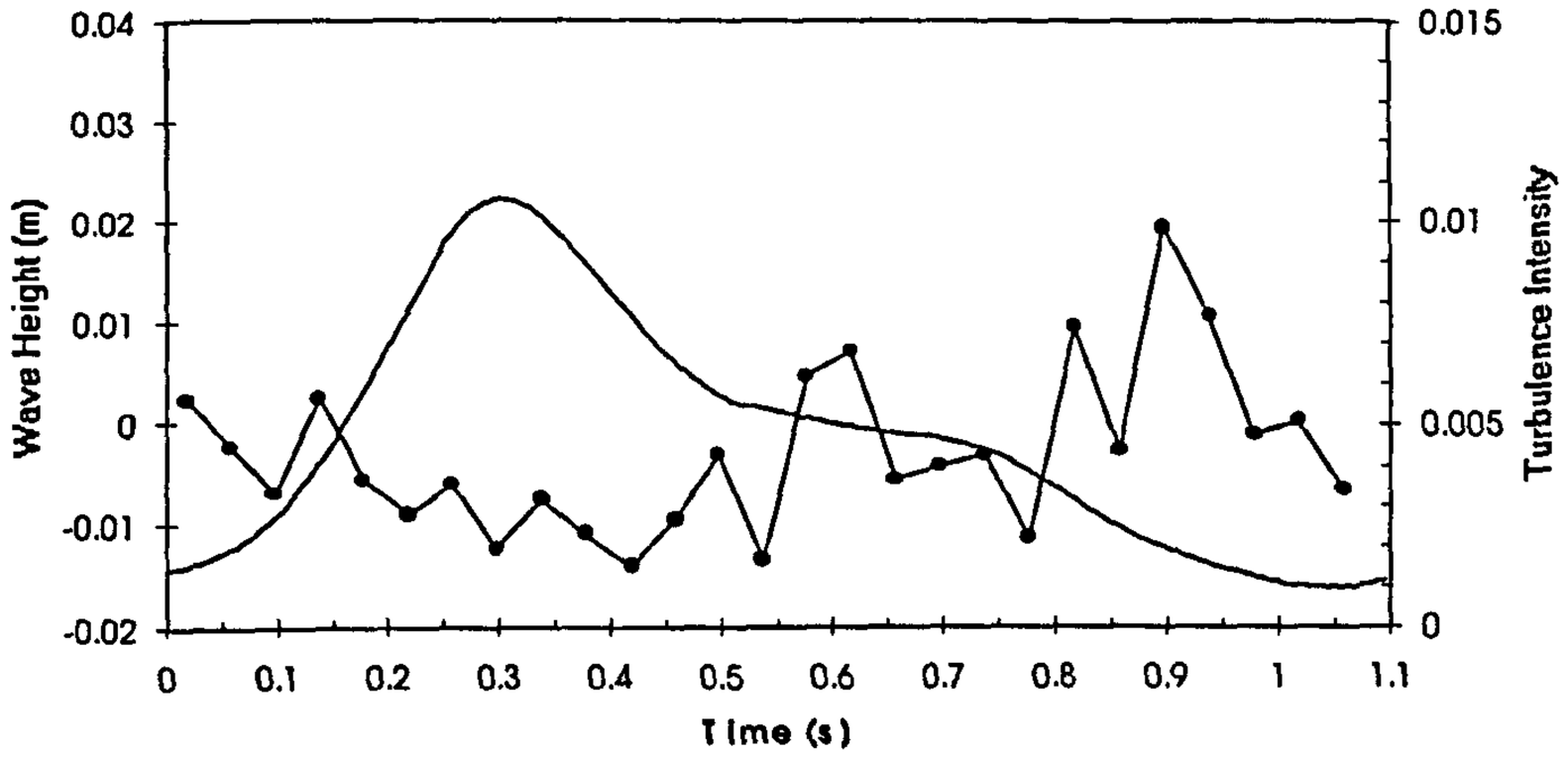

b)

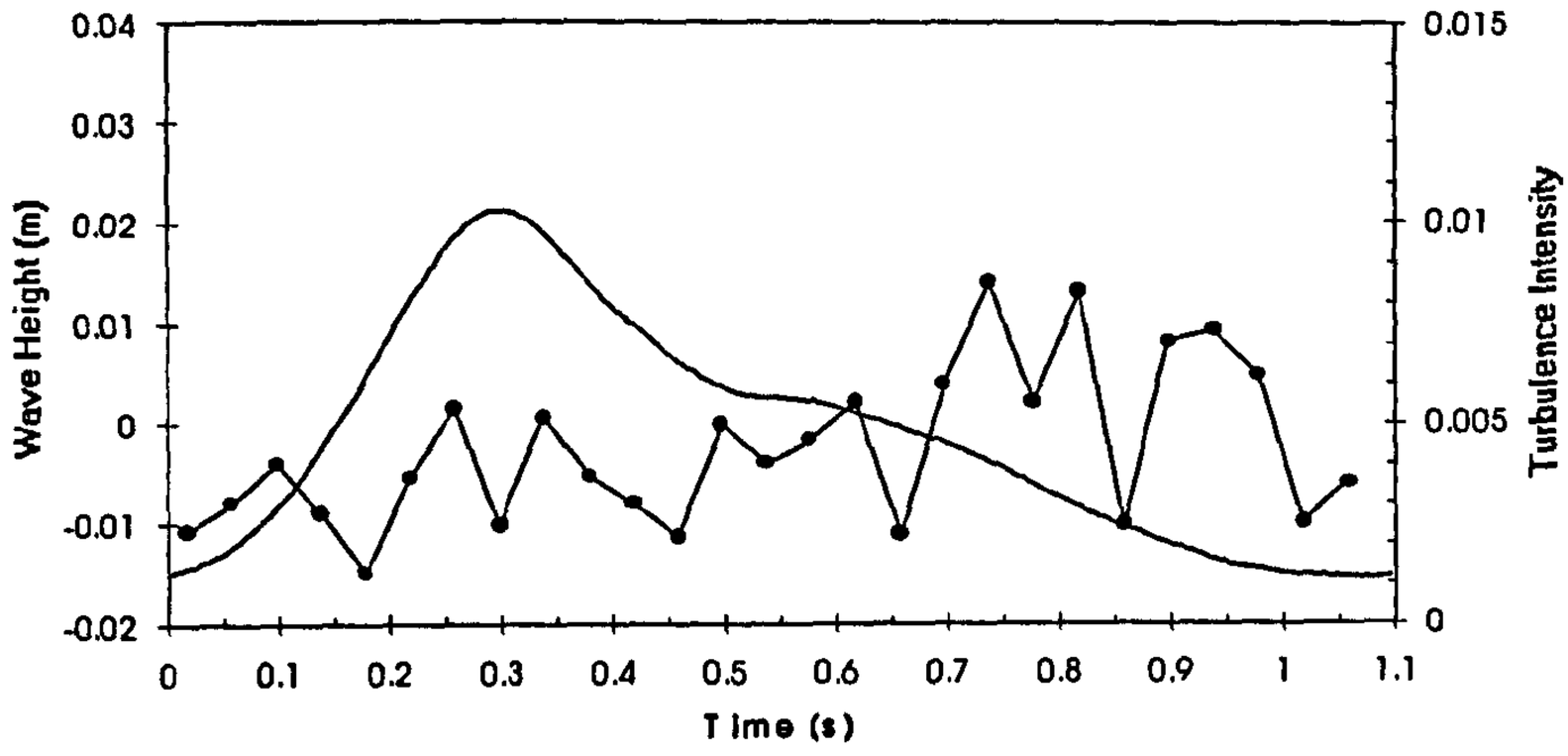

c)

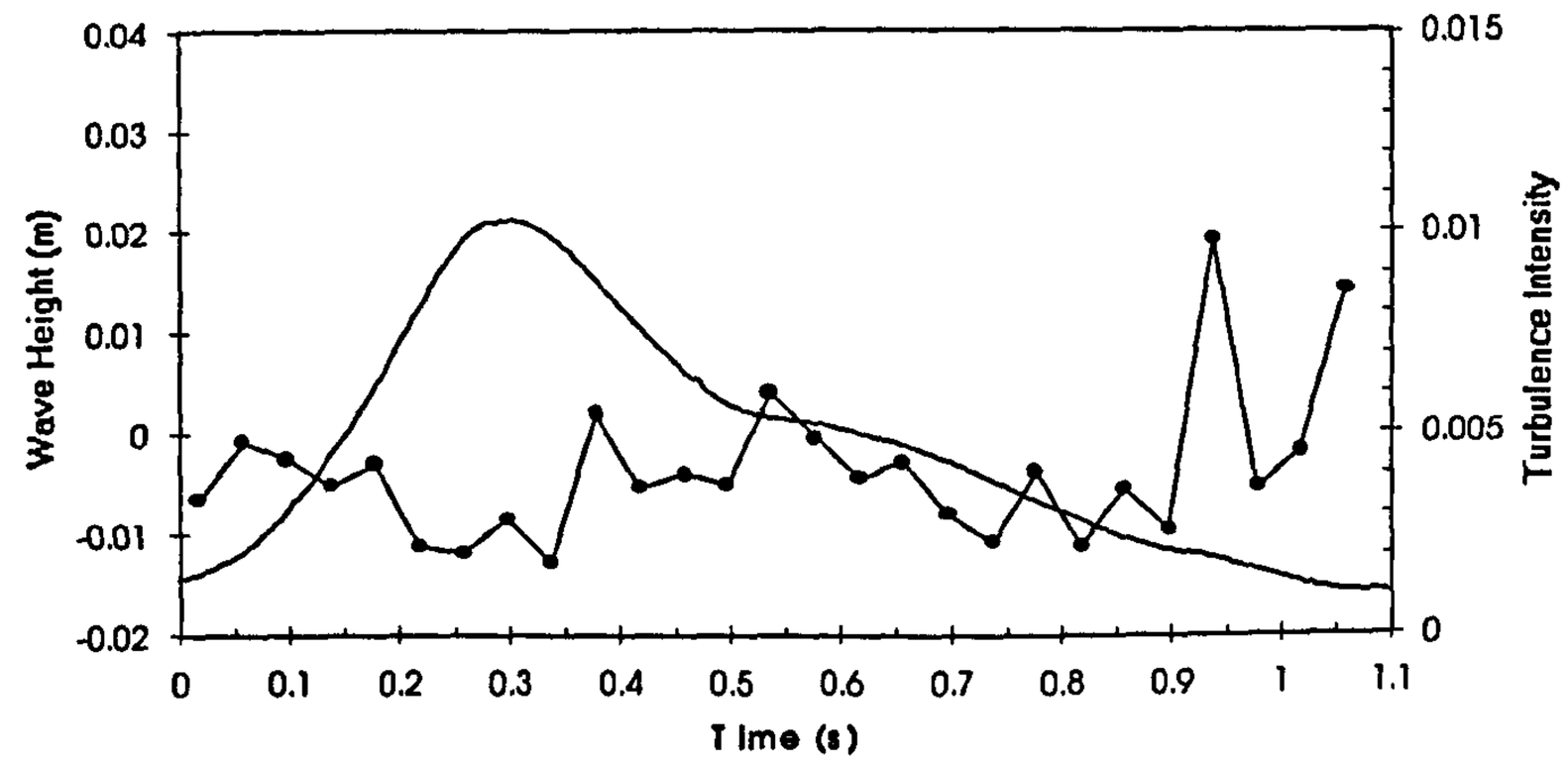

Figure 6.54 Phase-averaged turbulence intensity results for plunging waves under onshore winds at X=-1889mm.
Probe heights: a) 78 b) 58 c) 38mm

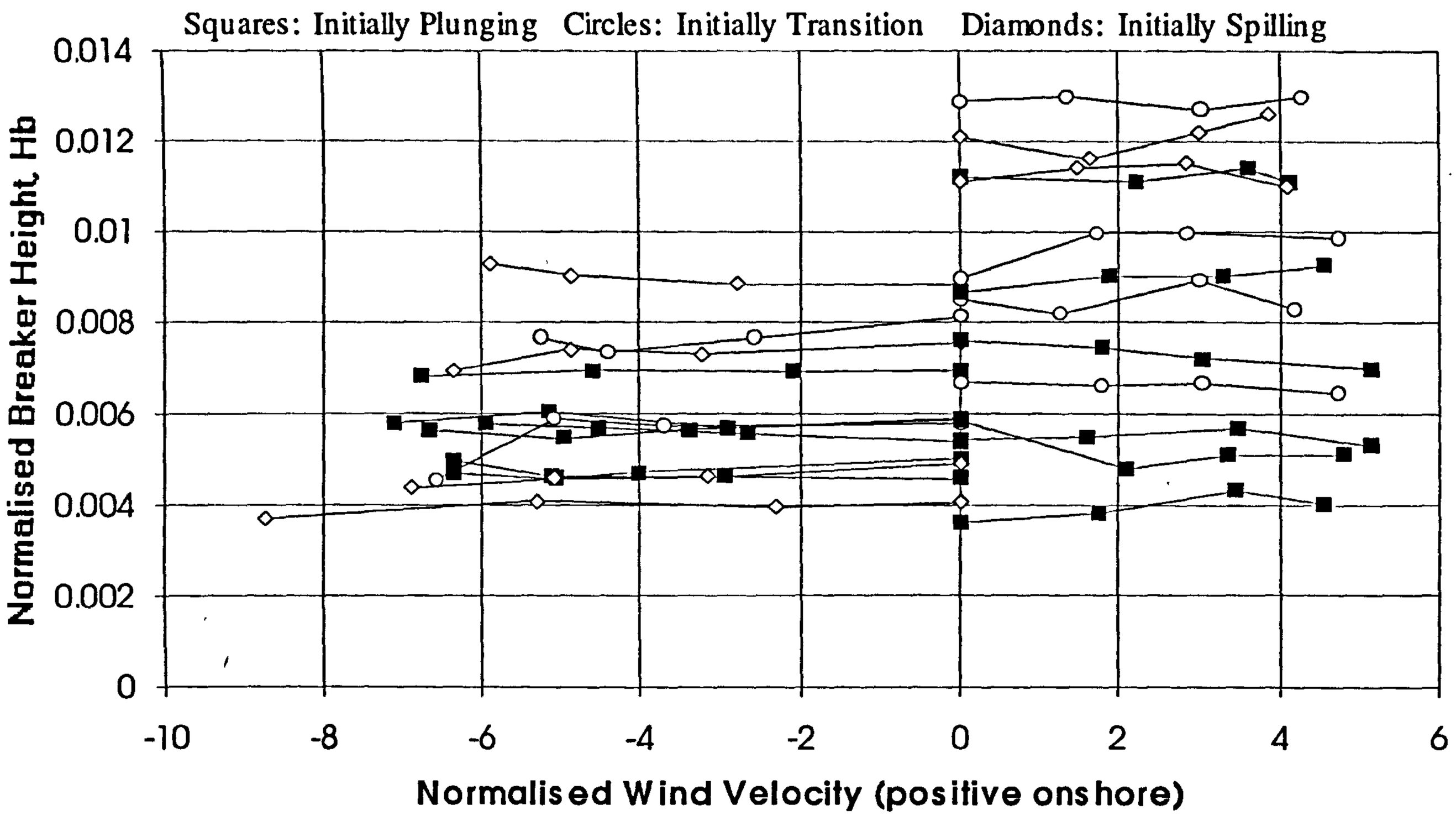

Figure 7.1 Wind effect on normalised breaker height, H_b/gT^2.

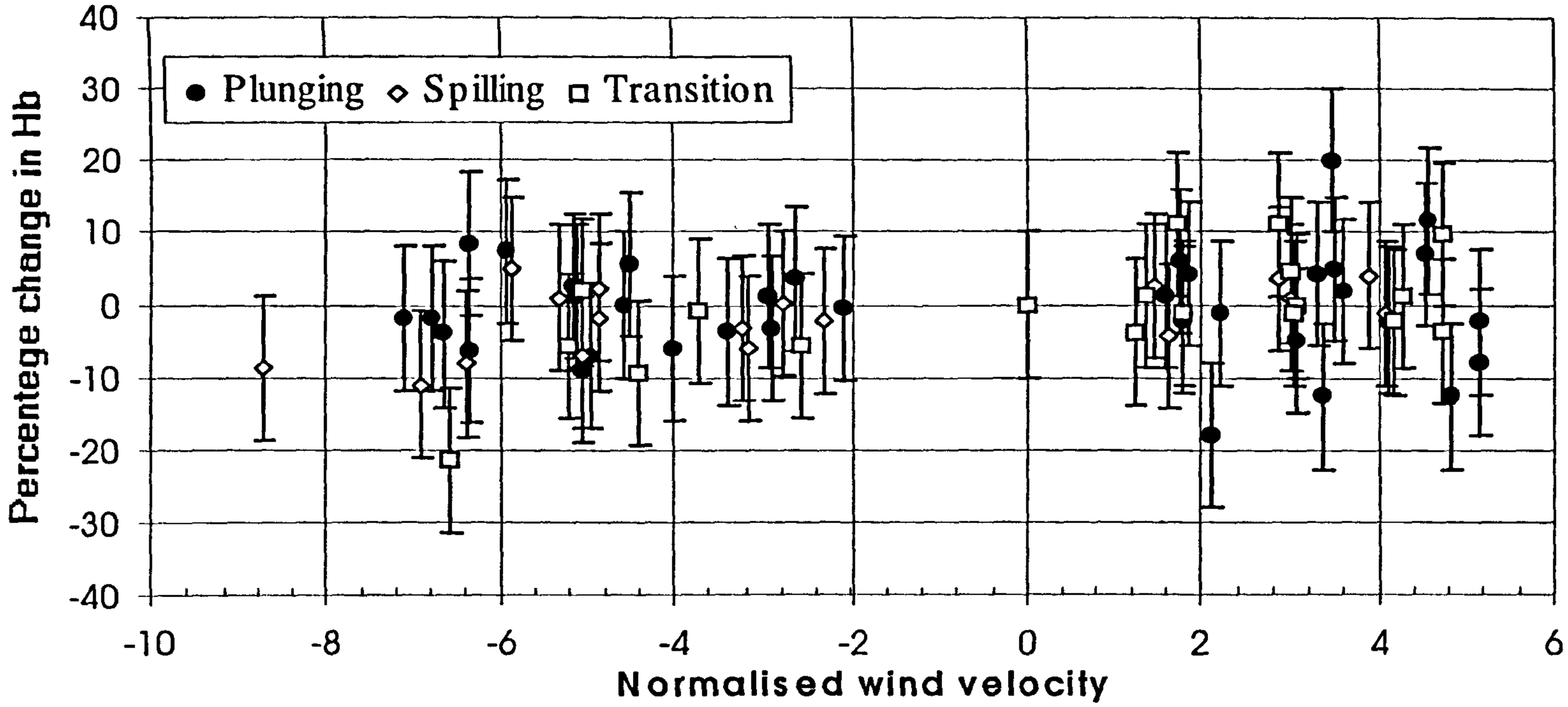

Figure 7.2 Percentage change in breaker height, H_b, against normalised wind velocity.

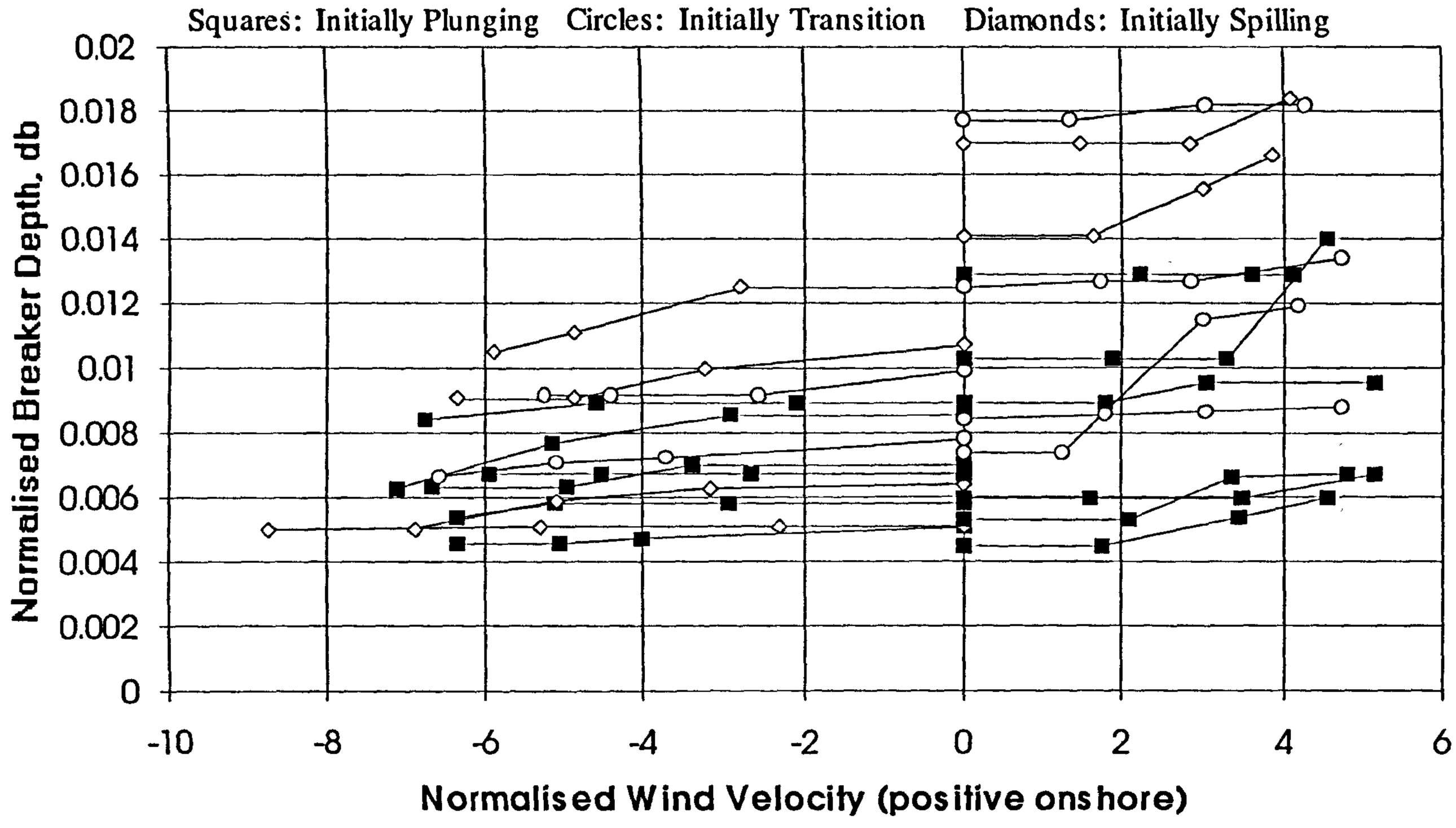

Figure 7.3 Wind effect on normalised breaker depth, d_b/gT^2.

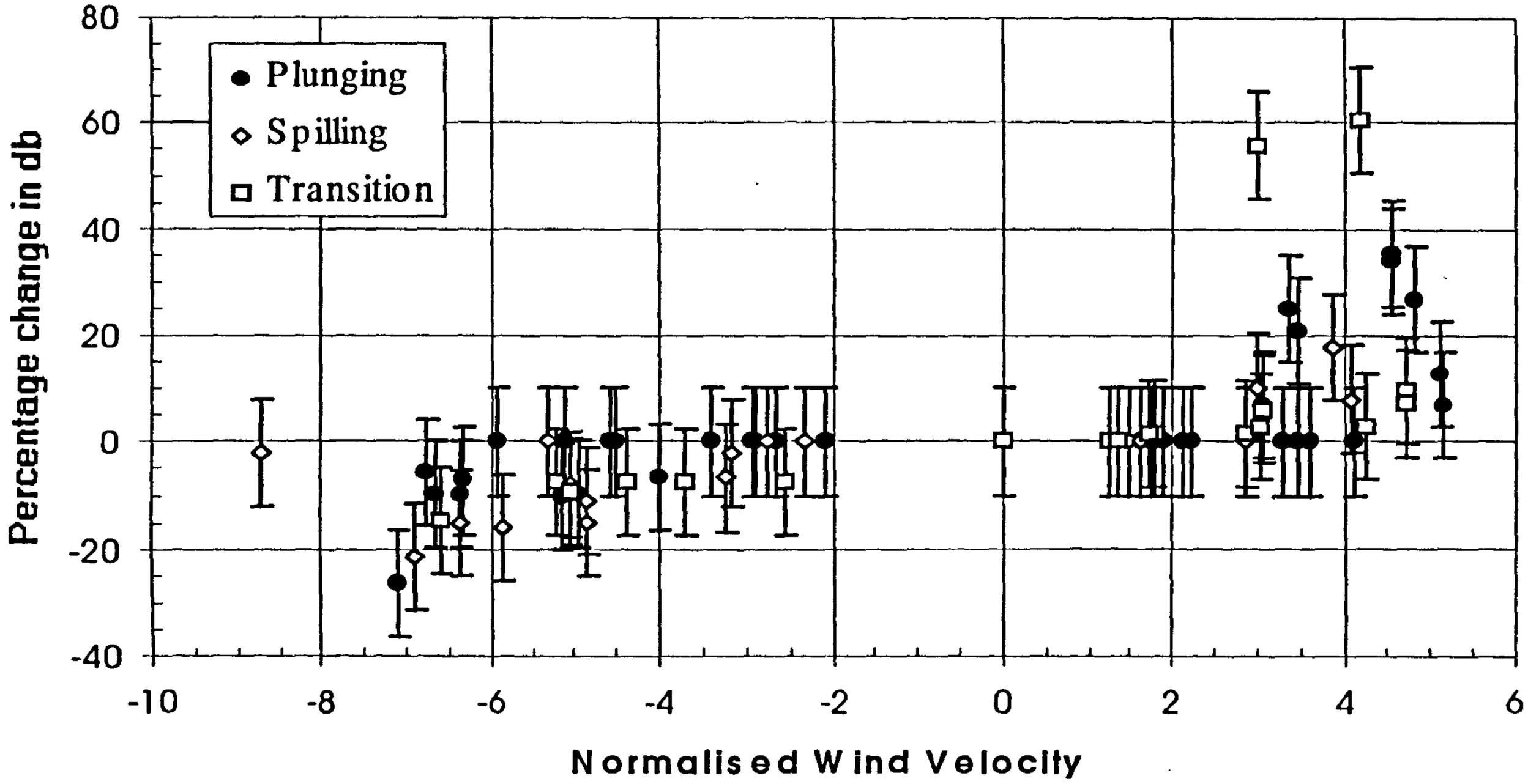

Figure 7.4 Percentage change in breaker depth, d_b, against normalised wind velocity.

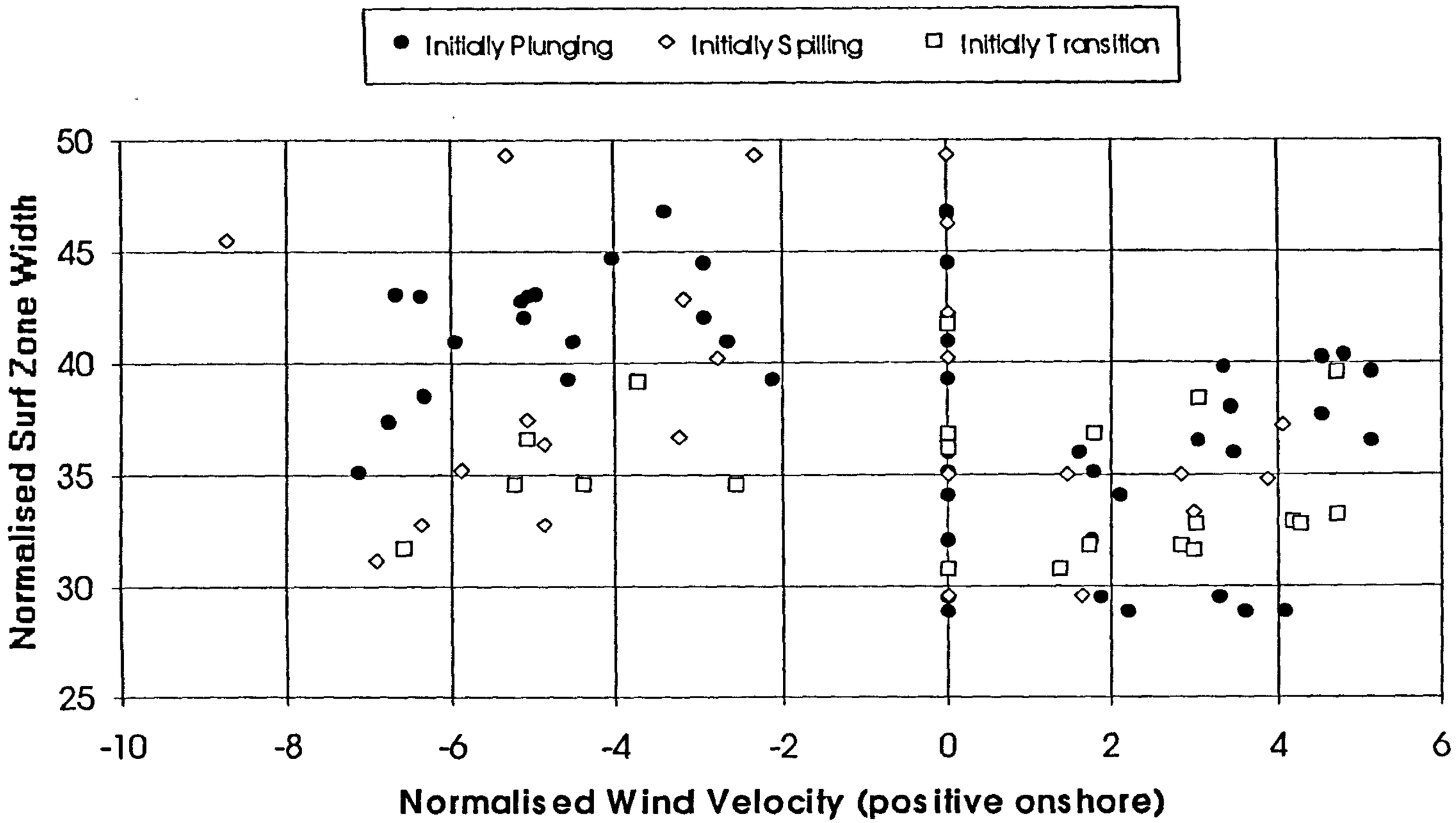

Figure 7.5 Wind effect on normalised surf zone width, X_s/H_p.

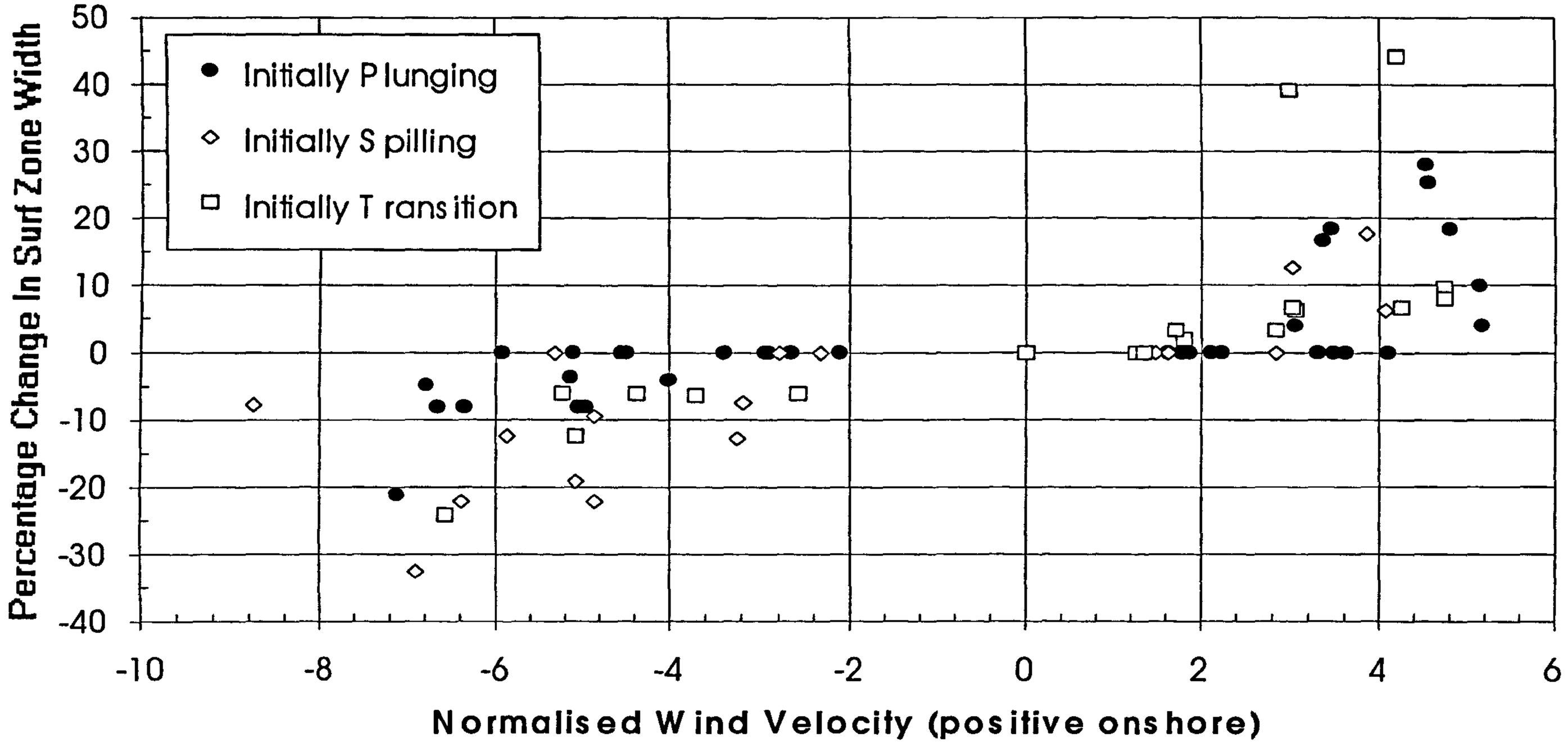

Figure 7.6 Percentage change in surf zone width due to wind influence.

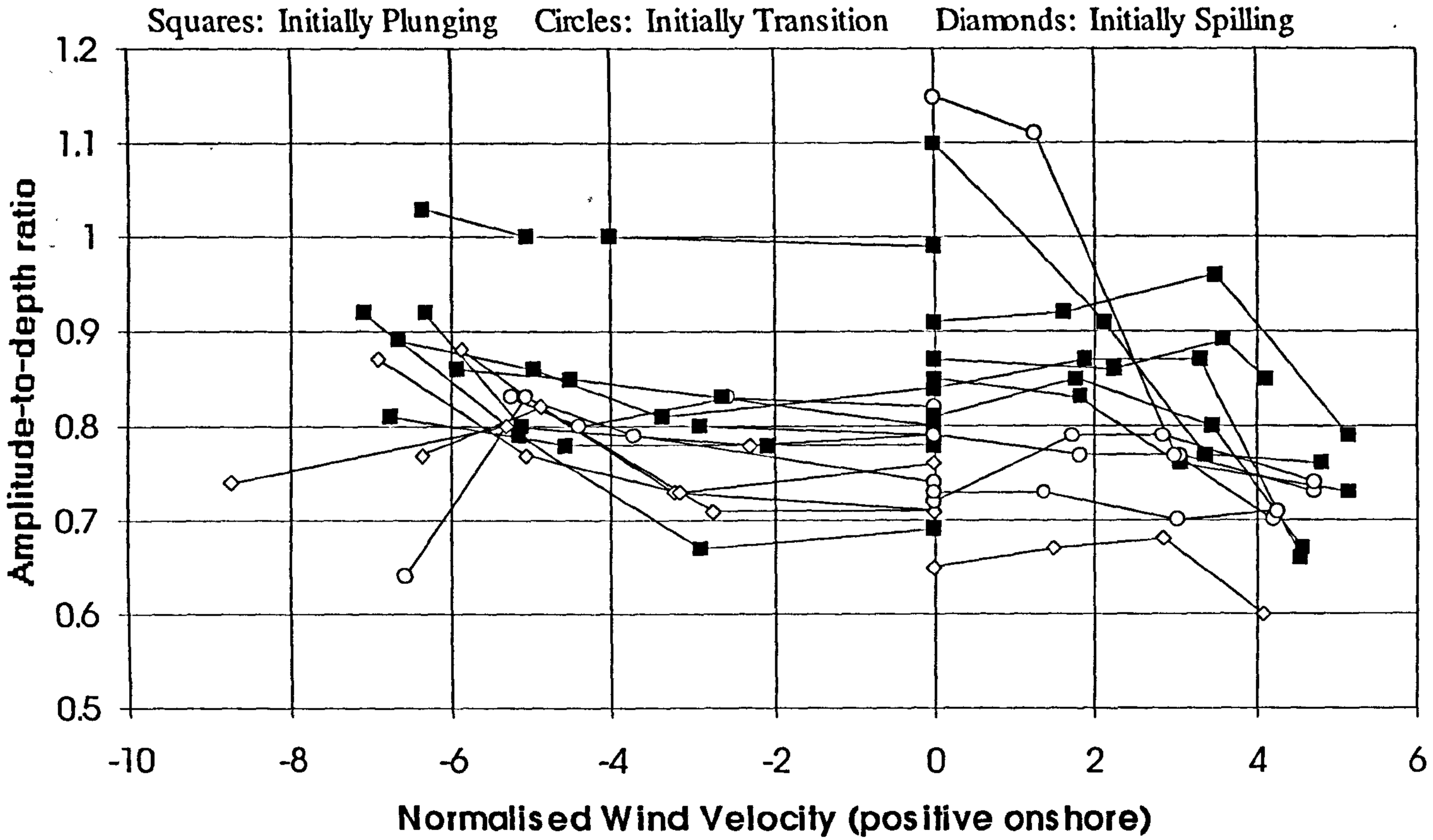

Figure 7.7 Wind effect on amplitude-to-depth ratio, H_b/d_b.

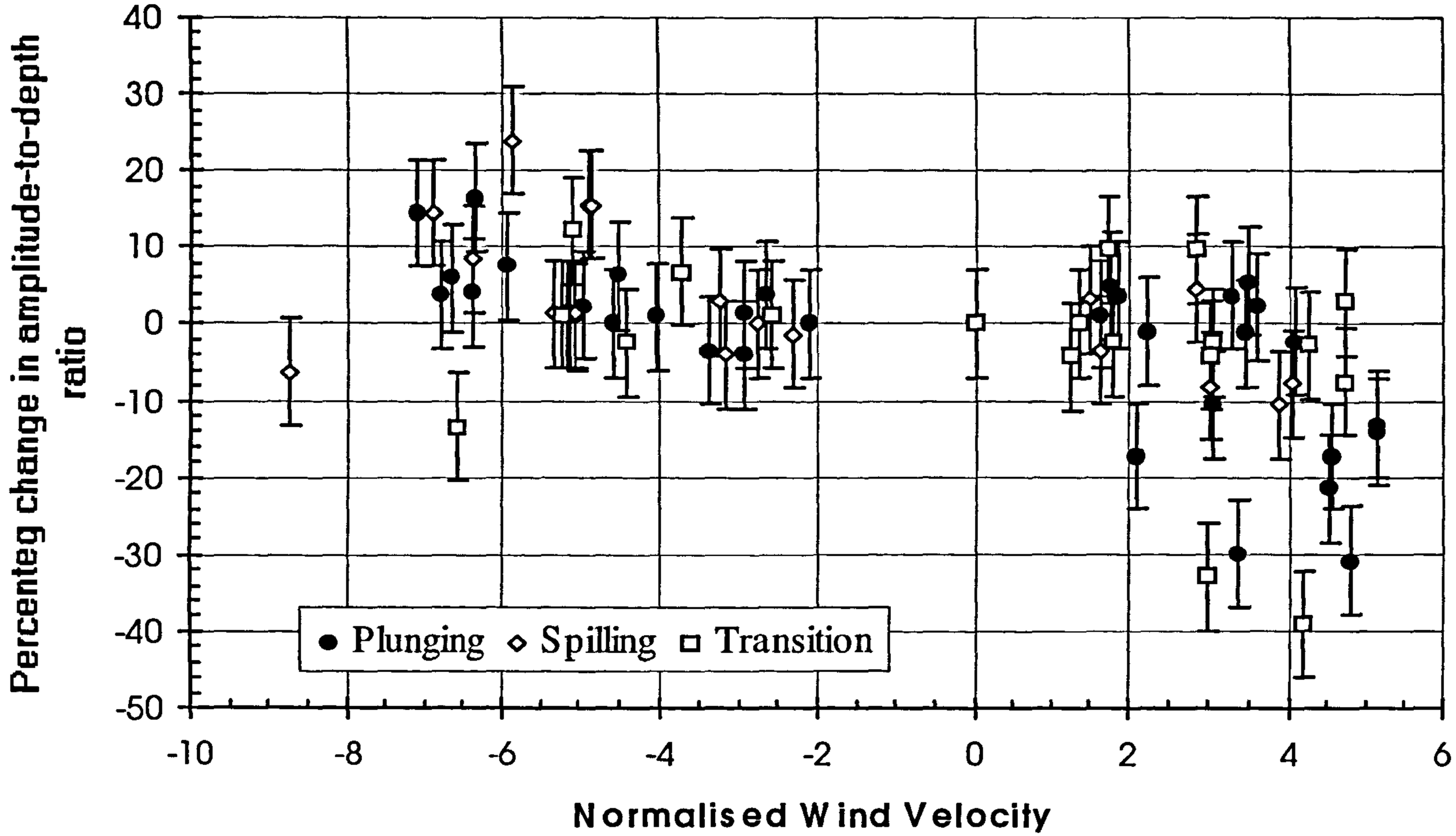

Figure 7.8 Percentage change in amplitude-to-depth ratio, H_b/d_b, against normalised wind velocity

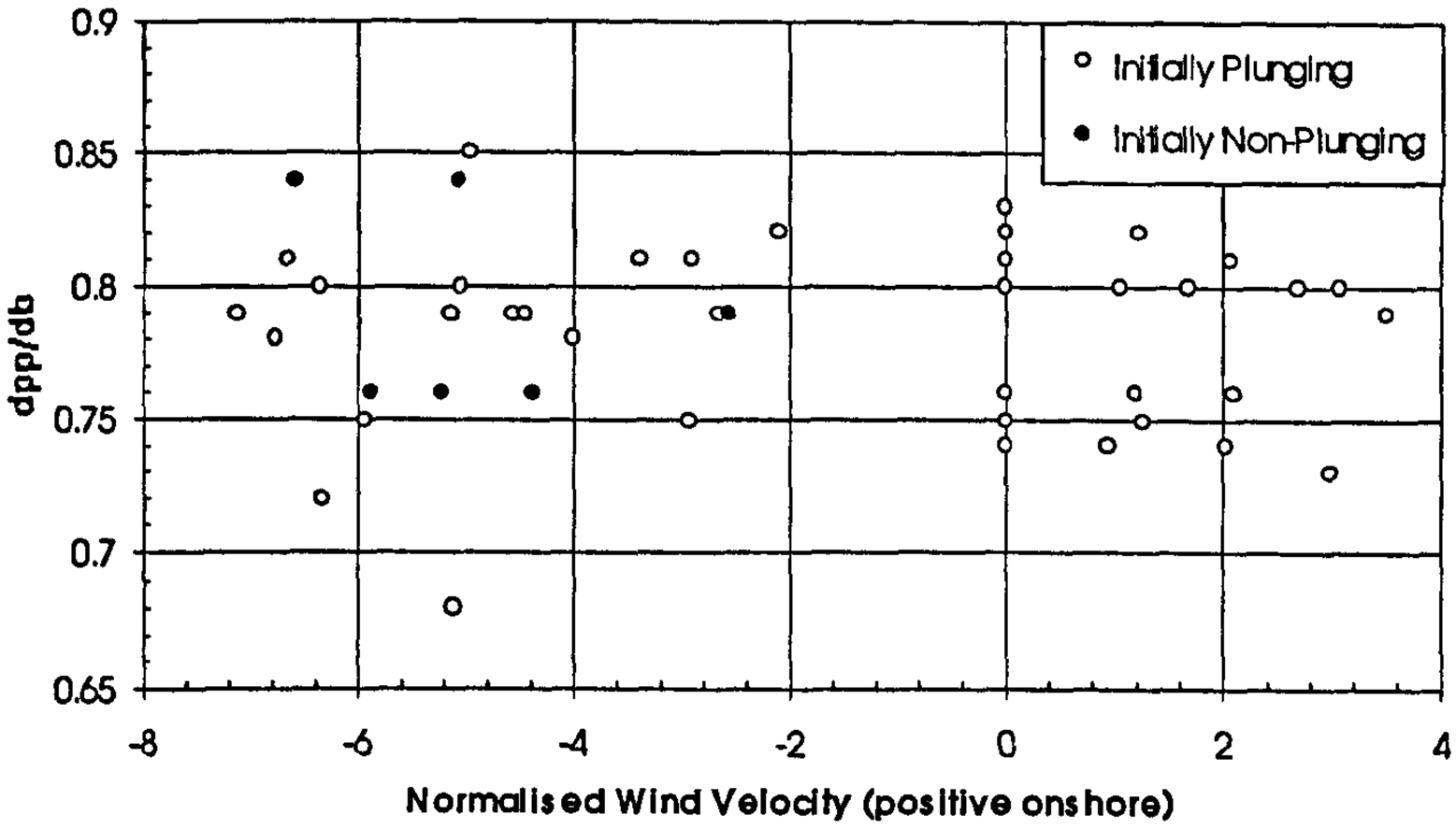

Figure 7.9 Wind effect on normalised plunge point depth, d_{pp}/d_b.

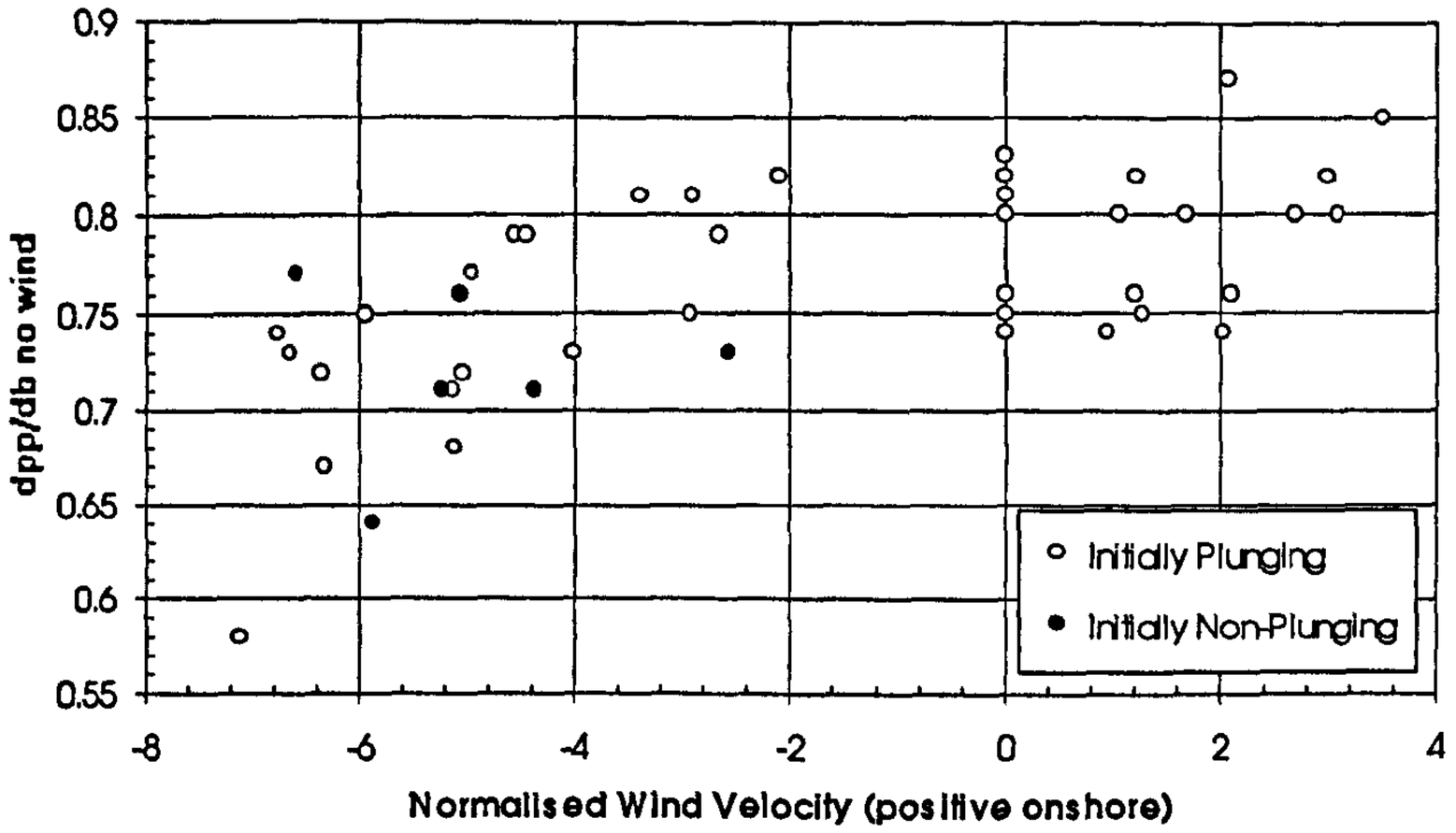

Figure 7.10 Wind effect on plunge point depth normalised by initial (no wind) breaker depth, (d_{pp}/d_b no wind).

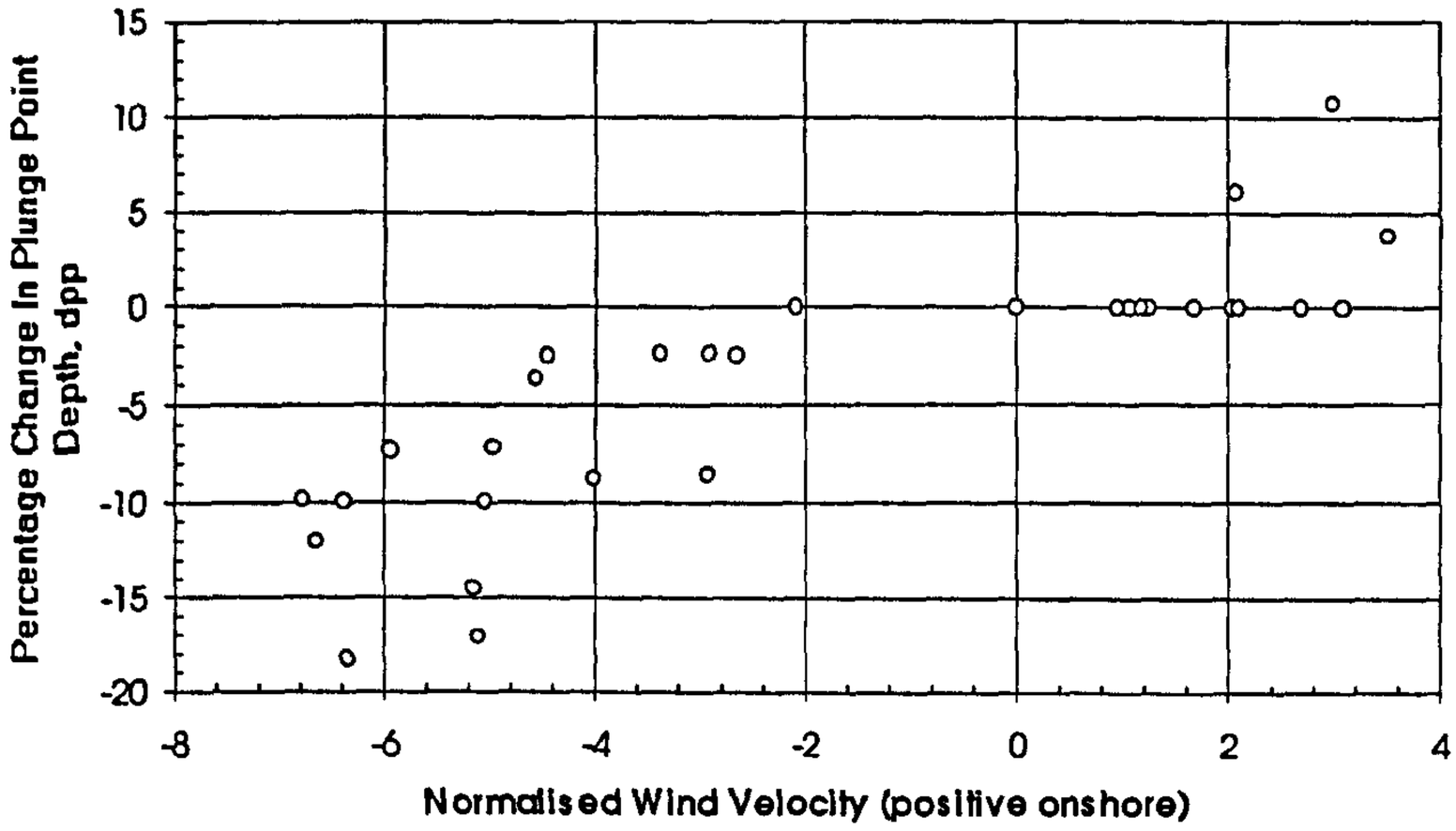

Figure 7.11 Percentage change in plunge point depth, d_{pp}. Only initially plunging waves considered.

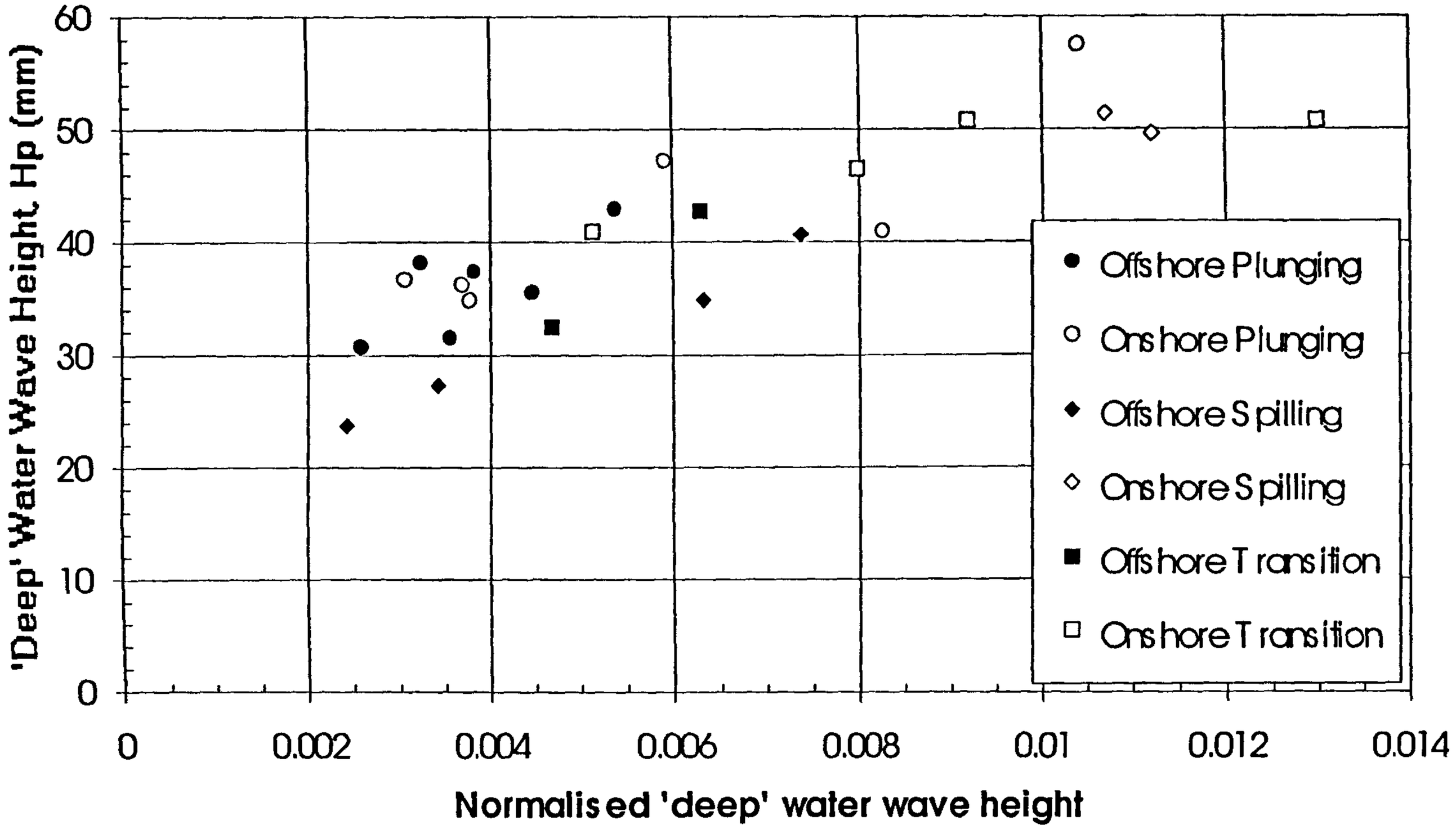

Figure 7.12 Distribution of breaker types (no wind) by normalised 'deep' water water wave height, H_p/gT^2.

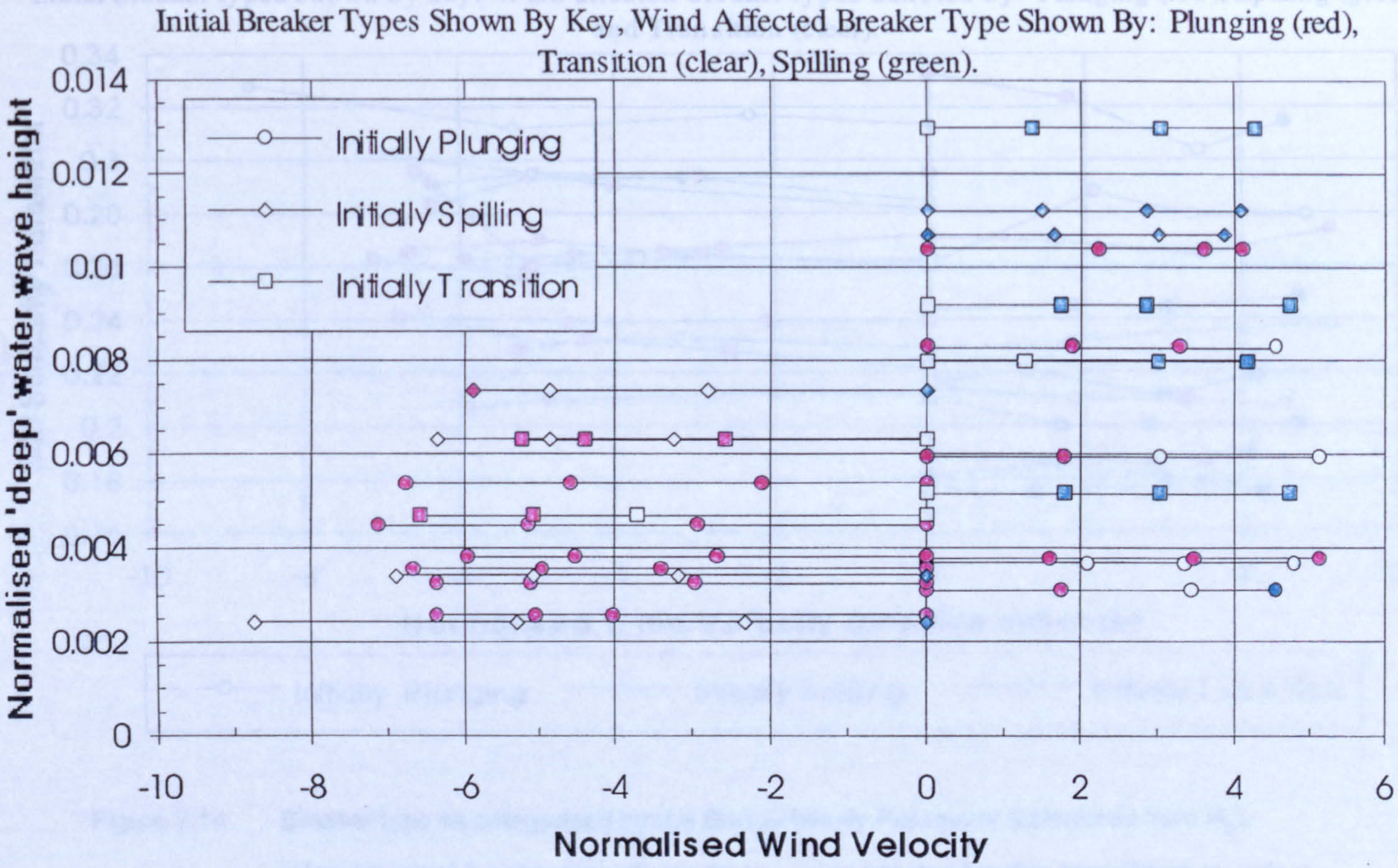

Figure 7.13 Wind effect on breaker type, categorized by normalised 'deep' water wave height, H_p/gT^2.

Initial Breaker types shown by key. Wind affected breaker types denoted by: Plunging (red), Spilling (green), and Transition (clear).

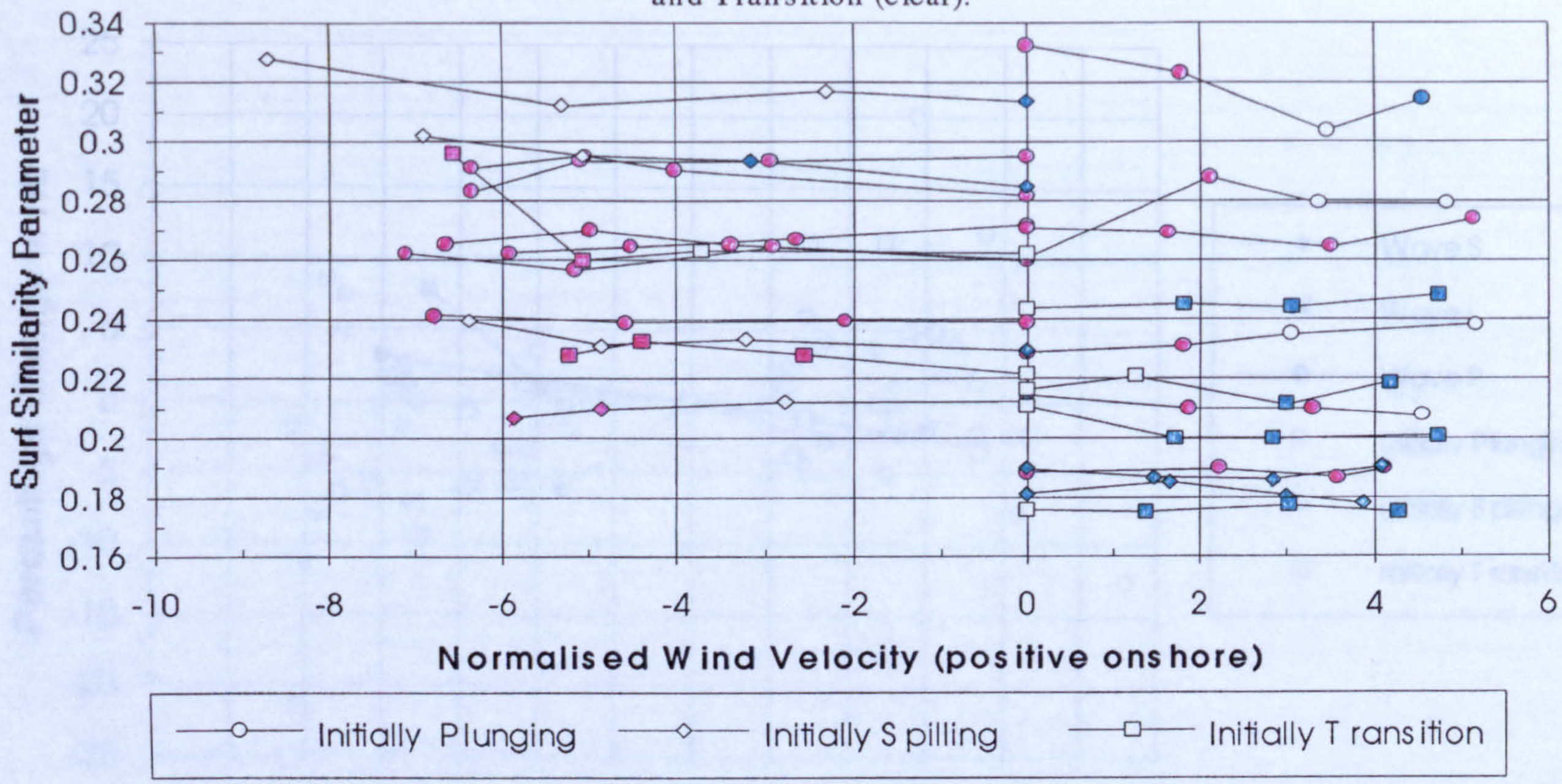

Figure 7.14 Breaker type as categorized by the Surf Similarity Parameter (calculated from H_b). Initial (no wind) breaker type shown by key, wind affected breaker type shown by colour.

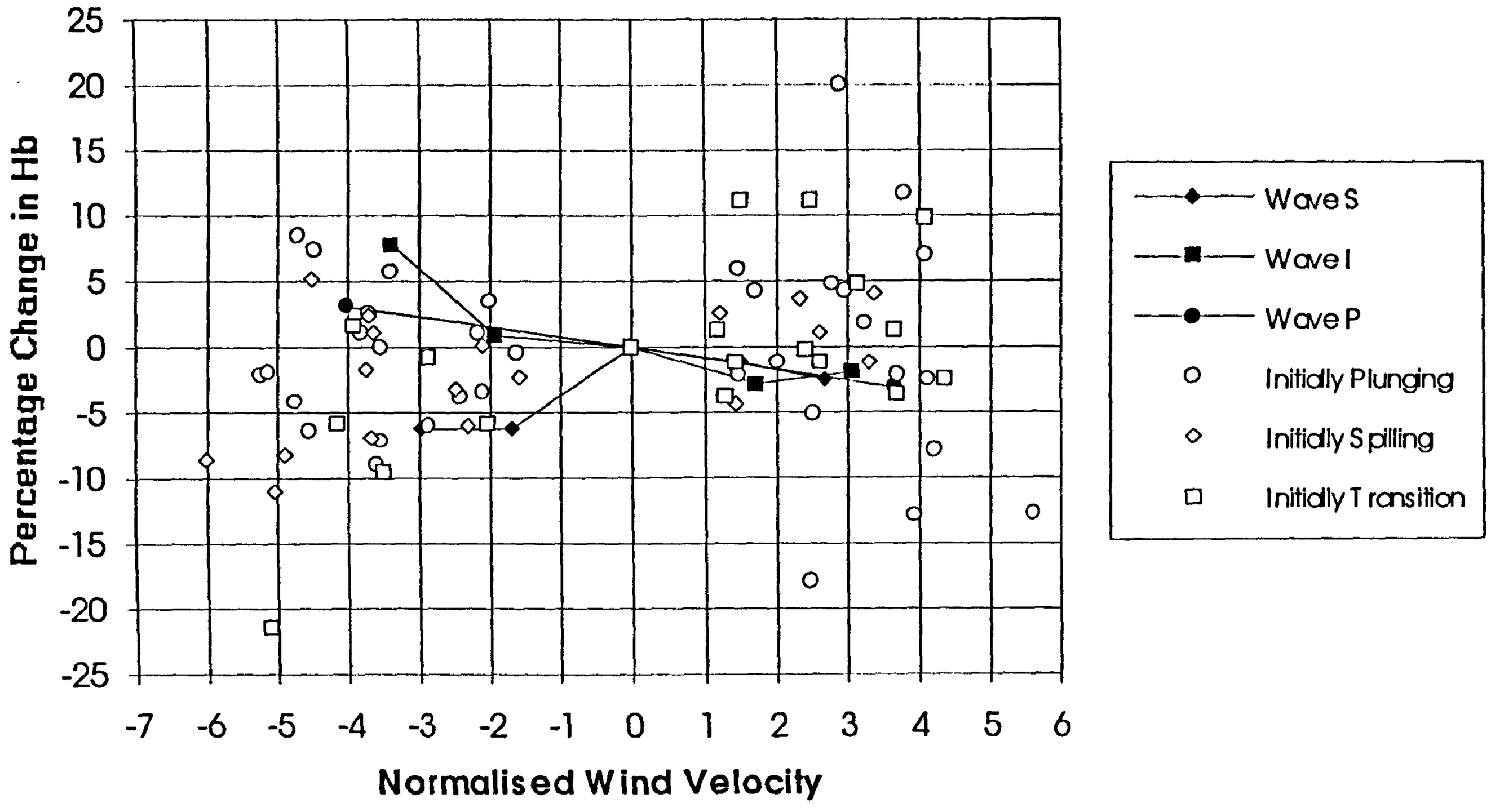

Figure 7.15 Percentage change in breaker height, H_b, comparison with Douglass (1989).

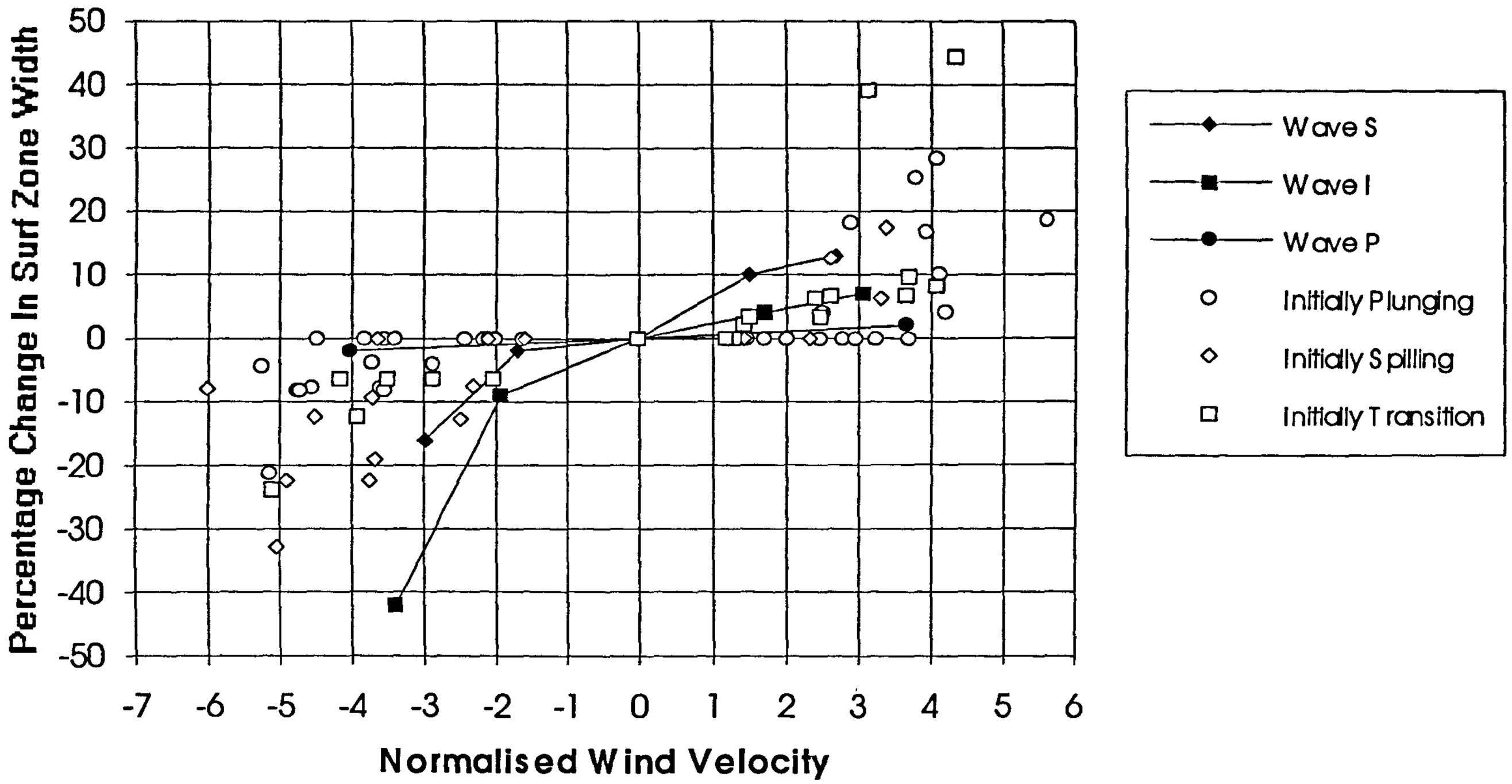

Figure 7.16 Percentage change in surf zone width, X_s, comparison with Douglass (1989).

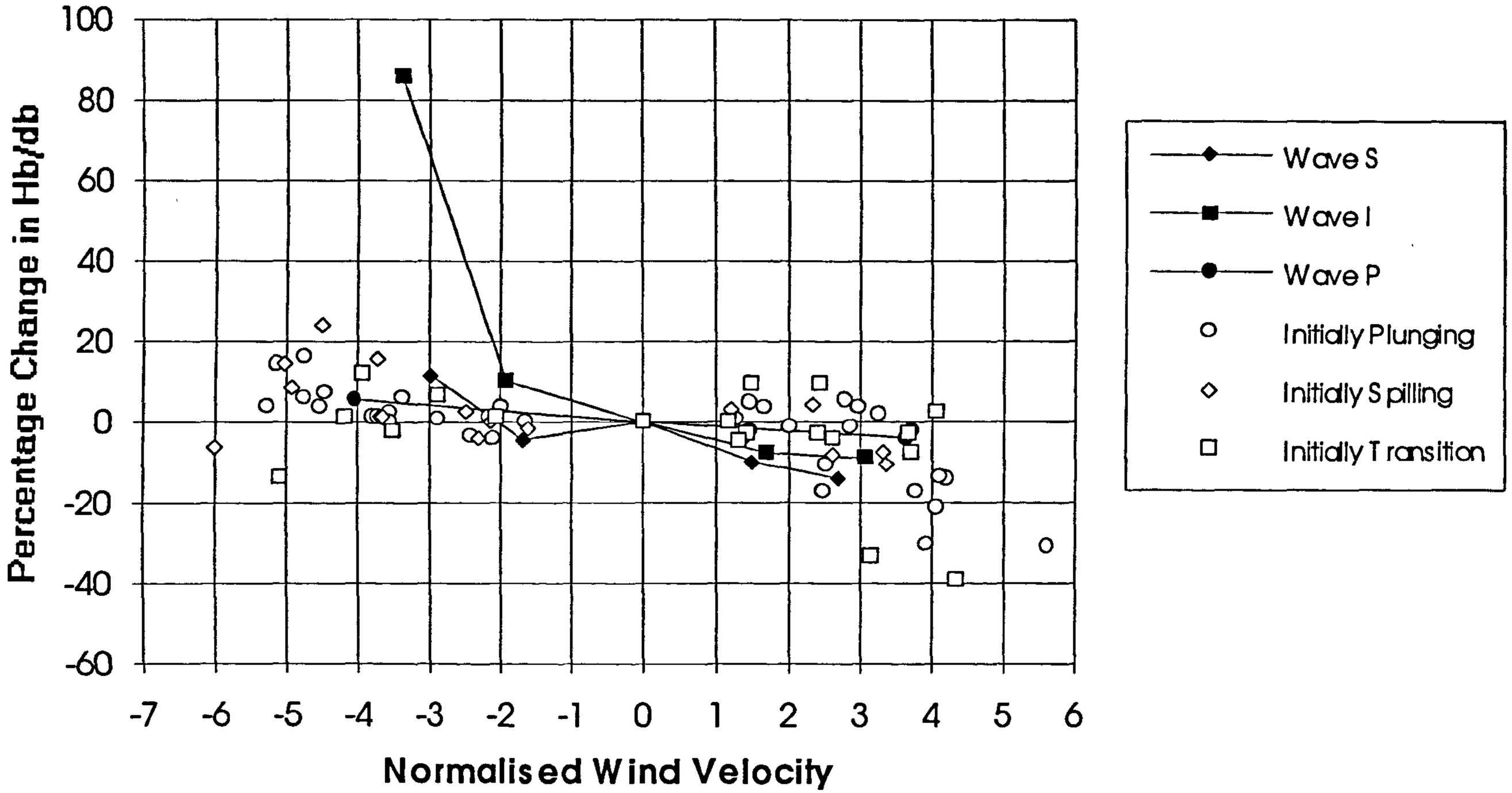

Figure 7.17 Percentage change in the amplitude-to-depth ratio, comparison with Douglass (1989).

a)

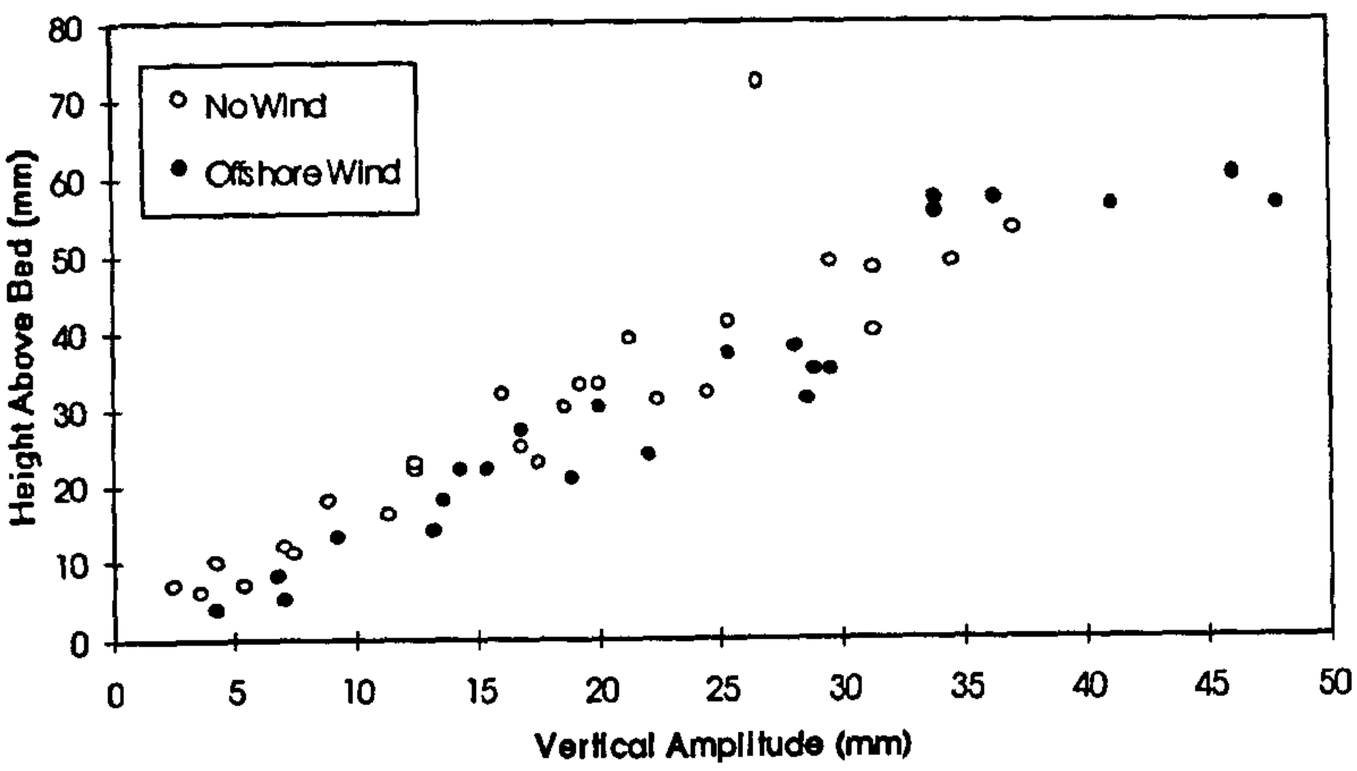

b)

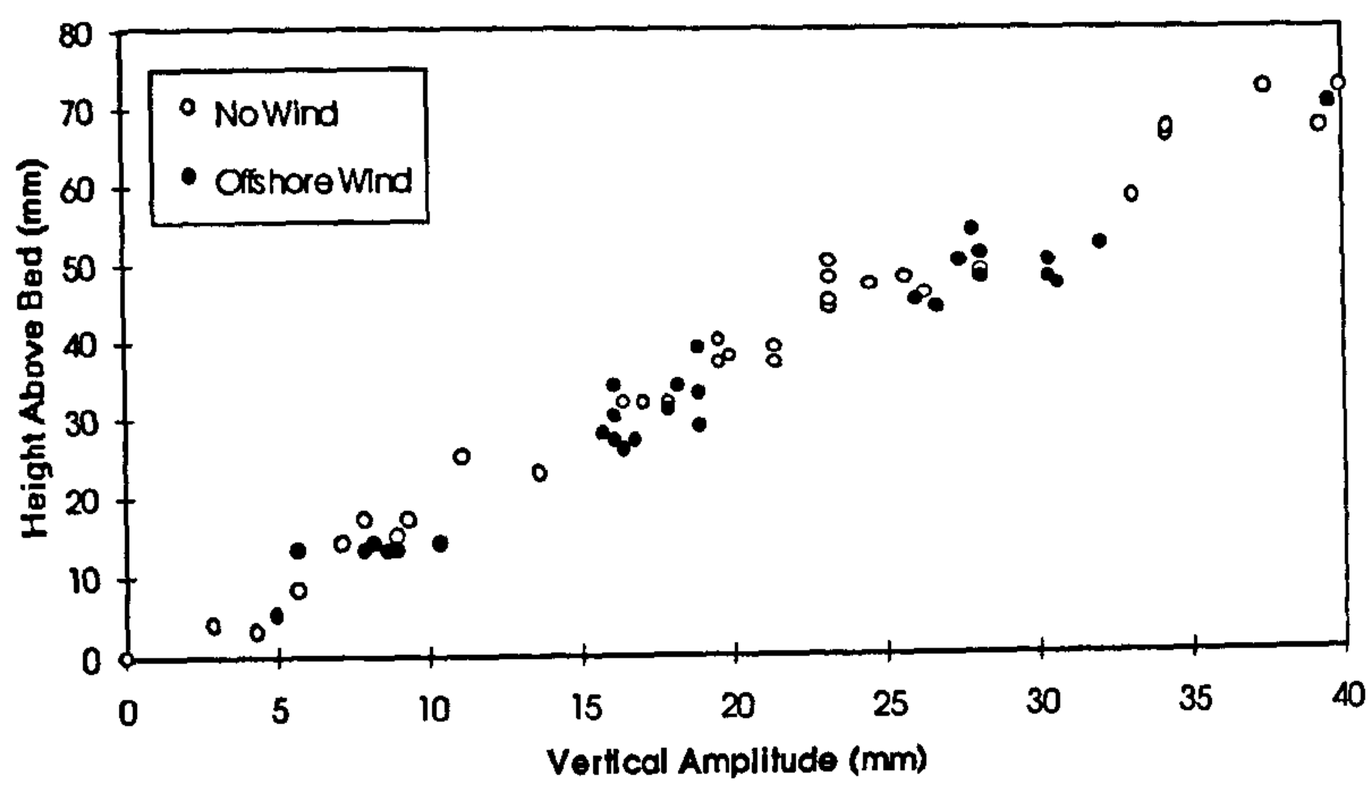

c)

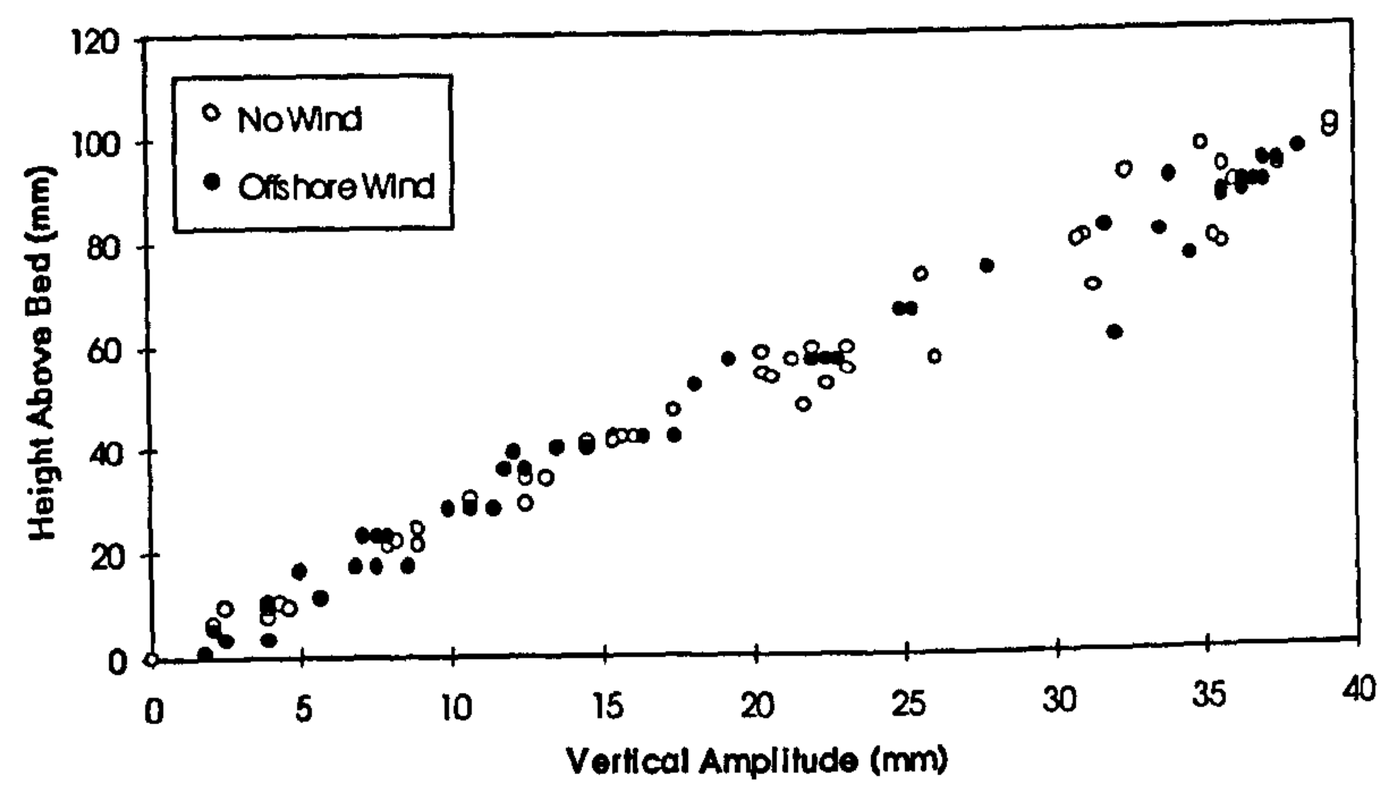

Figure 8.1 Vertical amplitude of particle motion for plunging waves under offshore winds: a) X=-1525mm b) X=-1755mm c) X=-2000mm

a)

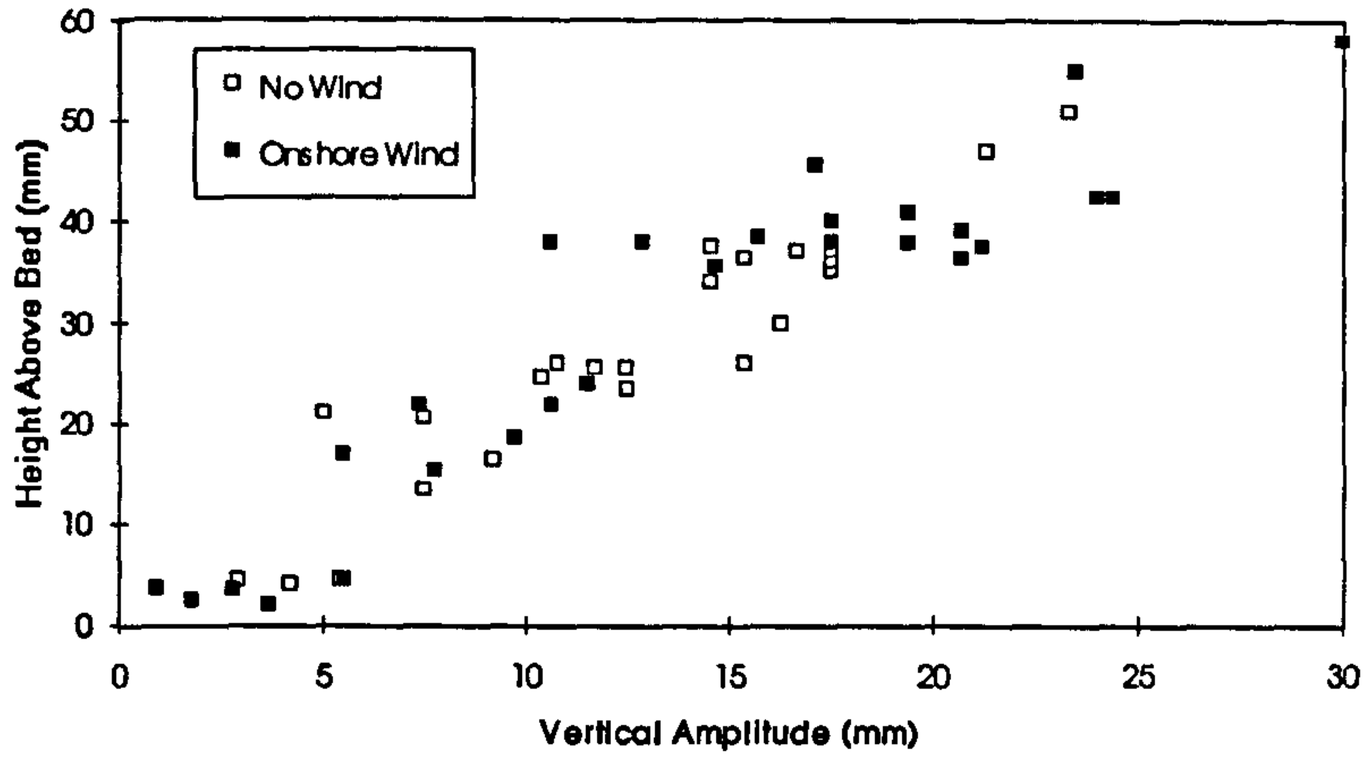

b)

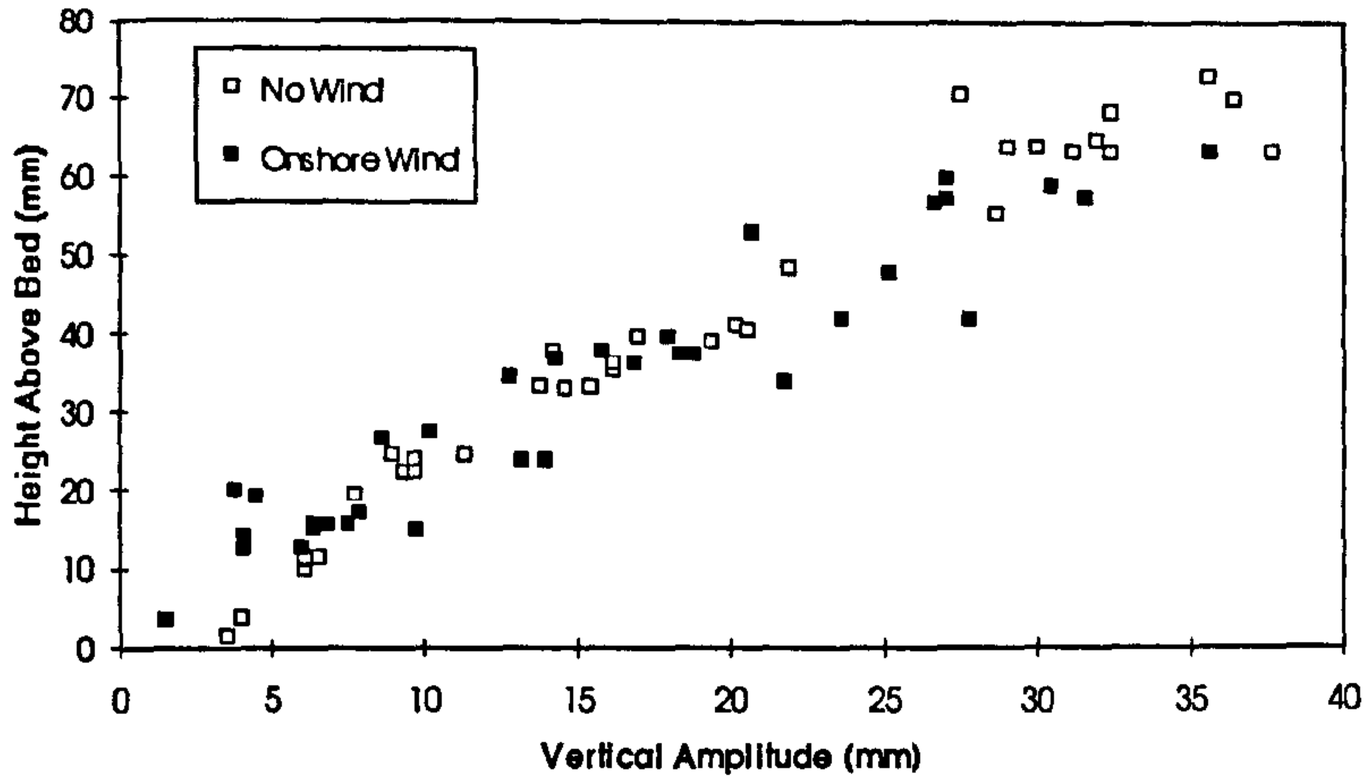

c)

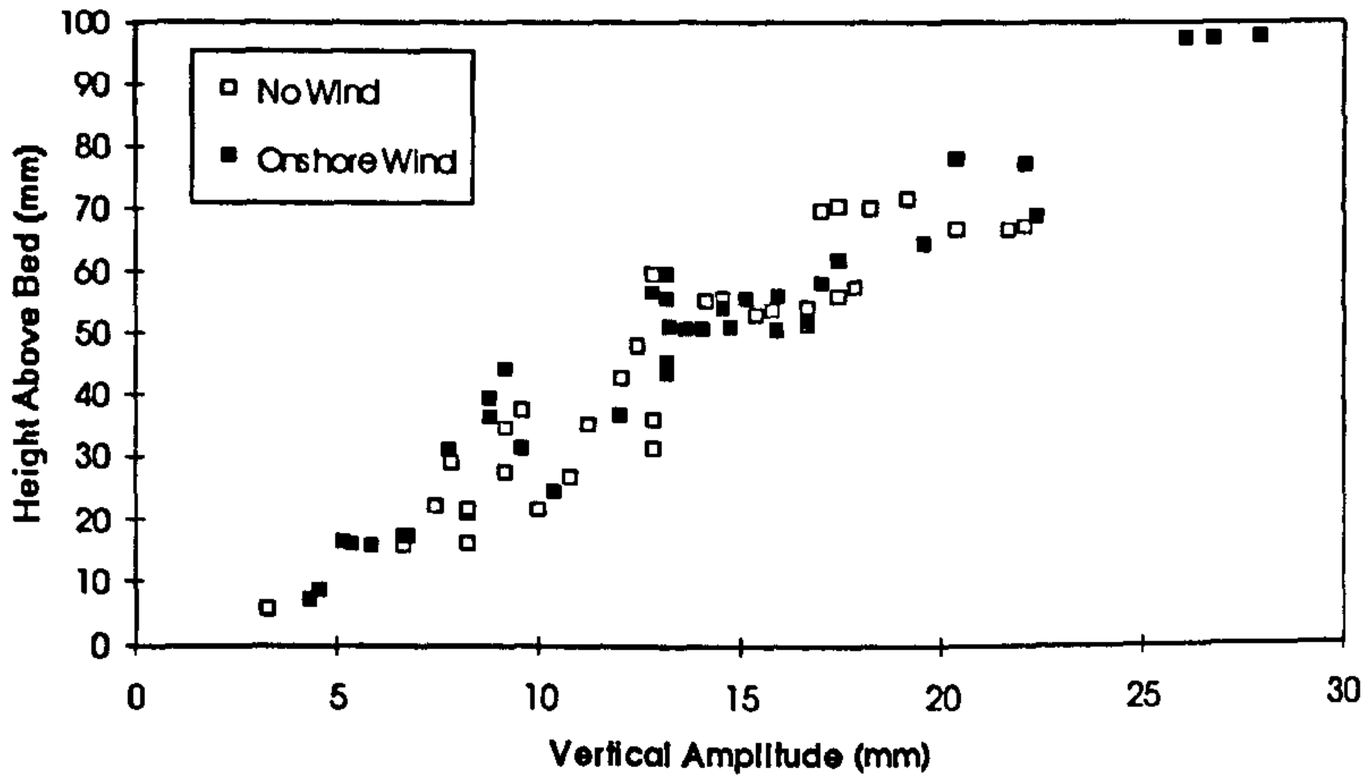

Figure 8.2 Vertical amplitude of particle motion for plunging waves under onshore winds: a) X=-1525mm b) X=-1755mm c) X=-2000mm

a)

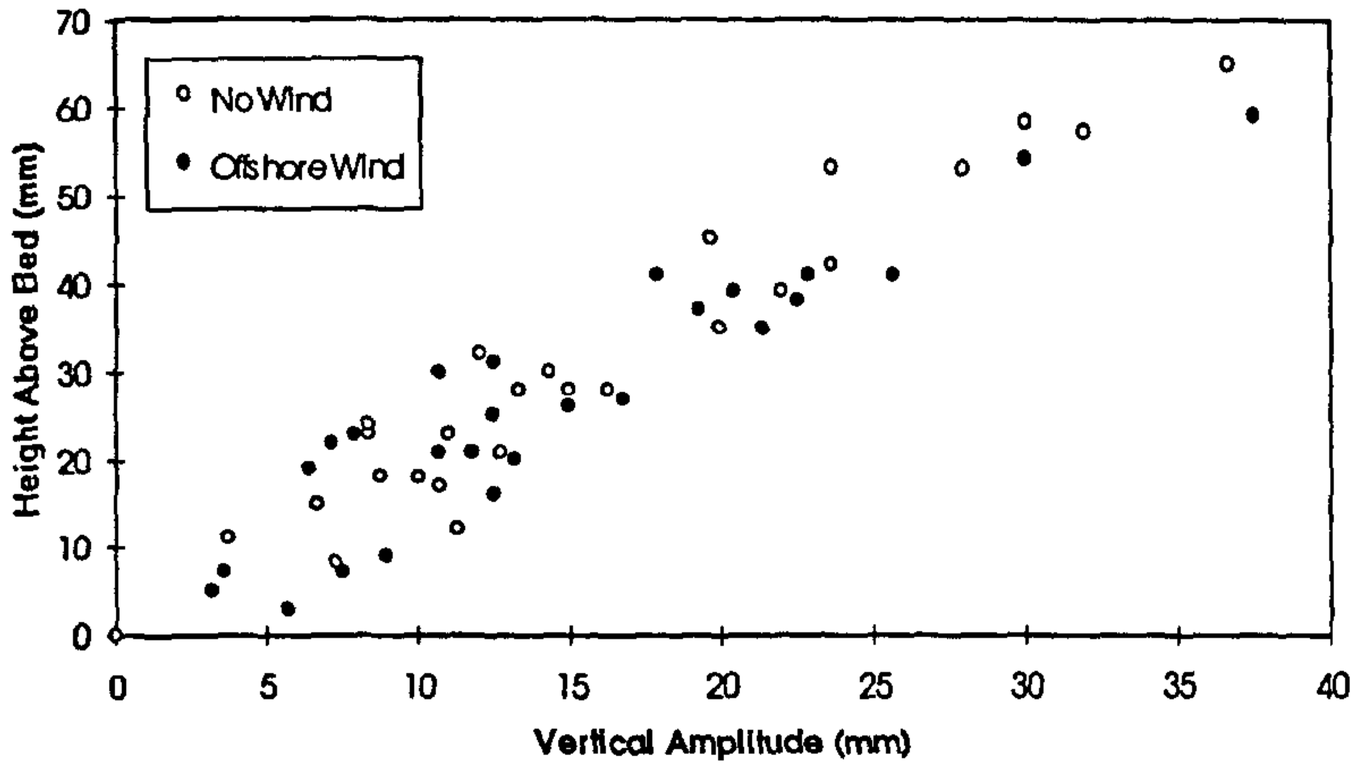

b)

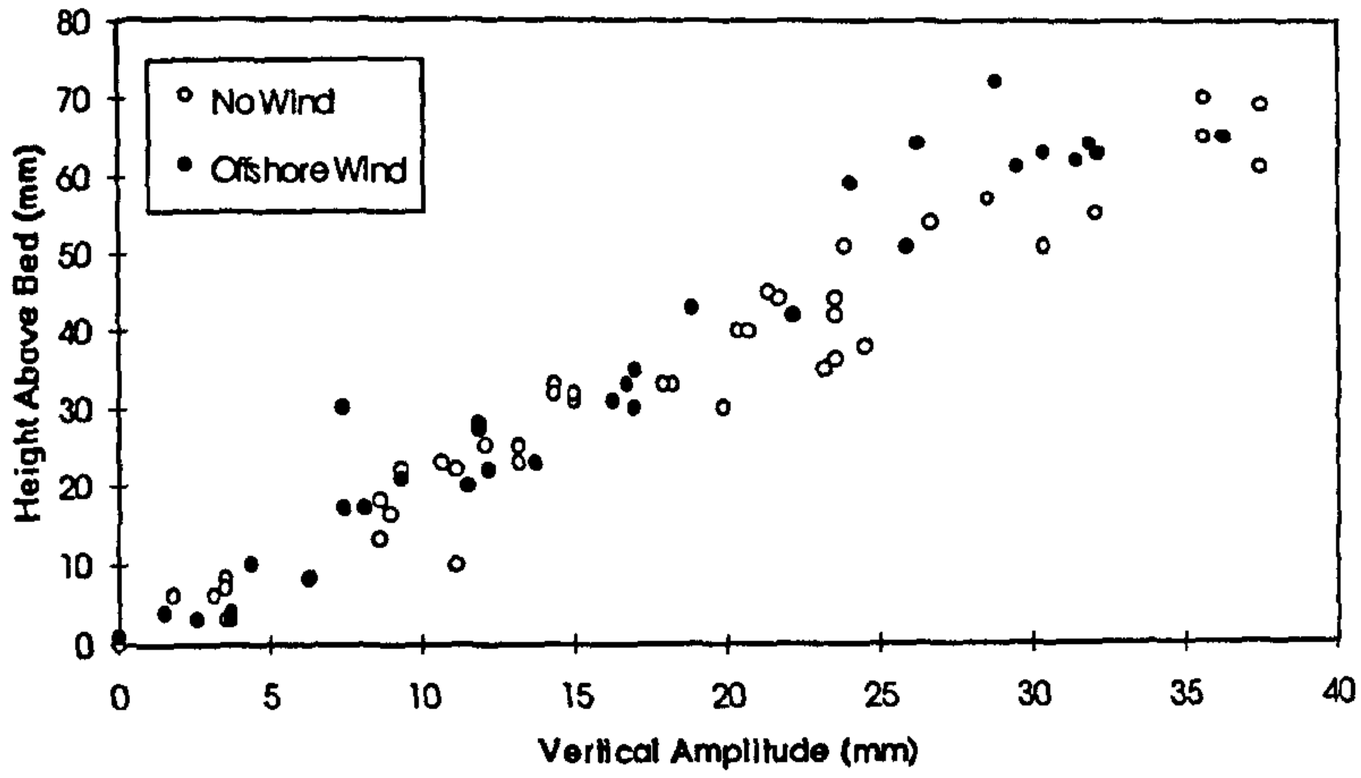

c)

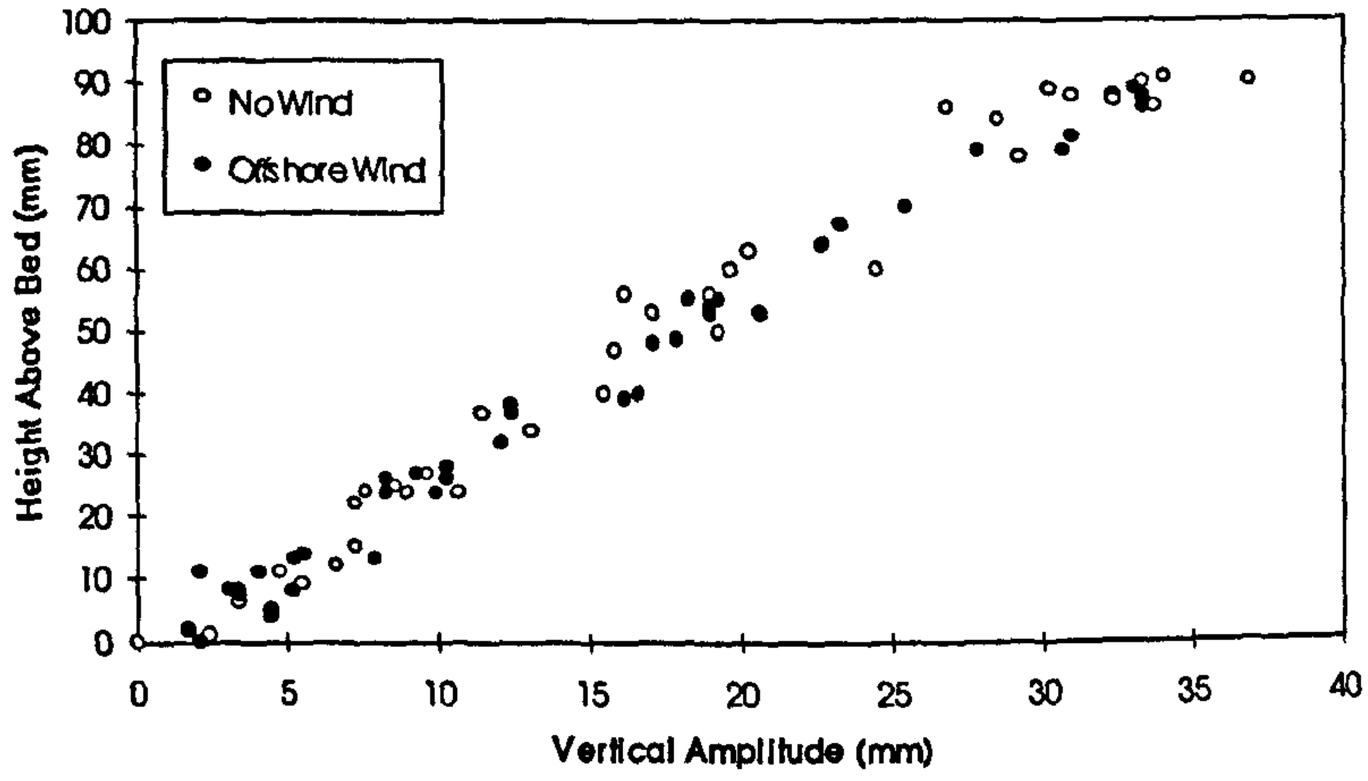

Figure 8.3 Vertical amplitude of motion for spilling waves under offshore winds:
a) X=-1525mm b) X=-1755mm c) X=-2000mm

a)

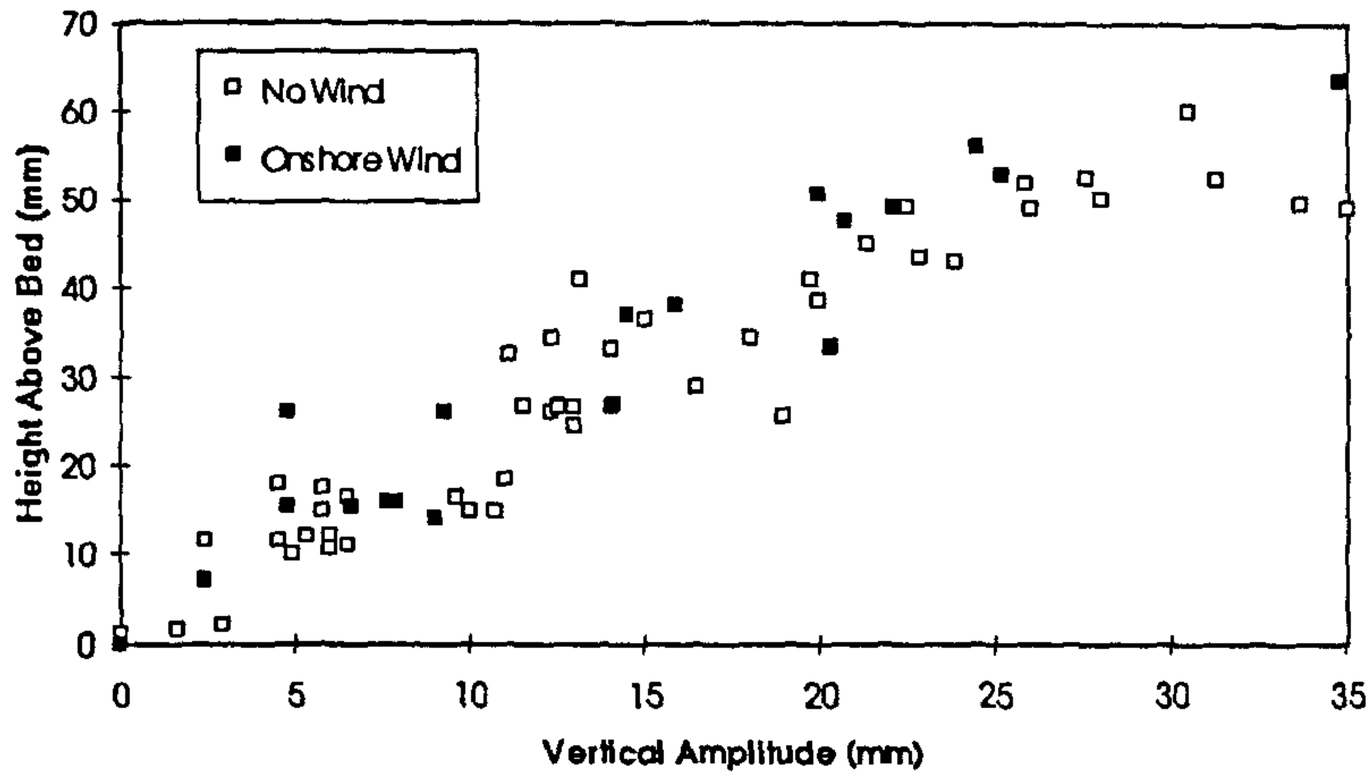

b)

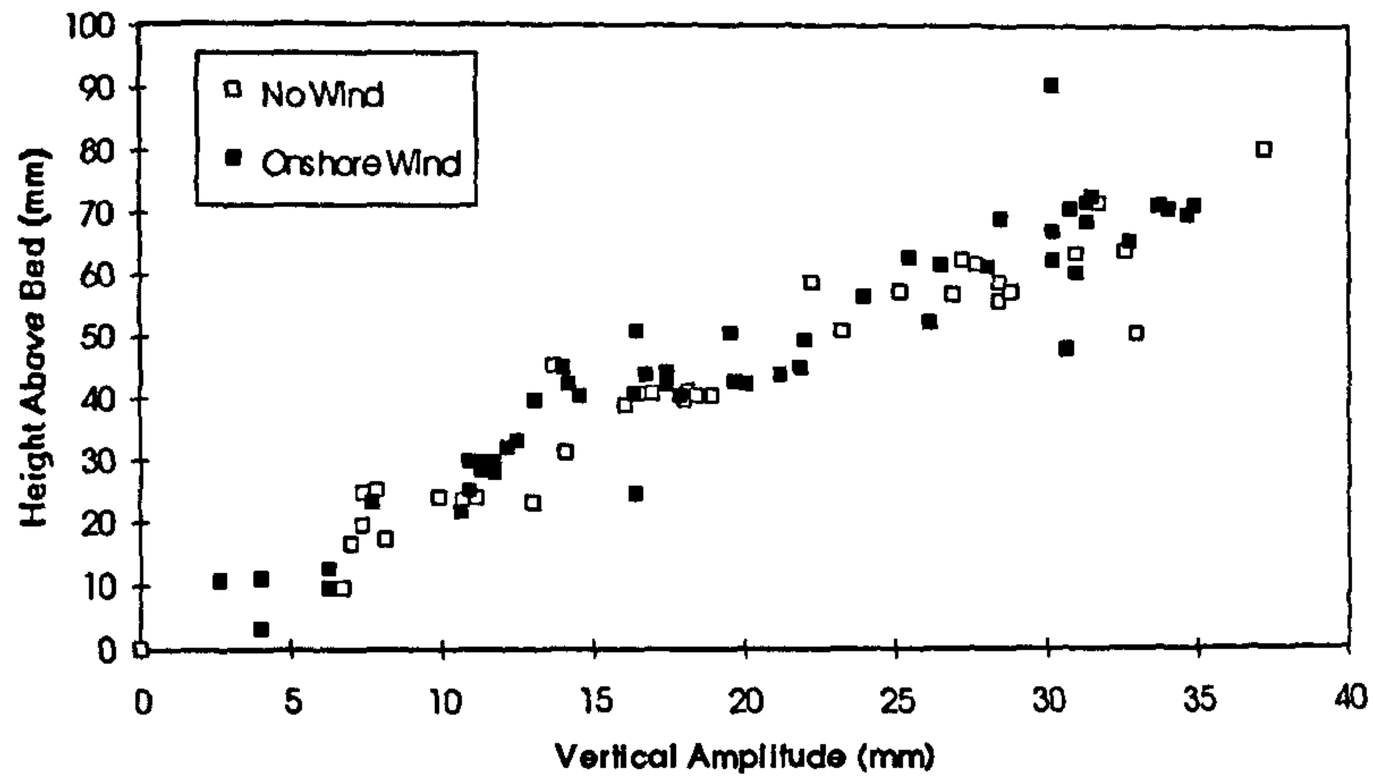

c)

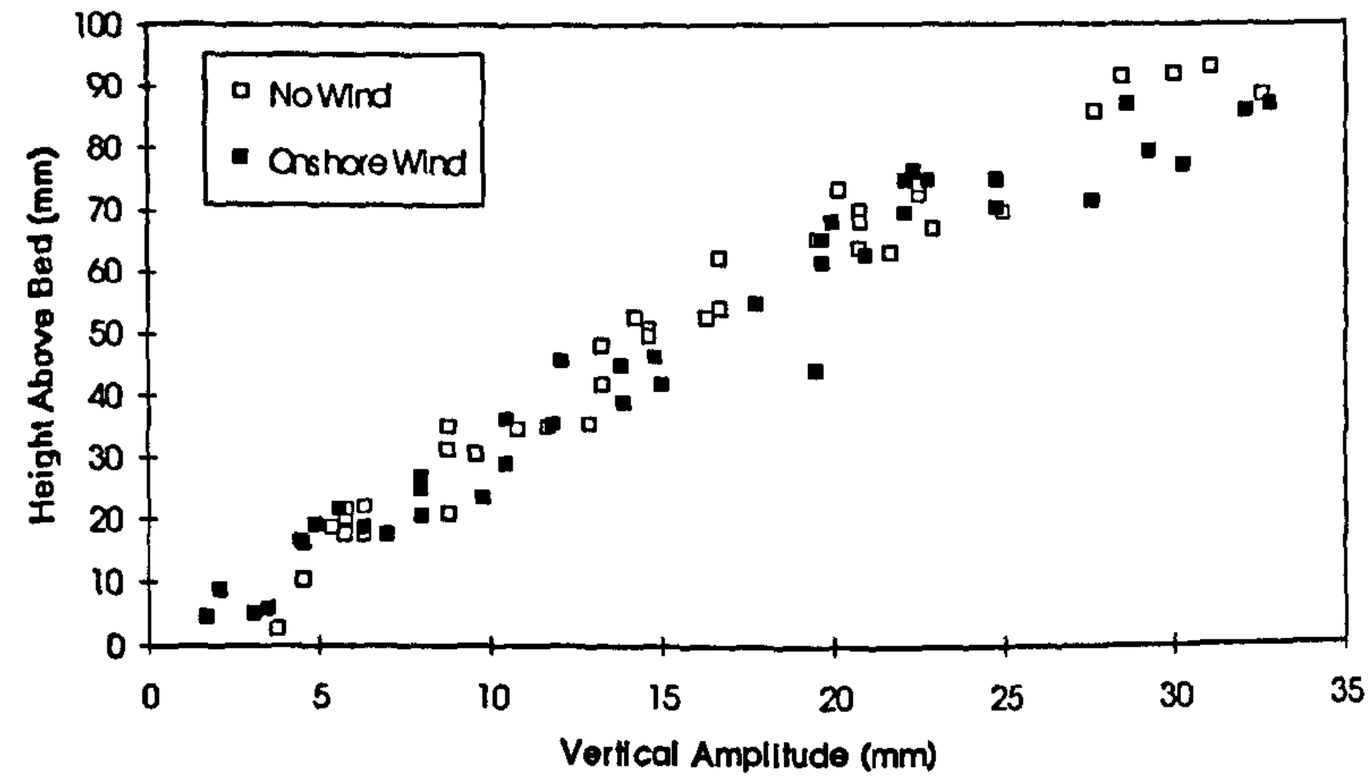

Figure 8.4 Vertical amplitude of motion for spilling waves under onshore winds:
a) X=-1525mm b) X=-1755mm c) X=-2000mm

a)

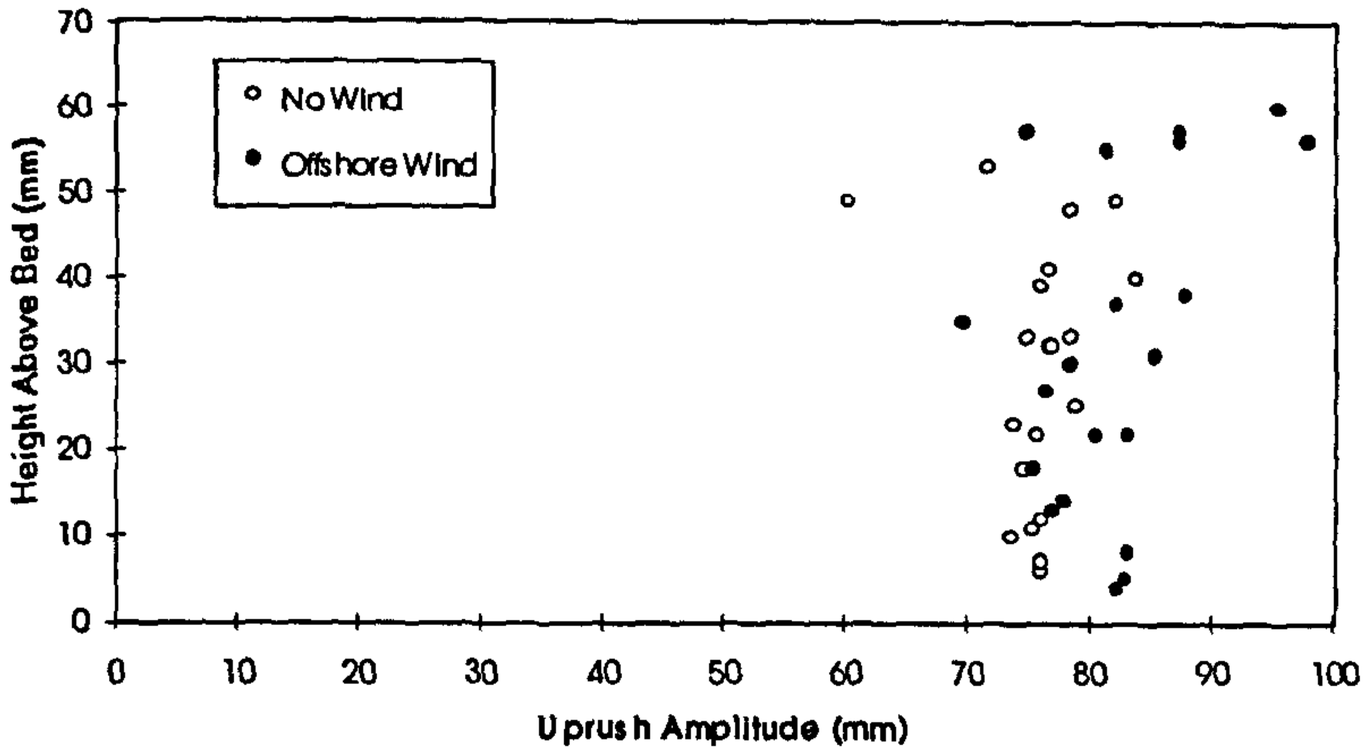

b)

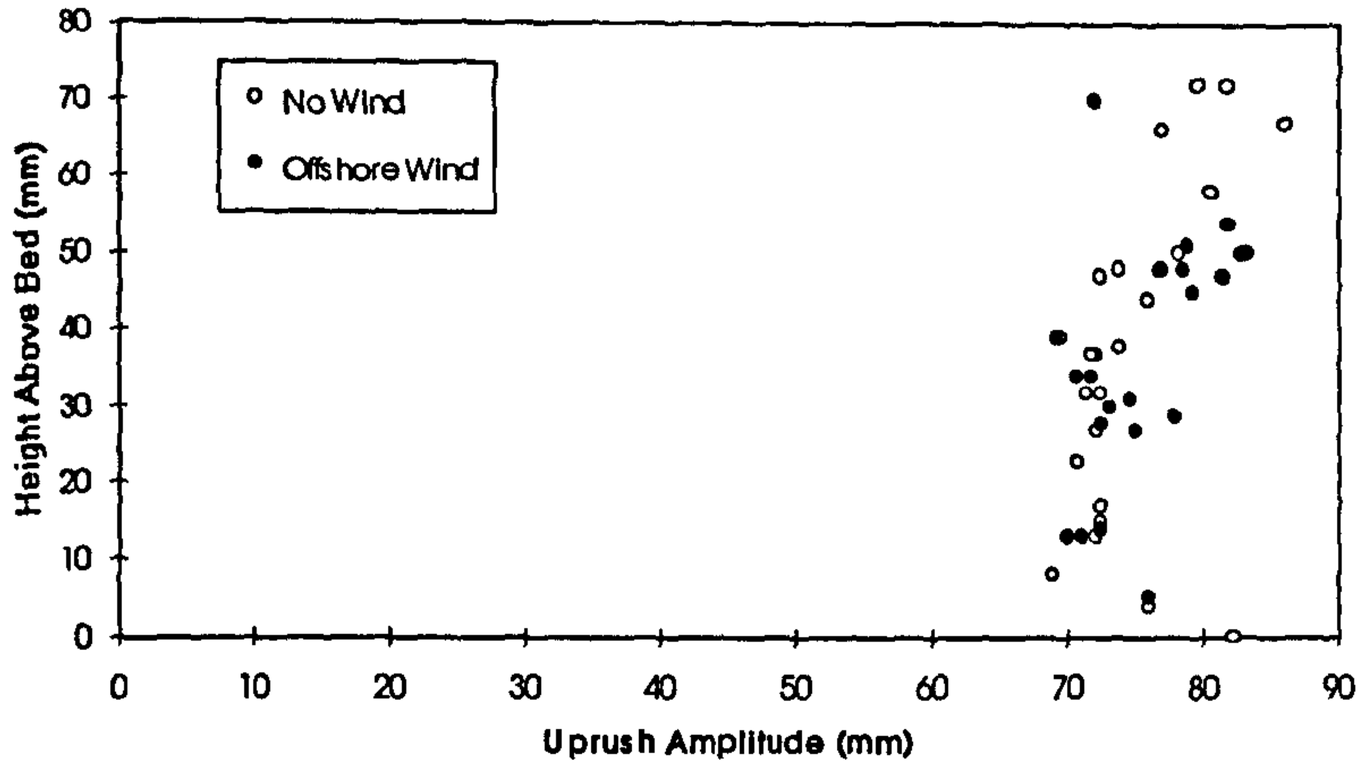

c)

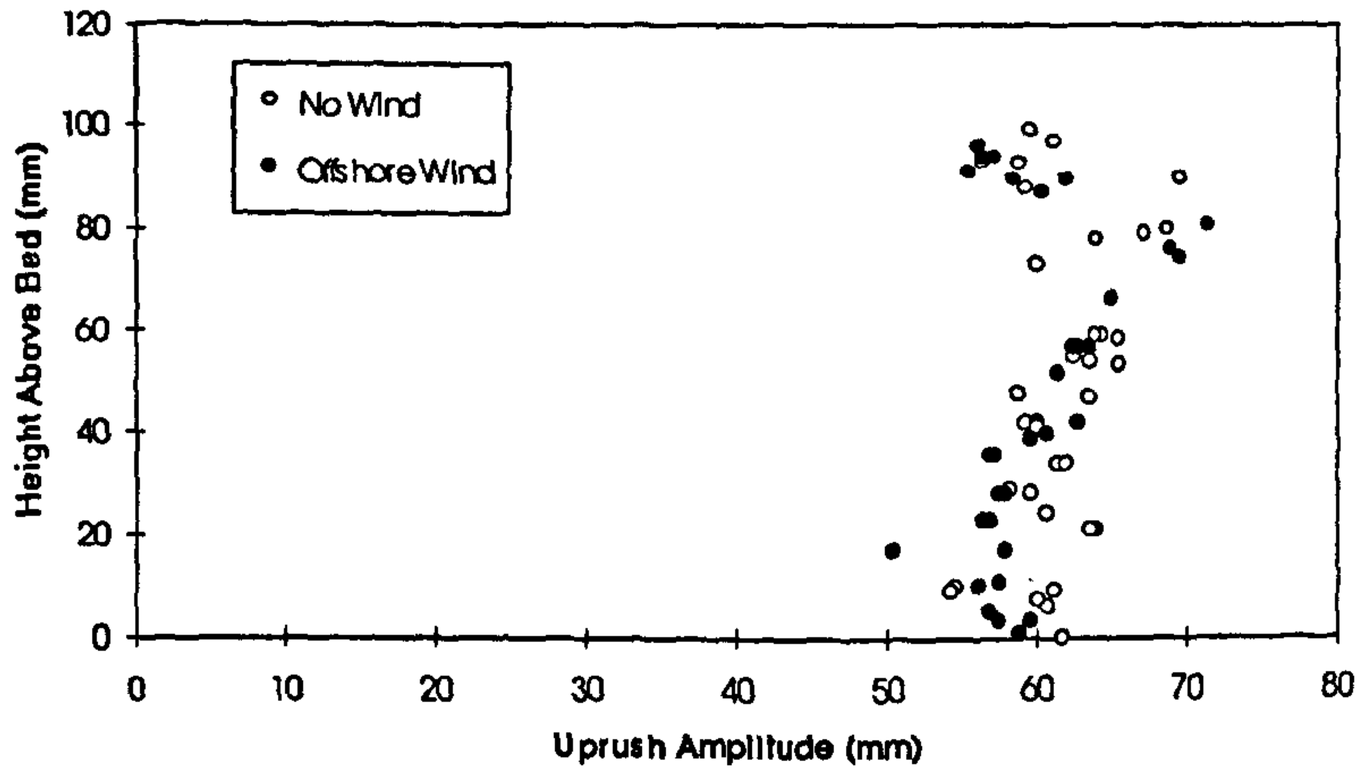

Figure 8.5 Uprush amplitude of particle motion for plunging waves under offshore winds: a) X=-1525mm b) X=-1755mm c) X=-2000mm

a)

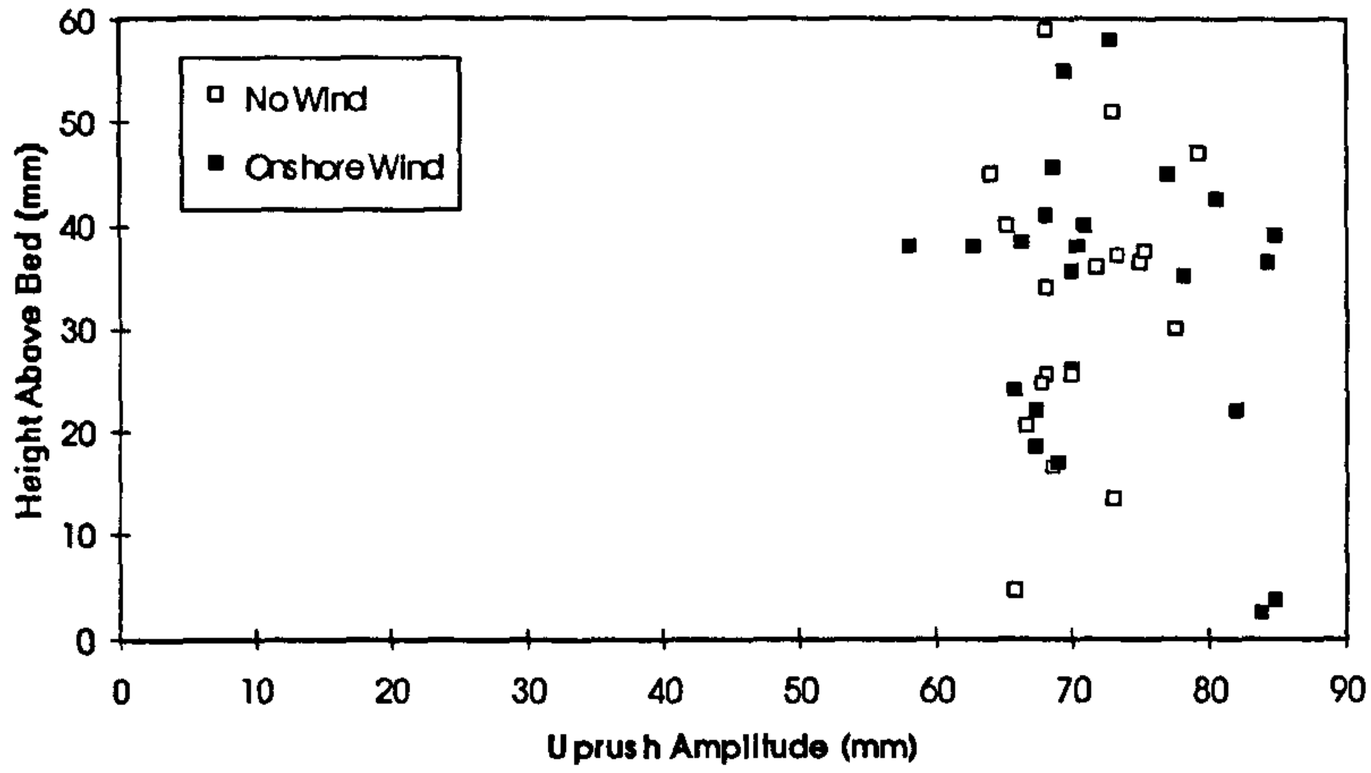

b)

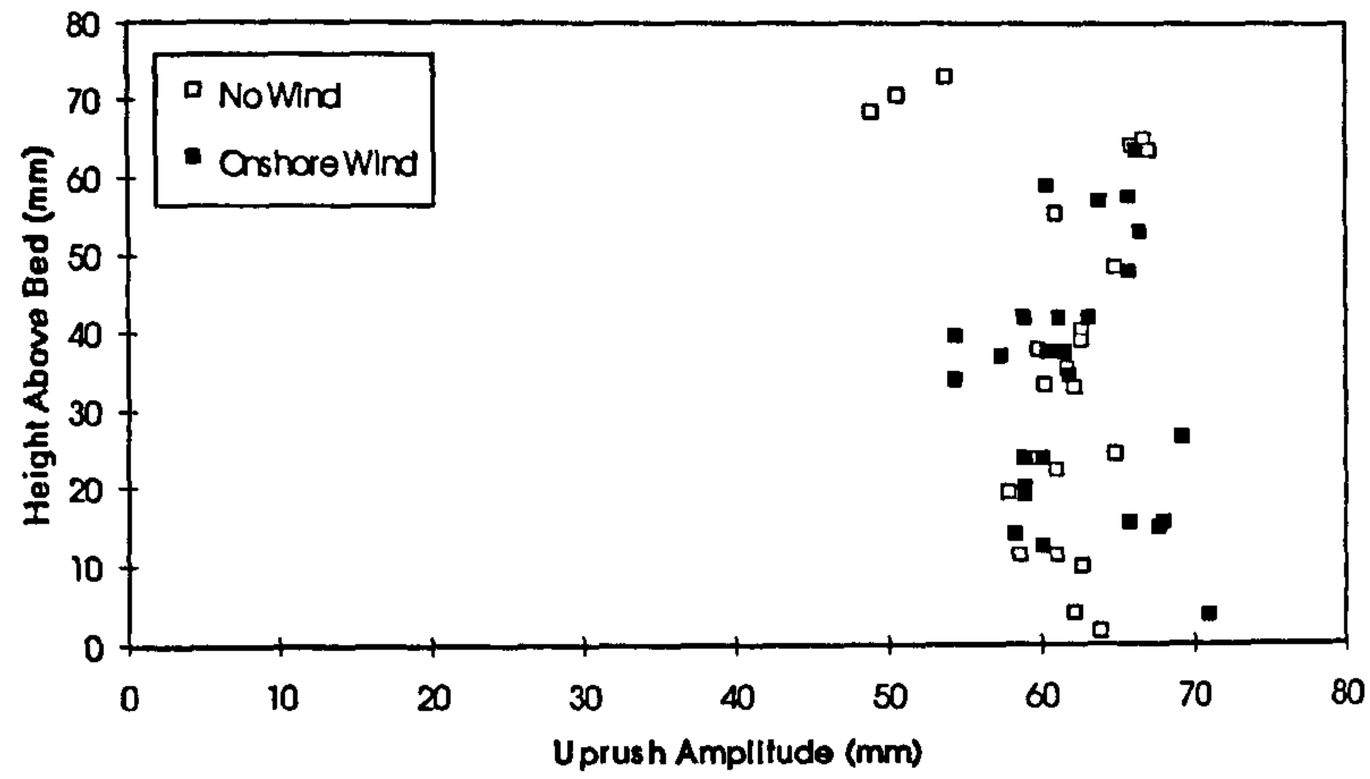

c)

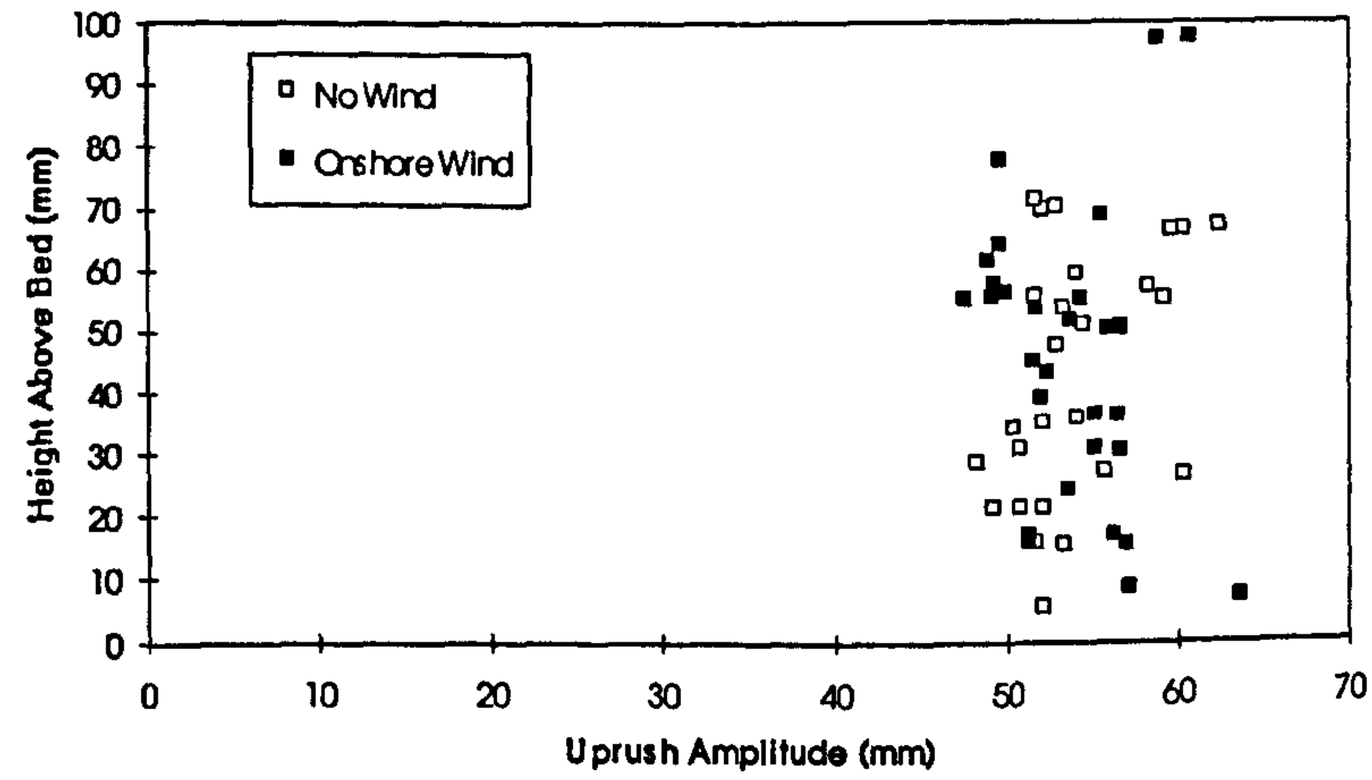

Figure 8.6 Uprush amplitude of particle motion for plunging waves under onshore winds: a) X=-1525mm b) X=-1755mm c) X=-2000mm

a)

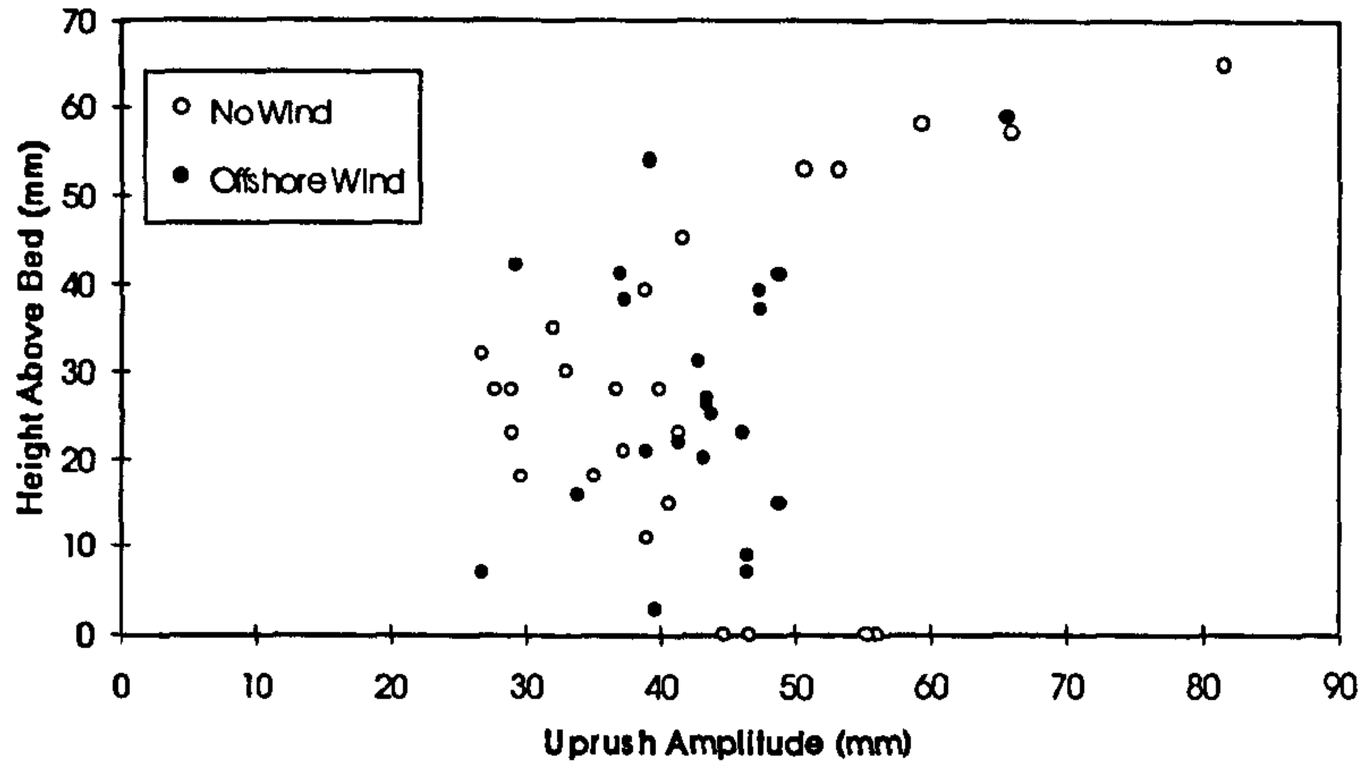

b)

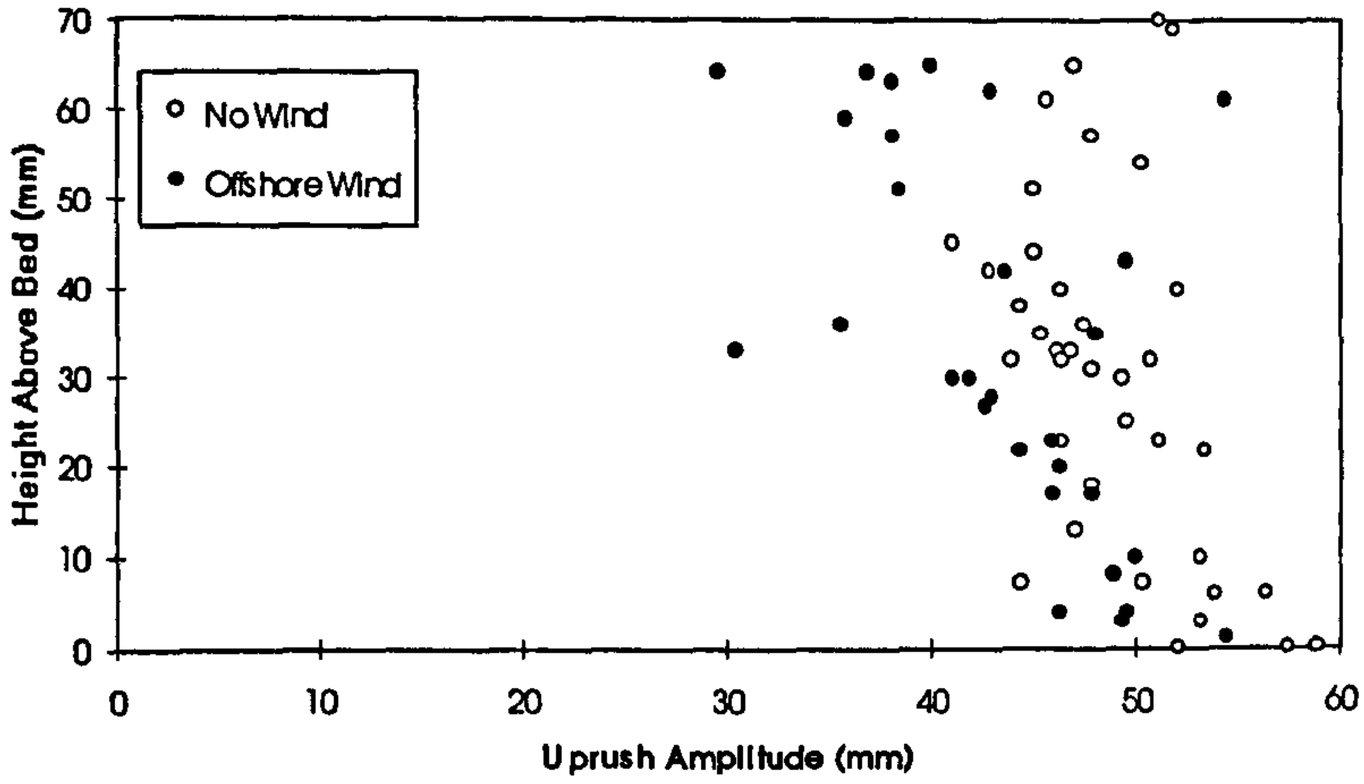

c)

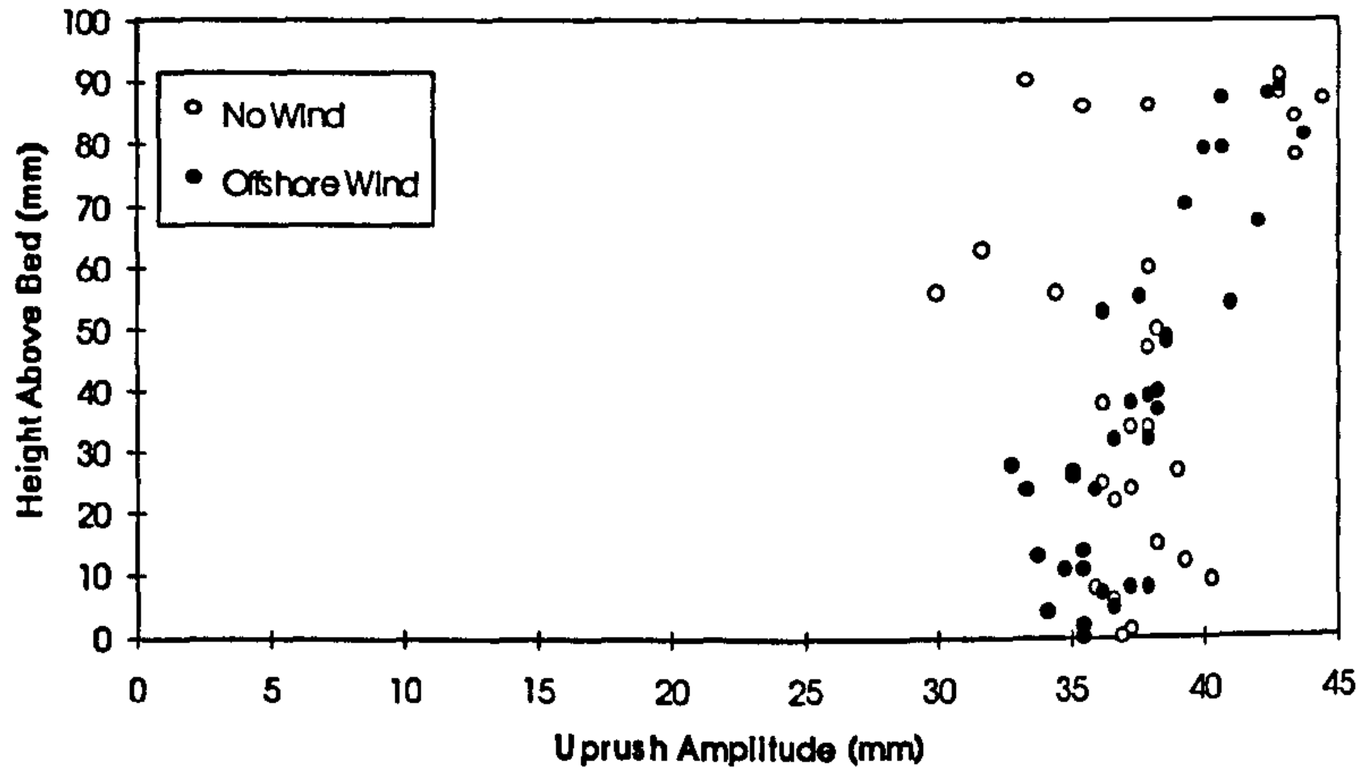

Figure 8.7 Uprush amplitude of particle motion for spilling waves under offshore winds: a) X=-1525mm b) X=-1755mm c) X=-2000mm

a)

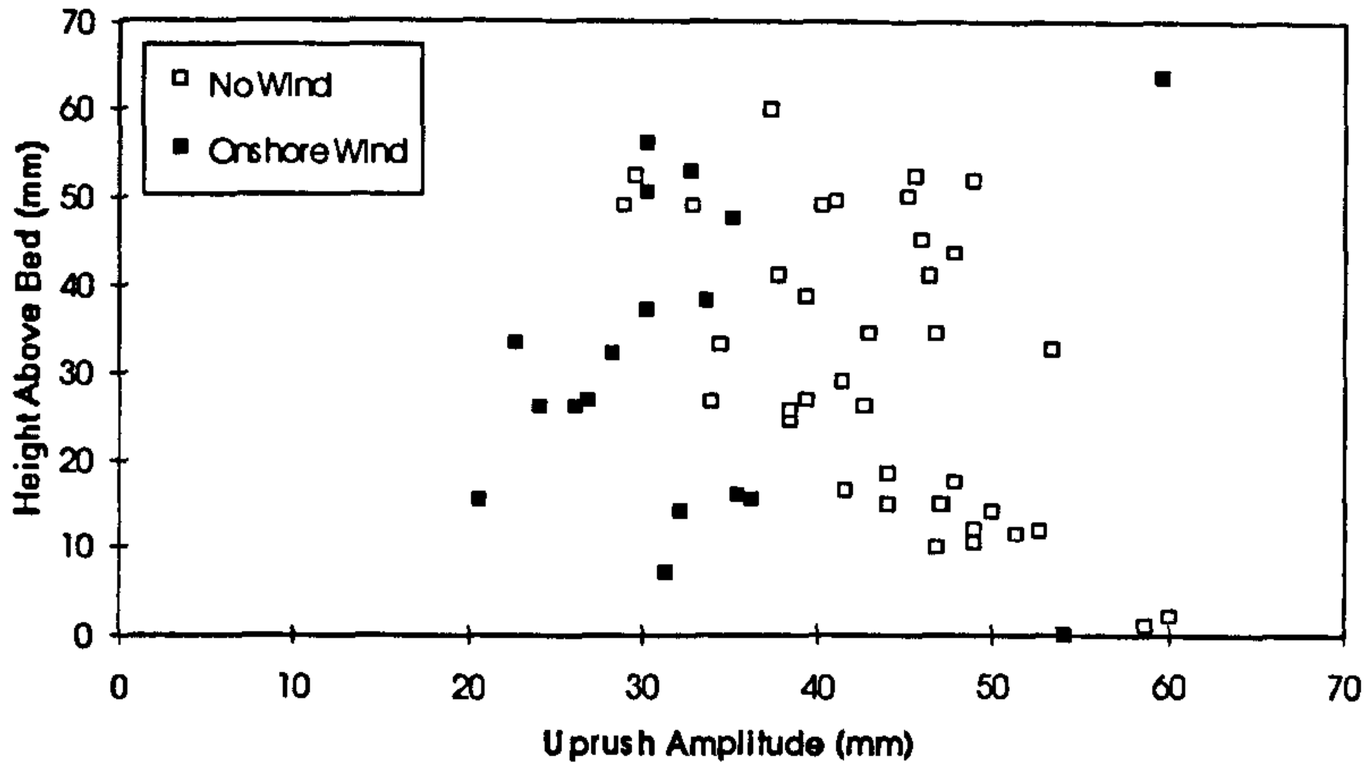

b)

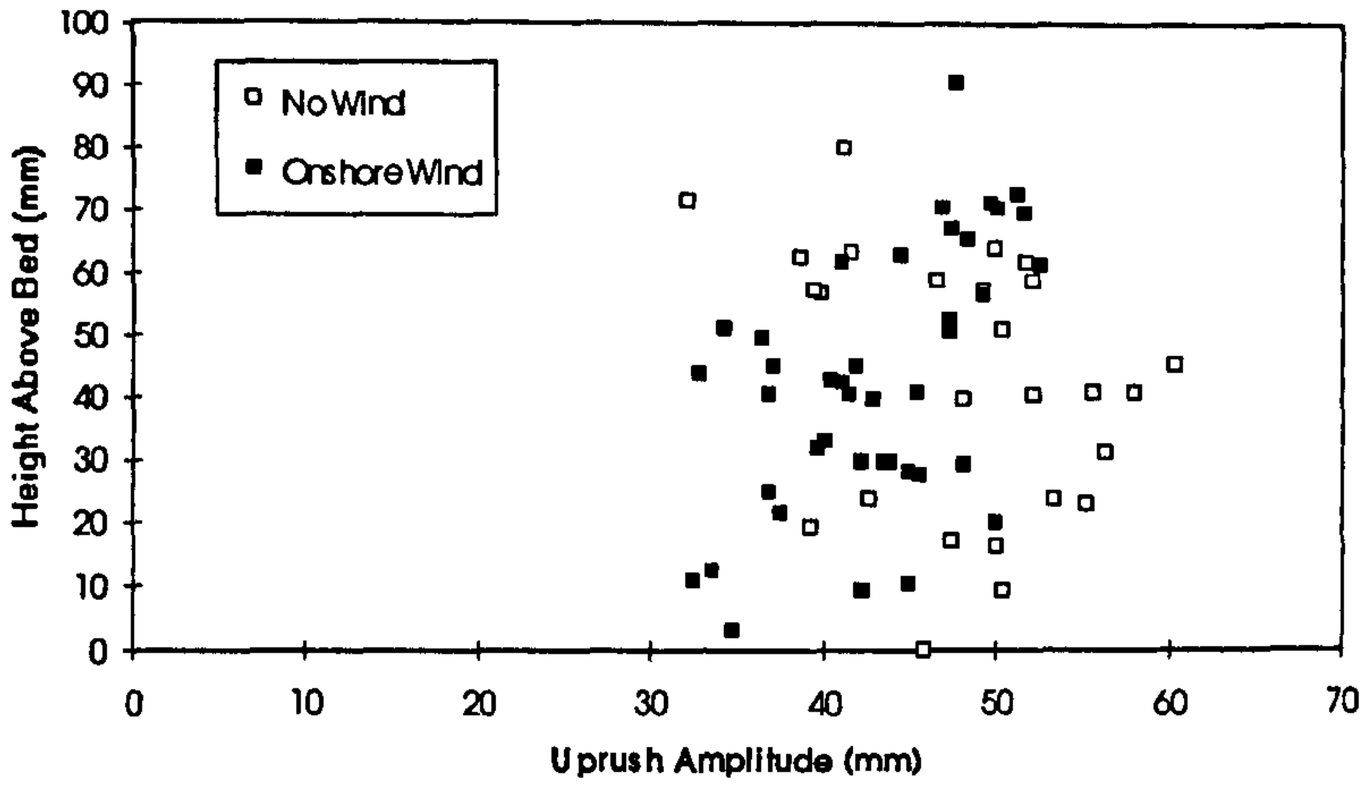

c)

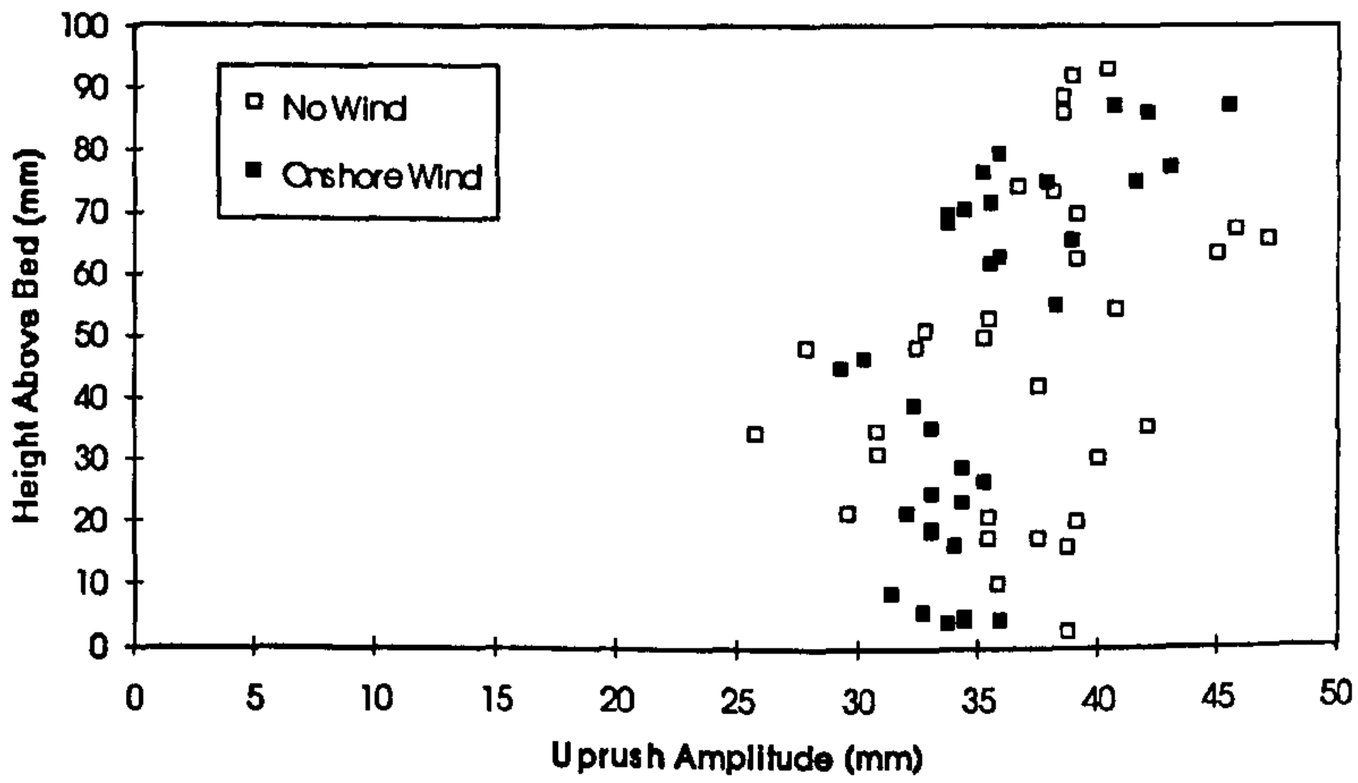

Figure 8.8 Uprush amplitude of particle motion for spilling waves under onshore winds: a) X=-1525mm b) X=-1755mm c) X=-2000mm

a)

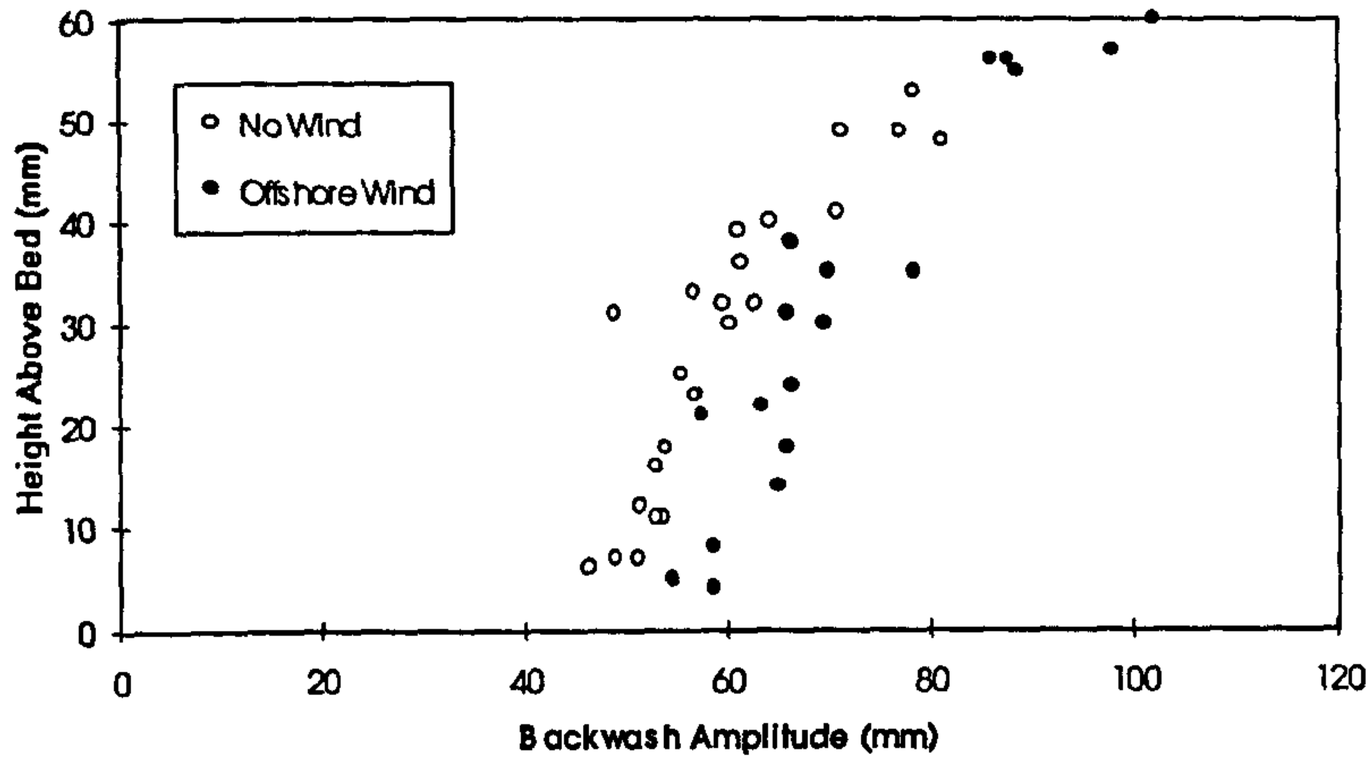

b)

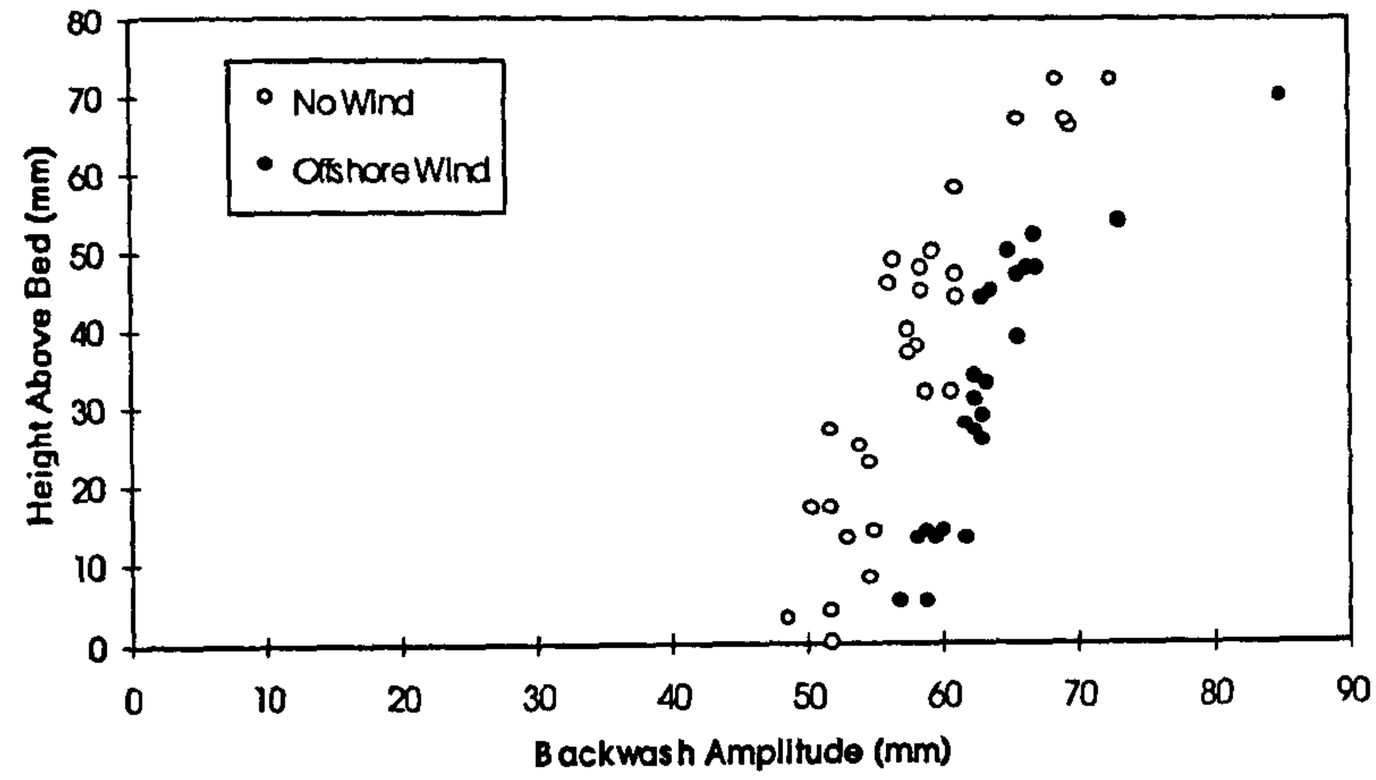

c)

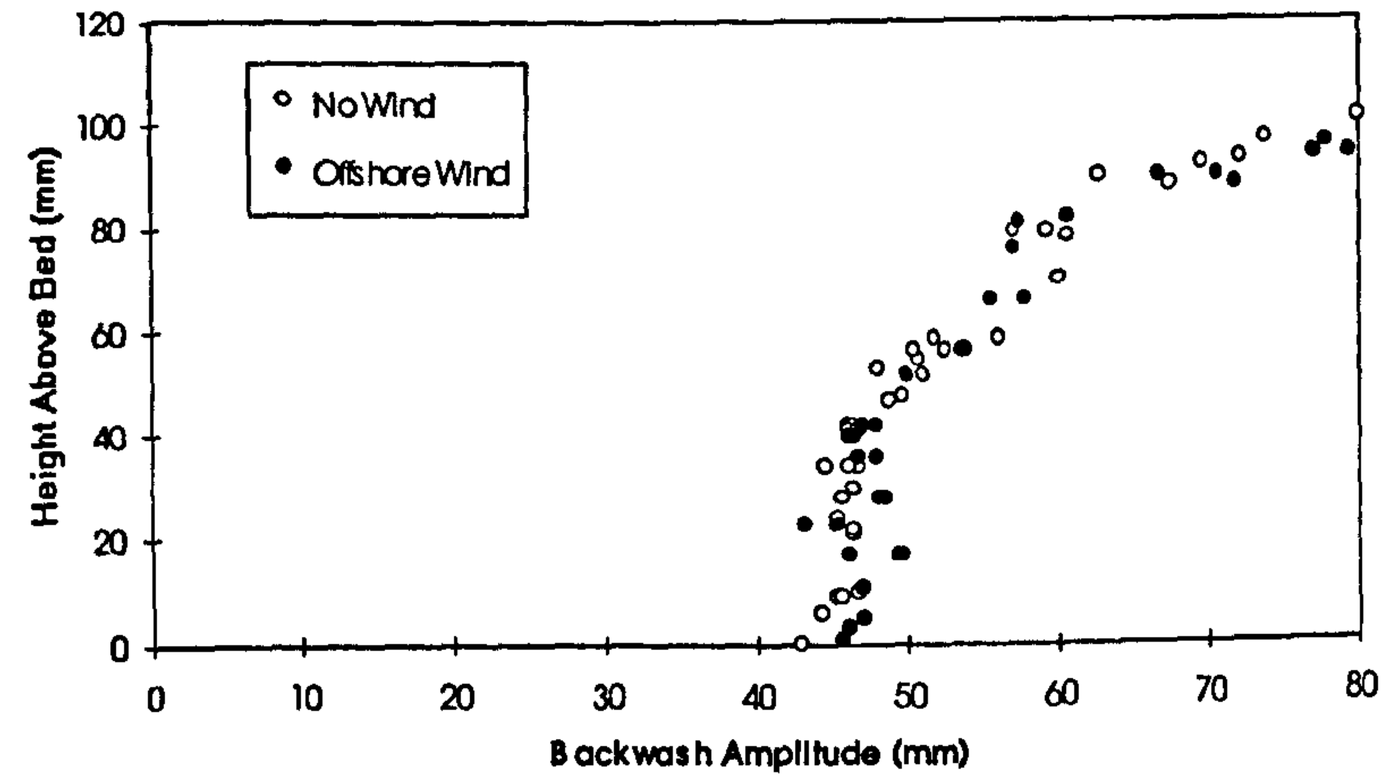

Figure 8.9 Backwash amplitude of motion for plunging waves under offshore winds: a) X=-1525mm b) X=-1755mm c) X=-2000mm

a)

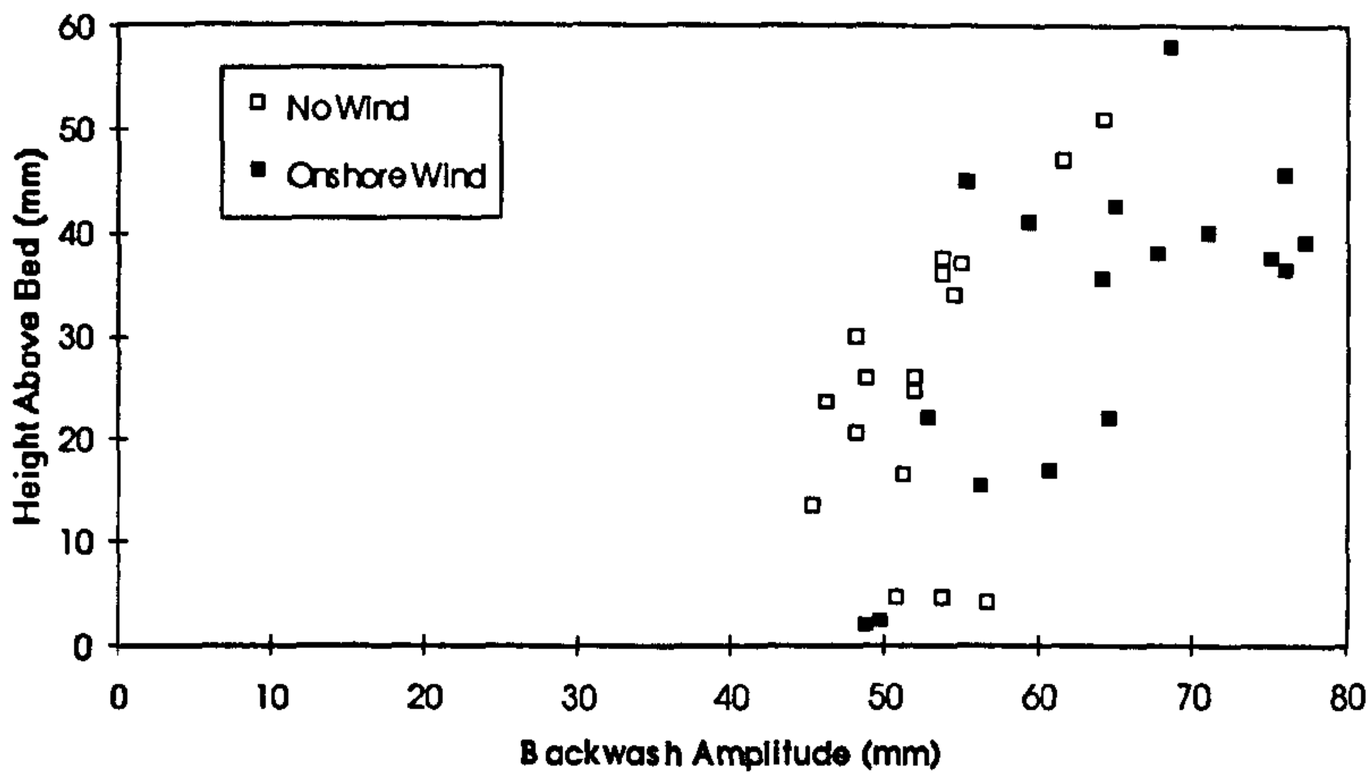

b)

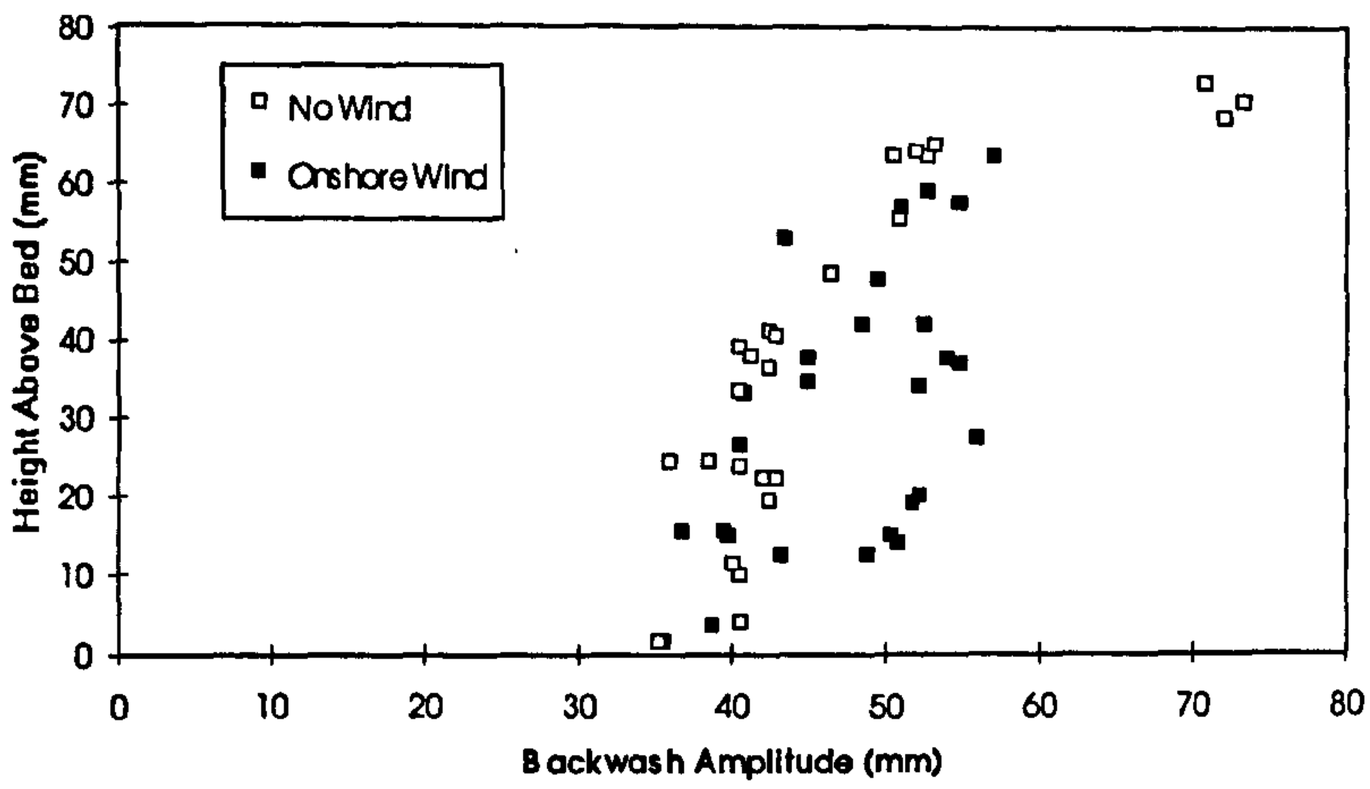

c)

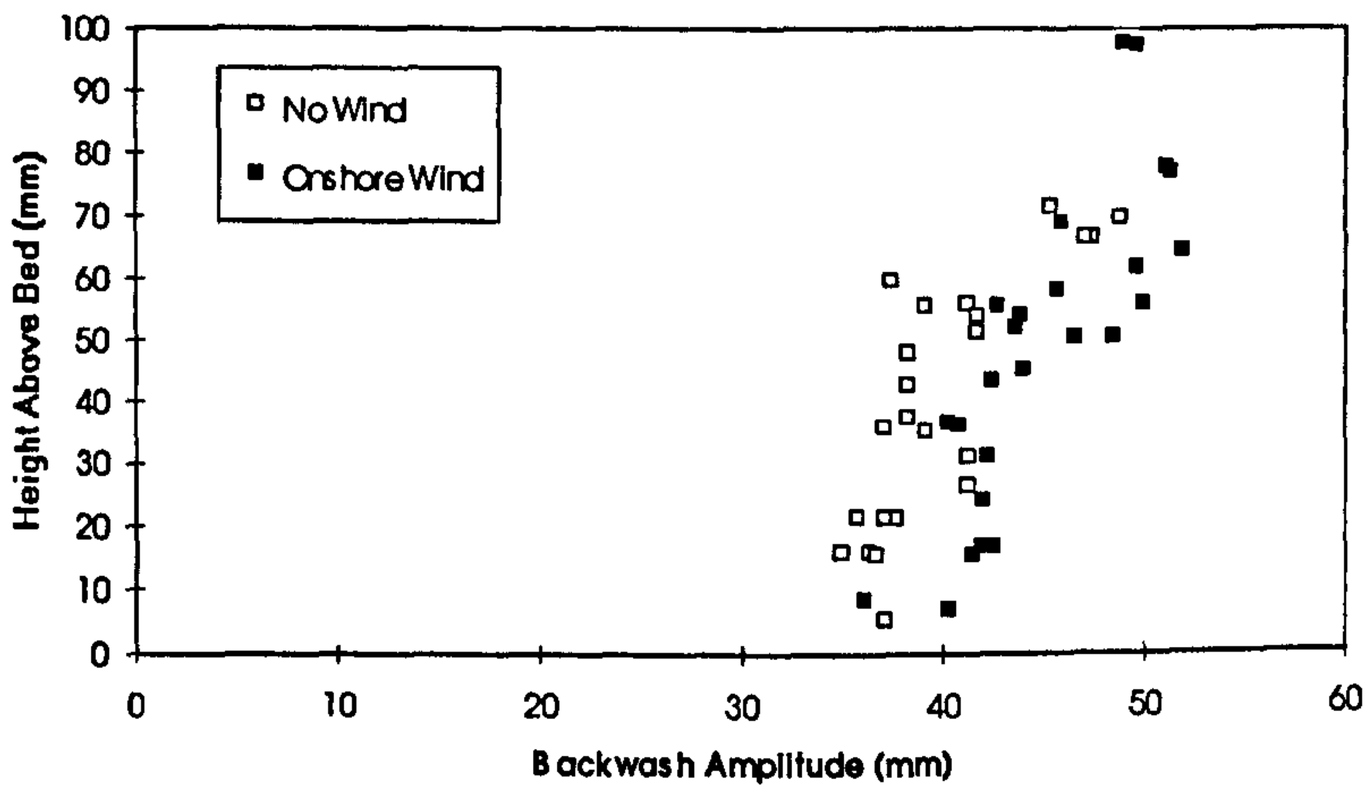

Figure 8.10 Backwash amplitude of motion for plunging waves under onshore winds: a) X=-1525mm b) X=-1755mm c) X=-2000mm

a)

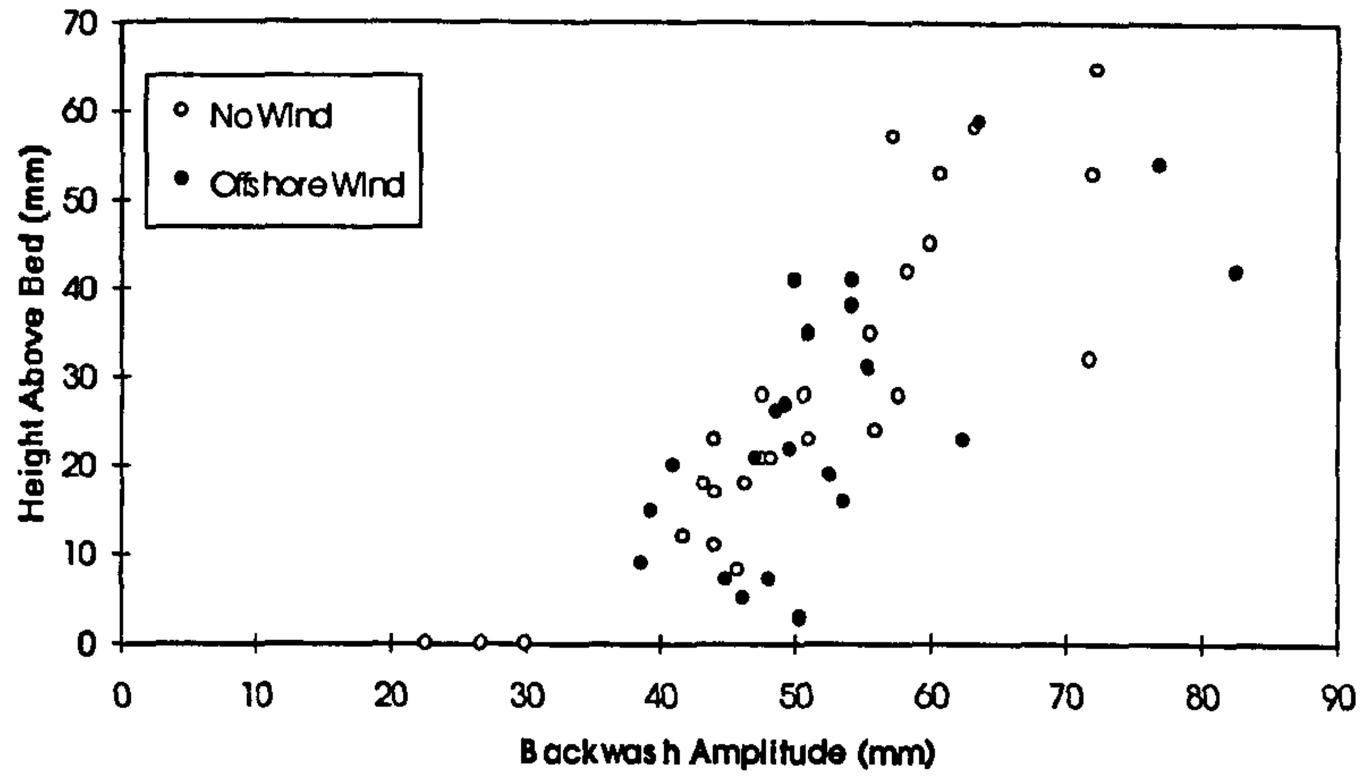

b)

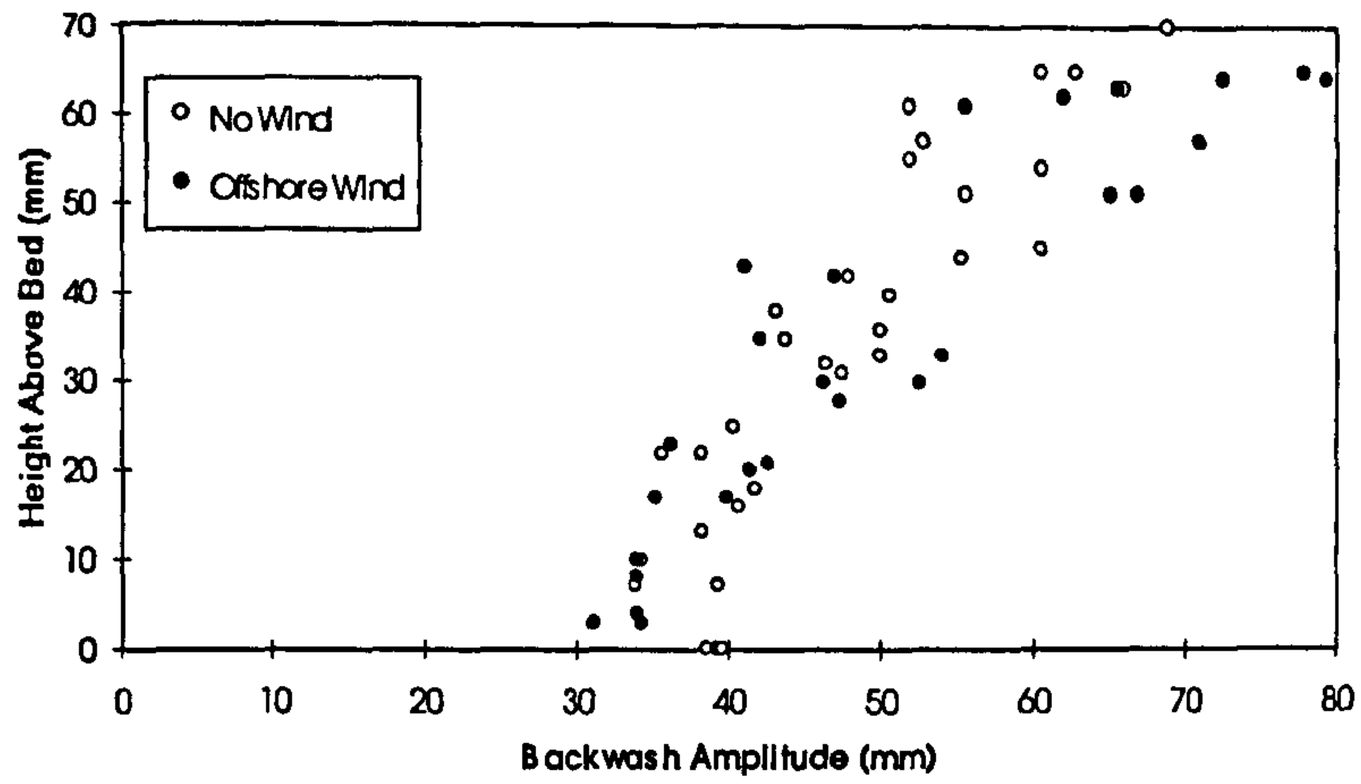

c)

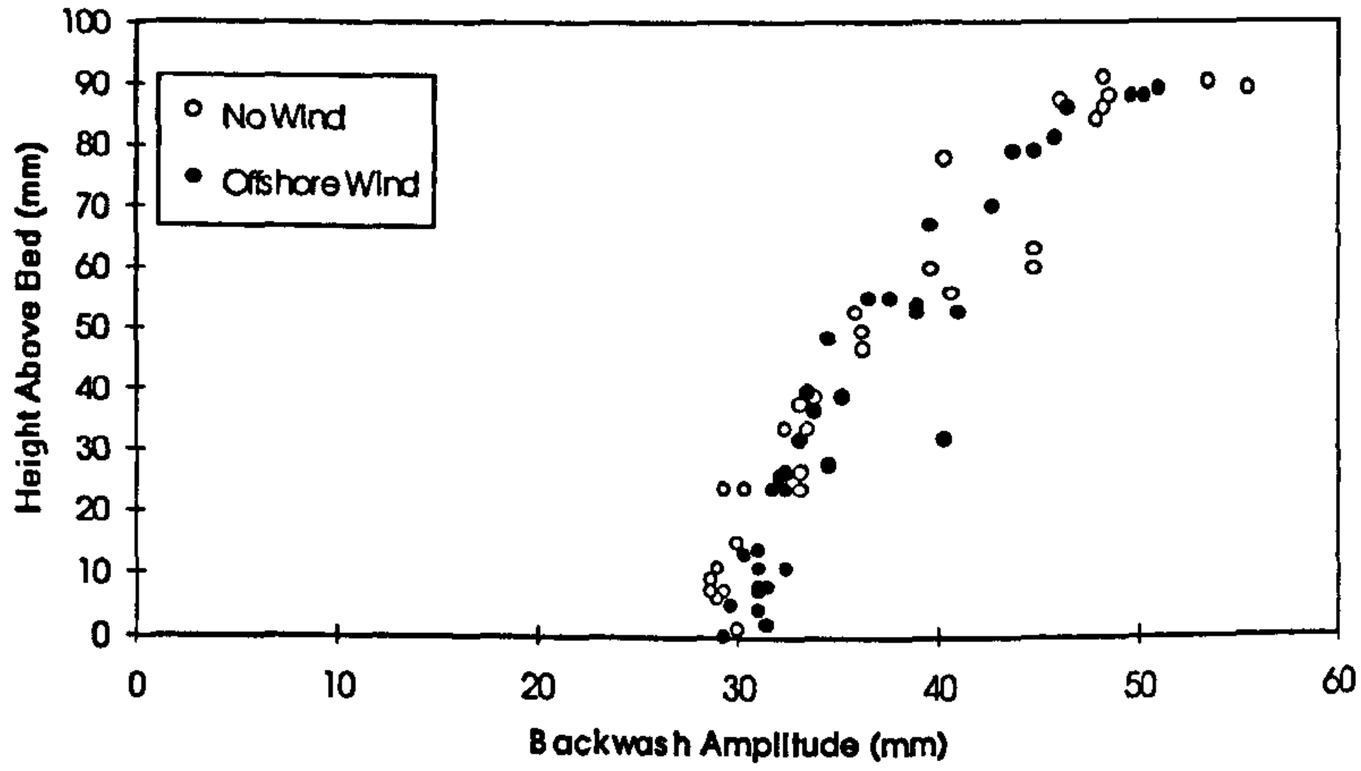

Figure 8.11 Backwash amplitude of particle motion for spilling waves under offshore winds: a) X=-1525mm b) X=-1755mm c) X=-2000mm

a)

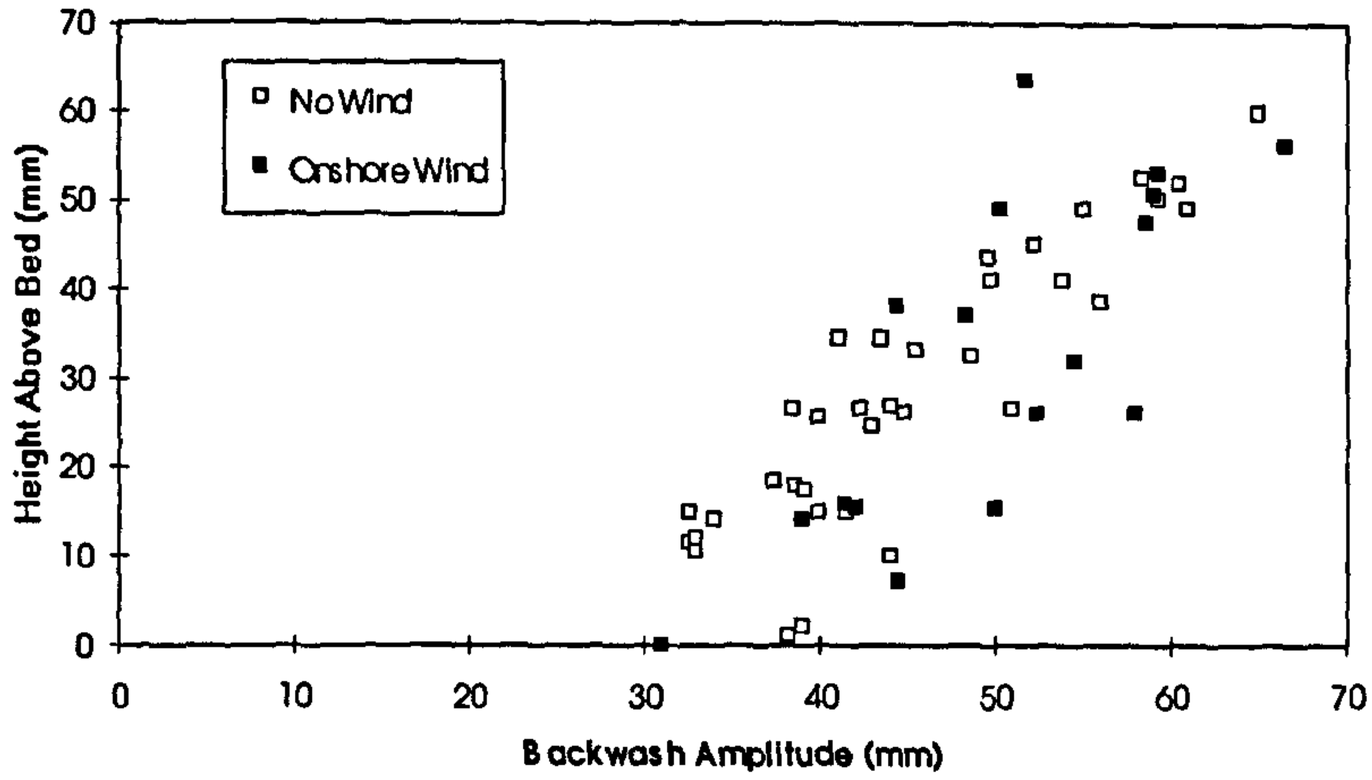

b)

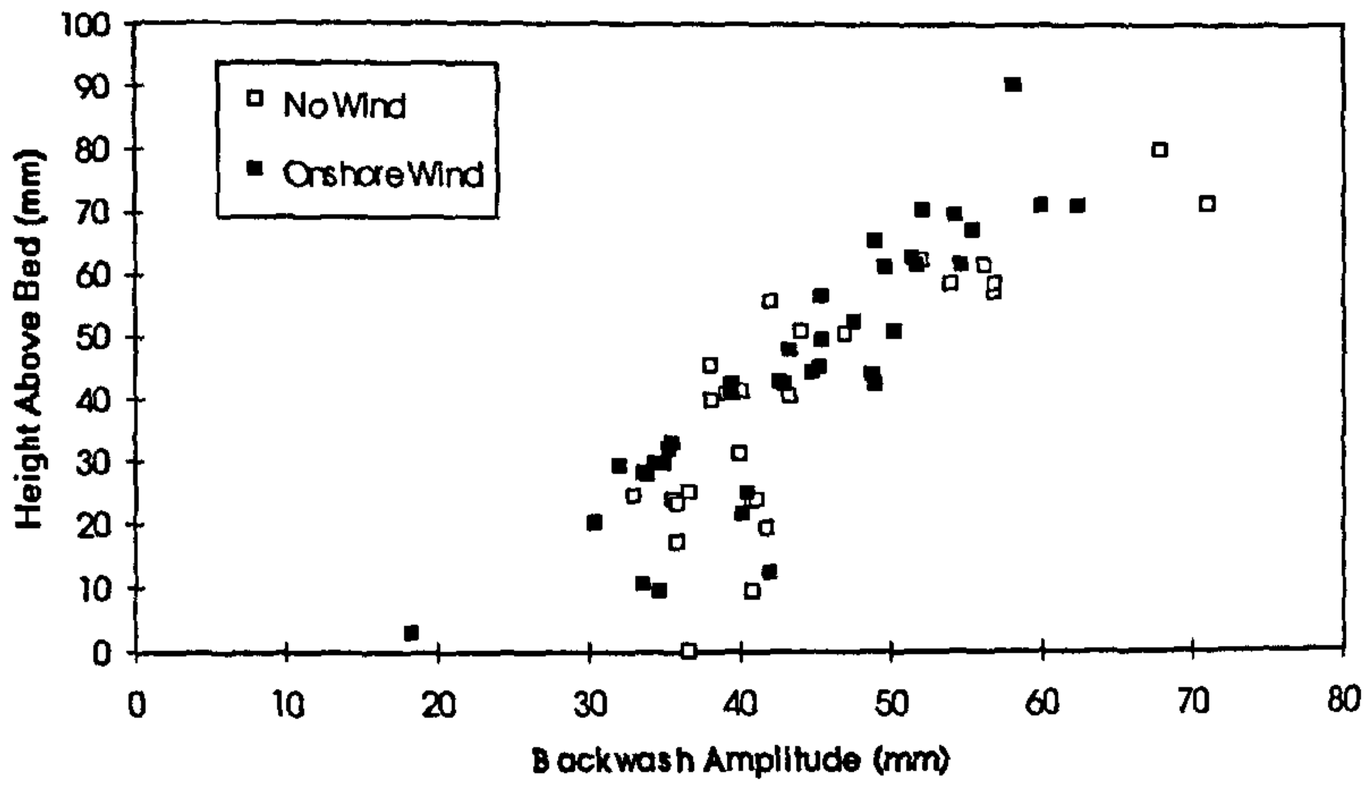

c)

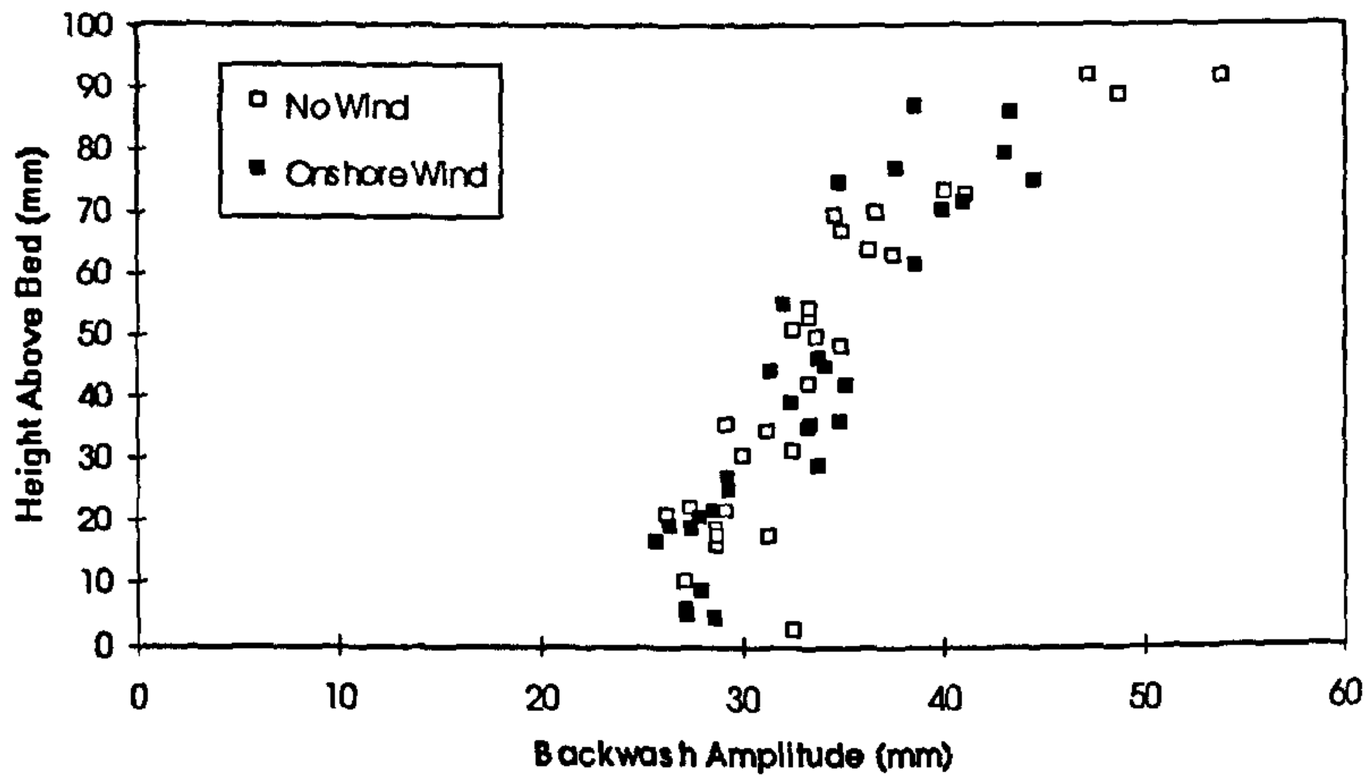

Figure 8.12 Backwash amplitude of particle motion for spilling waves under onshore winds: a) X=-1525mm b) X=-1755mm c) X=-2000mm

a)

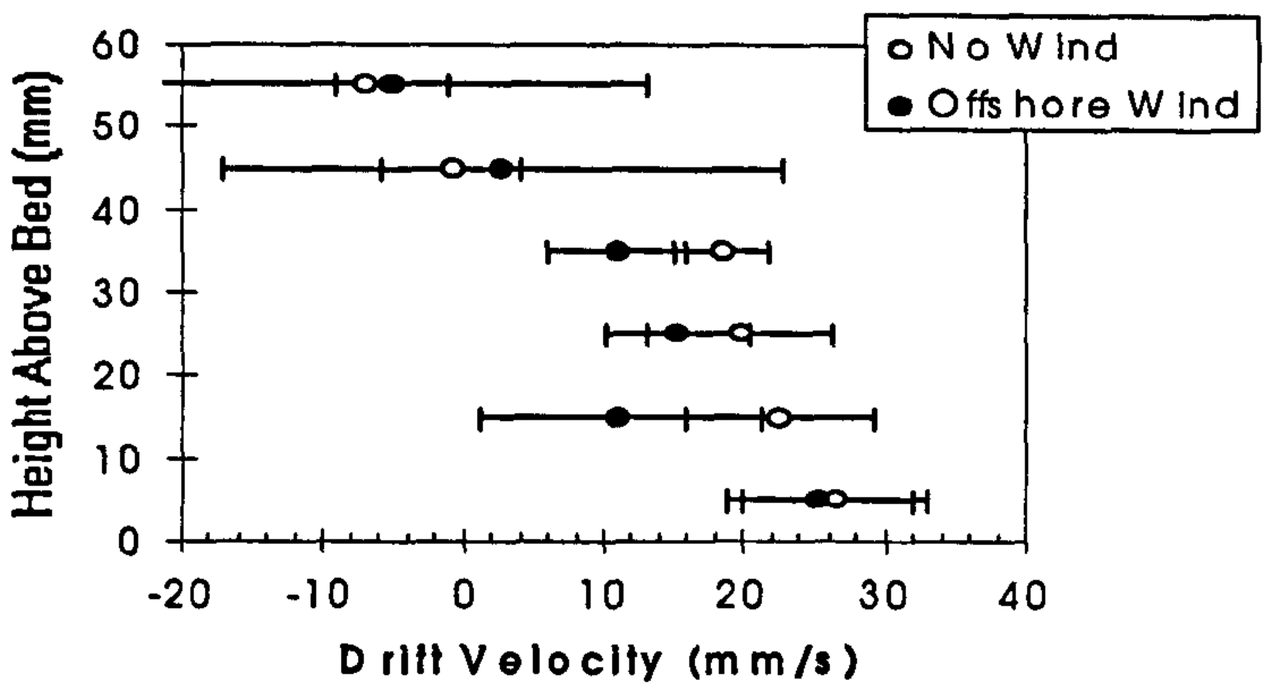

b)

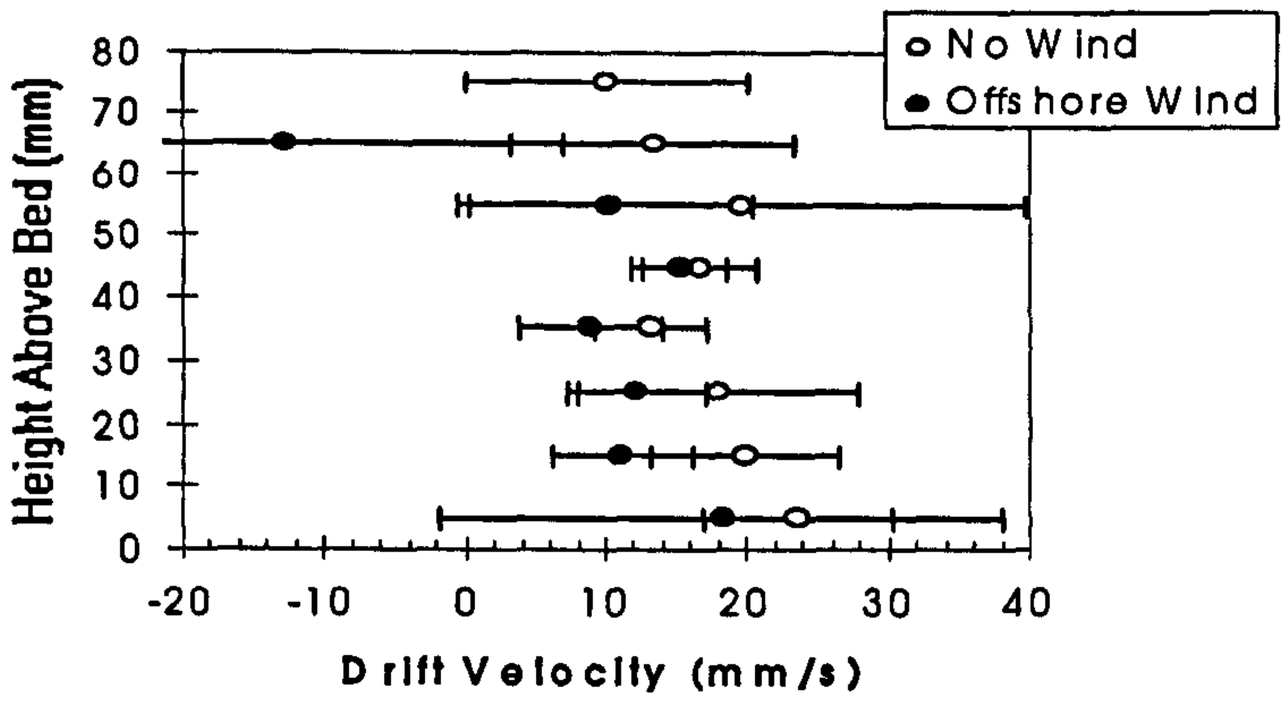

c)

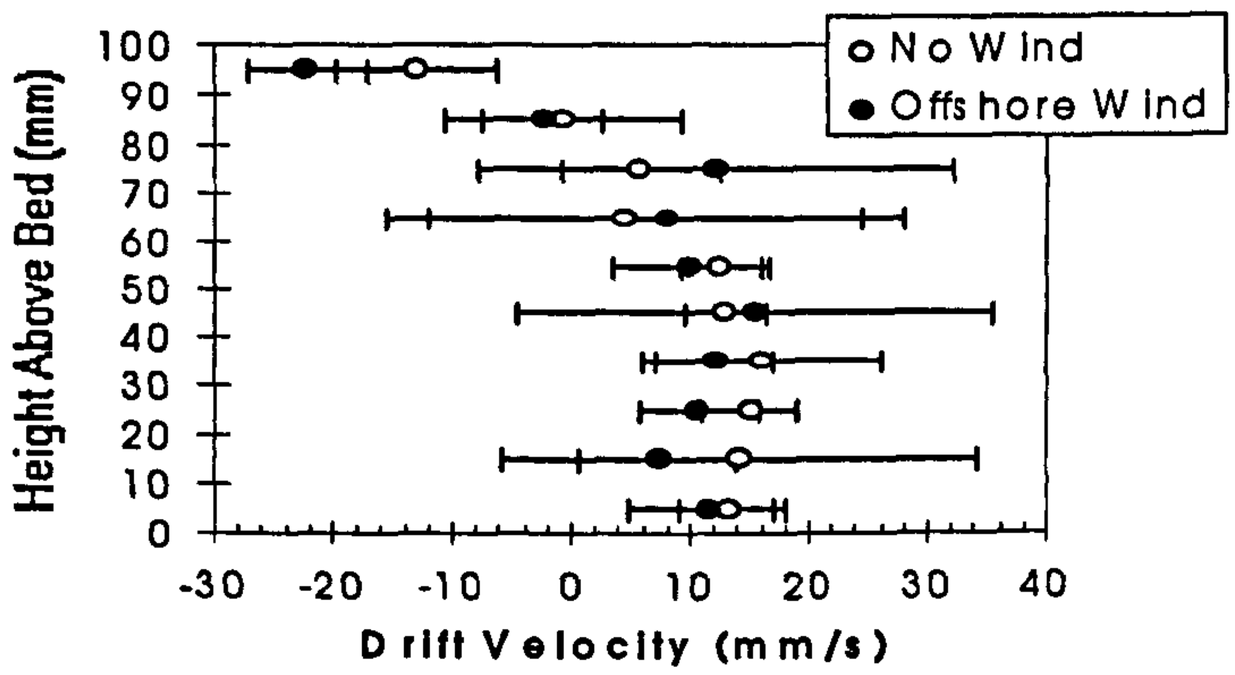

Figure 8.13 Horizontal particle drift velocities for plunging waves under offshore wind: a) X=-1525mm b) X=-1755mm c)X=-2000mm.

a)

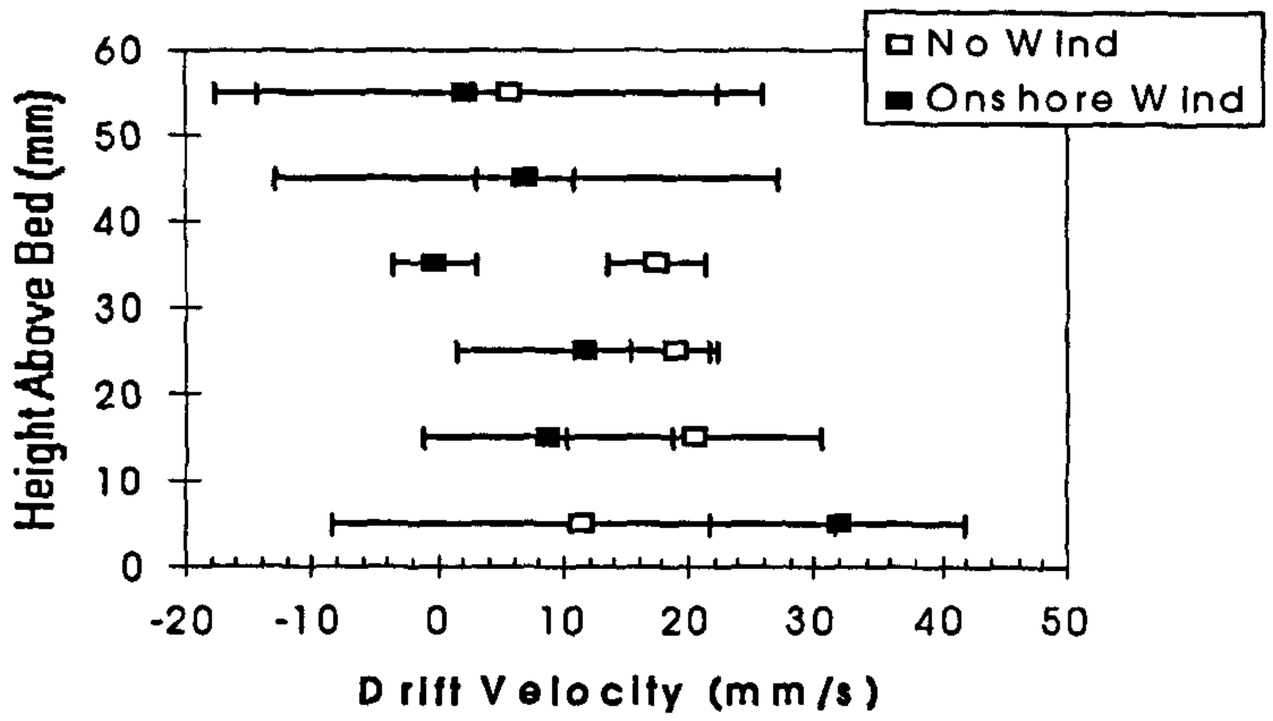

b)

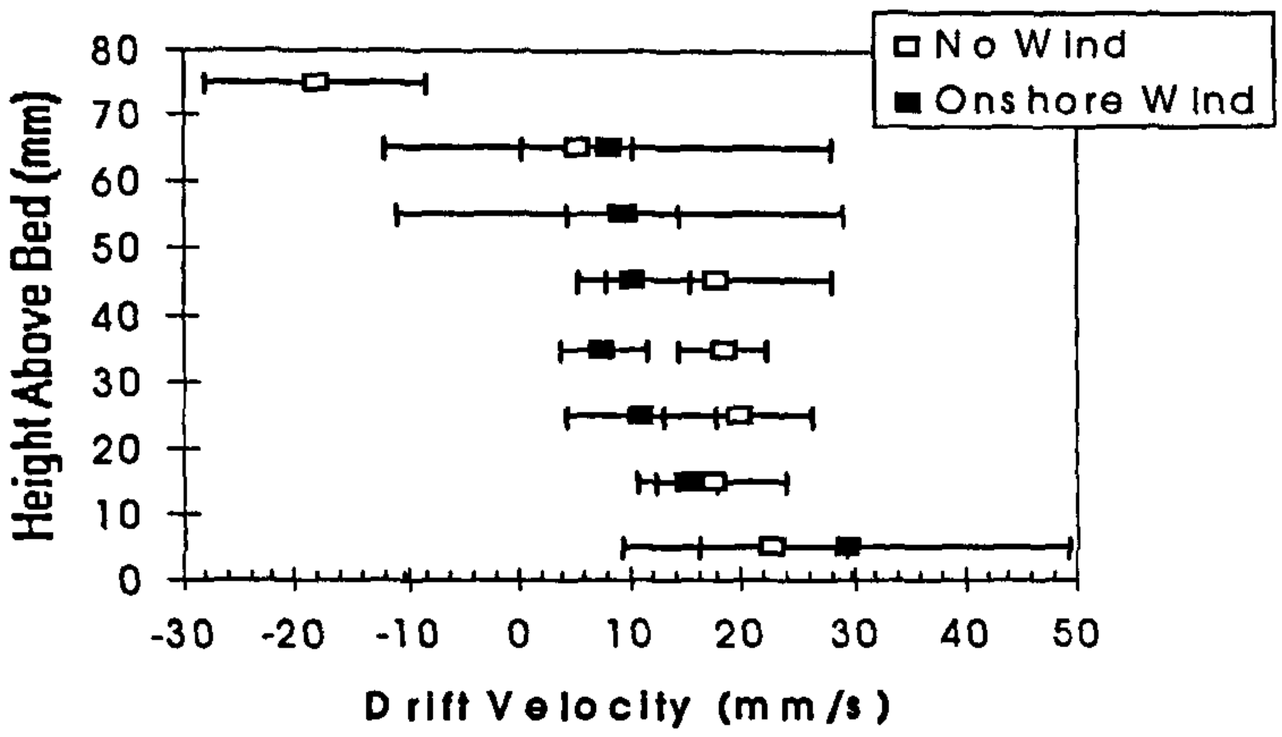

c)

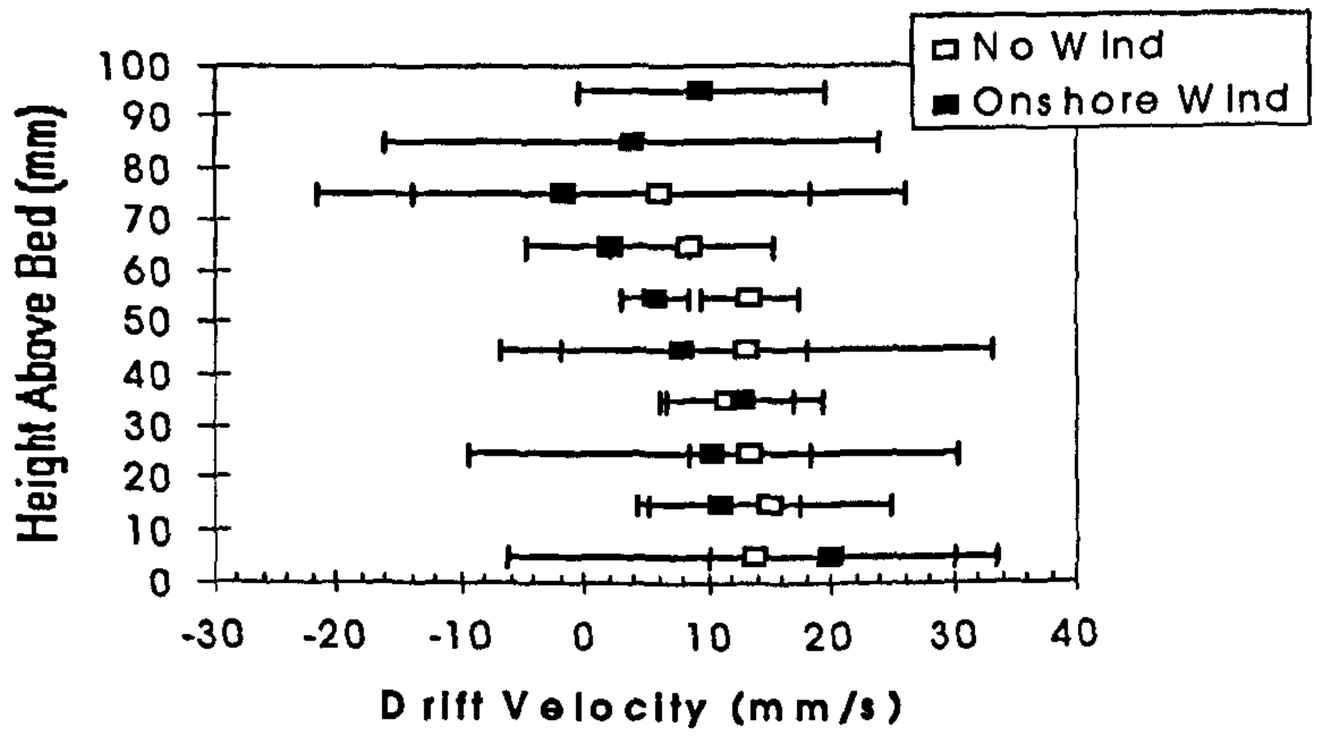

Figure 8.14 Horizontal particle drift velocities for plunging under onshore winds:
a) X=-1525mm b) X=-1755mm c) X=-2000mm

a)

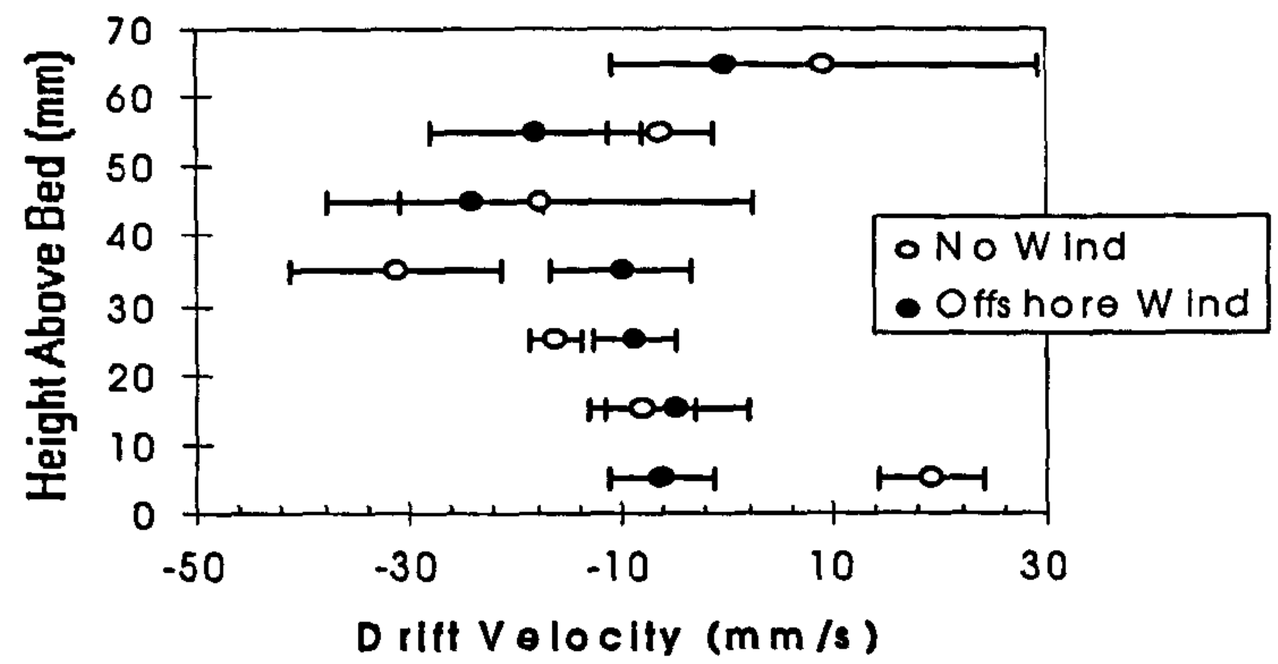

b)

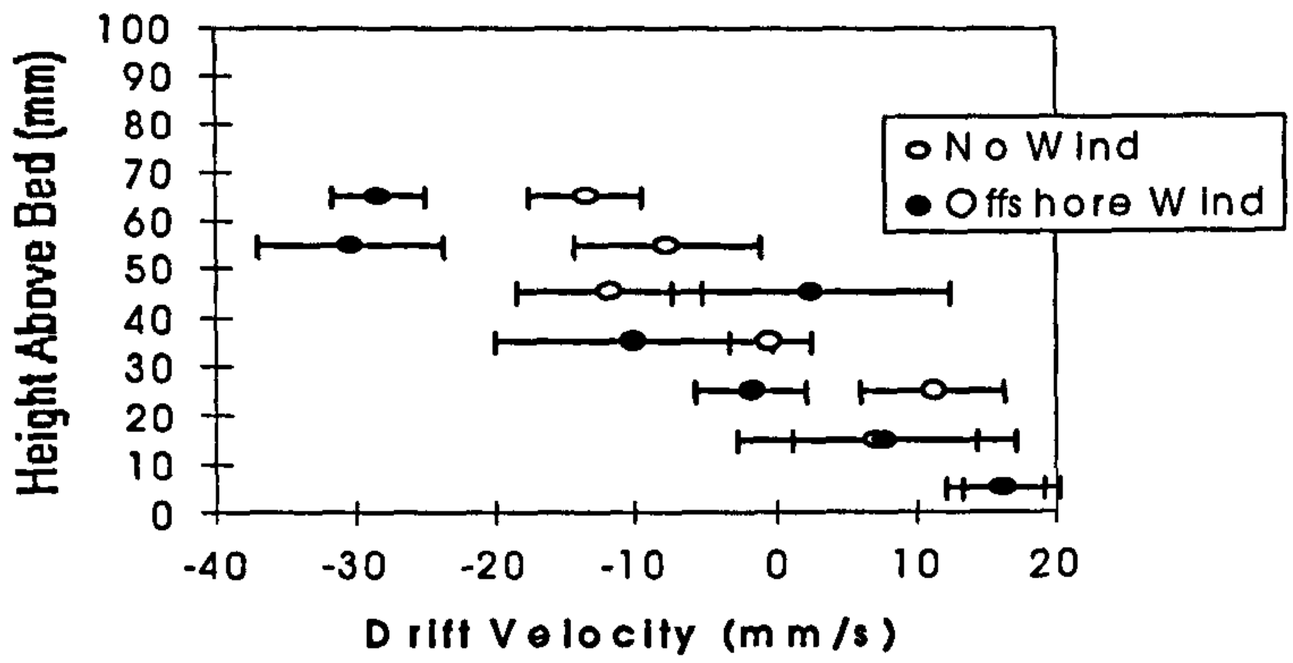

c)

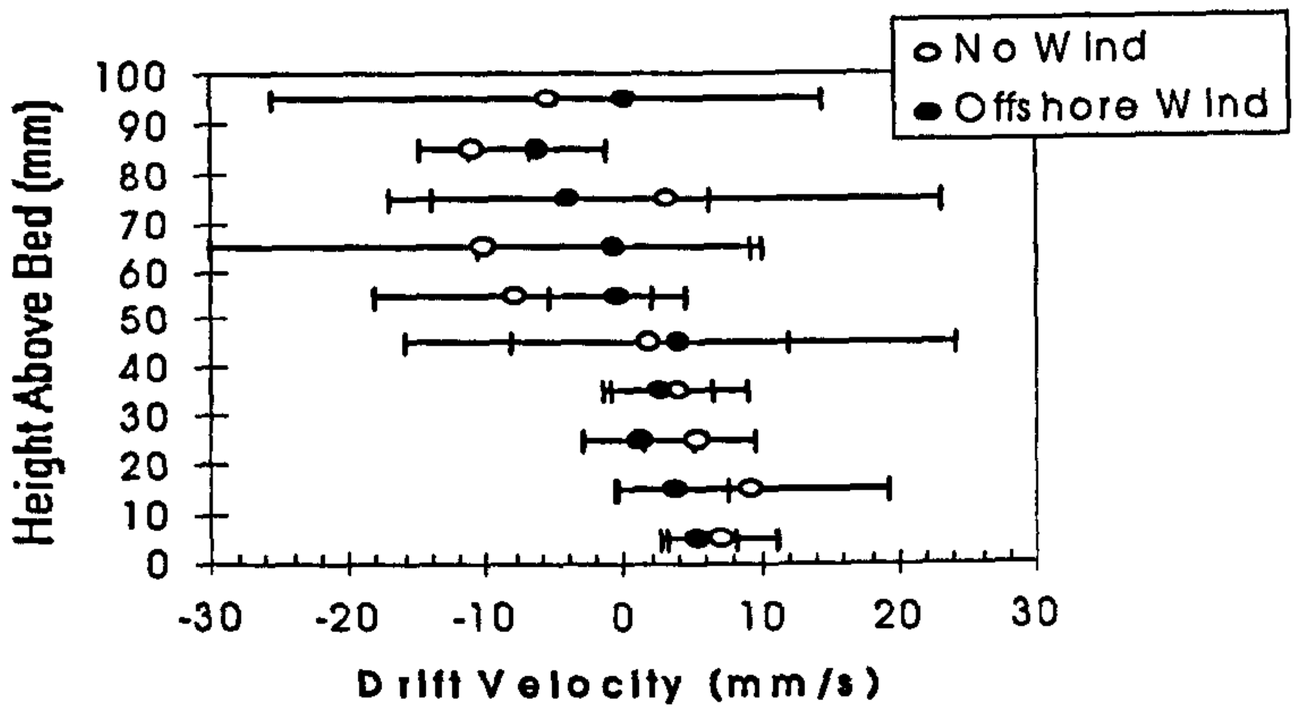

Figure 8.15 Horizontal particle drift velocities for spilling under offshore winds:
a) X=-1525mm b) X=-1755mm c) X=-2000mm

a)

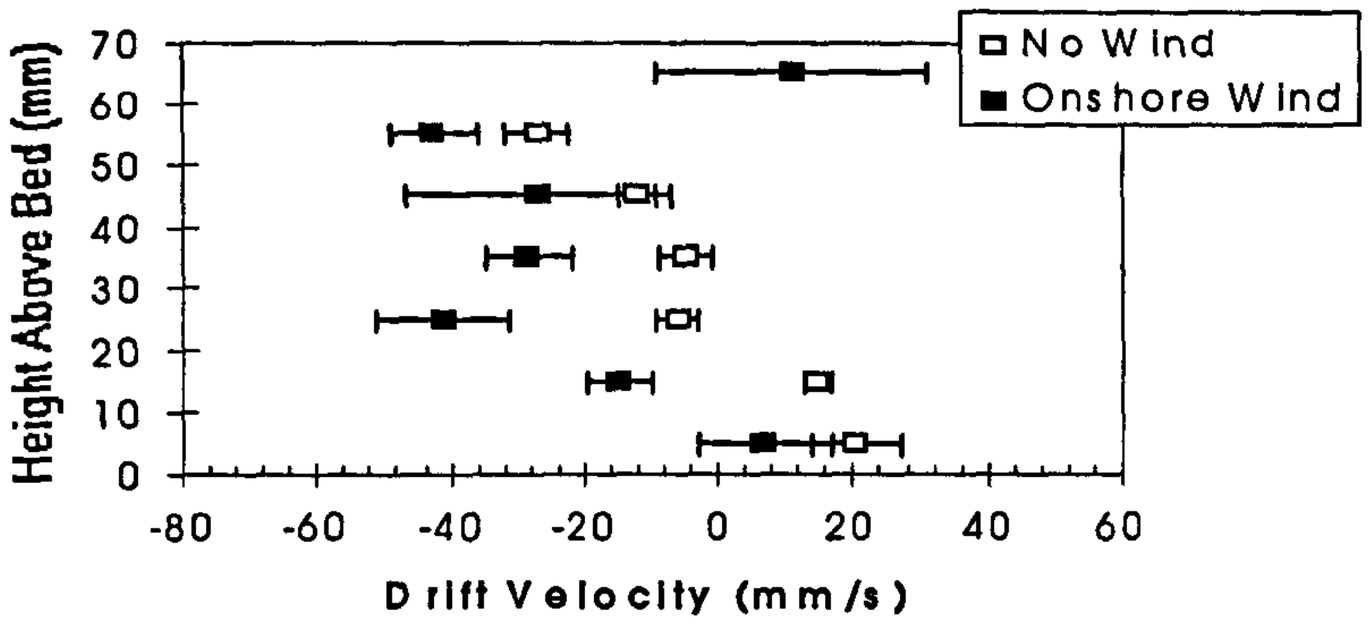

b)

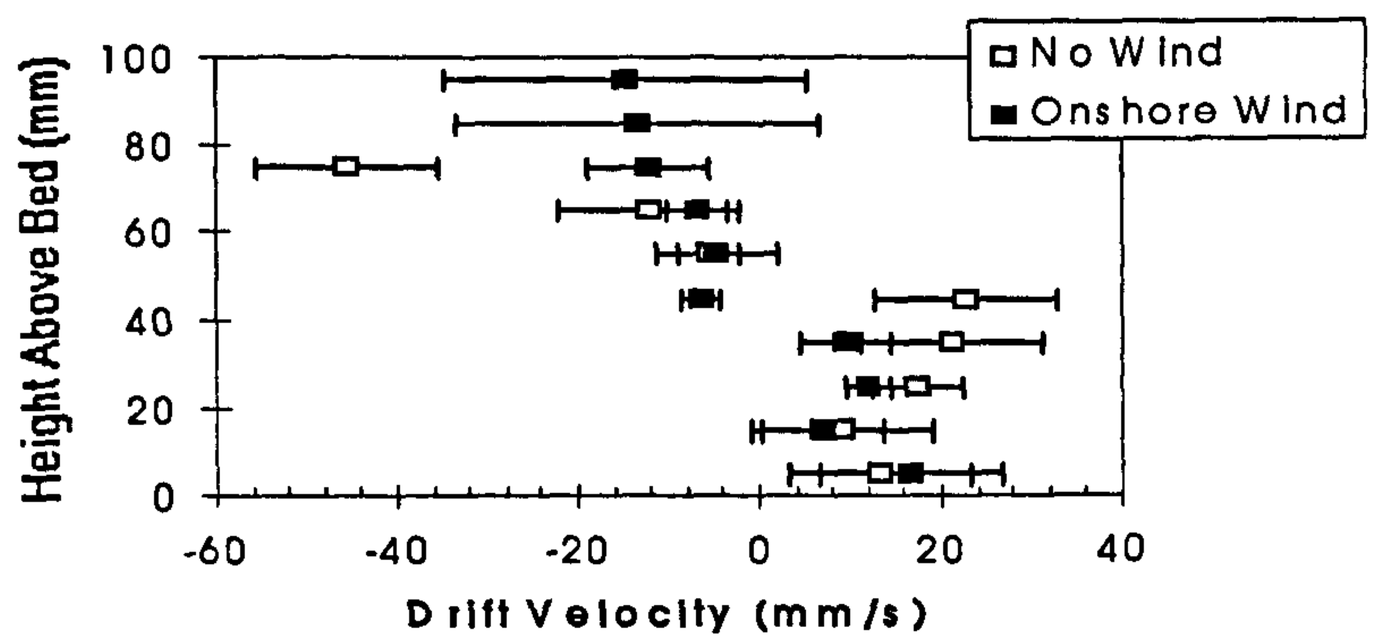

c)

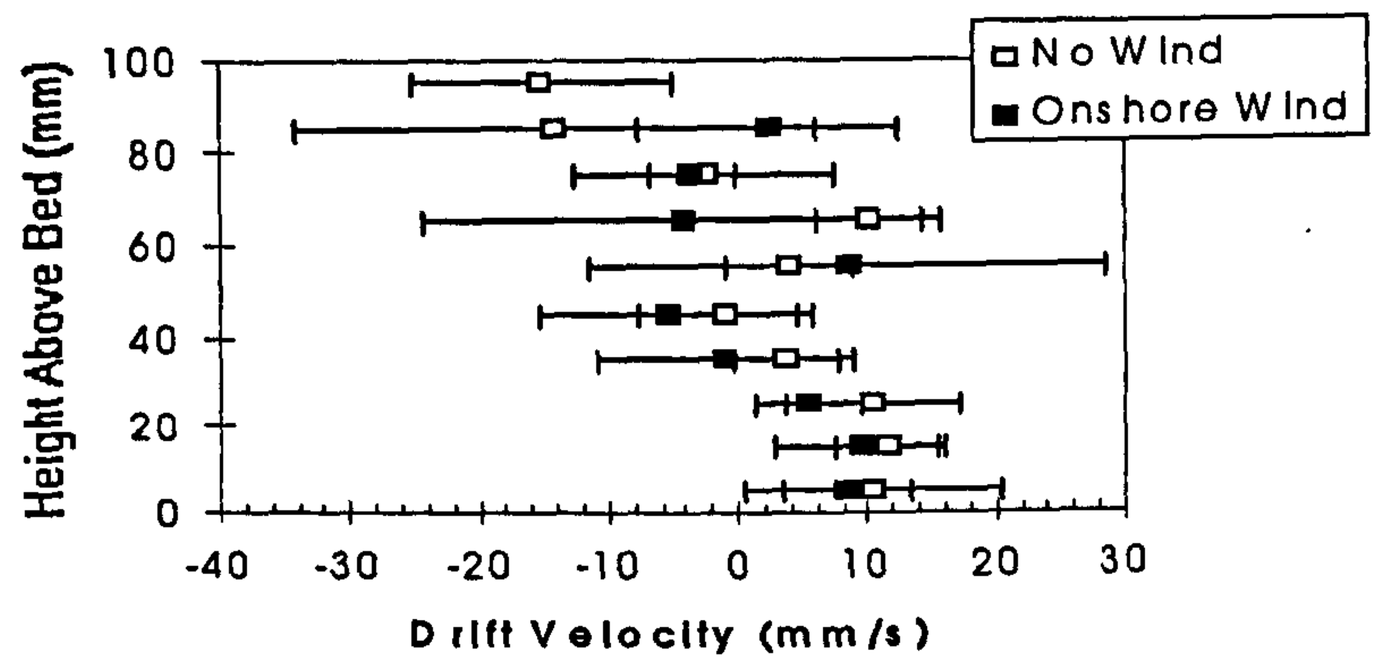

Figure 8.16 Horizontal particle drift velocities for spilling waves under onshore winds: a) X=-1525mm b) X=-1755mm c) X=-2000mm

a)

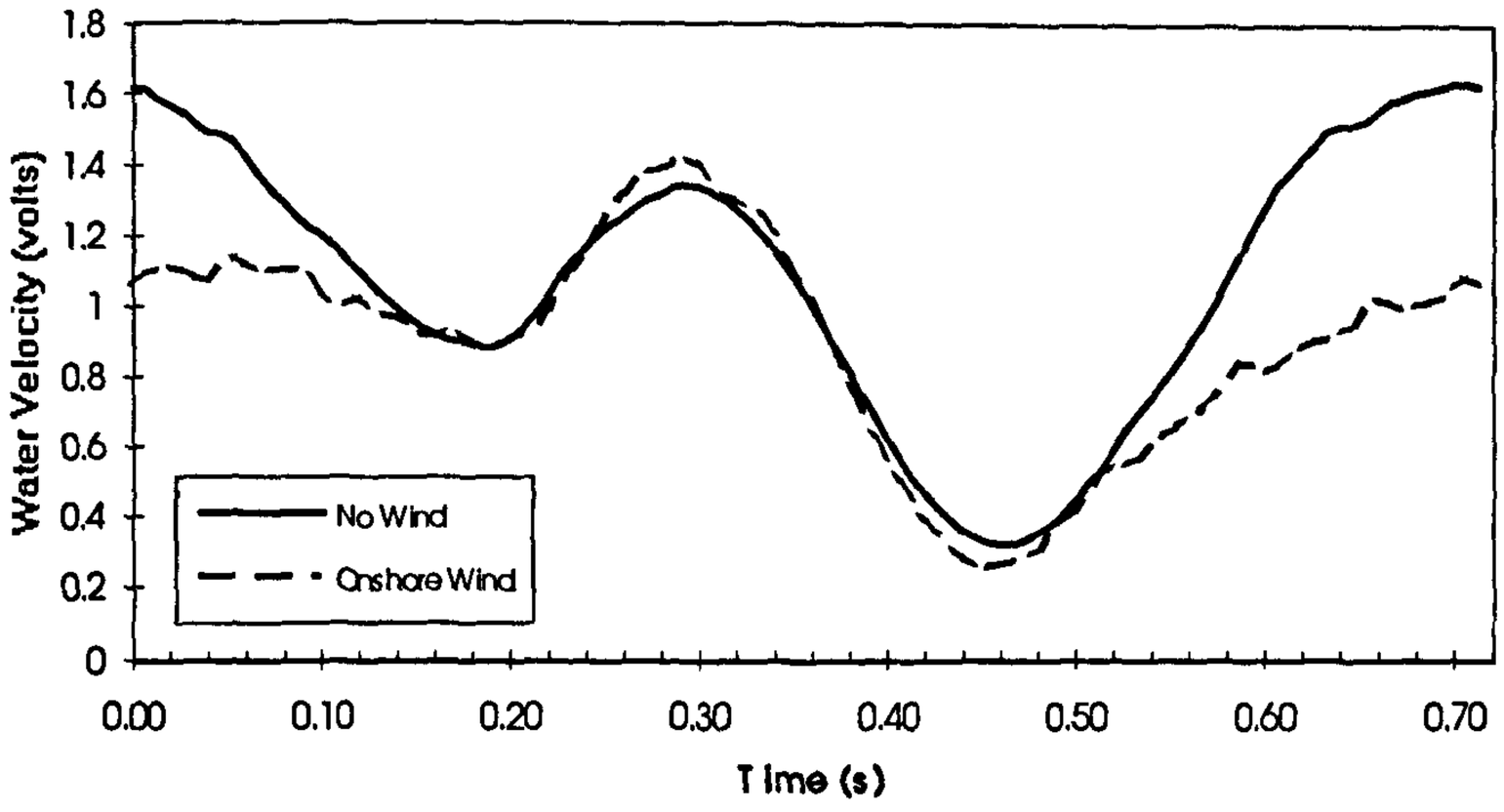

b)

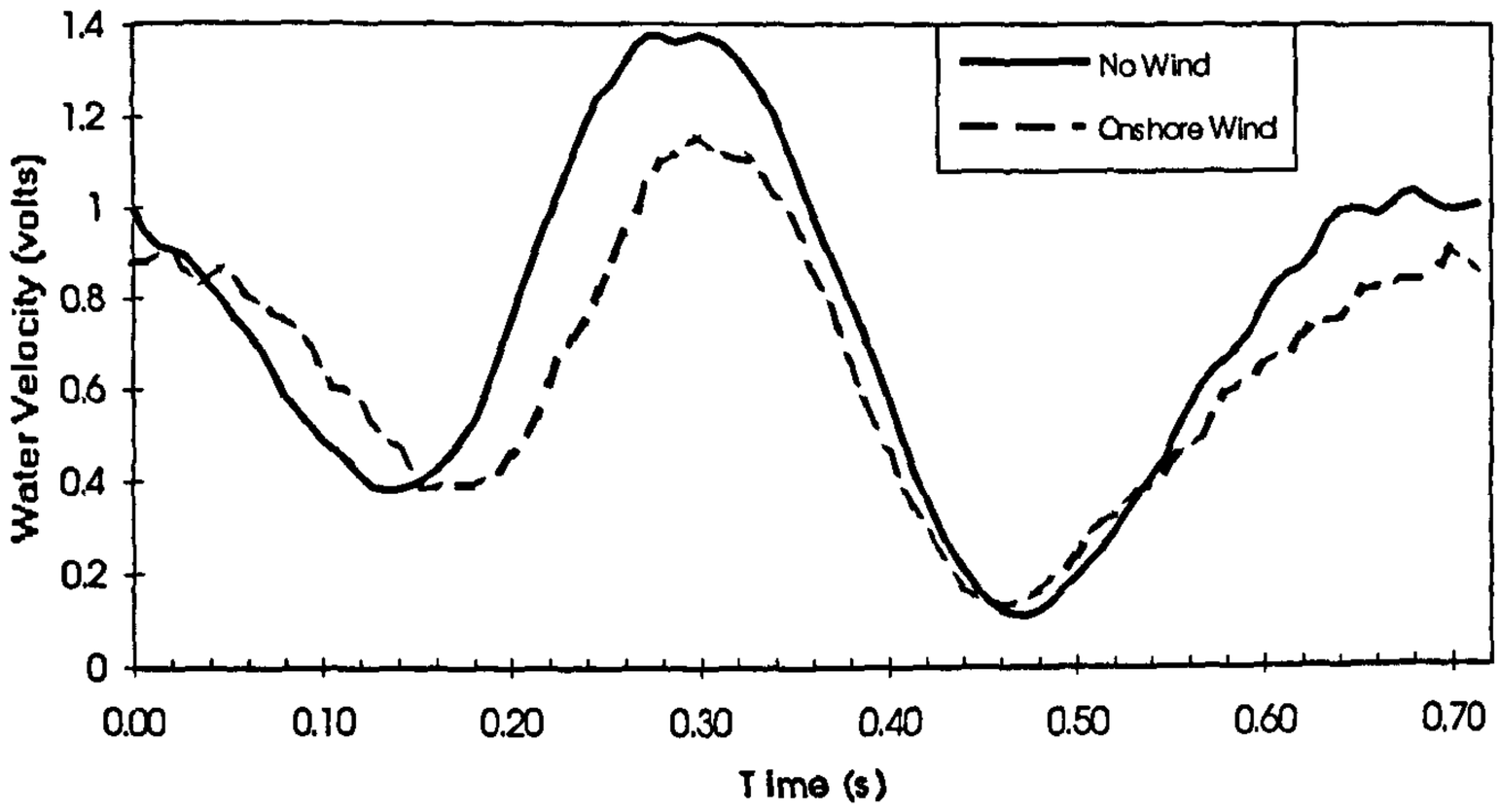

c)

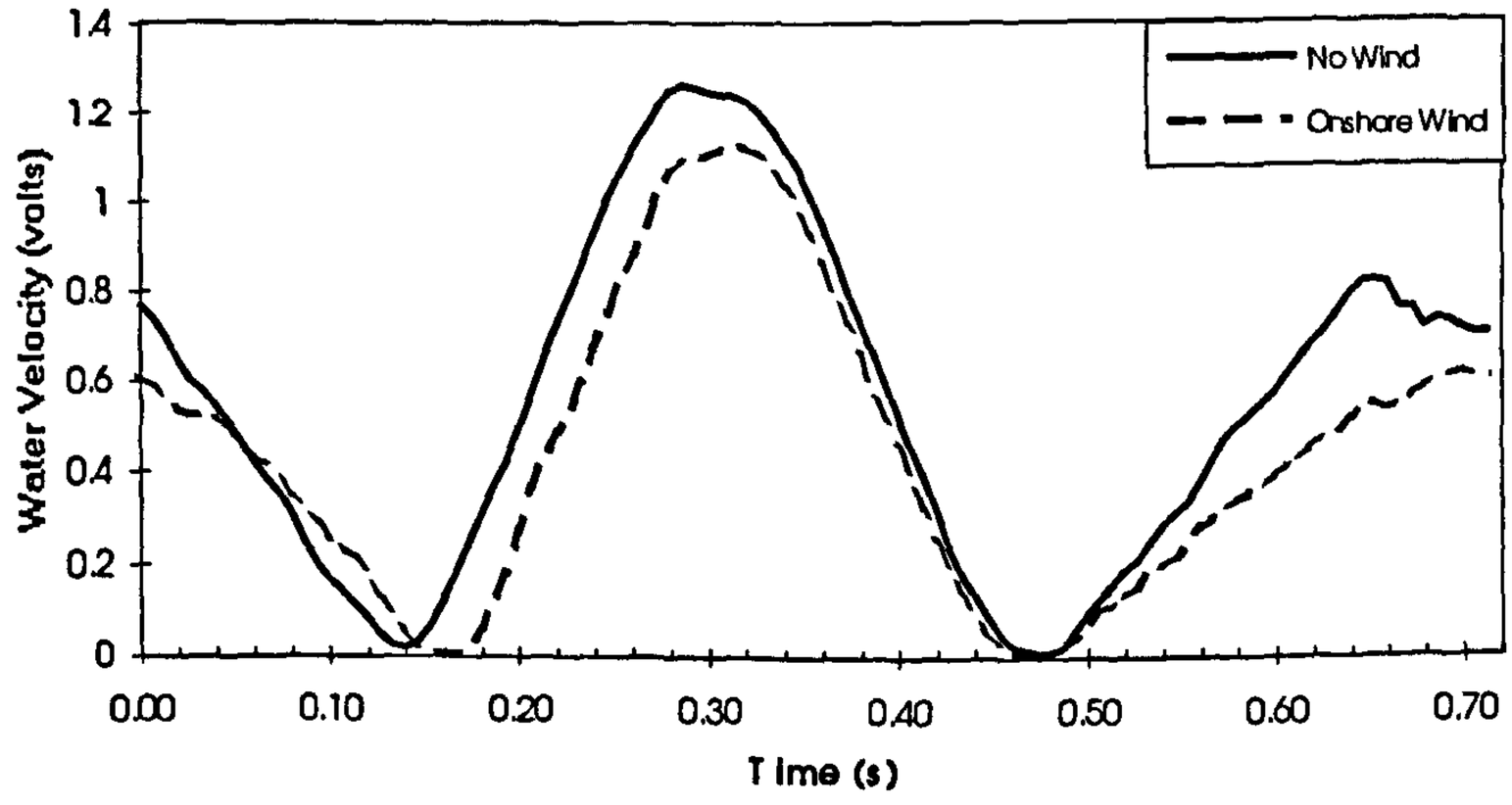

Figure 8.17 Onshore wind effect on internal water velocity for spilling waves at X=-1755mm. Height above bed: a) 50mm b) 30mm c) 10mm

a)

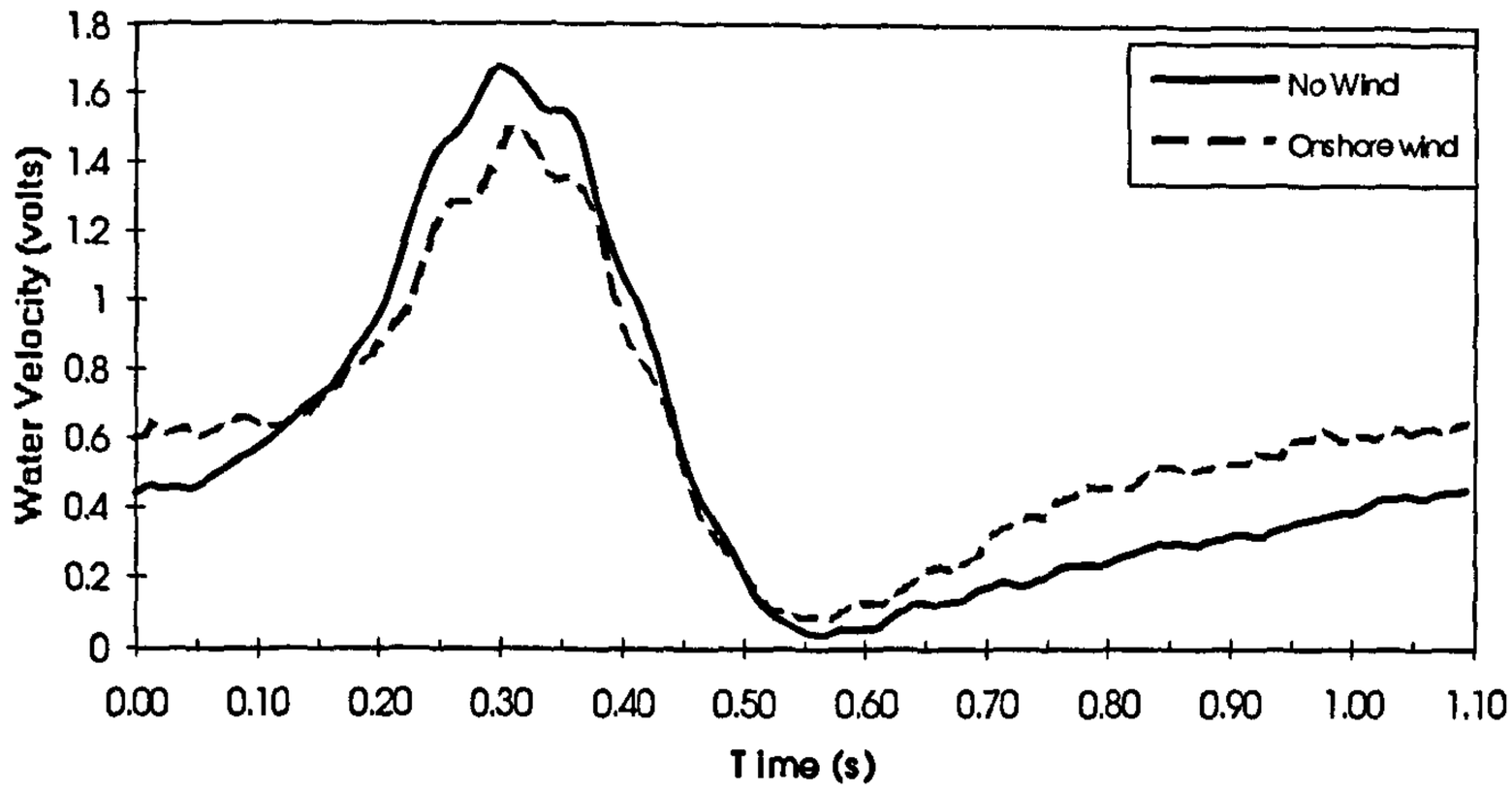

b)

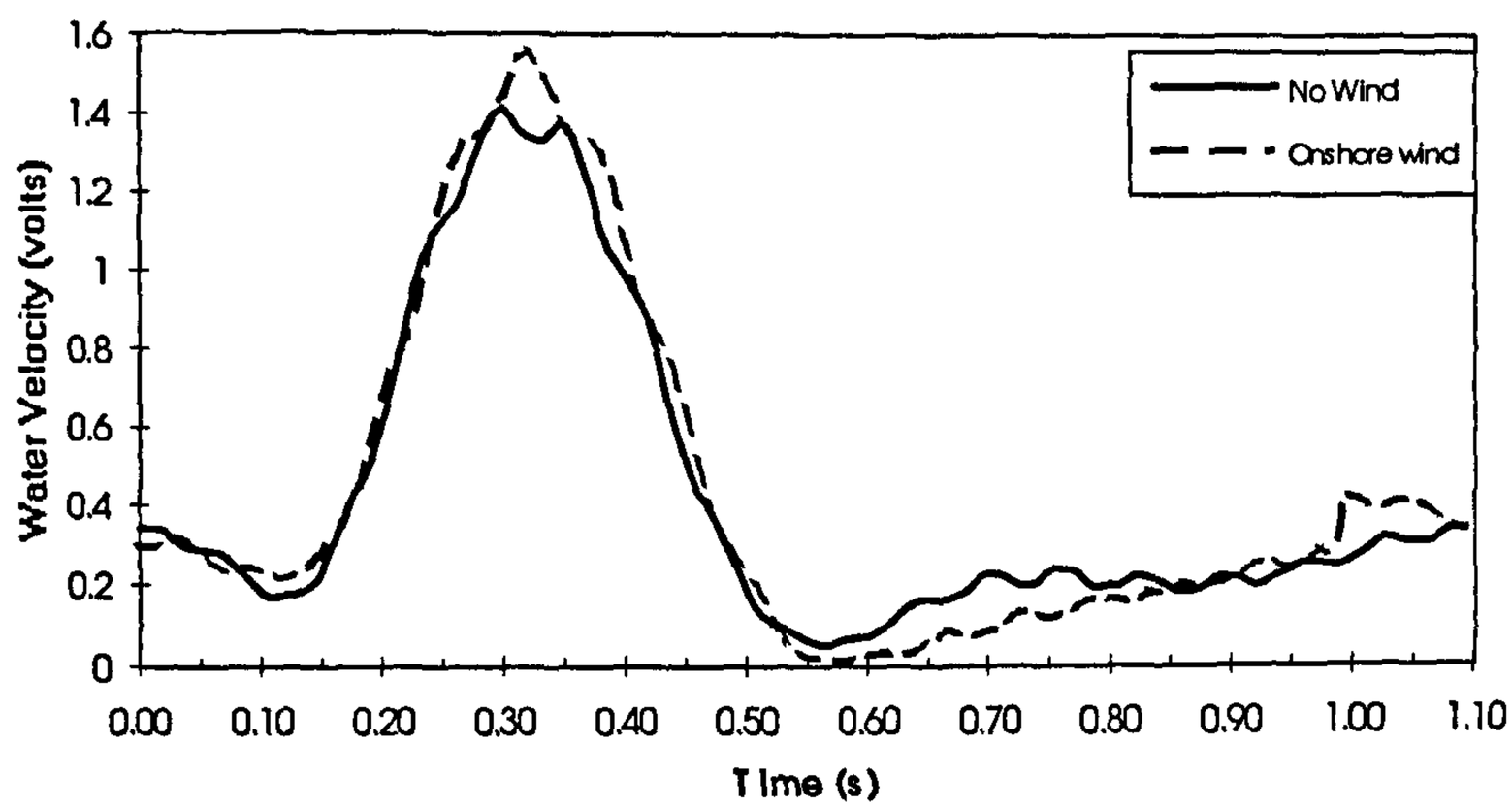

c)

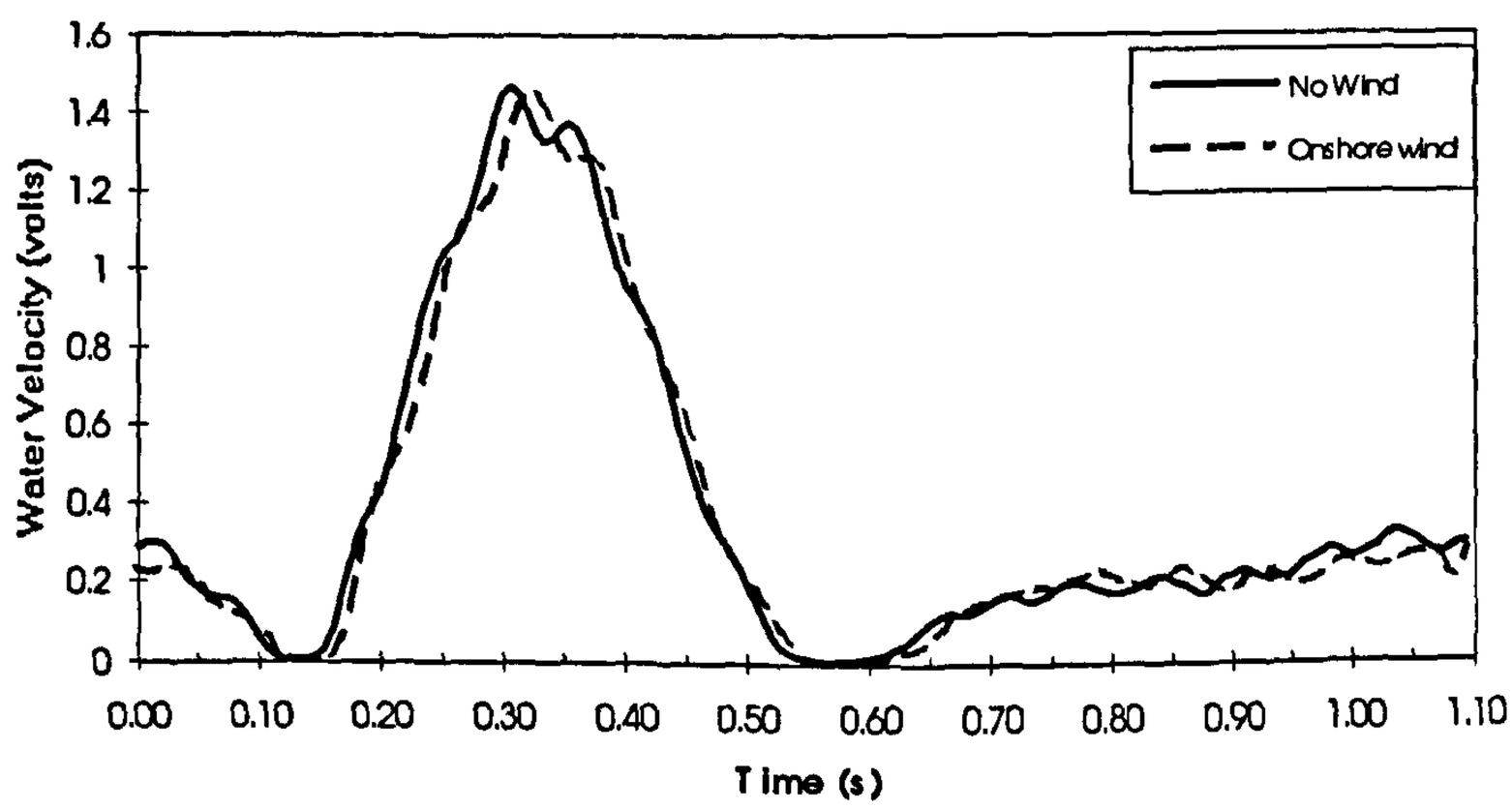

Figure 8.18 Onshore winds effect on internal water velocity for plunging waves at X=-1755mm. Height Above Bed: a) 50mm b) 30mm c) 10mm

a)

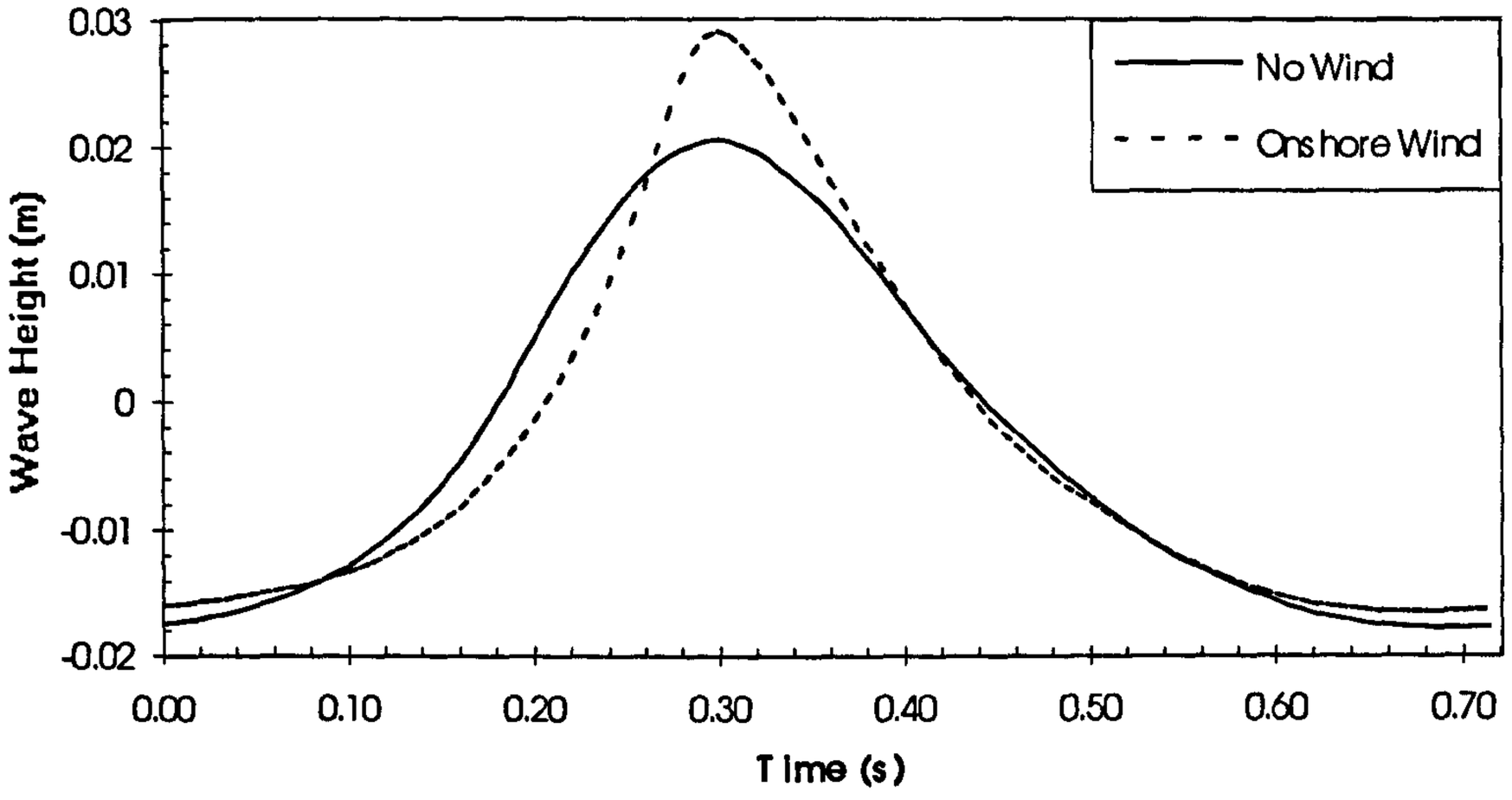

b)

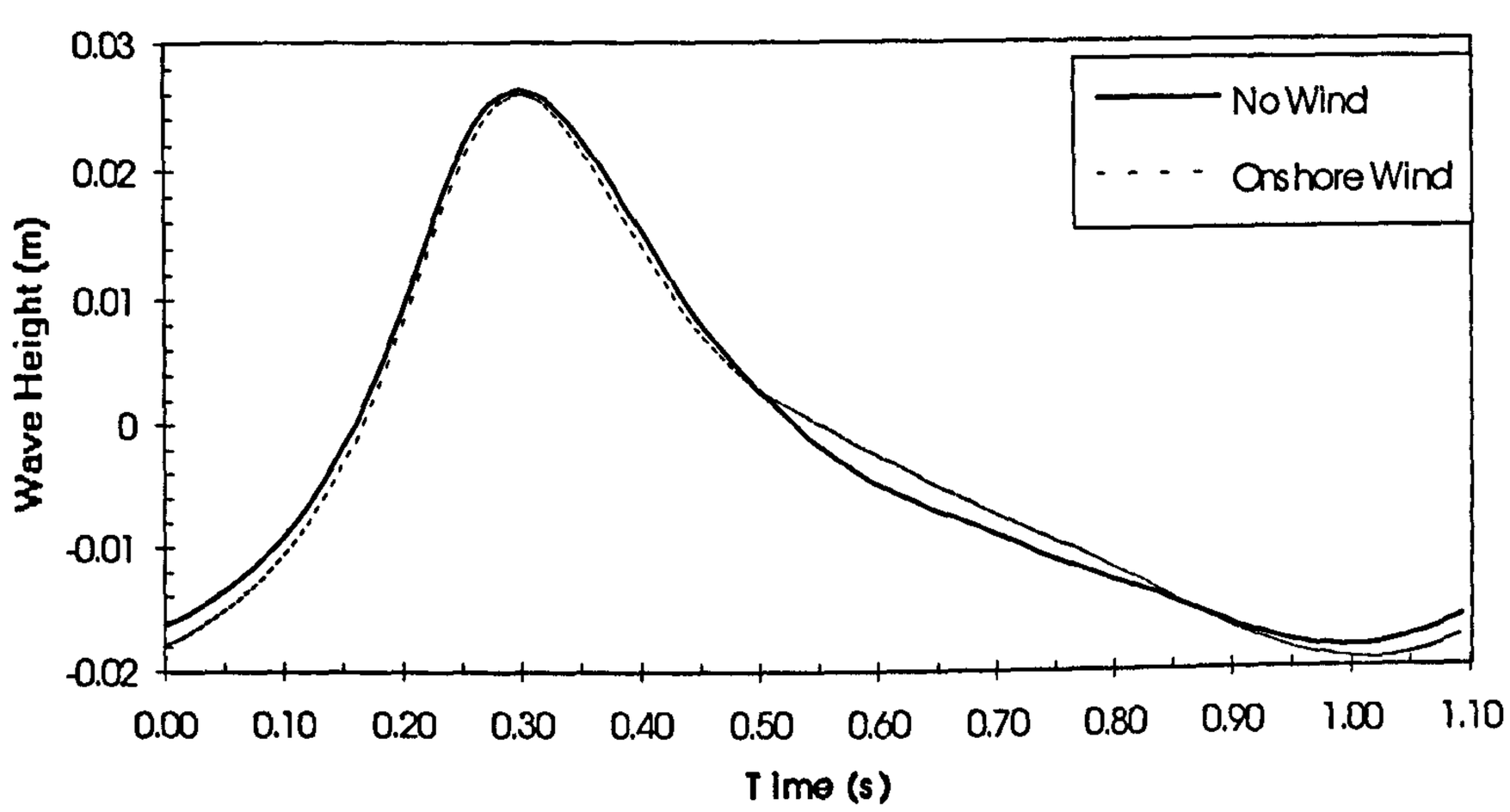

Figure 8.19 Onshore wind effect on phase-averaged wave profile at X=-1755mm. a) Spilling b) Plunging

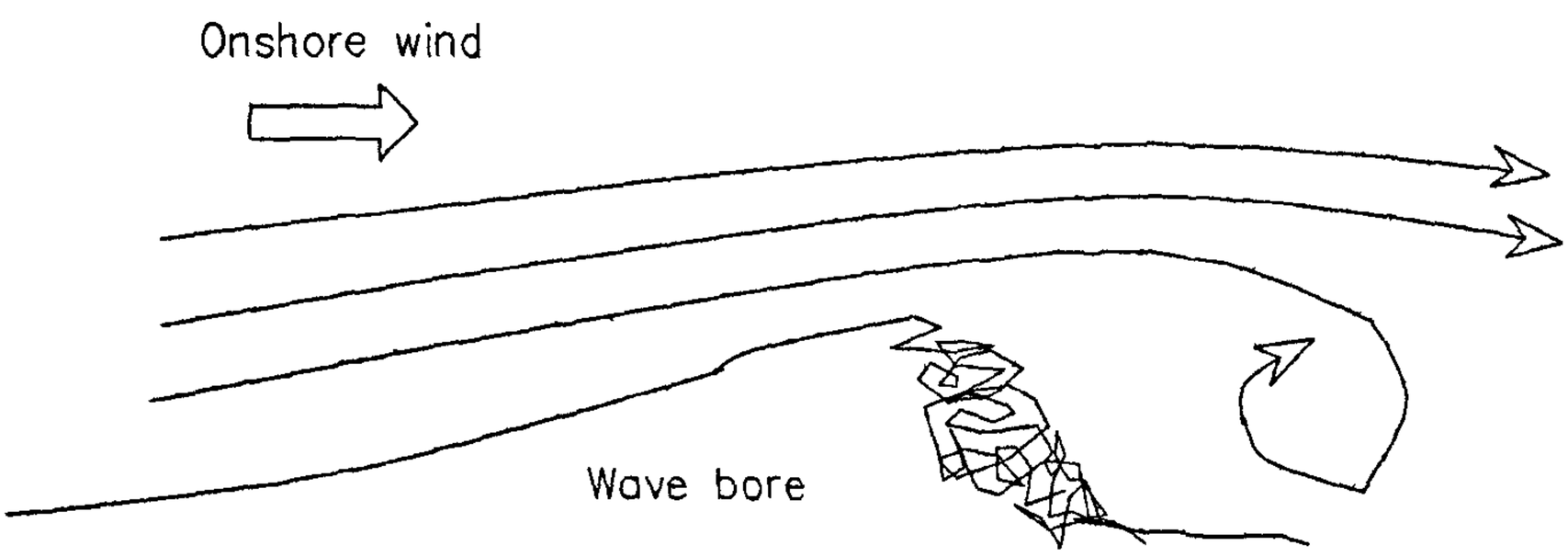

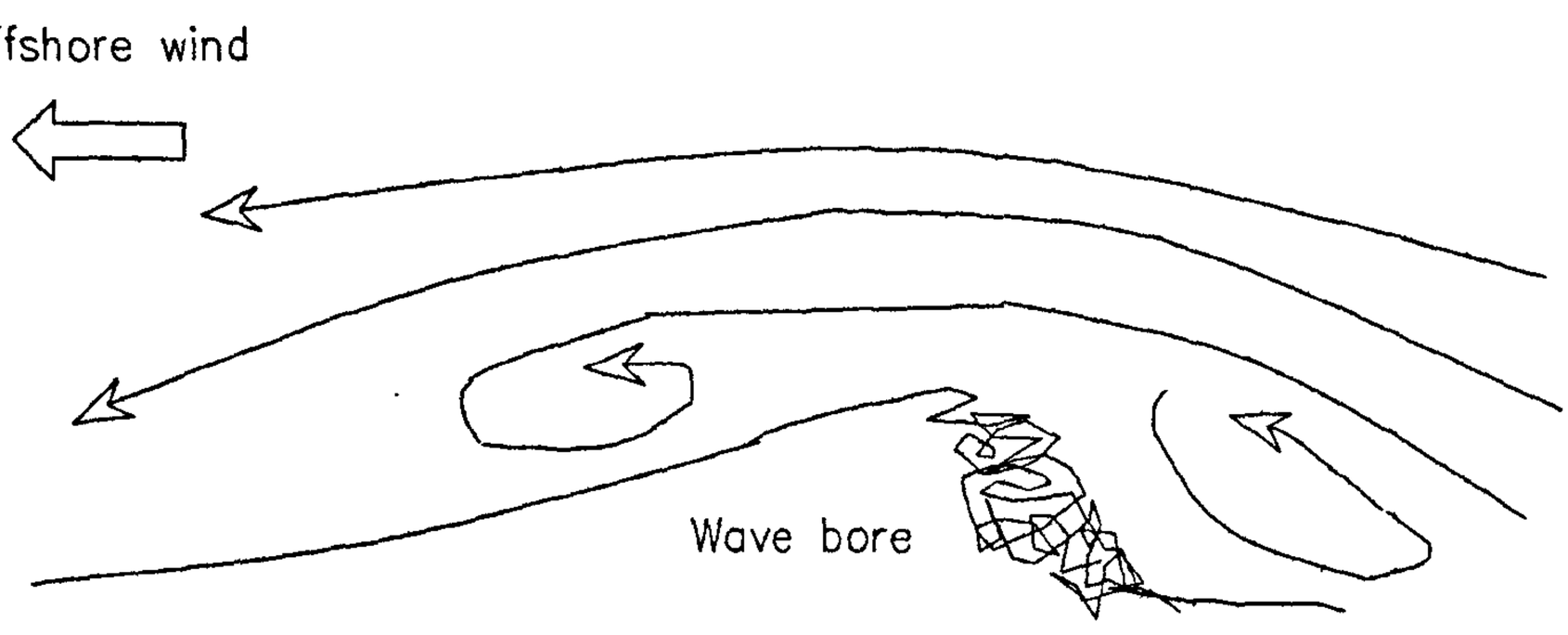

Figure 9.1 Possible effect of water turbulence at the front face of a wave bore on the air flow over the wave, for onshore and offshore winds.

APPENDICES

Appendix A

AIRY WAVE THEORY

Derived using the concepts of 2-D ideal fluid flow. Airy wave equations apply only to waves of small amplitude and do not give any information as to the wave height. This appendix contains a brief overview of the theory, some of which has been used in the main body of the thesis. For further details refer to Silvester (1974a).

For water depths where 0.5 > d/L > 0.04, (generally referred to as 'transitional' water depths), wave celerity is given by:

$$c = \frac{gT}{2\pi}\tanh\left(\frac{2\pi d}{L}\right) = c_o \tanh\left(\frac{2\pi d}{L}\right) \qquad \text{(A.1)}$$

where d is the water depth and L is the wavelength. The subscript 'o' denotes the value of that parameter in deep water.

At the extremes of water depth, where d/L<0.04 and d/L>0.5, the above equations can be simplified. The approximate, simplified equations are referred to as the shallow water and deep water approximations to the Airy wave theory.

Shallow Water Approximations

For d/L < 0.04, tanh(2πd/L) can be approximated by 2πd/L and therefore the equation for wave celerity can be expressed as in equation A.2.

$$c = \frac{gTd}{L} = \sqrt{gd} \qquad \text{(A.2)}$$

The shallow water limit ratio of water depth to wave length can be expressed in terms of d/L. Alternatively the limit can be expressed in the form: $d/L_0<0.004$,

(Silvester (1974a)). Working with L_o is easier since equation A.4 shows that it can be simply calculated from the wave period, T.

Deep Water Approximations

For d/L > 0.5 the equations can be expressed as in equations A.3 and A.4 since tanh(2πd/L) approaches unity.

$$c_o = \frac{gT}{2\pi} = \sqrt{\frac{gL_o}{2\pi}} \qquad \text{(A.3)}$$

and therefore

$$L_o = \frac{gT^2}{2\pi} \qquad \text{(A.4)}$$

Hence, in deep water the wave length and wave celerity are a function of wave period only.

It is useful to be able to calculate the ratio of d/L at a particular point, in order to be able to use certain equations which are defined in terms of d/L. The problem can be solved using the equation below, (Silvester (1974a)).

$$\frac{d}{L_o} = \frac{d}{L}\tanh\left(\frac{2\pi d}{L}\right) \qquad \text{(A.5)}$$

Thus for any water depth, d, the ratio of d/L can be calculated (assuming that the wave period is known so that L_o can be determined). Although Airy wave theory is strictly accurate only for waves of small amplitude, it provides a reasonable estimate of the deep water wavelength and ratio of d/L.

Silvester (1974a) provides a table of functions of d/L_o and this was used in order to estimate the difference between the 'true' deep water wave height, H_o, and the wave height in the deepest part of the wave tank, H_p. This showed that the ratio of H_p to H_o was roughly 0.92.

Appendix B

THE 2-D KOLMOGOROV-SMIRNOV TEST

The 2-D Kolmogorov-Smirnov test is a variation on the Kolmogorov-Smirnov test (or K-S test) for unbinned distributions that are functions of a single independent variable, (for example the lifetimes of lightbulbs). Data such as this can easily be converted to a cumulative distribution.

Different distribution functions (or sets of data) will give rise to different cumulative distributions functions. However since all cumulative distributions are identical at the smallest and largest allowable values of the variable (where the cumulative percentage of data is zero and 100% respectively). It is therefore the behaviour of the distribution between the largest and smallest values that distinguishes the distribution. The K-S test determines the maximum value of absolute difference between two cumulative distribution functions. Hence for a single set of data, the cumulative distribution function, (c.d.f.), must be compared with the known or expected c.d.f.

The 2-D K-S test is a variation on this in that each point in the 2-D distribution is categorized by an (x,y) pair of values. The cumulative difference between two sets of data is defined by the integrated probabilities in each of four quadrants around a given point.

Thus for two data sets: (a_i,b_i) and (c_j,d_j), each point in turn is taken as the origin and the relative proportions of data in each quadrant calculated. The maximum difference between the relative proportions is taken as the test statistic, D. For example if for point (a_n,b_n) data set one has in the first quadrant 0.56 of its data points and data set two has 0.12 of its data points, then the cumulative difference for that quadrant is 0.44. The test involves finding the maximum difference, for all quadrants and taking all data points as the origin. The maximum difference, D, is then used to calculate the significance level, which is given by:

$$\text{Prob. (D>observed)} \;=\; Q_{ks} \;=\; \frac{\sqrt{N}D}{1+\left[\sqrt{1-r^2}\left(0.25-\frac{0.75}{\sqrt{N}}\right)\right]} \qquad \text{(B.1)}$$

where: $\mathrm{N} = \dfrac{N_1 N_2}{N_1 + N_2}$

r = coefficient of correlation

N = sample size

The formulas are accurate enough when N>20 and when the significance level is less than approxmately 0.2. For significance levels greater than 0.2 the value may not be accurate, but the implication that the data sets are not significantly different is certainly correct.

For the work reported here, the K-S significance levels are calculated from the Fortran routines given in Press et al, (1992), ***Numerical Reciepes in Fortran: the art of scientific computing***, a full reference is included with the main reference section. A full listing of the working fortran program is presented in King & Baker (1993).

Appendix C

TABULATED RESULTS FOR AERODYNAMIC ROUGHNESS AND FRICTION VELOCITY

Appendix C contains the tabulated results from chapters 5 and 6. X and U_{ref} are as defined in chapter 4.

Table C.1. Flat Water Results

Wind	Probe Type	X (mm)	U_{ref} (m/s)	u_* (cm/s)	z_o (m)
Onshore	Single-film	100	1.823	11.9	4E-8
		-1265	1.714	20.5	5E-5
		-2164	1.513	21.7	1E-4
	X-film	100	1.256	5.6	1E-10
		-1265	0.951	8.2	1E-6
		-2164	0.856	14.9	4E-4
Offshore	single-film	-2658	1.703	20.9	5E-5
		-1265	1.687	17.7	1E-5
	X-film	-1265	1.091	5.1	3E-10
		-2312	1.289	9.3	1E-5

Table C.2. Results for Plunging waves

WIND	Probe Type	X (mm)	U_{ref} (m/s)	u_* (cm/s)	z_o (m)
Onshore	Single-film	100	1.750	12.4	3E-7
		-912	1.601	18.9	5E-5
		-1289	1.695	18.5	2E-5
		-1795	1.667	23.9	1E-4
	X-film	100	1.146	7.4	4E-8
		-912	1.323	18.2	1E-4
		-1289	1.363	17.0	6E-5
		-1800	1.112	16.6	2E-4
Offshore	Single-film	-912	1.703	18.5	3E-5
		-1404	1.713	30.8	7E-4
		-1811	1.522	36.3	2E-3
		-2640	1.325	22.1	3E-4
	X-film	-912	1.217	12.0	1E-5
		-1404	1.233	18.2	2E-4
		-1811	0.991	26.5	3E-3
		-2640	0.882	16.2	5E-4

Table C.3. Results for Spilling waves

WIND	Probe Type	X (mm)	U_{ref} (m/s)	u_* (cm/s)	z_0 (m)
Onshore	Single-film	100	1.809	14.5	8E-7
		-912	1.799	29.7	5E-4
		-1554	1.653	25.3	2E-4
		-1800	1.573	28.6	6E-4
	X-film	100	1.145	7.4	6E-8
		-912	1.263	21.9	6E-4
		-1554	1.163	17.4	2E-4
		-1800	1.142	21.9	9E-4
Offshore	Single-film	-2656	1.437	18.4	6E-5
		-1575	1.447	35.5	2E-3
		-1177	1.671	25.0	3E-4
		-912	1.700	24.3	2E-4
	X-film	-912	1.125	13.0	3E-5
		-1177	1.2	19.4	4E-4
		-1575	1.113	25.9	2E-3
		-2656	1.013	14.0	1E-4

Appendix D

TABULATED RESULTS FOR WAVE CHARACTERISTICS

Appendix D contains the normalised data for the winds' influence on the waves as presented in chapter 7. Table D.1 contains the data for offshore winds, table D.2 the data from the onshore configuration.

Table D.1. Offshore Winds

Wave	Breaker Type	T (s)	$\frac{U}{\sqrt{g H_p}}$	$\frac{H_p}{g T^2}$	$\frac{H_b}{g T^2}$	$\frac{d_b}{g T^2}$	X_s (mm)	X to plunge point (mm)
Wave 1	P	1.10	0.0	0.00258	0.00502	0.00505	1429	1185
	P		-4.015		0.00472	0.00472	1368	1120
	P		-5.037		0.00457	0.00455	1315	1097
	P		-6.363		0.00470	0.00455	1315	1097
Wave 2	S	0.75	0.0	0.00632	0.00756	0.01070	1472	-
	T		-3.223		0.00732	0.00997	1282	-
	T		-4.857		0.00743	0.00906	1143	-
	T		-6.371		0.00694	0.00906	1143	-
Wave 3	P	0.95	0.0	0.00356	0.00588	0.00700	1475	1265
	P		-3.382		0.00566	0.00700	1475	1245
	P		-4.954		0.00546	0.00632	1355	1185
	P		-6.656		0.00564	0.00632	1355	1138
Wave 4	T	0.83	0.0	0.00630	0.00812	0.00991	1570	-
	P		-2.568		0.00765	0.00917	1472	1215
	P		-4.379		0.00735	0.00917	1472	1180
	P		-5.222		0.00765	0.00917	1472	1180
Wave 5	P	1.10	0.0	0.00323	0.00458	0.00581	1609	1355
	P		-2.924		0.00463	0.00581	1609	1265
	P		-5.103		0.00463	0.00581	1609	1165
	P		-6.341		0.00497	0.00539	1476	1113
Wave 6	P	0.90	0.0	0.00539	0.00696	0.00894	1678	1425
	P		-2.096		0.00693	0.00894	1678	1425
	P		-4.565		0.00696	0.00894	1678	1380
	P		-6.770		0.00682	0.00843	1600	1305
Wave 7	S	0.90	0.0	0.00342	0.00491	0.00642	1259	-
	S		-3.161		0.00462	0.00629	1166	-
	T		-5.057		0.00457	0.00591	1019	-
	T		-6.898		0.00437	0.00503	848	-
Wave 8	S	1.00	0.0	0.00243	0.00405	0.00510	1175	-
	T		-2.310		0.00396	0.00510	1175	-
	T		-5.302		0.00409	0.00510	1175	-
	T		-8.727		0.00370	0.00499	1083	-
Wave 9	P	0.90	0.0	0.00447	0.00590	0.00856	1579	1340
	P		-2.906		0.00570	0.00856	1579	1315
	P		-5.138		0.00605	0.00768	1519	1260
	P		-7.107		0.00579	0.00629	1245	1035

Wave 10	T	0.84	0.0	0.00468	0.00579	0.00780	1352	-
	T		-3.705		0.00574	0.00722	1267	1023
	P		-5.061		0.00589	0.00708	1184	1023
	P		-6.582		0.00455	0.00665	1027	875
Wave 11	S	0.75	0.0	0.00736	0.00883	0.01250	1631	-
	T		-2.768		0.00884	0.01250	1631	-
	T		-4.852		0.00904	0.01110	1476	-
	P		-5.872		0.00928	0.01050	1429	1152
Wave 12	P	1.00	0.0	0.00381	0.00538	0.00673	1533	1287
	P		-2.646		0.00557	0.00673	1533	1254
	P		-4.494		0.00569	0.00673	1533	1254
	P		-5.937		0.00578	0.00673	1533	1197

Table D.2. Onshore Winds

Wave	Breaker Type	T (s)	$\frac{U}{\sqrt{g H_p}}$	$\frac{H_p}{g T^2}$	$\frac{H_b}{g T^2}$	$\frac{d_b}{g T^2}$	X_s (mm)	X to plunge point (mm)
Wave 1	P	1.10	0.0	0.00308	0.00360	0.00447	1174	964
	P		1.767		0.00381	0.00447	1174	964
	T		3.458		0.00432	0.00539	1388	-
	S		4.556		0.00402	0.00598	1472	-
Wave 2	P	0.90	0.0	0.00593	0.00760	0.00894	1654	1404
	P		1.801		0.00745	0.00894	1654	1404
	T		3.061		0.00722	0.00956	1719	1428
	T		5.155		0.00700	0.00956	1719	1398
Wave 3	T	0.90	0.0	0.00515	0.00670	0.00843	1478	1128
	S		1.803		0.00662	0.00856	1507	-
	S		3.053		0.00668	0.00868	1570	-
	S		4.728		0.00646	0.00881	1620	-
Wave 4	P	1.00	0.0	0.00368	0.00585	0.00530	1229	967
	P		2.114		0.00480	0.00530	1229	967
	T		3.366		0.00511	0.00663	1434	-
	T		4.814		0.00511	0.00673	1455	-
Wave 5	P	0.75	0.0	0.01040	0.01120	0.01290	1657	1372
	P		2.229		0.01110	0.01290	1657	1372
	P		3.598		0.01140	0.01290	1657	1372
	P		4.102		0.01100	0.01290	1657	1436
Wave 6	T	0.75	0.0	0.00919	0.00897	0.01250	1558	-
	S		1.724		0.00997	0.01270	1611	-
	S		2.860		0.00997	0.01270	1611	-
	S		4.729		0.00986	0.01340	1684	-
Wave 7	T	0.77	0.0	0.00798	0.00851	0.00739	1056	-
	T		1.248		0.00818	0.00739	1056	-
	S		3.007		0.00892	0.01150	1468	-
	S		4.181		0.00830	0.01190	1523	-
Wave 8	S	0.67	0.0	0.01120	0.01110	0.01700	1734	-
	S		1.472		0.01140	0.01700	1734	-
	S		2.859		0.01150	0.01700	1734	-
	S		4.068		0.01100	0.01840	1843	-
Wave 9	P	0.71	0.0	0.00827	0.00865	0.01030	1204	959
	P		1.876		0.00902	0.01030	1204	959
	P		3.307		0.00902	0.01030	1204	964
	T		4.537		0.00926	0.01400	1542	-
Wave 10	P	0.97	0.0	0.00377	0.00543	0.00596	1251	962
	P		1.616		0.00549	0.00596	1251	962
	P		3.488		0.00570	0.00596	1251	962
	P		5.141		0.00530	0.00672	1375	1039

Wave 11	S	0.70	0.0	0.01070	0.01210	0.01410	1517	-
	S		1.634		0.01160	0.01410	1517	-
	S		3.018		0.01220	0.01560	1709	-
	S		3.867		0.01260	0.01660	1782	-
Wave 12	T	0.63	0.0	0.01300	0.01290	0.01770	1557	-
	S		1.360		0.01300	0.01770	1557	-
	S		3.042		0.01270	0.01820	1661	-
	S		4.264		0.01300	0.01820	1661	-